NBSIR 83-2742

Photonuclear Data - Abstract Sheets 1955 - 1982 Volume V (Flourine - Magnesium)

U.S. DEPARTMENT OF COMMERCE
National Bureau of Standards
National Measurement Laboratory
Center for Radiation Research
Washington, DC 20234

March 1984

U.S. DEPARTMENT OF COMMERCE
NATIONAL BUREAU OF STANDARDS

NBSIR 83-2742

PHOTONUCLEAR DATA - ABSTRACT SHEETS 1955 - 1982 VOLUME V (FLOURINE - MAGNESIUM)

E. G. Fuller, Henry Gerstenberg

U.S. DEPARTMENT OF COMMERCE
National Bureau of Standards
National Measurement Laboratory
Center for Radiation Research
Washington, DC 20234

March 1984

U.S. DEPARTMENT OF COMMERCE, Malcolm Baldrige, *Secretary*
NATIONAL BUREAU OF STANDARDS, Ernest Ambler, *Director*

TABLE OF CONTENTS

Photonuclear Data-Abstract Sheets
1955-1982

I. Introduction

As used in connection with this collection of data-abstract sheets, the term photonuclear data is taken to mean any data leading to information on the electromagnetic matrix element between the ground state and excited states of a given nuclide. The most common types of reactions included in this compilation are: (e,e'), (γ,γ), (γ,γ'), (γ,n), (γ,p), etc. as well as ground-state particle capture reactions, e.g. (α,γ_0). Two reactions which fit the matrix element criterion are not included in the compilation because of their rather special nature. These are heavy particle Coulomb excitation and the thermal neutron capture reaction (n,γ_0). While the energy region of particular interest extends from 0 to 150 MeV, papers are indexed which report measurements in the region from 150 MeV to 4 GeV. Most of the experiments listed are concerned with the excitation energy range from 8 to 30 MeV, the region of the photonuclear giant resonance.

The hierarchical grouping of the photonuclear data-abstract sheets within the file is by: 1. Target Element, 2. Target Isotope, and 3. by the Bibliographic Reference Code assigned to the paper from which the data on the sheet were abstracted. In this file, colored pages are used to mark the beginning and end of the sheets for each chemical element. A brief historical sketch of the element is given on the divider sheet marking the start of each section; the information for this sketch was derived from references such as the Encyclopaedia Britannica. In those cases where the sheets for a given element make up a major part of a volume, colored pages are also used to delineate sections pertaining to the individual isotopes of the element. Each of the sections of the file, as delineated by two colored divider sheets, represents a 27 year history of the study of electromagnetic interactions in either a specific nuclide or a specifc element.

The data-abstract sheets are filed under the element and/or isotope in which the ground-state electromagnetic transition takes place. For example, the abstract sheet for a total neutron yield measurement for a naturally occurring copper sample would appear in the elemental section of the copper file. On the other hand, a measurement of the ^{62}Cu 9.73 minute positron activity produced in the same sample by photons with energies below the three-neutron separation energy for ^{65}Cu (28.68 MeV) would be filed with the sheets for ^{63}Cu. Similarly a measurement of the ground-state neutron capture cross section in ^{12}C would be filed under ^{13}C while the corresponding ground-state alpha-particle capture cross section would be filed under ^{16}O.

At the end of this volume there is a master list of the abbreviations that have been used in the index section of the abstract sheets. The listings are those used in the final published index, Photonuclear Data Index, 1973-1981, NBSIR 82-2543, issued in August 1982 by the U. S. Department of Commerce, National Bureau of Standards, Washington, DC 20234. In some cases two notations are entered for the same quantity. The second entry is the abbreviation that was used in one or more of the earlier published editions of the index.

FLUORINE
Z=9

Fluorine is the most reactive of all known chemical elements; this property hindered its original preparation and makes its handling even difficult today. This extreme reactivity brought agony and death to some of the pioneer investigators.

Georgius Agricola (1494-1555), a German scholar and man of science, wrote in his first mineralogical work Bermannus (1530), that fluorspar was used as a flux in metal smelting; the stones melted in the heat of the fire and caused the material in the fire to become more fluid. In 1670, Heinrich Schwanhard of Nuremberg treated the mineral with strong acids and discovered he could etch glass with the solution. He was a member of a family of glass cutters and raised the etching process to a high art by making scenes, in relief on glass, for Emperor Charles II. Scheele did extensive investigations of fluorspar and published papers in 1780 and 1786 claiming that fluorspar contained a peculiar acid; he called it "fluoric" (from the Latin "*fluo*", flow). This new acid immediately aroused widespread interest. Sir Humphry Davy (1778)-1829) and A. -M. Ampere (1775-1836) recognized in 1813 that the acid must be a compound of hydrogen and an unknown element for which the name "fluorine" was suggested by Ampere. Davy made numerous attempts to isolate the element and it was not until 1886 that Henri Moissan (1852-1907), made a successful preparation. This method used a platinum cell with platinum electrodes but the weight loss of the platinum exceeded the weight of the fluorine produced! The problem of making fluorine on a large scale was not solved until after 1939 when uranium hexafluoride became needed as part of the atomic energy program.

F
A=17

F
A=17

Ref. R.E. Segel, P.P. Singh, R.G. Allas, S. S. Hanna
Phys. Rev. Letters 10, 345 (1963)

Elem. Sym.	A	Z
F	17	9

Method Van de Graff; NaI

Ref. No. 63 Se 1 JHH

Reaction	E or ΔE	E_o	Γ	∫σdE	Jπ	Notes
$O^{16}(p,\gamma)$	E_p= 3.4-3.5					
	E_{po}= 3.473	E_{γ_o}= 3.86	Γ_γ = 0.11±0.02 eV		5/2⁻	This Γ_γ gives a radiative lifetime of (0.6±0.1) 10^{-14} sec.

Table I. Coefficients obtained in a least-squares fit of the expression $A_0(1+\sum_n A_n P_n)$ to the data in Fig. 3. The quantity A_0 is expressed in arbitrary units.

E_p (MeV)	A_0	A_1	A_2	A_3	A_4
3.473	1.55±0.02	0.00±0.02	0.47±0.03	0.01±0.04	-0.03±0.05
3.470	1.00±0.05	0.10±0.05	0.20±0.11	0.20±0.15	-0.05±0.17
3.465	0.52±0.05	-0.10±0.05	0.65±0.05	-0.25±0.06	0.03±0.07

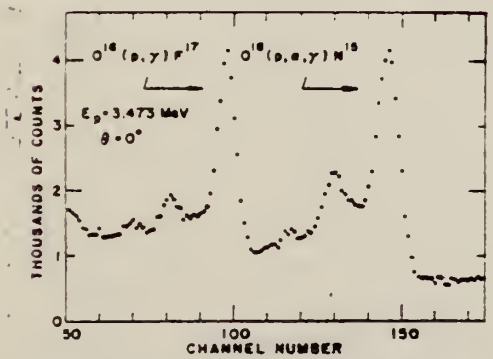

FIG. 1. NaI pulse-height spectrum for radiation emitted at 0° in proton bombardment (E_p=3.473 MeV) of a tantalum oxide target. The energy is 3.86 MeV for the resonant capture radiation.

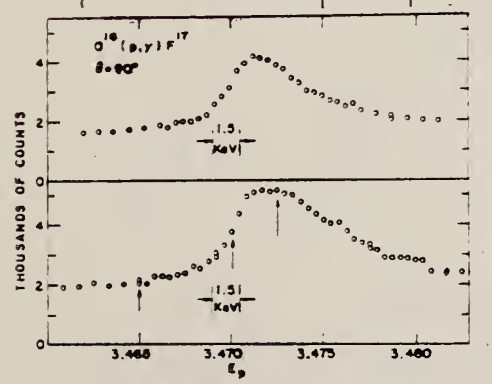

FIG. 2. Differential yield (θ = 90°) for $O^{16}(p,\gamma)F^{17}$ for two tantalum oxide targets of different thickness. Each point gives the total count in the channels corresponding to the 3.86-MeV peak; no background has been subtracted. Well below resonance the actual yield of 3.86-MeV radiation is less than 0.1 times the on-resonance value. The resonant energy is taken equal to 3.470 MeV. The arrows indicate points at which angu-

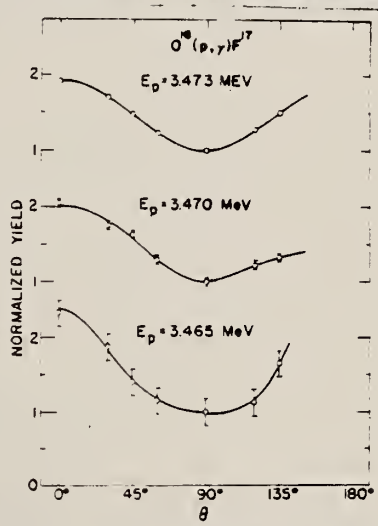

FIG. 3. Angular distributions measured with the target used in the lower part of Fig. 2. The distributions are normalized to unity at 90°. The indicated errors are statistical. The curves drawn are based on the coefficients of Table I.

REF. H. C. Chow, G. M. Griffiths, T. H. Hall
Can. J. Phys. 53, 1672 (1975)

ELEM. SYM.	A	Z
F	17	9

METHOD

REF. NO.	
75 Ch 1	hmg

REACTION	RESULT	EXCITATION ENERGY	SOURCE		DETECTOR		ANGLE
			TYPE	RANGE	TYPE	RANGE	
P,G	ABX	1- 3	D	0- 2	SCD-D		DST
		(.8 - 2.4)		(.4 - 2.0)			

.8 - 2.4 MEV

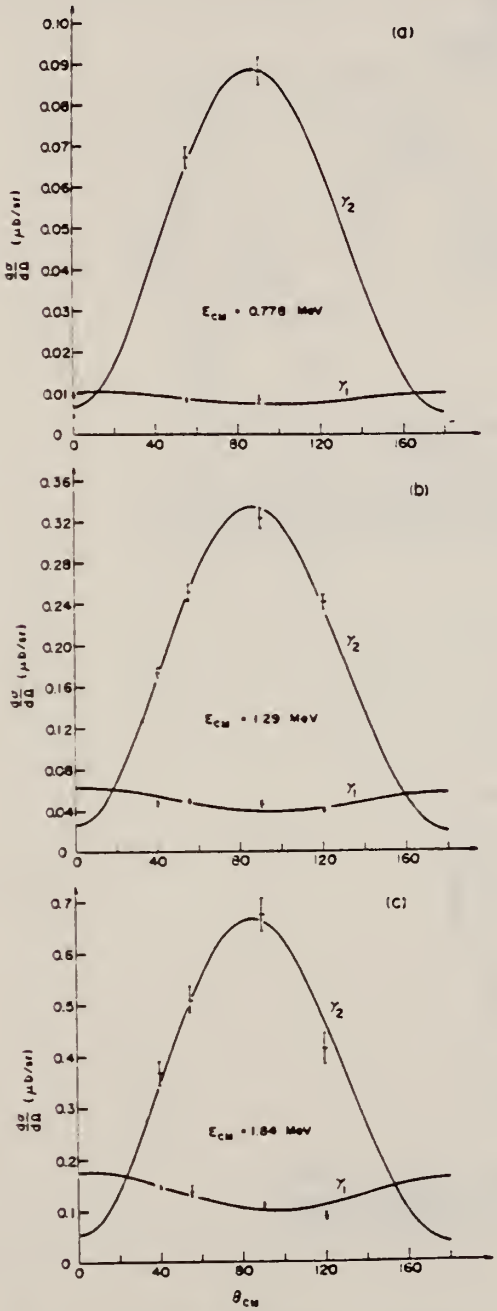

FIG. 6. The angular distributions of the $^{16}O(p,\gamma)^{17}F$ gamma rays at three energies. The experimental points have been normalized to give the best fit to the smoothed theoretical cross section.

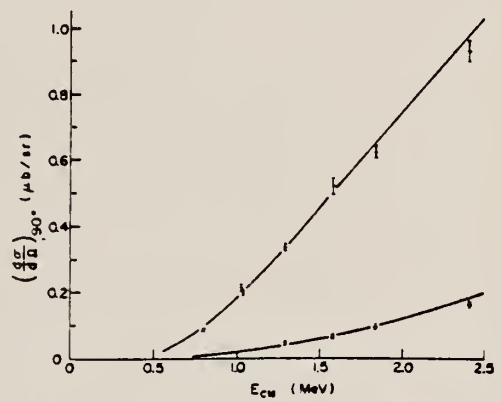

FIG. 7. $^{16}O(p,\gamma)^{17}F$ differential capture cross section at 90° for transitions to the $1/2^+$ first excited state (γ_2) and $5/2^+$ ground state (γ_1). The experimental cross sections have been normalized to the proton elastic scattering cross section. The solid curves are the theoretical cross sections.

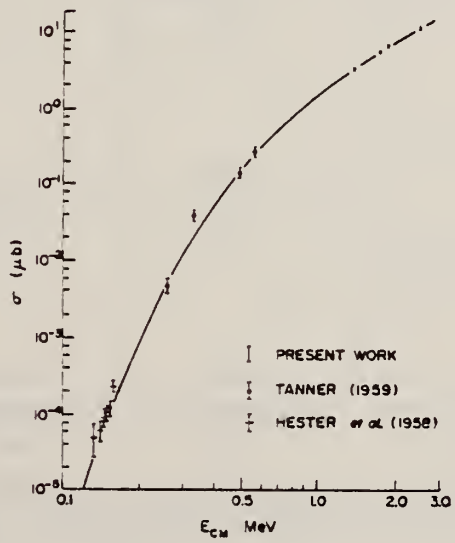

FIG. 8. $^{16}O(p,\gamma)^{17}F$ total cross section. The solid curve is the theoretical cross section. Data points above 1 MeV are from the present work; those between 250 and 600 keV are from Tanner (1959); and those below 200 keV are from Hester *et al.* (1958).

(over)

U.S. DEPARTMENT OF COMMERCE
NATIONAL BUREAU OF STANDARDS

TABLE 4. 90° differential and total cross sections for proton capture to the ground state (γ_1) and first excited state (γ_2) of ^{17}F

Mean CM energy (MeV)	γ_1		γ_2	
	$d\sigma/d\Omega$ (90°) (μb/sr)	σ (μb)	$d\sigma/d\Omega$ (90°) (μb/sr)	σ (μb)
0.795			0.086 ± 0.004	0.73 ± 0.04
1.024			0.212 ± 0.011	1.78 ± 0.09
1.029			0.195 ± 0.007	1.64 ± 0.06
1.288	0.046 ± 0.005	0.69 ± 0.08	0.337 ± 0.010	2.83 ± 0.08
1.572	0.066 ± 0.006	1.01 ± 0.09	0.521 ± 0.025	4.36 ± 0.21
1.836	0.096 ± 0.006	1.52 ± 0.10	0.628 ± 0.020	5.27 ± 0.17
2.404	0.164 ± 0.008	2.66 ± 0.13	0.940 ± 0.030	7.88 ± 0.25

REF.

M.N. Harakeh, P. Paul, and Ph. Gorodetzky
Phys. Rev. C11, 1008 (1975)

ELEM. SYM.	A	
F	17	9

METHOD

REF. NO.	
75 Ha 5	hmg

REACTION	RESULT	EXCITATION ENERGY	SOURCE		DETECTOR		ANGLE
			TYPE	RANGE	TYPE	RANGE	
P,G	ABX	15- 31	D	15- 32	NAI-D		DST

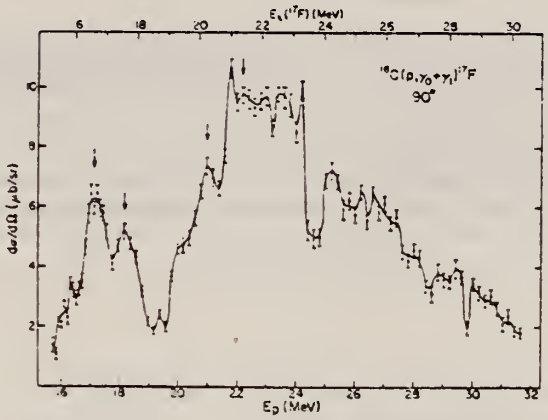

FIG. 3. Excitation curve for the summed transitions $\gamma_0+\gamma_1$. The solid line is drawn through the data to guide the eye. Arrows indicate energies where angular distributions were taken.

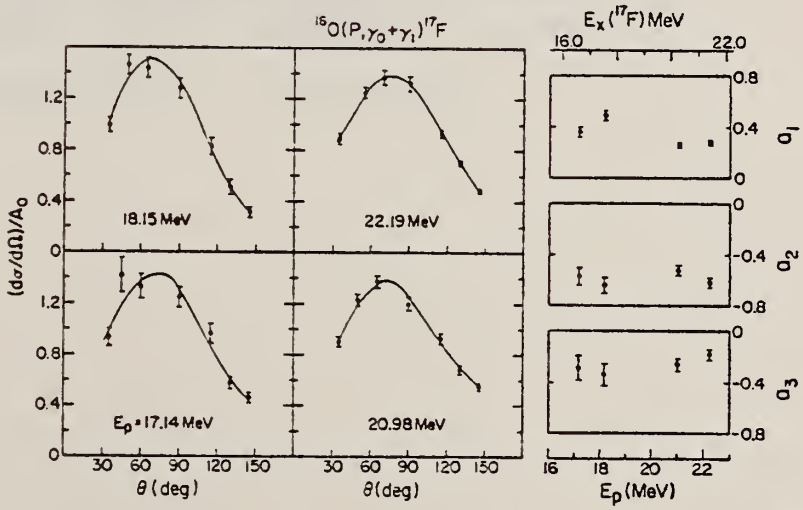

FIG. 4. Angular distributions of the $\gamma_0+\gamma_1$ yield at 17.14, 18.15, 20.98, and 22.19 MeV, i.e., the energies indicated by arrows in Fig. 3. Solid curves are fits with Legendre polynomials up to and including P_3 terms. The normalized Legendre coefficients a_1, a_2, and a_3 obtained from the fits are plotted on the right-hand side of the figure.

TABLE IV. Summary of theoretical and experimental results.

	General rules	1p and 2p-1h calc. [a]	Exp.
$\sigma_0 = \int \sigma dE$ (MeV mb)	$= 60\ NZ/A$ 254	$\sigma_0(T=\frac{1}{2}) = 129$ $\sigma_0(T=\frac{3}{2}) = 221$ $\sigma_0(\text{total}) = 350$	$\sigma_0(\gamma, p_0)$ ≤ 10.2
$\sigma_{-1} = \int \sigma/E dE$ (mb)	$= 0.36A^{4/3}$ 15.7	$\sigma_{-1}(T=\frac{1}{2}) = 6.0$ $\sigma_{-1}(T=\frac{3}{2}) = 8.9$ $\sigma_{-1}(\text{total}) = 14.9$	
$\sigma_{-1}(T+1)/\sigma_{-1}$	0.60 [b] 0.59 [c]	0.60	
$E_{GDR} = \sigma_0/\sigma_{-1}$ (MeV)		$E_{T=1/2} = 21.4(20.4)$ $E_{T=3/2} = 24.8$	$E_{T=1/2} = 22.0(15.4 - 30.4\ \text{MeV})$ $E_{T=1}(^{16}\text{O}) = 22.4(16.3 - 29\ \text{MeV})$ [d]
$\Delta E = E_{T=3/2} - E_{T=1/2}$ (MeV)	$= U(7_0 - 1)/A$ $= 5.3\ (U = 60\ \text{MeV})$ [e] $= 1.8\ (U \approx 20\ \text{MeV})$ [f]	3.4(4.4) $-U = 39$ MeV	

[a] Numbers in this column are from case I calculation except for numbers in parenthesis, which are from case II.
[b] See Ref. 17.
[c] See Ref. 18.
[d] Calculated from experimental data of Refs. 7 and 8.
[e] See Ref. 2.
[f] See Ref. 3.

[2] R.O. Akyuz and S. Fallieros, Phys. Rev. Lett. 27, 1016 (1971).

[3] Renzo Leonardi, Phys. Rev. Lett. 28, 836 (1972).

[7] W.J. O'Connell, Ph.D. Thesis, Stanford Univ. 1970 (unpublished).

[8] N.W. Tanner et al., Nucl. Phys. 52, 45 (1964).

[17] S. Fallieros and B. Goulard, Nucl. Phys. A147, 593 (1970).

[18] E. Hayward, B.F. Gibson, J.S. O'Connell, Phys. Rev. C5, 846 (1972).

REF. F.M. Khan, J. Lowe, J.M. Nelson, A.R. Barnett
Nucl. Phys. A322, 33 (1979)

ELEM. SYM.	A	Z
F	17	9

METHOD

REF. NO. 79 Kh 7 hg

REACTION	RESULT	EXCITATION ENERGY	SOURCE		DETECTOR		ANGLE
			TYPE	RANGE	TYPE	RANGE	
P,G	RLY	12,15	C	12-15	NAI-D		90
		(12.550,14.174)					

bstract: Measurements have been made of some parameters of the second and sixth $T = \frac{1}{2}$ states in ^{17}F. For the second state, the resonance energy was found to be $E_p = 12.707 \pm 0.001$ MeV ($E_x = 12.550 \pm 0.001$ MeV), which agrees with and improves on the accuracy of earlier work. For the sixth $T = \frac{1}{2}$ state, at $E_p = 14.435$ MeV, the γ-decay was determined to be predominantly γ_0 with a branch to the first excited state of $\Gamma(\gamma_1)/\Gamma(\gamma_0) \leqq 0.14$. Together with other work, this determines J^π to be $\frac{1}{2}^-$. The capture strength is found to be $(2J+1)\Gamma_p\Gamma_\gamma/\Gamma = 11.4 \pm 2.6$ eV.

BRANCHING RATIO, SPI

E NUCLEAR REACTIONS $^{16}O(p,\gamma)$, E = 12–15 MeV; measured $\sigma(E_p)$. ^{17}F deduced E_{res}, J^π, capture strength.

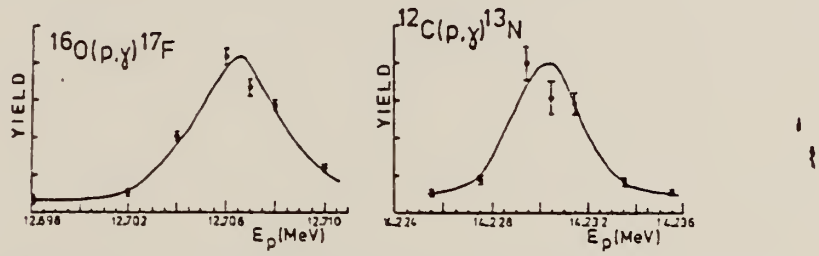

Fig. 2. Gamma yield for $T = \frac{1}{2}$ resonances in $^{16}O(p,\gamma_0)^{17}F$ and $^{12}C(p,\gamma_0)^{13}N$ as a function of proton energy at the target centre.

F
A=18

F
A=18

F
A=13

REF.

R. G. Couch, H. Spinka, T.A. Tombrello, T.A. Weaver
Nucl. Phys. A175, 300 (1971)

ELEM. SYM.	-	-
F	18	9

METHOD

REF. NO.	
71 Co 3	egf

REACTION	RESULT	EXCITATION ENERGY	SOURCE		DETECTOR		ANGLE
			TYPE	RANGE	TYPE	RANGE	
A,G	ABX	4-5	D	0-2	ACT-I		4PI

TABLE 1

Summary of $^{14}N(\alpha,\gamma)^{18}F$ results

E_x (MeV)	E_γ (MeV)	$J^\pi; T$	$(2J+1)\Gamma_\alpha\Gamma_{\gamma_0}/\Gamma$ eV(lab)	
			Present experiment	Parker [1]
0.310	4.656	$4^+; 1$	$< 2\times10^{-5}$	
0.417	4.739	$0^+; 1$	forbidden by selection rules	
0.559	4.849	$1^-; 0$	$2.79 \pm 0.5\times10^{-4}$	
0.698	4.957	$2^+; 1$	$< 0.5\times10^{-4}$	
1.140	5.301	$1^-, 2, 3, 4^+; 0$	0.108 ± 0.015	0.084 ± 0.004
1.395	5.501			0.027 ± 0.003
1.532	5.607	$(1^-; 0)$		4.80 ± 0.40
1.619	5.674	$(1^-; 0)$		1.35 ± 0.15

[1] Ref. [6]. - P.D. Parker, Phys. Rev. 173 (1968) 1021.

REF. J. C. Sens, A. Pape and R. Armbruster
Nucl. Phys. A199, 241 (1973)

ELEM. SYM.	A	Z
F	18	9

METHOD

REF. NO. 73 Se 3 egf

REACTION	RESULT	EXCITATION ENERGY	SOURCE TYPE	SOURCE RANGE	DETECTOR TYPE	DETECTOR RANGE	ANGLE
P,G	LFT	6- 7	D	0- 1	NAI-D		DST

6.14 MEV LEVEL

TABLE I
Electromagnetic decay properties for observed ^{18}F levels

Transition $E_i \to E_f$ (MeV)	$J_i^\pi \to J_f^\pi$	A_2	A_4	δ	$\Gamma'_{\gamma 1}$ (meV)	$\lvert M\rvert^2$ (W.u.) [a]
6.10 → 1.12	$4^- \to 5^+$	0.03±0.07	0.09±0.09	0.18±0.11	14± 11 [b]	(E1) (0.23±0.18)×10^{-3} (M2) ≲ 3
6.10 → 2.10	$4^- \to 2^-$	0.31±0.12	0.04±0.15	−0.07±0.11	6± 5 [b]	(E2) 2.5 ±1.9
6.14 → 0	$0^+ \to 1^+$	0.01±0.03	0.05±0.04	0	≧ 400±120	(M1) ≧ 0.08±0.02
6.14 → 1.70	$0^+ \to 1^+$	0.12±0.12	0.12±0.19	0	≧ 74± 8	(M1) ≧ 0.04±0.004
6.14 → 3.72	$0^+ \to 1^+$	0.05±0.08	0.10±0.11	0	≧ 270± 80	(M1) ≧ 0.9 ±0.3
6.16 → 0.94 → 0 [c]	$3^+ \to 3^+ \to 1^+$	0.27±0.07	−0.04±0.10	$0.11^{+1.1}_{-0.2}$	160± 50	(M1) (5.3 $^{+2.1}_{-1.7}$)×10^{-2}
6.24 → 2.10 [d]	$3^- \to 2^-$	−0.20±0.02	−0.01±0.05	−0.06±0.02	1900±860 [e]	(M1) 1.3 ±0.6 (E2) 2.1 ±1.7
6.24 → 2.10	$3^- \to 2^-$	0.06±0.05	0.06±0.06		1900±860 [e]	
6.24 → 3.79	$3^- \to (3^-)$	0.04±0.11	0.09±0.18		300±140 [e]	
6.28 → 0.94 → 0 [c]	$2^+ \to 3^+ \to 1^+$	−0.13±0.08	−0.01±0.10	0.06±0.04	350±120	(M1) (0.11±0.04) (E2) 0.12±0.12
6.39 → 0.94	$2, 3^- \to 3^+$	0.25±0.06	−0.05±0.09			
6.65 → 0.94	$2 \to 3^+$	0.00±0.05	−0.01±0.08		110± 55 [f]	
6.65 → 2.10	$2 \to 2^-$	−0.08±0.03	−0.06±0.04		640±310 [f]	
6.65 → 3.13	$2 \to 1^-$	0.11±0.07	0.06±0.09		140± 70 [f]	
6.78 → 0.94	$4^+ \to 3^+$	0.08±0.12	0.18±0.15	−0.13±0.11	11± 4	(M1) (2.6 ±0.9)×10^{-3} (E2) ≲ 0.03
6.78 → 1.12	$4^+ \to 5^+$	0.50±0.10	0.02±0.12	−1.1 ±0.3	29± 10	(M1) (3.3 ±1.6)×10^{-3} (E2) 1.2 ±0.5
6.78 → 4.65	$4^+ \to 4^+$	0.29±0.05	−0.05±0.08	−0.3 ±0.2	35± 12	(M1) 0.16±0.06 (E2) ≲ 80
6.87 → 0.94	$3, 4, 5 \to 3^+$	−0.1 ±0.2	0.7 ±0.3			
6.87 → 4.65	$3, 4, 5 \to 4^+$	0.19±0.05	0.06±0.06			

Angular distribution data A_1 are from the ^{17}O(p,γ)^{18}F reaction, and in the case of one transition from the 6.24 MeV level, from the ^{14}N(α,γ)^{18}F reaction. The energy shifts as functions of angle for the transitions from all of the resonant levels showed full Doppler shifts.

[a]) $\lvert M\rvert^2 = \Gamma_{\gamma\gamma}/\Gamma_w$ with $R_0 = 1.2$ fm.

[b]) The value used, $\Gamma_\gamma = 21 \pm 16$ meV, was calculated from the present strength, Brown's α-strength [19]), and Γ_α from Silverstein [18]). Berka [7]) gives $\Gamma_\gamma = 66 \pm 21$ meV. [c]) Angular correlation. [d]) From the ^{14}N(α,γ)^{18}F reaction. [e]) Using $\Gamma_\alpha \approx 1$ keV±30% given by Silverstein [18]).

[f]) With $\Gamma_\alpha\Gamma_\gamma/\Gamma = 0.58 \pm 0.20$ eV deduced from Phillips [20]).

[7] I. Berka et al., Bull. Am. Phys. Soc. 16, 510 (1971).

[18] E. A. Silverstein et al., Phys. Rev. 124, 868 (1961).

[19] R. E. Brown, Phys. Rev. 125, 347 (1962).

[20] W. R. Phillips, Phys. Rev. 110, 1408 (1958).

(over)

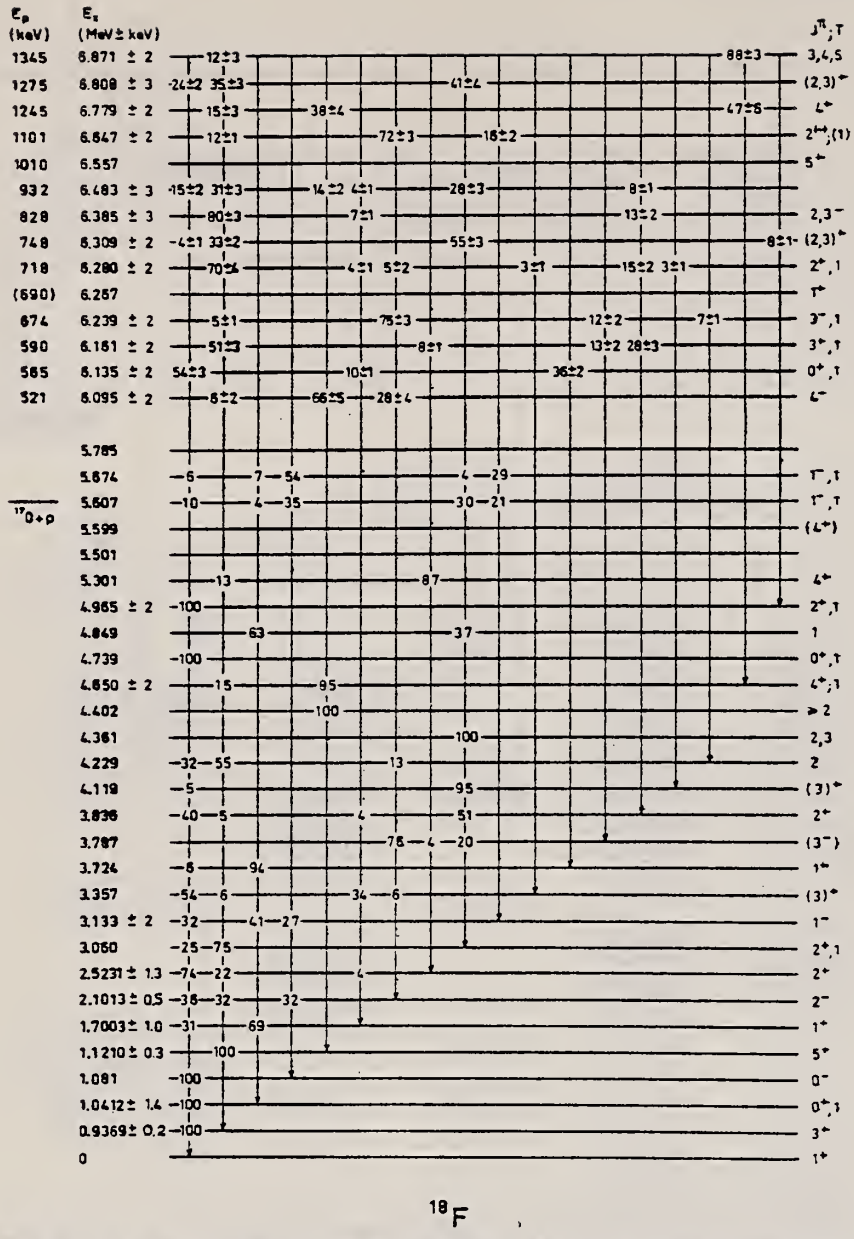

Fig. 2. Energy levels and γ-decay of ^{18}F. The uncertainty in E_p is 2 keV. Where an uncertainty is given for E_x this was determined from our observed γ-ray cascades. The figure includes all reported narrow levels. The J^π of the E_x = 5.30, 6.14 and 6.56 MeV levels are from refs. [36, 8]). The level at 6.27 MeV was not seen in (p,γ). Its J^π is from ref. [18]). Since the E_x = 6.56 MeV level was very weakly excited in the (p,γ) reaction, it was not possible to establish a decay scheme. The information on the E_p = 5.61 and 5.67 MeV doublet are from ref. [37]). All other data below E_x = 6 MeV are taken from ref. [35]).

[8] C. Rolfs et al., Bull.Am. Phys.Soc. 15, 782 (1970).

[35] F. Ajzenberg-Selove, Nucl.Phys. A190 (1972) 1.

[36] C. Rolfs et al., Bull.Am.Phys.Soc. 16, 510 (1971).

[37] E. K. Warburton et al., Isospin in nuclear physics, ed. D.H. Wilkinson (North-Holland, Amsterdam, 1969) p. 223.

REF. E. Bellptto. E. Fiorini, P. Negri, L. Zanotti
Il Nuovo Cimento 47A, 106 (1978)

ELEM. SYM.	A	Z
F	18	9

METHOD

REF. NO. 78 Be 16 hg

REACTION	RESULT	EXCITATION ENERGY	SOURCE		DETECTOR		ANGLE
			TYPE	RANGE	TYPE	RANGE	
A,G	LFT	6	D	2	SCD-D		90
		(6.138)		(2.215)			

Summary. — An experiment on the $^{14}N(\alpha,\gamma)^{18}F$ reaction leading to the parity- and isospin-forbidden 0^+ level at 6.138 MeV is reported. A ^{14}N gas target was exposed to a pulsed singly charged α-particle beam from the CN accelerator of the Laboratori Nazionali di Legnaro, and γ-rays emitted in coincidence with the beam were measured with a 90 cm³ Ge(Li) detector. A similar run with the same target as well as an activation experiment were carried out on the nearby parity-allowed resonance at 6.241 MeV, in order to test the electronic gain and the efficiency in the parity-violating experiment. The energy spectrum from the Ge(Li) shows no peak due to the decay of the 6.138 MeV state and allows to set an upper limit of $2 \cdot 10^{-3}$ eV for the parity-violating width of this resonance.

UP. LIM. WIDTH=.002EV

F
A=19

F
A=19

REF. R.J. Horsley, R.N.H. Haslam, and H.E. Johns
Phys. Rev. 87, 756 (1952)

ELEM. SYM.	A	Z
F	19	9

METHOD

REF. NO. 52 Ho 1 hmg

REACTION	RESULT	EXCITATION ENERGY	SOURCE		DETECTOR		ANGLE
			TYPE	RANGE	TYPE	RANGE	
G,N	ABX	10- 25	C	10- 25	ACT-I		4PI
G,2N	ABX	19- 26	C	19- 26	ACT-I		4PI

SEE 54TA1 FOR RE-ANALYSIS

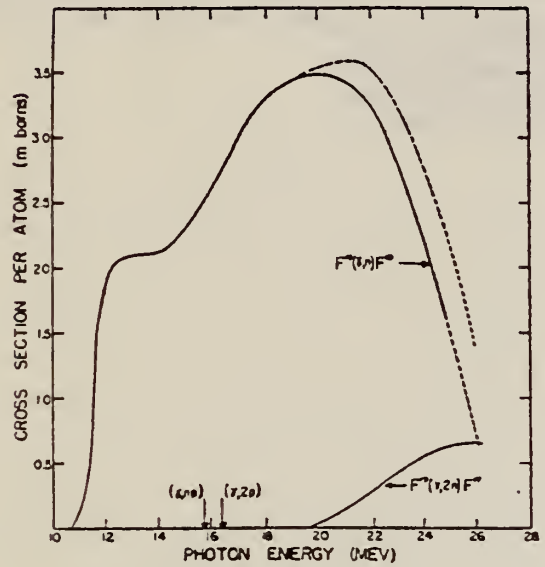

FIG. 2. Cross section vs energy curves for the reactions $F^{19}(\gamma, n)F^{18}$ and $F^{19}(\gamma, 2n)F^{17}$. The dotted line indicates the sum of the two reactions. The (γ, np) and $(\gamma, 2p)$ calculated thresholds are marked.

TABLE I. Information obtained from the $F^{19}(\gamma, n)F^{18}$ and $F^{19}(\gamma, 2n)F^{17}$ cross-sectional curves.

Reaction	$F^{19}(\gamma, n)F^{18}$		$F^{19}(\gamma, 2n)F^{17}$	
Peak position	20	Mev	26	Mev
Peak cross section	3.48	mb	0.66	mb
Width at half-maximum	12.9	Mev		—
Integrated cross section (to 26 Mev)	0.039	Mev-barns	0.0024	Mev-barns

REF. G. Ferguson, J. Halpern, R. Nathans, and P.F. Yergin
Phys. Rev. 95, 776 (1954)

ELEM. SYM.	A	Z
F	19	9

METHOD

REF. NO. 54 Fe 1 rs

REACTION	RESULT	EXCITATION ENERGY	SOURCE		DETECTOR		ANGLE
			TYPE	RANGE	TYPE	RANGE	
G,Sn	ABX	10-25	C	11-25	BF3-I		4PI

The direct detection of neutrons from (γ,n) reactions induced by betatron bremsstrahlung has been applied to cross-section determinations using gaseous targets at approximately 100 atmospheres pressure. Results from oxygen are consistent with other determinations. The remaining elements represent new results and show the familiar giant dipole resonance for the photoneutron process. Parameters of the resonances are determined and related to the systematic behavior previously reported for other elements.

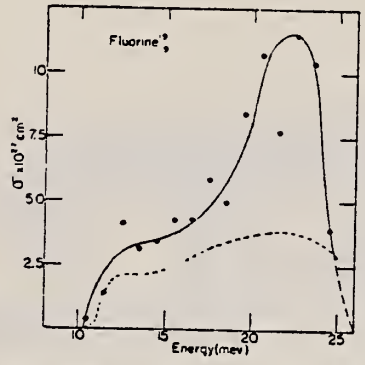

FIG. 7. Photoneutron excitation function for fluorine.

REF. J. G. V. Taylor, L. B. Robinson, and R. N. H. Haslam
Can. J. Phys. 32, 238 (1954)

ELEM. SYM.	A	Z
F	19	9

METHOD

REF. NO. 54 Ta 1 hmg

REACTION	RESULT	EXCITATION ENERGY	SOURCE		DETECTOR		ANGLE
			TYPE	RANGE	TYPE	RANGE	
G,N	ABX	10- 17	C	10- 17	ACT-I		4PI

Measurement is an extension of earlier work:
R.J. Horsley, R.N. Haslam, and H.E. Johns,
Phys. Rev. 87, 196 (1952)

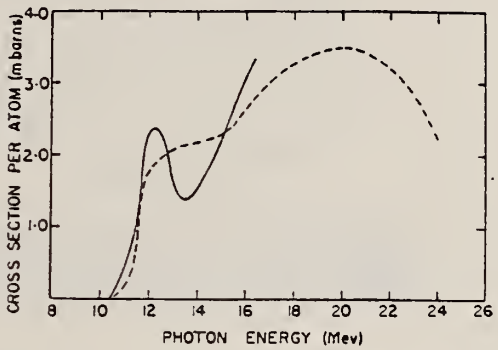

FIG. 1. Cross section for the reaction $F^{19}(\gamma, n)F^{18}$. The heavy line shows the cross-section curve determined in the present work, the dotted line the previously reported cross section (5).

REF. W. B. Lasich, E. G. Muirhead and G. G. Shute
Aust. J. Phys. 8, 456 (1955)

ELEM. SYM.	A	Z
F	19	9

METHOD

REF. NO. 55 La 1 JOC

REACTION	RESULT	EXCITATION ENERGY	SOURCE TYPE	SOURCE RANGE	DETECTOR TYPE	DETECTOR RANGE	ANGLE
G,P	SPC	10 - 17	C	17	EMU-D		DST

$$\int_{10}^{16.5} \sigma\ \gamma,p = 18\ \text{MeV-mb}$$

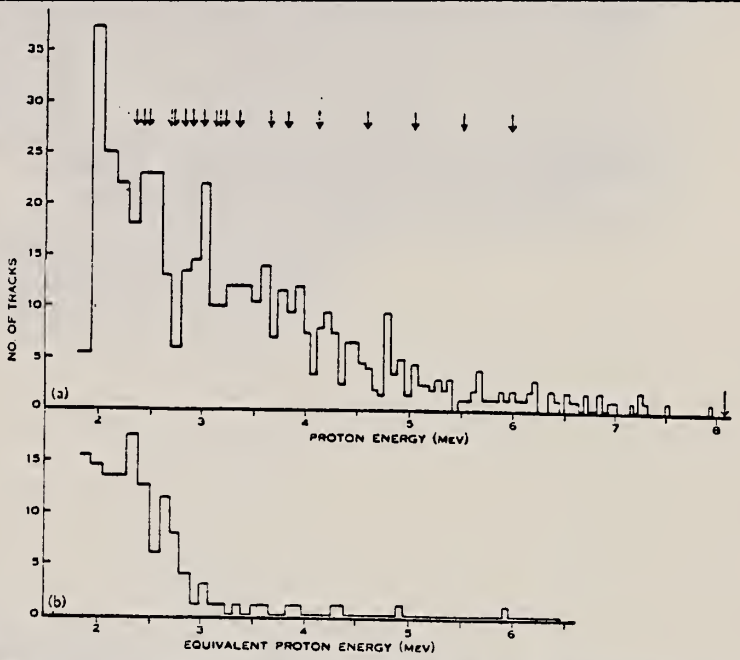

Fig. 2 (*a*).—Energy distribution of photoprotons from ^{19}F. The expected positions of proton groups botween known onorgy lovels in ^{19}F and ^{18}O are indicated by arrows above the histogram as follows:

↓ $^{19}F^{*}$ to ^{18}O (ground state),
↓ $^{19}F^{*}$ to $^{18}O^{*}$ (1·98 MeV state).

(Tho onorgy levels in ^{19}F were obsorvod in $^{18}O(p,n)^{18}F$ (Ajzonborg and Lauritsen 1955).) Tho limit of resolution is 0·3 MeV.

Fig. 2 (*b*).—Corresponding background tracks.

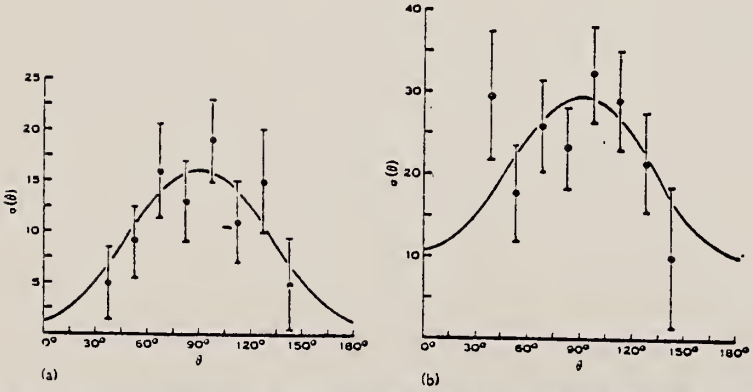

Fig. 3.—Angular distribution of photoprotons from ^{19}F. θ=angle botween incidont photon and tho proton, σ(θ)=difforontial cross section (arbitrary units). Vortical linos roprosont standard doviations of tho points.

(*a*) Enorgy rango 4·4–8·5 MoV. No. of tracks=75, porcontago background=10, least squarcs fit to data is shown by curvo $(1\pm5)+(15\mp7)\sin^2\theta$.

(*b*) Enorgy rango 2·9–4·4 MoV. No. of tracks=180, porcentage background=13½, least squarcs fit to data is shown by curve $(10\pm8)+(19\mp11)\sin^2\theta$.

U.S. DEPARTMENT OF COMMERCE
NATIONAL BUREAU OF STANDARDS

REF. D. Reagan
Phys. Rev. 100, 113-120 (1955)

ELEM. SYM.		
F	19	9

METHOD
Linac; counted delayed neutrons from N^{17}

REF. NO. 55 Re 1 | NVB

REACTION	RESULT	EXCITATION ENERGY	SOURCE		DETECTOR		ANGLE
			TYPE	RANGE	TYPE	RANGE	
G,2P	ABI	THR - 400	C	80-400	ACT-I		4PI

$$\int_{80}^{400} \sigma dE_\gamma = 0.0037 \text{ MeV-barns.}$$

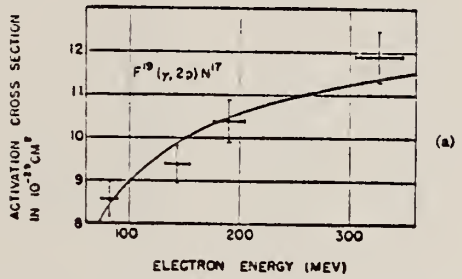

FIG. 3. Yields from the $O^{18}(\gamma,p)N^{17}$ and $F^{19}(\gamma,2p)N^{17}$ reactions, as functions of radiating electron energy. The solid lines are isochromats of characteristic energy 25 and 40 Mev, corresponding to integrated cross sections of 0.067 and 0.0037 Mev-barn, respectively.

Ref. W.L. Bendel, J. McElhinney, R.A. Tobin
Phys. Rev. 111, 1297 (1958)

Elem. Sym.	A	Z
F	19	9

Method: Betatron; neutron yield; radioactivity; ion chamber

Ref. No.: 58 Be 1 EH

Reaction	E or ΔE	E_o	Γ	$\int \sigma dE$	Jπ	Notes
$F^{19}(\gamma,n)$	Bremss. 10-11	10-11				Beak found at 10.47±0.02 based on (γ,n) thresholds in F^{19}, N^{14} and C^{12}.

REF. J. O'Connell, P. Dyal, J. Goldemberg
Phys. Rev. 116, 173 (1959)

ELEM. SYM.	A	L
F	19	9

METHOD: Betatron

REF. NO.: 59 Oc 1 NVB

REACTION	RESULT	EXCITATION ENERGY	SOURCE		DETECTOR		ANGLE
			TYPE	RANGE	TYPE	RANGE	
G,2N	RLI	THR-100	C	THR-100	ACT-I		4PI

REL TØ G,N

TABLE II. Relative integrated cross sections.

Element	(γ,n)	Position of the peak for (γ,n)	$(\gamma,2n)$	Position of the peak for $(\gamma,2n)$
C^{12}	1	23 Mev	0.003	42 Mev
N^{14}	1	24 Mev	0.007[a]	
O^{16}	1	22 Mev	0.002	40 Mev
F^{19}	1	20 Mev	0.14	32 Mev
Na^{23}	1	20 Mev	0.05	32 Mev
P^{31}	1	20 Mev	0.06 $(\gamma,2p)$	45 Mev $(\gamma,2p)$
			0.08 $(\gamma,2pn)$	50 Mev $(\gamma,2pn)$

[a] The (γ,n) integrated cross section was taken from reference 4.

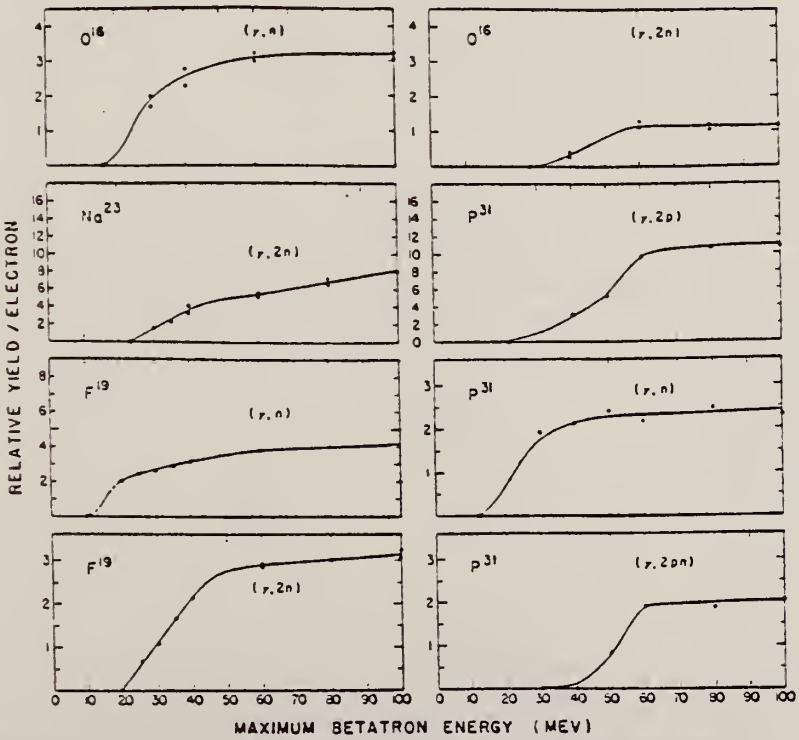

FIG. 1. The energy dependence of several photonuclear reactions. The relative yield scales of different graphs independent.

Ref. E.C. Booth
Nuclear Phys. 12, 426 (1960)

Elem. Sym.	A	Z
F	19	9

Method Van de Graaff; electron bremss.; Ring scatterer; NaI

Ref. No. 60 Bo 3 JHH

Reaction	E or ΔE	E_o	Γ	$\int \sigma dE$	Jπ	Notes
(γ,γ)	Bremss. 0.5-2.2	1.34			3/2	Mean lifetime t/g: $= (0.5 \pm 0.3) 10^{-13}$ sec [resonance scattering] where $g = (1+2I)/(1+2I_o)$. The 1.34 MeV resonance corresponds to a dipole transition between the 1.46 MeV state and the 0.109 MeV state (from yield curve data).

B. Forkman, I. Wahlström
Arkiv Fysik 18, 339 (1960)

ELEM. SYM.	A	Z
F	19	9

METHOD
Synchrotron; proton spectrum; angular distribution; nuclear emulsion; cross section.

REF. NO. 60 Fo 2 | NVB

REACTION	RESULT	EXCITATION ENERGY	SOURCE TYPE	SOURCE RANGE	DETECTOR TYPE	DETECTOR RANGE	ANGLE
G,P	RLX	10 - 18	C	16, 19	EMU-D		DST
				(15.5, 19)			

In Figure 8, $W(\theta) = 1 + 7\cos^2\theta - 6\cos^4\theta$

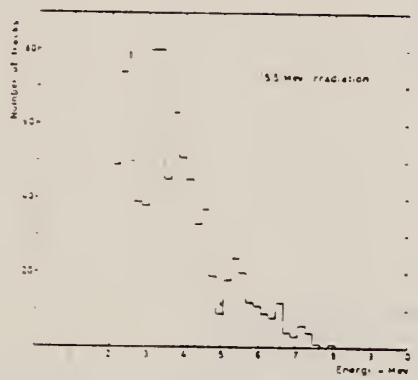

Fig. 3. The proton distribution from the 15.5 MeV irradiation after the background is subtracted.

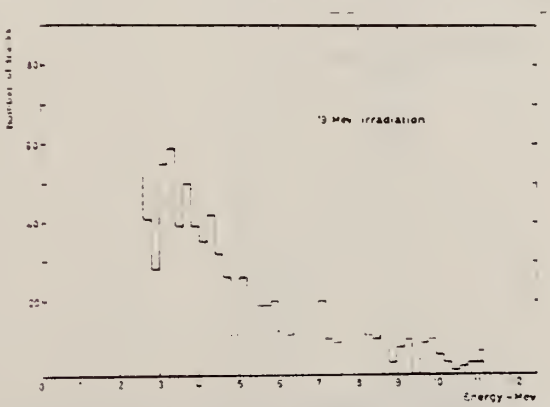

Fig. 4. The proton distribution from the 19 MeV irradiation after the background is subtracted.

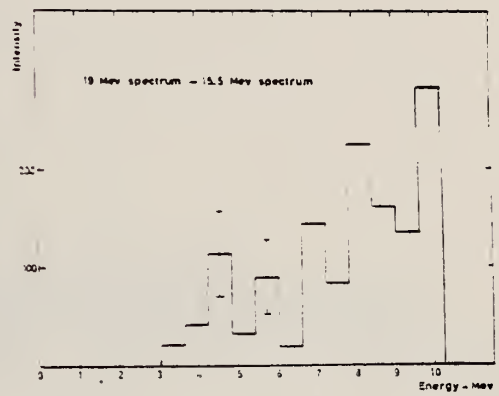

Fig. 5. The proton spectrum corresponding to photon absorption in the energy range 15.5–19 Me

Table I. The reported resonances (MeV) in F^{19} obtained by photo-excitation. The column headings give the references and methods employed.

Taylor *et al.* [3] (γ, n) activation curve	Goldemberg and Katz [4] (γ, n) neutron-yield curve	Bender *et al.* [5] (γ, n) activation curve	Bertozzi *et al.* [6] (γ, n) time of flight	Lasich *et al.* [7] (γ, p) nuclear emulsion	Present work (γ, p) nuclear emulsion
		10.47			10.4
10.6		—			—
10.9	11.0	—			—
11.2					—
11.5	11.5		11.5	11.1	11.4
11.9	11.9		12.0	12.0	11.9
12.2	—		12.2		
			13.0		12.8
	—		13.5	13.2	13.6
			14.1		
15.3	15.3		15.5		15.4
					16.5
					18.1

ELEM. SYM.	A	
F	19	9

METHOD

REF. NO.	
60 Fo 2	NVB

REACTION	RESULT	EXCITATION ENERGY	SOURCE		DETECTOR		ANGLE
			TYPE	RANGE	TYPE	RANGE	

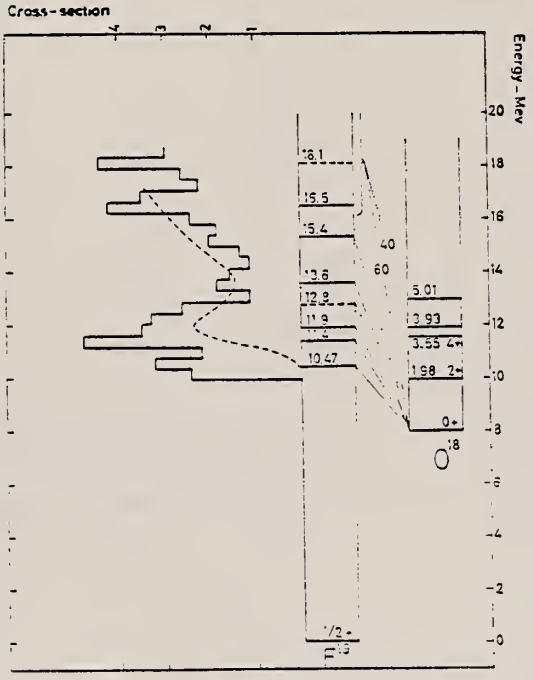

Fig. 7. The level scheme for the photo-disintegration of F^{19}. The histogram to the left gives the cross-section for (γ, p) in arbitrary units. The dotted curve shows the (γ, n) cross-section from [illegible] in millibarns. The numbers for some of the transitions to O^{18} denote the relative branching ratio in per cent.

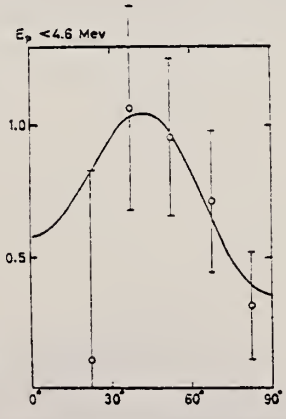

Fig. 8. The angular distribution of the protons with energies less than 4.6 MeV from the 15.5 MeV irradiation with thick teflon target.

Ref. K.N. Geller, J. Halpern, E.G. Muirhead
Phys. Rev. 119, 716 (1960)

Elem. Sym.	A	Z
F	19	9

Method
25 MeV Betatron; activation of Teflon; NaI counters for annih. rad. of positions from residual nuclei.

Ref. No. 60 Ge 2 JHH

Reaction	E or ΔE	E_o	Γ	$\int \sigma dE$	Jπ	Notes
(γ,n)	10.27 - 10.7					E_γ (threshold) = 10.45 ± 0.03 MeV to be compared with Everling's neutrc separation energy 10.442 ± 0.007 MeV from mass data. Observed break in yield curve (Figure 4) at: 10.53 MeV

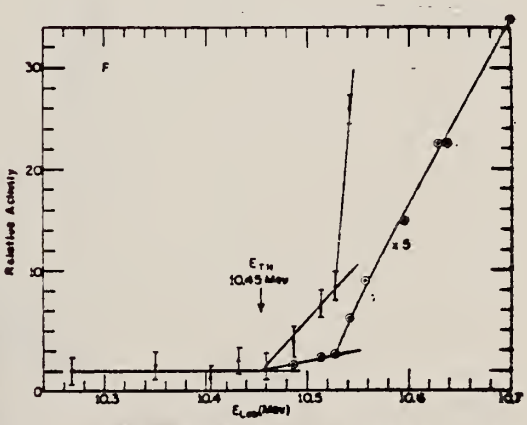

FIG. 4. Activation curve for the reaction $F^{19}(\gamma,n)F^{18}$.

J.D. King, R.N.H. Haslam, W.J. McDonald
Can. J. Phys. 38, 1069 (1960)

F	19	9

METHOD Betatron; neutron cross section; activity; $Cu^{63}(\gamma,n)$

REF. NO. 60 Ki 4 NVB

REACTION	RESULT	EXCITATION ENERGY	SOURCE TYPE	SOURCE RANGE	DETECTOR TYPE	DETECTOR RANGE	ANGLE
G,N	ABX	10-23	C	10-23	ACT-I		4PI
		(10.4-23.0)		(10.4-23.0)			

666

Peaks at:

E_γ = 10.6 MeV (very small)
12.4 MeV
14.0 MeV
16.1 MeV
17.2 MeV
19.3 MeV

Peaks at 14.0 and 19.3 MeV suggest split giant resonance, give quadropole moment
$Q_o = 0.30 \times 10^{-24} cm^2$.

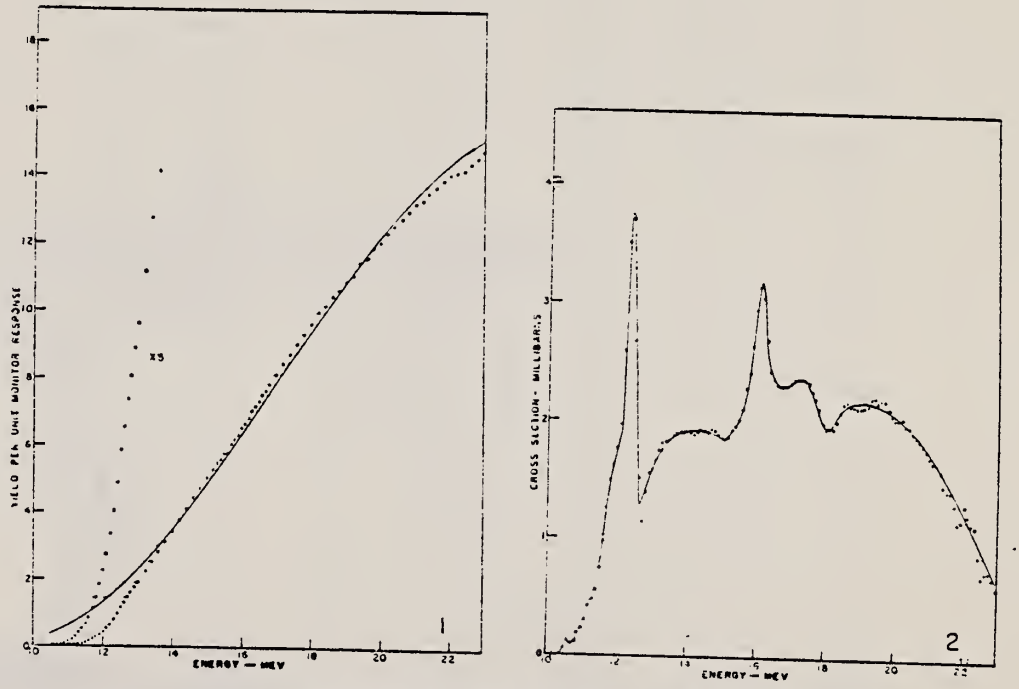

FIG. 1. Yield of F^{18} per unit monitor response as a function of the maximum energy in the X-ray spectrum. The full curve is an analytic function of the form $y = a[1+\sin b(E-c)]$.
FIG. 2. The cross section for $F^{19}(\gamma,n)F^{18}$ obtained from the smoothed yield curve.

Ref. K. Reibel, A.K. Mann
Phys. Rev. 118, 701 (1960)

Elem. Sym.	A	Z
F	19	9

Method
γ's from $F^{19}(\gamma,\alpha\gamma)$ reaction; protons from Van de Graaff; NaI

Ref. No. 60 Re 1 JHH

Reaction	E or ΔE	E_o	Γ	$\int \sigma dE$	Jπ	Notes
$F^{19}(\gamma,\gamma)$	~ 7					$\langle \bar{\sigma} \rangle (E_p = 2.05 \text{ MeV}) = < 0.03$ mb Assuming dipole transitions.

D. Sadeh
Compt. Rend. 250, 1632 (1960)

ELEM. SYM.	A	-
F	19	9

METHOD: Betatron; neutron yield; activity; ion chamber

REF. NO.: 60 Sa 2 | NVB

REACTION	RESULT	EXCITATION ENERGY	SOURCE		DETECTOR		ANGLE
			TYPE	RANGE	TYPE	RANGE	
G,N	RLY	10 - 12	C	10 - 12	ACT-I		4PI

Breaks in activation curves:

10.40 MeV
10.45 MeV
10.71 MeV
10.86 MeV
11.06 MeV
11.18 MeV
11.38 MeV
11.57 MeV
11.84 MeV
12.09 MeV

REF.

T.G. Walker, W.T. Morton
Proc. Phys. Soc. 75, 4 (1960)

ELEM. SYM.	A	Z
F	19	9

METHOD

Synchrotron; neutron cross section; radioactivity

REF. NO.	
60 Wa 2	NVB

REACTION	RESULT	EXCITATION ENERGY	SOURCE		DETECTOR		ANGLE
			TYPE	RANGE	TYPE	RANGE	
G,N	ABX	10-240	C	120-240	ACT-I		4PI
				(120,180,240)			

$\sigma = (3.5 \pm 0.3)\ 10^{-27}$ cm^2/equivalent quantrum

Data below 120 MeV from other workers; 50 MeV data is that of Barber et al, Phys. Rev. 98, 73 (1955).

Maximum bremsstrahlung energy (Mev)	Yield of ^{18}F from ^{19}F	^{23}Na	^{27}Al	^{12}C(γ, n)^{11}C yield
240	1·83(17)	0·18(9)	0·062(13)	1·62
180	1·78(16)	0·18(16)	0·058(16)	1·50
120	1·6(14)	0·15(14)	0·045(14)	1·34
100	1·5	—	—	1·27
70	1·4	0·11	—	1·15
50	1·22	0·07	—	1·0

E.C. Booth, K.A. Wright
Nuclear Phys. 35, 472 (1962)

Elem. Sym.	A	Z
F	19	9

'nod 4 MeV-electron Van de Graaff; bremss.; nuclear resonance scattering, ring scatterer; NaI

Ref. No. 62 Bo 6 — JHH

Reaction	E or ΔE	E_o	Γ	$\int \sigma dE$	Jπ	Notes
$F^{19}(\gamma,\gamma)$	Bremss. 0 - 4					

TABLE 3

Mean lifetimes of excited states deduced from the resonance scattering of bremsstrahlung

Nucleus	%	Energy (MeV)	Spins	g	Γ_o/Γ	W(θ)	$\tau \times 10^{18} \pm 35\%$ (sec)
F^{19}	100	1.46	$\frac{1}{2}^+ - ?$	?	0.13	(1)	$0.25g$
Na^{23}	100	2.08	$\frac{3}{2}^+ - \frac{1}{2}$	2	0.1	0.79	>0.04
		2.39	$-?$	?	0.53	(1)	$>1.6g$
		2.64	$-?$	?	0.6	(1)	$>0.3g$
		2.70	$-?$	?	(0.1)	(1)	$>0.008g$
		2.98	$-?$	?	0.46	(1)	$0.03g$
Al^{27}	100	2.73	$\frac{3}{2}^+ - \frac{1}{2}^+$	1	$\leqq 0.3$	0.91	>0.22
		2.98	$-\frac{1}{2}$	$\frac{1}{3}$	0.216	1	2.2×10^{-4}
Si^{28}	4.71	1.23	$\frac{1}{2}^+ - \frac{1}{2}^+$	2	1	0.88	1.5
		2.43	$-\frac{1}{2}^+$	2	(1)	0.88	0.2
P^{31}	100	1.26	$\frac{1}{2}^+ - \frac{1}{2}^+$	2	1	0.88	2.2
		2.23	$-\frac{3}{2}$	3	1	0.79	4.5
		3.13	$-\frac{1}{2}$	2	(1)	0.88	0.2
		3.29	$-\frac{3}{2}$	3	?	0.79	$>1.8(\Gamma_o/\Gamma)^2$
		3.41	$-?$	?	?	(1)	$>1.3g(\Gamma_o/\Gamma)^2$
		3.51	$-\frac{1}{2}$	2	?	0.88	$0.02(\Gamma_o/\Gamma)^2$
S^{32}	95	3.78	$0^+ - ?$	?	?	(1)	$>0.6g(\Gamma_o/\Gamma)^2$
S^{34}	4.2	2.127	$0^+ - 2$	5	1	0.63	>1.0
Cl^{35}	75.5	1.22	$\frac{3}{2}^+ - ?$	?	1	(1)	$6g$
		1.76	$-?$	?	(1)	(1)	$4g$
		2.7(2.65)	$-?$	?	?	(1)	$0.31g(\Gamma_o/\Gamma)^2$
		3.01	$-?$	?	?	(1)	$0.37g(\Gamma_o/\Gamma)^2$
Cl^{36}	75.5	3.1	?	?	?	(1)	$>0.74g(\Gamma_o/\Gamma)^2$
		3.17	?	?	?	(1)	$>1.5g(\Gamma_o/\Gamma)^2$
Cl^{37}	24.5	0.838	$\frac{3}{2}^+ - ?$	?	1	(1)	$>13\tau$
		1.72	$-?$	?	?	(1)	$>0.5g(\Gamma_o/\Gamma)^2$
K^{39}	93	2.53	$\frac{3}{2}^+ - ?$	?	1	(1)	$>1.6g$
		2.82	$-?$	?	1	(1)	$>1.5g$
		3.02	$-?$	?	1	(1)	$0.37g$
		3.60	$-?$	?	1	(1)	$>0.7g$
		3.88(3.94)	$-?$	?	?	(1)	$0.14g(\Gamma_o/\Gamma)^2$
		4.06–4.12	$-?$	?	?	(1)	$>0.2g(\Gamma_o/\Gamma)^2$
Ca^{40}	96	3.90	$0^+ - 2^+$	5	1	0.63	>0.48
Cu^{63}	69	1.33	$\frac{3}{2}^- - \frac{5}{2}$	2	(1)	0.8	$44>\tau>11$

The factor g equals $(2I+1)(2I_o+1)^{-1}$.

REF.
E. Braun
Z. Physik 166, 62 (1962)

ELEM. SYM.	A	Z
F	19	9

METHOD
Van de Graaff; proton spectrum, angular distribution; nuclear emulsion

REF. NO. 62 Br 3 NVB

REACTION	RESULT	EXCITATION ENERGY	SOURCE		DETECTOR		ANGLE
			TYPE	RANGE	TYPE	RANGE	
G,P	SPC	18	D	18	EMU-D	2-10	DST
		(17.6)		(17.6)			

In Figure 5, $W(\theta) = a + b \sin^2\theta$

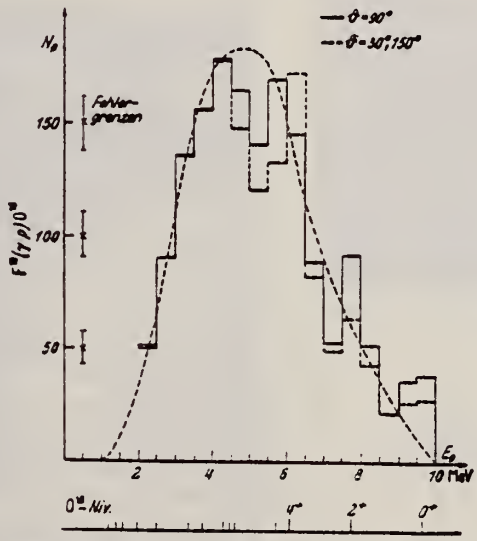

Fig. 4. Energieverteilung der Photoprotonen aus Fluor. Gestrichelte Kurve: Verteilung nach der statistischen Theorie, Stufenkurven: gemessenes Spektrum für $\theta = 90°$ bzw. Mittelwert der Spektren für $\theta = 30°, 150°$. Darunter: Niveauschema des Restkernes O^{16} (von rechts nach links)

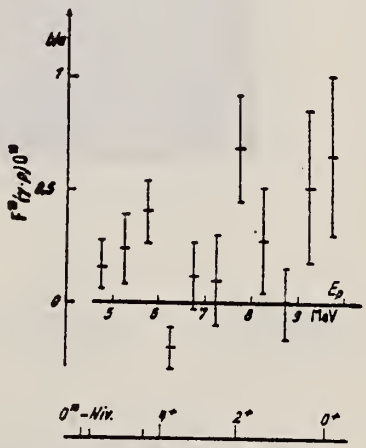

Fig. 5. Anisotropie-Faktor b/a in Abhängigkeit von der Protonenenergie mit statistischem Fehler, darunter Niveaus des Restkerns O^{16}

Ref. W.E. Del Bianco, [illegible]ephens
Phys. Rev. 126, 7[illegible])

Elem. Sym.	A	Z
F	19	9

Method Electrostatic ge[illegible] $H^3(p,\gamma)He^4$ reaction; activation of positron emitter; 2 [illegible]oincidence.

Ref. No. ~~GE Be 1~~ JHH

Reaction	E or ΔE	Γ	∫σdE	Jπ	Notes 664
(γ,n)	20.2-21.1				$\sigma(\gamma,n)$ = 3.30±0.41 mb at 20.48 MeV. Teflon sample. Fluctuations in Figure 7 may be due, in part, to carbon correction [10-50% of total $\sigma(\gamma,n)$].

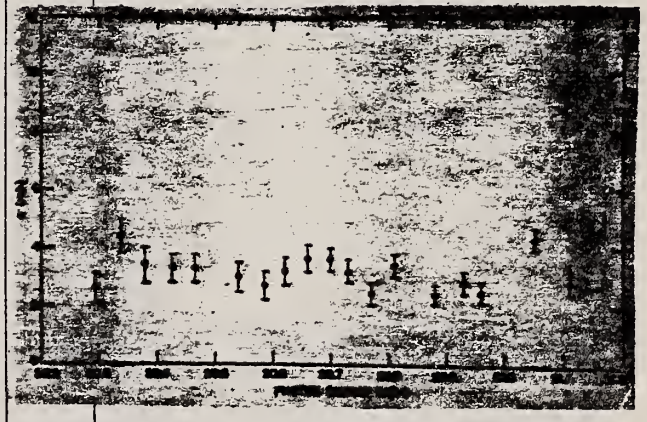

Figure 7: The $F^{19}(\gamma,n)F^{18}$ reaction cross section in millibarns as a function of photon energy in MeV.

Ref. W.R. Dodge, W. C. Barber
Phys. Rev. 127, 1746 (1962)

Elem. Sym.	A	Z
F	19	9

Method
Magnetic analysis of proton spectrum produced by electron bombardment

Ref. No. 62Do1 BG

Reaction	E or ΔE	E_o	Γ	$\int \sigma dE$	Jπ	Notes
(e,p)	18, 24.5 30	3.25 3.7 4.5 7.3 10.1		29^{+9}_{-3}) 23 * 10.5		For ground state transition E_γ= 11.42 11.90 12.74 15.70 18.70 *Calculated assuming 100% ground state transitions. Correspondence between (e, pe') reaction and (γ,p)reaction; assumed electron has associated with it a virtual photon spectrum. Electron production yields analyzed by use of E1 virtual photon spectrum to obtain σ (γ,p). Angular distribution measured; assume to be of form $A'+B'\cos\theta+C'\sin^2\theta+...$

803

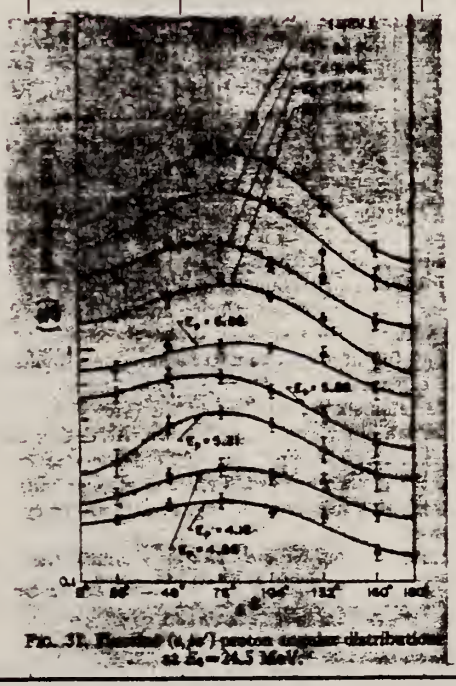

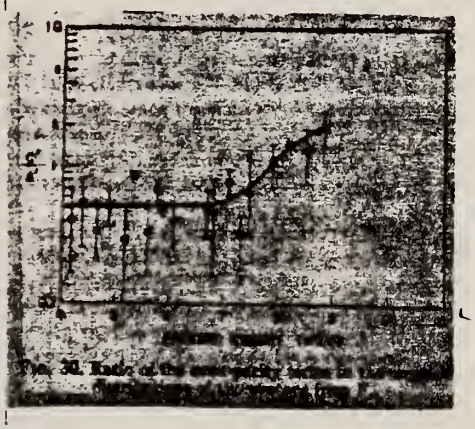

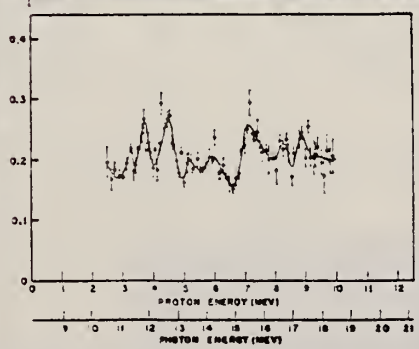

Ref. W.C.Barber, J.Goldemberg, G.A.Peterson, Y.Torizuka

Nuclear Phys. 41, 461 (1963); erratum to be published (as of 9/5/63)

Elem. Sym.	A	Z
F	19	9

Method: Linac (Stanford Mark II) - counter telescope

Ref. No. 63Bal 25

Reaction	E or ΔE	E_0	Γ	$\int \sigma dE$	Jπ	Notes
(e,e')	41.5	7.7	4.7	0.54		Inelastic scattering cross section at 180° = $2.0 \pm 25\% \times 10^{-32}$ cm^2/sr Rad. width corresponds to transiti from $\frac{1}{2}^+$ ground state to $\frac{3}{2}^+$ excited state.

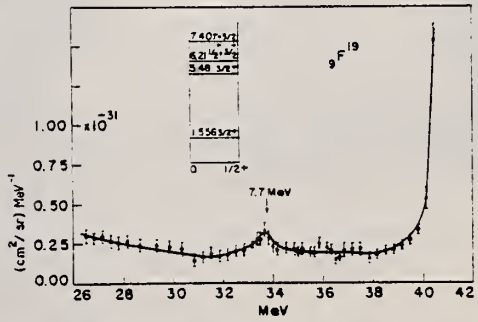

Fig. 9. Spectrum of 41.5 MeV electrons scattered from CF_2 at 180°.

Ref. K.M. Murray, W.L. Bendel
Phys. Rev. 132, 1134 (1963)

Elem. Sym.	A	Z
F	19	9

Method: 24 MeV betatron; proton spectrum; silicon-diode charged particle detector; r-chamber

Ref. No.: 63 Mu 1

Reaction	E or ΔE	E_o	Γ	$\int \sigma dE$	Jπ	Notes
(γ,p)	Bremss. 23.5					On basis of spectrum measured with absorber concludes there are some heavy charged particles present. Detector at 120°.

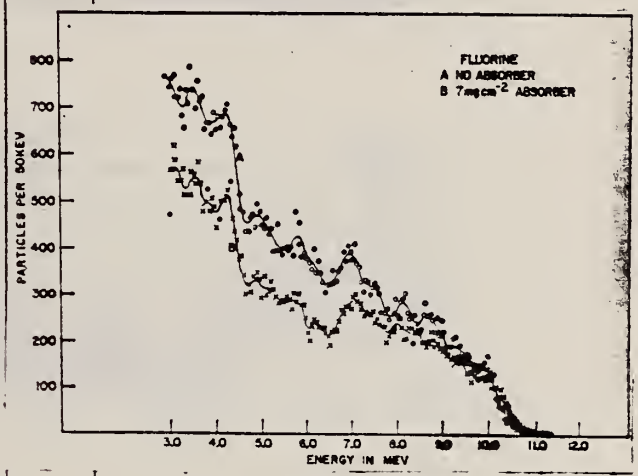

FIG. 7. Pulse-height distributions from fluorine. Curve A represents the smoothed value of data taken with no absorber. Curve B represents the smoothed value of data taken with 7 mg cm^{-2} of aluminum between target and detector, and was corrected in the same manner as in Fig. 5.

TABLE II. Proton energies and F^{18} levels, in MeV.

E_p	F^{19} to O^{18}	F^{19} to O^{16}	F^{19} to O^{18} ground state: Dodge[a] (e,pα')	Forkman[b] (γ,π)	Other (γ,π)
(2.98)			11.42	11.4	11.5[c,d]
3.58±0.06	11.80	15.44 to 3.63	11.90	11.9	11.9[c,d]
4.28±0.06	12.55		12.74	12.8	12.2[e]
(4.97)				13.6	
5.83±0.06	14.19				
(6.23)		(16.60 to 1.98)			
6.97±0.05	15.41		15.70	15.4	15.3[c,d]
(7.53)					
8.10±0.08	16.61			16.5	
(8.65)					

[a] See Ref. 11. [c] See Ref. 1.
[b] See Ref. 7. [d] See Ref. 3.

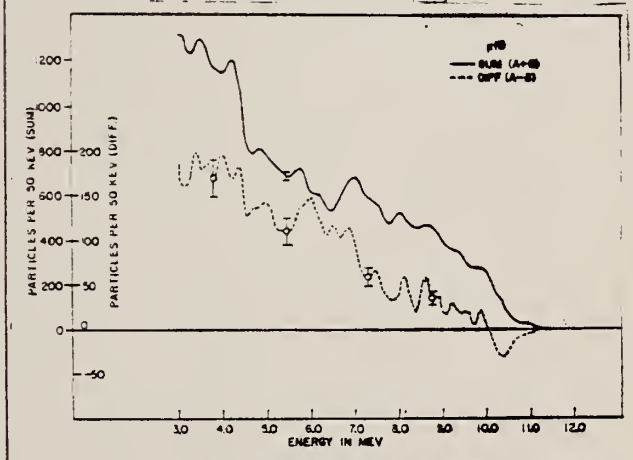

FIG. 8. The continuous curve represents the sum of curves A and B of Fig. 7, plotted against the ordinate scale at the left. The dashed curve is the difference (A−B), plotted against the inner scale.

REF. E. C. Booth, B. Chasan and K. A. Wright
Nucl. Phys. 57, 403-420 (1964)

ELEM. SYM.	A	Z
F	19	9

METHOD
Vam de Graaff; resonance fluorescence

REF. NO. 64 Bo 1 NVB

REACTION	RESULT	EXCITATION ENERGY	SOURCE		DETECTOR		ANGLE
			TYPE	RANGE	TYPE	RANGE	
G,G	LFT	1-3	C	1 - 3	NAI-D		100
		(0.5 - 3.0)		(0.5 - 3.0)			

ABI

TABLE 1
Cases of observed resonance fluorescence

Nucleus multipol.	State (MeV)	Spin	Γ_0/Γ	$T(g\omega\Gamma_0^2/\Gamma^2)^{-1}$ (sec).	Mean lifetime T BCW (sec)	Mean lifetime T other (sec)	Ref.	Γ_0/Γ_W BCW
F^{19}	0.00	$\frac{1}{2}^+$						
E1	1.46	$\frac{3}{2}^-$	0.15	$27\pm8\times10^{-14}\Gamma_1/\Gamma_0$	$6.2\pm2\times10^{-14}$	$5\pm1.5\times10^{-14}$	[6]	1.1×10^{-3}
M1[a])	1.56	$\frac{1}{2}^+$	(0.04)	$11\pm4\times10^{-14}\Gamma_2/\Gamma_0$	$20^{+10}_{-8}\times10^{-14}\Gamma_0/\Gamma$			1.5×10^{-3}

REF.

J. M. Loiseaux, M. Langevin and J. M. Maison
Proc. Paris Conf. 1048 (1964)

ELEM. SYM.	A	Z
F	19	9

METHOD

Betatron

REF. NO. 64 Lo 3 JDM

REACTION	RESULT	EXCITATION ENERGY	SOURCE		DETECTOR		ANGLE
			TYPE	RANGE	TYPE	RANGE	
G,G	ABX	10-30	C	10-30	NAI-D		140

The effective differential scattering cross section remains quite constant from 20-30 MeV.

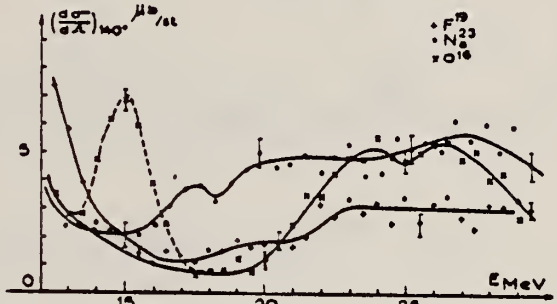

FIG. 2

REF.

S. Seki, M. Yamanouchi and M. Miwa
J. Phys. Soc. Japan 19, 1999 (1964)

ELEM. SYM.	A	Z
F	19	9

METHOD

REF. NO.	
64 Se 1	EGF

REACTION	RESULT	EXCITATION ENERGY	SOURCE		DETECTOR		ANGLE
			TYPE	RANGE	TYPE	RANGE	
G,XP	SPC	THR - 24	C	14-24	EMU-D	2-15	DST

Target thickness 3.4 mg/cm^2 and 5.7 mg/cm^2.

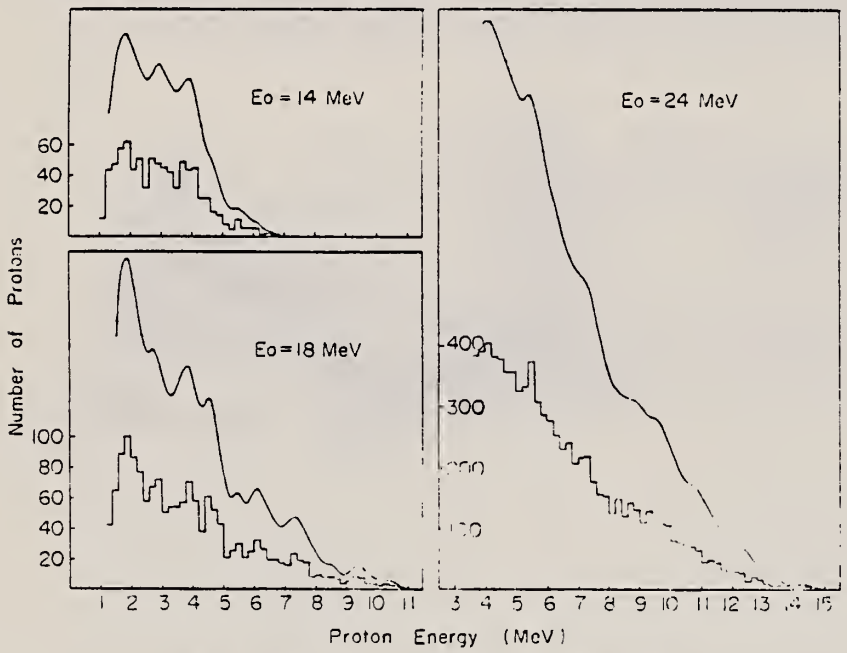

Fig. 2. Energy spectra of photoprotons from fluorine.

Table III. Coefficients a_i's of the Expression (2).

E_0	Energy region (MeV)	a_1	a_2	a_3	a_4
18 MeV	$3.2 \leqq E_p < 4.2$	0.45	−0.39	−0.32	−0.28
	$4.2 \leqq E_p < 5.2$	0.76	0.55	−0.64	−1.31
	$5.2 \leqq E_p < 10.0$	0.75	−0.65	−0.74	0.13
24 MeV	$8.0 \leqq E_p < 10.0$	0.25	0.14	−0.27	−0.67
	$10.0 \leqq E_p$	0.39	0.14	−0.27	−0.70

assuming an angular distribution of the form

$$1+a_1\cos\theta+a_2\cos^2\theta+a_3\cos^3\theta+a_4\cos^4\theta\,. \quad (2)$$

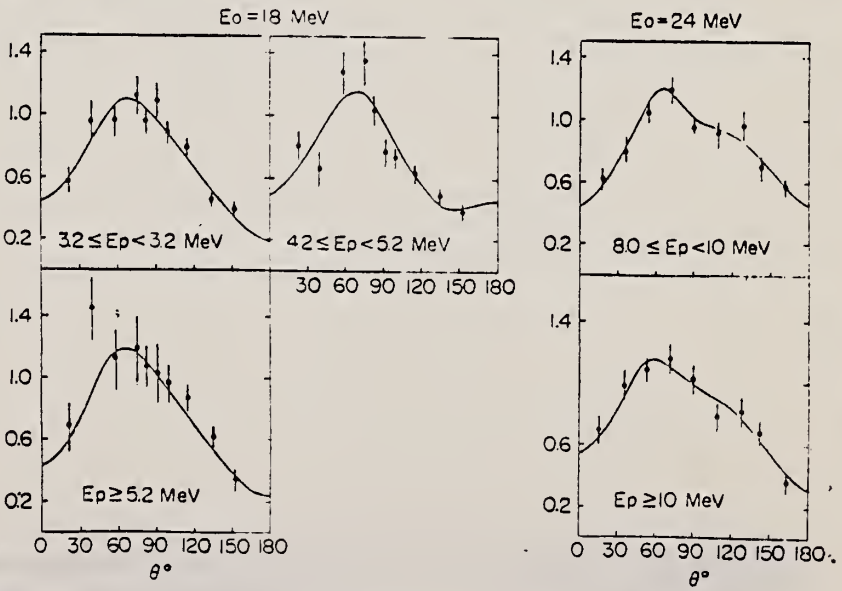

Fig. 4. Angular distributions of photoprotons from fluorine.

REF.

G. Tessler, W.E. Stephens
Phys. Rev. 135, B129-36 (1964)

ELEM. SYM.	A	Z
F	19	9

METHOD

Tandem, $T^3(p,\gamma)$

REF. NO. 64 Te 1 NVB

REACTION	RESULT	EXCITATION ENERGY	SOURCE		DETECTOR		ANGLE
			TYPE	RANGE	TYPE	RANGE	
G,MU-T	ABX	20-21	D	20-21	NAI-I		96

66

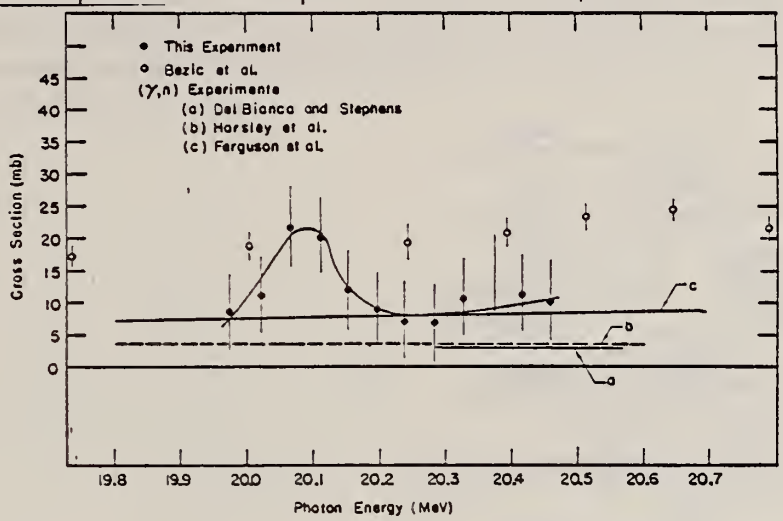

FIG. 10. Nuclear absorption cross section in F^{19} as a function of photon energy. The results of this experiment are plotted as dots. Other results are shown for comparison.

TABLE IV. Structure observed in the nuclear absorption cross section curves.

Element	E_{peak} (MeV)	σ_{peak} (mb)	Half-width (MeV)	$\int_{peak} \sigma dE$ (MeV-mb)
Be^9	20.47	6.8	0.13	0.45
	20.73	10.1	0.15	0.9
O^{16}	20.62	21.5	0.19	3.9
	21.02 {20.86 / 21.05}	23.5	~0.40	10.4
	>22			
F^{19}	20.09	21.9	0.16	3.5

REF.

F. I. Havliček and M. Modesto
Energ. Nucl. 12, 77 (1965)

ELEM. SYM.	A	Z
F	19	9

METHOD

REF. NO. 65 Ha 2 JOC

REACTION	RESULT	EXCITATION ENERGY	SOURCE		DETECTOR		ANGLE
			TYPE	RANGE	TYPE	RANGE	
G,A	SPC	THR-31	C	31	EMU-D	5-20	DST

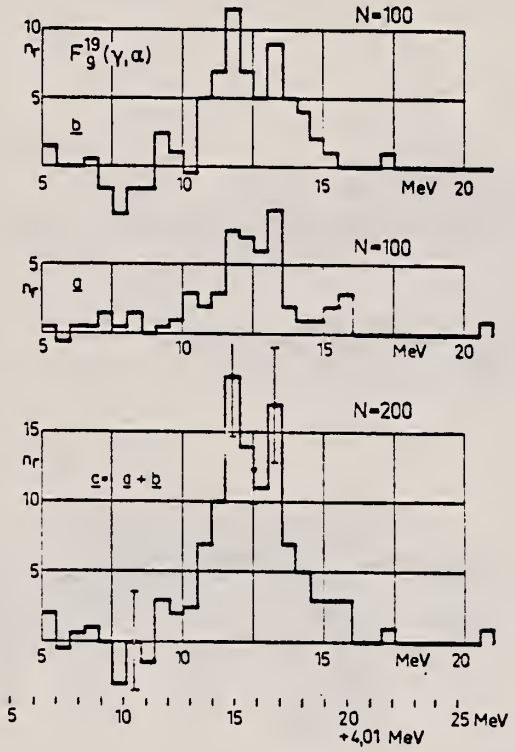

Fig. 8.

REF.

F.P. Denisov, A. Duisebaev, K.V. Kosareva, and P.A. Cerenkov
J. Nucl. Phys. (USSR) 1, 82 (1965)
Sov. J. Nucl. Phys. 2, 58 (1966)

ELEM. SYM.	A	Z
F	19	9

METHOD

Synchrotron; recoil nucleus method

REF. NO.: 66 De 5 JDM

REACTION	RESULT	EXCITATION ENERGY	SOURCE		DETECTOR		ANGLE
			TYPE	RANGE	TYPE	RANGE	
G,N	NOX	THR - 260	C	260	ACT-I		DST

Measured range of recoiling ^{18}F nuclei.

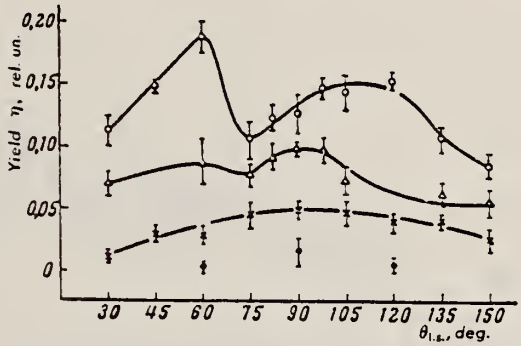

Angular and energy distribution of the F^{18} recoil nuclei; the points on the curves correspond to the following pressures (in centimeters mercury): ○ – pressure ~0; △ – 3.3; × – 10; ● – 15.

REF. B. S. Dolbilkin, V. A. Zapevalov, V. I. Korin, L. E. Lazareva and F. A. Nikolaev
Izv. Akad. Nauk fiz. 30, 349 (1966)
Bull. Acad. Sci. USSR-Phys. 30, 354 (1966)

ELEM. SYM.	A	Z
F	19	9

METHOD

REF. NO. 66 Do 2 EGF

REACTION	RESULT	EXCITATION ENERGY	SOURCE		DETECTOR		ANGLE
			TYPE	RANGE	TYPE	RANGE	
G-MU-T	ABX	8-30	C	260	MGP	6-30	4PI

Resolution 120 keV 10 MeV
220 keV 20 MeV

417

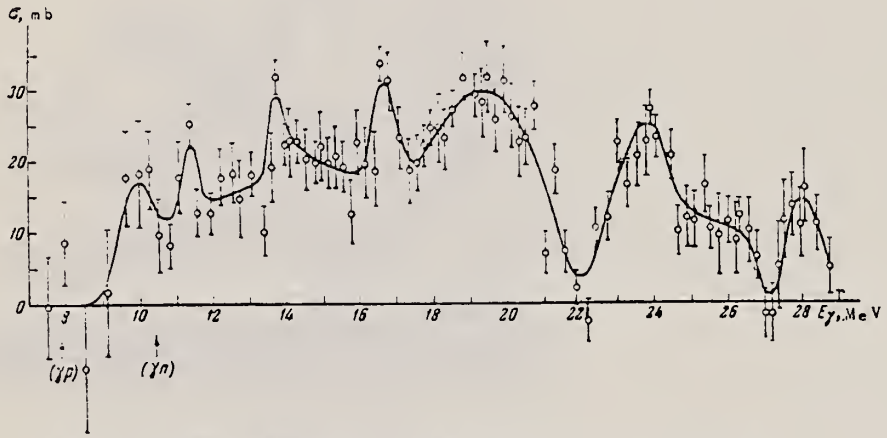

Fig.2. Nuclear absorption cross section of fluorine.

REF.

G. Baciu, D. Catana, C. Deberth, and I. Raileanu
Rev. Roum. Phys. 12, 385 (1967)

ELEM. SYM.	A	-
F	19	9

METHOD

REF. NO. 67 Ba 3 egf

REACTION	RESULT	EXCITATION ENERGY	SOURCE		DETECTOR		ANGLE
			TYPE	RANGE	TYPE	RANGE	
G,N	ABX	THR-25	C	THR-25	ACT-I		4PI

NSA 35223 BREAKS

35223 ON THE NUCLEAR SHAPE AND THE PHOTONEUTRON CROSS SECTION OF THE ^{19}F NUCLEUS. Baciu, G.; Catana, D.; Deberth, C.; Raileanu, I. (Inst. of Atomic Physics, Bucharest). Rev. Roum. Phys., 12: 385-91(1967).

The absolute cross section for the (γ,n) reaction on ^{19}F was measured by using the bremsstrahlung of the IFA betatron with a maximum energy of 25 MeV. The induced radioactivity in the samples of C_nF_{2n+2} (teflon) was recorded by means of a γ-γ scintillation spectrometer. The data supplied by the spectrometer were recorded by a SA-40 type (Intertechnique) multichannel analyzer. The yield points were taken at 0.25 MeV intervals. The betatron energy scale stability was controlled at least two times per day and a deviation smaller than ±10 keV was observed. The calculated cross-section shows several discrete resonances; those disposed in the giant resonance region were well described by three Gaussians. The maxima occur at 15.10, 18.55, and 19.90 MeV. From the fine structure of the giant resonance the nucleus deformation parameters and the intrinsic quadrupole moment were calculated. They are: $\gamma = 12°$, $\beta = 0.18$, and $Q_0 = 0.125$ mbarns. (auth)

REF.

J. M. Loiseaux, J. M. Maison, and M. Langevin
J. de Physique 28, 11 (1967)

ELEM. SYM.	A	Z
F	19	9

METHOD

REF. NO.	
67 Lo 1	JOC

REACTION	RESULT	EXCITATION ENERGY	SOURCE		DETECTOR		ANGLE
			TYPE	RANGE	TYPE	RANGE	
G,G/	ABX	14-32	C	34	NAI-D		DST

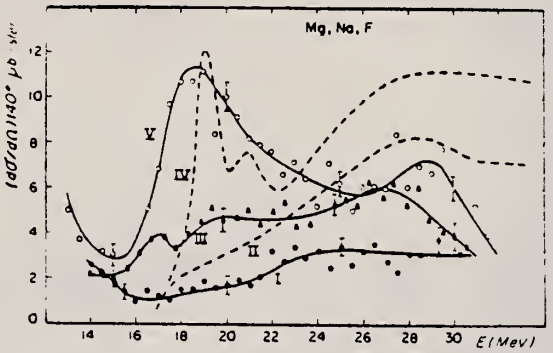

FIG. 6.

Sections efficaces différentielles de diffusion à 110° pour ^{19}F (I), ^{23}Na (III) et Mg (V).

Section efficace prévue par la relation de dispersion pour ^{23}Na (courbe II) et Mg (courbe IV).

REF.

K. Abe, E. Tanaka, N. Kawamura, M. Kanazawa and N. Mutsuro
J. Phys. Soc. Japan 25, 1507 (1968)

ELEM. SYM.	A	Z
F	19	9

METHOD

REF. NO. 68 Ab 1 egf

REACTION	RESULT	EXCITATION ENERGY	SOURCE		DETECTOR		ANGLE
			TYPE	RANGE	TYPE	RANGE	
G,XP	SPC	THR-22	C	22	SCD-D	3-13	90

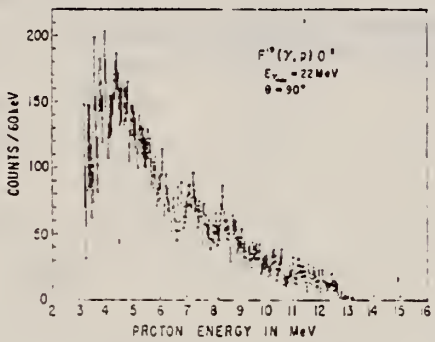

Fig. 2. Photoproton spectrum from a polytetrafluoroethylene target.

REF.

B.C. Cook and C.C. Jones
Nucl. Instr. & Methods 59, 229 (1968)

ELEM. SYM.	A	Z
F	19	9

METHOD

REF. NO. 68 Co 2 hmg

REACTION	RESULT	EXCITATION ENERGY	SOURCE		DETECTOR		ANGLE
			TYPE	RANGE	TYPE	RANGE	
G,N	ABI	10- 50	C	10- 50	MOD-I		4PI
G,2N	ABI	25- 50	C	20- 50	MOD-I		4PI

$\int_{TH}^{50} \sigma(\gamma,sn)dE = 221 \pm 20$ MeV-mb.

A 40" liquid scintillation detector was constructed for use in photonuclear work. Integrated cross sections for reactions in which one or two neutrons are emitted were measured up to 50 MeV for fluorine. The efficiency of the detector was about 60%.

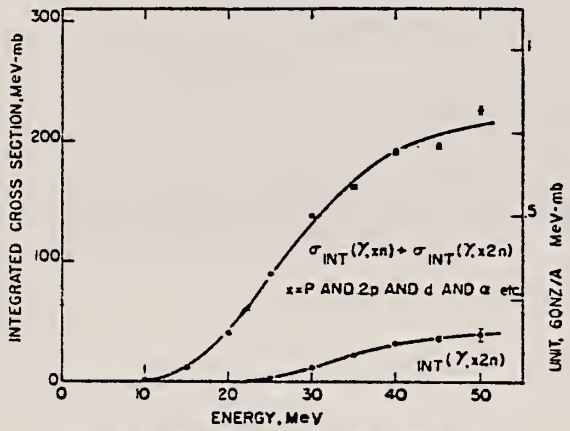

Fig. 9. Integrated cross sections for fluorine.

R. A. Meyer, W. B. Walters, J. P. Hummel
Nucl. Phys. A122, 606 (1968)

F	19	9

METHOD

REF. NO. 68 Me 4 | egf

REACTION	RESULT	EXCITATION ENERGY	SOURCE TYPE	SOURCE RANGE	DETECTOR TYPE	DETECTOR RANGE	ANGLE
G,2PN	ABX	THR-300	C	20-300	ACT-I		4PI

TABLE 1

Summary of integrated cross sections $\int_0^{E_{max}} \sigma dE$(MeV · mb) for the reactions studied

Reaction/E_{max}(MeV)	65	105	145	215	295
$^{16}O(\gamma, 2n)^{14}O$	0.42 ±0.02	0.57 ±0.04	0.56 ±0.05	0.63 ±0.09	1.29 ±0.16
$^{19}F(\gamma, 2pn)^{16}N$	3.7 ±0.2	5.0 ±0.3	6.1 ±0.5	8.4 ±1.0	13.6 ±1.5
$^{27}Al(\gamma, 2pn)^{24}Na$	8.3 ±0.3	13.3 ±0.7	17.1 ±1.2	24.1 ±2.3	31.2 ±3.3 a)
$^{51}V(\gamma, \alpha)^{47}Sc$	12.3 ±1.7	20.2 ±3.5	32.5 ±2.6	68.4 ±3.8	112 ±14
$^{51}V(\gamma, \alpha 3n)^{44}Sc$	0.7 ±0.2	6.0 ±0.9	12.2 ±1.3	34.1 ±4.1	91 ±11

a) E_{max} = 275 MeV.

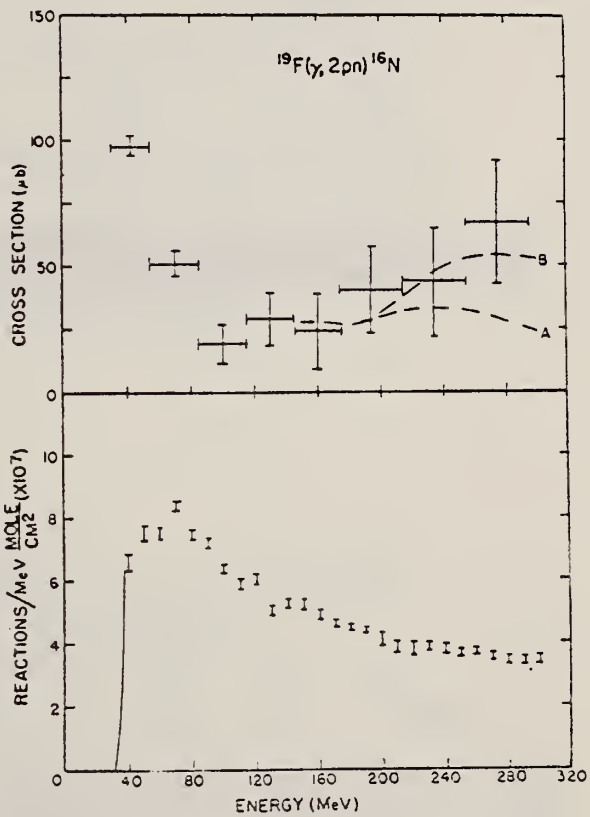

Fig. 2. Yields and cross sections for the $^{19}F(\gamma, 2pn)^{16}N$ reaction The solid line shows the assumed extrapolated yield curve behavio near the reaction threshold. The dashed lines have the same significance as in fig. 1.

The dashed lines show the cross sections expected for quasi-deuteron processes (curve A) and the sum of the cross sections expected for quasi-deuteron and pion emission processes (curve B).

REF. N. Bezić, D. Brajnik, D. Jamnik and G. Kernel
Nucl. Phys. A128, 426 (1969)

ELEM. SYM.	A	Z
F	19	9

METHOD

REF. NO. 69 Be 2 egf

REACTION	RESULT	EXCITATION ENERGY	SOURCE		DETECTOR		ANGLE
			TYPE	RANGE	TYPE	RANGE	
G,MU-T	ABX	10-30	C	35	MGC-D	10-30	4PI

107

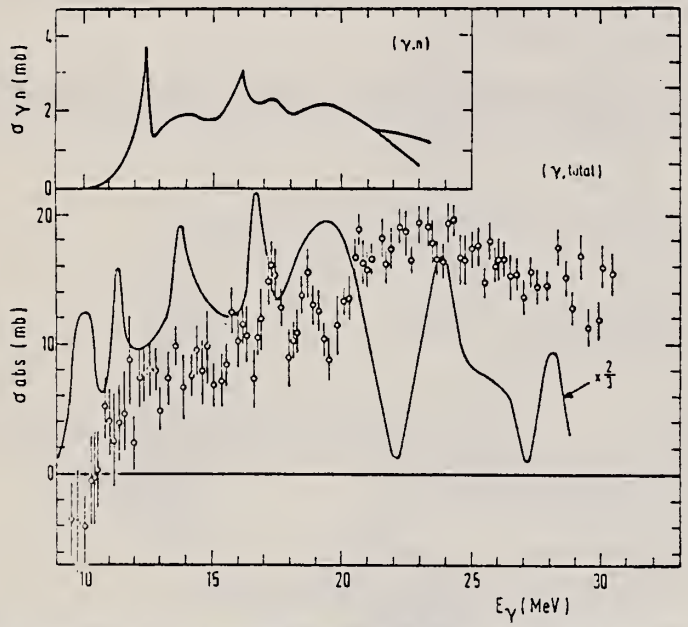

Fig. 4. The nuclear part of the photo-absorption cross section for ^{19}F. The inaccuracy of the zero line position is estimated to be the same as in case of ^{14}N. The solid line represents the photonuclear absorption cross section of Dolbilkin *et al.* [7]) multiplied by a factor of $\frac{2}{3}$. The (γ, n) cross section [35]) is shown in the upper left corner.

TABLE 1

Weighted energy-integrated total photonuclear cross sections

	σ_{int} (mb · MeV)	$\frac{\sigma_{int}}{60(NZ/A)}$ (mb · MeV)	σ_{-1} (mb)	$\frac{\sigma_{-1}}{0.30A^{\frac{4}{3}}\,mb}$	σ_{-2} (mb · MeV^{-1})	$\frac{\sigma_{-2}}{3.5\,A^{\frac{4}{3}}}$ (μb · MeV^{-1})
^{12}C	133±13	0.74±0.07	5.4±0.6	0.65±0.07	0.23±0.03	1.04±0.15
^{14}N	195±37	0.93±0.08	8.4±1.7	0.83±0.20	0.36±0.08	1.28±0.29
^{16}O	171±17	0.71±0.07	7.2±0.8	0.60±0.07	0.31±0.04	0.87±0.11
^{19}F	271±50	0.94±0.17	14.1±2.7	0.82±0.19	0.74±0.17	1.60±0.35
^{28}Si	360±30	0.86±0.07	17.5±1.7	0.68±0.07	0.83±0.10	0.93±0.11
^{40}Ca	580±60	0.96±0.10	29 ±3	0.71±0.08	1.5 ±0.2	0.92±0.12

The interval of integration is 10-30 MeV.

[7] B.S. Dolbilkin, V.A. Zapevalov, V.I. Korin, L.E. Lazareva and F.A. Nikolaev, Izv.Akad.Nauk SSSR(ser.fiz.) 30 (1966) 349.

[35] J.D. King, R.N. Haslam and W.J. McDonald, Can.J.Phys.38 (1960) 1069.

U.S. DEPARTMENT OF COMMERCE
NATIONAL BUREAU OF STANDARDS

T. Walcher and P. Strehl
Z. Physik 232, 342 (1970)

ELEM. SYM.	A	Z
F	19	9

METHOD

REF. NO. 70 Wa 1 egf

REACTION	RESULT	EXCITATION ENERGY	SOURCE		DETECTOR		ANGLE
			TYPE	RANGE	TYPE	RANGE	
E,E/	LFT	1-2	D	30-60	MAG-D	28-60	DST

1.56, 1.35 MEV

Tabelle 2. *Ergebnisse*

E_x (MeV)	Γ_γ^0 (eV)	Γ_γ^0/Γ_W	$B(q=0)$	R_{tr} (fm)
1,56 ($E2$)	$(1{,}76 \pm 0{,}15) \cdot 10^{-4}$	$7{,}65 \pm 0{,}61$	$(47{,}2 \pm 4{,}0)$ fm^4	$3{,}94 \pm 0{,}34$
1,35 ($E3$)	$(8{,}1 \pm 1{,}7) \cdot 10^{-10}$	$12{,}0 \pm 2{,}4$	(795 ± 160) fm^6	(4,2) vorgegeben

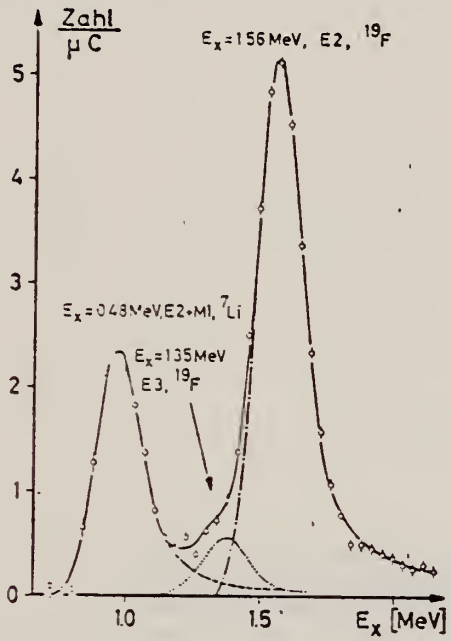

Fig. 1. Spektrum der unelastisch gestreuten Elektronen an LiF bei $E_0 = 58{,}0$ MeV und $\Theta = 117°$; Abszisse: Anregungsenergie im ^{19}F. Die Strahlungsschwänze der elastischen Linien sind abgezogen. Die gestrichelte, die punktierte und die strichpunktierte Kurve zeigen die Anteile aus der die angepaßte, durchgezogene Kurve zusammengesetzt ist

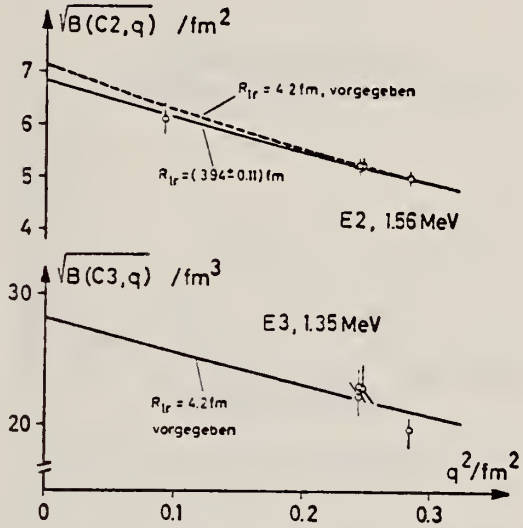

Fig. 2. Die reduzierten Übergangswahrscheinlichkeiten $B(C2, q)$ und $B(C3, q)$ als Funktion von q^2

Tabelle 1. *Experimentelle Daten*

Der Korrekturfaktor der DWBA-Analyse ist wie folgt definiert: $f_c(q, E_0, E_x) = (d\sigma/d\Omega)_{DWBA}/(d\sigma/d\Omega)_{BA}$

E_0(MeV)	Θ	$E2$, $E_x = 1{,}56$ MeV					$E3$, $E_x = 1{,}35$ MeV				
		q^2(fm^{-2})	σ/σ_{Ft} (10^{-3})	Fehler (%)	$d\sigma/d\Omega$ (10^{-6} fm^2/ster)	f_c	q^2(fm^{-2})	σ/σ_{Ft} (10^{-3})	Fehler (%)	$d\sigma/d\Omega$ (10^{-7} fm^2/ster)	f_c
57,99	117°	0.243	2,37	5,2	7,94	1,106	0,244	2,26	17,4	7,59	1,176
57,99	117°	0,243	2,35	5,1	7,87	1,106	0,244	2,45	15,5	8,21	1,176
58,29	117°	0,246	2,36	5,3	7,73	1,106	0,247	2,43	19,2	8,06	1,176
59,06	129°	0,283	3,26	5,0	5,02	1,097	0,284	3,17	17,7	4,88	1,162
36,01	117°	0,092	0,30	14,7	4,18	1,155	—	—	—	—	—

	Punched	Checked w/PO
IBM Card DATA	9/1/70	9/10/70
IBM Card REFERENCE	9/9/70	9/10/70

REF. R. J. Baglan, C. D. Bowman and B. L. Berman
Phys. Rev. C3, 672 (1971)

ELEM. SYM.	A	Z
F	19	9

METHOD

REF. NO. 71 Ba 2 hmg

REACTION	RESULT	EXCITATION ENERGY	SOURCE		DETECTOR		ANGLE
			TYPE	RANGE	TYPE	RANGE	
G,N	ABX	12-15	C	15	TOF-D		135
		(12.3-14.5)					

662

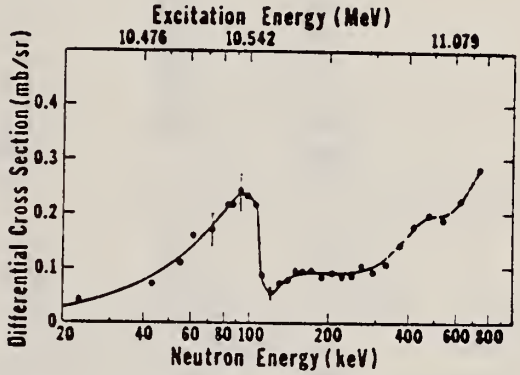

FIG. 18. The 135° differential threshold photoneutron cross section for ^{19}F (see caption to Fig. 4).

FIG. 4. The 135° differential threshold photoneutron cross section for ^{207}Pb at low energies versus the energy of the emitted neutron (lower scale) and the excitation energy (upper scale). The arrows indicate peaks which decay to excited states of the residual nucleus (ES), or peaks owing to contaminating isotopes in the photoneutron sample. The inset shows the $^{207}Pb(\gamma,n)$ cross section averaged with a square 40-keV wide smoothing function.

Also see:
R. J. Baglan et al.
Phys. Rev. C3, 2475
(1971)

[over]

TABLE VII. Resonance parameters for ^{24,25,26}Mg, ^{19}F, and ^{31}P. For all resonances, the area under the peak in the 135° differential cross section is multiplied by 4π to yield approximate values for $g_\gamma\Gamma_{\gamma 0}\Gamma_n/\Gamma \simeq g_\gamma\Gamma_{\gamma 0}$. For those resonances where J^π is known, the differential area is multiplied by the appropriate factor F from Table I to obtain $\Gamma_{\gamma 0}$. E_L is the laboratory neutron energy for the (γ,n) reaction and E_n is the corresponding laboratory neutron energy for a neutron-induced reaction. Column 5 labels the peak as a ground-state (GS) or excited-state (ES) transition as determined in this work alone.

Nucleus	E_L (keV)	E_{ex} (MeV)	$g_\gamma\Gamma_{\gamma 0}\Gamma_n/\Gamma$ (eV)	GS or ES	J^π	$\Gamma_{\gamma 0}$ (eV)	E_n (keV) (This work)
^{24}Mg	22	16.559	0.61		(1^-)	0.40	28
	55	16.596	2.4	GS	(1^-)	1.6	66
	110	16.656	4.0	GS	(1^-)	2.7	128
	312	16.871	10.7		(1^-)	7.1 [a]	354
	382	16.95					432
	717	17.30	19.5		(1^-)	13.0 [a]	804
	1210	17.83					1348
	1620	18.26					1799
	1955	18.61					2168
^{25}Mg	41.1	7.374	0.09	GS			46.8
	45.1	8.746	0.31	ES			
	74.9	7.410	0.36	GS	$\frac{3}{2}^-$ [b]	1.1	84.1 [b]
	208	8.920	0.29	ES			
	236	7.580	0.09	GS			261
	404	7.756	0.03				445
	439	7.793	0.05		$\frac{5}{2}^+$ [c]		484
	472	7.828	0.06				520
	515	7.873	0.46	GS	$\frac{3}{2}^+$ [c]		567
	601	7.964	0.18				661
	781	8.152	1.51	GS			857
	912	8.292	0.72				1003
	1236	9.999	2.4 [c]	ES	$\frac{3}{2}^+$ or $\frac{5}{2}^+$ [c]		
	1707	9.12					1869
	1764	9.18					1931
^{26}Mg	54.3	11.155	2.6	GS	$1^-(1^+,2^+)$	1.75	62.3
	63.2	11.164	0.05			0.034	72.2
	181	11.289	1.0	GS	$1^-(1^+,2^+)$	0.68	202
	222	11.333	1.9	GS	$1^-(1^+,2^+)$	1.3	248
	391	11.511	5.1	GS	$1^-(1^+,2^+)$	3.5	433
	621	11.753	32.5	GS	$1^-(1^+,2^+)$	22.2	684
	738		15.0 [d]	ES		5.1	
	1122	12.279	14.7	GS	$1^-(1^+,2^+)$	10.0	1232
^{19}F	100	10.542	1.8	GS			118
^{31}P	109	12.429	0.86				121
	280	12.609	0.60				307
	398	12.732	0.59				434
	678	13.026	0.90				737
	939	13.297	4.4				1013

[a] These values for $\Gamma_{\gamma 0}$, when increased by approximately a factor of 2 in order to include the relatively high cross sections in the valleys, agree very well with corresponding values from Ref. 8 (see Ref. 4).

[b] This resonance was seen at E_n = 83 and 84 keV in Refs. 24 and 25, respectively.

[c] Analogs of states in ^{25}Na (see text). The value for $g_\gamma\Gamma_{\gamma 0}\Gamma_n/\Gamma$ given in Ref. 26 was not corrected with the multiplicative factor in Table II.

[d] Assuming a first-excited-state transition.

[4] R.L. Van Hemert, C.D. Bowman, R.J. Baglan, and B.L. Berman (to be published); R.L. Van Hemert, University of California Lawrence Radiation Laboratory Report No. UCRL-50442, 1968 (unpublished).

[3] S.C. Fultz, M.A. Kelly, J.T. Caldwell, R.R. Harvey, and B.L. Berman, Bull. Am. Phys. Soc. 14, 103 (1969), and private communication.

[24] H.W. Newson, R.C. Block, P.F. Nichols, A. Taylor, A.K. Furr, and E. Merzbacher, Ann. Phys. (N.Y.) 8, 211 (1959).

[25] D.J. Hughes and R.B. Schwartz, Neutron Cross Sections (U.S. Government Printing Office, Washington, D.C., 1966), 2nd ed., 2nd Suppl., Vol. IIc.

REF. V. Di Napoli, D. Margadonna, F. Salvetti, H.G. De Carvalho, J.Benuzzi Martins
Nucl. Inst. Meth. 93, 77 (1971)

ELEM. SYM.	A	Z
F	19	9

METHOD

REF. NO. 71 Di 5 hg

REACTION	RESULT	EXCITATION ENERGY	SOURCE TYPE	SOURCE RANGE	DETECTOR TYPE	DETECTOR RANGE	ANGLE
G,N	ABY	10-999	C	300-999	ACT-I		4PI

999 = 1 GEV

The use of the $^{19}F(\gamma,n)^{18}F$, $^{27}Al(\gamma,x)^{24}Na$, $^{197}Au(\gamma,n)^{196}Au$, and $^{12}C(\gamma,x)^{7}Be$ reactions as absolute monitors for high-energy, high-intensity bremsstrahlung beams is discussed. The cross sections per equivalent quantum and the absolute cross sections, in the energy range 300-1000 MeV, are reported for these reactions. $^{19}F(\gamma,n)^{18}F$, $^{27}Al(\gamma,x)^{24}Na$, and $^{12}C(\gamma,x)^{7}Be$ reactions are proposed as very simple and suitable systems for monitoring purposes.

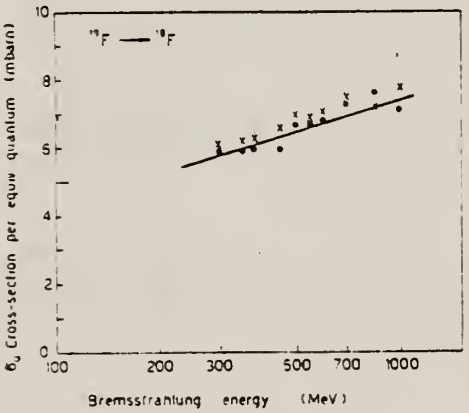

Fig. 1. $^{19}F \rightarrow {}^{18}F$ reaction cross sections per e.q. The circles represent values obtained by the Wilson quantameter; the straight line is a least-squares fit of these values. The crosses represent σ_Q values obtained by the $^{27}Al \rightarrow {}^{24}Na$ monitor.

TABLE 2

Energy (MeV)	σ_Q(mb) $^{19}F \rightarrow {}^{18}F$	$^{27}Al \rightarrow {}^{24}Na$	$^{197}Au \rightarrow {}^{196}Au$[a]	$^{12}C \rightarrow {}^{7}Be$[a]
260			270±14	
300	5.90±0.20	0.37±0.01	258±13	0.37±0.01
320		0.39±0.01		
350	5.90±0.20	0.39±0.01		0.38±0.01
380	5.95±0.20	0.41±0.01		
400				0.42±0.01
420		0.45±0.01		
450	5.95±0.20	0.48±0.01	249±12	0.44±0.02
500	6.65±0.20	0.49±0.01		
550	6.65±0.20	0.50±0.02		0.47±0.02
600	6.80±0.20	0.52±0.02		
650		0.52±0.02	266±13	0.47±0.02
700	7.20±0.30	0.56±0.02		
750		0.55±0.02		
850	7.60±0.30	0.60±0.02	246±12	0.49±0.03
900		0.59±0.02		
1000	7.10±0.30	0.66±0.02	249±12	0.51±0.03

[a] The values given in the last two columns are, in most cases, an average of two or more measurements (see figs. 3 and 4).

B. Friberg, G. Andersson, and B. Forkman
Nucl. Phys. A171, 551 (1971)

ELEM.		
F	19	9

METHOD

REF. NO. 71 Fr 1 egf

REACTION	RESULT	EXCITATION ENERGY	SOURCE		DETECTOR		ANGLE
			TYPE	RANGE	TYPE	RANGE	
G,N	ABY	10-800	C	100-800	ACT-I		4PI

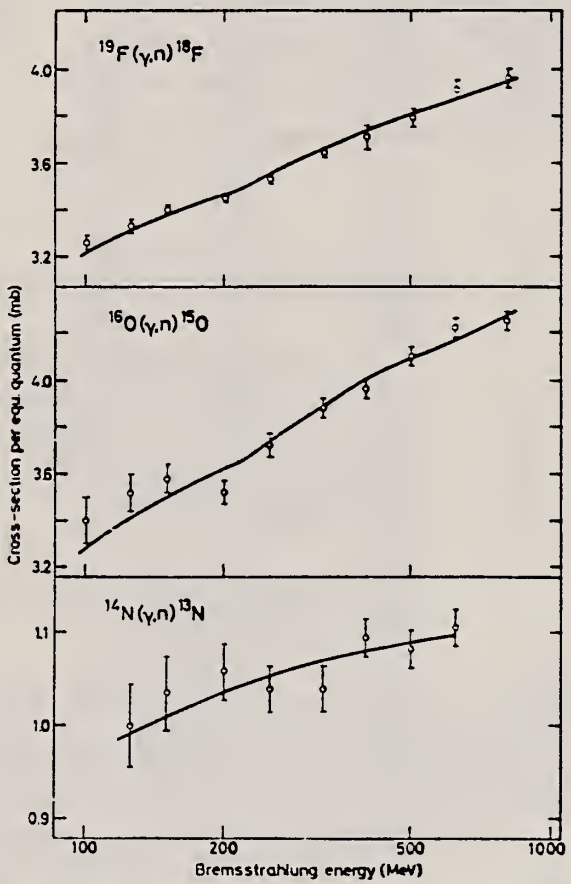

Fig. 1. Absolute yields for the (γ, n) reactions in ^{14}N, ^{16}O and ^{19}F. The solid lines are the least-squares fits of the yields from low-energy processes and photomeson yield.

REF.

M. R. Wormald and I. F. Wright
Particles & Nuclei 2, 168 (1971)

ELEM. SYM.	A	Z
F	19	9

METHOD

REF. NO.	
71 Wo 1	egf

REACTION	RESULT	EXCITATION ENERGY	SOURCE		DETECTOR		ANGLE
			TYPE	RANGE	TYPE	RANGE	
P,G	ABI	10	D	2	SCD-D		DST

10=10.129 MEV

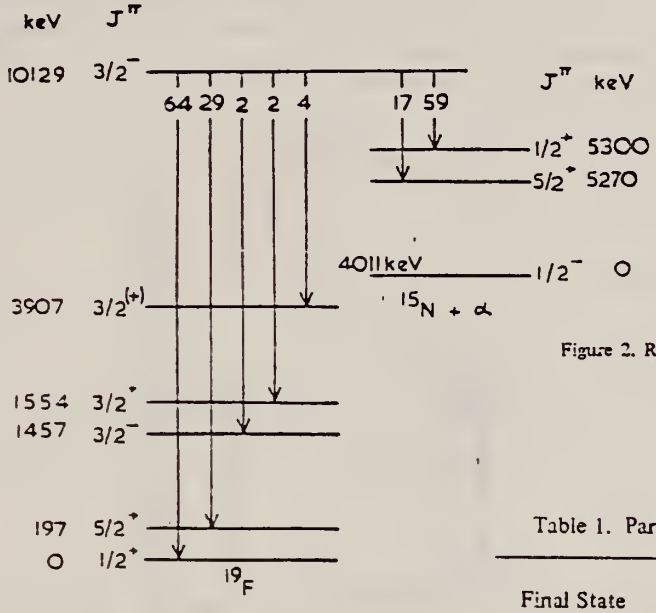

Figure 2. Relative intensities of the γ-rays observed from the 2260 keV resonance in $^{18}O + p$.

Table 1. Partial and Reduced Widths for the 2260 keV Resonance in $^{18}O + p$.

Final State (E_x, keV)	J^π	$\frac{\Gamma_p\Gamma_\gamma}{\Gamma}$ or $\frac{\Gamma_p\Gamma_{\alpha'}}{\Gamma}$ (eV)	Γ_γ, Γ_α or Γ_p (eV)	$\lvert M\rvert^2$ (W.u.)	θ_α^2 or θ_p^2 (MeV)
			see Note 1.		see Note 1
^{19}F (g.s.)	$1/2^+$	2.4	76	0.15 (E1)	
^{19}F (110)	$1/2^-$	<0.07	<2	<0.1 (M1)	
^{19}F (197)	$5/2^+$	1.1	35	0.08 (E1)	
^{19}F (1345)	$5/2^-$	<0.03	<1	<0.07 (M1)	
^{19}F (1457)	$3/2^-$	0.06	1.9	0.14 (M1)	
^{19}F (1554)	$3/2^+$	0.06	1.9	6.3×10^{-3} (E1)	
^{19}F (3907)	$3/2^{(+)}$	0.14	4.4	0.04 (E1)	
^{15}N (g.s)	$1/2^-$	-	7 ± 2 keV		0.021
^{15}N (5270)	$5/2^+$	0.65	20		(0.5)
^{15}N (5300)	$1/2^+$	2.3	71		(2.6)
^{18}O (g.s)	0^+	-	220		7×10^{-4}

NOTE: 1. Using $\Gamma_p/\Gamma = 0.032$ (see text). The errors in these widths are mainly due to the uncertainty in Γ_p/Γ, which is estimated to be ±50%.

2. The penetrabilities were calculated using an "effective radius" = $1.6(A_1^{1/3} + A_2^{1/3})$ fm (see text). The corresponding Wigner limit for α-particle emission is 2.9 MeV.

REF. T. Mo, R. A. Blue and H. R. Weller
Nucl. Phys. A197, 290 (1972)

ELEM. SYM.	A	Z
F	19	9

METHOD

REF. NO. 72 Mo 6 egf

REACTION	RESULT	EXCITATION ENERGY	SOURCE		DETECTOR		ANGLE
			TYPE	RANGE	TYPE	RANGE	
HE,G	RLX	19- 22	D	4- 7	NAI-D		DST

HR= HR3

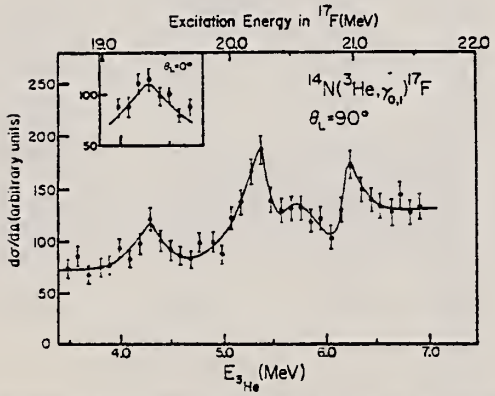

Fig. 5. Excitation functions for τ-capture γ-rays from a ^{14}N gaseous target. The data consist of the sum of γ_0 and γ_1 radiations to the ground and first excited states in ^{17}F. The indicated error bars are statistical errors. The solid curves were drawn through most of the data points for aiding the eye. The bombarding energies have been corrected for energy losses in the entrance foil and target gas, and correspond to incident energies at the center of the gas cell. The curve on the upper-left part is the excitation function measured at $\theta_L = 0°$ over the resonance at 4.3 MeV.

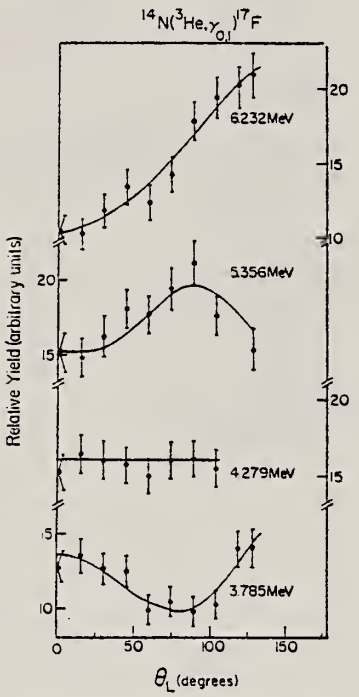

Fig. 6. Angular distributions for τ-capture γ-rays from a $^{14}N_2$ gaseous target. The bombarding energy attached on each angular distribution has been corrected for the energy loss through the entrance foil and target gas, and corresponds to the energy at the center of the gas cell. Statistical errors are indicated.

REF.

D.W.O. Rogers, R.P. Beukens, and W.T. Diamond
Can. J. Phys. 50, 2428 (1972)

ELEM. SYM.	A	Z
F	19	9

METHOD

REF. NO.: 72 Ro 3 | hmg

REACTION	RESULT	EXCITATION ENERGY	SOURCE TYPE	SOURCE RANGE	DETECTOR TYPE	DETECTOR RANGE	ANGLE
A,G	LFT	5-7	D	1-3	SCD-D		DST
		(5.3-6.2)		(1.6-2.7)			

J-PI ,4 LEVELS

TABLE 5. Transition strengths from states studied

E_i	J_i	E_f	J_f	Branching ratio	$\|M\|^2$ (W.u.) M1	E1	E2	M2
5336	1/2+1	0	1/2+	37 ± 4	0.18 ± 0.03			
		110	1/2−	42 ± 4		(10 ± 1.5) × 10^{-3}		
		197	5/2+	< 1			< 2	
		1346	5/2−	< 1.5				< 230
		1459	3/2−	20 ± 2		(12 ± 2) × 10^{-3}†		
		1554	3/2+	< 2	< 0.03			
5618	3/2−	0	1/2+	< 5		< 1.5 × 10^{-4}		
		110	1/2−	< 2	< 0.001			
		197	5/2+	39 ± 4		(9 ± 2) × 10^{-4}†		
		1346	5/2−	61 ± 4	0.068 ± 0.018†			
		1459	3/2−	< 25	< 0.025			
		1554	3/2+	< 25		< 1.5 × 10^{-3}		
5938	1/2+	0	1/2+	7 ± 4	(8.4 ± 4) × 10^{-3}			
		110	1/2−	20 ± 6		(1.1 ± 0.5) × 10^{-3}		
		197	5/2+	2 ± 1			0.7 ± 0.4	
		1459	3/2−	63 ± 6		(7.8 ± 2.6) × 10^{-3}†		
		1554	3/2+	< 2	< 0.006			
		3907	3/2+	8 ± 3	0.24 ± 0.10†			
6070	7/2+	197	5/2+	54 ± 5	0.077 ± 0.018		$1.1^{+0.6}_{-0.4}$	
		1346	5/2−	19 ± 2		(25 ± 6) × 10^{-4}		< 2
		1554	3/2+	$1^{+1}_{-0.5}$			$1.3^{+1.0}_{-0.7}$	
		2780	9/2+	23 ± 3	0.21 ± 0.05		< 3	
		3999	7/2−	< 2		< 3 × 10^{-3}		
		4032	9/2−	< 1		< 1.5 × 10^{-3}		
		4378	7/2+	4 ± 1	0.27 ± 0.08*		—	
6088	3/2−	0	1/2+	25 ± 4		(5 ± 1) × 10^{-3}		< 1.2
		110	1/2−	61 ± 5	0.31 ± 0.06		$0.15^{+0.28}_{-0.12}$	
		197	5/2+	14 ± 3		(32 ± 7) × 10^{-4}		< 2.7
		1346	5/2−	< 0.5	< 0.005			
		1459	3/2−	< 1.5	< 0.015			
		1554	3/2+	< 1		< 5 × 10^{-4}		
6160	7/2−	197	5/2+	31 ± 3		(17 ± 4) × 10^{-4}		$0.47^{+1.1}_{-0.40}$
		1346	5/2−	65 ± 4	0.16 ± 0.04		$0.34^{+0.15}_{-0.12}$	
		1459	3/2−	1.3 ± 0.6	—		0.12 ± 0.06	
		2780	9/2+	< 1		< 6 × 10^{-4}		
		3999	7/2−	1.6 ± 0.6	(5 ± 3) × 10^{-3}†			
		4032	9/2−	2.3 ± 0.3	(7 ± 3) × 10^{-3}†			
		4378	7/2+	< 1		< 1.5 × 10^{-4}		
		4681	5/2−	< 2	< 0.02			

*Assumed pure M1 although there is indication of a possible large E2 component.
†Assumed pure M1 or E1.

REF.

N. Shikazono and Y. Kawarasaki
Nucl. Phys. A188, 461 (1972)

ELEM. SYM.	A	Z
F	19	9

METHOD

REF. NO. 72 Sh 2 egf

REACTION	RESULT	EXCITATION ENERGY	SOURCE		DETECTOR		ANGLE
			TYPE	RANGE	TYPE	RANGE	
G,PG	SPC	0-14	C	14	SCD-D		87
G,AG	SPC	0-14	C	14	SCD-D		87
G,G/	SPC	0-14	C	14	SCD-D		87

TABLE 1

Gamma-rays resulting from the photon bombardment of a $(CF_2)_n$ (teflon) target

E_γ (MeV)	Observed peak	Relative intensity	Assignment	
			reaction	transition
1.66	F	38 ±11	$^{19}F(\gamma, p_1\gamma)^{18}O$	3.64 → 1.98 a)
1.94	F	20 ±10	$^{19}F(\gamma, p\gamma)^{18}O$	3.92 → 1.98 a)
1.98	F	158 ±10	$^{19}F(\gamma, p_0\gamma)^{18}O$	1.98 → 0 a)
3.91	D, F	17 ± 8	$^{19}F(\gamma,\gamma')^{19}F$	3.91 → 0
5.27	D, S, F	71 ± 2	$^{19}F(\gamma, \alpha\gamma)^{15}N$	5.27 → 0
5.30	D, S, F	93 ± 4	$^{19}F(\gamma, \alpha\gamma)^{15}N$	5.30 → 0
6.11	D, S, F	13.9± 1.3	$^{19}F(\gamma,\gamma')^{19}F$	7.66 → 1.56
7.66	D, S, F	11.5± 0.8	$^{19}F(\gamma,\gamma')^{19}F$	7.66 → 0

a) The transition is identified by comparing the transition energy with that from the level scheme for ^{18}O given in ref. [50]).

TABLE 5

Excitation energies and ground state transition widths obtained from the $^{19}F(\gamma,\gamma')^{19}F$ reaction

Excitation energy (keV)		$J^\pi; T$	$\Gamma_{\gamma 0}/\Gamma_\gamma$	$(2J+1)\Gamma_{\gamma 0}$ (eV) a)
present work	previous work			
3906 ± 6	3905 b)	$\frac{3}{2}^{(+)}$ b)	0.44 ± 0.10 b)	0.04 ± 0.03
7663 ± 4	7660 ± 3 c)	$\frac{3}{2}^+; T = \frac{1}{2}$ c)	0.49 ± 0.04 d)	2.6 ± 0.4

a) The error for $(2J+1)\Gamma_{\gamma 0}$ only includes the statistical error. An estimate of the uncertainty associated with the shape of the incident bremsstrahlung is not included. The ground state width of the 7663 keV level is normalized to the value obtained by Aitken *et al.* [10]) from the $^{15}N(\alpha,\gamma)^{19}F$ reaction: $\Gamma_{\gamma 0} = 0.65 \pm 0.11$ eV. The value of $\Gamma_\gamma\Gamma_\alpha/\Gamma = 1.5 \pm 0.3$ eV [ref. [10])] is used to estimate the ground state branching $\Gamma_{\gamma 0}/\Gamma$.

b) Refs. [11,12]).

c) Ref. [10]).

d) This value is calculated from the observed relative intensity at the scattering angle of 87° on the assumption that the transitions to the lower states are of pure dipole character.

10 J.H. Aitken et al. Phys.Lett. 30B (1969) 473.

11 H.G. Benson et al. Nucl.Phys. A126 (1969) 305.

12 K.W. Allen et al., quoted in ref. 11.

50 A.E. Litherland et al. Nucl.Phys. 44 (1963) 220.

REF. B.J. Thomas, A. Buchnea, J.D. Irish, and K.G. McNeil
Can. J. Phys. 50, 3085 (1972)

ELEM. SYM.	A	Z
F	19	9

METHOD

REF. NO.	
72 Th 5	hmg

REACTION	RESULT	EXCITATION ENERGY	SOURCE		DETECTOR		ANGLE
			TYPE	RANGE	TYPE	RANGE	
G,PG	ABI	8- 25	C	19- 25	SCD-D		DST
G,NG	ABI	10- 25	C	19- 25	SCD-D		DST
G,AG	ABI	4- 25	C	19- 25	SCD-D		DST

GAMMA DST

TABLE 2. Yields of gamma rays from the reaction $^{19}F(\gamma,x\gamma')$

Residual nucleus	State (MeV)	J^π	Known γ decay	Relative yield $E_0 = 19$ MeV $\theta = 90°$	$E_0 = 19$ MeV $\theta = 150°$	$E_0 = 21.5$ MeV $\theta = 90°$	$E_0 = 21.5$ MeV $\theta = 150°$	$E_0 = 25$ MeV $\theta = 90°$	$E_0 = 25$ MeV $\theta = 150°$	Estimate of $\int_{.25}^{} \frac{d\sigma(150)}{d\Omega} dE$ (MeV mb/sr)
^{18}F	0.940	3^+	GS	0.70	0.60	0.90	0.90	1.0	1.0	1.25 ± 0.3
	1.040	0^+	GS			0.25	0.20	0.35	0.35	0.45 ± 0.11
^{18}O	1.977	2^+	GS	0.28	0.65	0.85	1.10	0.90	1.40	1.75 ± 0.4
	3.630	0^+	1.977	0.20	0.25	0.25	0.45	0.50	0.70	0.9 ± 0.2
^{15}N	5.27	$5/2^+$	GS	0.07	0.09	0.45	0.35	0.55	0.60	0.75 ± 0.2

REF.

R. E. Van de Vyver, H. Ferdinande, G. Knuyt, R. Carchon, J. Devos
Nucl. Phys. A198, 144 (1972)

ELEM. SYM.	A	-
F	19	9

METHOD

REF. NO. 72 Va 2 egf

REACTION	RESULT	EXCITATION ENERGY	SOURCE		DETECTOR		ANGLE
			TYPE	RANGE	TYPE	RANGE	
G,XN	ABX	10-19	C	10-19	BF3-I		4PI

665

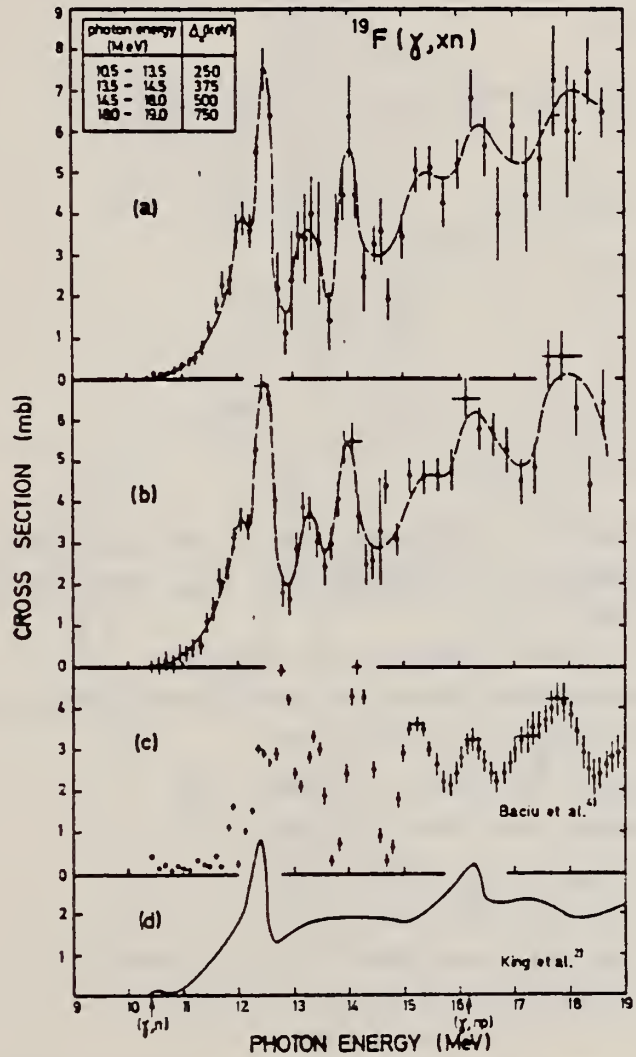

Fig. 3. Total photoneutron cross section $\sigma[(\gamma, n)+(\gamma, np)]$ for ^{19}F: (a) shows our results using the VBPL unfolding procedure, while (b) gives the results from a Cook analysis of the same data (the broken lines serve merely to guide the eye); (c) and (d) represent the other existing photoneutron cross-section data.

(OVER)

TABLE 1

Photonuclear resonance energies observed in ^{19}F

(γ, p)				(e, e'p)	(γ, T)		(γ, n)				
ref. [7])	ref. [9])	ref. [10])	ref. [11])	ref. [8])	ref. [12])	ref. [13])	ref. [2])	ref. [3])	ref. [4])	ref. [5])	this work
		10.0			(10.1)						
10.4							(10.6)				
		10.96				(10.9)		11.0			
11.4				11.42	11.4					(11.40)	
									11.56	(11.59)	
										(11.72)	
	11.8					(11.8)				(11.82)	
11.9		12.0		11.9					11.90	(11.90)	
								12.1		12.10	12.1
						12.5	12.4	12.5	12.42	12.38	12.5
	12.55		(12.6)							(12.65)	
(12.8)		12.85		12.74					12.88	(12.84)	
										(13.04)	
									13.28	(13.29)	13.3
13.6						13.7				13.82	
	14.19				14.0		14.0	14.0	14.08		14.0
		(14.45)				14.6					
15.4	15.41		15.5					15.5	15.23		15.4
		15.8		15.7							
						16.0	16.1		16.20	16.24	16.3
16.5	16.61		16.7		16.8						
						17.3	17.2	17.0	(17.12)		
(18.1)									17.91		18.0
			(18.8)	18.7		18.7			(19.06)		
			(19.8)		19.5		19.3				

2 J. D. King, R. N. H. Haslam & W. J. McDonald, Can. J. Phys. 38 (1960) 1069.

3 G. Baciu, D. Catana, C. Deberth & I. Raileanu, Rev. Roum. Phys. 12 (1967) 385; G. Baciu, St. Cerc. Fiz. 23 (1971) 773.

4 G. Baciu et al. Inst. for Atomic Physics report M-43-1969.

5 N. K. Sherman et al., National Res. Council of Canada report NRC-12180 (1972).

7 B. Forkman & I. Wahlstrom, Ark. Fys. 18 (1960) 339.

8 W. R. Dodge and W. C. Barber, Phys. Rev. 127 (1962) 1746.

9 K. M. Murray and W. L. Bendel, Phys. Rev. 132 (1963) 1134.

10 S. Seki et al., J. Phys. Soc. Jap. 19 (1964) 1999.

11 K. Abe et al., J. Phys. Soc. Jap. 25 (1968) 1507.

12 B. S. Dolbilkin et al., Izv. Akad. Nauk SSSR (fiz.) 30 (1966) 349.

13 N. Bezic et al., Nucl. Phys. A128 (1969) 426.

REF. R. Van de Vyver, H. Ferdinande, G. Knuyt, R. Carchon, J. Devos
PICNS-72, p.307 Sendai

ELEM. SYM.	A	Z
F	19	9

METHOD

REF. NO. 72 Va 3 hvm

REACTION	RESULT	EXCITATION ENERGY	SOURCE		DETECTOR		ANGLE
			TYPE	RANGE	TYPE	RANGE	
G,XN	ABX	10- 19	C	10- 19	BF3-I		4PI

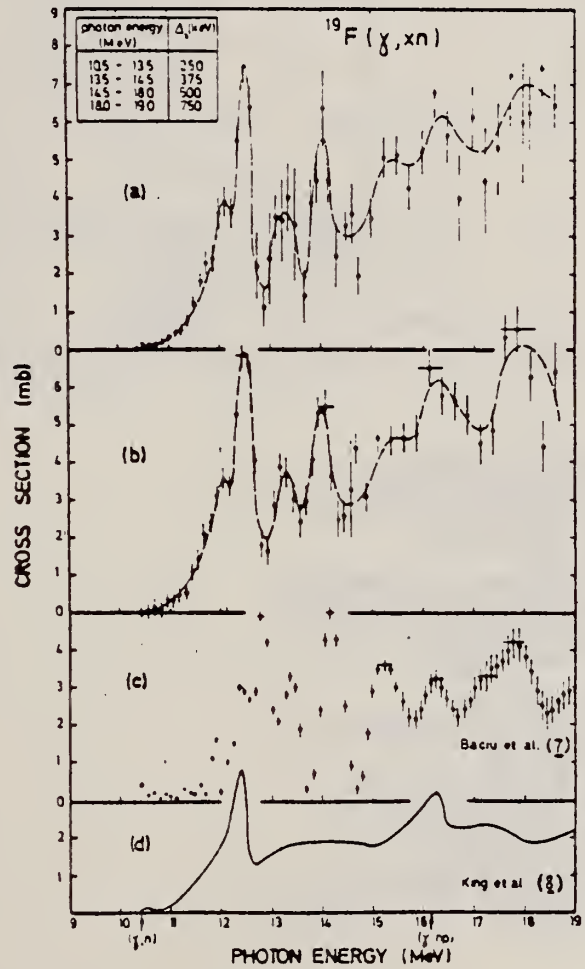

Fig. 1. Total photoneutron cross section for ^{19}F. Our results following (a) the VEPL method and (b) the Cook analysis. Previous data (c) by Baciu et al. (7) and (d) by King et al.(8)

(over)

Table 1. Photonuclear resonance energies observed in ^{19}F

(γ,p)				(e,e'p)	(γ,T)		(γ,n)				
Forkman (13)	Murray (14)	Seki (15)	Abe (16)	Dodge (17)	Dolbilkin (9)	Bezić (10)	King (8)	Baciu (7)	Baciu (18)	Sherman (11)	This work
		10.0			(10.1)						
10.4							(10.6)				
		10.96				(10.9)		11.0			
11.4				11.42	11.4					(11.40)	
									11.56	(11.59)	
										(11.72)	
	11.8					(11.8)				(11.82)	
11.9		12.0		11.9					11.90	(11.90)	
								12.1		12.10	12.1
						12.5	12.4	12.5	12.42	12.38	12.5
	12.55		(12.6)							(12.65)	
(12.8)		12.85		12.74					12.88	(12.84)	
										(13.04)	
									13.28	(13.29)	13.3
13.6						13.7				13.82	
	14.19				14.0		14.0	14.0	14.08		14.0
		(14.45)				14.6					
15.4	15.41		15.5					15.5	15.23		15.4
		15.8		15.7							
						16.0	16.1		16.20	16.24	16.3
16.5	16.61		16.7		16.8						
						17.3	17.2	17.0	(17.12)		
(18.1)									17.91		18.0
			(18.8)	18.7		18.7			(19.06)		
			(19.8)		19.5		19.3				

References

(1) R.A. Alvarez et al., Phys. Rev. C4 (1971) 1673
(2) J.S. Pruitt and S.R. Domen, NBS Monograph 48 (1962)
(3) E. Bramanis et al., Nucl. Instr. and Meth. 100 (1972) 59
(4) B.C. Cook, Nucl. Instr. and Meth. 24 (1963) 256
(5) L.I. Schiff, Phys. Rev. 83 (1951) 252
(6) B. Cook and C. Jones, Nucl. Instr. and Meth. 59 (1968) 229
(7) G. Baciu et al., Institute for Atomic Physics rep. M-43-1969
(8) J.D. King et al., Can. J. Phys. 38 (1960) 1069
(9) B.S. Dolbilkin et al., Izv. Akad. Nauk. SSSR (ser. fiz.) 30 (1966) 349
(10) N. Bezić et al., Nucl. Phys. A128 (1969) 426
(11) N. Sherman et al., Nat. Res. Council of Can. NRC-12180 (1972)
(12) S. Fujii, Prog. Theor. Phys. 21 (1959) 511
(13) B. Forkman and I. Wahlström, Ark. Fys. 18 (1960) 339
(14) K.M. Murray and W.L. Bendel, Phys. Rev. 132 (1963) 1134
(15) S. Seki et al., J. Phys. Soc. Jap. 19 (1964) 1999
(16) K. Abe et al., J. Phys. Soc. Jap. 25 (1968) 1507
(17) W.R. Dodge and W.C. Barber, Phys. Rev. 127 (1962) 1746
(18) G. Baciu et al., Rev. Roum. Phys. 12 (1967) 385 ; G. Baciu St. Cerc. Fiz. 23 (1971) 773.

REF. R. Bergere, H. Beil, P. Carlos, A. Lepretre, A. Veyssiere
PICNS-73, Vol.I, p.525 Asilomar

ELEM. SYM.	A	Z
F	19	9

METHOD

REF. NO.	
73 Be 10	hmg

REACTION	RESULT	EXCITATION ENERGY	SOURCE		DETECTOR		ANGLE
			TYPE	RANGE	TYPE	RANGE	
G,N	ABX	11- 29	D	11- 29	BF3-I		4PI
G,2N	ABX	22- 29	D	22- 29	BF3-I		4PI

217+

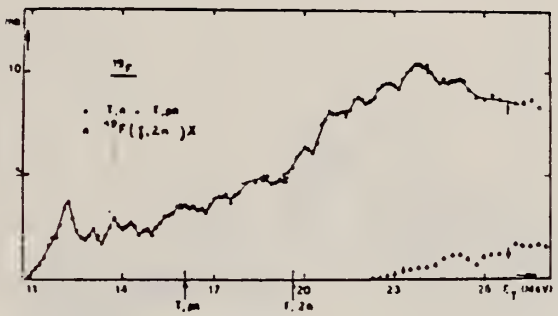

Fig. 10 Partial $\sigma(\gamma,n) + \sigma(\gamma,pn)$ and $\sigma(\gamma,2n \ldots)$ of ^{19}F.

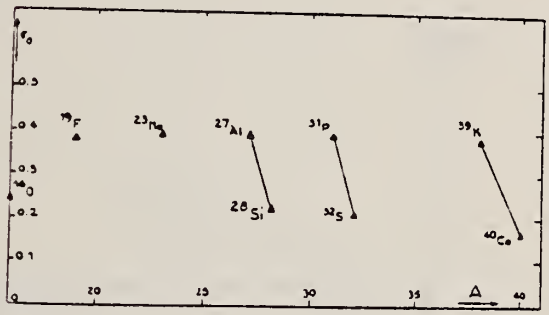

Fig. 13 Integrated photoneutron cross-sections for s-d shell nuclei.

REF. D. Catană, G. Baciu, C. Iliescu, and V. I. R. Niculescu
Z. Physik 261, 125 (1973)

ELEM. SYM.	A	Z
F	19	9

METHOD

REF. NO. 73 Ca 5 egf

REACTION	RESULT	EXCITATION ENERGY	SOURCE		DETECTOR		ANGLE
			TYPE	RANGE	TYPE	RANGE	
G,XN	ABX	10- 25	G	10- 25	BF3-I		4PI

726

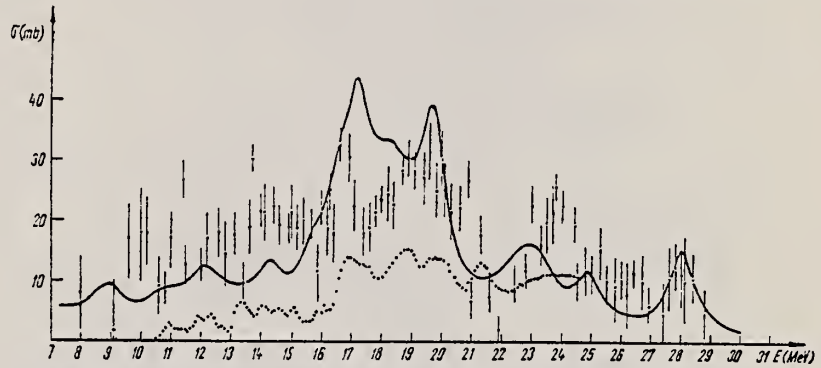

Fig. 6. Theoretical $E1$ photoabsorption cross section for ^{19}F (full line). Experimental photoabsorption cross section reported by Dolbilkin [10] (points with errors). Cross section of $^{19}F(\gamma, xn)$ reaction (point line)

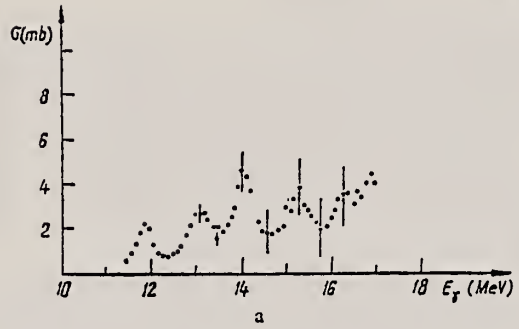

a

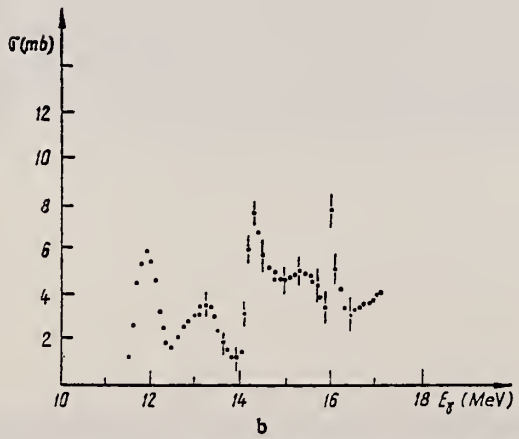

b

Fig. 3a and b. Penfold and Leiss solution for $^{19}F(\gamma, xn)$ cross section. a Schiff bremsstrahlung spectrum, b FDTTB spectrum

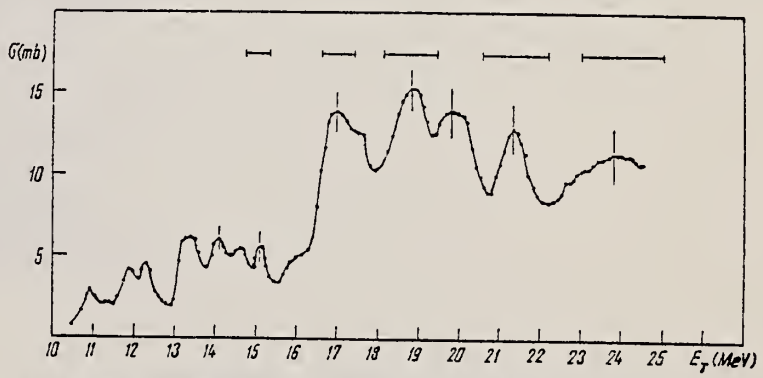

Fig. 4. Least structure solution for $^{19}F(\gamma, xn)$ cross section. The statistical errors and the resolution function are shown at representative energies

U.S. DEPARTMENT OF COMMERCE
NATIONAL BUREAU OF STANDARDS

REF. V. di Napoli, F. Salvetti, M.L. Terranova, H.G. de Carvalho, and J.B. Martins
Phys. Rev. C8, 206 (1973)

ELEM. SYM.	A	Z
F	19	9

METHOD

REF. NO. 73 Di 4 hmg

REACTION	RESULT	EXCITATION ENERGY	SOURCE TYPE	SOURCE RANGE	DETECTOR TYPE	DETECTOR RANGE	ANGLE
G,SPL	ABY	THR-999	C	999	ACT-I		4PI

999 = 1 GEV

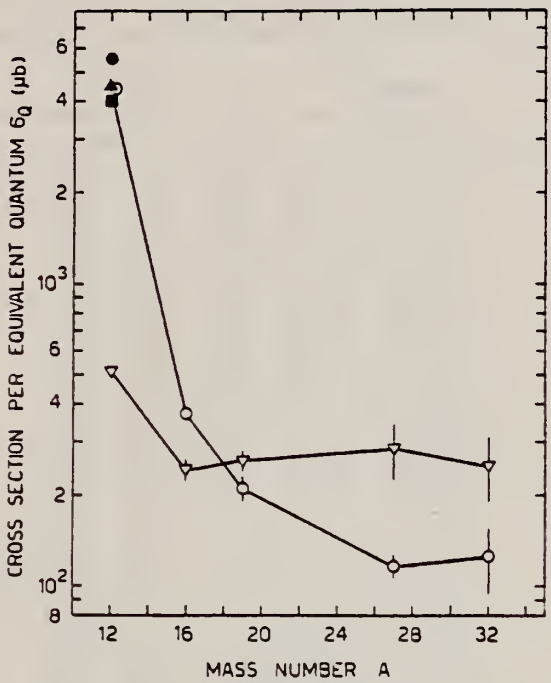

FIG. 3. Yields of ^{11}C and ^{7}Be versus the mass number of the target nucleus. Filled circle: ^{11}C, Ref. 16. Filled triangle: ^{11}C, Ref. 17. Filled square: ^{11}C, Ref. 8. Open circles: ^{11}C, present work. Reversed open triangles: ^{7}Be, present work.

[8] G. Andersson et al., Nucl. Phys. A197, 44 (1972).

[16] V. di Napoli et al., Nuovo Cimento 55B, 95 (1968).

[17] A. Masaike, J. Phys. Soc. Japan 19, 427 (1964).

REF. F. L. Halloweli, W. Bertozzi, J. Heisenberg, S. Kowalski, X. Maruyama, C. P. Sargent, W. Turchinetz, C. F. Williamson, S. P. Fivozinsky, J. W. Lightbody, Jr., and S. Penner
Phys. Rev. C7, 1396 (1973)

ELEM. SYM.	A	Z
F	19	9

METHOD

REF. NO. 73 Ha 1

hmg

REACTION	RESULT	EXCITATION ENERGY	SOURCE TYPE	SOURCE RANGE	DETECTOR TYPE	DETECTOR RANGE	ANGLE
E,E/	FMF	0- 2	D	61-121	MAG-D		DST

3 LEVELS .2-1.6 ME

TABLE II. Elastic and inelastic electron scattering form factors for ^{19}F.

Level	θ (deg) [a]	E (MeV) [b]	q (fm^{-1})	$F^2(q)$ Value	$F^2(q)$ standard deviation [c]
$\frac{1}{2}^+$ (g.s.)	110.75	66.02	0.550	0.4352	0.001 00
	110.75	71.02	0.592	0.3463	0.001 10
	110.64	71.03	0.591	0.3721	0.000 94
	110.64	86.05	0.716	0.219 04	0.000 53
	110.40	101.21	0.841	0.118 34	0.001 02
	110.64	101.17	0.842	0.117 90	0.000 91
	110.64	121.00	1.006	0.045 09	0.000 80
	145.82	60.88	0.589	0.3993	0.001 05
	145.79	68.55	0.663	0.2875	0.001 70
	145.82	73.94	0.715	0.2297	0.001 17
	145.70	74.45	0.720	0.2201	0.001 32
	145.40	87.96	0.849	0.112 78	0.000 89
	145.79	104.59	1.011	0.041 40	0.000 119
	145.70	104.65	1.011	0.040 98	0.000 102
	163.21	85.41	0.855	0.117 75	0.003 84
$\frac{1}{2}^+$ (0.197 MeV)	110.64	86.05	0.712	3.20×10^{-3}	0.44×10^{-3}
	110.40	101.21	0.838	3.52×10^{-3}	0.37×10^{-3}
	110.64	121.00	1.003	3.52×10^{-3}	0.34×10^{-3}
	145.82	73.94	0.711	3.52×10^{-3}	0.93×10^{-3}
	145.70	74.45	0.717	3.18×10^{-3}	1.02×10^{-3}
	145.40	87.96	0.846	3.98×10^{-3}	0.37×10^{-3}
	145.79	104.59	1.006	4.01×10^{-3}	0.36×10^{-3}
	163.21	85.41	0.851	4.28×10^{-3}	0.78×10^{-3}
$\frac{5}{2}^-$ (1.346 MeV)	110.75	66.02	0.543	1.19×10^{-4}	0.52×10^{-4}
	110.75	71.02	0.585	1.84×10^{-4}	0.45×10^{-4}
	110.64	86.05	0.709	3.97×10^{-4}	0.83×10^{-4}
	110.40	101.21	0.833	6.54×10^{-4}	0.86×10^{-4}
	110.64	121.00	0.998	10.58×10^{-4}	0.60×10^{-4}
	145.82	60.88	0.580	2.14×10^{-4}	0.80×10^{-4}
	145.82	73.94	0.705	3.91×10^{-4}	1.10×10^{-4}
	145.40	87.96	0.840	6.85×10^{-4}	0.72×10^{-4}
	145.79	104.59	1.001	9.80×10^{-4}	0.62×10^{-4}
	163.21	85.41	0.846	6.30×10^{-4}	1.92×10^{-4}
$\frac{1}{2}^+$ (1.554 MeV)	110.75	66.02	0.542	1.34×10^{-3}	0.12×10^{-3}
	110.75	71.02	0.584	1.52×10^{-3}	0.14×10^{-3}
	110.64	86.05	0.708	2.57×10^{-3}	0.11×10^{-3}
	110.40	101.21	0.832	2.76×10^{-3}	0.11×10^{-3}
	110.64	121.00	0.997	2.36×10^{-3}	0.07×10^{-3}
	145.82	60.88	0.579	1.75×10^{-3}	0.20×10^{-3}
	145.82	73.94	0.704	2.33×10^{-3}	0.27×10^{-3}
	145.50	87.96	0.839	2.55×10^{-3}	0.10×10^{-3}
	145.79	104.59	1.000	2.42×10^{-3}	0.08×10^{-3}
	163.21	85.41	0.844	3.41×10^{-3}	0.26×10^{-3}

[a] Laboratory angle.
[b] Laboratory kinetic energy.
[c] Standard deviation for statistical errors only; estimated ±2% systematic error not included.

TABLE IV. Transition charge parameters for ^{19}F.

Level	$B(EL, 0)\uparrow$ (e^2 fm^{2L})	$\lvert M^2\rvert$ (W.u.)	$\langle r^2_\alpha\rangle^{1/2}$ (fm)	$\langle r^4_\alpha\rangle^{1/4}$ (fm)
$\frac{1}{2}^+$ (0.197)	52^{+30}_{-24}	$5.73^{+3.30}_{-2.64}$	$3.75^{+1.08}_{-1.56}$	$3.60^{+0.79}_{-3.60}$
$\frac{5}{2}^-$ (1.346)	608^{+221}_{-187}	$9.45^{+3.43}_{-2.91}$	$4.30^{+0.88}_{-1.10}$	$4.13^{+0.68}_{-1.48}$
$\frac{1}{2}^+$ (1.554)	$35.5^{+3.8}_{-3.7}$	$5.89^{+0.65}_{-0.61}$	$3.44^{+0.29}_{-0.32}$	$2.99^{+0.37}_{-0.61}$

(over)

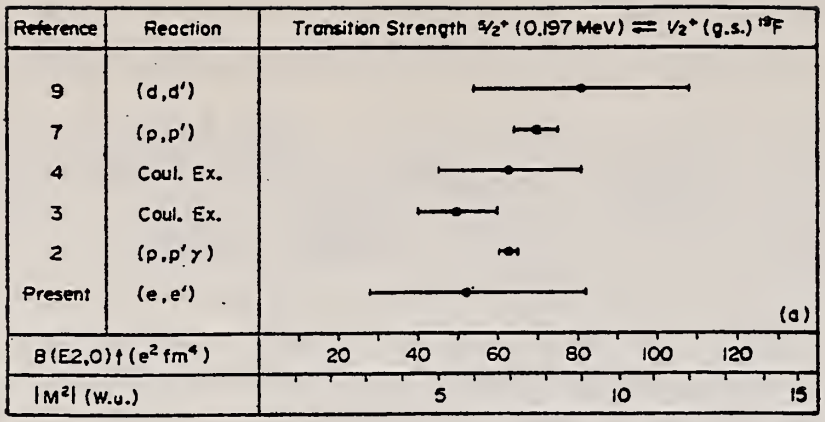

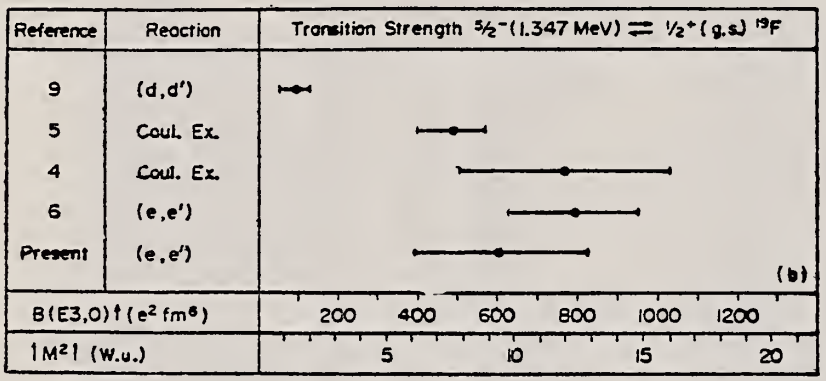

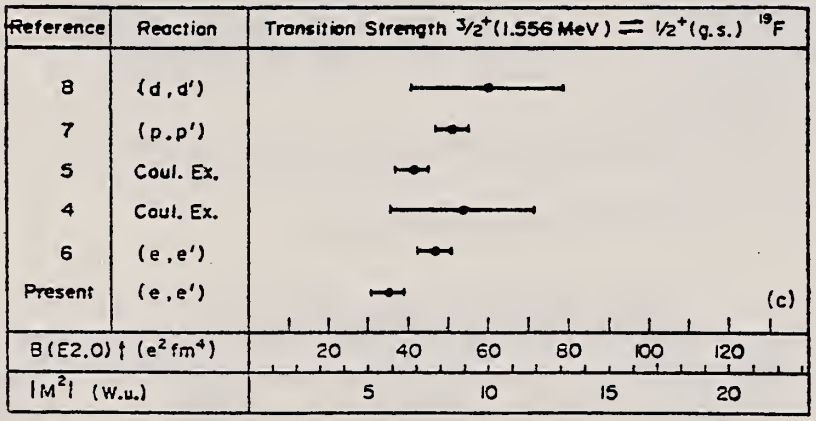

FIG. 4. Comparison of transition strengths for ^{19}F levels derived by various workers. (a) $\frac{5}{2}^+$ (0.197-MeV) level. (b) $\frac{5}{2}^-$ (1.347-MeV) level. (c) $\frac{3}{2}^+$ (1.556-MeV) level.

REF. P.L. Hallowell, W. Bertozzi, J. Heisenberg, S. Kowalski, X. Maruyama, C.P. Sargent, W. Turchinetz, C.F. Williamson, S.P. Fivozinsky, J.W. Lightbody,Jr., and S. Penner
Phys. Rev. C7, 1396 (1973)

ELEM. SYM.	A	Z
F	19	9

METHOD

REF. NO. 73 Ha 1 hmg

REACTION	RESULT	EXCITATION ENERGY	SOURCE		DETECTOR		ANGLE
			TYPE	RANGE	TYPE	RANGE	

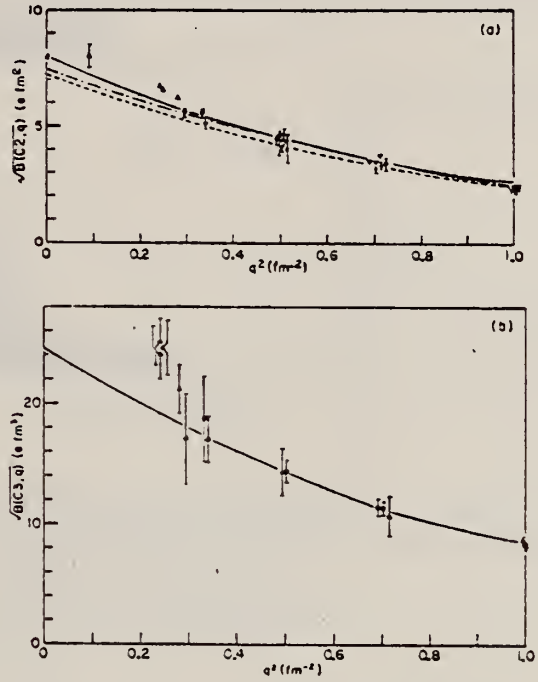

FIG. 3. Analysis of inelastic electron scattering from ^{19}F. (a) $\frac{1}{2}^+$ (0.197-MeV) and $\frac{3}{2}^+$ (1.554-MeV) levels. ●, present data, $\frac{1}{2}^+$ level. ▼, present data, $\frac{3}{2}^+$ level; ordinate scaled by $(\frac{3}{2})^{1/2}$. ▲, data of Ref. 6; ordinate scaled by $(\frac{3}{2})^{1/2}$. ■, lifetime measurement, $\frac{1}{2}^+$ level, of Ref. 2. ----, model independent fit, $\frac{1}{2}^+$ level. -·-·-, model independent fit, $\frac{3}{2}^+$ level; ordinate scaled by $(\frac{3}{2})^{1/2}$. ——, rotational model fit based on the measured ground-state charge distribution and the lifetime measurement of Ref. 2. The ordinate as given applies to the $\frac{1}{2}^+$ state. Ordinates for the $\frac{3}{2}^+$ state are obtained by multiplying the plotted ordinates by $(\frac{3}{2})^{1/2}$. (b) $\frac{1}{2}^-$ (1.346-MeV) level. ●, present data. ▲, data of Ref. 6. ——, model independent fit.

[2]J.A. Becker, J.W. Olness, and D.H. Wilkinson. Phys. Rev. 155, 1089 (1967).

[6]T. Walcher and P. Strehl, Z. Physik 232, 342 (1970).

REF. J.R. Moreira, E. Wolynec, G. Moscati
PICNS-73, Vol.I, p.165 Asilomar

ELEM. SYM.	A	Z
F	19	9

METHOD

REF. NO. 73 Mo 9 hmg

REACTION	RESULT	EXCITATION ENERGY	SOURCE		DETECTOR		ANGLE
			TYPE	RANGE	TYPE	RANGE	
G,N	RLY	10- 39	C	10- 39	ACT-I		4PI
E,N	RLY	10- 39	D	10- 39	ACT-I		4PI

YIELD/PHOTO/ELECTRO

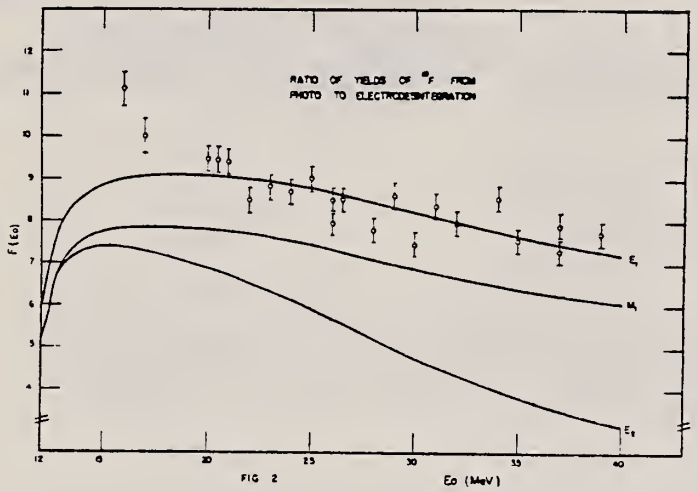

FIG 2

REF. N. K. Sherman, K. H. Lokan, and R. W. Gellie
PICNS-73, Vol. I, p. 167 Asilomar

ELEM. SYM.	A	Z
F	19	9

METHOD

REF. NO.	
73 Sh 9	hmg

REACTION	RESULT	EXCITATION ENERGY	SOURCE		DETECTOR		ANGLE
			TYPE	RANGE	TYPE	RANGE	
G,N	ABX	11- 21	C	13- 21	TOF-D		90

GND AND EXCIT STATE

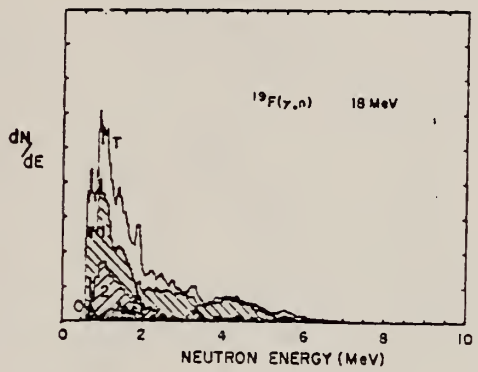

Figure 1 - Photoneutron spectrum of ^{19}F due to 18 MeV bremsstrahlung, labelled "T". The numbered curves result from folding the photon spectrum with: "0" - the ground-state cross section (stippled); "1" - the cross section to 1.04 MeV excitation in ^{18}F. The remainder is "2".

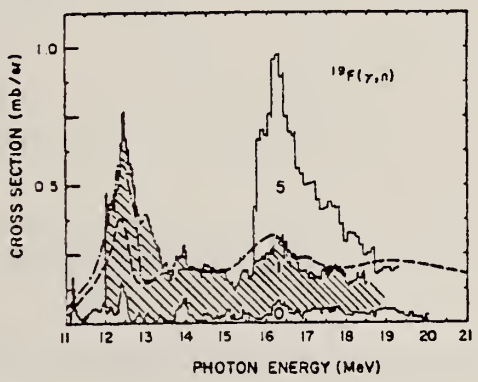

Figure 2 - The 90° differential cross section for (γ,n) processes in ^{19}F. The region "0" is $\sigma(\gamma,n_0)$. The hatched region "1" is $\sigma(\gamma,n_1)$. The region "5" results from curve 2 of Fig. 1 assuming transitions to the 4.74 MeV (T = 1) level of ^{18}F. The dashed curve derives from King et al.[3], assuming d → f and d → p transitions. The dash-dot curve assumes p → d transitions. If region "5" is due to the $^{19}F(\gamma,an)$ reaction, there is no disagreement.

REF.

D. M. Skopik and Y.M. Shin
Nucl. Phys. A223, 409 (1974)

ELEM. SYM.	A	-
F	19	9

METHOD

REF. NO.	
74 Sk 4	egf

REACTION	RESULT	EXCITATION ENERGY	SOURCE		DETECTOR		ANGLE
			TYPE	RANGE	TYPE	RANGE	
E,T	ABX	18- 23	D	UKN	MAG-D		DST

$^{19}F(\gamma, t)$

GROUND STATE

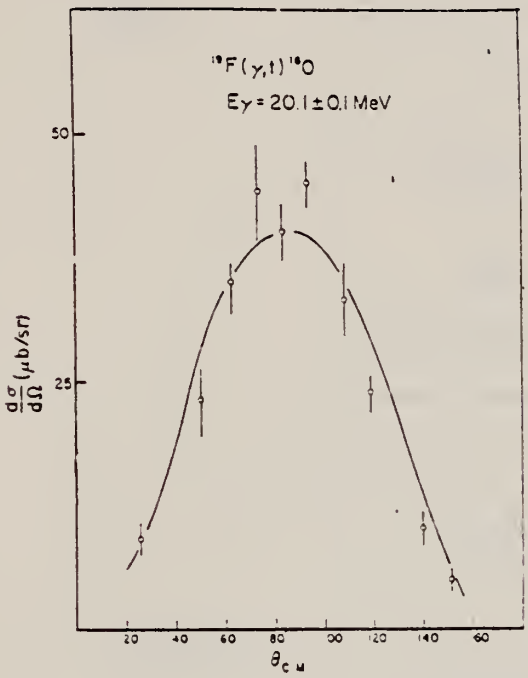

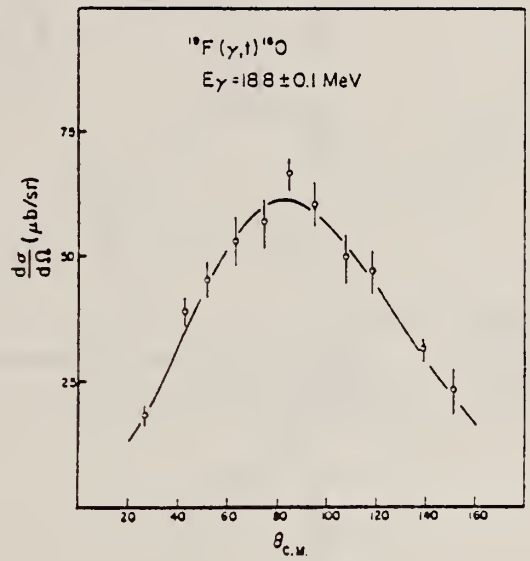

Fig. 3. Angular distributions of tritons at the two observed resonances. The solid line is the least squares fit to eq. (1).

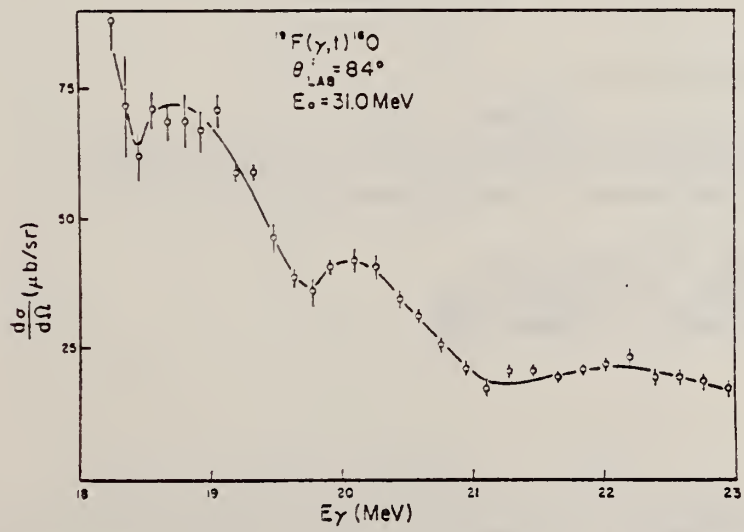

Fig. 4. The differential cross section at 84° for $E_0 = 31$ MeV. For $E_\gamma \leqq 25$ MeV non-ground-state transitions are possible.

(over)

TABLE 1

Integrated cross sections for ^{19}F in MeV · mb

	Total absorption	(γ, xn)	(γ, t)
$\int_{18}^{23} \sigma dE$	≈ 170 [a]		1.2
$\int_{20.1 \text{ resonance}} \sigma dE$	3.5 [b]	≈ 2 [c]	0.1

[a]) Ref. [2]). [b]) Ref. [9]). [c]) Ref. [1]).

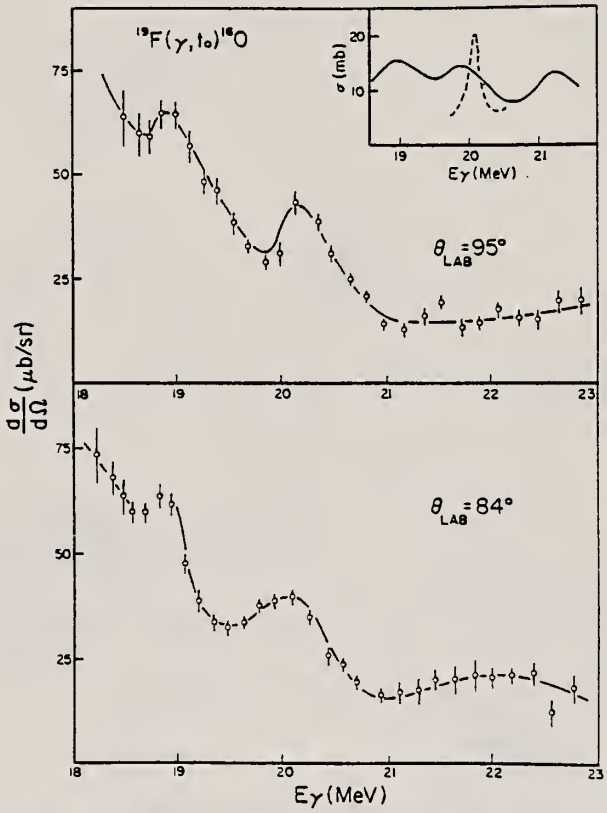

Fig. 2. The $^{19}F(\gamma, t)^{16}O$ ground state differential cross section at $\theta_{Lab} = 84°$ and 95°. The solid line in the inset is taken from the $^{19}F(\gamma, xn)$ work of Catana *et al.* [ref. [1])]; the dashed line is the total absorption measurement of Tessler and Stephens [ref. [9])].

1) D. Catana et al., Z. Phys. 261 (1973) 125
2) N. Bezic et al., Nucl. Phys. A128 (1969) 426
9) G. Tessler et al., Phys. Rev. 135 (1964) B129

REF.

A. Veyssiere, H. Beil, R. Bergere, P. Carlos, A. Lepretre, and A. De Miniac
Nucl. Phys. A227, 513 (1974)

ELEM. SYM.	A	Z
F	19	9

METHOD

REF. NO. 74 Ve 1 egf

REACTION	RESULT	EXCITATION ENERGY	SOURCE		DETECTOR		ANGLE
			TYPE	RANGE	TYPE	RANGE	
* G,N	ABX	10- 28	D	10- 28	BF3-I		4PI
** G,2N	ABX	20- 28	D	20- 28	BF3-I		4PI

* 881
** 880 +

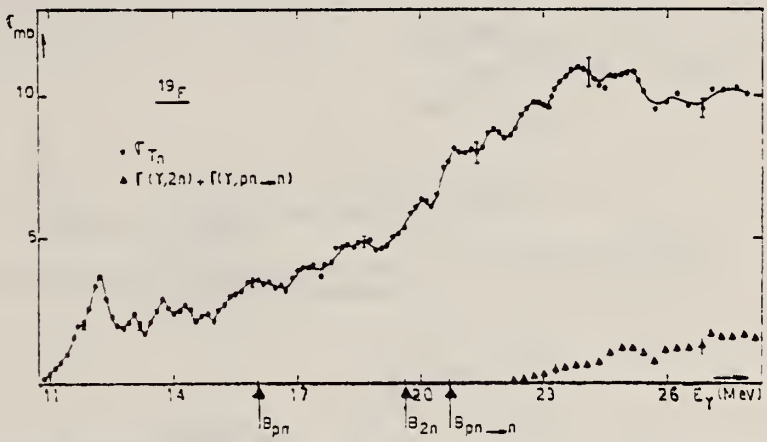

Fig. 3. Photoneutron cross sections $\sigma_{(\gamma,n)}$ and $[\sigma(\gamma, 2n)+\sigma(\gamma, pn \rightarrow n)]$ of ^{19}F.

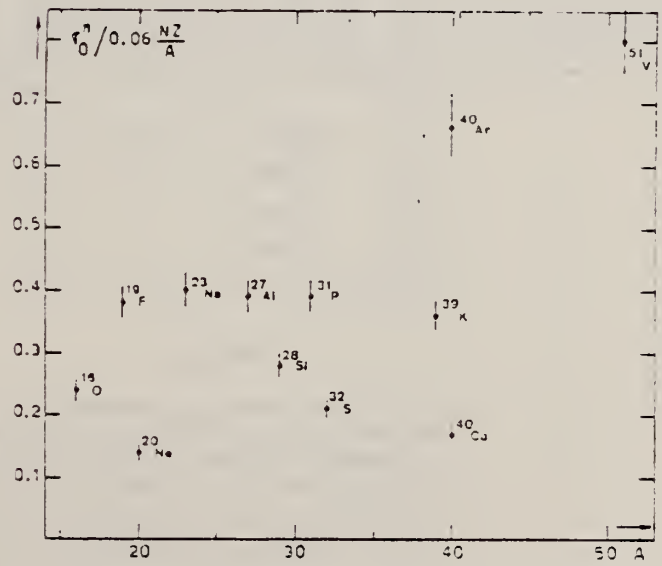

Fig. 22. Ratio of experimental integrated photoneutron cross section $\sigma_0{}^n$ over the Thomas, Reiche and Kuhn sum rule [0.06 NZ/A]. Numerical values and upper integration limits E_M are taken from table 3. Also $\Delta\sigma_0{}^n = \pm 7\%$ for all nuclei.

(over)

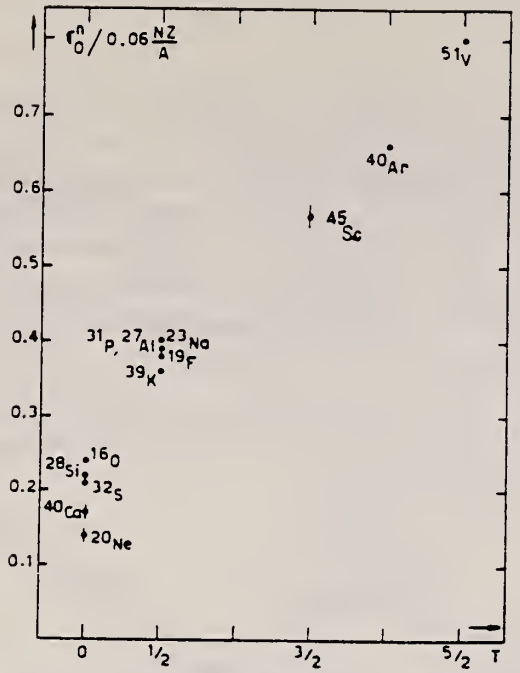

Fig. 24. The $[\sigma_0^n/(0.06\,NZ/A)]$ ratio as a function of isospin T. Possible overall errors of $\pm 7\%$ are to be applied to all nuclei shown.

TABLE 3

Experimental integrated photoneutron cross sections $\sigma_0^n = \int_0^{E_M} \sigma_{Tn}(E)\mathrm{d}E$ compared with the classical sum rule $[0.06\,NZ/A]$ of Thomas, Reich and Kuhn

	$T=0$					$T=\frac{1}{2}$					$T=\frac{3}{2}$	$T=2$	$T=\frac{5}{2}$
Nucleus	^{16}O	^{20}Ne	^{28}Si	^{32}S	^{40}Ca	^{19}F	^{23}Na	^{27}Al	^{31}P	^{39}K	^{45}Sc	^{40}Ar	^{51}V
σ_0^n (MeV · mb)	58 ±4	42 ±3	94 ±7	98 ±7	100 ±7	108 ±7	137 ±9	158 ±10	182 ±12	210 ±14	383 ±25	393 ±28	60 ±42
$\sigma_0^n/(0.06NZ/A)$	0.24	0.14	0.22	0.21	0.17	0.38	0.40	0.39	0.39	0.36	0.57	0.66	0.3
E_M (MeV)	30	26.7	30	30	29.5	29	30	30	29	30	28.1	26.7	28

REF. M. Oyamada, T. Terasawa, K. Nakahara, Y. Endo, H. Saito, E. Tanaka
Phys. Rev. C11, 1578 (1975)

ELEM. SYM.	A	Z
F	19	9

METHOD

(Page 1 of 4)

REF. NO. 75 Oy 1 hmg

REACTION	RESULT	EXCITATION ENERGY	SOURCE		DETECTOR		ANGLE
			TYPE	RANGE	TYPE	RANGE	
E,E/	FMF	1- 6	D	134-250	MAG-D		DST

B(Eλ) 7 STATES

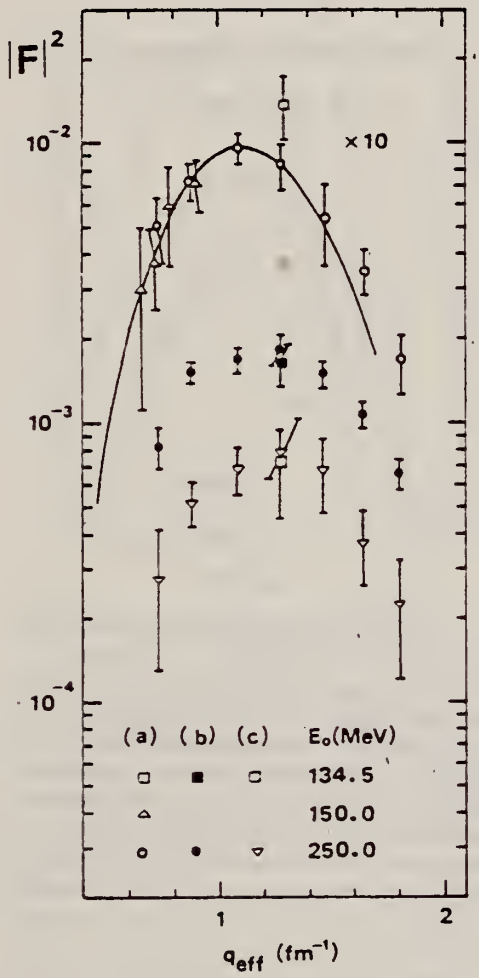

FIG. 7. Experimental squared form factors for (a) the 1.35-MeV $\frac{5}{2}^-$, (b) 5.43-MeV $\frac{7}{2}^-$, and (c) 5.63-MeV states in ^{19}F. The solid curve represents the calculated $C3$ form factor Eq. (8) fitted to the data points for the 1.35-MeV state in the region of $q < 1.3$ fm^{-1}. From this curve the value of $B(E3)$ was deduced. The values of the squared form factors for (a) are multiplied by 10 in the figure.

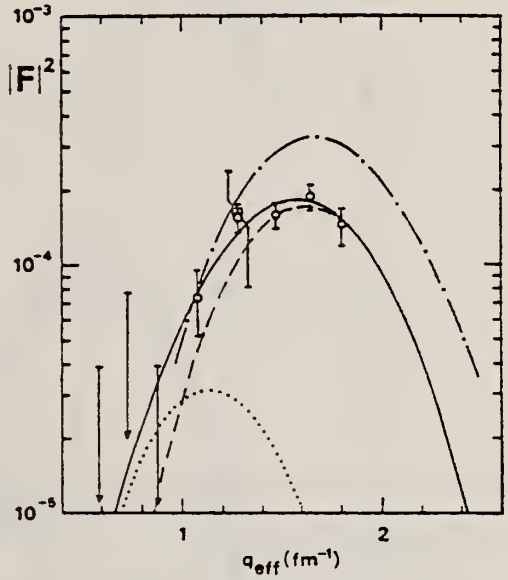

FIG. 8. Squared form factors for the 4.0-MeV peak which results from the excitations of the 4.00-MeV $\frac{7}{2}^-$ and 4.03-MeV $\frac{9}{2}^-$ states. The square denotes the data point at $E_0 = 134.5$ MeV, $\theta = 135°$. The $C3$ and $C5$ squared form factors given by Eq (9) are fitted to experimental data points and shown with the solid curve ($C3 + C5$), dotted curve ($C3$), and dashed curve ($C5$). $R = 3.2$ fm, $g = 1.0$ fm. The dash-dotted curve represents the calculated $C5$ form factor for the $1g_{9/2}1p_{1/2}^{-1}$ particle-hole excitation of the doubly closed ^{16}O core (harmonic oscillator model, $b = 1.85$ fm). Vertical lines with arrows indicate upper limits of the experimental form factors.

(over)

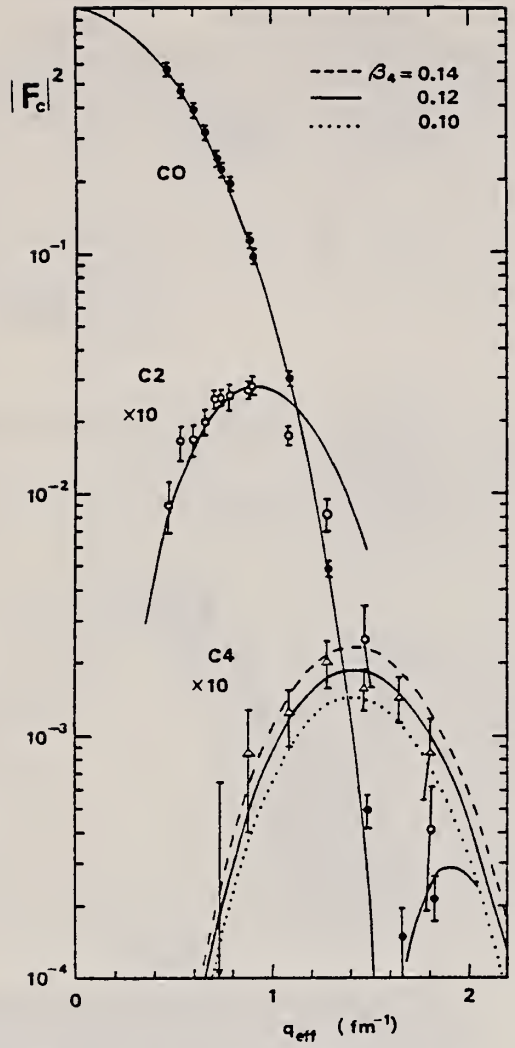

FIG. 9. The $C0$, $C2$ ($\frac{1}{2}^+ \rightarrow \frac{1}{2}^+$), and $C4$ ($\frac{1}{2}^+ \rightarrow \frac{9}{2}^+$) squared form factors calculated in the rigid-rotor model using the deformed Fermi distribution with $c = 2.60$ fm, $z = 0.527$ fm, $\beta_2 = 0.43$, and $\beta_4 = 0.12 \pm 0.2$. The experimental points are as follows: $C0$: the ground state (closed circles); $C2$: the 1.55-MeV state (open circles); $C4$: the 2.78-MeV state (triangles, after subtraction of the transverse component). The upper limit of the experimental $C4$ form factor at $q_{eff} = 0.73$ fm^{-1} is indicated by a vertical line with arrow.

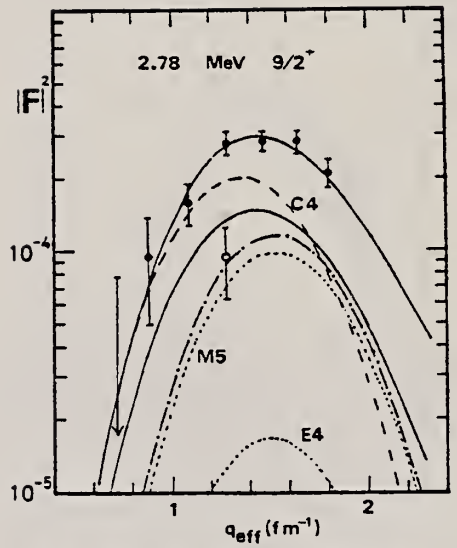

FIG. 12. Experimental and theoretical squared form factors for the 2.78-MeV $\frac{9}{2}^+$ state in ^{19}F. The curves are the theoretical values calculated in the RPC model. The closed circles and upper solid curve represent total form factors for $E_0 = 250$ MeV; the dashed curve is $C4$; the open circle and the dash-dotted curve are transverse $E4 + M5$; the dotted curves are $E4$ (lower) and $M5$ (upper). The lower solid curve shows the total form factor calculated without RPC using the same parameters as those in the RPC case ($E_0 = 250$ MeV). A vertical line with arrow indicates the upper limit of the experimental total form factor at $E_0 = 250$ MeV, $\theta = 33°$.

ION Y	SOURCE TYPE	SOURCE RANGE	DETECTOR TYPE	DETECTOR RANGE	ANGLE

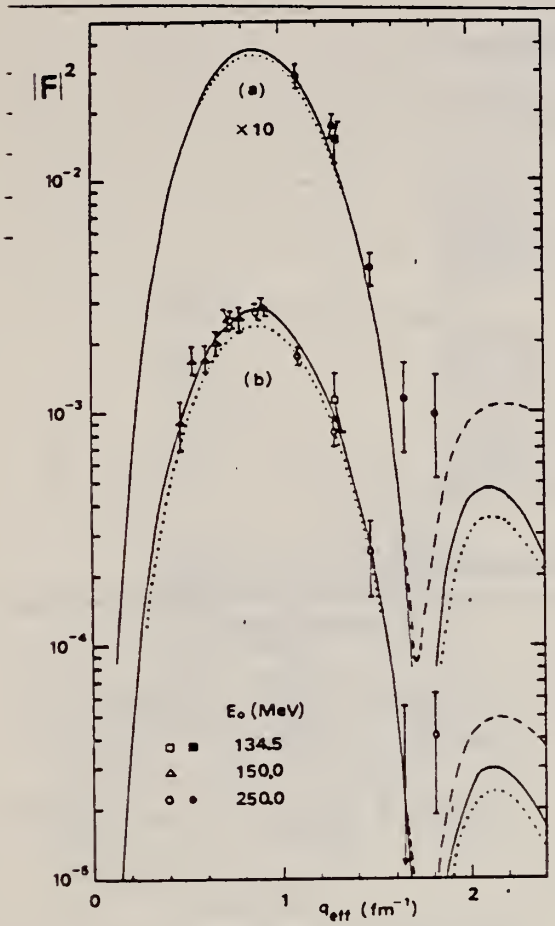

FIG. 11. Experimental and theoretical squared form factors for (a) the 0.197-MeV $\frac{5}{2}^-$ state and (b) the 1.55-MeV $\frac{1}{2}^+$ state in ^{19}F. The solid curves represent the $C2$ form factors squared, calculated in the RPC model. The dotted curves show the calculation of the $C2$ form factors squared, without RPC, using the same parameters of the single-particle field as those in the case of the RPC model. The dashed curves are the total form factors including small transverse components calculated for $E_0 = 250$ MeV. The experimental and theoretical squared form factors for (a) are multiplied by 10 in the figure. The upper limit of the experimental form factor for (b) at $q_{eff} = 1.65$ fm^{-1} is indicated by a vertical line with arrow.

TABLE II. Experimental values of total form factors for negative-parity states in ^{19}F. Errors are statistical only.

E_0 (MeV)	ϑ (deg)	$\lvert F(q,\theta)\rvert^2 \times 10^4$ $E_x = 1.35$	$E_x = 4.0$	$E_x = 5.43$	$E_x = 5.63$
134.5	135.0	13.8 ± 3.5	1.6 ± 0.8	16.3 ± 2.9	7.3 ± 2.8
150.0	35.0	<1.0			
150.0	40.0	<1.8			
150.0	45.0	<3.0	<0.39		
150.0	50.0	3.0 ± 1.9			
150.0	55.0	3.7 ± 1.2			
150.0	60.0	5.9 ± 2.3			
150.0	70.0	7.1 ± 1.5			
250.0	33.0	5.0 ± 1.3	<0.77	8.2 ± 1.4	2.7 ± 1.4
250.0	40.0	7.3 ± 1.1	<0.39	15.1 ± 1.0	5.1 ± 0.9
250.0	50.0	9.5 ± 1.1	0.73 ± 0.22	16.7 ± 1.6	6.8 ± 1.3
250.0	60.0	8.3 ± 1.5	1.54 ± 0.20	18.3 ± 2.1	7.7 ± 1.6
250.0	70.0	5.3 ± 1.7	1.57 ± 0.18	14.9 ± 1.6	6.7 ± 2.0
250.0	80.0	3.50 ± 0.66	1.88 ± 0.22	10.7 ± 1.1	3.7 ± 1.1
250.0	90.0	1.65 ± 0.39	1.44 ± 0.25	6.56 ± 0.75	2.19 ± 0.97

(over)

TABLE I. Experimental values of total form factors for positive-parity states in ^{19}F. Errors are statistical only.

E_0 (MeV)	θ (deg)	$\lvert F(q,\theta)\rvert^2$ elastic	$\lvert F(q,\theta)\rvert^2 \times 10^4$ inelastic $E_x = 0.197$	$E_x = 1.55$	$E_x = 2.78$	$E_x = 4.56$
134.5	135.0	$(4.95 \pm 0.46) \times 10^{-3}$	14.9 ± 3.1	11.3 ± 3.2	8.0 ± 1.6	3.8 ± 1.3
150.0	35.0	$(5.71 \pm 0.03) \times 10^{-1}$ [a]		9.1 ± 2.5		
150.0	40.0	$(4.56 \pm 0.05) \times 10^{-1}$ [a]		16.9 ± 2.7		2.20 ± 1.04
150.0	45.0	$(3.88 \pm 0.05) \times 10^{-1}$ [a]		17.5 ± 2.8		3.21 ± 0.77
150.0	50.0	$(3.08 \pm 0.03) \times 10^{-1}$ [a]		20.0 ± 2.2		3.37 ± 0.85
150.0	55.0	$(2.46 \pm 0.02) \times 10^{-1}$ [a]		25.0 ± 2.5		4.97 ± 0.93
150.0	60.0	$(1.97 \pm 0.02) \times 10^{-1}$ [a]		25.3 ± 3.1		4.87 ± 0.72
150.0	70.0	$(1.01 \pm 0.03) \times 10^{-1}$ [a]		28.5 ± 2.2		
250.0	33.0	$(2.26 \pm 0.02) \times 10^{-1}$ [a]		24.9 ± 1.9	<0.78	5.44 ± 0.58
250.0	40.0	$(1.17 \pm 0.01) \times 10^{-1}$ [a]		26.9 ± 1.4	0.94 ± 0.44	4.96 ± 0.29
250.0	50.0	$(3.01 \pm 0.05) \times 10^{-2}$	29 ± 3	17.4 ± 1.3	1.59 ± 0.32	4.02 ± 0.29
250.0	60.0	$(4.85 \pm 0.20) \times 10^{-3}$	17.3 ± 2.2	8.2 ± 1.2	2.80 ± 0.31	2.31 ± 0.22
250.0	70.0	$(4.86 \pm 0.75) \times 10^{-4}$	4.15 ± 0.68	2.5 ± 0.9	2.83 ± 0.24	1.28 ± 0.17
250.0	80.0	$(1.47 \pm 0.48) \times 10^{-4}$	1.15 ± 0.48	<0.55	2.84 ± 0.28	1.32 ± 0.18
250.0	90.0	$(2.16 \pm 0.45) \times 10^{-4}$	0.97 ± 0.45	0.41 ± 0.22	2.14 ± 0.31	0.51 ± 0.18

[a] Including the 0.197-MeV state component.

TABLE III. Experimental values of electric transition strengths $J^\pi \to \frac{1}{2}^+$ (ground state).

Mode	E_x (MeV)	J^π	Present experiment $B(E\lambda, \uparrow)\ e^2\ \mathrm{fm}^{2\lambda}$ (e,e')	Present experiment $\lvert M\rvert^2$	Other experiments $\lvert M\rvert^2$ (e,e')	Coul. ex.	(p,p')	(d,d')
$E2$	1.55	$\frac{3}{2}^+$	24.4 ± 3.0	8.1 ± 1.0	7.84 ± 0.67 [a] $5.89^{+0.65}_{-0.61}$ [e]	9 ± 3 [b] 6.8 ± 0.7 [f]	8.4 ± 0.7 [c]	10 ± 3 [d]
$E2$	4.56	$\frac{5}{2}^+$	3.1 ± 0.7	1.0 ± 0.2				
$E3$	1.35	$\frac{5}{2}^-$	$(2.4 \pm 0.6) \times 10^2$	11 ± 3	12.4 ± 2.5 [a] $9.45^{+3.43}_{-2.31}$ [e]	12 ± 4 [b] 7.6 ± 1.3 [f]		1.4 ± 0.6 [d]
$E3$	4.00	$\frac{7}{2}^-$	<8	<0.4				
$E3$	5.43	$\frac{7}{2}^-$	$(3.3 \pm 0.9) \times 10^2$	15 ± 4				
$E4$	2.78	$\frac{9}{2}^+$	$(9.4 \pm 2.0) \times 10^2$	5.8 ± 1.3				
$E5$	4.03	$\frac{9}{2}^-$	$(2.0 \pm 0.9) \times 10^4$	16 ± 7				

[a] Reference 10.
[b] Reference 3.
[c] This value was calculated using the β_2 value and Eq. (7) in Ref. 7.
[d] Reference 9.
[e] Reference 11.
[f] Reference 4.

[3] A.E. Litherland, M.A. Clark, C. Broude, Phys. Lett. 3, 204 (1963).

[4] T.K. Alexander, O. Hausser, K.W. Allen, A.E. Litherland, Can. J. Phys. 47, 2335 (1969).

[7] C.M. Crawley, G.T. Garvey, Phys. Rev. 167, 1070 (1968).

[9] D. Dehnhard, N.M. Hintz, Phys. Rev. C1, 460 (1970).

[10] T. Walcher, P. Strehl, Z. Phys. 232, 342 (1970).

[11] P.L. Hallowell et al., Phys. Rev. C7, 1396 (1973).

REF. H. Tsubota, N. Kawamura, S. Oikawa, J. Uegaki
J. Phys. Soc. Japan 38, 299 (1975)

ELEM. SYM.	A	Z
F	19	9

METHOD

REF. NO. 75 Ts 1 egf

REACTION	RESULT	EXCITATION ENERGY	SOURCE TYPE	SOURCE RANGE	DETECTOR TYPE	DETECTOR RANGE	ANGLE
E,P	ABX	13- 25	D	13- 26	MAG-D		90

Photo cross sections obtained using Barber's El virtual photon spectrum. CONVERTS TO PHOTO SIG

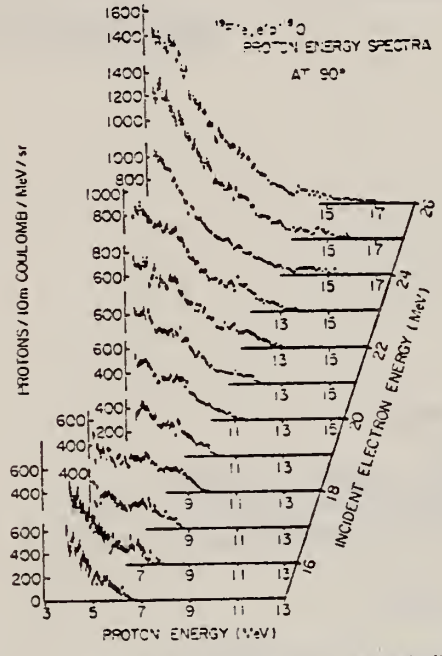

Fig. 2. Proton energy spectra of the $^{19}F(e,e'p)^{15}O$ reaction at 90°.

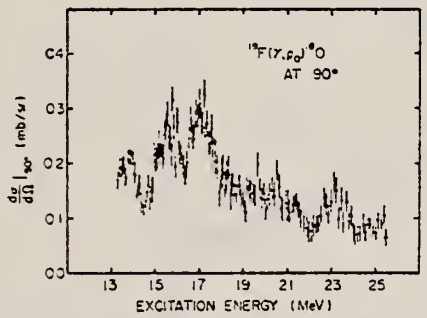

Fig. 4. The (γ, p_0) differential cross section at 90° for the ^{19}F nucleus.

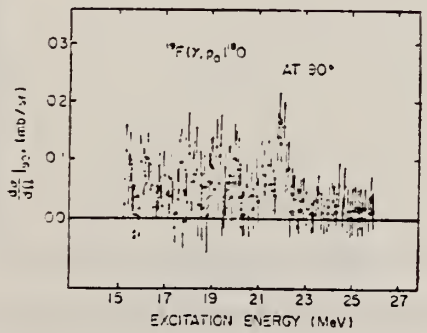

Fig. 5. The (γ, p_1) differential cross section at 90° for the ^{19}F nucleus.

Table II. Integrated differential cross sections at 90° (MeV-mb/sr).

	$\int \frac{d\sigma(\gamma, p_0)}{d\Omega} dE$ *	$\int \frac{d\sigma(\gamma, p_1)}{d\Omega} dE$ *	
^{19}F	1.80 ± 0.27 (25.39 / 13.29)	0.50 ± 0.45 (25.96 / 15.23)	present work
^{20}Ne	~1.99 (25.7 ** / 15.8)		ref. 1
	~2.23 (20.5 / 16.4)		ref. 2

* Superscripts and subscripts are the limits of integration.

** The integrated differential cross section is calculated from total cross section assuming isotropy.

[1] R. E. Segal et al., Nucl. Phys. A93, 31 (1967).

[2] N. W. Tanner et al., Nucl. Phys. 52, 29 (1964).

REF. E. Wolynec, G. Moscati, J. R. Moreira, O. D. Goncalves, M. N. Martins
Phys. Rev. C11, 1083 (1975)

ELEM. SYM.	A	Z
F	19	9

METHOD

REF. NO. 75 Wo 2 hmg

REACTION	RESULT	EXCITATION ENERGY	SOURCE		DETECTOR		ANGLE
			TYPE	RANGE	TYPE	RANGE	
G,N	RLY	16- 40	C	16- 40	ACT-I		4PI

RATIO (G,N)/(E,N)

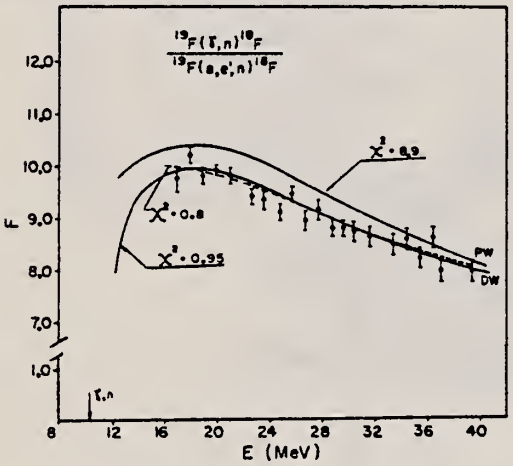

FIG. 2. Measured F for $^{19}F(\gamma, n)$. Dashed curve is a polynomial fit to the points. Full curves are F_{PW} and F_{DW} predictions.

$$F_{PW}^{(E1)} = (N_\tau / Z_\tau^2 r_e^2 N_\tau) \times \frac{\int_0^{E_1 - m_e} \sigma_\gamma(\omega)\phi(E_1, \omega, Z_\tau)(d\omega/\omega)}{\int_0^{E_1 - m_e} \sigma_\gamma(\omega) N_{PW}^{E1}(E_1, \omega)(d\omega/\omega)}, \quad (10)$$

$$F_{DW}^{(E1)} = (N_\tau / Z_\tau^2 r_e^2 N_\tau) \times \frac{\int_0^{E_1 - m_e} \sigma_\gamma(\omega)\phi(E_1, \omega, Z_\tau)(d\omega/\omega)}{\int_0^{E_1 - m_e} \sigma_\gamma(\omega) N_{DW}^{E1}(E_1, \omega, Z_t)(d\omega/\omega)}, \quad (11)$$

REF.		ELEM. SYM.	A	Z
	D. W. Anderson, R. F. Petry, H. J. Fischbeck Nucl. Phys. A262, 91 (1976)	F	19	9
METHOD		REF. NO.		
		76 An 2		egf

REACTION	RESULT	EXCITATION ENERGY	SOURCE		DETECTOR		ANGLE
			TYPE	RANGE	TYPE	RANGE	
G,2N	ABX	20- 60	C	19- 60	ACT-I		4PI

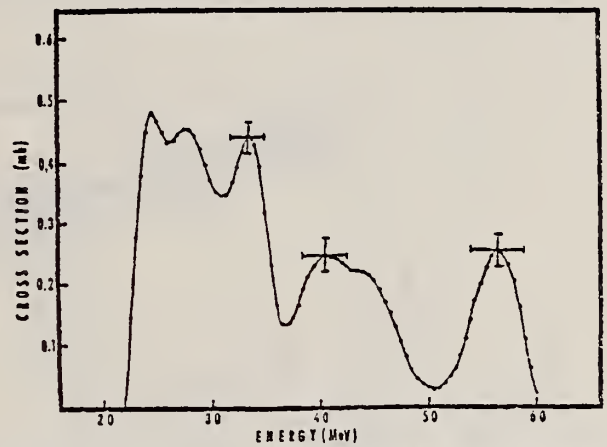

Fig. 2. Cross section for the $^{19}F(\gamma, 2n)^{17}F$ reaction. Vertical bars indicate standard deviations in the cross section. Horizontal bars indicate the minimum width for analysis of a single isolated resonance.

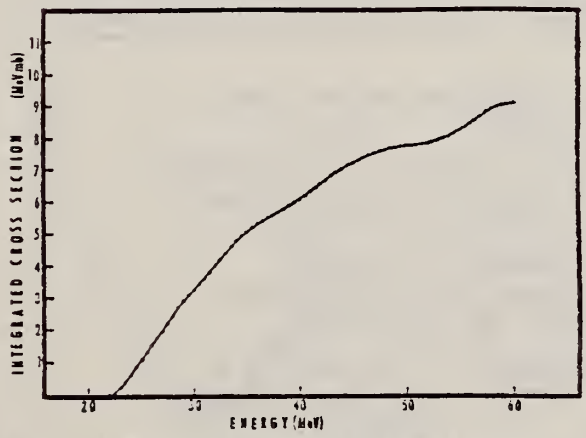

Fig. 3. Integrated cross-section curve for the $^{19}F(\gamma, 2n)^{17}F$ reaction as a function of energy.

REF. J.B. Martins, O.A.P. Tavares, M.L. Terranova, and V. Di Napoli
Lett. Nuovo Cimento 15, 364 (1976)

ELEM. SYM.	A	Z
F	19	9

METHOD

REF. NO. 76 Ma 10 egf

REACTION	RESULT	EXCITATION ENERGY	SOURCE		DETECTOR		ANGLE
			TYPE	RANGE	TYPE	RANGE	
G,N13	ABY	THR-999	C	300-999	ACT-I		4PI

999=1 GEV

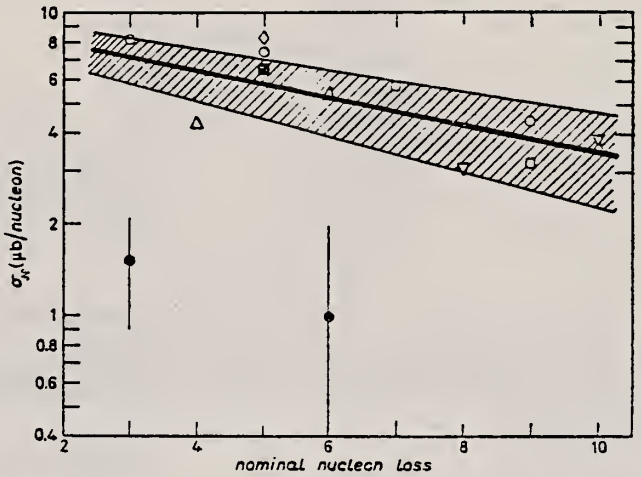

Fig. 1. – Values of mean absolute cross-section *per* nucleon σ_N as a function of the nominal nucleon loss (semi-logarithmic plot). Open circles: ^{27}Al target, ref. ([9,10,16]); open triangles: ^{28}Si target, ref. ([3]); open rhomb: ^{23}Na target, ref. ([3]); open reversed triangles: ^{32}S target, ref. ([3]); open squares: ^{31}P target, ref. ([3]); filled square: ^{16}O target, ref. ([2]). The straight line is a least-squares fit of all the experimental points. The shaded area represents the standard deviation. Filled circles with error bars: present-work results for ^{16}O and ^{19}F targets.

[2] V. Di Napoli and M.L. Terranova: Journal Inorg. Nucl. Chem., 36, 3633 (1974)

[3] V. Di Napoli, G. Rosa, F. Salvetti, M.L. Terranova, H.G. De Carvalho, J.B. Martins and O.A.P. Tavares: Journal. Inorg. Nucl. Chem., 37, 1101 (1975)

[12] V. Di Napoli, A.M. Lacerenza, F. Salvetti, S.M. Terenzi, H.G. De Carvalho and J.B. Martins: Joural Inorg. Nucl. Chem. 35, 1419 (1973)

[16] V. Di Napoli, A.M. Lacerenza, F. Salvetti, H.G. De Carvalho and J.B. Martins: Lett. Nuovo Cimento, 1, 835 (1971)

REF.

N.K. Sherman, K.H. Lokan, and R.W. Gellie
Can. J. Phys. 54, 1178 (1976)

ELEM. SYM.	A	Z
F	19	9

METHOD

REF. NO.	
76 Sh 5	hmg

REACTION	RESULT	EXCITATION ENERGY	SOURCE		DETECTOR		ANGLE
			TYPE	RANGE	TYPE	RANGE	
G,N	ABX	10- 19	C	13- 21	TOF-D		90

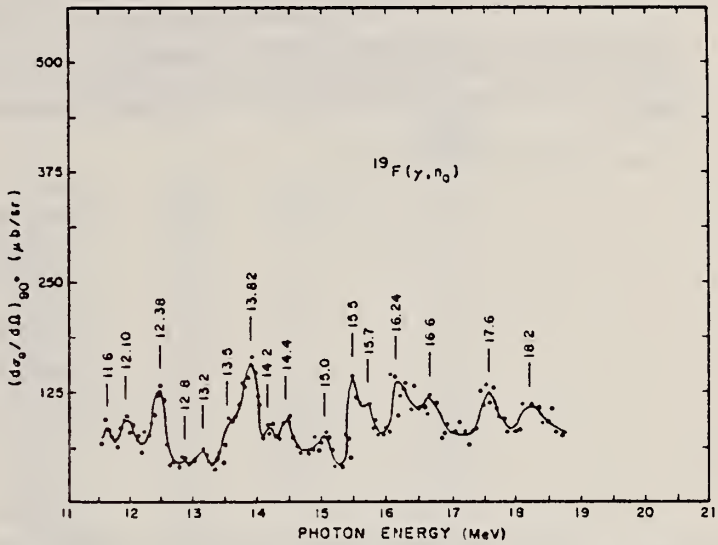

FIG. 4. Ground-state photoneutron cross section $d\sigma_0/d\Omega$ synthesized from the neutron data of Fig. 2, using the photon spectra of Fig. 3.

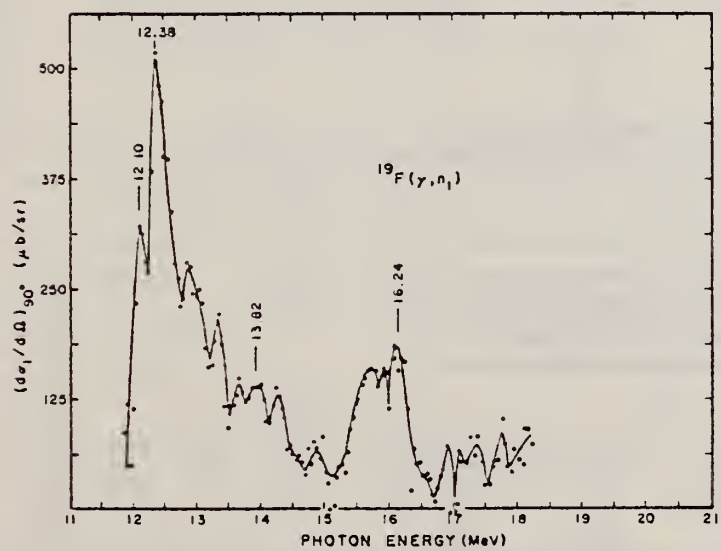

FIG. 5. First-excited-state photoneutron cross section $d\sigma_1/d\Omega$ obtained from the curves of Fig. 2 after subtracting away the ground-state components.

(over)

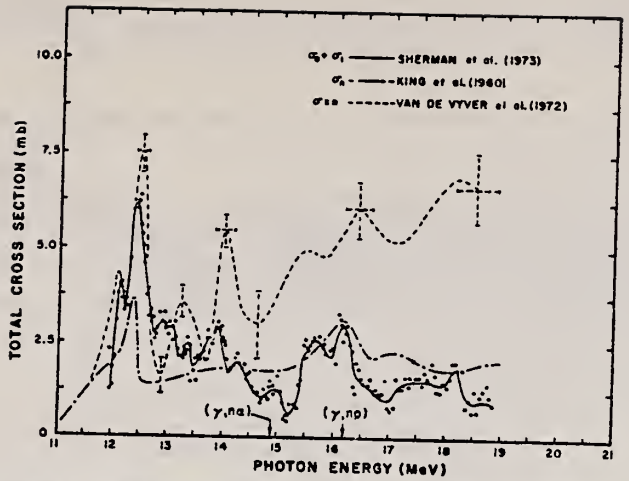

FIG. 6. Comparison of the sum of $((d\sigma_0/d\Omega) + (d\sigma_1/d\Omega))$ integrated over angle (solid line), with the single-neutron cross section σ_n (dash–dot line) of King *et al.* (1960) and with the total-neutron cross section σ_{xn} (dashed line) of Van de Vyver *et al.* (1972). The angular distribution is assumed to be $6 + 5 \sin^2 \theta$.

$$\sigma_{tot} = 10.66\ (d\sigma/d\Omega)_{90^0}$$

TABLE 1. Correlation of resonances at photon energy k in the ground-state cross section with observed neutron peaks at energies T_{n0} and T_{n1}, ascribed to ground- and first-excited-state transitions. The measured resonance width is Γ, and the 90° branching ratio to the first-excited-state group is σ_1/σ_0

k (MeV)	T_{n0} (MeV)	T_{n1} (MeV)	Γ (keV)	σ_1/σ_0
11.6	1.10	—	(150)	—
12.10 ± 0.04	1.579 ± 0.020	0.64	200 ± 50[a]	2.46
12.38 ± 0.04	1.842 ± 0.025	0.92	167 ± 50[a]	3.70
(12.65)	2.10	—	(200)	—
12.79	2.24	—	(200)	(10.1)
13.29	2.71	—	(250)	(3.0)
(13.5)	—	—	—	(1.3)
13.82 ± 0.05	3.22 ± 0.04	2.47	250 ± 100	0.85
(14.2)	—	—	—	—
14.4	3.79	—	(300)	(0.88)
(15.0)	—	—	(550)	(0.75)
15.5	4.64	—	(450)	(2.8)
(15.7)	—	—	—	(0.2)
16.24 ± 0.05	5.49 ± 0.07	4.26	300 ± 150	1.04
16.6	—	—	—	(0.5)
17.6	—	—	—	(0.6)
18.2	—	—	—	—

[a]Sherman *et al.* (1972).

TABLE 2. Approximate total integrated cross sections $\int\sigma_T$ for the principal transitions at photon energies k. The integrated 90° differential ground-state cross section $\int d\sigma_0/d\Omega$, the product of statistical factor g_r and radiative width $\Gamma_{\gamma 0}$, and the radiative width $\Gamma_{\gamma 0}$(E1) assuming electric dipole transitions, and spin parity J^π are also tabulated

k (MeV)	$\int \frac{d\sigma_0}{d\Omega}$ (MeV mb sr^{-1})	$\int\sigma_T$ (MeV mb)	$g_r\Gamma_{\gamma 0}$ (eV)	$\Gamma_{\gamma 0}$(E1) (eV)	J^π
12.10	0.0334	1.21	23.1	11.6	1/2⁻
12.38	0.0514	2.53	50.6	25.3	1/2⁻
13.82	0.0505	0.98	24.4	24.4	3/2⁻
16.24	0.0616	1.32	45.4	45.4	3/2⁻

W.R. Dixon and R.S. Storey
Nucl. Phys. A284, 97 (1977)

ELEM. SYM	A	Z
F	19	9

METHOD	REF. NO.
	77 Di 4 egf

REACTION	RESULT	EXCITATION ENERGY	SOURCE		DETECTOR		ANGLE
			TYPE	RANGE	TYPE	RANGE	
A,G	LFT	6 - 7	D	2-4	SCD-D		DST
		(6.28-7.17)		(2.87-3.99)			

6.28-7.17 MeV

TABLE 1
Resonances in the $^{15}N+\alpha$ system in the energy range E_x = 2.8–4.0 MeV

E_x (keV)	E_x (keV)	From $^{15}N(\alpha,\gamma)^{19}F$[a] $\omega\gamma$ (eV)[b]	From $^{15}N(\alpha,\gamma)^{19}F$[a] J^π	From $^{15}N(\alpha,\alpha)^{15}N$[c] J^π	From $^{15}N(\alpha,\alpha)^{15}N$[c] Γ(lab) (keV)
2873 ± 3	6281 ±2	1.0 ±0.2	$\frac{1}{2}^+$	$\frac{1}{2}^+$	3
2935 ± 3	6330 ±2	0.76±0.15	$\frac{1}{2}^+$ ($\frac{3}{2}^+$)	$\frac{3}{2}^+$	3
3060 ±10	6429 ±8			$\frac{1}{2}^-$	358
3146.8± 1.5	6497.4±1.5	1.7 ±0.3	$\frac{1}{2}^+$		
3149.8± 1.5	6499.8±1.5	2.3 ±0.4	$\frac{11}{2}^+$		
3183 ± 2	6526 ±2	2.4 ±0.4	$\frac{1}{2}^+$	$\frac{1}{2}^+$	5
3218 ± 2	6553 ±2	0.63±0.13	$\frac{1}{2}^+$	$\frac{1}{2}^+$	2
3267 ± 2	6592 ±2	1.6 ±0.3	$\frac{1}{2}^+$		
3511 ± 3	6785 ±2	10.9 ±1.5	$\frac{1}{2}^-$	$\frac{1}{2}^-$	3
3576 ± 3	6836 ±2	1.0 ±0.2	$\frac{1}{2}^+$	$\frac{1}{2}^+$ ($\frac{3}{2}^+$)	1.5
3645 ± 5	6891 ±4	6.1 ±1.3	$\frac{1}{2}^-$	$\frac{1}{2}^-$	35
3688 ± 3	6925 ±2	9.7 ±1.4	$\frac{1}{2}^+$	$\frac{1}{2}^-$ ($\frac{3}{2}^-$)	3
3770 ±10	6989 ±8			$\frac{1}{2}^-$	64
3930 ±10	7116 ±8			$\frac{1}{2}^+$	≈ 40
3993 ± 2	7165.7±1.0	1.5 ±0.2	$\frac{11}{2}^-$		

[a]) This work and refs. [11, 6]).
[b]) $\omega\gamma = \frac{1}{3}(2J+1)\Gamma_\alpha\Gamma_\gamma/\Gamma$. Measured relative to the strength of the E_x = 1.68 MeV reonance [5]).
[c]) Refs. [7, 8]). The α-particle energies taken from the elastic-scattering work (3.07, 3.78 and 3.94 MeV) have been adjusted downwards by 10 keV to correspond to the other (α, γ) resonances, and arbitrarily assigned errors of ±10 keV.

TABLE 2
Branching ratios (percentages) for states (E_x in MeV) in ^{19}F in the energy range E_x = 6.3–7.2 MeV

	g.s. $\frac{1}{2}^+$	0.11 $\frac{1}{2}^-$	0.20 $\frac{3}{2}^+$	1.35 $\frac{3}{2}^-$	1.46 $\frac{5}{2}^-$	1.55 $\frac{5}{2}^+$	2.78 $\frac{3}{2}^+$	3.91 $\frac{3}{2}^+$	4.00 $\frac{7}{2}^-$	4.03 $\frac{5}{2}^-$	4.38 $\frac{7}{2}^+$	Other
6.28	14±2		4.2±1.0	36 ±2	26±2	20 ±2						
6.33			56 ±3	17 ±2		8.5±1.5					18±2	
6.50	38±2	14±2	9 ±2	14 ±2	25±2							
6.50							55					4.65 (45%)
6.53	29±2	59±3										4.55 (12±2%)
6.55			19 ±2	55 ±4			26 ±3					
6.59			13 ±2				63 ±3				24±2	
6.79	15±2	39±2	13 ±2	5.3±0.8	25±2			2.6±1.0				
6.84	9±5	9±5	27 ±6	10 ±7	45±8							
6.89	9±2	< 8	< 5	61 ±5	30±5							
6.93			73 ±3	22 ±2			2.4±0.5		1.3±0.5	1.3±0.5		
7.17									6 ±2	94 ±2		

(OVER)

TABLE 3

Angular-distribution coefficients, mixing ratios and some transition strengths for the main γ-decay branches for ^{19}F states with $E_x = 6.3$–7.0 MeV

$E_i \to E_f$	$J_i \to J_f$	A_2/A_0 [a]	A_4/A_0 [a]	Mixing ratio, δ [b]	$\lvert M\rvert^2$ (W.u.) [c]
6.28 → 0	$\frac{5}{2}^+ \to \frac{1}{2}^+$	0.612	0.469	−0.05±0.07	1.9±0.4 (E2)
→ 1.35	$\to \frac{5}{2}^-$	0.468	0.000	−0.01±0.09	(2.0±0.4) × 10^{-3} (E1)
→ 1.46	$\to \frac{3}{2}^-$	−0.350	0.000	−0.02±0.04	(1.6±0.3) × 10^{-3} (E1)
→ 1.55	$\to \frac{3}{2}^+$	−0.617	0.008	0.11±0.06	0.030−0.006 (M1)
6.33 → 0.20	$\frac{7}{2}^+ \to \frac{5}{2}^+$	0.195	0.045	−0.27±0.04	0.021±0.004 (M1)
					0.35±0.10 (E2)
→ 1.35	$\to \frac{5}{2}^-$	−0.306	0.000	−0.02±0.03	(5.4±1.1) × 10^{-4} (E1)
→ 1.55	$\to \frac{3}{2}^+$	0.510	−0.367	0.00±0.14	2.8±0.6 (E2)
→ 4.38	$\to \frac{7}{2}^+$	0.443	−0.001	0.04±0.20	0.22±0.05 (M1)
6.50 → 0	$\frac{3}{2}^+ \to \frac{1}{2}^+$	−0.396		−0.06±0.04	0.056±0.010 (M1)
				or 2.00±0.17	9±2 (E2)
→ 0.11	$\to \frac{1}{2}^-$	−0.507		0.00±0.03	(9±2) × 10^{-4} (E1)
→ 0.20	$\to \frac{5}{2}^+$	0.320		0.3 −1.8	0.003−0.014 (M1)
					0.3−2.4 (E2)
→ 1.35	$\to \frac{5}{2}^-$	−0.236		−0.11±0.09	(1.8±0.4) × 10^{-3} (E1)
→ 1.46	$\to \frac{3}{2}^-$	0.400		0.00±0.07	(3.4±0.7) × 10^{-3} (E1)
6.53 → 0	$\frac{3}{2}^+ \to \frac{1}{2}^+$	−0.915		0.32±0.04	0.053±0.009 (M1)
				or 0.90±0.06	5±1 (E2)
→ 0.11	$\to \frac{1}{2}^-$	−0.510		0.00±0.02	(5.4±0.9) × 10^{-3} (E1)
→ 4.55	$\to \frac{5}{2}^+$	−0.368		-0.23±0.13	20–220 (E2)
	$\frac{7}{2}^+ \to \frac{5}{2}^+$	−0.371	0.000	0.01±0.07	0.43±0.10 (M1)
6.55 → 0.20	$\frac{7}{2}^- \to \frac{5}{2}^+$	−0.414	0.001	0.03±0.05	
→ 1.35	$\to \frac{5}{2}^-$	−0.371	0.000	0.01±0.03	
→ 2.78	$\to \frac{3}{2}^+$	−0.088	0.000	0.05±0.07	
6.59 → 0.20	$\frac{3}{2}^+ \to \frac{5}{2}^+$	0.633	−0.046	−0.13±0.13	1.6±0.4 (E2)
→ 2.78	$\to \frac{3}{2}^+$	0.584	−0.022	−0.20±0.20	0.17±0.04 (M1)
→ 4.38	$\to \frac{7}{2}^+$	−0.369	0.000	0.02±0.07	0.35±0.08 (M1)
6.79 → 0	$\frac{1}{2}^- \to \frac{1}{2}^+$	−0.348		−0.08±0.03	(5.4±1.0) × 10^{-3} (E1)
→ 0.11	$\to \frac{1}{2}^-$	−0.670		0.11±0.02	0.33±0.05 (M1)
					0.8±0.3 (E2)
→ 0.20	$\to \frac{5}{2}^+$	−0.044		0.05±0.06	(5.1±1.1) × 10^{-3} (E1)
→ 1.46	$\to \frac{3}{2}^-$	0.594		−0.13±0.08	0.43±0.07 (M1)
6.84 → 0.20	$\frac{5}{2} \to \frac{5}{2}^+$	0.760	−0.078	−0.5 ±0.5	
→ 1.46	$\to \frac{3}{2}^-$	−0.359	0.000	−0.02±0.11	
6.89 → 1.35	$\frac{3}{2}^- \to \frac{5}{2}^-$	0.296		0.22−2.2	0.09–0.50 (M1)
					6–120 (E2)
→ 1.46	$\to \frac{3}{2}^-$	0.165		0.15±0.12	0.26±0.07 (M1)
6.93 → 0.20	$\frac{7}{2}^- \to \frac{5}{2}^+$	−0.328	0.000	−0.01±0.03	(12±2) × 10^{-3} (E1)
→ 1.35	$\to \frac{5}{2}^-$	−0.371	0.000	0.01±0.02	0.15±0.03 (M1)
→ 2.78	$\to \frac{3}{2}^+$	−0.172	0.000	0.00±0.16	(1.7±0.4) × 10^{-3} (E1)

[a]) The experimental angular distributions are fitted to $A_0 + A_2 Q_2 P_2 + A_4 Q_4 P_4$, where P_2 and P_4 are the usual Legendre polynomials, and Q_2 and Q_4 are attenuation coefficients giving the effect of the finite solid angle of the detector (typically 0.90–0.95 and 0.78–0.83, respectively). The fitting procedure requires minimization of χ^2 with respect to the mixing ratio δ, of which A_2/A_0 and A_4/A_0 are known functions.

[b]) The phase convention is that of Rose and Brink [23]). The 68 % errors are assigned by the (χ^2+1) rule or by the "external-error" method [24]), whichever is larger.

[c]) Weisskopf units as defined by Wilkinson [25]).

REF. V. Di Napoli, J. B. Martins, G. Rosa, F. Salvetti, O. A. P. Tavares, M. L. Terranova and H. G. De Carvalho
J. Inorg. Nucl. Chem. 40, 1619 (1978)

ELEM. SYM.	A	Z
F	19	9

METHOD

REF. NO. 78 Di 10 hg

REACTION	RESULT	EXCITATION ENERGY	SOURCE TYPE	SOURCE RANGE	DETECTOR TYPE	DETECTOR RANGE	ANGLE
G,C11	ABY	33(33.08)-999	C	300-999	ACT-I		4PI
G,Be7	ABY	30(30.63)-999	C	300-999	ACT-I		4PI

Abstract—Mean cross sections for the photoproduction of ^{7}Be and ^{11}C from ^{19}F, ^{27}Al, ^{28}Si and ^{32}S targets, ^{7}Be from ^{10,11}B, and ^{11}C from ^{14}N and ^{16}O targets have been measured using bremsstrahlung beams in the energy range 0.3–1.0 GeV. The results have been compared with previous measurements and an excellent agreement has been found. In most cases, the values obtained turned out to be much larger than those expected from a simple spallation mechanism. A fragmentation and/or a fission-like process has been suggested in explaining the mechanism of such reactions.

999=1 GEV

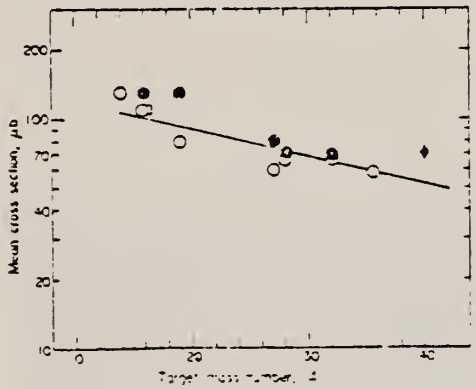

Fig. 1. Mean cross sections per photon, $\bar{\sigma}_{\gamma}$, of ^{11}C photoproduction vs the target mass number A. Experimental data are taken from: ●, Ref. [9]; □, Ref. [13]; ◆, Ref. [2]; ○, present work. The straight line is a least squares fit of the experimental points.

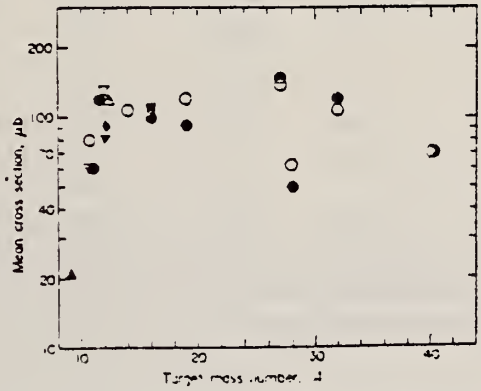

Fig. 2. The same as in Fig. 1 for ^{7}Be photoproduction. Experimental data are taken from: ▲, Refs. [6, 7]; ▽, Ref. [8]; ⊖, Ref. [9]; △, Ref. [10]; ◆, Ref. [11]; ▼, Ref. [12]; □, Ref. [13]; ■, Ref. [14]; ◇, Ref. [2]; ○, present work.

Table 1. Cross sections per equivalent quantum of ^{11}C photoproduction

E_0 (GeV)	Cross Section, σ_Q (μb) ^{14}N	^{16}O	^{19}F	^{27}Al	^{28}Si	^{32}S	^{35,37}Cl
0.30	520±30	200±20	110±20	29±10	35±10	45±10	30±10
0.32	520±30	210±20	120±20	30±10	42±10	50±10	30±10
0.35	530±30	230±20	125±20	38±10	45±10	60±10	40±10
0.40	530±30	230±20	130±20	42±10	52±10	65±10	50±10
0.48	550±30	255±20	150±20	60±10	70±10	80±10	60±10
0.55	570±30	260±20	160±20	60±10	78±10	85±10	60±10
0.65	600±30	290±20	180±20	70±10	85±10	98±10	75±10
0.75	620±30	300±20	180±20	79±10	95±10	110±10	85±10
0.90	650±30	320±20	190±20	90±10	110±10	120±10	95±10
1.00	680±30	330±20	210±20	100±10	115±10	125±10	100±10

Table 2. Cross sections per equivalent quantum of ^{7}Be photoproduction

E_0 (GeV)	Cross Section, σ_Q (μb) ^{10,11}B	^{14}N	^{16}O	^{19}F	^{27}Al	^{28}Si	^{32}S
0.30	150±20	200±20	113±20	152±20	40±20	20±20	50±20
0.32	160±20	200±20	120±20	150±20	45±20	30±20	54±20
0.35	160±20	210±20	130±20	159±20	42±20	30±20	60±20
0.40	175±20	225±20	145±20	170±20	98±20	20±20	70±20
0.48	190±20	245±20	163±20	186±20	100±20	50±20	140±20
0.55	200±20	260±20	187±20	200±20	93±20	48±20	90±20
0.65	220±20	280±20	197±20	214±20	140±20	68±20	130±20
0.75	225±20	300±20	215±20	227±20	180±20	70±20	130±20
0.90	240±20	318±20	230±20	245±20	166±20	88±20	165±20
1.00	250±20	330±20	242±20	260±20	200±20	97±20	190±20

Table 3. Comparison between experimentally determined and calculated cross sections of ^{7}Be and ^{11}C photoproduction and indication of the dominant reaction channels

Target Nucleus	Product Nucleus	Nominal Nucleon Loss, ΔA	$\Delta A/A_t$ (x10^{4})	$\bar{\sigma}_{exp}$ (*) (μb)	$\bar{\sigma}_{CDMD}$ (**) (μb)	$\frac{\bar{\sigma}_{exp}}{\bar{\sigma}_{CDMD}}$	Apparent Threshold (Exp.) E_{th}(MeV)	Possible Mechanism of Production
$^{10,11}B$	^{7}Be	(3).	(30).36	67	28	2	$\leq$ 50	Spallation
^{12}C	^{7}Be	5	42	110	20	5	$\leq$ 50	Spallation
^{14}N	^{7}Be	7	50	108	12	9	$\leq$ 50	Fission Spallation
^{14}N	^{11}C	3	21	130	60	2	$\leq$ 50	Spallation
^{16}O	^{7}Be	9	56	107	8	13	50<E_{th}<200	Fission Fragmentation
^{16}O	^{11}C	5	31	117	33	3	$\leq$ 50	Spallation
^{19}F	^{7}Be	12	63	106	5	21	50<E_{th}<200	Fission Fragmentation
^{19}F	^{11}C	8	42	105	16	7	50<E_{th}<200	Fission Fragmentation Spallation
^{27}Al	^{7}Be	20	74	142	2	71	> 200	Fragmentation
^{27}Al	^{11}C	16	59	70	5	14	50<E_{th}<200	Fission Fragmentation
^{28}Si	^{7}Be	21	75	56	2	28	> 200	Fragmentation
^{29}Si	^{11}C	17	61	68	4	17	50<E_{th}<200	Fission Fragmentation
^{32}S	^{7}Be	25	78	114	2	57	> 200	Fragmentation
^{32}S	^{11}C	21	66	68	3	23	50<E_{th}<200	Fission Fragmentation
$^{35,37}Cl$	^{11}C	24.(26)	69.(70)	59	3	20	50<E_{th}<200	Fission Fragmentation
^{40}Ca	^{7}Be	33	83	70	1	70	> 200	Fragmentation
^{40}Ca	^{11}C	29	73	70	2	35	> 200	Fragmentation

(*) Mean values of the different measurements (see Figs. 1 and 2).

(**) Calculated values according to Ref. [9].

REF.

T.J.M. Symons, L.K. Fifield, M.J. Hurst, F. Watt, C.H. Zimmerman and K.W. Allen
J. Phys. G 4, 411 (1978)

ELEM. SYM.	A	Z
F	19	9

METHOD

REF. NO.	
78 Sy 2	rs

REACTION	RESULT	EXCITATION ENERGY	SOURCE		DETECTOR		ANGLE
			TYPE	RANGE	TYPE	RANGE	
A,G	LFT	8- 10	D	5- 8	SCD-D		55

Abstract. The $^{15}N(\alpha,\gamma)^{19}F$ reaction has been studied for α-particle bombarding energies from 5·2 to 8·4 MeV using a differentially-pumped gas target. Forty-two resonances have been identified in the gamma ray yield, of which 32 have been observed to decay by gamma emission to known states in ^{19}F. The remaining ten resonances were found to arise from the $^{15}N(\alpha,\alpha'\gamma)^{15}N$ and $^{15}N(\alpha,p\gamma)^{18}O$ reactions. Decay schemes, widths and values of $\omega\gamma$ have been measured for many of these states. The data obtained are compared with previous published work on the ^{19}F nucleus.

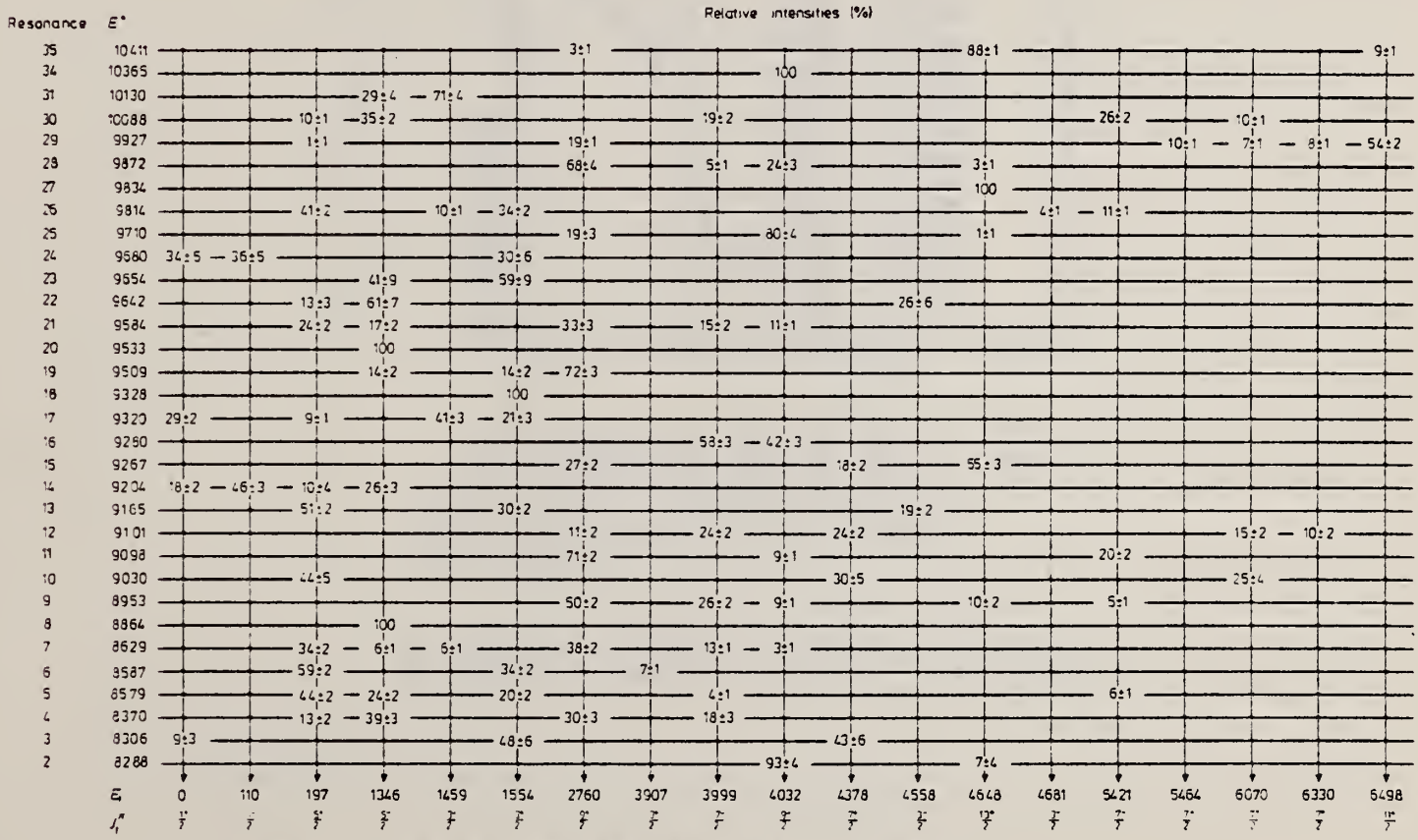

Figure 6. Relative intensities at 55° of the decays of resonances observed in the $^{15}N(\alpha,\gamma)^{19}F$ reaction.

over

Table 1. Properties of capture resonances.

Resonance	E^* (keV)	E_γ (keV)	Γ (keV)	$\omega\gamma(55^\circ)$ (eV)	J^π
2	8288 ± 4	5415 ± 5	<1	0·58 ± 0·1	$\frac{13}{2}^-$
3	8306 ± 4	5439 ± 5	<1	2·1 ± 0·5	$\frac{5}{2}^+$
4	8370 ± 4	5520 ± 5	7·5 ± 1·5	0·54 ± 0·2	$\frac{7}{2}^-, \frac{5}{2}^+$
5	8579 ± 4	5784 ± 5	~1	5·1 ± 1·3	$\frac{5}{2}$
6	8587 ± 3	5794 ± 4	2·1 ± 0·1[a]	1·6 ± 0·35	$\frac{3}{2}$
7	8629 ± 4	5487 ± 5	<1	2·5 ± 0·4	$\frac{7}{2}^+$
8	8864 ± 4	6145 ± 5	<1	0·2 ± 0·05	$<\frac{9}{2}$
9	8953 ± 3	6261 ± 4	~1	0·85 ± 0·2	$\frac{11}{2}^-, (\frac{9}{2}^+)$
10	9030 ± 5	6356 ± 5	4·2 ± 1	0·53 ± 0·26	$\frac{5}{2}, \frac{7}{2}$
11	9098 ± 4	6442 ± 5	0·57 ± 0·03[a]	0·48 ± 0·15	$\frac{7}{2}^+$
12	9101 ± 4	6445 ± 5	~1	0·40 ± 0·1	$\frac{7}{2}, \frac{9}{2}$
13	9165 ± 5	6526 ± 6	9·9 ± 1·5	1·4 ± 1	$\frac{1}{2}, \frac{3}{2}$
14	9204 ± 7	6576 ± 6	10·2 ± 1·5	1·5	$\frac{3}{2}$
15	9267 ± 4	6656 ± 5	2 ± 1	0·15 ± 0·04	$\frac{11}{2}^+, \frac{9}{2}^+$
16	9280 ± 5	6672 ± 6	<1·5	0·38 ± 0·09	$\frac{7}{2}, \frac{9}{2}$
17	9320 ± 4	6722 ± 5	3·4 ± 1	3·4 ± 1·7	$\frac{1}{2}^+$
18	9329 ± 4	6735 ± 5	~6	—	$<\frac{5}{2}$
19	9509 ± 4	6963 ± 5	<1	0·7 ± 0·2	$\frac{5}{2}^+, \frac{7}{2}^+$
20	9533 ± 6	6993 ± 7	6·3 ± 1·5	0·5	$\frac{3}{2}, \frac{5}{2}, \frac{7}{2}$
21	9584 ± 4	7057 ± 5	9·6 ± 1·5	5·2 ± 3	$\frac{7}{2}$
22	9642 ± 6	7131 ± 7	~8	~1	$\frac{3}{2}, \frac{5}{2}$
23	9654 ± 6	7146 ± 6	~6	~2	$\frac{3}{2}, \frac{5}{2}$
24	9680 ± 6	7179 ± 7	~4	~1	$\frac{1}{2}, \frac{3}{2}$
25	9710 ± 4	7217 ± 5	<1	4 ± 0·7	$\frac{9}{2}^+, \frac{11}{2}$
26	9814 ± 4	7349 ± 5	<1·5	3·5 ± 0·8	$\frac{5}{2}^+$
27	9834 ± 3	7376 ± 4	<1	0·51 ± 0·1	$\frac{11}{2}, \frac{13}{2}, \frac{15}{2}$
28	9872 ± 3	7422 ± 4	~1·5	3·6 ± 0·6	$\frac{9}{2}^+, \frac{11}{2}^-$
29	9926 ± 3	7491 ± 4	~1	19·3 ± 3·0	$\frac{9}{2}^+$
30	10088 ± 5	7696 ± 6	<1·5	2·37 ± 0·5	$\frac{5}{2}, \frac{7}{2}$
31	10130 ± 6	7749 ± 6	3·2 ± 1	1·3 ± 0·4	$\frac{3}{2}, \frac{5}{2}$
34	10365 ± 4	8047 ± 5	3 ± 1·5	0·9 ± 0·4	$\frac{7}{2}, \frac{9}{2}, \frac{11}{2}$
35	10411 ± 3	8105 ± 4	<1·5	15·0 ± 3·0	$\frac{11}{2}^+, \frac{13}{2}^+$

[a] These values are from the measurements of Yagi (1962).

Yagi, K. 1962, J. Phys. Soc. Japan 17, 604.

REF. C.F. Williamson, F.N. Rad, S. Kowalski, J. Heisenberg, H. Crannell, J.T. O'Brien, and H.C. Lee
Phys. Rev. Lett. 40, 1702 (1978)

ELEM. SYM.	A	Z
F	19	9

METHOD

REF. NO. 78 Wi 2 rs

REACTION	RESULT	EXCITATION ENERGY	SOURCE TYPE	SOURCE RANGE	DETECTOR TYPE	DETECTOR RANGE	ANGLE
E,E/	FMF	0- 5	D	1* 3	MAG-D		DST

*Q=0.5-2.5FM-1

Cross sections for the electroexcitation of the ground-state rotational band in ^{19}F have been measured over the momentum transfer range $0.5 \leq q \leq 2.5$ fm^{-1} and are compared to calculations based on the variation-after-projection, Hartree-Fock approximation. The data support the predicted predominance of $\vec{L}\cdot\vec{S}$ coupling for this band. The 5464-keV level is unambiguously identified as the $\frac{1}{2}^+$ member of the ground-state band.

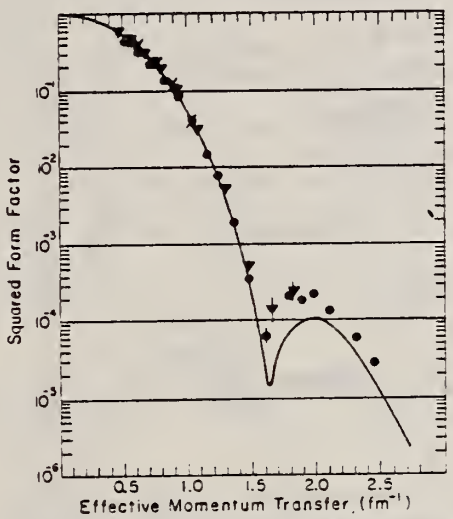

FIG. 1. Squared form factors for elastic scattering in ^{19}F. Solid circles, present data; crosses, data of Ref. 1; inverted triangles, data of Ref. 2; solid line, VPHF calculation.

[2] M. Oyamada, T. Terasawa, K. Nakahara, Y. Endo, H. Saito, E. Tanaka, Phys. Rev. C 11, 1578 (1975).

over

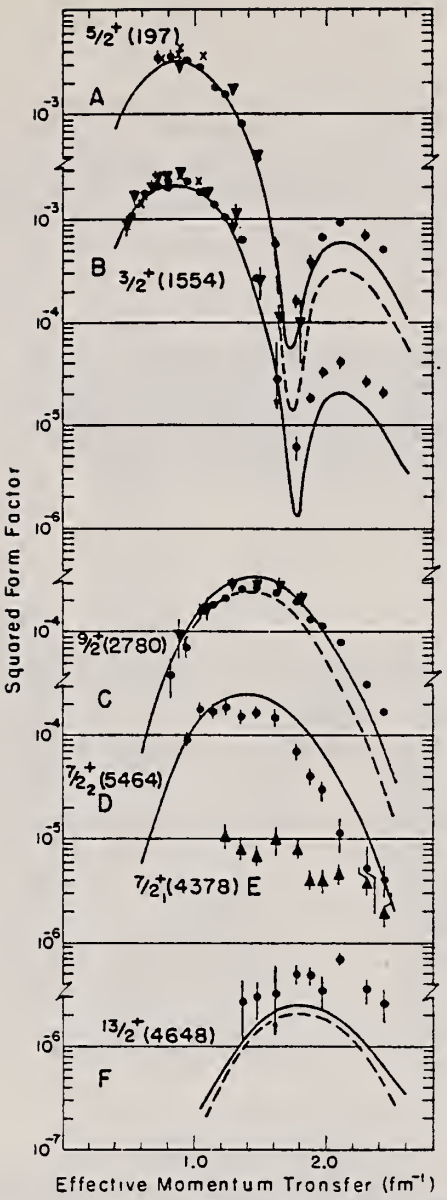

FIG. 2. Squared form factors for inelastic scattering in ^{19}F. Circles and triangles, present data; crosses, data of Ref. 1; inverted triangles, data of Ref. 2; solid line, VPHF calculation including both longitudinal and transverse magnetic components; in *B* and *D* the magnetic components are predicted to be negligibly small; dashed line, VPHF calculation including longitudinal components only.

[1] P.L. Hallowell, W. Bertozzi, J. Heisenberg, S. Kowalski, X. Maruyama, C.P. Sargent, W. Turchinetz, C.F. Williamson, S.P. Fivozinsky, J.W. Lightbody, Jr., and S. Penner, Phys. Rev. C 7, 1346 (1973).

[2] M. Oyamada, T. Terasawa, K. Nakahara, Y. Endo, H. Saito, E. Tanaka, Phys. Rev. C 11, 1578 (1975).

REF. J.E.M. Thomson and M.N. Thompson
Nucl. Phys. A330, 66 (1979)

ELEM. SYM.	A	Z
F	19	9

METHOD

REF. NO. 79 Th 1 hg

REACTION	RESULT	EXCITATION ENERGY	SOURCE		DETECTOR		ANGLE
			TYPE	RANGE	TYPE	RANGE	
G,PG	ABX	14-30	C	14-30	SCD-D		150
G,NG							
G,AG							

Abstract: Cross sections and integrated cross sections for photodisintegration of ^{19}F to excited residual states following emission of protons, neutrons and α-particles have been measured. The size of the photo-α cross sections appear to be too large to be explained by a semidirect reaction mechanism.

DE-EXCIT G-RAYS

E NUCLEAR REACTIONS $^{19}F(\gamma, n)$, $^{19}F(\gamma, p)$, $^{19}F(\gamma, \alpha)$, bremsstrahlung E_{max} = 14–30 MeV; measured σ, $\int\sigma dE$, de-excitation γ-rays. ^{18}F, ^{18}O, ^{15}N deduced levels, J, π. Natural target.

TABLE I

Cross sections integrated to 30 MeV for photoreaction in ^{19}F leading to the levels indicated

Level (MeV)	J^π, T	$\int_{th}^{30}\left(\frac{d\sigma}{d\Omega}\right)_{150°} dE$ this work (MeV · mb/sr)	$\int_{th}^{23}\left(\frac{d\sigma}{d\Omega}\right)_{150°} dE$ ref. [8]) (MeV · mb/sr)	Rel. strength following irradiation with 14 MeV bremsstrahlung [1])
^{18}O				
1.982	$2^+, 1$	1.6 ±0.2 [a])	1.75	158 ± 10
3.553	$4^+, 1$	< 0.1		
3.632	$0^+, 1$	0.4 ±0.2 [a])	0.90	38 ± 11
3.919	$2^+, 1$	0.2 ±0.1 [c])		
4.448	$1^-, 1$	0.6 ±0.2 [c])		20 ± 10
^{19}F				
0.936	$3^+, 0$	1.0 ±0.2 [b])	1.25	
1.042	$0^+, 1$	0.9 ±0.2 [b])	0.45	
1.081	$0^-, 0$	0.2 ±0.1 [b])		
1.128	$5^+, 0$	?		
1.701	$1^+, 0$	< 0.05		
2.101	$2^-, 0$	< 0.1 [c])		
2.524	$2^+, 0$	≲ 0.04 [c])		
3.059	$2^+, 1$	0.3 ±0.15 [c])		
3.135	$1^-, 0$	0.3 ±0.1 [c])		
4.739	$3^+, 0$	0.07 ± 0.02 [c])		
^{15}N				
5.270	$\frac{1}{2}^+$	0.1 ±0.03 [a])		71 ± 2
5.270 + 5.299 [a])	$(\frac{1}{2}^+ + \frac{1}{2}^+)$	0.33 ± 0.13 [a])	0.75	184 ± 6

[a]) Evaluated by direct integration of cross section.
[b]) Evaluated from yield at 30 MeV.
[c]) Evaluated by comparing the strength of the peaks to that from 1.98 MeV level in ^{18}O in summed spectrum.

(OVER)

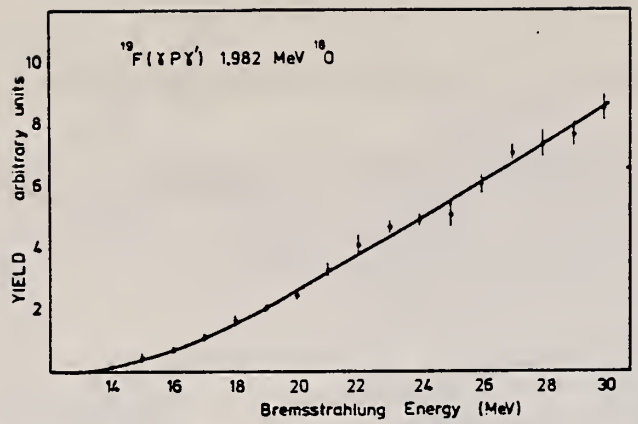

Fig. 2a. The yield curve for the photoreaction $^{19}F(\gamma, p)$ to the 1.982 MeV state in ^{18}O

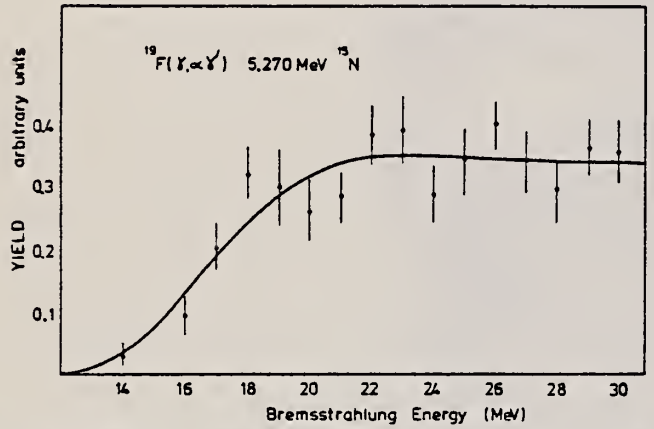

Fig. 2b. The yield curve for the photoreaction $^{19}F(\gamma, \alpha)$ to the 5.270 MeV state in ^{15}N.

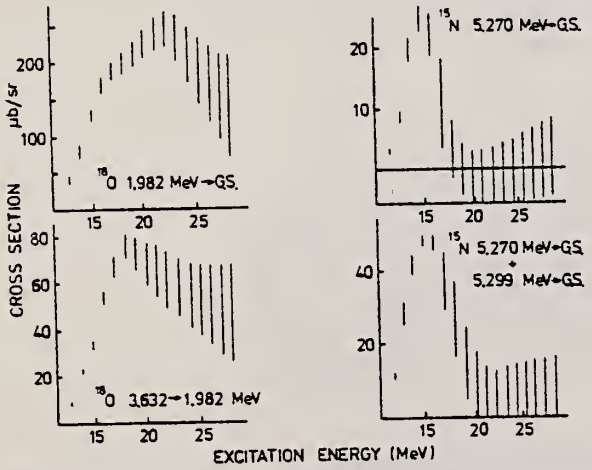

Fig. 3. Cross sections for photoreactions in ^{19}F leading to the emission of the de-excitation γ-rays indicated. No corrections for feeding from higher states has been made to those data.

REF. J.R. Calarco, P.M. Kurjan, G.A. Fisher, S.S. Hanna
Phys. Lett. 92B, 67 (1980)

ELEM. SYM.	A	Z
F	19	9

METHOD

REF. NO. 80 Ca 4 hg

REACTION	RESULT	EXCITATION ENERGY	SOURCE TYPE	SOURCE RANGE	DETECTOR TYPE	DETECTOR RANGE	ANGLE
$ P,G	ABX	15-23	D	3-10	NAI-D		DST

$ POLARIZED PROTONS

The striking intermediate structure observed in the giant E1 resonance of ^{20}Ne has been studied with the polarized and unpolarized ^{19}F(p, γ_0)^{20}Ne reaction. A heuristic model of four intermediate doorway resonances is found to fit the data.

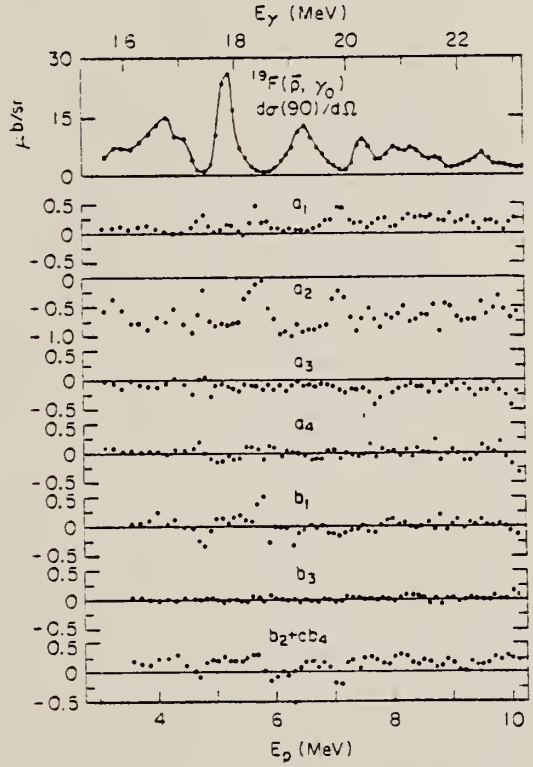

Fig. 1. Shown from the top to bottom are the observed differential cross sections of ^{19}F(p, γ_0)^{20}Ne at 90° along with the angular distribution coefficients discussed in the text.

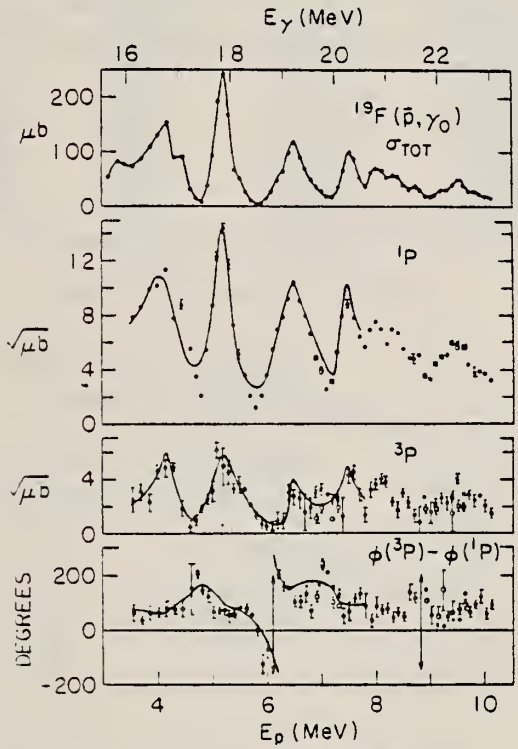

Fig. 2. Shown from top to bottom are the extracted total (p, γ_0) cross sections, the ^{1}P and ^{3}P amplitudes, normalized so that $|^1P|^2 + |^3P|^2 = \sigma(p, \gamma_0)$, and the relative phase. To keep the plotted values of these phases between $\pm\pi$ they are changed by 2π at the discontinuity. Indefinite values are indicated by the vertical double arrows. The top curve is simply drawn through the points. The other curves are fits obtained with the four-resonance model discussed in the text.

REF. M. Yagi, R. Amano
Int. J. Applied Radiat. Isotopes 31, 559 (1980)

ELEM. SYM.	A	Z
F	19	9

METHOD

REF. NO.	
80 Ya 2	hg

REACTION	RESULT	EXCITATION ENERGY	SOURCE		DETECTOR		ANGLE
			TYPE	RANGE	TYPE	RANGE	
G,F18	YLD	THR-60	C	30-60	ACT-I		4PI

The production rates of ^{18}F by the $^{20}Ne(\gamma, pn)^{18}F$ plus $^{20}Ne(\gamma, 2n)^{18}Ne \rightarrow {}^{18}F$, $^{23}Na(\gamma, \alpha n)^{18}F$, and $^{19}F(\gamma, n)^{18}F$ reactions were determined as a function of the maximum bremsstrahlung energies between 30 and 60 MeV. In addition, a simple and fast method to prepare anhydrous $H^{18}F$ was studied by using KHF_2 target.

TABLE I. Photonuclear reactions for ^{18}F production

Target nuclide (abundance, %)	Reaction type	Threshold energy (MeV)	Product nuclide
^{20}Ne (90.51)	$(\gamma, 2n)$	28.50	$^{18}Ne \rightarrow {}^{18}F$
^{21}Ne (0.27)	$(\gamma, 3n)$	35.27	$^{18}Ne \rightarrow {}^{18}F$
^{22}Ne (9.22)	$(\gamma, 4n)$	45.63	$^{18}Ne \rightarrow {}^{18}F$
^{20}Ne (90.51)	(γ, pn)	23.26	^{18}F
^{21}Ne (0.27)	$(\gamma, p2n)$	29.93	^{18}F
^{22}Ne (9.22)	$(\gamma, p3n)$	40.38	^{18}F
^{23}Na (100)	$(\gamma, \alpha n)$	20.89	^{18}F
^{19}F (100)	(γ, n)	10.43	^{18}F

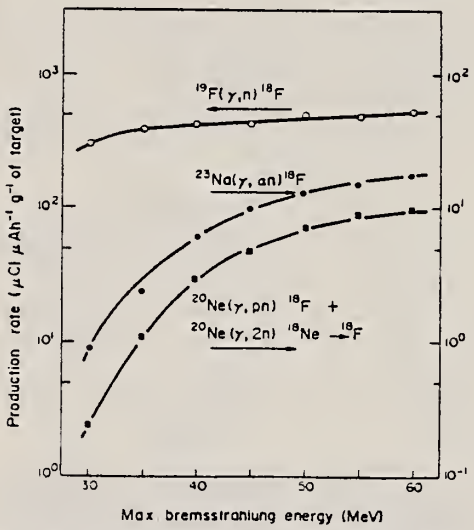

FIG. 1. Production rates of ^{18}F on Ne, Na and F targets as a function of the maximum bremsstrahlung energy.

F
A=20

F
A=20

F
A=20

REF. I. Bergqvist, J. A. Biggerstaff, J. H. Gibbons, W. M. Good
Phys. Rev. 158, 1049 (1967)

ELEM. SYM.	A	Z
F	20	9

METHOD

REF. NO.: 67 Be 7 egf

REACTION	RESULT	EXCITATION ENERGY	SOURCE		DETECTOR		ANGLE
			TYPE	RANGE	TYPE	RANGE	
N,G	LFT	6-7	D	0-1	NAI-D	0-7	90

SOURCE 27,50 KEV

TABLE I. Gamma rays from $^{19}F(n,\gamma)^{20}F$; $E_n = 27$ keV, $J^\pi = 2^-$.

E_γ (MeV)	I_γ (per 100 captures)	Assignment	$J_i^\pi \rightarrow J_f^\pi$	Γ_{γ_i} (meV)	$1000\|M\|^2$
5.98	6±2	$C \rightarrow 0.65$	$2^- \rightarrow (2,3)^+$	65	0.6
5.31	32±2	$C \rightarrow 1.31$	$2^- \rightarrow 2^+$	350	4.6
4.66	50±2	$C \rightarrow 1.97 (C \rightarrow 1.85)$	$2^- \rightarrow ?, (2^- \rightarrow ?)$	550	11
(4.09)[a]	(4)	$(4.08 \rightarrow 0)$	$[(0,1)^+ \rightarrow 2^+]$		
3.5	4±2	$(3.5 \rightarrow 0)$			
3.1	8±1	$(C \rightarrow 3.55, 3.49, 3.59)$		(90)	
2.60	5±2	$C \rightarrow 4.08$	$[2^- \rightarrow (0,1)^+]$	55	6
1.98	8±3	$1.97 \rightarrow 0$	$? \rightarrow 2^+$		
1.85	15±4	$1.85 \rightarrow 0$	$? \rightarrow 2^+$		
1.32	57±2	$1.31 \rightarrow 0$ $1.97 \rightarrow 0.65$	$2^+ \rightarrow 2^+$ $? \rightarrow (2,3)^+$		
1.15	16±2	$1.97 \rightarrow 0.83$	$? \rightarrow (1.2,3)^+$		
(0.95)[a]	(4)	$(1.06 \rightarrow 0, 0.99 \rightarrow 0)$			
0.84	4±2	$0.83 \rightarrow 0$	$(1,2,3)^+ \rightarrow 2^+$		
0.65	~30	$0.65 \rightarrow 0$	$(2,3)^+ \rightarrow 2^+$		

[a] Parentheses imply marginal credibility.

TABLE II. Gamma rays from $^{19}F(n,\gamma)^{20}F$; $E_n = 50$ keV, $J^\pi = 1^-$.

E_γ (MeV)	I_γ (per 100 captures)	Assignment	$J_i^\pi \rightarrow J_f^\pi$	Γ_{γ_i} (meV)	$1000\|M\|^2$
6.60(?)	5±3	$C \rightarrow 0$	$1^- \rightarrow 2^+$	80	0.6
6.0	9	$C \rightarrow 0.65$	$1^- \rightarrow (2,3)^+$	~140	~1.3
5.6	13 ; 34±3	$C \rightarrow$ 0.83 / 0.99 / 1.06		(~200)	
5.35	12	$C \rightarrow 1.31$	$1^- \rightarrow 2^+$	~190	~2.5
4.60	42±2	$C \rightarrow 2.05$ $(C \rightarrow 1.97$ weak)	$1^- \rightarrow (1,2,3)^+$	670	14
3.7 3.5	13±3	(3.59) 3.53 $\rightarrow 0$ (3.49)			
3.09	20±2	$(C \rightarrow 3.59, 3.53)$		(320)	
2.5–2.6	7±3	3.59 / 3.53 / 3.49 $\rightarrow$ 1.06 / 0.99 / 0.83			
2.1	8±3	$2.05 \rightarrow 0$	$(1,2,3)^+ \rightarrow 2^+$		
1.9	6±3				
1.38	37±3	$2.05 \rightarrow 0.65$ $(1.31 \rightarrow 0)$[b] $(1.97 \rightarrow 0.65)$	$(1,2,3)^+ \rightarrow 2^+$ $[2^+ \rightarrow 2^+][? \rightarrow (2,3)^+]$[b]		
1.15	3±2	$1.97 \rightarrow 0.83$			
1.06	7±3	$1.06 \rightarrow 0$	$(0,1)^+ \rightarrow 2^+$		
0.9–1.0	6±3				
0.65	≳30	$0.65 \rightarrow 0$	$(2,3)^+ \rightarrow 2^+$		

[a] Unresolved structure. [b] Parentheses imply marginal credibility.

NEON
Z=10

Neon (Greek *neos*, new) was discovered by Sir William Ramsay (1852-1916), and his assistant Morris William Travers. Argon and helium had been discovered with atomic weight of 40 and 4 respectively; Ramsay thought there might be an intermediate gas with an atomic weight of 20. Ramsay and Travers tried, unsuccessfully, to find this gas by heating rare minerals. The rare gases could not be detected by chemical means since they are inert and they could not be detected by spectroscopy because of their high dilution in air. It was first necessary for them to remove the carbon dioxide, oxygen, and nitrogen by chemical means. Next they liquified and then solidified the argon by surrounding it with liquid air under reduced pressure. They then allowed the argon to volatize and collected the portion that distilled off first. The vacuum tube containing this volatile fraction of gas was subject to the Plücker tube for spectroscopic analysis. The blaze of crimson light (now so familiar to us as the light from a neon tube) convinced them that they had discovered a new gas.

Ne

Ne

REF. G. Ferguson, J. Halpern, R. Nathans, and P.F. Yergin
Phys. Rev. 95, 776 (1954)

ELEM. SYM.	A	Z
Ne		10

METHOD

REF. NO. 54 Fe 1 rs

REACTION	RESULT	EXCITATION ENERGY	SOURCE		DETECTOR		ANGLE
			TYPE	RANGE	TYPE	RANGE	
G,SN	ABX	10-25	C	11-25	BF3-I		4PI

The direct detection of neutrons from (γ,n) reactions induced by betatron bremsstrahlung has been applied to cross-section determinations using gaseous targets at approximately 100 atmospheres pressure. Results from oxygen are consistent with other determinations. The remaining elements represent new results and show the familiar giant dipole resonance for the photoneutron process. Parameters of the resonances are determined and related to the systematic behavior previously reported for other elements.

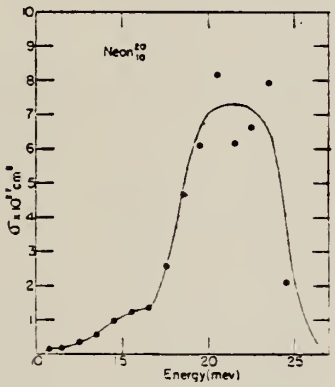

FIG. 8. Photoneutron excitation function for neon.

[1] Horsley, Haslam, and Johns, Phys. Rev. 87, 756 (1952).
[2] R. Nathans and J. Halpern, Phys. Rev. 92, 940 (1953).

REF.
D. Reagan
Phys. Rev. 100, 113-120 (1955)

Ne		10

METHOD
Linac; counted delayed neutrons from N^{17}

REF. NO.
55 Re 1

NVB

REACTION	RESULT	EXCITATION ENERGY	SOURCE		DETECTOR		ANGLE
			TYPE	RANGE	TYPE	RANGE	
G,N17	ABI	THR - 400	C	90-400	ACT-I		4PI

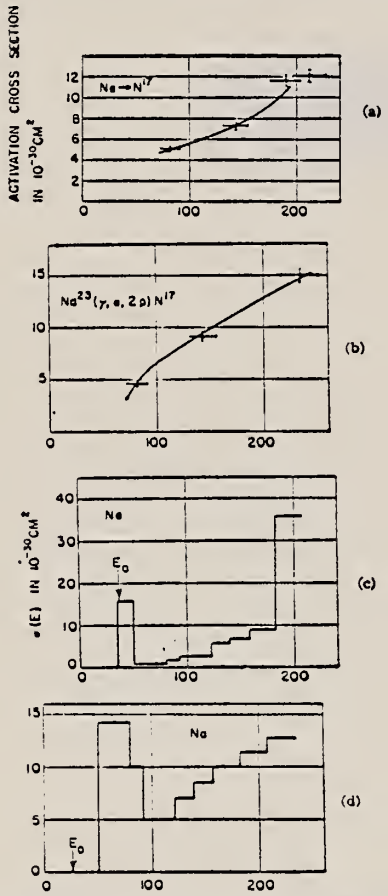

FIG. 4. Experimental N^{17} activation points for neon and sodium are plotted in the upper graphs. The lower graphs are the photon cross sections, which were calculated as indicated in the text. The activation cross sections indicated by the solid lines are reconstructions from the photon cross sections shown. The photon cross sections for energies below 80 Mev were chosen arbitrarily.

Ref. A.P. Komar, I.P. Iavor
Zhur. Eksp. i Teoret. Fiz. 32, 614 (1957)
Soviet Phys. JETP 5, 508 (1957)

Elem. Sym.	A	Z
Ne		10

Method: Cloud chamber at 1.4 atm; 80 MeV synchrotron

Ref. No.: 57 Ko 1 | EGF

Reaction	E or ΔE	E_o	Γ	$\int \sigma dE$	Jπ	Notes
Ne (γ,p)	Bremss					For E_p(1-15 MeV), $\frac{d\sigma}{dr} = a+b \sin^2 \theta$,
Ne(γ,pn)	80					$b/a \simeq 2.5$
Ne(γ,2p)						$\int\sigma_{(\gamma,p)} = 0.16\pm0.08$ MeV-b based on
Ne(γ,2α)						Gaerttner and Yeater [Phys. Rev. 83,
Ne(γ,αp)						146 (1951)].
Ne(γ,5α)						

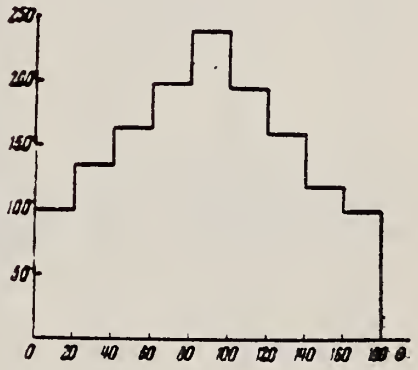

(γ,p)

The number of observed cases for the separate types of reactions is as follows:

Type of disintegration:	(γp)	(γpn)	(γ2p)	(γ2α)	(γαp)	(γ5α)
Number of cases:	352	137	64	21	143	2

Ref. W. R. Dodge, W. C. Barber
Phys. Rev. 127, 1746 (1962)

Elem. Sym.	A	Z
Ne		10

Method: Magnetic analysis of proton spectron produced by eletron bombardment

Ref. No.: 62Do1

BG

Reaction	E or ΔE	E_o	Γ	$\int \sigma dE$	Jπ	Notes
((e,p))	18-30	3.20 3.70 4.58 5.80 6.65 7.75 8.65 9.40 11.40 (see Table V)	0.50 0.58 0.54 0.49	11.4 11.1 7.6 6.1 (see Table VI) 65^{+13}_{-10}) $^{27}_{16}$ * Calculated assuming 100% ground state transitions		Correspondence between (e,pe') reaction and (γ,p)reaction; assumed electron has associated with it a virtual photo spectrum. Electron production yields analyzed by use of E1 virtual photon spectrum to obtain σ (γ,p). Angular distribution of proton measured. Target 90.9% Ne^{20} Angular distribution of proton produced by photon assumed to be $A' + B' \cos\theta + C' \sin^2\theta + \ldots$

797

TABLE VI. Summary of the properties of the major Ne peaks.

Proton energy of peak (MeV)	Photon energy of peak (MeV)	Peak height at 76° (mb/sr)	Photon width at half-height (MeV)	$\int \sigma(\gamma,p)dE_\gamma$ under resonance curve (MeV-mb)	$\% \int_{16}^{27} \sigma(\gamma,p)dE_\gamma$
4.58	17.70	1.45	0.50	11.4	19.0
5.80	18.87	1.11	0.58	11.1	16.7
6.65	19.87	0.90	0.54	7.6	12.7
7.75	21.02	0.77	0.49	6.1	10.3
				Total 36.2	58.9

TABLE V. Summary of the excitation characteristics of the Ne protons.

Proton energy (MeV)	Ground state transition energy (MeV)	Experimental threshold (MeV)	Electron energy at which a deviation from an E1 isochromat occurs (MeV)	Branching ratio (%)	Energy of excited state (MeV)
4.56	17.68	17.7±0.3	21.8±0.5	17±8	4.1±0.5
5.20	18.35	19.4±0.6	21.8±0.7; $27.8_{-1}^{+1.2}$	25±5; 39±10	3.5±0.7; $9.5_{-1}^{+1.2}$
5.57	18.74	19.5±0.7	...	...	...
5.81	18.99	19.6±0.6	...	...	...
6.74	19.97	20.0±0.4	...	...	...
7.22	20.47	20.4±0.4	...	...	...
7.77	21.00	21.4±0.5	29.8±1	26±10	8.8±1
8.30	21.61	21.9±0.5	26.0±1	29±10	4.4±1
8.72	22.05	22.3±0.5	26.5±1	29±10	4.5±1
9.20	22.56	23.0±0.6	28.2±1.5	29±10	5.2±1.5
9.49	22.86	23.0±0.5	27.6±1.5*	...	4.7±1.5*
9.86	23.25	23.6±0.6	...	...	...

* Slight evidence.

(See page 2 for figures)

Ref. W. R. Dodge, W. C. Barber
Phys. Rev. 127, 1746 (1962)

Elem. Sym.	A	Z
Ne		10

Method

Magnetic analysis of proton spectrum produced by electron bombardment

Ref. No. 62 Do 1 BG

Reaction	E or ΔE	E_0	Γ	$\int \sigma dE$	Jπ	Notes

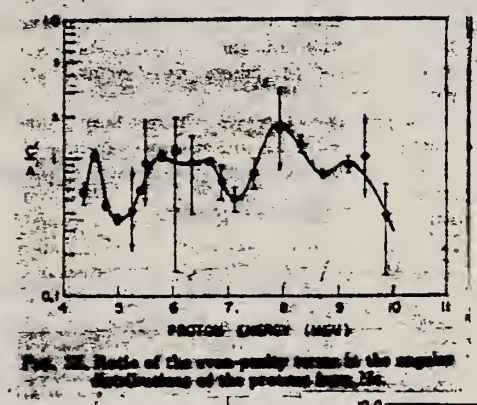

Fig. 33. Ratio of the even-parity terms to the angular distributions of the protons from Ne.

Fig. 18. Neon (e,pe') cross section at $E_0=30$ MeV and $\theta=76°$, under the assumption of 100% ground-state transitions.

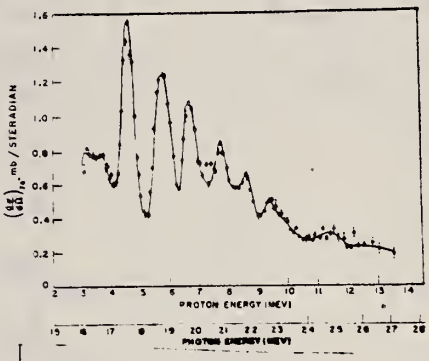

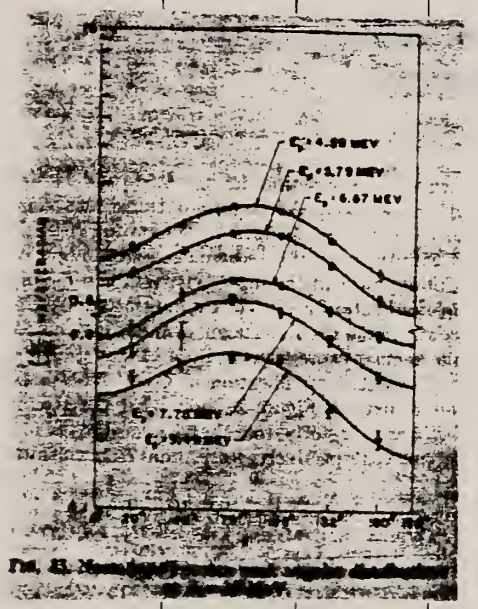

Fig. 34. Ne (e,p_0') proton angular distributions from the low- and high-energy sides of the peaks at $E_0=30$ MeV.

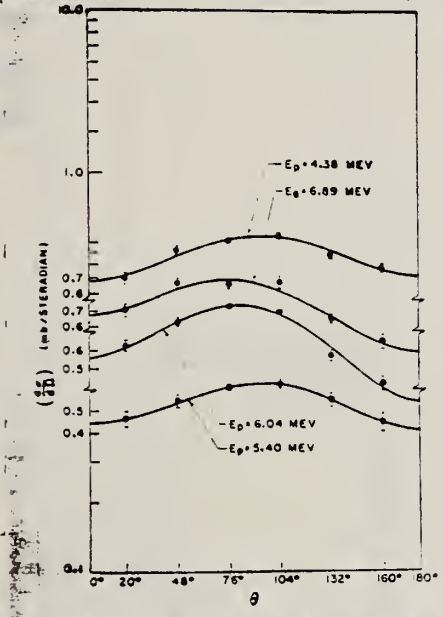

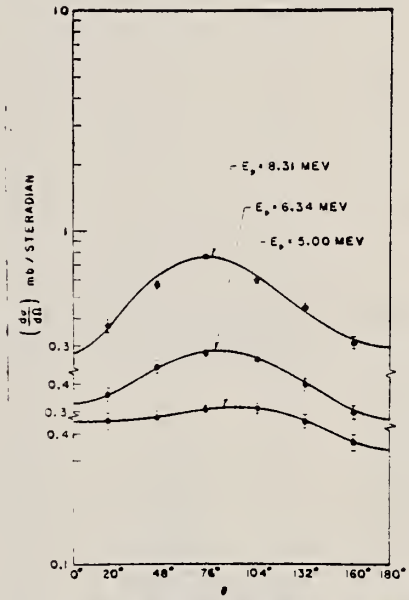

G. 35. Neon (e,p_0') proton valley angular distributions at $E_0=30$ MeV.

Ref. L.E.Sarkisov, V.A.Zaborenkin, V.A.Osipova, V.I.Silaeva, P.A.Cherenkov
Zhur.Eksptl. i Teoret.Fiz. 42, 787 (1962);
Soviet Phys. JETP 15, 550 (1962)

Elem. Sym.	A	Z
Ne		10

Method: synchrotron - cloud chamber

Ref. No.: 6281 | BG

Reaction	E or ΔE	E_o	Γ	∫σdE	Jπ	Notes
(γ,p)	$E_{\gamma max}$=		$165)^{170}_{0}$	MeV-mb		$\sigma_{-1} = \int \sigma(E) E^{-1} dE$ (Table IV)
(γ,n)	170		$115)^{170}_{0}$			$\sigma_{-2} = \int \sigma(E) E^{-2} dE$ (Table IV)
(γ,pn)			$66)^{170}_{0}$			Absolute value of yields given in the article.
(γ,d)			$6)^{170}_{0}$			(γ,n) and (γ,2n) could not be distinguished - all were taken to be (γ,n); similarly (γ,p) and (γ,d) were all taken to be (γ,p).
(γ,pα)			$38)^{170}_{0}$			Charge distribution parameters were determined.
(γ,Hyp)			$600)^{170}_{0}$			

Table I

Reaction	Reaction Threshold, MeV			Reaction	Reaction Threshold, MeV		
	N	O	Ne		N	O	Ne
(γ, n)	10.54	15.60	16.79	(γ, 2α)	16.06	—	11.92
(γ, p)	7.54	12.11	12.79	(γ, pαn)	19.86	34.56	27,61
(γ, d)	19.26	20.72	20.99	(γ, 2pn)	28.44	30.68	28.81
(γ, t)	11.61	7.15	4.67	(γ, 2αn)	—	—	30.53
(γ, pn)	12.49	22.34	23.22	(γ, 4α)	—	14.43	
(γ, 2n)	20.05	25.86	20.26	(γ, 3αpn)	19.77	—	
(γ, pα)	18.20	23.10	16.78	(γ, 2p2n3α)	—	42.71	
(γ, 2p)	25.08	22.32	20.76				

Table IV

Reaction type	σ_0, MeV-mb				σ_{-1}, mb				σ_{-2}, mb·MeV^{-1}			
	He^4	N^{14}	O^{16}	Ne	He^4	N^{14}	O^{16}	Ne	He^4	N^{14}	O^{16}	Ne
(γ, p)	38	38	129	165	1.09	2.5	5.3	6.5	0.035	0.14	0.22	0.25
(γ, n)	44	31	105	115	1.09	1.5	3.4	3.5	0.031	0.06	0.11	0.10
(γ, pn)	12	128	59	66	0.18	5.1	1.3	1.4	0.003	0.18	0.03	0.03
(γ, t)	—	9	4	6	—	0.3	0.3	0.6	—	0.01	0.02	0.07
(γ, 2n)	—	5	15	38	—	0.1	0.3	1.0	—	0.003	0.005	0.02
Stars:												
3-prong	—	53	71	151	—	1.2	1.4	4.2	—	0.03	0.03	0.12
4-prong	—	70	27	34	—	1.6	0.5	0.5	—	0.04	0.01	0.01
5-prong	—	14	23	15	—	0.2	0.3	0.2	—	0.002	0.003	0.003
6-prong	—	—	5	10	—	—	0.03	0.1	—	—	0.001	0.001
σ_{exp}*	95±7	347	438	600	2.40±0.15	12.5	12.8	18.0	0.07±0.005	0.48	0.43	0.60
σ_{theor}**	60	210	240	300	2.3	12.1	13.1	19.5	0.023	0.18	0.23	0.33
$\sigma_{exp}/\sigma_{theor}$	1.6	1.65	1.8	2.0	1.04	1.03	0.98	0.9	3.0	2.6	1.8	1.8

* σ_{exp}—experimental value of the integrated absorption cross sections σ_0, σ_{-1} and σ_{-2}.
** The theoretical values σ_{theor} have been calculated by means of the expressions: $\sigma_0 = 60(NZ/A)$MeV-mb; $\sigma_{-1} = 0.36\ A^{4/3}$ mb; $\sigma_{-2} = 2.25\ A^{4/3}$ μb·MeV^{-1}.

REF. B.N. Sung
J. Phys. Soc. Japan 17, 1811 (1962)

ELEM. SYM.	A	Z
Ne		10

METHOD Betatron; proton spectrum; cross section; nuclear emulsions

REF. NO.	
62 Su 1	NVB

REACTION	RESULT	EXCITATION ENERGY	SOURCE		DETECTOR		ANGLE
			TYPE	RANGE	TYPE	RANGE	
G,XP	SPC	16-23	C	23	EMU-D	2-13	90
				(23.5)			

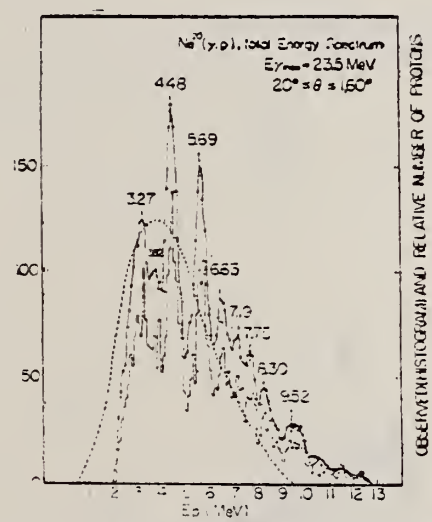

Fig. 1. Energy distributions of photoprotons from Ne^{20}. This histogram is for the total number of detected protons. The solid line is a smoothed curve by Valoshek's method. The broken line is a calculated curve using the statistical theory with Weisskopf's level density

$$w = C \exp[2\sqrt{0.245\,E}]\ \mathrm{MeV}^{-1}.$$

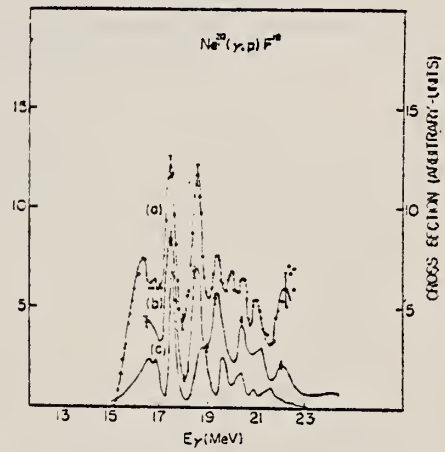

Fig. 2. Comparison of experiments for $Ne^{20}(\gamma, p)F^{19}$, $Ne^{20}(e, e'p)$ and $F^{19}(p, \gamma_0)$.

Curve (a)—present work, the observed energy spectrum is devided by number of photons, assuming all proton transitions are to the ground state of F^{19}.

Curve (b)—$Ne^{20}(e, e'p)$ by Dodge and Barber.

Curve (c)—$Ne^{20}(\gamma_0, p)$ reduced from $F^{19}(p, \gamma_0 + \gamma_1)$ using the detailed balance by Tanner and Thomas.

E. Finckh, R. Kosiek, K.H. Lindenberger, K. Maier,
U. Meyer-Berkhout, M. Schechter, J. Zimmerer
Z. Physik 174, 337 (1963)

Ne		10

METHOD
Betatron; proton spectrum, cross section; CsI spectrometer

REF. NO. 63 Fi 4 | NVB

REACTION	RESULT	EXCITATION ENERGY	SOURCE		DETECTOR		ANGLE
			TYPE	RANGE	TYPE	RANGE	
G,XP	SPC	15-29	C	31	SCI-D	2-15	90

796

Maxima: E_p = 3.5 MeV
= 3.95 MeV
= 4.65 MeV
= 5.8 MeV
= 7.1 MeV
= 7.7 MeV
= 8.5 MeV
= 9.3 MeV
= 11.25 MeV
= 12.4 MeV

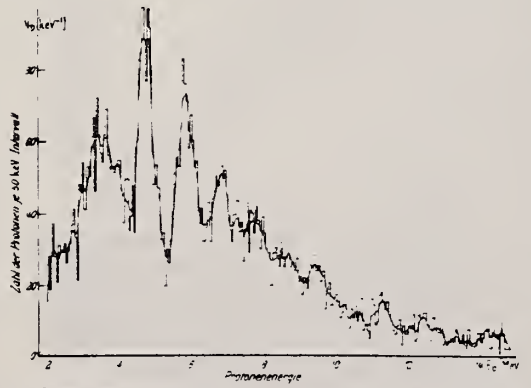

Fig. 7. Energieverteilung der Photoprotonen aus Neon. Das Histogramm stellt die auf Energieverlust korrigierten Meßwerte dar, die ausgezogene Kurve wurde nach einem Mittelungsverfahren gewonnen. Nähere Erläuterungen im Text

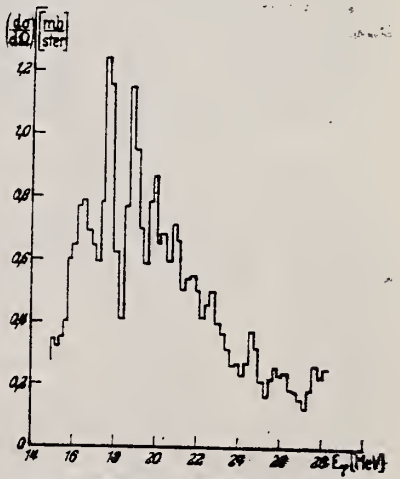

Fig. 8. Differentieller Wirkungsquerschnitt für Photoprotonenemission aus Neon unter 90° zum γ-Strahl unter der Annahme, daß nur Grundzustandsübergänge aus Ne^{20} in F^{19} vorliegen.

REF.

A. Veyssiere, H. Beil, R. Bergere, P. Carlos, A. Lepretre, and A. De Miniac
Nucl. Phys. A227, 513 (1974)

ELEM. SYM.	A	Z
Ne		10

METHOD

REF. NO.	
74 Ve 1	egf

REACTION	RESULT	EXCITATION ENERGY	SOURCE		DETECTOR		ANGLE
			TYPE	RANGE	TYPE	RANGE	
G,N *	ABX	16- 26	D	16- 26	BF3-I		4PI
G,2N **	ABX	18- 26	D	18- 26	BF3-I		4PI

* 869+
** 870+

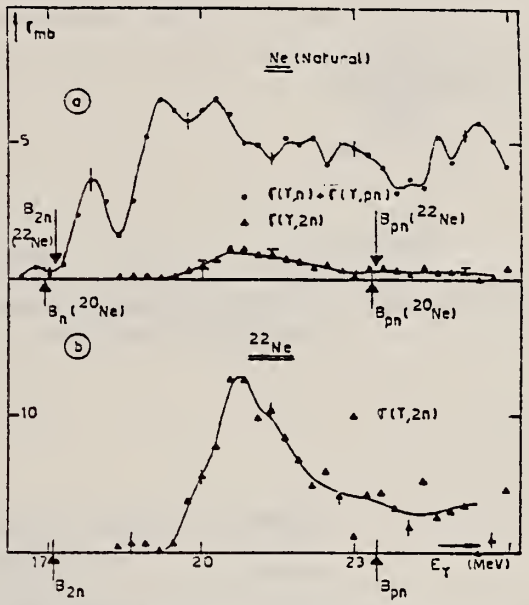

Fig. 4. (a) Photonuclear cross sections $[\sigma(\gamma, n)+\sigma(\gamma, pn)]$ and $\sigma(\gamma, 2n)$ for natural Ne. (b) Partial photoneutron cross section $\sigma(\gamma, 2n)$ of ^{22}Ne.

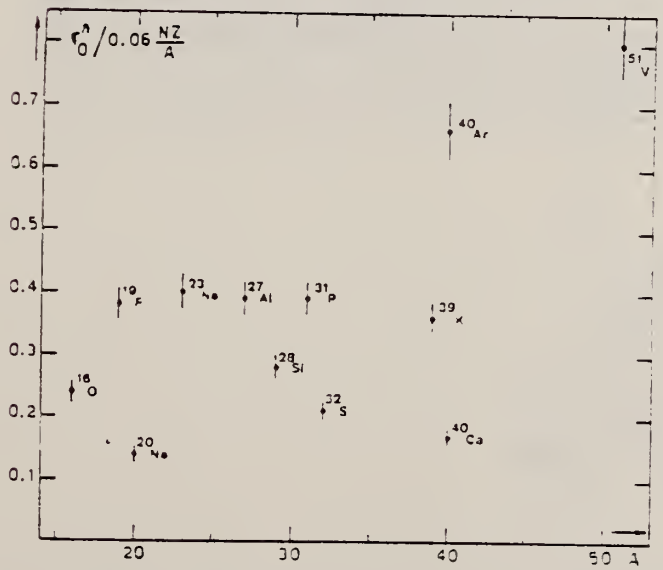

Fig. 22. Ratio of experimental integrated photoneutron cross section $\sigma_0{}^n$ over the Thomas, Reiche and Kuhn sum rule $[0.06\ NZ/A]$. Numerical values and upper integration limits E_M are taken from table 3. Also $\Delta\sigma_0{}^n = \pm 7\%$ for all nuclei.

(over)

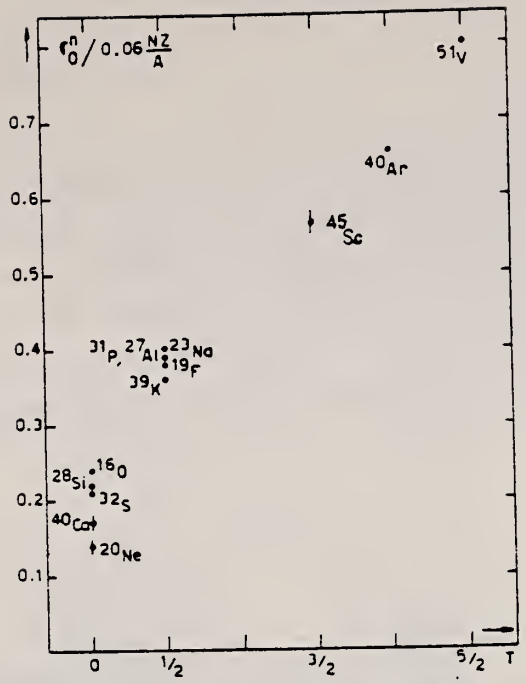

Fig. 24. The $[\sigma_0^n/(0.06\,NZ/A)]$ ratio as a function of isospin T. Possible overall errors of $\pm 7\%$ are to be applied to all nuclei shown.

TABLE 3

Experimental integrated photoneutron cross sections $\sigma_0^n = \int_0^{E_M} \sigma_{Tn}(E)\mathrm{d}E$ compared with the classical sum rule $[0.06\,NZ/A]$ of Thomas, Reich and Kuhn

	$T=0$					$T=\frac{1}{2}$					$T=\frac{3}{2}$	$T=2$	$T=\frac{5}{2}$
Nucleus	^{16}O	^{20}Ne	^{28}Si	^{32}S	^{40}Ca	^{19}F	^{23}Na	^{27}Al	^{31}P	^{39}K	^{45}Sc	^{40}Ar	^{51}V
σ_0^n (MeV · mb)	58 ±4	42 ±3	94 ±7	98 ±7	100 ±7	108 ±7	137 ±9	158 ±10	182 ±12	210 ±14	383 ±25	393 ±28	602 ±42
$\sigma_0^n/(0.06NZ/A)$	0.24	0.14	0.22	0.21	0.17	0.38	0.40	0.39	0.39	0.36	0.57	0.66	0.8
E_M (MeV)	30	26.7	30	30	29.5	29	30	30	29	30	28.1	26.7	2[illegible]

REF. J. G. Woodworth, J. W. Jury, K. H. Lokan, N. K. Sherman
Can. J. Phys. 53, 795 (1975)

ELEM. SYM.	A	Z
Ne		10

METHOD

REF. NO. 75 Wo 3 hmg

REACTION	RESULT	EXCITATION ENERGY	SOURCE TYPE	SOURCE RANGE	DETECTOR TYPE	DETECTOR RANGE	ANGLE
G,N	ABX	17- 31	C	19- 32	TOF-D		90

NORMALIZED TO D(G,N)

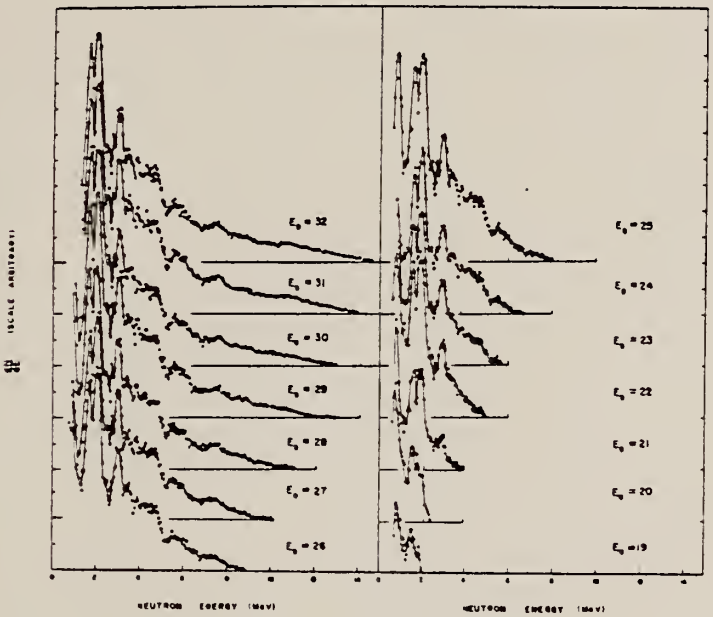

FIG. 3. Photoneutron spectra from ^{20}Ne.

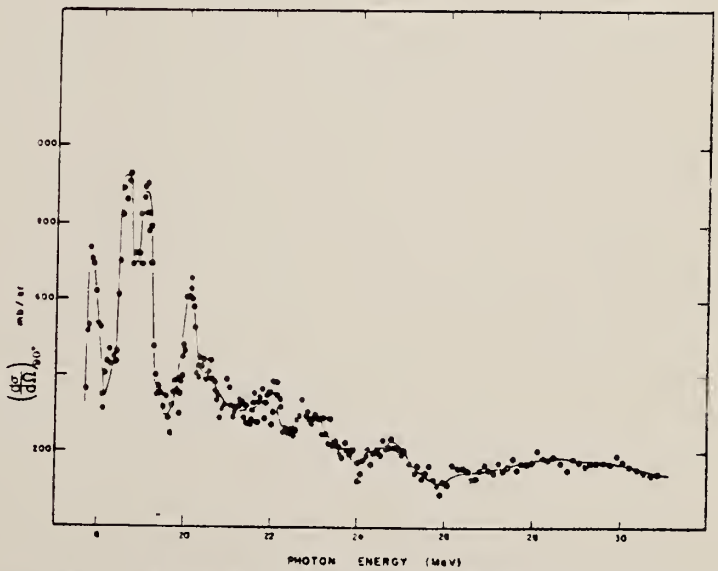

FIG. 5. The cross section for the reaction ^{20}Ne($\gamma, n_0 + n_1 + n_2$)^{19}N.

N_E
A=20

N_E
A=20

Ref. H.J. Hay, J.B. Warren
Can. J. Phys. 37, 1153 (1959)

Elem. Sym.	A	Z
Ne	20	10

Method: 500 keV Cockcroft-Walton cascade generator; photodisintegration; $Li^7(p,\gamma)$ reaction.

Ref. No.: 59 Ha 1 EH

Reaction	E or ΔE	E_o	Γ	$\int \sigma dE$	Jπ	Notes
						Cross Section — State
$Ne^{20}(\gamma,\alpha)$	17.63					0.05 mb — ground state O^{16}
						0.67 mb — 6.06 + 6.19
						1.80 mb — 6.91 + 7.12
	14.8					0.086 mb — ground state
						~ 1.0 mb — 6.06 + 6.14
$Ne^{20}(\gamma,2\alpha)$	17.6					
	14.8					
$Ne^{20}(\gamma,\alpha p)$						
$Ne^{20}(\gamma,p)$	17.6					21 mb — ground state and low levels at 0.100, 0.197 MeV
						~ 5 mb — 1.35 + 1.57
	14.8					

REF.

C. Broude, H.E. Gove
PICNS, 754 (1960)

Ne	20	10

METHOD

Tandem van de Graaff; inverse; NaI spectrometer

REF. NO. 60 Br 1 | NVB

REACTION	RESULT	EXCITATION ENERGY	SOURCE TYPE	SOURCE RANGE	DETECTOR TYPE	DETECTOR RANGE	ANGLE
P,G	RLY	17-23	D	4-11	NAI-D		0KN
		(16.9-22.9)					

873+

Peaks: 18.1 MeV
19.4 MeV
20.45 MeV
21.2 MeV
22.2 MeV

All have
$\Gamma \approx 350$ keV

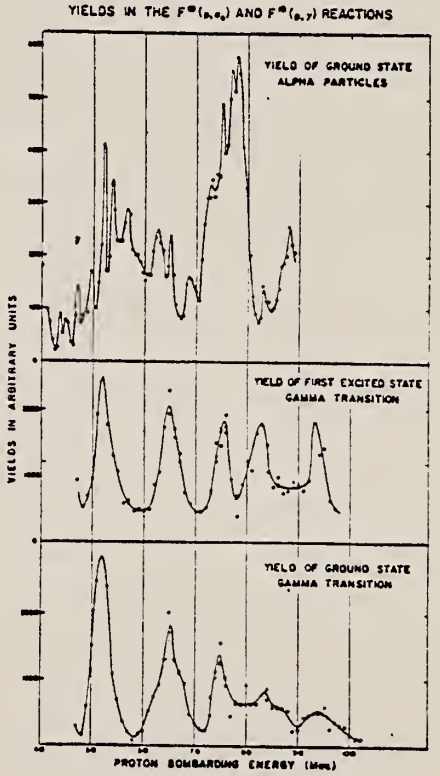

Fig. 1:

REF.

J. M. Reid and B. Lalovic
Proc. Phys. Soc. (London) 76, 65 (1960)

ELEM. SYM.	A	Z
Ne	20	10

METHOD

REF. NO. 60 Re 2 EGF

REACTION	RESULT	EXCITATION ENERGY	SOURCE		DETECTOR		ANGLE
			TYPE	RANGE	TYPE	RANGE	
G,XP	RLY	100-240	C	240	CCH		

185 events (γ,p) (γ,pn). Recorded only events where proton with $20 \leq E \leq 120$ MeV was emitted.

REF.

M. A. Clark, H. E. Gove and A. E. Litherland
Proc. Ruth. Int. Conf. Manchester 807 (1961)

ELEM. SYM.	A	Z
Ne	20	10

METHOD

Doppler-Shift Attenuation Method

REF. NO.	
61 Cl 1	JDM

REACTION	RESULT	EXCITATION ENERGY	SOURCE		DETECTOR		ANGLE
			TYPE	RANGE	TYPE	RANGE	
G,G	LFT	1-3	D	1-3	NAI-D	1-3	0

TABLE I

Lifetimes obtained for the first three excited states in Ne^{20} using the Doppler shift attenuation technique. α is the characteristic slowing down time for the target backings listed and $|M|^2$ is the ratio of the measured gamma-ray transition probability to the Weiskopf value.

Level (MeV)	1·63	4·25	4·97	
E_γ (MeV)	1·63	2·62	3·34	
Slowing materials	Mg, Al	Al, Cu	Mg, Al	
α (10^{-13} sec)	8·9, 5·9	5·9, 2·9	8·9, 5·9	
$\tau_{exp.}$ (10^{-13} sec)	$5{\cdot}6 \pm {}^{2{\cdot}8}_{1{\cdot}2}$	$0{\cdot}76 \pm {}^{0{\cdot}72}_{0{\cdot}52}$	$19 \pm {}^{35}_{10}$	
Assumed multipolarity	$E2$	$E2$	$M1, E2$	$E1, M2$
$\lvert M \rvert^2$	38	26	$4{\cdot}4\times10^{-4}$, $1{\cdot}6\times10^{-3}$,	$1{\cdot}6\times10^{-5}$, $3{\cdot}3\times10^{-5}$

Ref.	Elem. Sym.	A	Z
R.C.Barber, J.Goldemberg, S.A.Petersen, Y.Torizuka Nuclear Phys. 41, 461 (1963); erratum to be published (as of 9/9/63)	Ne	20	10

Method	Ref. No.
Linac (Stanford Mark II) - counter telescope	63Bal 25

Reaction	E or ΔE	E_o	Γ	$\int \sigma dE$	Jπ	Notes
			eV			Inelastic electron scattering cross section at 180°(cm^2/sr x10^{-32})
(e,e')	41.5					
		~9	7.1	0.9		3.0±20%
		~13	16.6	1.0		2.0±20%
						The rad. widths correspond to transitions from the 0^+ state to 1^+ excited states.

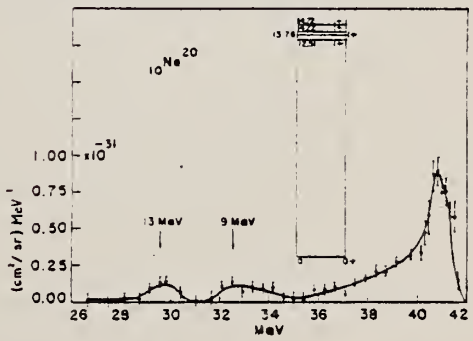

ig. 10. Spectrum of 41.5 MeV electrons scattered from a neon gas target at 180°.

REF.	ELEM. SYM.	A	Z
R.G. Allas, S.S. Hanna, L. Meyer-Schützmeister, R.E. Segel, P.P. Singh, and Z. Vager Phys. Rev. Letters 13, 628 (1964)	Ne	20	10

METHOD	REF. NO.	
$Al^{27}(p,\gamma_o)Si^{28}$; tandem	64 Al 3	JOC

REACTION	RESULT	EXCITATION ENERGY	SOURCE		DETECTOR		ANGLE
			TYPE	RANGE	TYPE	RANGE	
P,G	NØX	17 - 22	D	4 - 9	NAI-D		DST

Table I. Summary of experimental results on the (p,γ) giant resonance (references 9-11). The angular distributions that are quoted generally characterize the data to within 15% throughout the giant-resonance region.

Nucleus	Type of observation	Energy interval and range	Result
C^{12}	90° yield curve	50-keV steps 4.0-14 MeV	Broad ($\Gamma \approx 1$ MeV) overlapping levels; no correlation between γ_0 and γ_1.
	Angular distribution[a]	50-keV steps 4.0-14 MeV	$W(\theta)_{\gamma_0} = 1 + 0.15P_1 - 0.6P_2$ $W(\theta)_{\gamma_1} = 1 + 0.15P_1$
Ne^{20}	90° yield curve	30-keV steps 4.3-9.1 MeV	Broad ($\Gamma \approx 400$ keV) levels usually well isolated, γ_0 and γ_1 well correlated.
	Angular distribution	100-keV steps 4.0-10.5 MeV	$W(\theta)_{\gamma_0} = 1 + 0.05P_1 - 0.7P_2$ $W(\theta)_{\gamma_1} = 1 + 0.05P_1 + 0.2P_2$
Si^{28}	90° yield curve	15-keV steps 4.0-12.5 MeV	Narrow ($\Gamma \approx 50$ keV) Ericson fluctuations, superimposed on intermediate structure; no correlation between γ_0 and γ_1.
	Angular distribution	15-keV steps 4.0-4.32 MeV 6.0-6.62 MeV 8.0-8.54 MeV 10.0-10.28 MeV 11.54-11.58 MeV	$W(\theta)_{\gamma_0} = 1 + 0.07P_1$ $W(\theta)_{\gamma_1} = 1 + 0.1P_1 - 0.45P_2 - 0.1P_3$

[a]The coefficients of P_1 are average values. They actually increase by about 0.03/MeV over the giant resonance.

N. W. Tanner, G. C. Thomas and E. D. Earle
Nucl. Phys. 52, 29-44 (1964)

Ne	20	10

METHOD $F^{19}(p,\gamma)Ne^{20}$

REF. NO. 64 Ta 1 JOC

REACTION	RESULT	EXCITATION ENERGY	SOURCE TYPE	SOURCE RANGE	DETECTOR TYPE	DETECTOR RANGE	ANGLE
P,G	ABX	17-24	D	4-11	NAI-D		90

40

At E_p = 5.25 MeV $\left.\frac{d\sigma\gamma_0}{d\Omega}\right|_{90}$ = 350±110 μb/4πsr

From detailed balance:

$$\int_{16.4}^{20.5} \sigma(\gamma,Po)dE\gamma = 28\pm9 \text{ MeV - mb}$$

Comparison with several other (p,γ) results

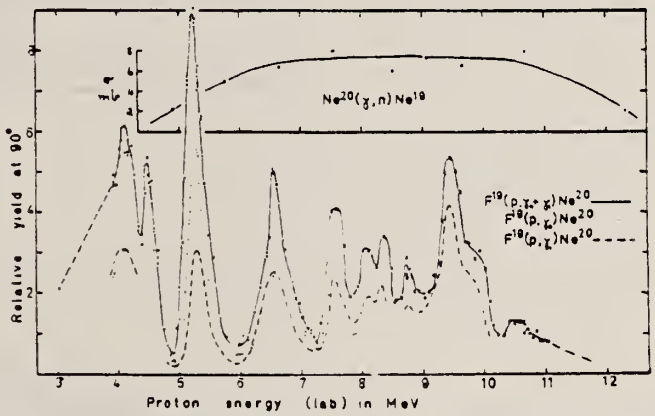

Fig. 4. The excitation function at 90° of $F^{19}(p, \gamma_1+\gamma_0)Ne^{20}$. The data shown in table 2 were used to sketch in the curves for γ_0 and γ_1 separately. The $Ne^{20}(\gamma, n)Ne^{19}$ data from ref. [8]) are shown, using an energy scale so that excitation energies in Ne^{20} correspond.

REF.

A.W. Parker, R.R. Whitehead, and G.G. Shute
Aust. J. Phys. 19, 147 (1966)

ELEM. SYM.	A	Z
Ne	20	10

METHOD

Cyclotron

REF. NO. 66 Pa 3 JDM

REACTION	RESULT	EXCITATION ENERGY	SOURCE		DETECTOR		ANGLE
			TYPE	RANGE	TYPE	RANGE	
P,G	NOX	17.8	D	5.2	SCI-D		DST

$W(\theta) \sim 1 + a_1 P_1 + a_2 P_2$

TABLE 1

ANGULAR DISTRIBUTIONS CORRECTED FOR SOLID-ANGLE EFFECTS, AND CROSS-SECTION RATIOS

E_p (MeV)	γ	a_1	a_2	Cross-section Ratio R
5·20	γ_0	$+0·18 \pm 0·03$	$-0·75 \pm 0·05$	$1·53 \pm 0·04$
	γ_1	$+0·05 \pm 0·01$	$+0·22 \pm 0·02$	
5·40	γ_0	$+0·10 \pm 0·03$	$-0·63 \pm 0·03$	$0·62 \pm 0·03$
	γ_1	$+0·11 \pm 0·04$	$+0·33 \pm 0·04$	

REF. R. E. Segel, Z. Vager, L. Meyer-Schutzmeister, P. P. Singh and R. G. Allas
Nucl. Phys. A93, 31 (1967)

ELEM. SYM.	A	Z
Ne	20	10

METHOD: Proton capture

[Page 1 of 2]

REF. NO.: 67 Se 1 | EGF

REACTION	RESULT	EXCITATION ENERGY	SOURCE TYPE	SOURCE RANGE	DETECTOR TYPE	DETECTOR RANGE	ANGLE
P,G	ABX	16-25	D	3-13	NAI-D		DST

131

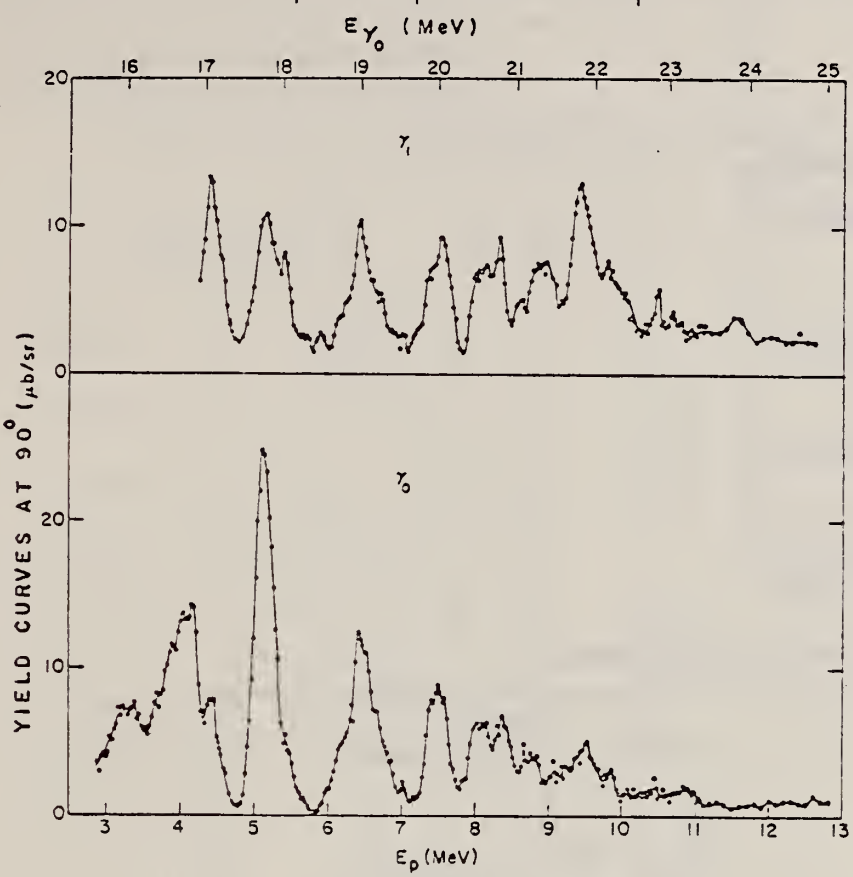

Fig. 5. Yield curves at 90° for $^{19}F(p, \gamma_0)^{20}Ne$ and $^{19}F(p, \gamma_1)^{20*}Ne$.

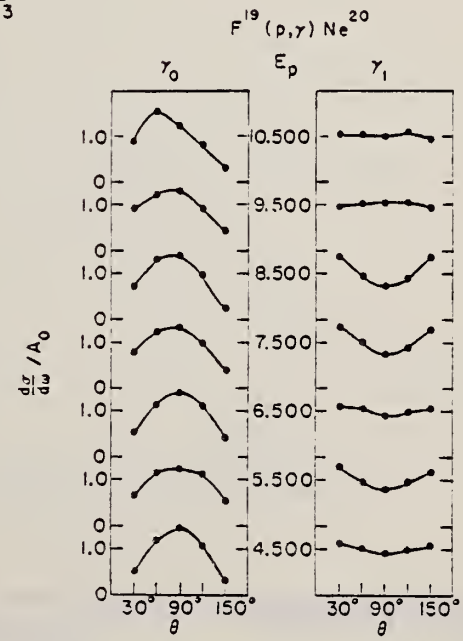

Fig. 8. Sample angular distributions for $^{19}F(p, \gamma_0)^{20}Ne$ and $^{19}F(p, \gamma_1)^{20*}Ne$.

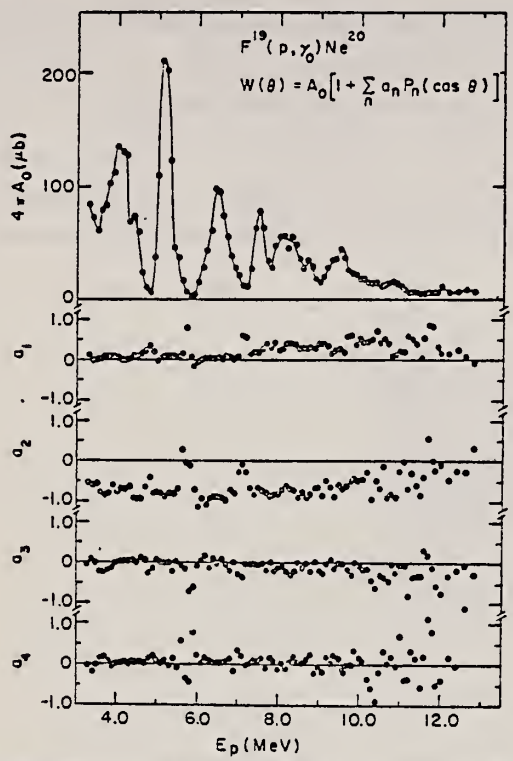

Fig. 9. Coefficients obtained in fitting series of Legendre polynomials to the angular distributions for $^{19}F(p, \gamma_0)^{20}Ne$.

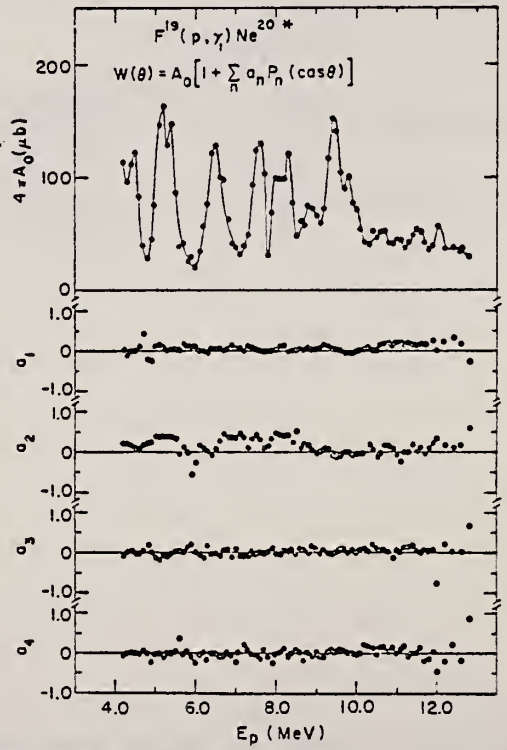

Fig. 10. Coefficients obtained in fitting series of Legendre polynomials to the angular distributions for $^{19}F(p, \gamma_1)^{20*}Ne$.

W. Hofmann, R. Kosiek, G. Kraft and R. Mundhenke
Z. Physik 225, 303 (1969)

Ne	20	10

METHOD

REF. NO. 69 Ho 1 egf

REACTION	RESULT	EXCITATION ENERGY	SOURCE		DETECTOR		ANGLE
			TYPE	RANGE	TYPE	RANGE	
G,XP	ABY	THR- 33	C	24-33	SCI-D	3-14	90

795

Tabelle 1. *Daten zu den einzelnen Reaktionen. Die Werte für den integrierten Wirkungsquerschnitt wurden unter der Annahme ausschließlicher Grundzustandsübergänge berechnet. Für ^{23}Na und ^{39}K als Ausnahme s. Text*

Target	Anreicherungsgrad %	(γ, p)-Schwelle MeV	Druck oder Dicke	Endenergie MeV	Zahl gemess. Protonen	Ausbeute µb/MeV sr	$\int_{32.5}\sigma(E)dE$ MeVmb	Figur
^{18}O	99	16,0	230 Torr	32,5	36074	58 ± 7	38 ± 6	1, 2
^{20}Ne	90,9	12,8	450 Torr	28,0	3175	7,4 ± 1	–	–
			610 Torr	32,5	6293	14,9 ± 2	61 ± 11	5, 6
^{22}Ne	99,9	15,3	240 Torr	24,0	1960	2,3 ± 0,4	–	4, 5
				28,0	4790	3,6 ± 0.6	–	4, 5
				32,5	5210	6,7 ± 0,9	45 ± 8	4, 5
^{23}Na	100	8,8	65µ	24,0	14182	6,3 ± 1,0	–	7
			60µ	32,5	11152	12,8 ± 2,0	117 ± 30	7
^{36}Ar	99	8,5	250 Torr	32,5	45173	57 ± 6	270 ± 40	8, 10
^{40}Ar	99,6	12,5	230 Torr	32,5	29559	14,2 ± 15	104 ± 15	9, 11
^{39}K	93,1	6,4	80µ	24,0	24230	17,4 ± 2,8	–	12
			90µ	32,5	24941	41,9 ± 6,7	405 ± 100	12
^{84}Kr	99	10,7	170 Torr	32,5	35515	12,7 ± 2,0	80 ± 20	14
Kr	natürl.	10	170 Torr	32,5	13570	12,5 ± 2,0	75 ± 20	13
Ne	natürl.	9	150 Torr	32,5	7553	7,6 ± 0,9	40 ± 7	15

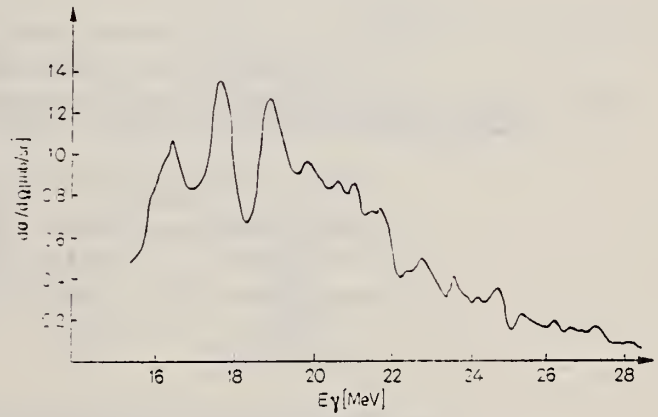

Fig. 5. Der (γ, p)-Wirkungsquerschnitt für ^{20}Ne

REF. W.L. Bendel, L.W. Fagg, S.K. Numrich, E.C. Jones, Jr., H.F. Kaiser
Phys. Rev. C3, 1821 (1971)

ELEM. SYM.	A	Z
Ne	20	10

METHOD

REF. NO.: 71 Be 1 hmg

REACTION	RESULT	EXCITATION ENERGY	SOURCE		DETECTOR		ANGLE
			TYPE	RANGE	TYPE	RANGE	
E,E/	ABX	11	D	39,56	MAG-D		180

11.23, 11.58 MEV

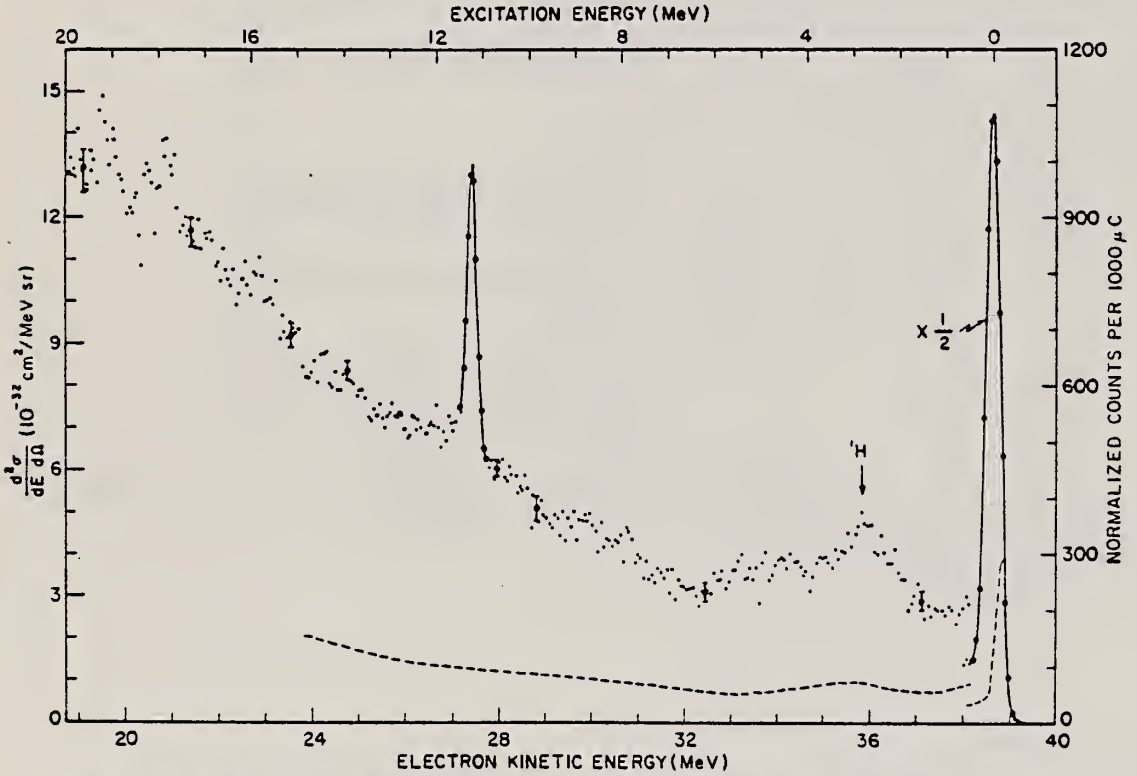

FIG. 2. Spectrum obtained by 180° scattering of 39-MeV electrons from ^{20}Ne. The dashed line shows the spectrum obtained with an evacuated chamber, in terms of counts per 1000 μC only.

TABLE I. Values of differential cross sections, spin and parity, transition radius, and radiation width for levels excited in ^{20}Ne, with DWBA corrections.

Level energy (MeV)	$(d\sigma/d\Omega)_{56}$ (10^{-34} cm^2/sr)	$(d\sigma/d\Omega)_{39}$ (10^{-34} cm^2/sr)	J^π	R (fm)	Γ_0 (eV)
11.235[a]	145 ± 5	219 ± 10	1^+	2.53 ± 0.15	$11.2^{+2.1}_{-1.8}$
11.58 ± 0.03	16 ± 4	13 ± 4	1^+	<1.8[b]	0.65 ± 0.18[b]
			2^+	<2.7[b]	0.40 ± 0.13[b]
			2^-	$4.1^{+1.0}_{-1.6}$	0.016 ± 0.009

[a] See Refs. 14 and 15.

[b] The value calculated for R^2 is negative, with a positive upper limit. Therefore, the value of Γ_0 is calculated assuming that R is between zero and the maximum value consistent with the data.

[14] R.C. Ritter, J.T. Parson, D.L. Bernard: Phys. Letters 28B, 588 (1969).

[15] B.T. Lawergren, A.T.G. Ferguson, G.C. Morrison, Nucl. Phys. A108, 325 (1968).

Y. Horikawa, Y. Torizuka, A. Nakada, S. Mitsunobu, Y. Kojima, and M. Kimura
Phys. Letters 36B, 9 (1971)

Ne	20	10

METHOD

REF. NO. 71 Ho 1 | egf

REACTION	RESULT	EXCITATION ENERGY	SOURCE TYPE	SOURCE RANGE	DETECTOR TYPE	DETECTOR RANGE	ANGLE
E,E/	FMF	1,4	D	183,250	MAG-D		DST

1.63, 4.25 MEV

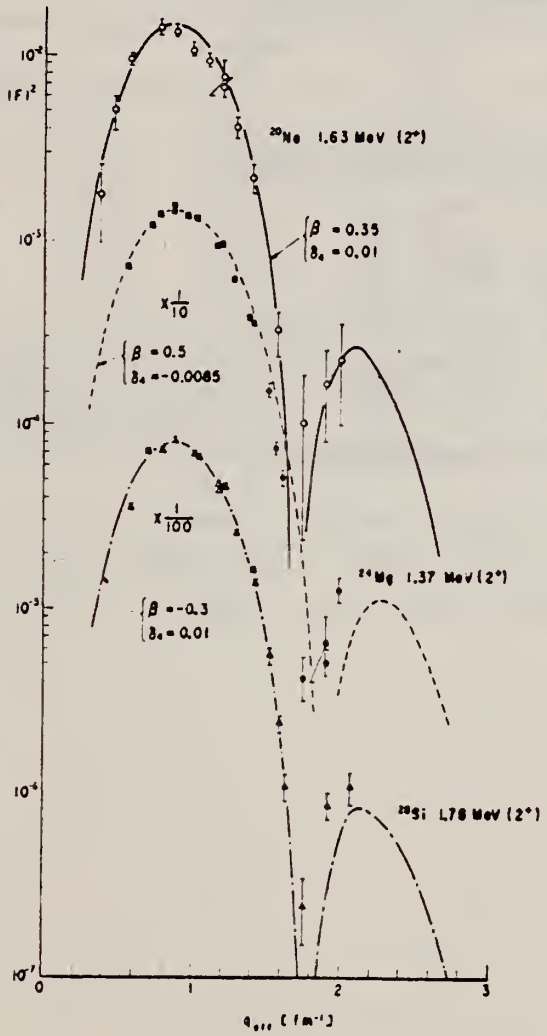

Fig.1. The experimental form factors for the 2$^+$ members of the ground-state rotational bands in ^{20}Ne. ^{24}Mg and ^{28}Si are shown as a function of the q_{eff} [3].

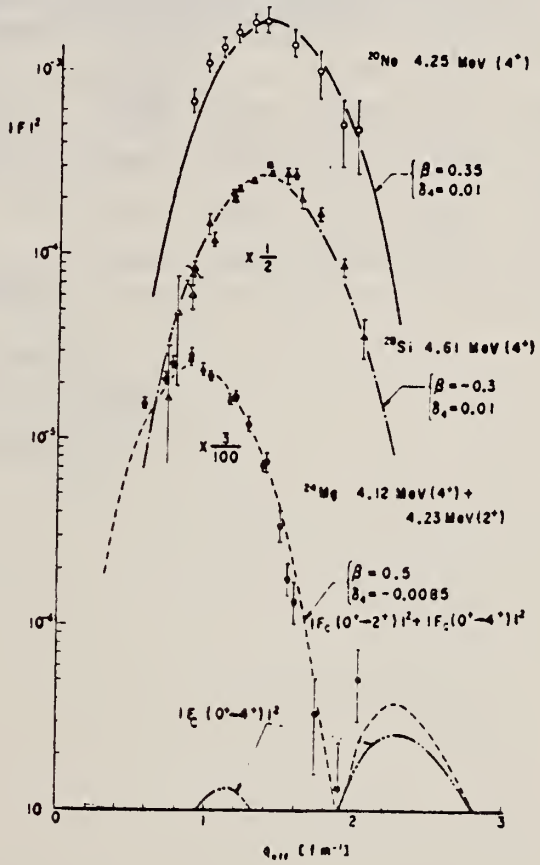

Fig.2. The same as for fig. 1 except for the 4$^+$ members. The unresolved data of the 4.12 MeV (4$^+$) and 4.23 MeV (2^+_2) states is presented in the case of ^{24}Mg.

(over

(2) R. de Swiniarski, D. Glashausser, D. L. Hendrie, J. Sherman, A. D. Bacher, and E. A. McClatchie, Phys. Rev. Letters 23 (1964) 317.
(3) D. G. Ravenhall, quoted in: R. Hofstater, Rev. Mod. Phys. 28 (1956) 214.
(5) H. Rebel, G. W. Schweimer, J. Specht, G. Schatz, R. Lohken, D. Habs, G. Hanser and H. Klewe-Nebenius, Phys. Rev. Letters 26 (1971) 1190.

Table 1
The values obtained from the Nilsson orbits which provide the best fit form factors. The signs of the moments were determined by the characteristic of the orbits. The β_2 and β_4 values of the present study are compared with those of the (p, p') [2] and (α, α') [5] reactions.

	$\langle r^2 \rangle^{1/2}$	$\langle r^4 \rangle^{1/4}$	Q_o	H_o	β_2			β_4		
	(fm)	(fm)	(efm^2)	(efm^4)	present (e, e')	(p, p')	(α, α')	present (e, e')	(p, p')	(α, α')
^{20}Ne	2.91	3.14	+58 ± 3	+249 ± 27	+0.40	+0.47	+0.35 ±0.01	+0.19	+0.28 ±0.05	+0.11 ±0.01
^{24}Mg	3.03	3.24	+69 ± 3	+ 48 ± 16	+0.45	+0.47		-0.06	-0.05 ±0.08	
^{28}Si	3.14	3.35	-64 ± 3	+205 ± 33	-0.39	-0.37	-0.32 ±0.01	+0.10	+0.25 ±0.08	+0.08 ±0.01

REF.

T.K. Alexander, B.Y. Underwood, N. Anyas-Weiss, N.A. Jelley, J. Szucs, S.P. Dolan, M.R. Wormald, and K.W. Allen
Nucl. Phys. A197, 1 (1972)

ELEM.	A	Z
Ne	20	10

METHOD

REF. NO.: 72 A1 4 egf

REACTION	RESULT	EXCITATION ENERGY	SOURCE TYPE	SOURCE RANGE	DETECTOR TYPE	DETECTOR RANGE	ANGLE
A,G	LFT	7 - 9	D	3 - 5	SCD-D		DST

4 LEVELS

TABLE 2
Summary of γ-ray decay measurements

E_x (keV)	$J_i^\pi \to J_f^\pi$	Branching (%)	$\omega\gamma$ (meV)	Γ_γ (meV)	$\lvert M(E2)\rvert^2$ (W.u.)
7191	$0^+ \to 2^+$	100	4.35±0.75 [a])	4.35±0.75	0.37±0.07
7420	$2^+ \to 2^+$	≧ 90.6±1.4	146 ±19 [a])	29 ±4	1.65±0.27 [b])
	$2^+ \to 0^+$	≦ 9.4±1.4 [b])	≦ 15.2 ±2.6 [a])	≦ 3.0 ±0.6	≦ 0.05±0.01
	$2^+ \to 4^+$	< 7.6	< 11	< 2.2	< 2.6
7826	$2^+ \to 2^+$	17 ±1	58 ± 8 [c])	11.7 ±1.6	0.48±0.07 [d])
	$2^+ \to 0^+$	83 ±1	285 ±34 [c])	57 ±7	0.73±0.09
	$2^+ \to 4^+$	< 3	< 10	< 2	< 1.3
9029	$4^+ \to 2^+$	100	3050 ±375 [e])	340 ±42	5.8 ±0.7
	$4^+ \to 4^+$	< 2	< 61	< 6.8	< 1 [d])

[a]) Measured relative to $\omega\gamma(6^+) = 1.36\pm0.14$ eV, refs. [22,23]).
[b]) $\delta(E2/M1) = -8.36^{+\infty}_{+1.3}$, $|M(M1)|^2 = (1.0\pm0.3)\times10^{-4}$ W.u.
[c]) Measured relative to $\omega\gamma(2^+, T=1) = 22.2\pm2.4$ eV, ref. [16]).
[d]) Assumed to be pure E2.
[e]) Considered an upper limit since off-resonance intensity was not measured.

[16] J. D. Pearson et al., Nucl. Phys. 54 (1964) 434
[22] W. T. Diamond et al., Can. J. Phys. 49 (1971) 1589
[23] D. W. O. Rogers et al., Can. J. Phys. 49 (1971) 1397

REF.

S. Mitsunobu and Y. Torizuka
Phys. Rev. Letters 28, 920 (1972)

ELEM. SYM.	A	Z
Ne	20	10

METHOD

REF. NO.
72 Mi 4
hmg

REACTION	RESULT	EXCITATION ENERGY	SOURCE		DETECTOR		ANGLE
			TYPE	RANGE	TYPE	RANGE	
E,E/	FMF	6-8	D	120-250	MAG-D		DST

6.72-7.84 MEV LEVELS

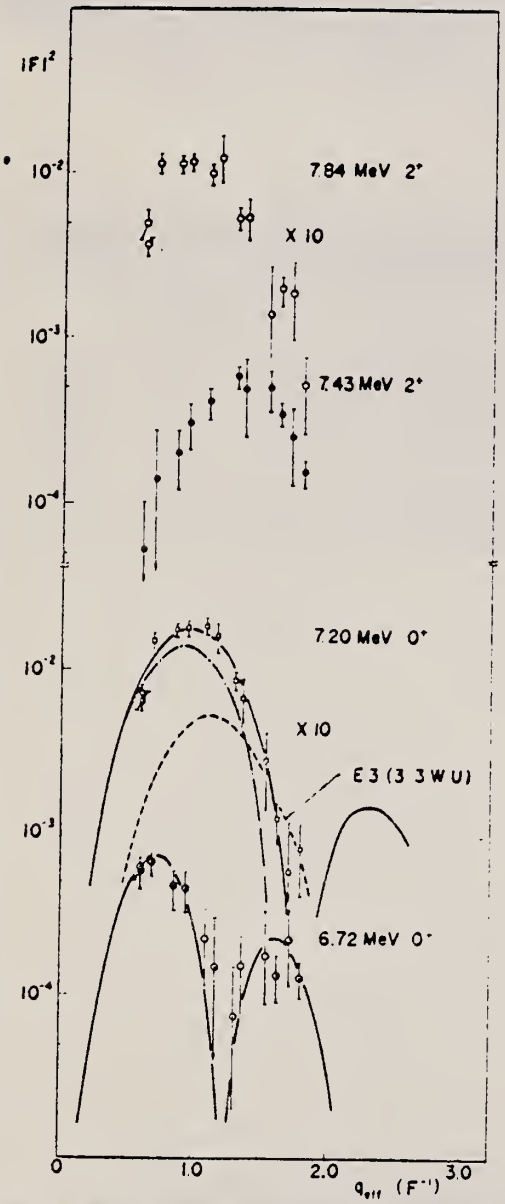

FIG. 2. Experimental form factors for the 6.72- (0^+), 7.20- (0^+), 7.43- (2^+), and 7.84-MeV (2^+) states, plotted against q_{eff}.

TABLE I. Matrix elements M, transition radii R_{tr}, and reduced transition probabilities $B(E2)$.

	E_x (MeV)	J^π	M (F^2)	$R_{tr}/A^{1/3}$ (F)	$B(E2)/B_{s.p.}$
^{20}Ne	6.72	0^+	7.37 ± 1.97	2.11 ± 0.48	
^{20}Ne	7.20	0^+	6.90 ± 1.44	1.69 ± 0.52	
^{28}Si	4.98	0^+	6.63 ± 2.43	1.81 ± 0.51	
			6.82 ± 0.52 [a]	1.86 ± 0.09 [a]	
^{20}Ne	7.43	2^+			0.13 ± 0.03
^{20}Ne	7.84	2^+			0.83 ± 0.13

[a] Ref. 12.

P. Strehl and T.H. Schucan, Phys. Lett. 27B, 641 (1968).

REF.

R.P. Singhal, H.S. Caplan, J.R. Moreira, and T.E. Drake
Can. J. Phys. 51, 2125 (1973)

Ne	20	10

METHOD

REF. NO. 73 Si 15 hmg

REACTION	RESULT	EXCITATION ENERGY	SOURCE TYPE	SOURCE RANGE	DETECTOR TYPE	DETECTOR RANGE	ANGLE
E,E/	FMF	1- 8	D	77-115	MAG-D		DST

6 LEVELS

TABLE 1. Experimental form factors for ^{20}Ne

		Square of experimental form factor × 10^4 (errors in %)					
				5.63 MeV 3_1^- +		7.17 MeV 3_2^- +	
E_0 (MeV)	θ (deg)	1.625 MeV 2_1^+	4.24 MeV 4_1^+	5.78 MeV 1^-	6.72 MeV 0_2^+	7.20 MeV 0_3^+	7.84 MeV 2_2^+
81.28	60	31.62 (15)					
81.28	75	46.28 (15)					
102.40	60	60.56 (15)		4.956 (15)	2.480 (25)		
102.40	75	93.41 (10)					
77.00	125	86.50 (10)					
81.28	125	113.5 (10)					
77.00	140	115.2 (10)					
102.40	90	103.5 (10)	1.833 (25)	18.64 (15)	3.165 (20)	7.090 (20)	4.340 (20)
102.40	110	110.0 (10)	3.940 (20)	24.74 (15)	2.730 (20)	11.20 (20)	5.244 (20)
114.40	110	86.34 (10)					
102.40	140	108.8 (10)		32.00 (15)			
110.50	140	60.33 (20)					

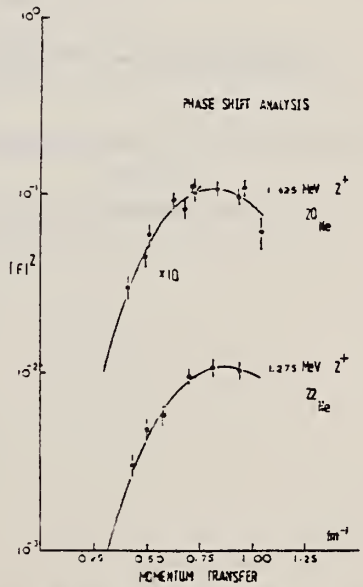

FIG. 6. The result of best fits to the 1.625 MeV, 2^+ state in ^{20}Ne and 1.275 MeV, 2^+ state in ^{22}Ne. Tassie model has been used in a phase shift code for the fits.

REF.		ELEM. SYM.	A	Z
	I.I. Chkalov, N.G. Shevchenko, A.Yu. Buki, A.A. Khomich, A.S. Litvinenko, and V.N. Polishchuk Yad. Fiz. 22, 893 (1975) Sov. J. Nucl. Phys. 22, 464 (1976)	Ne	20	10

METHOD	REF. NO.
	75 Ch 4 hmg

REACTION	RESULT	EXCITATION ENERGY	SOURCE		DETECTOR		ANGLE
			TYPE	RANGE	TYPE	RANGE	
E,E/	SPC	0- 35	D	151,164	MAG-D		DST

Experimental results are presented of a study of the fine structure of the giant resonance in the nuclei ^{20}Ne and ^{40}Ar by the method of inelastic scattering of electrons. A correlation is observed between the energy positions of the maxima of the fine structure of the giant resonance in the nuclei ^{20}Ne and ^{40}Ar, on the one hand, and the positions of the discrete levels in the respective nuclei ^{19}F and ^{39}Ar, on the other.

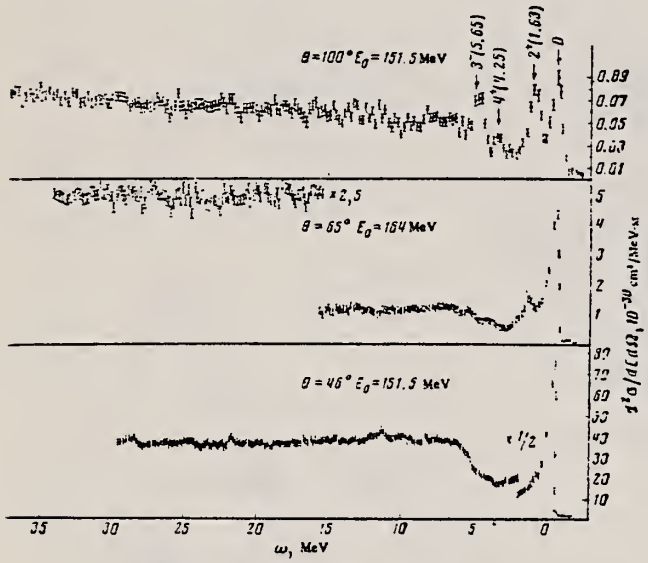

FIG. 1. Spectra of electrons scattered by ^{20}Ne.

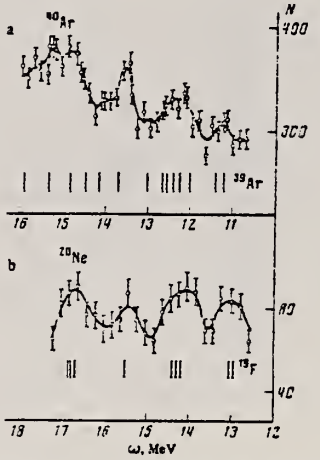

FIG. 3. Fine structure of the giant resonance in the nuclei ^{40}Ar (a) and ^{20}Ne (b) at $\theta = 100°$ and $E_0 = 152$, and the discrete-level schemes of the nuclei ^{39}Ar and ^{19}F.

REF. D. M. Skopik, Y. M. Shin, and J. J. Murphy, II
Can. J. Phys. 53, 1398 (1975)

ELEM. SYM.	A	Z
Ne	20	10

METHOD

REF. NO. 75 Sk 10 hmg

REACTION	RESULT	EXCITATION ENERGY	SOURCE		DETECTOR		ANGLE
			TYPE	RANGE	TYPE	RANGE	
E,A	ABX	15- 24	D	UKN	MAG-D		DST

GND STATE SIGMA

The electrodisintegration cross sections, $^{16}O(e,\alpha_0)^{12}C,e'$ and $^{20}Ne(e,\alpha_0)^{16}O,e'$, have been measured and, by using virtual photon analysis, a comparison with photodisintegration experiments has been made. Satisfactory agreement with earlier $^{12}C(\alpha,\gamma_0)^{16}O$ experiments was found and the $^{20}Ne(\gamma,\alpha_0)^{16}O$ reaction reveals several pronounced resonances.

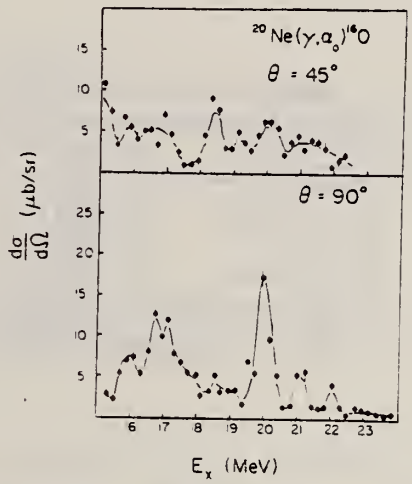

FIG. 2. Comparison of the $^{20}Ne(\gamma,\alpha_0)$ cross sections at θ = 45° and 90°.

REF. L.K. Fifield, F. P. Calaprice, C. H. Zimmerman, M. J. Hurst, A. Pakkanen, T. J. M. Symons, F. Watt and K. W. Allen
Nucl. Phys. A288, 57 (1977)

ELEM. SYM.	A	Z
Ne	20	10

METHOD

REF. NO.: 77 Fi 6 | egf

REACTION	RESULT	EXCITATION ENERGY	SOURCE		DETECTOR		ANGLE
			TYPE	RANGE	TYPE	RANGE	
A,G	LFT	10	D	6	SCD-D		55

Abstract: The radiative widths for decays of the ^{20}Ne $T = 1$, 2^- (10.27 MeV) state were measured by resonance α-capture in the reaction ^{16}O(α, γ)^{20}Ne. A special windowless gas-cell target yielded a low-background spectrum enabling six γ-branches to be observed with a Ge(Li) detector. The six branches correspond to decays from the 10.27 MeV level to the following levels: 2^+(7.83 MeV), 2^+(7.42 MeV), 3^-(5.62 MeV), 2^-(4.97 MeV), 2^+(1.63 MeV) and 0^+(g.s.). The branching ratios and radiative widths Γ_γ to these levels are: 7.83 MeV [(0.22±0.06)%, 0.008±0.002 eV], 7.42 MeV [(6.9±0.4)%, 0.31±0.04 eV], 5.62 MeV [(2.1±0.2)%, 0.097±0.014 eV], 4.97 MeV [(1.3±0.1)%, 0.060±0.008 eV], 1.63 MeV [(88.9±0.5)%, 4.08±0.43 eV] and 0.0 MeV [(0.64±0.14)%, 0.029±0.008 eV]. The radiative widths to the 1.63 MeV and 7.42 MeV levels are used to determine the CVC predictions of the weak magnetism form factors and their effects on certain β-decay observables are evaluated.

10=10.27 MeV

TABLE 2

Branching ratios and transition energies for the 6.93 MeV resonance

Transition	$E_\gamma^{(0)}$ (keV)	Branch (%)
$R \rightarrow 0$	10266.1±5.0	0.65±0.14
$R \rightarrow 1.63$	8636.3±3.2	88.9 ±0.5
$R \rightarrow 4.97$	5305.2±3.8	1.3 ±0.1
$R \rightarrow 5.62$	4649.6±2.2	2.1 ±0.2
$R \rightarrow 7.42$	2847.9±1.2	6.9 ±0.4
$R \rightarrow 7.83$	2442.9±2.6	0.22±0.06
$4.97 \rightarrow 1.63$	3332.0±1.9	

TABLE 4

Transition strengths for the 6.93 MeV resonance

Transition	Type	$\omega\gamma$ (eV)	Γ_γ (eV)	$\lvert M\rvert^2$	$\lvert M\rvert^2$ (W.u.)
$R \rightarrow 0.0$	E2	0.14±0.04	0.029±0.008	0.32 ±0.09 $e^2 \cdot fm^4$	0.10 ±0.03
$R \rightarrow 1.63$	M1	19.7 ±2.1	4.08 ±0.44	0.55 ±0.06 μ_N^2	0.31 ±0.03
$R \rightarrow 4.97$	E1	0.29±0.04	0.060±0.008	(3.8 ±0.5)×$10^{-4} e^2 \cdot fm^2$	(8.3 ±1.0)×10^{-4}
$R \rightarrow 5.62$	E1	0.47±0.07	0.097±0.014	(9.2 ±1.3)×$10^{-4} e^2 \cdot fm^2$	(2.0 ±0.3)×10^{-3}
$R \rightarrow 7.42$	M1	1.5 ±0.2	0.31 ±0.04	1.16 ±0.15 μ_N^2	0.65 ±0.08
$R \rightarrow 7.83$	M1	0.04±0.01	0.008±0.002	0.050±0.012 μ_N^2	0.027±0.006

REF. J.M. Davidson and M.M. Lowry
Phys. Rev. C 18, 2776 (1978)

ELEM. SYM.	A	Z
Ne	20	10

METHOD

REF. NO. 78 Da 5 hg

REACTION	RESULT	EXCITATION ENERGY	SOURCE		DETECTOR		ANGLE
			TYPE	RANGE	TYPE	RANGE	
A,GO	LFT	11	D	8	SCD-D		DST
		(11.278)		(8.18)			

The properties of the 1^-, $T = 1$ state of ^{20}Ne at 11278 ± 4 keV excitation were studied by means of the $^{16}O(\alpha,\gamma)^{20}Ne$ reaction. The level parameters determined for this state are not in complete agreement with those reported in a recent study. The implication of this discrepancy for the feasibility of a measurement of parity nonconservation in ^{20}Ne is discussed.

TABLE I. Properties of the lowest 1^-, $T=1$ state of ^{20}Ne.

Reference	$\omega\gamma\zeta^{-m}$ (eV)	E_x (keV)
Ref. 3	0.7 ± 0.3[a]	11270 ± 30
Ref. 1	0.58 ± 0.05	11259 ± 8
Ref. 12	1.2 ± 0.3	
Present work	1.0 ± 0.3	11278 ± 4

[a]The value quoted in Ref. 3 has been multiplied by $\frac{16}{20}$ to express it in the center-of-mass system.

1
D.J. Steck, Phys. Rev. C 17, 1034 (1978)
3
J.D. Pearson and R.H. Spear, Nucl. Phys. 54, 434 (1964)
12
K. Fifield, Nuclear Physics Laboratory, Oxford University, private communication

REF. Z.M. Szalata, K. Itoh, G.A. Peterson, J. Flanz, S.P. Fivozinsky, F.J. Kline, J.W. Lightbody, Jr., X.K. Maruyama & S. Penner
Phys. Rev. C17, 435 (February 1978)

ELEM. SYM.	A	Z
Ne	20	10

METHOD

REF. NO. 78 Sz 7

hmg 11/18/80

REACTION	RESULT	EXCITATION ENERGY	SOURCE TYPE	SOURCE RANGE	DETECTOR TYPE	DETECTOR RANGE	ANGLE
E,E/	FMF	12-23	D	59-120	MAG-D	---	DST

Electrons at five energies between 60 and 120 MeV were used to study the giant electric-dipole and -quadrupole resonances in ^{20}Ne. Prominent electric-dipole peaks were found at 17.7, 19.1, 20.2, and 23 MeV in good agreement with photoreaction results. In addition our analysis reveals weaker fragmented electric-dipole strength in the region between 12.5 and 15 MeV. Prominent electric-quadrupole peaks were found at 13.0, 13.7, and 16.2 MeV, and a broad peak was found from 14.2 to 15.9 MeV. Two different analyses reveal a broad quadrupole excitation between 16 and 25 MeV. The dipole and quadrupole resonances deplete about 65% and 100% of the energy-weighted sum rule, respectively.

Q 0.35-0.9 FM-1

TABLE I. Reduced transition probabilities $B(CL)\uparrow$ obtained by (A) photoreaction subtraction and (B) multipole expansion using the Goldhaber-Teller model and the Steinwedel-Jensen model (square brackets) for the $B(C1)\uparrow$ and the Tassie model for the $B(C2)\uparrow$. Model errors are not included.

Dipole reduced transition probabilities

E_x (MeV)	A. Photoreaction subtraction (Ref. 12) $B(C1)\uparrow$ (e^2 fm^2)	B. Multipole expansion $B(C1)\uparrow$ (e^2 fm^2)
10–16		0.33 ±0.02 [0.35 ±0.02]
16–25	1.65 ±0.13	2.1 ±0.1 [2.2 ±0.1]
16–17.2	0.16	0.17 ±0.02
17.7	0.29	0.20 ±0.02
19.1	0.34	0.33 ±0.03
20.2	0.33	0.43 ±0.04
20.9–25.0	0.53	0.99 ±0.10

Quadrupole reduced transition probabilities

A. Photoreaction subtraction E_x (MeV)	$B(C2)\uparrow$ (e^2 fm^4)	B. Multipole expansion E_x (MeV)	$B(C2)\uparrow$ (e^2 fm^4)
1.63	188 ±9[a]		
7.80	18.1 ±0.9		
10–16	128 ±19	10–18	110 ±5 [105 ±5]
		10.4–11.2	10 ±1
		11.9	11 ±1
		13.0	19 ±2
		13.7	17 ±2
		14.5, 15.0, 15.4	30 ±3
		16.2	24 ±2
16–25	119 ±18	18–25	88 ±5 [72 ±5]

[a] Obtained by using Helm model (Ref. 24) in a comparison to the elastic scattering.

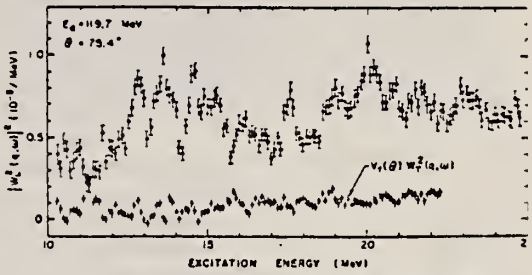

FIG. 2. The radiatively unfolded longitudinal (solid points) and transverse (open circle) differential form factors in the giant resonance region of ^{20}Ne obtained by scattering 119.7 MeV electrons through 75.4°. The transverse form factor $V_T(\theta)W_T^2(q,\omega)$ was obtained by a matching-q experiment.

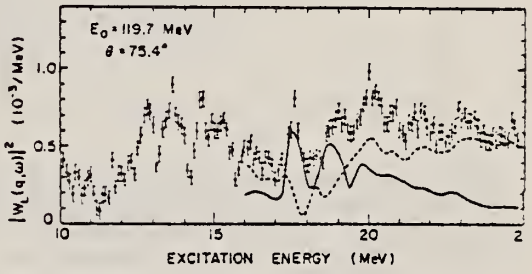

FIG. 3. The longitudinal differential form factor of ^{20}Ne obtained by scattering 119.7 MeV electrons through an angle of 75.4° is shown by the points with error bars. The dipole contribution obtained as described in Sec. IIIA is shown by the solid curve, and the residual contribution is shown by the dashed curve.

(OVER)

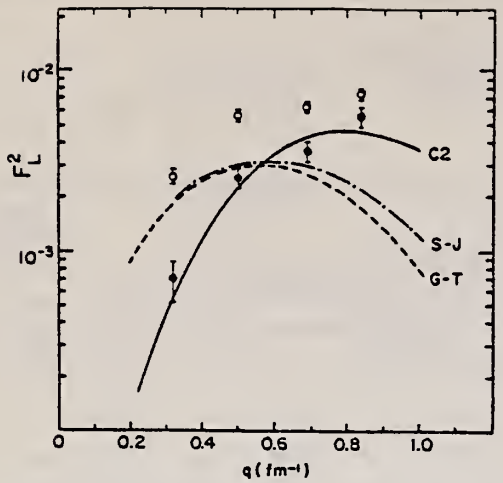

FIG. 4. The longitudinal form factor integrated from 16 to 26 MeV is shown by the open circles and the residual form factor obtained by the subtraction of the dipole form factor is shown by the black circles. The residual form factors can be explained by quadrupole excitations. The curve labeled GT (SJ) is the dipole form factor calculated using the Goldhaber-Teller (Steinwedel-Jensen) model.

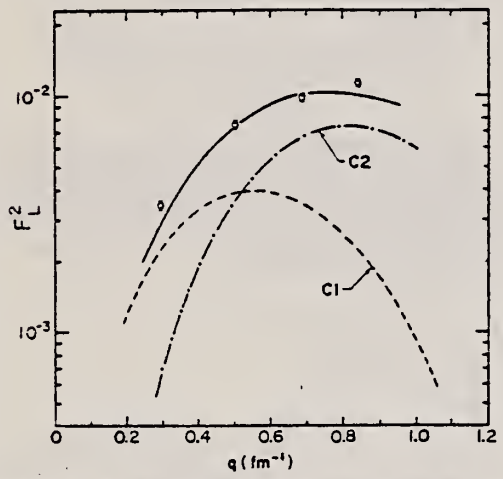

FIG. 6. The results of the multipole expansion method, showing the longitudinal form factor squared integrated from 10 to 25 MeV. The dashed, dash-dotted, and solid lines are dipole and quadrupole components, and their sum, respectively.

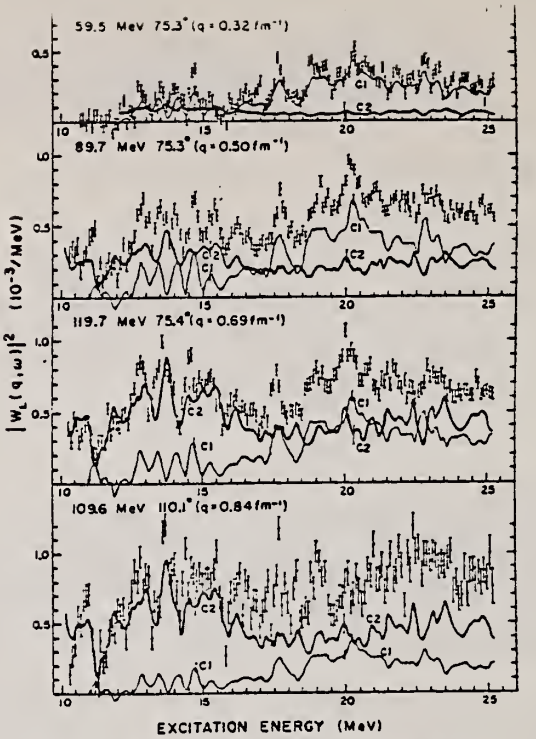

FIG. 5. The longitudinal differential form factor of ^{20}Ne at various momentum transfers. The points with error bars show the experimental results. The thin curve shows the dipole form factor and the thick curve shows the quadrupole form factor obtained by the multipole expansion method. The occasional error bars on the $C1$ and $C2$ curves indicate statistical errors only. In addition there are model dependent and unexplored systematic errors.

TABLE III. The percentages of the electric-quadrupole isoscalar energy-weighted sum rule S_2 (Isoscalar) as obtained by the multipole expansion method, in comparison with (α,α') results (Ref. 7), and calculations using an excited core model (Ref. 35). Results are also given assuming the excitations were of monopole rather than of quadrupole character. Model errors are not included in the present results.

Present results		Quadrupole (α,α')		Theory	
E_x (MeV)	S_2 (Isoscalar) (%)	E_x (MeV)	S_2 (Isoscalar) (%)	E_x (MeV)	S_2 (Isoscalar) (%)
1.63	8.2±0.5	1.63	16.3		
7.80	3.7 ±0.3				
10–18	41 ±2	12.9–16.4	19.5	15–29	29.8
10.4–11.2	2.8			15.8	7.9
				21.1	8.9
11.9	3.3			23.5	1.1
13.0	6.4			25.5	4.0
				26.1	4.1
13.7	6.2	12.9	4	27.2	0.19
				28.1	2.9
		13.9	5	28.9	0.66
14.2–15.9	12	15.2	6		
15.9–18.0	11	16.4	≤4.5		
18–25	50 ±3	18.1–28.2	$35^{+8.7}_{-9.2}$		

Monopole (isoscalar and isovector)			
E_x (MeV)	S_0 (%)	E_x (MeV)	S_0 (%)
10–18	34	15–30	40
18–25	40	15.0	6.5
		25.2	3.3
		26.6	27.7
		29.9	2.4

REACTION	RESULT	EXCITATION ENERGY	SOURCE		DETECTOR		ANGLE
			TYPE	RANGE	TYPE	RANGE	

TABLE II. The percentages of the electric-dipole isovector energy-weighted sum rule S_1 (Isovector) as obtained by the multipole expansion method, in comparison with the results of photoreactions. Model errors are not included.

Dipole		
Present results		Photoreaction
E_x (MeV)	S_1 (Isovector) (%)	S_1 (Isovector (%)
10–15.6	6.0 ±4	
11.2	0.39	
12.3	1.0	
13.4	1.1	
14.1	1.2	
14.7	1.4	
15.3	0.91	
15.6–25.0	59 ±3	
15.6–17.2	3.6	3.5
17.7	4.8	6.9
19.1	8.3	3.6
20.2	11.7	8.8
20.9–25.0	30.6	16.1

able fragmentation between 11 and 17 MeV, although the presence of some monopole strength in this region cannot be excluded. Thus the quadrupole strength in ^{20}Ne spreads over a wide energy region and is not concentrated in a well-defined GQR as in medium and heavy nuclei. This seems to be a feature of other light nuclei.

An excited core model calculation for ^{20}Ne, wherein the low-lying excited states of the valence nucleons are coupled to the giant multipole resonance of the ^{16}O core, was performed by Knüpfer *et al.*[35] We have compared the results of this calculation with our experimental results in Table III. One of the characteristic results of this calculation is the splitting of C0 and C2 strength into a higher and a lower energy component (14 and 21 MeV), which is in qualitative agreement with the present experimental results as well as the results of (α, α') experiments. The splitting of the GQR in deformed nuclei such as ^{20}Ne has also been examined by the coupling of

REF. J.D. MacArthur, H.C. Evans, J.R. Leslie, H.-B. Mak
Phys. Rev. C22, 356 (1980)

ELEM. SYM.	A	Z
Ne	20	10

METHOD

REF. NO. 80 Ma 5 hg

REACTION	RESULT	EXCITATION ENERGY	SOURCE		DETECTOR		ANGLE
			TYPE	RANGE	TYPE	RANGE	
G,A	LFT	7	D	3	SCD-D		DST
		(7.158)		(3.036)			

LFT LIMIT 7.156 MEV

In an alpha capture experiment on an ^{16}O gas target, the 3^-, 7.156 MeV state in ^{20}Ne has been observed to decay to the 1^-, 5.782 MeV and the 4^+, 4.248 MeV states with gamma ray branches of $45 \pm 5\%$ and $55 \pm 5\%$, respectively. The strengths of the 1374 and 2908 keV transitions were deduced to be $B(E2) = 51 \pm 8$ W.u. and $B(E1) = 79 \pm 9$ μW.u., respectively. The strongly enhanced $E2$ rate for the 3^- to 1^- transition is convincing evidence for these two states being the first members of this $K^\pi = 0^-$ band in ^{20}Ne. From resonance scattering experiments, the alpha widths for these two states were determined to be 28 ± 3 eV and 8.1 ± 0.3 keV, respectively; values in agreement with cluster calculations of alpha widths in ^{20}Ne.

[NUCLEAR REACTIONS Measured $\sigma(E,\vartheta)$ for $^{16}O(\alpha,\alpha)^{16}O$ and $\sigma(E_R)$ for $^{16}O(\alpha,\gamma)^{20}Ne$; deduced Γ_α for $E_x = 5.782$ and 7.156 MeV and radiative transition rates from $E_x = 7.156$ MeV.]

TABLE I. Transitions from the 3^- state at $E_x = 7.156$ MeV excited in the $^{16}O(\alpha,\gamma)^{20}Ne$ reaction at $E_\alpha = 3.036$ MeV. Energies with errors are for gamma rays actually observed. The strengths are deduced assuming pure transitions.

Final state E_x (keV)	J^π	E_γ (keV)	Γ_γ (meV)	Strength
0	0^+	7156	<0.05	<5.0 W.u. $E3$
1634	2^+	5523	<0.08	<0.9 μW.u. $E1$
4248	4^+	2908.4 ± 0.4	0.97 ± 0.11	79 ± 9 μW.u. $E1$
4963	2^-	2188	<0.05	<0.23 mW.u. $M1$
5621	3^-	1535	<0.05	<0.66 mW.u. $M1$
5782	1^-	1374.3 ± 0.4	0.64 ± 0.10	51 ± 8 W.u. $E2$

REF. M. Yagi, R. Amano
Int. J. Applied Radiat. Isotopes 31, 559 (1980)

ELEM. SYM.	A	Z
Ne	20	10

METHOD

REF. NO. 80 Ya 2 hg

REACTION	RESULT	EXCITATION ENERGY	SOURCE		DETECTOR		ANGLE
			TYPE	RANGE	TYPE	RANGE	
G,F18	YLD	THR-60	C	30-60	ACT-I		4PI

The production rates of ^{18}F by the $^{20}Ne(\gamma, pn)^{18}F$ plus $^{20}Ne(\gamma, 2n)^{18}Ne \rightarrow {}^{18}F$, $^{23}Na(\gamma, xn)^{18}F$, and $^{19}F(\gamma, n)^{18}F$ reactions were determined as a function of the maximum bremsstrahlung energies between 30 and 60 MeV. In addition, a simple and fast method to prepare anhydrous $H^{18}F$ was studied by using KHF_2 target.

TABLE I. Photonuclear reactions for ^{18}F production

Target nuclide (abundance, %)	Reaction type	Threshold energy (MeV)	Product nuclide
^{20}Ne (90.51)	$(\gamma, 2n)$	28.50	$^{18}Ne \rightarrow {}^{18}F$
^{21}Ne (0.27)	$(\gamma, 3n)$	35.27	$^{18}Ne \rightarrow {}^{18}F$
^{22}Ne (9.22)	$(\gamma, 4n)$	45.63	$^{18}Ne \rightarrow {}^{18}F$
^{20}Ne (90.51)	(γ, pn)	23.26	^{18}F
^{21}Ne (0.27)	$(\gamma, p2n)$	29.93	^{18}F
^{22}Ne (9.22)	$(\gamma, p3n)$	40.38	^{18}F
^{23}Na (100)	(γ, xn)	20.89	^{18}F
^{19}F (100)	(γ, n)	10.43	^{18}F

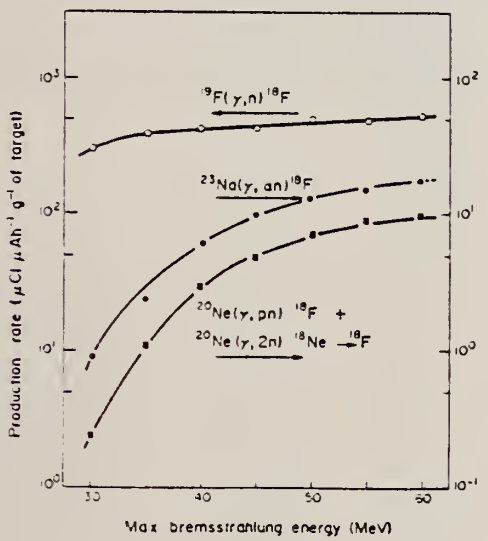

FIG. 1 Production rates of ^{18}F on Ne, Na and F targets as a function of the maximum bremsstrahlung energy

REF. P.D. Allen, E.G. Muirhead, D.V. Webb
Nucl. Phys. A357, 171 (1981)

ELEM. SYM.	A	Z
Ne	20	10

METHOD

REF. NO. 81 A1 5 hg

REACTION	RESULT	EXCITATION ENERGY	SOURCE		DETECTOR		ANGLE
			TYPE	RANGE	TYPE	RANGE	
G,1N,	ABX	16-29	C	16-29	BF3-I		4PI

ENRICHED NEON-20 TARG

Abstract: The photoneutron cross section of ^{20}Ne has been measured over a photon energy range 16 to 29 MeV in steps of 100 keV. The giant dipole resonance is resolved into three strong peaks below 21 MeV and at least two broader resonances at higher excitations. This structure is consistent with earlier measurements of poorer resolution and shows a correlation with the recent calculations of Schmid and Do Dang. Comparisons with high-resolution neutron time-of-flight and electron scattering data indicate the existence of regions of structure, roughly 2–3 MeV wide, which exhibit localised characteristics related to the excitation mechanisms. The role of deformation and configuration splitting effects in the cross section is discussed and possible directions of further study are noted which might clarify the situation more fully.

E NUCLEAR REACTIONS ^{20}Ne(γ, n), bremsstrahlung, E = 16 - 29 MeV; measured $\sigma(E)$; deduced σ, σ^* and differential form factor. $B^{10}F_3$ detector. Enriched target.

TABLE 1

Photonuclear integrated cross sections

Ref.	Reaction	Upper energy limit (MeV)	Integrated cross section (MeV · mb)	Fractional dipole sum *
Melbourne	(γ, n)	20.6	20 ± 2	0.07
		26.7	49 ± 5	0.16
		28.5	58 ± 6	0.19
Veyssière *et al.* [3])	(γ, n)	20.6	15.8	0.05
		26.7	42 ± 3	0.14
Woodworth *et al.* [5])	(γ, n)	31.0	56.9–76.8	0.19–0.26
Ferguson *et al.* [15])	(γ, n)	27	52	0.17
Gorbunov *et al.* [38])	(γ, n)	170	115	0.38
Dodge and Barber [6])	(γ, p)	27	65^{13}_{-10}	0.22
Hofmann *et al.* [20])	(γ, p)	32.5	61 ± 11	0.20
Komar and Iavor [39])	(γ, p)	80	160 ± 80	0.53
Gorbunov *et al.* [38])	(γ, p)	170	165	0.55
Tanner *et al.* [22])	(γ, p_0)	20.5	28 ± 9	0.09
Segel *et al.* [7])	(γ, p_0)	25.7	25	0.08
Gorbunov *et al.* [38])	(γ, tot)	170	600	2

* Dipole sum = $60NZ/A$ = 300 MeV · mb.

(OVER)

TABLE 3

Comparison of the integrated cross section under the 17.6 MeV peak for the $^{20}Ne(\gamma, n_0+n_1+n_2)$ reactions

Ref.	$\int \sigma dE$ (MeV · mb)
present experiment	3.3±0.3
Woodworth *et al.* [5])	3.3±0.5
Veyssière *et al.* [3])	2.6±0.3

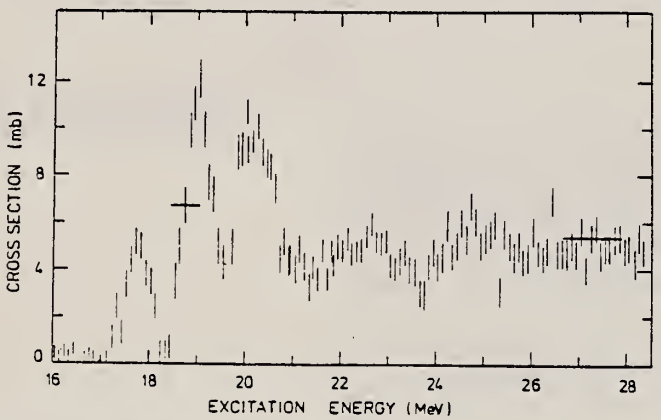

Fig. 3. The measured $^{20}Ne(\gamma, tn)$ cross section. The vertical bars indicate statistical errors while the horizontal bars show the variation of resolution over the energy range.

Ne
A=22

Ne
A=22

Ne
A=22

Ref. H.J. Hay, J.B. Warren
Can. J. Phys. 37, 1153 (1959)

Elem. Sym.	A	Z
Ne	22	10

Method 500 keV Cockcroft-Walton cascade generator; photodisintegration; $Li^7(p,\gamma)$ reaction.

Ref. No. 59 Ha 1 EH

Reaction	E or ΔE	E_o	Γ	$\int \sigma dE$	Jπ	Notes
$Ne^{22}(\gamma,\alpha)$	17.63 14.8					Cross Section: 0.76 mb; State: ground state α's dectected in neon filled proportional counters.

A.P. Komar, Ya. Krzhemenek, I.P. Yavor
Dokl. Akad. Nauk SSSR 135, 291 (1960); Soviet Phys. Doklady 5, 1234 (1961)

ELEM. SYM.	A	Z
Ne	22	10

METHOD: Synchrotron; proton, n-p spectra; angular distribution; cross sections; cloud chamber

REF. NO.: 60 Ko 2 | NVB

REACTION	RESULT	EXCITATION ENERGY	SOURCE TYPE	SOURCE RANGE	DETECTOR TYPE	DETECTOR RANGE	ANGLE
G,P	SPC	THR-90	C	90	CCH-D	2-24	DST
G,NP	SPC	THR-90	C	90	CCH-D	2-20	DST

89% Ne^{22}, 10% Ne^{20}, 1% Ne^{21}

SEP ISOTPS

$$\int_0^{90} \sigma_t dE = 0.44 \text{ MeV-b}$$

In Figure 3:

$$\frac{d\sigma}{d\Omega} = 0.29 + 0.11 \sin^2\theta$$

In Figure 4:

$$\frac{d\sigma}{d\Omega} = [0.22 + 0.07 \sin^2\theta] + [0.085 \cos\theta]$$

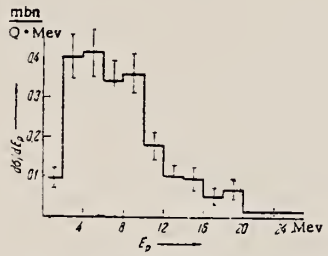

Fig. 1. Energy distribution of the photoprotons from the reaction (γ, p).

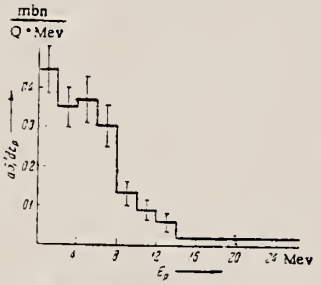

Fig. 2. Energy distribution of the photoprotons from the reaction (γ, pn).

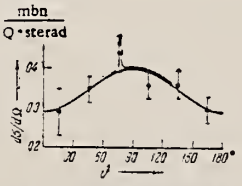

Fig. 3. Angular distribution of the photoprotons from the reaction (γ,p) with energies exceeding 0.5 Mev.

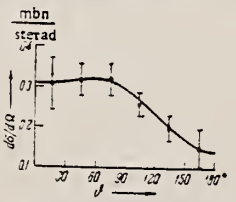

Fig. 4. Angular distribution of the photoprotons from the reaction (γ,pn) with energies exceeding 0.5 Mev.

TABLE 1

Relative Outputs for the Photodisintegration of Neon

Reaction	Ne^{20} thresh. Mev.	Ne^{22} thresh. Mev.	Ne^{20} output %	Ne^{22} output %
γ, p	12.9	15.3	39	22
γ, n	16.9	10.4	17	30
γ, 2n	(24.1)	(17.1)	—	—
γ, α	4.7	9.7	1	7
γ, pn	23.3	23.4	6	18
γ, αp	16.9	25.6	22	1.5
γ, αn	21.2	17.7	7.5	8.5
Other stars	—	—	7.5	13
No. of cases			1928	1759
$\int_0^{90} \sigma\, dE$, Mev. mbn			430	440

J. Graff, G. Chouraqui, M. Port, J. M. Thirion, S. Jang and T. Muller
J. Physique 29, 141 (1968)

Ne	22	10

METHOD

REF. NO. 68 Gr 1 egf

REACTION	RESULT	EXCITATION ENERGY	SOURCE		DETECTOR		ANGLE
			TYPE	RANGE	TYPE	RANGE	
A,G	LFT	12,13	D	2,3	NAI-D	8-13	DST

12,13=11.89,12.28 MEV

TABLEAU I

CARACTÉRISTIQUES DES NIVEAUX ÉTUDIÉS
LES VALEURS DE $E_{rés}$, E_x ET Γ ONT ÉTÉ RELEVÉES DANS LES RÉFÉRENCES [4, 5]

				TRANSITION γ_0		TRANSITION γ_1			
$E_{rés}$ MeV	E_x (^{23}Ne) MeV	J^π	Γ keV	Γ_{γ_0} eV	$\lvert M\rvert^2$ UNITÉS DE WEISSKOPF	x = COEFFICIENT DE MÉLANGE M2/E1	Γ_{γ_1} eV	$\lvert M\rvert^2$ UNITÉS DE WEISSKOPF	$\Gamma_{\gamma_0}/\Gamma_{\gamma_1}$
2,71	11,89	1⁻	13	0,36 ± 0,14	0,38 × 10^{-3}	— 0,267 ± 0,047	0,35 ± 0,11	0,28 × 10^{-3}	1,09 ± 0,13
3,19	12,28	1⁻	80	2,4 ± 1,0	2,1 × 10^{-3}	— 0,327 ± 0,067	2,3 ± 1,0	1,7 × 10^{-3}	1,04 ± 0,14

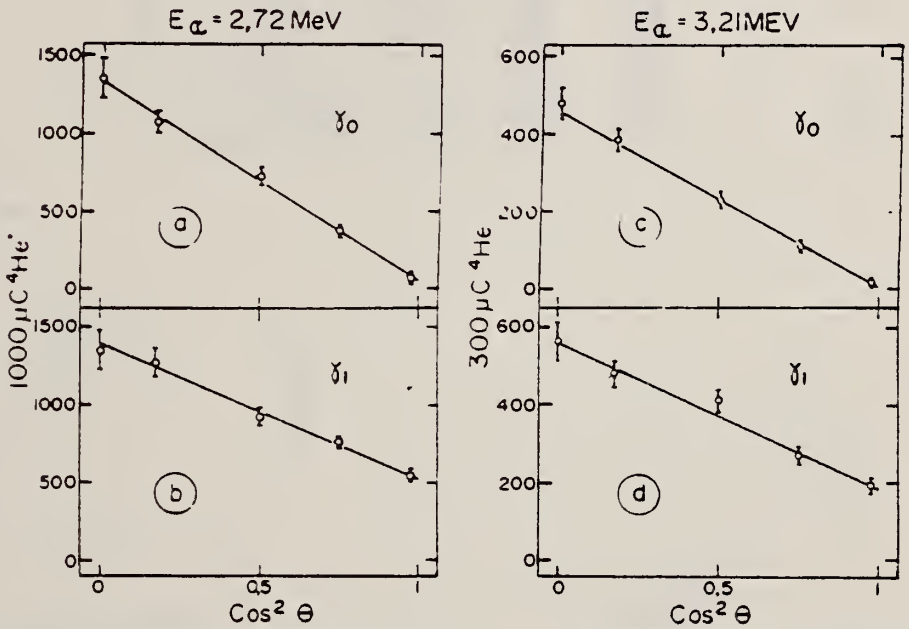

FIG. 2. — Distributions angulaires des rayonnements γ_0 et γ_1. Les barres d'erreur sont d'origine statistique et tiennent compte des diverses corrections appliquées. Les droites représentent les ajustements obtenus par la méthode des moindres carrés.

W. Hofmann, R. Kosiek, G. Kraft and R. Mundhenke
Z. Physik 225, 303 (1969)

Ne	22	10

METHOD

REF. NO. 69 Ho 1 egf

REACTION	RESULT	EXCITATION ENERGY	SOURCE		DETECTOR		ANGLE
			TYPE	RANGE	TYPE	RANGE	
G,XP	ABY	THR-33	C	24-33	SCI-D	3-14	90

Tabelle 1. *Daten zu den einzelnen Reaktionen. Die Werte für den integrierten Wirkungsquerschnitt wurden unter der Annahme ausschließlicher Grundzustandsübergänge berechnet. Für ^{23}Na und ^{39}K als Ausnahme s. Text*

Target	Anreicherungsgrad %	(γ, p)-Schwelle MeV	Druck oder Dicke	Endenergie MeV	Zahl gemess. Protonen	Ausbeute µb MeV sr	$\int_{32.5}\sigma(E)dE$ MeVmb	Figur
^{16}O	99	16,0	230 Torr	32,5	36074	58 ± 7	38 ± 6	1, 2
^{20}Ne	90,9	12,8	450 Torr	28,0	3175	7,4 ± 1	—	—
			610 Torr	32,5	6293	14,9 ± 2	61 ± 11	5, 6
^{22}Ne	99,9	15,3	240 Torr	24,0	1960	2,3 ± 0,4	—	4, 5
				28,0	4790	3,6 ± 0,6	—	4, 5
				32,5	5210	6,7 ± 0,9	45 ± 8	4, 5
^{23}Na	100	8,8	65µ	24,0	14182	6,3 ± 1,0	—	7
			60µ	32,5	11152	12,8 ± 2,0	117 ± 30	7
^{36}Ar	99	8,5	250 Torr	32,5	45173	57 ± 6	270 ± 40	8, 10
^{40}Ar	99,6	12,5	230 Torr	32,5	29559	14,2 ± 15	104 ± 15	9, 11
^{39}K	93,1	6,4	80µ	24,0	24230	17,4 ± 2,8	—	12
			90µ	32,5	24941	41,9 ± 6,7	405 ± 100	12
^{84}Kr	99	10,7	170 Torr	32,5	35515	12,7 ± 2,0	80 ± 20	14
Kr	natürl.	10	170 Torr	32,5	13570	12,5 ± 2,0	75 ± 20	13
Ne	natürl.	9	150 Torr	32,5	7553	7,6 ± 0,9	40 ± 7	15

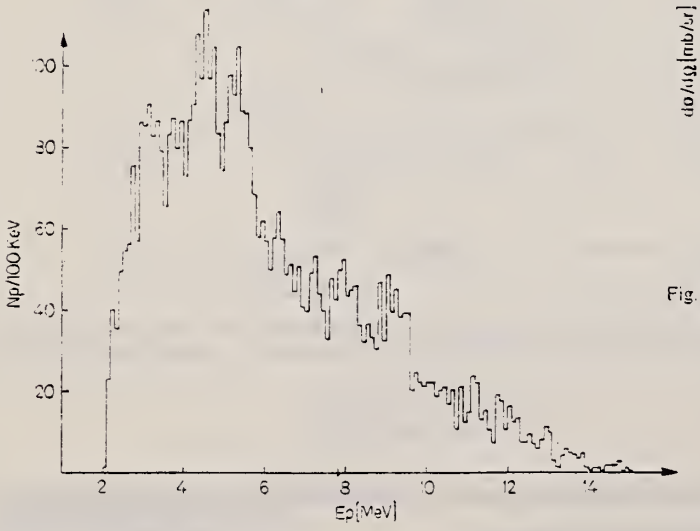

Fig. 3. Energieverteilung der Photoprotonen aus ^{22}Ne. $E_0 = 32.5$ MeV

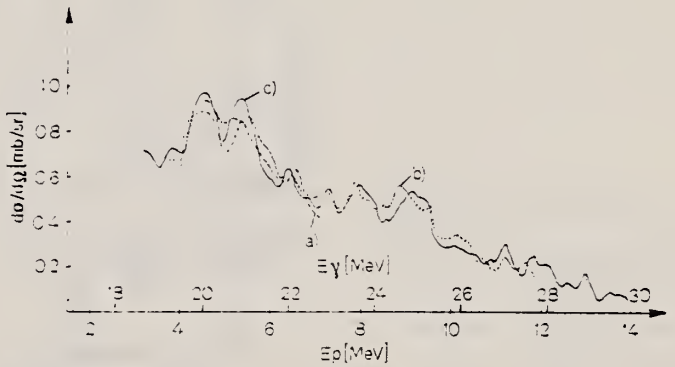

Fig. 4. Der (γ, p)-Wirkungsquerschnitt für ^{22}Ne, berechnet aus den Bestrahlungen bei *a* 24 MeV, *b* 28 MeV und *c* 32,5 MeV

REF.

R. P. Singhal, H. S. Caplan, J. R. Moreira, and T. E. Drake
Can. J. Phys. 51, 2125 (1973)

ELEM. SYM.	A	-
Ne	22	10

METHOD

REF. NO.: 73 Si 15 hmg

REACTION	RESULT	EXCITATION ENERGY	SOURCE		DETECTOR		ANGLE
			TYPE	RANGE	TYPE	RANGE	
E,E/	FMF	1	D	77-115	MAG-D		DST
		(1,275)					

LEVEL AT 1.275 MEV

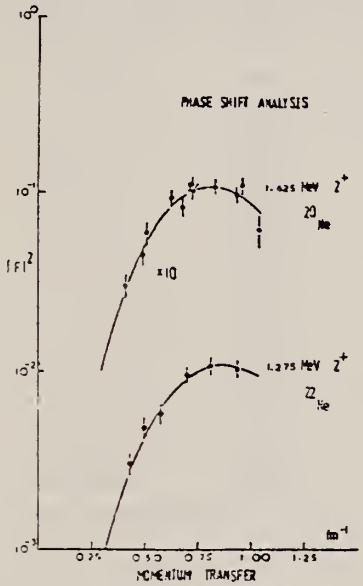

FIG. 6. The result of best fits to the 1.625 MeV, 2^+ state in ^{20}Ne and 1.275 MeV, 2^+ state in ^{22}Ne. Tassie model has been used in a phase shift code for the fits.

TABLE 2. Experimental form factors for the 1.275 MeV state in ^{22}Ne

E_0 (MeV)	θ (deg)	Square of experimental form factor × 10^3 (errors in %)	
60.3	90	3.12	(15)
60.3	110	4.96	(15)
114.7	60	5.73	(15)
114.7	75	9.54	(10)
114.7	90	10.52	(10)
114.7	110	10.20	(10)

REF.

X.K. Maruyama, R.A. Lindgren, W.L. Bendel, E.C. Jones, Jr., and L.W. Fagg
Phys. Rev. C10, 2257 (1974)

SUBJECT		
Ne	22	10

METHOD

REF. NO.	
74 Ma 8	hmg

REACTION	RESULT	EXCITATION ENERGY	SOURCE		DETECTOR		ANGLE
			TYPE	RANGE	TYPE	RANGE	
E,E/	ABX	0- 19	D	37- 60	MAG-D		180

B(EL),J-PI

FOR ERRATUM SEE 78 Ma 6

TABLE III. Summary of results of this experiment showing excitation energy, spin and parity, transition radius, reduced matrix elements, electromagnetic width to the ground state, and transition strength. The Weisskopf unit is defined in Ref. 12. Where two J^π assignments are made, the data are compatible with either designation.

Level energy (MeV)	J^π	R (fm)	$B(\lambda L)\uparrow$ (e^2 fm^{2L} or μ_0^2 fm^{2L-2})	Γ_γ (eV)	Transition strength (Weisskopf units)
5.31 ± 0.03	1^-	$2.51^{+0.18}_{-0.31}$	0.074 ± 0.013	0.127 ± 0.022	0.040 ± 0.007
6.82 ± 0.03	1^+	$2.24^{+0.24}_{-0.42}$	0.166 ± 0.026	0.611 ± 0.096	0.092 ± 0.014
9.14 ± 0.03	1^+	$2.85^{+0.11}_{-0.14}$	0.320 ± 0.030	2.83 ± 0.26	0.176 ± 0.016
10.84 ± 0.06	1^+	$2.86^{+0.25}_{-0.30}$	$0.045^{+0.015}_{-0.012}$	$0.66^{+0.21}_{-0.17}$	$0.025^{+0.009}_{-0.006}$
10.08 ± 0.03	1^-	$3.15^{+0.15}_{-0.19}$	0.095 ± 0.016	1.13 ± 0.14	0.042 ± 0.007
	1^-	$1.89^{+0.84}_{-1.89}$	$0.031^{+0.029}_{-0.007}$	33^{+10}_{-7}	$0.061^{+0.017}_{-0.014}$
12.56 ± 0.06	1^+	$3.14^{+0.32}_{-0.66}$	$0.058^{+0.027}_{-0.028}$	$1.3^{+0.85}_{-0.65}$	$0.032^{+0.021}_{-0.015}$
	1^-	$2.60^{+0.51}_{-2.60}$	$0.21^{+0.011}_{-0.009}$	44^{+33}_{-17}	$0.042^{+0.026}_{-0.016}$
7.63 ± 0.03	2^-	3.69 ± 0.30	$10.1^{+2.5}_{-2.3}$	$(2.84^{+0.57}_{-0.51}) \times 10^{-3}$	$0.78^{+0.19}_{-0.17}$
8.54 ± 0.03	2^-	$3.07^{+0.53}_{-1.10}$	$3.5^{+2.1}_{-1.2}$	$(1.48^{+0.57}_{-0.53}) \times 10^{-3}$	$0.27^{+0.16}_{-0.09}$
11.86 ± 0.08	2^-	$4.10^{+0.25}_{-0.53}$	$6.9^{+2.9}_{-2.1}$	$(1.49^{+0.6}_{-0.5}) \times 10^{-3}$	$0.52^{+0.22}_{-0.18}$

TABLE II. Reduced matrix element extracted from fitting the data assuming an electric quadrupole transition.

Level energy (MeV)	$B(E2)\uparrow$ (e^2 fm^4)
5.31 ± 0.03	22.9 ± 5.6
6.82 ± 0.03	32.0 ± 6.2
9.14 ± 0.03	38.2 ± 4.9
10.08 ± 0.08	$8.0^{+1.6}_{-0.9}$
10.84 ± 0.06	3.5 ± 0.9
12.56 ± 0.06	$3.0^{+1.9}_{-1.4}$

TABLE I. Values of differential cross sections for states observed in this experiment in units of 10^{-32} cm^2/sr. The incident electron energies are 37.39, 50.65, and 60.85 MeV.

Excitation energy (MeV)	$(d\sigma/d\Omega)_{37}$	$(d\sigma/d\Omega)_{50}$	$(d\sigma/d\Omega)_{60}$
1.27 ± 0.15	≤0.16	≤0.14	≤0.020
5.31 ± 0.03	0.268 ± 0.033	0.185 ± 0.020	0.109 ± 0.012
6.82 ± 0.03	0.640 ± 0.069	0.510 ± 0.053	0.337 ± 0.034
7.63 ± 0.03	0.191 ± 0.029	0.209 ± 0.024	0.171 ± 0.021
8.54 ± 0.03	≤0.19	0.116 ± 0.015	0.127 ± 0.017
9.14 ± 0.03	0.992 ± 0.103	0.607 ± 0.062	0.326 ± 0.035
10.08 ± 0.08	0.257 ± 0.036	0.107 ± 0.016	0.068 ± 0.011
10.84 ± 0.06	0.134 ± 0.028	0.092 ± 0.012	0.039 ± 0.008
11.86 ± 0.08	0.097 ± 0.030	0.107 ± 0.016	0.072 ± 0.010
12.56 ± 0.06		0.087 ± 0.017	0.040 ± 0.009
13.55 ± 0.10			0.029 ± 0.009
14.49 ± 0.15			0.163 ± 0.020
15.68 ± 0.25			0.068 ± 0.015
16.93 ± 0.20 / 17.43 ± 0.10 / 17.98 ± 0.08			0.157 ± 0.024
18.73 ± 0.20			0.112 ± 0.018

(over)

TABLE IV. Excitation energies (MeV) and spin and parity of states observed in the present experiment, compared with states observed in other experiments.

Present work, level energy, and J^π	(t,p) [a]	(d,p) [b]	$(^7\mathrm{Li},t)$ [c]	(t,α) [d]	Currently-accepted [e] level energy and J^π
1.27 ± 0.15					1.275 2^+
5.31 ± 0.03 1^+		5.331		5.350	5.335 ± 0.009 $(1,2)^+$
	5.340	5.359	5.370	5.360	5.360 ± 0.003 2^+
	6.823	6.821	6.820	6.800	6.819 ± 0.007 2^+
6.82 ± 0.03 1^+	6.860	6.858		6.840	6.855 ± 0.003 $(1,2)^+$
	7.633	7.630	7.640		7.632 ± 0.003 $(1,2)^+$
7.63 ± 0.03 2^-	7.663	7.658			7.660 ± 0.003 $(0-3)^-$
8.54 ± 0.03 2^-		8.548			8.548 ± 0.010 $(0-4)^+$
	8.575	8.585	8.590		8.583 ± 0.003 $(1,2)^+$
9.14 ± 0.03 1^+	9.174				9.174 ± 0.015
	$(\alpha,\eta\gamma)$ [f]	(α,α) [g]	$(t,^3\mathrm{He})$ [h]		Currently-accepted [e] level energy and J^π
	11.745				11.75 ± 0.01
	11.751	11.76			11.76 ± 0.01 1^-
11.86 ± 0.03 2^-	11.89	11.89			11.89 ± 0.01 1^-
					11.92 ± 0.01 (2^+)
		12.48			12.48 ± 0.01 (2^+)
12.56 ± 0.06 $(1^+,1^-)$		12.58			12.58 ± 0.01 (1^-)
		12.61			12.61 ± 0.01 $(1^-,2^+)$
15.68 ± 0.25			15.400 ± 0.040, $T=2$		
			15.610 ± 0.060, $T=2$		

[a] $^{20}\mathrm{Ne}(t,p)^{22}\mathrm{Ne}$, Ref. 22.
[b] $^{21}\mathrm{Ne}(d,p)^{22}\mathrm{Ne}$, Ref. 24.
[c] $^{18}\mathrm{O}(^7\mathrm{Li},t)^{22}\mathrm{Ne}$, Ref. 25.
[d] $^{23}\mathrm{Na}(t,\alpha)^{22}\mathrm{Ne}$, Ref. 23.
[e] Reference 21.
[f] $^{18}\mathrm{O}(\alpha,\eta\gamma)^{21}\mathrm{Ne}$, Ref. 27.
[g] $^{18}\mathrm{O}(\alpha,\alpha)^{18}\mathrm{O}$, Ref. 28.
[h] $^{22}\mathrm{Ne}(t,^3\mathrm{He})^{22}\mathrm{F}$, Ref. 20.

[20] R. H. Stokes and P. G. Young, Phys. Rev. 178, 1789 (1969).
[21] P. M. Endt and C. Van der Leun, Nucl. Phys. A214, 1 (1973), and references therein.
[22] M. G. Silbert and N. Jaramie, Phys. Rev. 123, 221 (1961).
[23] S. Hinds, private communication to Ref. 21.
[24] P. Neogy, R. Middleton, and W. Scholz, Phys. Rev. C 6, 885 (1972).
[25] W. Scholz, P. Neogy, K. Bethge, and R. Middleton, Phys. Rev. C 6, 893 (1972).
[26] W. Kutschera, D. Pelte, and G. Schrieder, Nucl. Phys. A111, 529 (1968).
[27] G. Chouraqui, Th. Muller, M. Port, and J. M. Thirion, J. Phys. (Paris) 31, 249 (1970).
[28] S. Corodetzky, M. Port, J. Graff, J. M. Thirion, and G. Chouraqui, J. Phys. (Paris) 29, 271 (1968).
[12] See, for example, S. J. Skorka, J. Hertel, and T. W. Retz-Schmidt, Nucl. Data A 2, 347 (1966).

REF.

A. Veyssiere, H. Beil, R. Bergere, P. Carlos, A. Lepretre, and A. De Miniac
Nucl. Phys. A227, 513 (1974)

ELEM. SYM.	A	Z
Ne	22	10

METHOD

REF. NO.	
74 Ve 1	egf

REACTION	RESULT	EXCITATION ENERGY	SOURCE		DETECTOR		ANGLE
			TYPE	RANGE	TYPE	RANGE	
G,2N *	ABX	18- 26	D	18- 26	BF3-I		4PI

*871

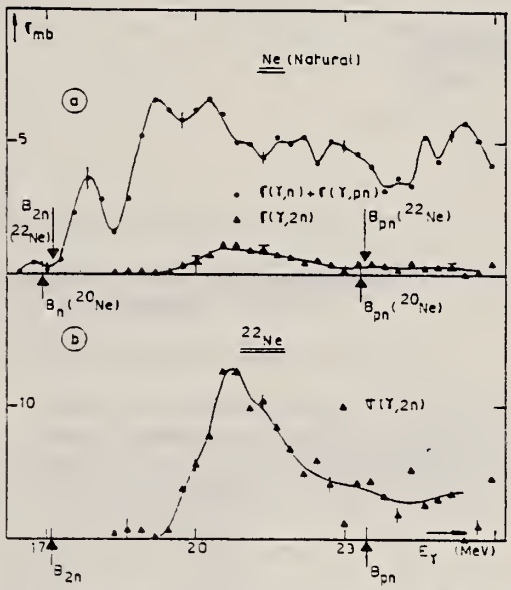

Fig. 4. (a) Photonuclear cross sections $[\sigma(\gamma, n)-\sigma(\gamma, pn)]$ and $\sigma(\gamma, 2n)$ for natural Ne. (b) Partial photoneutron cross section $\sigma(\gamma, 2n)$ of ^{22}Ne.

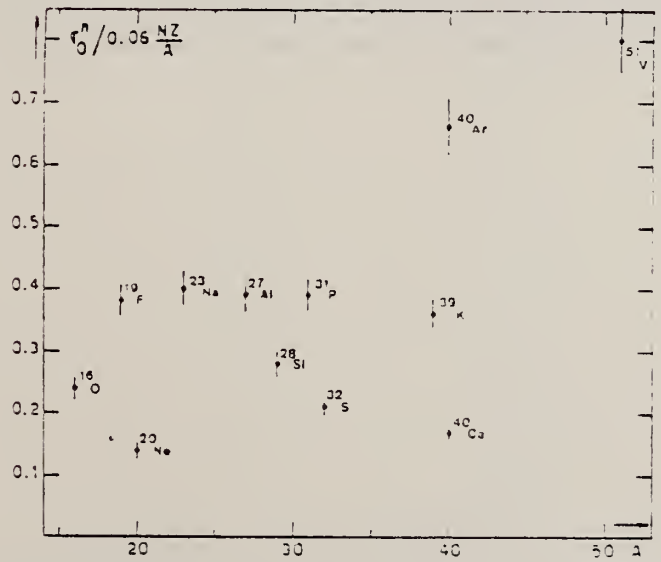

Fig. 22. Ratio of experimental integrated photoneutron cross section σ_0^n over the Thomas, Reiche and Kuhn sum rule $[0.06\,NZ/A]$. Numerical values and upper integration limits E_M are taken from table 3. Also $\Delta\sigma_0^n = \pm 7\%$ for all nuclei.

(over)

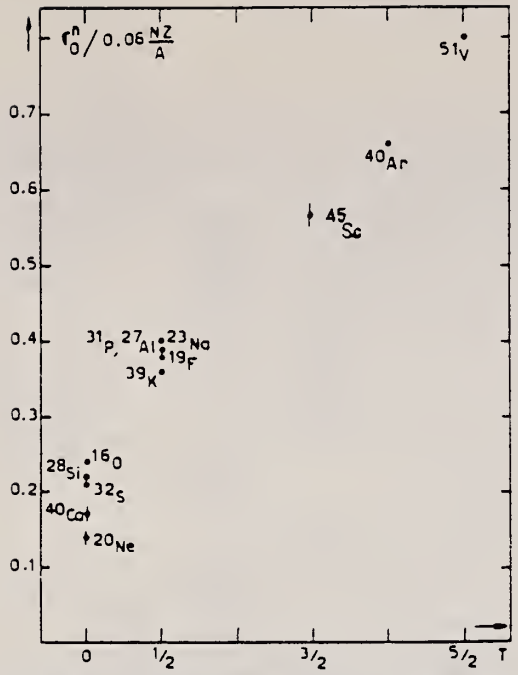

Fig. 24. The $[\sigma_0^n/(0.06\,NZ/A)]$ ratio as a function of isospin T. Possible overall errors of $\pm 7\%$ are to be applied to all nuclei shown.

TABLE 3

Experimental integrated photoneutron cross sections $\sigma_0^n = \int_0^{E_M} \sigma_{Tn}(E)\mathrm{d}E$ compared with the classical sum rule $[0.06\,NZ/A]$ of Thomas, Reich and Kuhn

	$T=0$					$T=\frac{1}{2}$					$T=\frac{3}{2}$	$T=2$	$T=\frac{5}{2}$
Nucleus	^{16}O	^{20}Ne	^{28}Si	^{32}S	^{40}Ca	^{19}F	^{23}Na	^{27}Al	^{31}P	^{39}K	^{45}Sc	^{40}Ar	^{51}V
σ_0^n (MeV · mb)	58 ±4	42 ±3	94 ±7	98 ±7	100 ±7	108 ±7	137 ±9	158 ±10	182 ±12	210 ±14	383 ±25	393 ±28	602 ±42
$\sigma_0^n/(0.06NZ/A)$	0.24	0.14	0.22	0.21	0.17	0.38	0.40	0.39	0.39	0.36	0.57	0.66	0.8
E_{int} (MeV)	30	26.7	30	30	29.5	29	30	30	29	30	28.1	26.7	28

REF. X.K. Maruyama, R.A. Lindgren, W.L. Bendel, E.C. Jones, Jr., and L.W. Fagg
Phys. Rev. C 17, 856 (1978)

ELEM. SYM.	A	Z
Ne	22	10

METHOD

REF. NO. 78 Ma 6 hg

REACTION	RESULT	EXCITATION ENERGY	SOURCE		DETECTOR		ANGLE
			TYPE	RANGE	TYPE	RANGE	
E,E/	ABX	0- 19	D	37- 60	MAG-D		180

ERRATUM SEE 74Ma8

Erratum: Excitation of $M1$ and $M2$ states in ^{22}Ne by 180° electron scattering [Phys. Rev. C 10, 2257 (1974)]

X. K. Maruyama, R. A. Lindgren, W. L. Bendel, E. C. Jones, Jr., and L. W. Fagg

Cross sections, reduced matrix elements, electromagnetic widths to the ground state, and transition strengths for ^{22}Ne deduced from the experimental data should be multiplied by 2. The published results were obtained with a miscalculation of the relative densities of ^{22}Ne and H_2. On p. 2262, first paragraph, right hand column, last two lines, there is a typographical error; $2.79\mu_0$ and $-1.91\mu_0$ should be interchanged.

REF. H.P. Trautvetter, M. Wiescher, K.-U. Kettner, C. Rolfs & J.W. Hammer
Nucl. Phys. A297, 489 (1978)

ELEM. SYM.	A	Z
Ne	22	10

METHOD

REF. NO.: 78 Tr 3 | hmg

REACTION	RESULT	EXCITATION ENERGY	SOURCE TYPE	SOURCE RANGE	DETECTOR TYPE	DETECTOR RANGE	ANGLE
A,G	SPC	10-12	D	0-3	SCD-D		DST
		(10.2-11.47)		(.66-2.20)			

Abstract: The $^{18}O(\alpha, \gamma)^{22}Ne$ capture reaction has been studied at E_α = 0.6–2.3 MeV. The known resonance at E_α = 2.20 MeV has been established and fourteen new resonances have been found in the energy range covered. The E_α = 1.16, 1.32, 1.45, 1.53, 1.87, 1.96 and 2.15 MeV resonances correspond to resonances observed previously in the $^{18}O(\alpha, n)^{21}Ne$ reaction. The E_α = 0.77, 1.25 and 1.27 MeV resonances represent new compound states in ^{22}Ne. Information on branching ratios, $\omega\gamma$ values and total widths is reported. Transition strength arguments and analyses of γ-ray angular distribution data together with results from previous work resulted in the most likely J^π assignments for the resonances.

The E_α = 1.66 and 1.78 MeV resonances are good candidates for the two $J^\pi = 8^+$ states predicted at $E_x \approx$ 11–12 MeV and are probably members of the $K^\pi = 0^+$ (ground state) and $K^\pi = 2^+$ rotational bands in ^{22}Ne.

The investigated energy range of E_α together with that of previous work corresponds to stellar temperatures of $T = (0.3-4.3) \times 10^9$ K. The astrophysical reaction rate determined from these data is compared with predictions based in part on the nuclear optical model. The rate is also compared with that of the competing $^{18}O(\alpha, n)^{21}Ne$ reaction.

10.2, 10.92, 11.47 MEV

E NUCLEAR REACTIONS $^{18}O(\alpha, \gamma)$, E = 0.6–2.3 MeV; measured E_α, E_γ, I_γ, $I_\gamma(\theta)$, $I_\gamma(E)$. ^{22}Ne deduced resonances, resonance strength, Γ, J, π, δ, γ-ray branching ratios, astrophysical reaction rate. Enriched ^{18}O targets. Ge(Li) detector.

TABLE 2

Summary of the angular distribution results for $^{18}O(\alpha, \gamma)^{22}Ne$ resonances

E_α (MeV)	Transition (MeV)	a_2 [a]	a_4 [a,b]
1.45	R → 1.27	0.9 ±0.3	−0.5 ±0.5
	1.27 → 0	0.4 ±0.3	
1.53	R → 0	−1.0 ±0.3	
	R → 1.27	−0.15 ±0.13	
	1.27 → 0	0.35 ±0.12	
1.87	R → 1.27	0.3 ±0.4	
	R → 8.90	−0.1 ±0.2	
	8.90 → 1.27	0.1 ±0.3	
	1.27 → 0	−0.1 ±0.1	
1.96	R → 3.36	1.2 ±0.4	
	R → 6.34	0.1 ±0.4	
	6.34 → 3.36	0.8 ±0.2	−0.3 ±0.4
	3.36 → 1.27	0.4 ±0.2	
	1.27 → 0	0.7 ±0.2	
2.20	R → 0	−1.06 ±0.11	0.08 ±0.12
	R → 1.27	−0.28 ±0.14	
	R → 5.15	−0.14 ±0.10	−0.15 ±0.11
	5.15 → 1.27	0.74 ±0.18	−0.3 ±0.3
	4.46 → 1.27	0.20 ±0.10	
	1.27 → 0	0.24 ±0.02	−0.03 ±0.05

[a]) Corrected for finite solid angle of the Ge(Li) detector and finite size of the beam spot on the target.
[b]) A_4 terms are included only in the analyses, if the a_2 term alone could not fit the data ($\chi^2_{norm} \geqq 1.4$). The errors are obtained by variation of the a_4 terms within the statistical errors of the data.

(OVER)

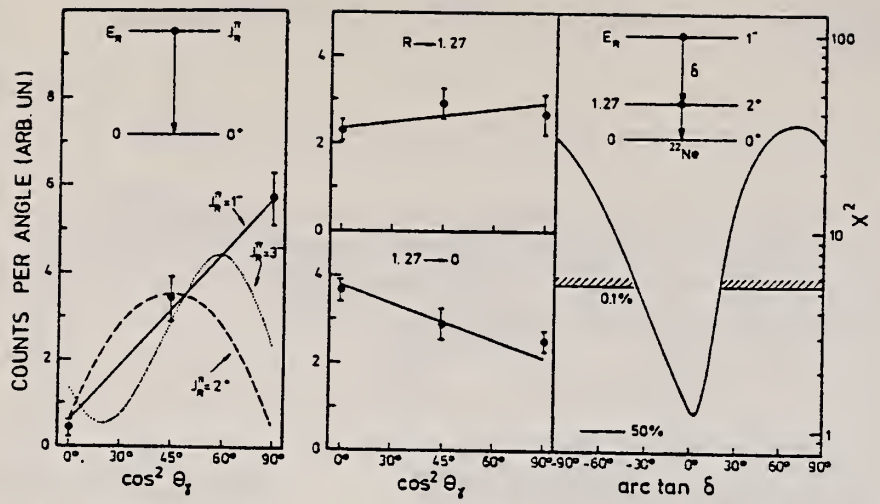

Fig. 6. The γ-ray angular distributions for the R → 0 and R → 1.27 → 0 transitions obtained at the E_x = 1.53 MeV resonance are shown together with their analyses.

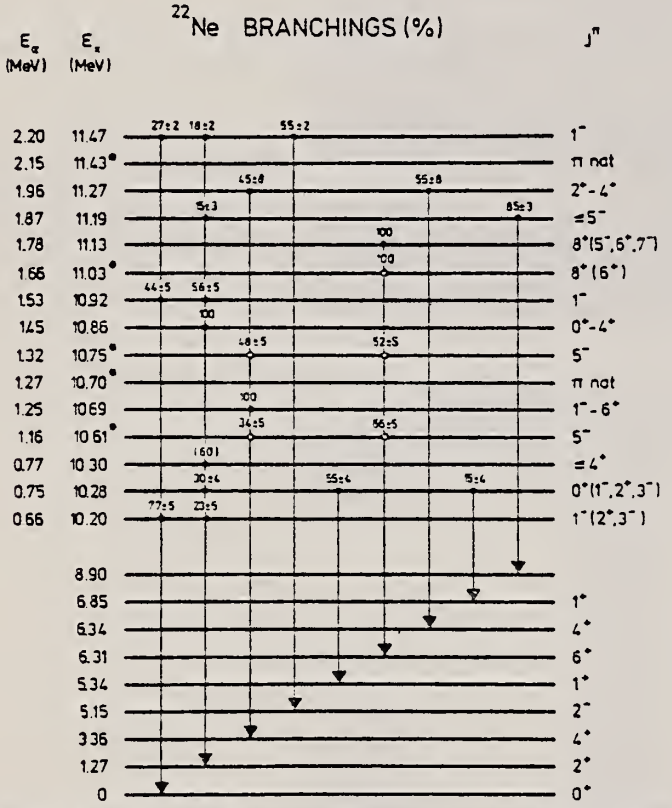

Fig. 7. Summary of results on branching ratios and J^π assignments to states in ^{22}Ne above the α-particle threshold. The stars on the E_x values mark those resonance states, which have been established in the present work only through the 1.27 MeV secondary γ-ray transition. The open circles indicate that the branching ratios for these states are taken from ref. [9]). Information on E_x and J^π values for the bound states are obtained from refs. [9, 10, 22, 25]).

REF. U. E. P. Berg, K. Wienhard
Nucl. Phys. A318, 453 (1979)

EL EM. SYM.	A	Z
Ne	22	10

METHOD

REF. NO. 79Be7 hg

REACTION	RESULT	EXCITATION ENERGY	SOURCE TYPE	SOURCE RANGE	DETECTOR TYPE	DETECTOR RANGE	ANGLE
G,G	ABI	5-11	C	UKN-18	SCD-D		DST
		(5.328-10.203)					

Abstract: States at 5.328, 6.851, 8.553, 9.165 and 10.203 MeV in ^{22}Ne have been observed in a nuclear resonance fluorescence experiment using bremsstrahlung and high resolution Ge(Li) diodes. Photon scattering cross sections, γ-ray decay widths to the ground and first excited states, and lifetimes are derived. The results are compared with inelastic electron scattering data and shell model calculations.

LFT

E NUCLEAR REACTION ^{22}Ne($\vec{\gamma}$, γ). $E < 18$ MeV; measured E_γ, $\sigma(\vec{\gamma}, \gamma)$. ^{22}Ne deduced mean lives, Γ_{γ_0}, B(M1) values. Enriched target.

TABLE I

Total photon scattering cross sections I_s, γ-ray decay widths Γ, mean lives, and M1 transition probabilities in ^{22}Ne from resonance fluorescence

E_x (keV)	E_γ at 127° (keV)	Decay mode	I_s (MeV mb)	Γ_0 (eV)	Γ_1 (eV)	$\left(\frac{\Gamma_i}{\Gamma}\right)_s$	Mean lives (fs)	B(M1, $1^- \rightarrow 0^-$) (μ_N^2)
5328 ± 5	5326	→ g.s.	0.10 ± 0.04	0.25 ± 0.10		1	$2.6^{+1.8}_{-0.9}$	0.15 ± 0.06
6851 ± 3	6849	→ g.s.	0.32 ± 0.11	1.65 ± 0.65		0.79	$0.31^{+0.35}_{-0.09}$	0.44 ± 0.15
	5576	6851 → 1275	0.085 ± 0.049		0.44 ± 0.28	0.21		
8553 ± 3	8549	→ g.s.	0.20 ± 0.08	1.28 ± 0.51		1	$0.51^{+0.34}_{-0.14}$	0.18 ± 0.07
9165 ± 3	9161	→ g.s.	0.75 ± 0.25	5.44 ± 1.81		1	$0.12^{+0.06}_{-0.03}$	0.61 ± 0.20
10203 ± 4	10198	→ g.s.	0.87 ± 0.29	9.38 ± 3.25		0.84	$0.059^{+0.033}_{-0.016}$	
	8923	10203 → 1275	0.17 ± 0.07		1.83 ± 0.78	0.16		

REF. X. K. Maruyama, F. J. Kline, J. W. Lightbody, Jr., S. Penner, W. J. Briscoe, M. Lunnon, H. Crannell
Phys. Rev. C19, 1624 (1979)

ELEM. SYM.	A	Z
Ne	22	10

METHOD

REF. NO.	
79Ma3	hg

REACTION	RESULT	EXCITATION ENERGY	SOURCE		DETECTOR		ANGLE
			TYPE	RANGE	TYPE	RANGE	
E,E/	FMF	1-9	D	60-110	MAG-D	51-109	DST
		(1.275-8.59)					

The states of ^{22}Ne below 8.6 MeV excitation energy have been studied using the technique of inelastic electron scattering. Ratios of inelastic to elastic scattering cross sections were measured with incident electron energies between 60 and 110 MeV and scattering angles of 110° and 128°. Form factors for 14 inelastic transitions were measured for the momentum transfer range 0.4 to 1.0 fm^{-1}. Reduced transition probabilities for these states have been deduced and assignments of spin and parity have been made.

14 LEVELS, J-PI, B(CL)

Comparison of J^{π} results with assignments given in 7 other references is made in Table VIII.

[NUCLEAR REACTIONS ^{22}Ne(e,e'), E=60 to 110 MeV; measured $\sigma(E)$ at 110° and 128° up to 8.6 MeV in excitation energy; deduced J, π, $B(CL)$. Enriched ^{22}Ne target.]

TABLE IV. Squared longitudinal form factors, F_L^2 obtained from this experiment. Coulomb correction factors f_c have been applied to all states. For the state at 6.27 MeV, no Coulomb correction factor was applied. F_L^2 for the states at 6.70, 7.46, 8.17, and 8.59 MeV are tabulated assuming $J^{\pi}=3^-$; to compute F_L^2 assuming $J^{\pi}=2^+$ for these states, multiply by the ratio $f_c(2^+)/f_c(3^-)$ from the values of Table III.

E_0 (MeV)	θ (deg)	$F_L^2 \times 10^3$				
		E_x (MeV), J^{π} 1.275, 2$^+$	3.36, 4$^+$	4.46, 2$^+$	5.91, 3$^-$	6.14, 2$^+$
59.59	110.39	4.30 ± 0.21	···	0.215 ± 0.027	0.075 ± 0.021	0.083 ± 0.020
59.59	110.39	4.85 ± 0.26	···	0.204 ± 0.015	0.080 ± 0.013	0.047 ± 0.014
59.59	110.39	4.57 ± 0.20	···	0.232 ± 0.019	0.070 ± 0.023	0.051 ± 0.012
69.69	110.45	6.56 ± 0.28	···	0.304 ± 0.020	0.163 ± 0.013	···
69.91	110.39	7.68 ± 0.32	···	0.309 ± 0.025	0.157 ± 0.019	0.078 ± 0.023
85.13	110.36	9.89 ± 0.42	0.004 ± 0.011	0.430 ± 0.024	0.287 ± 0.021	0.098 ± 0.015
100.34	110.36	11.61 ± 0.49	0.163 ± 0.012	0.462 ± 0.026	0.736 ± 0.035	0.134 ± 0.021
110.61	110.28	10.86 ± 0.46	0.229 ± 0.075	0.496 ± 0.028	0.974 ± 0.045	0.139 ± 0.023
63.84	128.16	6.48 ± 0.33	···	0.257 ± 0.023	···	···
77.42	128.17	9.39 ± 0.39	0.045 ± 0.026	0.386 ± 0.029	0.362 ± 0.020	0.115 ± 0.015
110.56	128.05	10.84 ± 0.57	0.386 ± 0.045	0.461 ± 0.040	1.377 ± 0.075	0.151 ± 0.031
		E_x (MeV), J^{π} 6.27, 0$^+$	6.70, (3$^-$,2$^+$)	6.90, 1$^-$	7.06, 2$^+$	7.46, (3$^-$,2$^+$)
59.59	110.39	0.089 ± 0.022	0.090 ± 0.021	0.156 ± 0.030	···	···
59.59	110.39	0.087 ± 0.016	0.082 ± 0.013	0.130 ± 0.020	···	···
59.59	110.39	0.083 ± 0.019	0.055 ± 0.014	0.103 ± 0.025	0.052 ± 0.016	···
69.91	110.39	0.102 ± 0.026	0.121 ± 0.018	0.175 ± 0.028	0.068 ± 0.019	0.052 ± 0.010
85.13	110.36	0.097 ± 0.016	0.180 ± 0.013	0.164 ± 0.021	0.072 ± 0.011	0.116 ± 0.012
110.34	110.36	0.138 ± 0.020	0.319 ± 0.021	0.152 ± 0.037	0.120 ± 0.016	0.206 ± 0.017
110.61	110.28	0.156 ± 0.021	0.344 ± 0.024	0.083 ± 0.042	0.115 ± 0.021	0.271 ± 0.021
77.42	128.17	0.133 ± 0.015	0.207 ± 0.015	0.165 ± 0.043	0.079 ± 0.010	0.121 ± 0.011
110.56	128.05	0.170 ± 0.028	0.451 ± 0.032	0.031 ± 0.073	0.120 ± 0.034	0.308 ± 0.028
		E_x (MeV), J^{π} 7.65, 2$^+$	7.93, 2$^+$	8.17, (3$^-$,2$^+$)	8.59, (3$^-$,2$^+$)	
59.59	110.39	0.282 ± 0.025	0.072 ± 0.013	0.021 ± 0.012	0.131 ± 0.012	
69.91	110.39	0.467 ± 0.030	0.127 ± 0.018	···	0.235 ± 0.021	
85.13	110.36	0.782 ± 0.038	0.195 ± 0.014	0.074 ± 0.012	0.371 ± 0.034	
100.34	110.36	0.921 ± 0.049	0.213 ± 0.019	0.075 ± 0.016	0.557 ± 0.034	
110.61	110.28	1.007 ± 0.053	0.201 ± 0.021	0.113 ± 0.019	0.653 ± 0.037	
77.42	128.17	0.731 ± 0.045	0.179 ± 0.018	0.063 ± 0.014	0.396 ± 0.042	
110.56	128.05	1.122 ± 0.073	0.151 ± 0.025	0.126 ± 0.023	0.917 ± 0.064	

(continued)

TABLE VI. Excitation energies and reduced transition probabilities. The energies of states from the literature identified with the experimentally observed states are presented along with the assumed J^π and deduced $B(CL)\uparrow$. The $B(CL)\uparrow$ are averages of those in Table V. The uncertainties associated with $B(CL)\uparrow$ reflect the range of values including fitting errors allowed by the models considered. Where fewer than four of the models considered allowed a satisfactory fit, the uncertainties are not presented. The reduced transition probabilities for those states are to be considered approximate values.

No.	E_x (lit.) (keV)	E_x (expt.) (MeV)	J^π	$B(CL)\uparrow$ (e^2 fm^{2L})
1	1274.57 ± 0.02	1.275 ± 0.010	2^+	271 ± 36
2	3357.2 ± 0.4	3.36 ± 0.02	4^+	17 000 ± 4000
3	4456.7 ± 1.6	4.46 ± 0.02	2^+	13 ± 2
9	5909.9 ± 1.8	5.91 ± 0.02	3^-	870 ± 250
10	6115 ± 6	6.14 ± 0.04	2^+	3.2 ± 1.5
11	6237 ± 5	6.27 ± 0.05	0^+	3.8 ± 1.1
15	6691 ± 4	6.70 ± 0.02	2^+	3.9 ± 1.5
			3^-	750 ± 400
18	6904 ± 1.6	6.90 ± 0.03	1^-	0.08 ± 0.04
19	7052 ± 7	7.06 ± 0.03	2^+	2.1 ± 1.2
25	7470 ± 20	7.46 ± 0.03	2^+	1.6
			3^-	350 ± 250
29	7644 ± 4	7.65 ± 0.02	2^+	18 ± 3
32	7924 ± 6	7.93 ± 0.02	2^+	5.7 ± 2.4
35	8162 ± 4	8.17 ± 0.02	2^+	1.3 ± 1.3
			3^-	270 ± 270
41	8593 ± 7	8.59 ± 0.02	2^+	7
			3^-	1 700

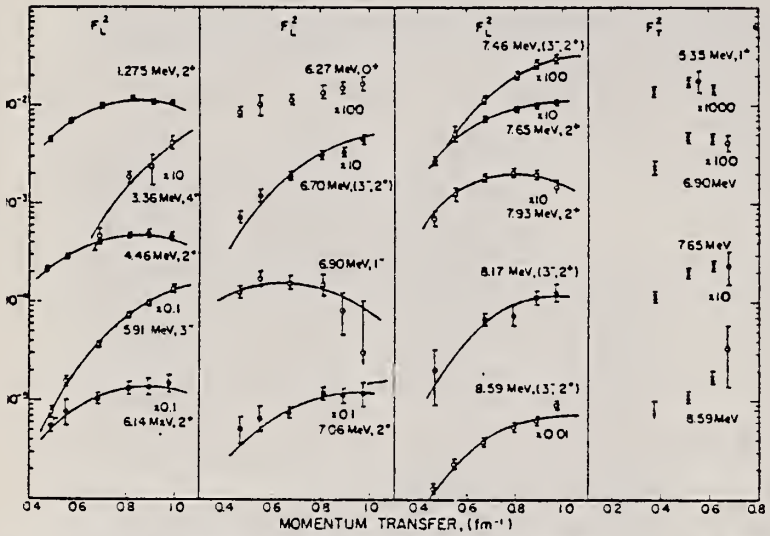

FIG. 2. Born approximation form factors for states observed in this experiment. F_L^2 for all states except at 6.27 MeV are the longitudinal squared form factors with Coulomb distortion corrections f_c applied. F_T^2 are the transverse squared form factors without Coulomb distortion corrections. The circles are measurements obtained in this experiment. Open and closed circles are used to aid in distinguishing among the various states. The solid line through the data are fits obtained using the generalized Helm model (model 4 of Table V). The crosses represent the 180° electron scattering data of Ref. 8.

SODIUM
Z=11

Sir Humphry Davy isolated sodium in the fall of 1807 and announced its discovery before the Royal Society in London in November of that year. He did electrolysis of sodium hydroxide to obtain the metal. The following year, Joseph Gay-Lussac (1778-1850) and Louis Thénard used a chemical process to reduce sodium hydroxide by iron at a high temperature. These two methods for sodium production produced a conflict that raged for over a century and was not resolved until the introduction of the Downs process in 1921 which made sodium the cheapest non-ferrous metal available. The incentive for all this activity was provided by Hans Christian Oersted's (1777-1851) discovery that sodium could be used to prepare pure aluminum by the reduction of aluminum chloride.

NA
A=21

NA
A=21

Ref. R.E. Benenson, L.J. Lidofsky
Phys. Rev. 123, 939 (1961)

Elem. Sym.	A	Z
Na	21	11

Method: Van de Graaff; NaI

Ref. No.: 61 Be 2 JHH

Reaction	E or ΔE	E_o	Γ	$\int \sigma dE$	Jπ	Notes
(p,γ)	1.17	3.61±0.06				

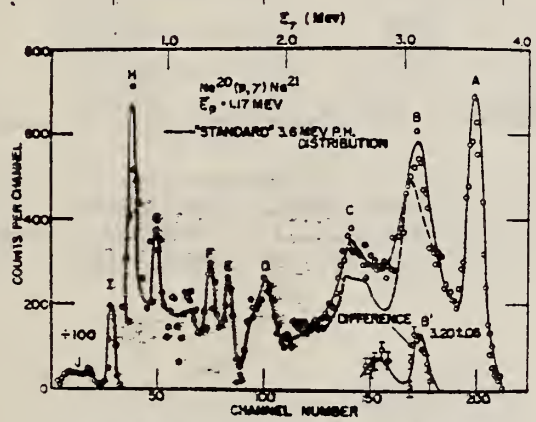

FIG. 7. Single 3×3 NaI crystal spectrum of gamma rays following capture of 1.17-Mev protons by Ne^{20}.

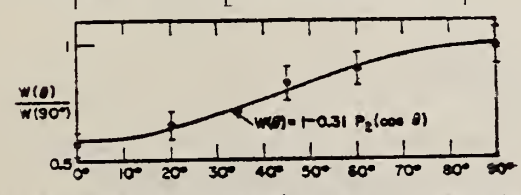

FIG. 8. Angular distribution of gamma rays corresponding to peak *A* of Fig. 7.

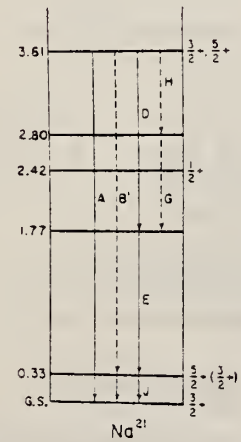

FIG. 11. Energy-level scheme of Na^{21} from present work. Gamma-ray transitions are labeled by letters corresponding to peaks in Fig. 7. Dashed lines indicate transitions based purely on energy differences with no further supporting evidence.

REF. R. C. Bearse, J. C. Legg, G. C. Morrison, and R. E. Segel
Phys. Rev. C 1, 608 (1970)

ELEM. SYM.	A	Z
Na	21	11

METHOD

REF. NO. 70 Be 3 hmg

REACTION	RESULT	EXCITATION ENERGY	SOURCE TYPE	SOURCE RANGE	DETECTOR TYPE	DETECTOR RANGE	ANGLE
P,G	LFT	8-10	D	6-8	SCD-D	0-9	90
				(6.850-7.215)			

8.973,9.216 MEV

The γ decays of the two lowest $T=\frac{3}{2}$ states in Na^{21} at 8.97 and 9.22 MeV were studied as resonances in the $Ne^{20}(p,\gamma)$ reaction by use of a gas cell and a 30-cc Ge(Li) detector. For the lower resonance, we find three branches: to the $\frac{3}{2}^+$ ground state (11%), to the $\frac{1}{2}^+$ first excited state (50%), and to the $\frac{5}{2}^+$ second excited state (39%). These results imply that $J=\frac{3}{2}^+$ for the $T=\frac{3}{2}$ state. On the simple rotational model, transitions from states of the $K=\frac{1}{2}$ (Nilsson orbit #6) band are possible only to the ground-state $K=\frac{1}{2}$ (#7) band. A $J=\frac{1}{2}^+$, $K=\frac{1}{2}$ assignment for the lowest $T=\frac{3}{2}$ state fits the observed branching ratios. The second resonance decays predominantly to the ground state, and there is at most a 9% branch to the $\frac{1}{2}^+$ state at 2.41 MeV. The second resonance is assigned $J=\frac{1}{2}^+$, $K=\frac{1}{2}$. If the 2.41-MeV state is $K=\frac{1}{2}$ (#9), no transition to it is expected. On both resonances, transitions to higher excited states are obscured by background.

TABLE I. Radiative widths for the various observed transitions. In calculating the widths for the decay of the 8.973-MeV state, the proton branching ratio estimated from the work of Hardy and Bell[a] has been used; for the 9.216-MeV state,[a] the branching ratio given by McDonald *et al.*[b] has been used.

$E_i(T=\frac{3}{2})\rightarrow E_f(T=\frac{1}{2})$	$J_i^\pi\rightarrow J_f^\pi$	$\frac{(2J_i+1)}{(\Gamma_p\Gamma_\gamma/\Gamma)}$ (eV)	Γ_γ (eV)	$\lvert M_{M1}\rvert^2$
8.973→0	$\frac{5}{2}^+\rightarrow\frac{3}{2}^+$	1.1	0.73±0.3	0.06±0.03
8.973→0.338	$\frac{5}{2}^+\rightarrow\frac{5}{2}^+$	5.1	3.3±0.6	0.31±0.06
8.973→1.72	$\frac{5}{2}^+\rightarrow\frac{7}{2}^+$	4.1	2.7±0.5	0.39±0.08
9.216→0	$\frac{1}{2}^+\rightarrow\frac{3}{2}^+$	8.7	9.5±1.9	0.68±0.13
9.216→2.41	$\frac{1}{2}^+\rightarrow\frac{1}{2}^+$	<0.8	<0.9	<0.17

[a] Reference 8. [b] Reference 7.

a[8] J. C. Hardy and R. E. Bell, Can. J. Phys. 43, 1671 (1965).
b[7] A. B. McDonald, J. R. Patterson, and H. Winkler, Bull. Am. Phys. Soc. 13, 652 (1968); and (to be published).

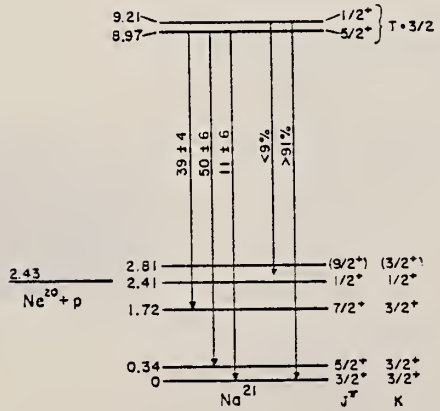

FIG. 3. γ-ray branching ratios for the two lowest $T=\frac{3}{2}$ states in Na^{21}. In computing the branching ratios, the angular distributions have been assumed to be those for pure $M1$ transitions.

REF. C. Rolfs and H. Winkler
Phys. Lett. 52B, 317 (1974)

ELEM. SYM.	A	Z
Na	21	11

METHOD

REF. NO. 74 Ro 4 egf

REACTION	RESULT	EXCITATION ENERGY	SOURCE TYPE	SOURCE RANGE	DETECTOR TYPE	DETECTOR RANGE	ANGLE
P,G	ABX	2- 3	D	1- 2	SCD-D		90

The high-energy tail of the $J^{\pi} = 1/2^+$, 2425 keV state in ^{21}Na, bound by 7 keV against proton decay, has been observed in the ^{20}Ne(p, γ)^{21}Na reaction at $E_p = 0.5-1.5$ MeV. The observed excitation function is consistent with a single-level Breit–Wigner shape with $\Gamma_\gamma = 0.31 \pm 0.07$ eV at $E_x = 2425$ keV.

$S(E) = \sigma(E) E_{cm} \exp(2\pi\eta)$

η = Coulomb parameter

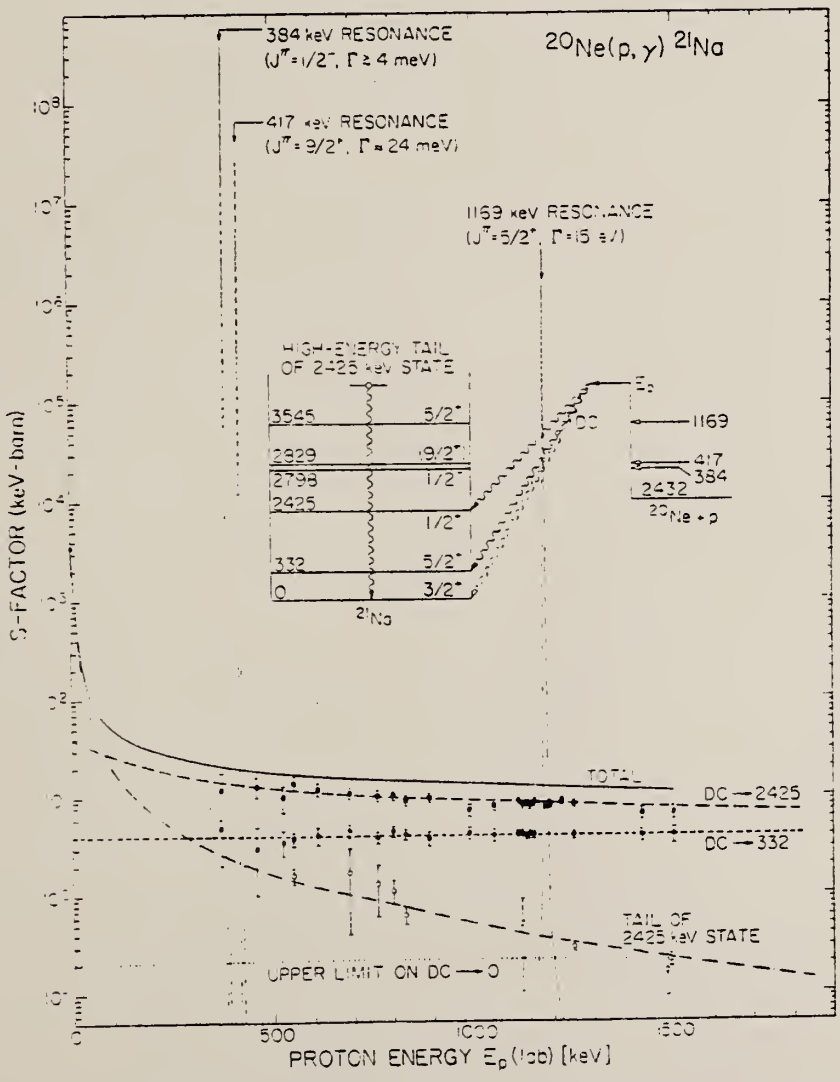

[2] C. Rolfs et al. to be published.

[3] P.M. Endt and C. Van der Leun, Nucl. Phys. A214 (1973) 1.

Fig. 2. Astrophysical *S*-factor for the ^{20}Ne(p, γ)^{21}Na reaction. The dashed lines through the DC → 332 and DC → 2425 keV data points taken from ref. [2] are model predictions. The dashed-dotted line is the theoretical prediction of the high-energy tail of the 2425 keV bound state. A possible DC process to the ground state would have almost the same energy dependence as the DC → 332 keV transition and is indicated as a dotted line. Shown also for comparison are the S-factor curves for the $J^{\pi} = (5/2)^+$, 1169 keV resonance [3] and for the new low-energy resonances at $E_p(J^{\pi}) = 384$ (1/2$^+$) and 417 (9/2$^+$) keV, observed in ref. [2].

NA
A=22

NA
A=22

Ref. R.W. Krone, J.J. Singh
Phys. Rev. 117, 1562 (1960)

Elem. Sym.	A	Z
Na	22	11

Method
Proton capture; NaI detector

Ref. No. 60 Kr 1 JH

Reaction	E or ΔE	E_o	Γ	$\int \sigma dE$	Jπ	Notes
(p,γ)	E_p=0.6-1.5M	E_p = 0.776 Mev 0.865 1.010 1.120 1.215 1.296 1.354				$Na^{22}\gamma$ mostly to ground state. $Na^{22}\gamma$ mostly to 2.25 MeV level.

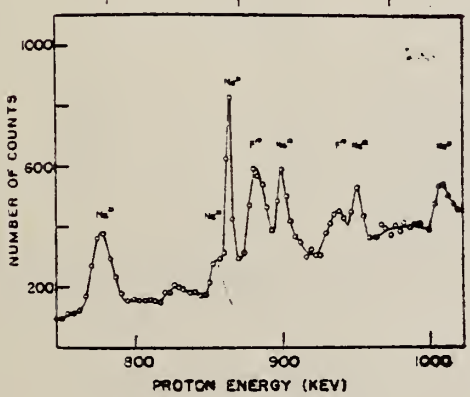

FIG. 1. Excitation curve for $Ne^{22}(p,\gamma)$ for E_p = 750 kev to 1020 kev.

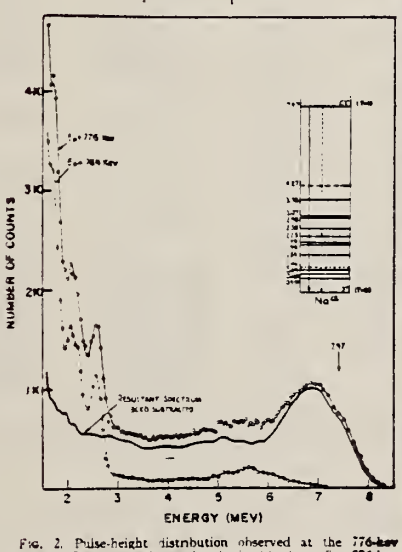

FIG. 2. Pulse-height distribution observed at the 776-kev resonance. Plotted are the results obtained both for E_p = 776 kev and E_p = 764 kev. The resultant genuine spectrum is indicated by the heavy line.

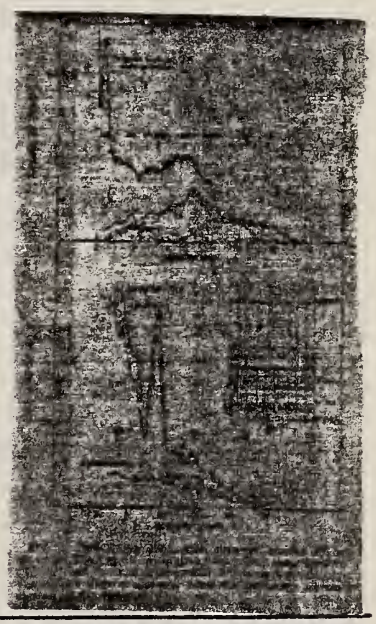

N. W. Tanner
Nuclear Phys. 61, 297 (1965)

Na	22	11

METHOD

REF. NO. 65 Ta 1 | EGF

REACTION	RESULT	EXCITATION ENERGY	SOURCE		DETECTOR		ANGLE
			TYPE	RANGE	TYPE	RANGE	
P,G	NØX	7	D	0-1	NAI-D	0-8	90
		(7.5 ± 0.1)		.3-1.0			
		(7.23 ± 0.1)					

Resonances in excitation function at E_p = 520 ± 5 keV and 766 keV

LEVELS, SPIN-PARITY

at E_γ = 7240 ± 10 kev and 7474 ± 5 keV

766 level as 2^-

520 level has small g.s. width

REF. R. Hentelä, J. Keinonen
Phys. Scrip. 17, 421 (1978)

ELEM. SYM.	A	Z
Na	22	11

METHOD

REF. NO. 78 He 3 hg

REACTION	RESULT	EXCITATION ENERGY	SOURCE TYPE	SOURCE RANGE	DETECTOR TYPE	DETECTOR RANGE	ANGLE
P,G	LFT	7-9	D	0-2	SCD-D		DST
		(7.47-8.50)		(.768-1.840)			

Angular distribution measurements of gamma-rays from unbound $T = 1$ states in ^{22}Na. R. Hentelä and J. Keinonen (Department of Physics, University of Helsinki, Helsinki, Finland).
Physica Scripta (Sweden) 17, 421–424, 1978.

J-PI

Angular distributions have been measured at six ^{21}Ne$(p,\gamma)^{22}$Na analogue resonances, with $E_p = 0.70$, 0.77, 1.09, 1.21, 1.56 and 1.84 MeV, and at a candidate for analogue resonance with $E_p = 1.11$ MeV. Gamma-ray mixing ratios have been obtained for the first time for the decays of these levels with determination of spin-parity assignments. The spins and parities for the bound states at 1.98 and 4.36 MeV have been deduced. Transition strengths provide information on the isoscalar and isovector strengths in the self-conjugated nucleus ^{22}Na.

Table I. *Results of the angular distribution measurements, spins and parities of the resonance states, the experimental angular distribution coefficients corrected for finite solid angle, χ^2-values and channel spin (τ) and γ-ray (δ) mixing ratios. Except when otherwise indicated, the energy and final state spin values are as given in ref. [4]*

E_p (keV)	E_i (keV)	E_f (keV)	J_i^π	J_f^π	A_2	A_4	χ^2	τ	δ
702	7411	583	1⁺	1⁺	0.00 ± 0.04	+ 0.01 ± 0.04	3.3	0.3	+ 0.19 ± 0.10
		1937		1⁺	+ 0.02 ± 0.03	− 0.01 ± 0.03	5.5	0.3	+ 0.29 ± 0.11
		3060		2⁺	+ 0.03 ± 0.04	− 0.03 ± 0.04	3.2	0.3	− 0.3 ± 0.3
		3944		1⁺	+ 0.06 ± 0.03	+ 0.02 ± 0.03	5.0	0.3	+ 1.3 ± 0.9
		4360		1⁻[a]	+ 0.06 ± 0.02	− 0.02 ± 0.01	4.5	0.3	$+0.4\ {}^{+0.4}_{-0.1}$
768	7474	0	2⁺	3⁺	+ 0.005 ± 0.009	− 0.02 ± 0.01	9.8	16	+ 0.2 ± 0.2
		1937		1⁺	+ 0.02 ± 0.02	− 0.01 ± 0.02	3.0	16	− 0.2 ± 0.2
1089	7780	1937[b]	(1, 2)⁻	1⁺	− 0.12 ± 0.04	− 0.05 ± 0.04	5.0	1.6	+ 0.05 ± 0.10 (1⁻)
							5.5	1.6	− 0.1 ± 0.3 (2⁻)
		2211		1⁻	− 0.14 ± 0.03	− 0.02 ± 0.03	4.0	1.6	+ 0.03 ± 0.03 (1⁻)
							4.5	1.6	+ 0.01 ± 0.06 (2⁻)
1113	7803	0	2⁺(1⁺)	3⁺	+ 0.01 ± 0.05	− 0.03 ± 0.05	3.0	6	> − 0.35
							(3.3)	(0.4)	(isotropic)
		1952		2⁺	+ 0.03 ± 0.03	− 0.04 ± 0.03	6.0	6	+ 0.15 ± 0.09
							(5.3)	(0.4)	(− 0.2 ± 0.2)
1205	7891	891	4⁺	4⁺	+ 0.40 ± 0.02	− 0.01 ± 0.02	1.3	300	− 0.01 ± 0.02
		1528		5⁺	− 0.09 ± 0.03	− 0.01 ± 0.03	2.6	300	+ 0.03 ± 0.02
		1983		3⁺[a,c]	− 0.14 ± 0.05	− 0.07 ± 0.05	6.4	300	− 0.08 ± 0.03
1564	8234	0	2⁺	3⁺	0.00 ± 0.04	0.00 ± 0.04	2.1	∞	isotropic
		583		1⁺	+ 0.02 ± 0.05	+ 0.03 ± 0.05	3.6	∞	isotropic
1840[b]	8495[b]	0	(1, 2)⁺	3⁺	+ 0.04 ± 0.03	+ 0.04 ± 0.03	6.7	0	isotropic
							6.7	∞	isotropic

[a] Present work (see text). [b] Ref. [9]. [c] Ref. [12].

(over)

Table II. *Electromagnetic transition strengths in ^{22}Na. Except when otherwise indicated, the branching ratios are taken from ref. [4]. The γ-ray widths Γ_γ are from ref. [3].*

E_i (MeV)	E_f (MeV)	$J_i^\pi(T_i)$	$J_f^\pi(T_f)$	Branching ratio (%)	δ	Γ_γ (eV)	Multipolarity	Γ_γ/Γ_w (W.u.)(n)[a]
7.41	0.58	1⁺(1)	1⁺(0)	8 ± 1	+ 0.19 ± 0.10	0.20 ± 0.04	M1	(2.9 ± 0.7) (− 2)
	1.94		1⁺(0)	15 ± 2	+ 0.29 ± 0.11	0.33 ± 0.07	M1	(0.9 ± 0.2) (− 1)
	3.06		2⁺(0)	28 ± 2	− 0.3 ± 0.3	0.70 ± 0.14	M1	(3.7 ± 1.0) (− 1)
	3.94		1⁺(0)	18 ± 2	+ 1.3 ± 0.9	0.45 ± 0.09	M1	> 3.5 (1)
	4.36		1⁺(0)	31 ± 2	$+0.4\ ^{+0.4}_{-0.1}$	0.75 ± 0.15	M1	$(1.1\ ^{-0.3}_{+0.1})$ (0)
7.47	0	2⁺(1)	3⁺(0)	78 ± 3	+ 0.2 ± 0.2	5.3 ± 1.1	M1	(6.0 ± 1.4) (− 1)
	1.94		1⁺(0)	10 ± 2	− 0.2 ± 0.2	0.7 ± 0.1	M1	(1.9 ± 0.3) (− 1)
7.78	1.94	(1, 2)⁻(1)	1⁺(0)	28 ± 3[b]	+ 0.05 ± 0.10	0.17 ± 0.03	E1	(1.6 ± 0.3) (− 3)
					− 0.1 ± 0.3	0.10 ± 0.02	E1	(0.9 ± 0.2) (− 3)
	2.21		1⁻(0)	60 ± 3[b]	+ 0.03 ± 0.03	0.40 ± 0.08	M1	(1.1 ± 0.2) (− 1)
					+ 0.01 ± 0.06	0.24 ± 0.05	M1	(0.7 ± 0.1) (− 1)
7.80	0	2⁺(1⁺)(0)	3⁺(0)	15 ± 2	> − 0.35	0.18 ± 0.05	M1	(1.0 ± 0.2) (− 2)[c]
					(isotropic)		(E2)	((2.1 ± 0.5) (0))
	1.95		2⁺(1)	69 ± 3	+ 0.15 ± 0.09	0.81 ± 0.16	M1	(1.9 ± 0.4) (− 1)
					(− 0.2 ± 0.2)		M1	((1.9 ± 0.4) (− 1))
7.89	0.89	4⁺(1)	4⁺(0)	34 ± 3	− 0.01 ± 0.02	0.51[d]	M1	7(− 2)
	1.53		5⁺(0)	48 ± 3	+ 0.03 ± 0.02	0.72[d]	M1	1.4(− 1)
	1.98		3⁺(0)	14 ± 2	− 0.08 ± 0.03	0.21	M1	5(−2)
8.23	0	2⁺(1)	3⁺(0)	55 ± 3	isotropic	1.2 ± 0.2	M1	(1.0 ± 0.2) (− 1)
	0.58		1⁺(0)	12 ± 2	isotropic	0.26 ± 0.06	M1	(2.8 ± 0.6) (− 2)
8.50	0	2⁺(1)	3⁺(0)	97 ± 5[b]	isotropic	5.2 ± 1.4	M1	(4.1 ± 1.1) (− 1)
		1⁺(0)			isotropic		E2	(4.0 ± 1.1) (+ 1)

[a] (n) means × 10^n. [b] Ref. [9]. [c] Calculated for the pure transition. [d] Estimated from ref. [3].

NA
A=23

NA
A=23

REF.

D. Reagan
Phys. Rev. 100, 113-120 (1955)

ELEM.	A	Z
Na	23	11

METHOD

Linac; counted delayed neutrons from N^{17}

REF. NO. 55 Re 1 NVB

REACTION	RESULT	EXCITATION ENERGY	SOURCE		DETECTOR		ANGLE
			TYPE	RANGE	TYPE	RANGE	
G,N17	ABI	THR - 400	C	90-400	ACT-I		4PI

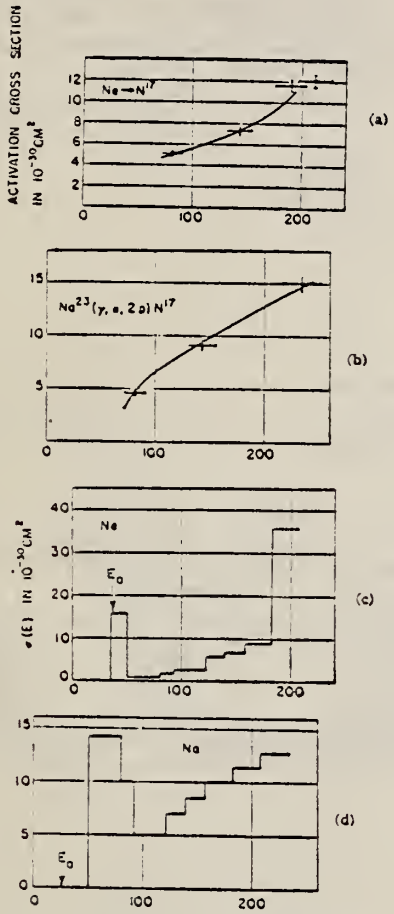

FIG. 4. Experimental N^{17} activation points for neon and sodium are plotted in the upper graphs. The lower graphs are the photon cross sections, which were calculated as indicated in the text. The activation cross sections indicated by the solid lines are reconstructions from the photon cross sections shown. The photon cross sections for energies below 80 Mev were chosen arbitrarily.

Ref. E.G. Fuller, E. Hayward
Phys. Rev. 101, 692 (1956)

Elem. Sym.	A	Z
Na	23	11

Method: Betatron; photon scattering; NaI spectrometer

Ref. No.: 56 Fu 1 | NVB

Reaction	E or ΔE	E_o	Γ	$\int \sigma dE$	Jπ	Notes
$Na^{23}(\gamma,\gamma)$	Bremss. 4-40					Detector at 120°. Cross sections given here are 13% too high due to erroneous cos β factor in denominator of Eq. (5). [See footnote 8 in Phys. Rev. 106, 993 (1957)].

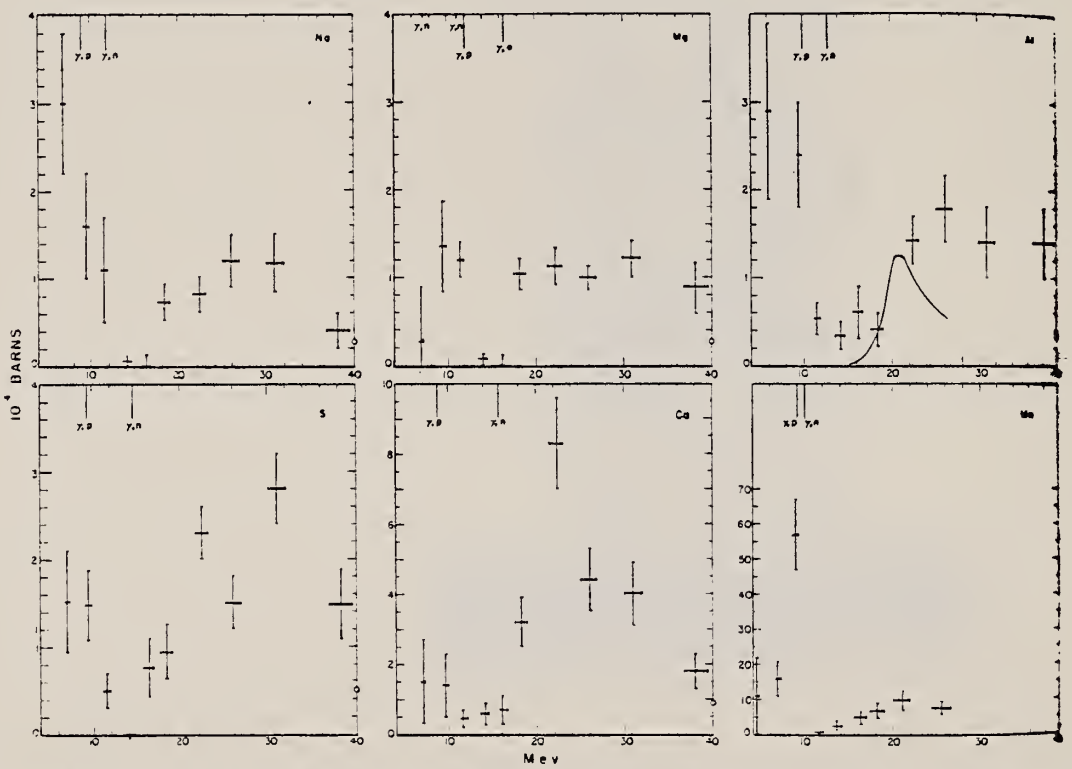

FIG. 4. The elastic scattering cross sections for Na, Mg, Al, S, Ca, and Mn. The indicated spread in energy is the width of the differential discriminator channel, and the standard deviations are based only on the number of counts. The vertical lines at the top represent the particle thresholds for the most important isotopes. The open circles at the extreme right indicate the magnitude of the Thomson cross section for Z free protons scattering coherently. The solid curve superimposed on the Al data is the scattering cross section calculated from the dispersion relation by substituting for $\sigma_a(E)$ in Eq. (6) the sum of the neutron and proton yield cross sections.

B.G. Chidley, L. Katz, S. Kowalski
Can. J. Phys. 36, 407 (1958)

ELEM. S/M.	A	Z
Na	23	11

METHOD: Betatron

REF. NO.: 58 Ch 2 | NVB

REACTION	RESULT	EXCITATION ENERGY	SOURCE		DETECTOR		ANGLE
			TYPE	RANGE	TYPE	RANGE	
G,N	RLY	THR	C	THR	BF3-I		4PI

THRESHØLD

TABLE I

MEASURED PHOTONEUTRON THRESHOLDS

Reaction	Measured Q value, Mev.	Other Q values, Mev.	Method	Reference
$Na^{23}(\gamma, n)Na^{22}$	12.47±0.05 (12.46±0.08)			
		12.05 ±0.20	Threshold	Sher *et al.* (1951)
		12.42 ±0.05	Mass data	Wapstra (1955)
		12.417±0.014	Review	Mattauch *et al.* (1956)

See 58 Ka 1 for Cross sections

TABLE II

COMPARISON OF THRESHOLDS FROM MASS DATA AND FROM PHOTONEUTRON REACTIONS

Reaction	Photoneutron threshold, Mev.	Mass data threshold, Mev.	Difference, Mev.
$Na^{23}(\gamma, n, Na^{22}$	12.47±0.05	12.417±0.014	−0.05±0.05
$Al^{27}(\gamma, n)Al^{26}$	12.96±0.06	13.03 ±0.06	−0.07±0.08
$P^{31}(\gamma, n)P^{30}$	12.48±0.05	12.39 ±0.03	−0.09±0.06
$Co^{59}(\gamma, n)Co^{58}$	10.44±0.05	10.49 ±0.05	+0.05±0.05
$Pr^{141}(\gamma, n)Pr^{140}$	9.46±0.05	9.30 ±0.06	−0.16±0.08

Ref. L. Keszthelyi, J. Erő
Nuclear Phys. 8, 650 (1958)

Elem. Sym.	A	Z
Na	23	11

Method
NaI(Tℓ) detector; Li(p,γ) source

Ref. No. 58 Ke 1 | EH

Reaction	E or ΔE	E_0	Γ	$\int \sigma dE$	Jπ	Notes
(γ,p)	17.6					

TABLE 1

Nucleus	N_e	σ_0 (b)	N_p	N_{23}	σ(γ, p) (mb)	σ(17.6) (mb)
$_{11}Na^{23}$	$4.2 \cdot 10^{6}$	10.7	1176 ± 96	240	2.4 ± 1.1	3.6 ± 1.5
$_{19}K^{39}$	3×10^{6}	11 s	3378 ± 98	230	10 ± 3.5	15 ± 5.8
$_{53}I^{127}$	$1.7 \cdot 10^{6}$	20 s	130 ± 10	10	1.5 ± 0.6	1.5 ± 0.6
$_{55}Cs^{133}$	$1.7 \cdot 10^{6}$	20 s	130 ± 10	10	1.5 ± 0.6	1.5 ± 0.6

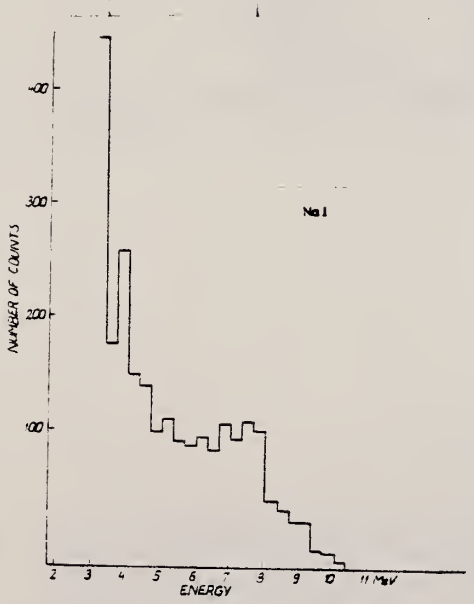

Fig. 6. Pulse spectrum of NaI crystal.

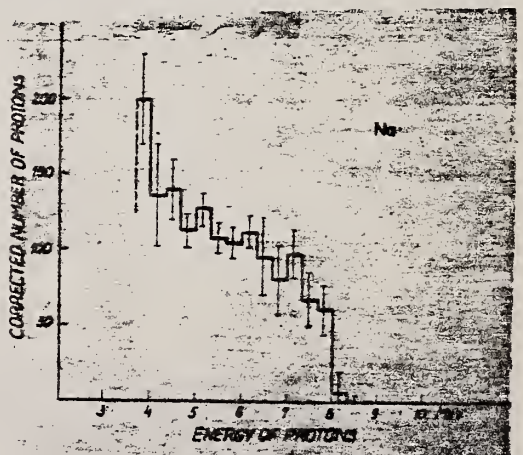

Fig. 9. Energy spectrum of protons from Na.

Ref. T.R. Ophel, I.F. Wright
Proc. Phys. Soc. 71, 389 (1958)

Elem. Sym.	A	Z
Na	23	11

Method: γ-rays from $Li^7(p,\gamma)$ radiation; NaI(Tℓ) scintillator; proton spectra

Ref. No.: 58 Op 1 EH

Reaction	E or ΔE	E_o	Γ	$\int \sigma dE$	Jπ	Notes
$Na^{23}(\gamma,p)$		17.6				Energies of protons incident in Li were varied to permit identification of protons produced by 17.6 MeV component.

Outgoing Proton E	Excitation of Ne^{22}	σ(mb)
8.4	0	0.31
7.2	1.3	2.5
5.2	3.3	0.6
4.1	4.4	0.9
3.2	5.4	~ 2.0
2.9	5.7	

REF.

J. O'Connell, P. Dyal, J. Goldemberg
Phys. Rev. 116, 173 (1959)

ELEM.		
Na	23	11

METHOD

Betatron

REF. NO. 59 Oc 1 | NVB

REACTION	RESULT	EXCITATION ENERGY	SOURCE		DETECTOR		ANGLE
			TYPE	RANGE	TYPE	RANGE	
G,2N	RLI	THR-100	C	THR-100	ACT-I		4PI

REL TØ G,N

TABLE II. Relative integrated cross sections.

Element	(γ,n)	Position of the peak for (γ,n)	$(\gamma,2n)$	Position of the peak for $(\gamma,2n)$
C^{12}	1	23 Mev	0.003	42 Mev
N^{14}	1	24 Mev	0.007[a]	
O^{16}	1	22 Mev	0.002	40 Mev
F^{19}	1	20 Mev	0.14	32 Mev
Na^{23}	1	20 Mev	0.05	32 Mev
P^{31}	1	20 Mev	0.06 $(\gamma,2p)$	45 Mev $(\gamma,2p)$
			0.08 $(\gamma,2pn)$	50 Mev $(\gamma,2pn)$

[a] The (γ,n) integrated cross section was taken from reference 4.

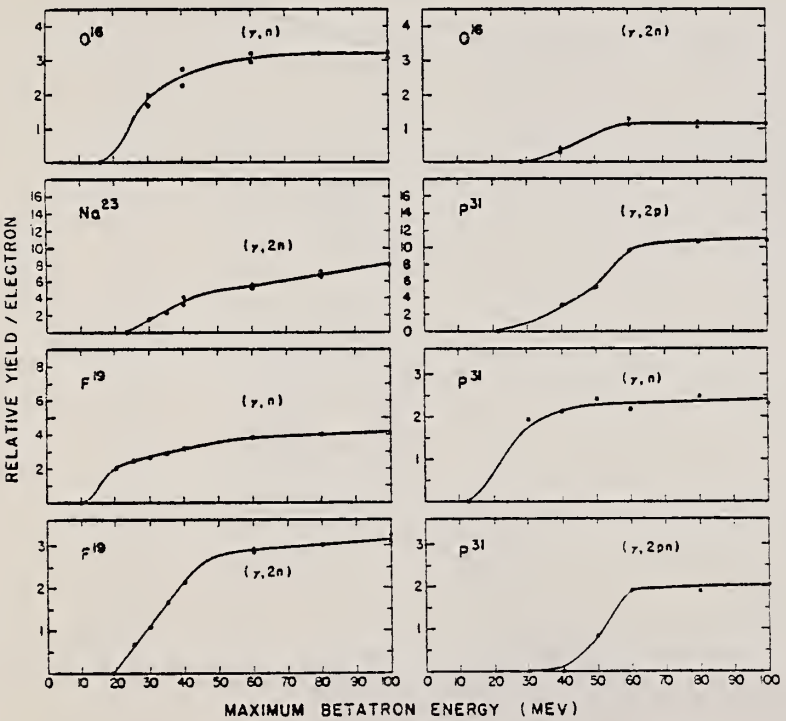

FIG. 1. The energy dependence of several photonuclear reactions. The relative yield scales of different graphs are independent.

Ref. V.K. Rasmussen, F.R. Metzger, C.P. Swann
Nuclear Phys. 13, 95 (1959)

Elem. Sym.	A	Z
Na	23	11

Method $Na^{23}(p,p')$ photon scattering; NaI spectrometer

Ref. No. 59 Ra 1 | NVB

Reaction	E or ΔE	E_o	Γ	$\int \sigma dE$	Jπ	Notes
$Na^{23}(\gamma,\gamma)$	2.78	440 keV				Detectors at 115°, 151°. Intensity ratio: $\frac{I(151^\circ)}{I(115^\circ)} = 1.10 \pm 0.04$ Lifetime of first excited state: $\tau = (1.8^{+0.4}_{-0.3}) \times 10^{-12}$ sec.

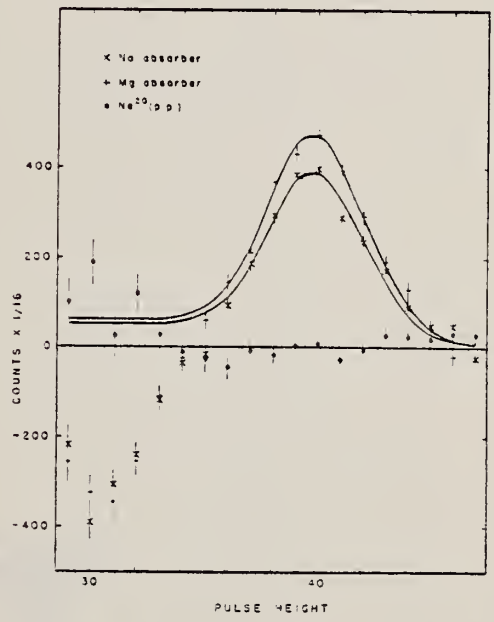

Fig. 4. Sodium scatterer-magnesium scatterer differences from the data shown in fig. 3. The shape of the solid curves is that observed with the 440-keV γ-ray from Tl^{202} adjusted slightly in pulse height to match the experimental points (it is *not* to be inferred that a precise comparison of the energies of these two γ-rays has been obtained). The negative differences at lower pulse heights result from small errors in the placement of the scatterers, as explained in the text. The sum of counts from pulse height 38 to 42 is taken to be proportional to the resonance effect.

Ref. W.L. Mouton, P.B. Smith
Nuclear Phys. 16, 206 (1960)

Elem. Sym.	A	Z
Na	23	11

Method 800 kev cascade generator; γ's from $Ne^{22}(p,\gamma)$; NaI

Ref. No. 60 Mo 1 JHH

Reaction	E or ΔE	E_o	Γ	$\int \sigma dE$	Jπ	Notes
(γ,γ)	9.40		2.7±1.1 ev			$\Gamma_{\gamma o}$ by absorption integral.
			2.0±0.5 ev			$\Gamma_{\gamma o}$ by yield measurement from $Ne^{22}(p,\gamma)$
						E_p = 637 kev; γ energy varied to Doppler - compensate by changing angle with respect to proton beam.

REF.
T.R. Walker, W.T. Morton
Proc. Phys. Soc. 75, 4 (1960)

ELEM. SYM.		
Na	23	11

METHOD
Synchrotron; proton-neutron cross section; radioactivity

REF. NO.	
60 Wa 2	NVB

REACTION	RESULT	EXCITATION ENERGY	SOURCE		DETECTOR		ANGLE
			TYPE	RANGE	TYPE	RANGE	
G,3N2P	ABX	THR-240	C	120-240	ACT-I		4PI
				(120,180,240)			

$\sigma = (0.33 \pm 0.03)\ 10^{-27}\ cm^2$/equivalent quantrum

Data (in Table) below 120 MeV from other workers; 50 MeV data is that of Barber et al., Phys. Rev. 98, 73 (1955).

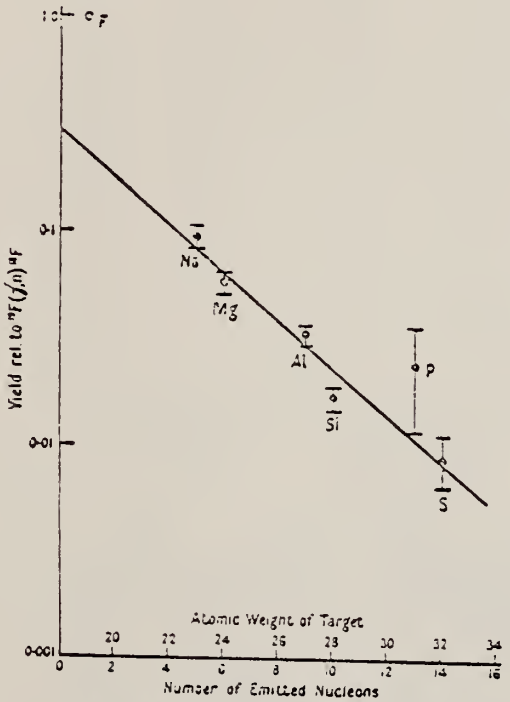

Yields relative to $^{19}F(\gamma, n)^{18}F$ at 240 Mev.

Maximum bremsstrahlung energy (Mev)	Yield of ^{18}F from ^{19}F	^{23}Na	^{27}Al	$^{12}C(\gamma, n)^{11}C$ yield
240	1·83(17)	0·18(9)	0·062(13)	1·62
180	1·78(16)	0·18(16)	0·058(16)	1·50
120	1·6(14)	0·15(14)	0·045(14)	1·34
100	1·5	—	—	1·27
70	1·4	0·11	—	1·15
50	1·22	0·07	—	1·0

REF. B. Ambrozy, A. Faudrowicz, A. Jasinski, J. Kownacki, H. Lancman and J. Ludziejewski
Proc. Int. Conf. Manchester 281 (1961)

ELEM. SYM.	A	Z
Na	23	11

METHOD

Resonance Fluorescence

REF. NO.	
61 Am 1	JDM

REACTION	RESULT	EXCITATION ENERGY	SOURCE		DETECTOR		ANGLE
			TYPE	RANGE	TYPE	RANGE	
G,G	LFT	1	D		NAI-D		120

Mean life of first excited state is $\tau = 1.5\binom{+\ 0.3}{-\ 0.2}\ 10^{-12}$ sec.

E.C. Booth, K.A. Wright
Nuclear Phys. 35, 472 (1962)

Elem. Sym.	A	Z
Na	23	11

Method 4 MeV electron Van de Graaff; bremss.; nuclear resonance scattering, ring scatterer; NaI

Ref. No. 62 Bo 6 JHH

Reaction	E or ΔE	E_o	Γ	$\int \sigma dE$	Jπ	Notes
$Na^{23}(\gamma,\gamma)$	Bremss. 0 - 4					$\theta = 110^\circ$

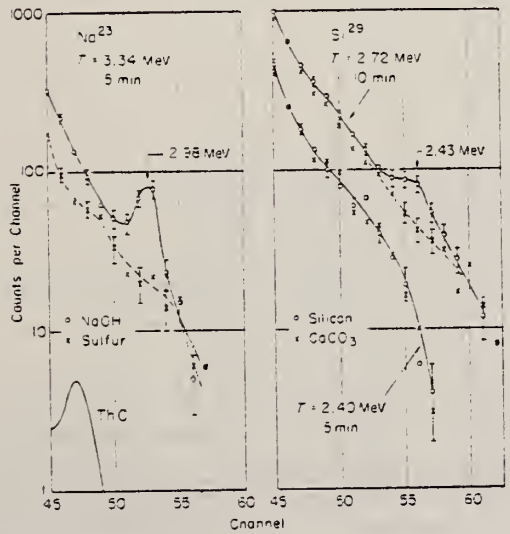

Fig. 3. Resonance fluorescence from the 2.98 MeV state of Na^{23} and the 2.43 MeV state of Si^{29}. The ThC peak is at 2.615 MeV. T is the maximum bremsstrahlung energy.

TABLE 3
Mean lifetimes of excited states deduced from the resonance scattering of bremsstrahlung

Nucleus	I_0	Energy (MeV)	Spins	g	Γ_0/Γ	W(90°)/W(0)	$\tau \times 10^{15} \pm 35\%$ (sec)
F^{19}	100	1.46	$\frac{1}{2}^+ - \frac{1}{2}^+$	2	0.13	(1)	$0.25g$
Na^{23}	100	2.08	$\frac{3}{2}^+ - \frac{3}{2}^+$	2	0.1	0.79	>0.04
		2.39	$-^?$	?	0.53	(1)	$>1.6g$
		2.64	$-^?$	?	0.6	(1)	$>0.3g$
		2.70	$-^?$	?	(0.1)	(1)	$>0.008g$
		2.98	$-^?$	?	0.46	(1)	$0.03g$
Al^{27}	100	2.73	$\frac{1}{2}^+ - \frac{1}{2}^+$	1	≤ 0.3	0.91	>0.22
		2.98	$-\frac{3}{2}$	$\frac{3}{5}$	0.216	1	2.2×10^{-4}
Si^{29}	4.71	1.28	$\frac{1}{2}^+ - \frac{1}{2}^+$	2	1	0.88	1.5
		2.43	$-\frac{3}{2}^+$	2	~1)	0.88	0.2
P^{31}	100	1.28	$\frac{1}{2}^+ - \frac{1}{2}^+$	2	1	0.88	2.2
		2.23	$-\frac{3}{2}$	3	1	0.79	4.5
		3.13	$-\frac{1}{2}$	2	(1)	0.88	0.2
		3.29	$-\frac{3}{2}$	3	?	0.79	$>1.8g(\Gamma_0/\Gamma)^2$
		3.41	$-^?$	?	?	(1)	$>1.3g(\Gamma_0/\Gamma)^2$
		3.51	$-\frac{1}{2}$	2	?	0.88	$0.02g(\Gamma_0/\Gamma)^2$
S^{32}	95	3.78	$0^+ - ?$	?	?	(1)	$>0.6g(\Gamma_0/\Gamma)^2$
S^{34}	4.2	2.127	$0^+ - 2$	5	1	0.63	>1.0
Cl^{35}	75.5	1.22	$\frac{1}{2}^+ - ?$	?	1	(1)	$0g$
		1.76	$-^?$	?	(1)	(1)	$4g$
		2.7(2.65)	$-^?$	?	?	(1)	$0.31g(\Gamma_0/\Gamma)^2$
		3.01	$-^?$	?	?	(1)	$0.37g(\Gamma_0/\Gamma)^2$
Cl^{36}	75.5	3.1	?	?	?	(1)	$>0.74g(\Gamma_0/\Gamma)^2$
		3.17	?	?	?	1)	$>1.5g(\Gamma_0/\Gamma)^2$
Cl^{37}	24.5	0.838	$\frac{3}{2}^+ - ?$	?	1	(1)	$>13g$
		1.72	$-^?$	?	?	(1)	$>0.82g(\Gamma_0/\Gamma)^2$
K^{39}	93	2.53	$\frac{1}{2}^+ - ?$	?	1	(1)	$>1.0g$
		2.82	$-^?$	?	1	(1)	$>1.5g$
		3.02	$-^?$	?	1	(1)	$0.47g$
		3.60	$-^?$	?	1	(1)	$>0.7g$
		3.88(3.94)	$-^?$	?	?	(1)	$0.14g(\Gamma_0/\Gamma)^2$
		4.06–4.12	$-^?$	?	?	(1)	$>0.25g(\Gamma_0/\Gamma)^2$
Ca^{40}	96	3.90	$0^- - 2^-$	5	1	0.63	<0.46
Ca^{42}	69	1.33	$\frac{1}{2}^- - \frac{5}{2}$	2	(1)	0.8	$44 > \tau > 11$

The factor g equals $(2I+1)/(2I_0+1)^{-1}$.

Ref. D.W. Braben, L.L. Green, J.C. Willmott
Nuclear Phys. 32, 584 (1962)

Elem. Sym.	A	Z
Na	23	11

Method
"Liverpool University H.T. set"; NaI

Ref. No.
62 Br 2 JHH

Reaction	E or ΔE	E_o	Γ	$\int \sigma dE$	Jπ	Notes
$Ne^{22}(p,\gamma)$	440-1030 keV	9.43±0.05			$\frac{1}{2}^+$ ($\frac{1}{2}^-$)	E_{p_o} = 636 keV; 82% to ground state.
		9.59±0.05			$3/2^+$	= 854 keV; 28% to ground state.
		9.67±0.03			$5/2^+$	= 902 keV; 37% to ground state.
		9.70±0.04			$3/2^+$	= 952 keV; 50% to ground state.
		9.78±0.04			$3/2^+$	= 1014 keV; 10% to ground state.
						$W(\theta) = a_o P_o(\cos\theta) + a_2 P_2(\cos\theta) + a_4 P_4(\cos\theta)$; parameters in Table 6.

TABLE 6
Angular distributions

Resonance	Transition	a_2/a_0	a_4/a_0
636 keV		all isotropic	
854 keV	7 → 0	0.70±0.03	0.01±0.02
	7 → 1	−0.14±0.03	−0.03±0.03
902 keV	7 → 0	0.47±0.06	0.17±0.06
	7 → 1	0.53±0.11	0 ±0.04
	7 → 7	−0.04±0.07	0.07±0.08
	7 → 11	−0.16±0.03	−0.05±0.03
	11 → 1	−0.02±0.02	−0.08±0.03
	7 → 1	−0.05±0.06	−0.06±0.07
	4 → 0	0.17±0.06	0.08±0.07
952 keV	7 → 0	0.28±0.05	0.02±0.04
	7 → 1	−0.04±0.03	0.03±0.04
	7 → 4	−0.46±0.09	−0.05±0.1
	7 → 6	0.30±0.09	0.07±0.2
	6 → 0	0.13±0.05	−0.02±0.09
	6 → 1	0.06±0.05	0.09±0.06
	4 → 0	−0.02±0.05	0.08±0.06
1014 keV	7 → 0	0.23±0.01	0.04±0.01
	7 → 1	−0.09±0.04	−0.07±0.04
	7 → 4	−0.24±0.03	0.04±0.03
	7 → 7	0.36±0.05	0.12±0.05
	7 → 1	−0.03±0.02	0 ±0.05
	4 → 0	0.02±0.02	0.01±0.02
	Triple correlations		
636 keV	7 → 0 → 0, types I and II	0.28±0.06	−0.05±0.2
	7 → 7 → 1, types I and II	0.04±0.1	0.01±0.2
	7 → 10 → 0 types I and II	0.06±0.1	0 ±0.1
854 keV	7 → 1 → 0 type I	−0.19±0.01	−0.01±0.01
	7 → 1 → 0 type II	−0.21±0.01	−0.01±0.01
902 keV	7 → 1 → 0, type I	0.53±0.05	−0.04±0.03
	7 → 1 → 0 type II	0.02±0.03	−0.02±0.04
	7 → 7 → 1, type II	−0.04±0.07	−0.06±0.09
1001 keV	7 → 11 → 1 type I	−0.04 ±0.06	0.04±0.08
	7 → 11 → 1, type II	0.01 ±0.05	−0.09±0.07
	7 → 11 → 2 type II	0.34 ±0.15	−0.17±0.20
952 keV	7 → 1 → 0 type I	−0.02±0.04	0 ±0.04
	7 → 1 → 0 type II	−0.21±0.02	−0.03±0.02
	7 → 4 → 0 type I	−0.20±0.32	−0.02±0.20
	7 → 4 → 0 type II	0.06±0.16	0.06±0.18
1014 keV	7 → 1 → 0 type I	−0.18±0.01	0 ±0.03
	7 → 4 → 0 type I	−0.33±0.04	0.02±0.02
	7 → 4 → 0 type II	−0.01±0.04	−0.02±0.04

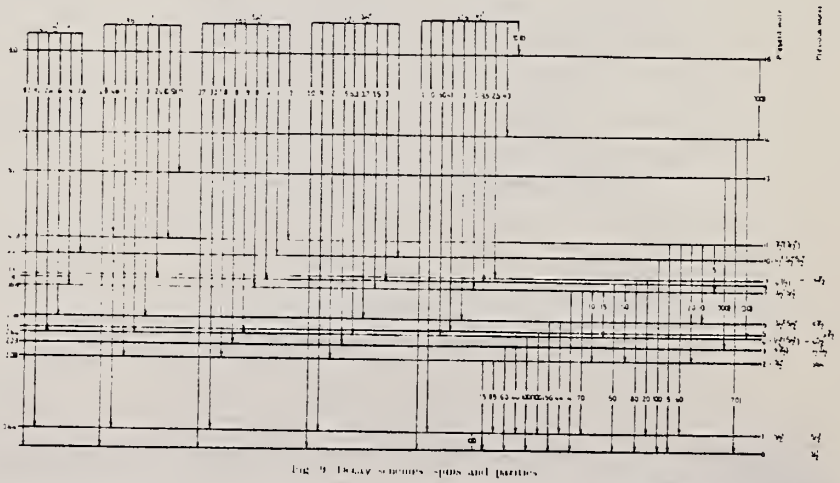

Fig. 9. Decay schemes, spins and parities.

Ref. W.L. Mouton, J.P.F. Sellschop, R.J. Keddy
Phys. Rev. 128, 2745 (1962)

Elem. Sym.	A	Z
Na	23	11

Method 1.4 MeV electron accelerator; NaI

Ref. No 62 Mo 1 JHH

Reaction	E or ΔE	E_o	Γ	∫σdE	Jπ	Notes
$Na^{23}(\gamma,\gamma')$	Bremss; 600 kev	440 kev	(3.66±0.50) X 10^{-4} ev			This Γ gives a mean lifetime of t = (1.80±0.28) X 10^{-12} sec. Scattering angle 130°

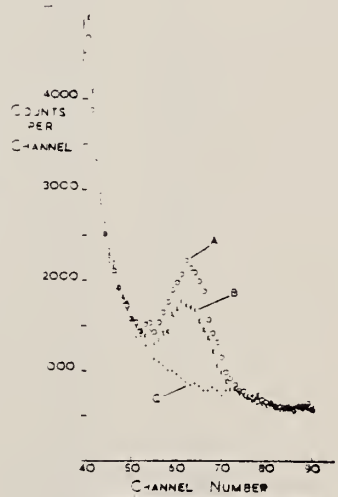

FIG. 3. Results for scattering from sodium. Curve A: sodium scatterer with aluminum absorber. Curve B: sodium scatterer with sodium absorber. Curve C: aluminum scatterer with sodium absorber.

Ref. M. Odera

J. Phys. Soc. Japan 17, 1675 (1962)

Elem. Sym.	A	Z
Na	23	11

Method

Synchrotron; foils; emulsions

Ref. No. 620d1 BG

Reaction	E or ΔE	E_o	Γ	$\int \sigma dE$	Jπ	Notes
(γ,p)	bremss.; $E_{\gamma max}$ = 18MeV			1.1×10^5 protons/mol/roentgen		Energy (Fig.1) and angular distribution (Fig.2) Angular distributions fit $A(1 + \cos^2\theta)$

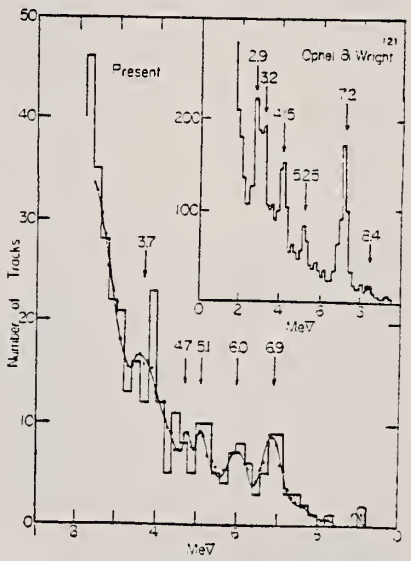

Fig. 1. Energy spectrum of photoprotons from Na. Irradiation by 18 MeV bremmsstrahlung. The inset shows the result of Ophel and Wright.[2]

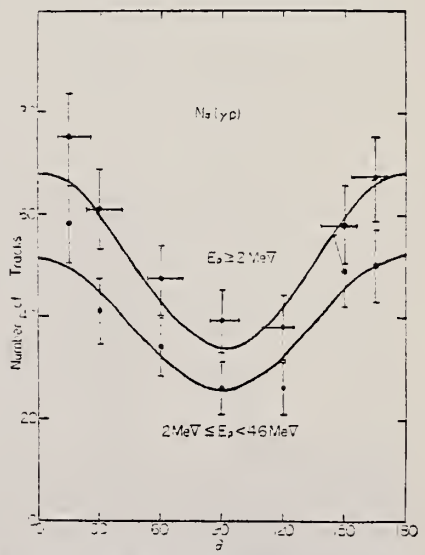

Fig. 2. Angular distributions of photoprotons from Na. Upper one is for all protons measured and lower one is for those below 4.6 MeV. Solid curves are $A(1+\cos^2\theta)$.

* Present address: Institute of Physical and Chemical Research. Bunkyo-ku. Tokyo.

Ref.	Elem. Sym.	A	Z
W.C.Barber, J.Goldemberg, G.A.Peterson, Y.Torizuka Nuclear Phys. 41, 461 (1963); erratum to be published (as of 9/5/63)	Na	23	11

Method	Ref. No.	
Linac (Stanford Mark II) - counter telescope	63Bal	BG

Reaction	E or ΔE	E_o	Γ	$\int \sigma dE$	Jπ	Notes
(e,e')	41.5		determined see Table II		see Table II	inelastic scattering cross section $(cm^2/sr) \times 10^{-32}$ at 180°
		3.0		0.02 MeV-mb		0.2±50%
		4.6		0.07		0.5±40%
		6.1		0.20		1.0±40%
		8.0		0.68		2.5±30%

TABLE 2

Isotope	Energy of level (MeV)	Spin and parity: Ground state	Spin and parity: Excited state	Inelastic electron scattering cross section (cm^2/sr) $\times 10^{-28}$: Estimated error (%)	Inelastic electron scattering cross section (cm^2/sr) $\times 10^{-28}$: MeV-mb	Radiation width to ground state (eV): This experiment [a]	Radiation width to ground state (eV): Weisskopf
$_3Li^6$	3.56	1+	0+	4.0	20	0.42	4.7	0.82
	5.7		0+ 1+ 2-	0.15	50	0.03	0.9 0.3 0.16	3.6
	9.3		0+ 1+ 2-	0.6	30	0.20	15 5 3	16
	14.0		0+ 1+ 2-	0.25	50	0.14	24 8 5	58
	15.8		0+ 1+ 2-	0.25	50	0.17	37.5 12.5 7.5	80
$_3Li^7$	9.6	3/2-	1/2- 3/2- 5/2-	0.18	50	0.06	3.4 1.7 1.1	18
	10.5		1/2- 3/2- 5/2-	0.78	30	0.30	19.2 9.6 6.4	23
	14.0		1/2- 3/2- 5/2-	0.48	40	0.27	31.2 15.6 10.4	58
$_7N^{14}$	9.3	1+	0+ 1+ 2-	0.92	30	0.30	23.4 7.8 4.6	17
	10.6		0+ 1+ 2-	0.65	30	0.25	24.6 8.2 4.9	25
$_8O^{16}$	19.0	0+	1-	0.45	40	0.41	14.1	145
$_9F^{19}$	7.7	1/2+	1/2-	2.0	25	0.54	4.7	9.0
$_{10}Ne^{20}$	≈ 9	0+	1-	3.0	20	0.9	7.1	14.5
	≈13		1-	2.0	20	1.0	16.6	48
$_{11}Na^{23}$	3.0	3/2+	1/2- 1/2-	0.2	50	0.02	0.05 0.035	0.45
	4.6		1/2-	0.5	40	0.07	0.43	1.8
	6.1		1/2-	1.0	40	0.20	4.4	4.6
	8.0		1/2- 1/2-	2.5	30	0.68	12.3 8.6	10.8
$_{12}Mg^{24}$	11.0	0+	1-	4.4	20	1.76	21.0	29
	≈14		1-	1.5	30	0.83	15.8	58
$_{13}Al^{27}$	4.3	5/2+	1/2- 3/2- 5/2-	0.7	30	0.10	1.0 0.67 0.50	2.1
	8.0		1/2- 3/2- 5/2-	1.9	30	0.50	14.0 8.3 7.0	10.8

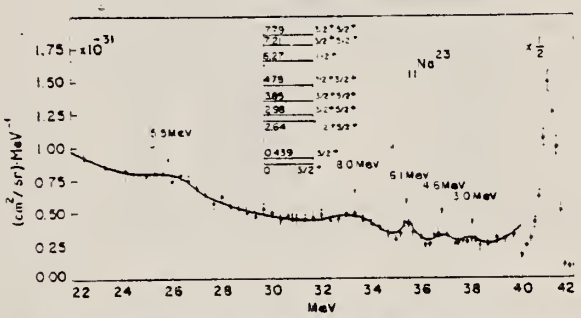

Fig. 11. Spectrum of 41.5 MeV electrons scattered from Na^{23} at 180°.

Ref.		Elem. Sym.	A	Z
	S. Costa, F. Ferrero, S. Ferroni, B. Minetti, C. Molino R. Malvano Phys. Letters 6, 226 (1963)	Na	23	11

Method		Ref. No.	
	100 MeV Synchrotron; 4 π neutron detector; calculated integrated cross sections - fitted with polynomial of degree η	63 Co 3	EGF

Reaction	E or ΔE	E_o	Γ	$\int \sigma dE$	J π	Notes
$Na^{23}(\gamma, xn)$						$\sigma_b = \int \frac{\sigma(E)}{E} dE$ gets $\langle \bar{\nu}_p \cdot \bar{\nu}_n - \bar{\nu}_n \cdot \bar{\nu}_{n1} \rangle$ $= \left(Rc^2 - Rp^2 - \frac{3}{\pi^2} \frac{tr\ c}{e^2} \sigma_b \frac{A-1}{A^2} \right) X \frac{2}{A-2}$ See "Boron" for plots of this and $\int \sigma dE / 60\ NZ/A$.

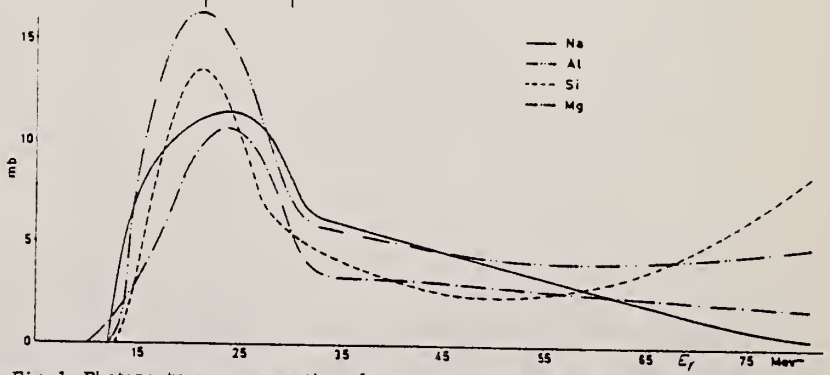

Fig. 1. Photoneutron cross sections for several light elements versus γ-ray energy.

K. Sato
J. Phys. Soc. Japan 18, 1353 (1963)

Na	23	11

METHOD: Betatron; neutron cross sections; BF_3 counters; ion chamber

REF. NO.: 63 Sa 1 | NVB

REACTION	RESULT	EXCITATION ENERGY	SOURCE TYPE	SOURCE RANGE	DETECTOR TYPE	DETECTOR RANGE	ANGLE
G,XN	ABX	12 - 24	C	12 - 24	BF_3 - I		4 PI

781

a,b in Table I refer to two Lorentz shaped peaks in the split giant resonance.

Quadrupole moment $Q_o = 0.3 \times 10^{-24}$ cm^2, based on Danos' theory.

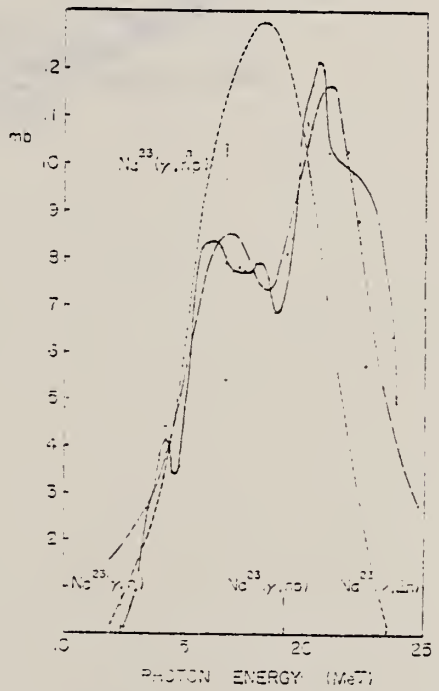

Fig. 2. The $(\gamma, n)+(\gamma, np)$ cross sections for Na^{23} and fitting the cross section to the superposition of two Lorentz lines.

Sold line: present data obtained from the yield curve for the summation of the 7 runs.
Dotted line: data of Montalbetti et al[8].
Broken line: the superposition of two Lorentz lines which is calculated from the parameters given in Table. 1.
The arrows in the figure show the threshold energies.

Table I. Resonance Parameters

	Na^{23}	Si^{28}
E_a	16.5 Mev	18.75 Mev
σ_a	6.8 mb	11.0 mb
Γ_a	4.0 Mev	2.0 Mev
E_b	21.0 Mev	20.75 Mev
σ_b	10.5 mb	13.0 mb
Γ_b	4.0 Mev	2.6 Mev

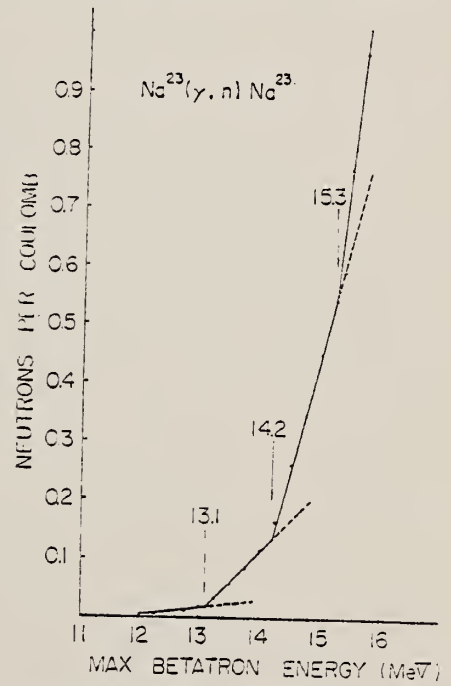

Fig. 4. The breaks in the Na^{23} (γ, n) Na^{22} yield curve.

8) R. Montalbetti, L. Katz and J. Goldemberg: Phys. Rev. 91 (1953) 659.

REF.

J. M. Loiseaux, M. Langevin and J. M. Maison
Proc. Paris Conf. 1048 (1964)

ELEM. SYM.		
Na	23	11

METHOD

Betatron

REF. NO.

64 Lo 3 JDM

REACTION	RESULT	EXCITATION ENERGY	SOURCE		DETECTOR		ANGLE
			TYPE	RANGE	TYPE	RANGE	
G,G	ABX	10-30	C	10-30	NAI-D		140

The effective differential scattering cross section remains quite constant from 20-30 MeV.

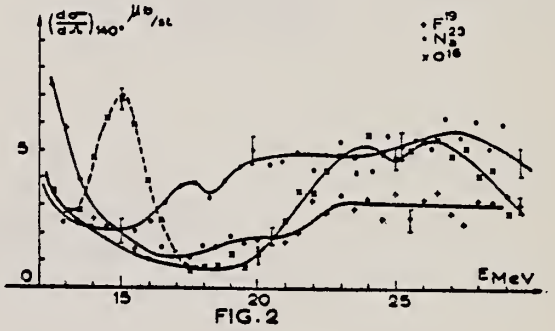

FIG. 2

REF.

F.R. Metzger
Phys. Rev. 136, B374-79(1964)

ELEM.	SYM.	
Na	23	11

METHOD
Van de Graaff; $N^{15}(p,\alpha)C^{12*}$ source.

REF. NO.
64 Me 1 NVB

REACTION	RESULT	EXCITATION ENERGY	SOURCE		DETECTOR		ANGLE
			TYPE	RANGE	TYPE	RANGE	
G,G	LFT	4	D	4	NAI-D		DST
		(4.431)		(4.431)			

J-PI, WIDTH

$J^{\pi} = \frac{1}{2}^-$ for 4.431 MeV level.

Γ^{o} = (2.14 ± 0.10)eV (partial width for ground state transitions)

Γ = (2.25 ± 0.20)eV, or $\tau = (2.9 \pm 0.3) \times 10^{-16}$ sec.

REF.

F. R. Metzger
Proc. Paris Conference 392 (1964)

ELEM. SYM.	A	Z
Na	23	11

METHOD

Resonance Scattering $^{15}N(p,\alpha\gamma)^{12}C$

REF. NO.

64 Me 2 JDM

REACTION	RESULT	EXCITATION ENERGY	SOURCE		DETECTOR		ANGLE
			TYPE	RANGE	TYPE	RANGE	
G,G	LFT	4	D	4	NAI-D	4	DST

The 4.431 MeV state in ^{23}NA has spin $\frac{1}{2}$ and $\Gamma_o = (2.1\pm0.1)$eV.

C. P. Swann
Phys. Rev. 136, B1355-59 (1964)

Na	23	11

METHOD
Van de Graaff; $F^{19}(p,\alpha)O^{16*}$ source

REF. NO.
64 Sw 1

NVB

REACTION	RESULT	EXCITATION ENERGY	SOURCE TYPE	SOURCE RANGE	DETECTOR TYPE	DETECTOR RANGE	ANGLE
G,G	NØX	7	D	7,7	NAI-D		DST
		(7.10±0.02)	(6.91. 7.12)				

J-PI, WIDTH

Found level energy to be 7.10 ± 0.02 MeV.

Angular distribution

$W(\theta) = 1 + (0.47 \pm 0.09)P_2 + (0.32 \pm 0.03)P_4$.

$J^{\pi} = \frac{5}{2}^{+}$

Γ_o = (0.62 ± 0.07)eV (partial width for ground state transition)

Γ = (0.98 ± 0.12)eV (total width)

Quadrupole-dipole amplitude ratio (E2-M1)δ:

$-1.3 < \delta < -2.2$

or $2.5 < \delta < 3.0$

REF.

W. C. Barber and G. J. Vanpraet
Nuclear Phys. 72, 63 (1965)

ELEM. SYM.	A	Z
Na	23	11

METHOD

REF. NO. 65 Ba 4 JOC

REACTION	RESULT	EXCITATION ENERGY	SOURCE		DETECTOR		ANGLE
			TYPE	RANGE	TYPE	RANGE	
E,E/	ABX	4	D	59	MAG-D	50-59	180

$\int \sigma\gamma d\epsilon$ = 63.3 μb-MeV

$g\Gamma_o$ = .32 ± .03 eV

Level at 4.431 MeV.

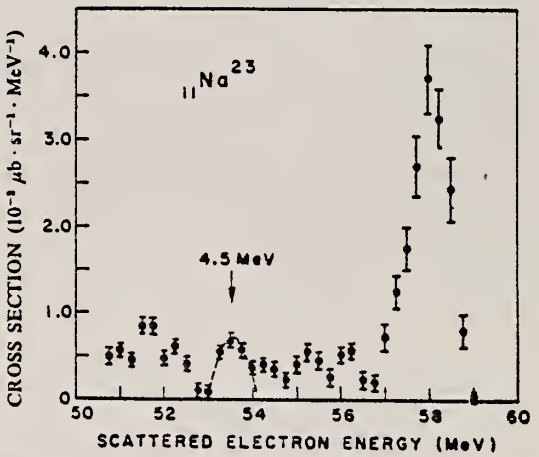

Fig. 1. Energy distribution of 58.5 MeV electrons, scattered elastically and inelastically at 180° from a ^{23}Na target, after correction for radiative effects. The dashed curve shows the area used in evaluating the cross section.

REF.

J.M. Wyckoff, B. Ziegler, H.W. Koch, and R. Uhlig
Phys. Rev. 137, B576-94 (1965)

ELEM.		
Na	23	11

METHOD

Synchrotron; ion chamber monitor

REF. NO.	
65 Wy 1	NVB

REACTION	RESULT	EXCITATION ENERGY	SOURCE		DETECTOR		ANGLE
			TYPE	RANGE	TYPE	RANGE	
G,MU-T	ABX	10 - 35	C	90	SCI-D		4PI

47

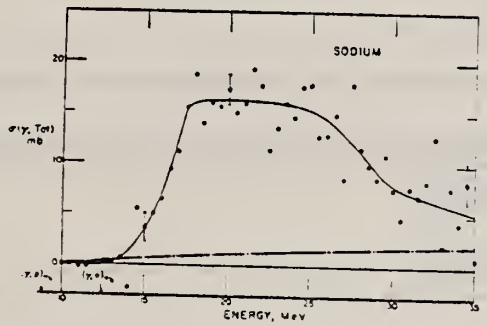

FIG. 11. Sodium total photonuclear cross section.

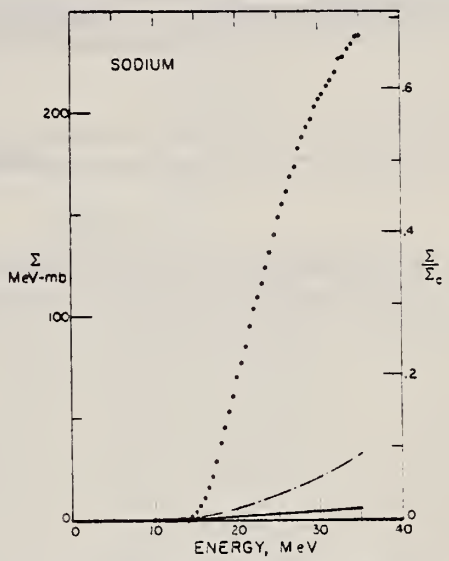

FIG. 12. Sodium total photonuclear cross section integrated over energy.

REF.

E. Wernbom-Selin and S.E. Arnell
Ark. Fysik 31, 113 (1966)

ELEM. SYM.	A	Z
Na	23	11

METHOD

REF. NO.	
66 We 1	JDM

REACTION	RESULT	EXCITATION ENERGY	SOURCE TYPE	SOURCE RANGE	DETECTOR TYPE	DETECTOR RANGE	ANGLE
P,G	SPC	9 - 10	D	1 - 2	NAI-D	1 - 10	DST

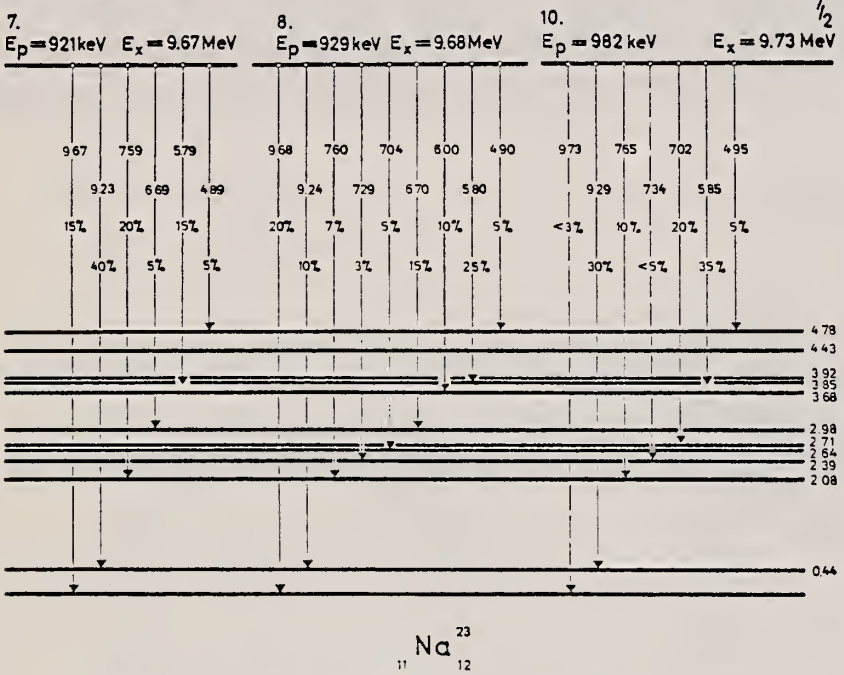

Fig. 22. Decay schemes of the 921 keV, 929 keV and 982 keV resonances.

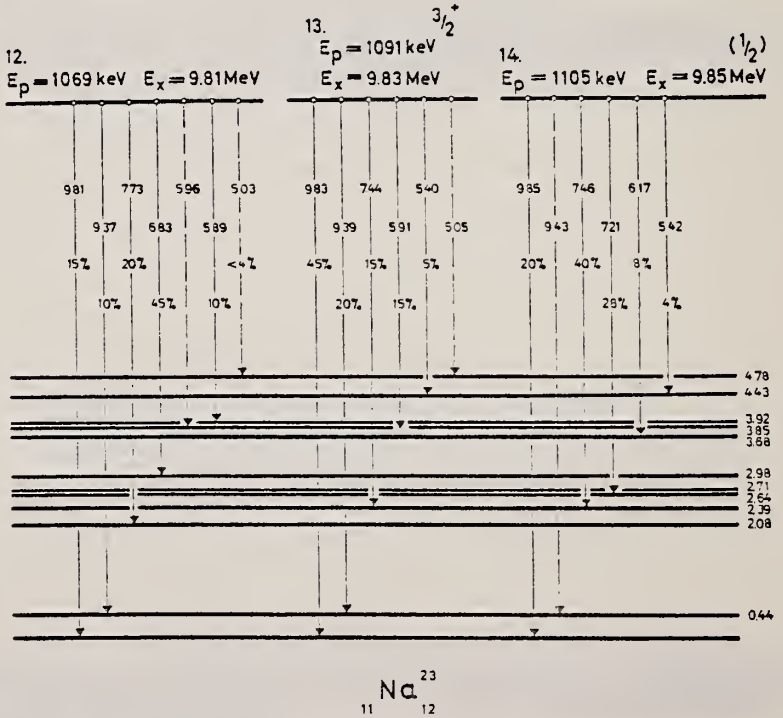

Fig. 23. Decay schemes of the 1069 keV, 1091 keV and 1105 keV resonances.

REF.

E. Wernbom-Selin and S.E. Arnell
Ark. Fysik 31, 113 (1966)

ELEM. SYM.	A	Z
Na	23	11

METHOD

REF. NO.	
66 We 1	JDM

DETECTOR		ANGLE
TYPE	RANGE	

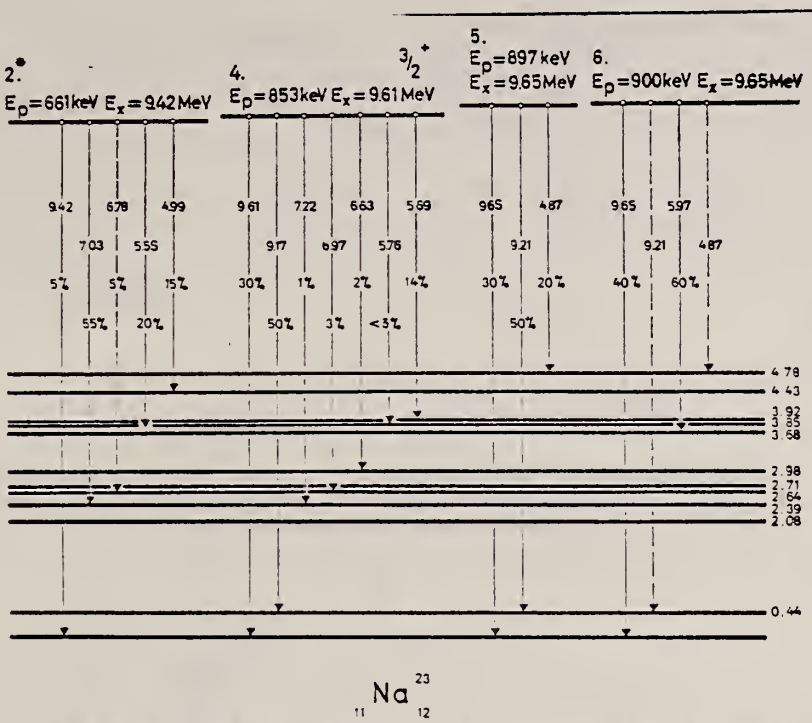

Fig. 21. Decay schemes of the 661 keV, 853 keV, 897 keV and 900 keV resonances. The spin value of the 853 keV capturing state from Braben *et al.* [3].

*The figure refers to the resonance number given in ref. 1.

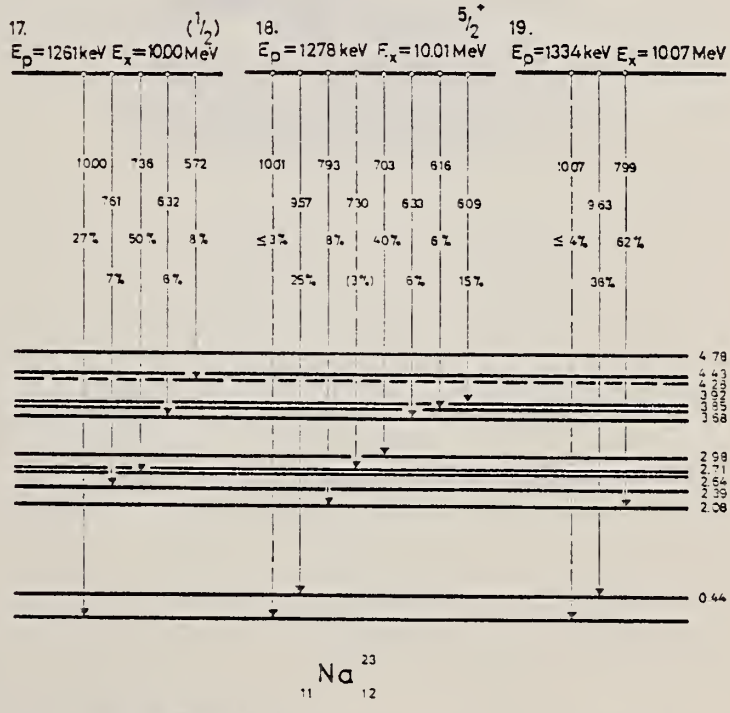

Fig. 24. Decay schemes of the 1261 keV, 1278 keV and 1334 keV resonances.

REF.
W. Feldman, D. W. Heikkinen and W. E. Meyerhof
Phys. Letters 25B, 593 (1967)

ELEM. SYM.	A	Z
Na	23	11

METHOD

REF. NO.: 67 Fe 3 EGF

REACTION	RESULT	EXCITATION ENERGY	SOURCE		DETECTOR		ANGLE
			TYPE	RANGE	TYPE	RANGE	
O,G	ABX	23-29	D	12-31	NAI-D	20-30	90

LI7 + 016

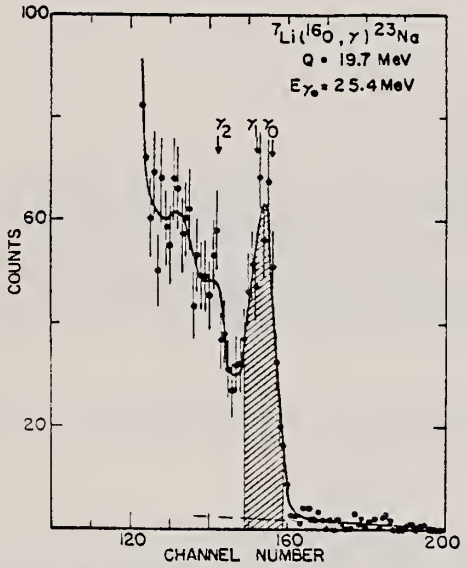

Fig. 1. The high-energy portion of a γ ray spectrum from $^7Li(^{16}O,\gamma)^{23}Na$ for $E(^{16}O)$ = 19.4 MeV. The shaded region was summed for the excitation function. The cosmic-ray background in the peak region is indicated by a dashed line.

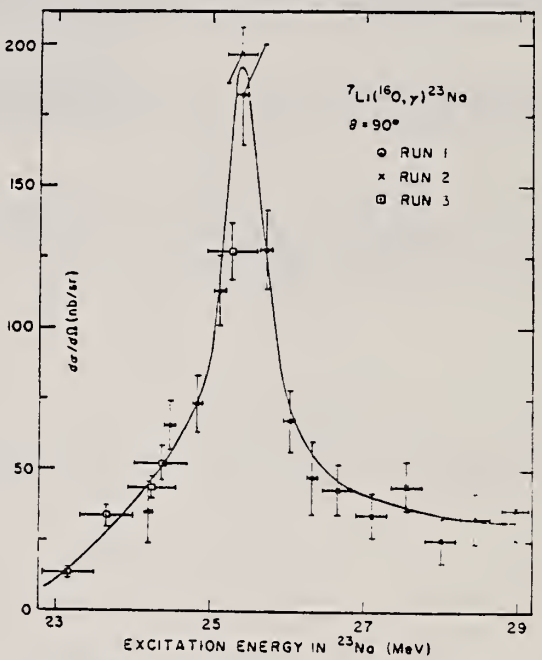

Fig. 2. The excitation function of the unresolved gamma transitions to the ground- and first-excited states of ^{23}Na for the reaction $^7Li(^{16}O,\gamma)^{23}Na$.

REF.

J. M. Loiseaux, J. M. Maison, and M. Langevin
J. de Physique 28, 11 (1967)

ELEM. SYM.	A	Z
Na	23	11

METHOD

REF. NO.	
67 Lo 1	JOC

REACTION	RESULT	EXCITATION ENERGY	SOURCE		DETECTOR		ANGLE
			TYPE	RANGE	TYPE	RANGE	
G,G/	ABX	15-30	C	34	NAI-D		DST

TABLEAU I

COEFFICIENT a DES DISTRIBUTIONS ANGULAIRES

$$W(\theta) = 1 - a\cos^2\theta$$

^{18}O.....	a(19-25 MeV)	$= 1$	$\pm 0,1$					
^{23}Na.....	a(15-18 MeV)	$= 0,1$	$\pm 0,1$	a(18,5-23 MeV)	$= 0,4$	$\pm 0,15$	a(25-30 MeV)	$= 0,85 \pm 0,2$
^{24}Mg	a(16,5-20 MeV)	$= 0,3$	$\pm 0,1$	a(20-25 MeV)	$= 0,5$	$\pm 0,1$	a(25,5-32 MeV)	$= 0,5 \pm 0,1$
^{28}Si	a(15-17,5 MeV)	$= 0,87$	$\pm 0,1$	a(18-23 MeV)	$= 0,7$	$\pm 0,1$	a(25,5-32 MeV)	$= 0,5 \pm 0,1$
^{39}K	a(14,5-18,5 MeV)	$= 0,5$	$\pm 0,1$	a(19-24,5 MeV)	$= 1$	$\pm 0,1$	a(25-32 MeV)	$= 1 \pm 0,1$

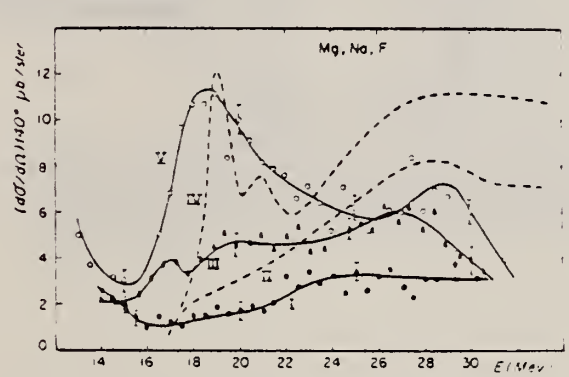

FIG. 6.

Sections efficaces différentielles de diffusion à 110° pour ^{19}F (I), ^{23}Na (III) et Mg (V).

Section efficace prévue par la relation de dispersion pour ^{23}Na (courbe II) et Mg (courbe IV).

REF.

G. A. Savitskii, N. G. Afanas'ev, I. S. Gul'karov, V. D. Kovalev, I. V. Andreeva, V. M. Khvastunov, N. G. Shevchenko
Ukr. Fiz. Zhur. 13, 1648 (1968)
Ukr. J. Phys. 13, 1174 (1969)

ELEM. SYM.	A	Z
Na	23	11

METHOD

REF. NO.	
68 Sa 3	egf

REACTION	RESULT	EXCITATION ENERGY	SOURCE		DETECTOR		ANGLE
			TYPE	RANGE	TYPE	RANGE	
E,E/	FMF	2,7	D	225	MAG-D		DST

2=2.08,7=6.27+7.10

TABLE 3. Squared Form Factor for Inelastic Scattering with Excitation of the 2.08 MeV Level in Na^{23}

q', fermi^{-1}	$F^2 \cdot 10^4$	q', fermi^{-1}	$F^2 \cdot 10^4$
0.41	13.9±13.9	1.26	14.5±1.2
0.51	25.3±15.7	1.365	11.1±0.9
0.61	24.2±14.7	1.41	7.46±0.67
0.71	32.1±9.1	1.45	7.20±0.50
0.71	22.0±10.3	1.48	6.52±0.51
0.80	15.8±10.8	1.51	5.71±0.43
0.90	70.3±9.1	1.54	4.43±0.35
0.90	31.0±8.9	1.73	1.37±0.15
0.99	46.3±5.0	1.865	1.11±0.11
1.08	31.2±2.9	1.98	0.91±0.12
1.17	29.8±1.7	2.08	1.67±0.20

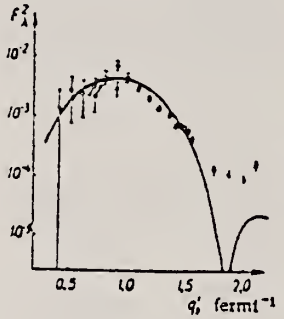

Fig. 3. Form factor for inelastic scattering of electrons with excitation of the 2.08 MeV level in Na^{23}.

TABLE 4. Differential Cross Sections for Inelastic Scattering of Electrons Having an Initial Energy of 225 MeV with Excitation of the 6.27 and 7.10 MeV Levels in Na^{23}, Which Were Not Resolved Experimentally

θ	$\sigma_{exp} \cdot 10^{32}$, cm^2/sr	θ	$\sigma_{exp} \cdot 10^{33}$, cm^2/sr
30	667±251	74	47.7 ±5.2
35	456±125	76	46.2 ±4.2
35	351±131	78	40.6 ±3.6
40	132±54	78	36.8 ±3.3
45	76.2±17.0	80	30.5 ±2.7
45	78.0±16.9	82	27.1 ±2.5
50	42.8± 9.9	85	12.1 ±1.5
55	25.1± 4.4	95	8.20±1.08
60	20.7± 2.4	105	5.30±0.85
65	9.01±1.10	115	2.70±0.64
70	6.96±0.98	125	1.35±0.46

REF.

K. Shoda, K. Abe, T. Ishizuka, N. Kawamura, M. Oyamada, and Baik-Nung Sung
J. Phys. Soc. Japan 25, 664 (1968)

ELEM. SYM.	A	Z
Na	23	11

METHOD

REF. NO.: 68 Sh 3 | egf

REACTION	RESULT	EXCITATION ENERGY	SOURCE		DETECTOR		ANGLE
			TYPE	RANGE	TYPE	RANGE	
G,XP	SPC	20-24	D	20,24	EMU-D	2-14	DST

Table III. Anisotropic factor B/A of angular distributions estimated for the groups of strong transitions.

	Assumed residual Energy (MeV)	E_γ (MeV)	B/A	Used data[a]
^{22}Na	1.27	18.8–20.5	0.5±0.4	20.5
	3.3	20.8–22.1	∞[b]	*D*
		22.1–24	∞[b]	24.0
	7.0	20.7–22.7	1.5±0.3	*D*
^{24}P	0	15.7–21	∞[b]	24.0,19.0
	7.0	17.4–20.2	0.5±0.6	*D*
		20.2–22.7	1.3±1.3	*D*
^{22}S	0	14–20	∞[b]	(*p*, γ_0)
		14–14.8	2.4±0.7	17.0
		14.8–16.2	∞[b]	17.0
		16.2–17.1	∞[b]	17.0
	5.0	19.2–20.1	0.5±0.2	*D*
		20.1–21.3	0.4±0.2	*D*
^{40}Ca	0	17.1–20.5	1.5±0.2	20.5
	2.8	17.4–19.9	2.6±0.3	20.5
	6.0	17.2–18.7	0.05±0.09	20.5
		18.7–20.5	0.6±0.1	20.5

a) The numerical number indicates the maximum energy of the bremsstrahlung irradiated for the data. *D* shows the difference between the two distributions. (*p*, γ_0) shows the inverse reaction data.

b) The notation ∞ indicates that the distribution is almost $\sin^2\theta$, *i.e.*, the result has stronger maximum than $1+10\sin^2\theta$.

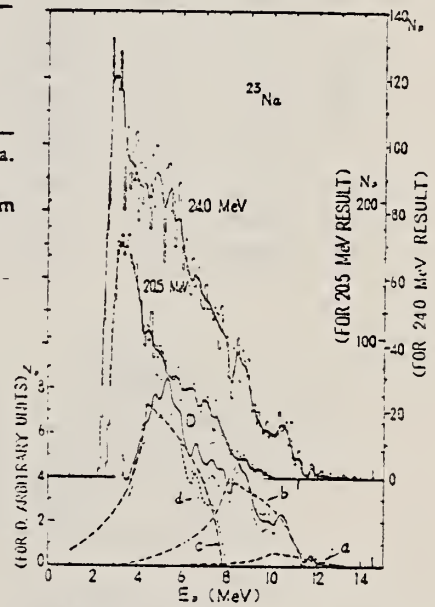

Fig. 1. Energy distributions of photoprotons from ^{23}Na irradiated with 20.5 MeV and 24.0 MeV bremsstrahlung. Curve *D* and its error brackets (dotted curves) show the spectrum made by difference of the two results. Curves *a*, *b* and *c*, respectively showing the transitions leaving the residual nucleus in 1.27, 3.3 and 7.0 MeV, are component spectra for curve *D*. Curve *d* is the difference spectrum between curve *b* and curve *D*.

Table II. Anisotropic factor B/A of angular distributions determined by least-squares fits with $A+B\sin^2\theta$.

^{23}Na					
($E_{\gamma\,max}$=20.5 MeV)		($E_{\gamma\,max}$=24.0 MeV)		(Curve *D* in Fig. 1)	
E_p(MeV)	B/A	E_p(MeV)	B/A	E_p(MeV)	B/A
2.5–4.6	1.6±0.6	4.7–6.5	1.3±0.2	4.7–6.6	1.5±0.3
4.6–6.7	1.0±0.2	6.5–8.3	3.4±1.1	6.6–8.3	6.1±1.3
6.7–8.4	1.6±0.7	8.3–9.6	9.6±6.1	8.3–9.6	∞[a]
8.4≦	0.5±0.4	9.6≦	∞[a]	9.6≦	∞[a]
2.5≦	1.4±0.4	3.5≦	1.9±0.3		

a) The notation ∞ indicates that the distribution is almost $\sin^2\theta$. It is used when the result has stronger maximum than that of $1+10\sin^2\theta$.

W. Hofmann, R. Kosiek, G. Kraft and R. Mundhenke
Z. Physik 225, 303 (1969)

Na	23	11

METHOD

REF. NO. 69 Ho 1 egf

REACTION	RESULT	EXCITATION ENERGY	SOURCE		DETECTOR		ANGLE
			TYPE	RANGE	TYPE	RANGE	
G,XP	ABY	THR- 33	C	24-33	SCI-D	3-14	90

Tabelle 1. *Daten zu den einzelnen Reaktionen. Die Werte für den integrierten Wirkungsquerschnitt wurden unter der Annahme ausschließlicher Grundzustandsübergänge berechnet. Für ^{23}Na und ^{39}K als Ausnahme s. Text*

Target	Anreicherungsgrad %	(γ, p)-Schwelle MeV	Druck oder Dicke	Endenergie MeV	Zahl gemess. Protonen	Ausbeute µb/MeV sr	$\int_{32,5}^{\sigma}\sigma(E)dE$ MeVmb	Figur
^{18}O	99	16,0	230 Torr	32,5	36074	58 ± 7	38 ± 6	1, 2
^{20}Ne	90,9	12,8	450 Torr	28,0	3175	7,4 ± 1	–	–
			610 Torr	32,5	6293	14,9 ± 2	61 ± 11	5, 6
^{22}Ne	99,9	15,3	240 Torr	24,0	1960	2,3 ± 0,4	–	4, 5
				28,0	4790	3,6 ± 0,6	–	4, 5
				32,5	5210	6,7 ± 0,9	45 ± 8	4, 5
^{23}Na	100	8,8	65µ	24,0	14182	6,3 ± 1,0	–	7
			60µ	32,5	11152	12,8 ± 2,0	117 ± 30	7
^{36}Ar	99	8,5	250 Torr	32,5	45173	57 ± 6	270 ± 40	8, 10
^{40}Ar	99,6	12,5	230 Torr	32,5	29559	14,2 ± 15	104 ± 15	9, 11
^{39}K	93,1	6,4	80µ	24,0	24230	17,4 ± 2,8	–	12
			90µ	32,5	24941	41,9 ± 6,7	405 ± 100	12
^{84}Kr	99	10,7	170 Torr	32,5	35515	12,7 ± 2,0	80 ± 20	14
Kr	natürl.	10	170 Torr	32,5	13570	12,5 ± 2,0	75 ± 20	13
Xe	natürl.	9	150 Torr	32,5	7553	7,6 ± 0,9	40 ± 7	15

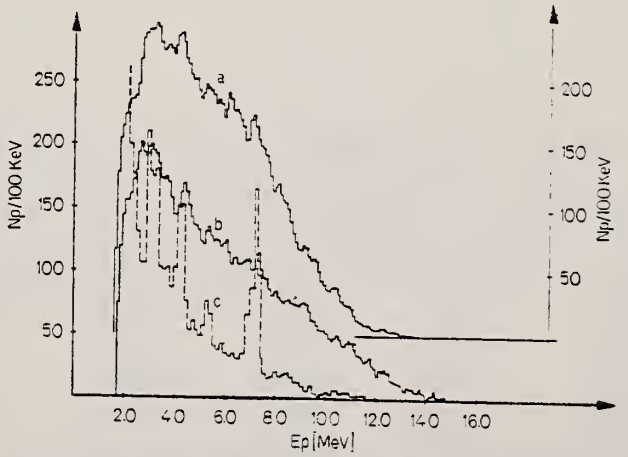

Fig. 7. Energieverteilung der Photoprotonen aus ^{23}Na. *a* Für $E_0 = 24$ MeV, *b* für $E_0 = 32,5$ MeV, *c* nach OPHEL und WRIGHT[28]

G. A. Savitskii, N. G. Afanas'ev, I. S. Gul'karov, V. D. Kovalev, V. M. Khvastunov, N. G. Shevchenko, I. V. Andreeva
Izv. Akad. Nauk Fiz. 33, 60 (1969)
Bull. Acad. Sci. USSR-Phys. 33, 56 (1969)

Na	23	11

METHOD

REF. NO. 69 Sa 3 hmg

REACTION	RESULT	EXCITATION ENERGY	SOURCE TYPE	SOURCE RANGE	DETECTOR TYPE	DETECTOR RANGE	ANGLE
E,E/	FMF	2	D	99-227	MAG-D	99-227	DST
		(2.08)					

B(EL) 2.08 MEV

Table 2

Squared form factors for inelastic scattering of electrons with excitation of levels in ^{23}Na and ^{39}K

2,08 MeV ^{23}Na		3,6 MeV ^{39}K		6,5 MeV ^{39}K	
q', fermi^{-1}	F_λ^2, 10^{-4}	q', fermi^{-1}	F_λ^2, 10^{-4}	q', fermi^{-1}	F_λ^2, 10^{-4}
0,41	13,9±13,9	0,72	7,43±7,95	0,41	77,5±22,9
0,51	26,3±18,7	0,72	4,18±11,12	0,52	45,4±14,1
0,61	24,2±14,7	0,82	10,9±5,5	0,62	43,1±15,1
0,71	32,4± 9,4	0,91	18,5±3,3	0,72	23,9±5,7
0,71	22,0±10,3	0,91	14,6±4,4	0,72	23,3±7,8
0,80	45,8±10,8	0,92	12,6±3,3	0,82	18,2±4,1
0,90	70,3±9,1	1,01	18,4±2,4	0,91	6,7±2,0
0,90	31,0±8,9	1,10	24,7±2,4	0,91	11,4±2,8
0,99	46,3±5,0	1,19	18,9±1,7	0,92	9,2±2,4
1,08	31,2±2,9	1,28	17,0±1,7	1,01	7,5±1,9
1,17	20,8±1,7	1,37	11,8±1,2	1,19	6,3±1,5
1,26	14,5±1,2	1,44	8,66±0,87	1,28	4,45±1,09
1,35	11,1±0,9	1,53	5,50±0,75	1,37	3,78±0,88
1,41	7,46±0,67	1,61	4,56±0,52	1,44	2,77±0,57
1,45	7,20±0,50	1,75	1,35±0,35		
1,48	5,52±0,51				
1,51	5,71±0,43				
1,54	4,43±0,35				
1,73	1,37±0,15				
1,86	1,11±0,14				
1,98	0,91±0,12				
2,08	1,07±0,20				

Table 4

Characteristics of transitions excited by high-energy electrons in ^{23}Na and ^{39}K

Method	Parameters and method of determination	2,03 MeV ^{23}Na (λ=2)	3,6 MeV ^{39}K (λ=3)	6,5 MeV ^{39}K (λ=1)
1	β_λ, 10^{-2}	11,6±2,5	13,1±2,8	3,40±0,69
	$B(E\lambda, I_i \to I_f)e^2$ fermi$^{2\lambda}$	107±23	11800±2500	14,3±2,9
	G	13,7±3,0	19±4	6,4±1,3
2	A_λ, fermi$^{\lambda-2}$	1,55±0,10	1,39±0,04	1,79±0,15
	B_λ, fermi^2	0,45±0,07	0,34±0,09	0,79±0,17
	$B(E\lambda, I_i \to I_f)$, e^2 fermi$^{2\lambda}$	80±11	6300±400	8,5±1,5
	G	10,2±1,4	10±1	3,8±0,7
	R_{trans}, fermi	3,93±0,57	4,38±0,06	3,89±0.22

REF. N. Shikazono and Y. Kawarasaki
Phys. Letters 32B, 473 (1970)

ELEM. SYM.	A	Z
Na	23	11

METHOD

REF. NO. 70 Sh 2 egf

REACTION	RESULT	EXCITATION ENERGY	SOURCE		DETECTOR		ANGLE
			TYPE	RANGE	TYPE	RANGE	
G,G	LFT	7	C	14	SCD-D		

7 = 7.895 MEV

Table 1
Comparison between experimental log ft values and radiative widths: Γ_{th} represents the width estimated only from the spin part with eq. (1); R denotes the ratio of the reduced matrix element of the spin part to that of the orbital part.

	E_i (keV)	(T, J^π)	E_f (keV)	(T, J^π)	log ft	Γ_{th} (eV)	Γ_{obs} (eV) [a]	R
^{23}Na	7895	$(\frac{1}{2}, \frac{1}{2}^+)$	0	$(\frac{1}{2}, \frac{1}{2}^+)$	5.3	0.21	1.02 ± 0.37	5.5 ± 1.2
^{23}Na	7895	$(\frac{1}{2}, \frac{5}{2}^+)$	439	$(\frac{1}{2}, \frac{1}{2}^+)$	5.4	0.14	0.57 ± 0.21	4.8 ± 1.1
^{31}P	6381	$(\frac{1}{2}, \frac{3}{2}^+)$	0	$(\frac{1}{2}, \frac{1}{2}^+)$	5.5	0.07	≤ 0.11	≤ 1.2

a) In the estimate of Γ_{obs}, the branching ratio Γ_0/Γ for ^{23}Na and ^{31}P were assumed to be 0.64 and 0.18, respectively.

REF. R. A. Alvarez, B. L. Berman, D. R. Lasher, T. W. Phillips, and S. C. Fultz
Phys. Rev. C4, 1673 (1971)

ELEM. SYM.	A	Z
Na	23	11

METHOD

REF. NO.	
71 A1 1	hmg

REACTION	RESULT	EXCITATION ENERGY	SOURCE		DETECTOR		ANGLE
			TYPE	RANGE	TYPE	RANGE	
G,N 347	ABX	12-27	D	12-27	BF3-I		4PI *
G,2N 350+	ABX	23-27	D	23-27	BF3-I		4PI

* INCLUDES G,NP 347

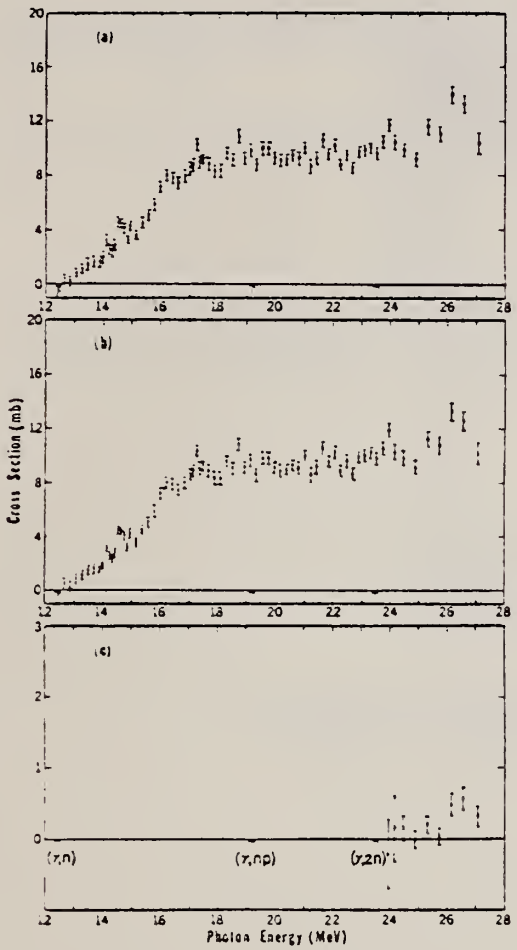

FIG. 2. Cross sections for ^{23}Na. (a) Total photoneutron cross section, $\sigma[(\gamma,n)+(\gamma,np)+(\gamma,2np)]$. (b) Single-photoneutron cross section, $\sigma[(\gamma,n)+(\gamma,np)]$. (c) Double-photoneutron cross section, $\sigma(\gamma,2n)$. The thresholds (arrows) are taken from Mattauch *et al.* (see Table I).

TABLE II. Integrated total photoneutron cross sections and their moments.

Nucleus	$E_{\gamma max}$ (MeV)	σ_{int} [a] (MeV mb)	σ_{-1} [b] (mb)	σ_{-2} [b] (mb MeV^{-1})
^{23}Na	27	119	5.74	0.288
^{25}Mg	29	249	11.7	0.584

[a] $\sigma_{int} \equiv \int_{E_{thr}}^{E_{\gamma max}} \sigma_{tot} dE$.

[b] $\sigma_{-n} \equiv \int_{E_{thr}}^{E_{\gamma max}} \sigma_{tot} E^{-n} dE$.

(over)

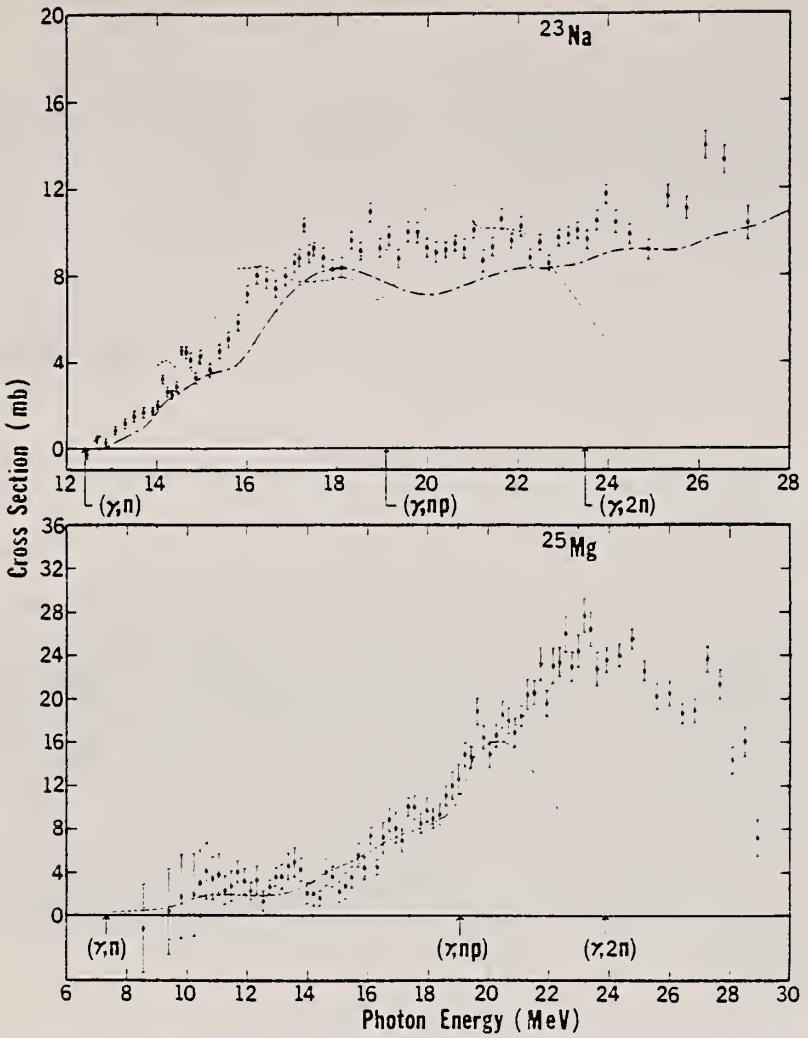

FIG. 4. Comparison of the present total photoneutron cross sections with previous measurements. The dashed curves indicate the results of Sato (Ref. 11) for ^{23}Na and of Nathans and Yergin (Ref. 13) for ^{25}Mg; the dash-dot curve represents the ^{23}Na data of Fielder, Bolen, and Whitehead (Ref. 12).

REF.

M. Piiparinen, A. Anttila, and M. Viitasalo
Z. Physik 247, 400 (1971)

Na	23	11

METHOD

REF. NO. 71 Pi 2 egf

REACTION	RESULT	EXCITATION ENERGY	SOURCE TYPE	SOURCE RANGE	DETECTOR TYPE	DETECTOR RANGE	ANGLE
P,G	RLX	9-10	D	0-2	SCD-D		DST

9.61 MEV LEVEL,J-PI

Table. *Angular distribution coefficients and mixing ratios measured at the E_p=853 keV*

E_i (MeV)	J_i^π	E_f (MeV)	J_f^π	Legendre polynomial coefficients a_2	a_4	δ
9.61	$3/2^+$	0	$3/2^+$	0.60 ± 0.04	-0.04 ± 0.04	0.15 ± 0.07 or 2.2 ± 0.4
		0.44	$5/2^+$	-0.18 ± 0.01	0.00 ± 0.01	0.07 ± 0.06 or -7.0 ± 1.5
		3.91	$5/2^+$	-0.16 ± 0.02	-0.01 ± 0.02	0.05 ± 0.05 or -6.0 ± 1.5
3.91	$5/2^-$	0	$3/2^+$	0.00 ± 0.02	0.00 ± 0.02	-0.20 ± 0.08 or 10.0 ± 2.0

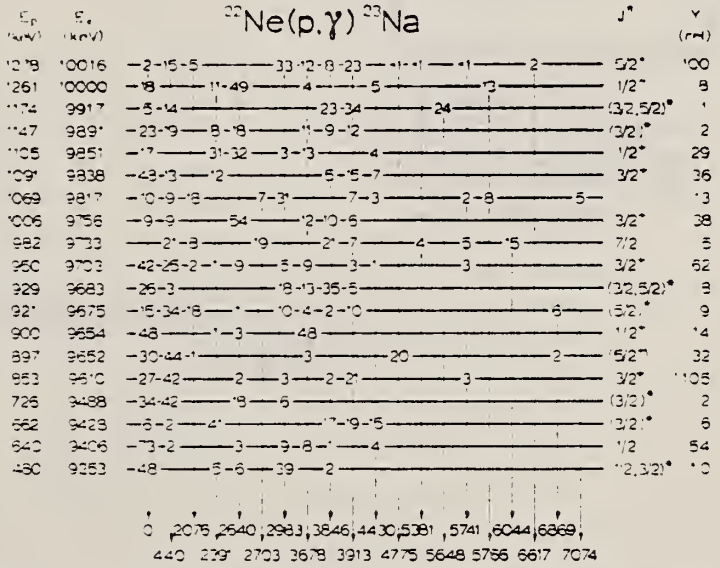

Fig. 1. Decay modes of the excited states in ^{23}Na proposed in the present work. The J^π assignments are from Refs.[1-9], except those marked with an asterisk, which are from the present work (see discussion). Errors in E_x values are ± 2 keV

(over)

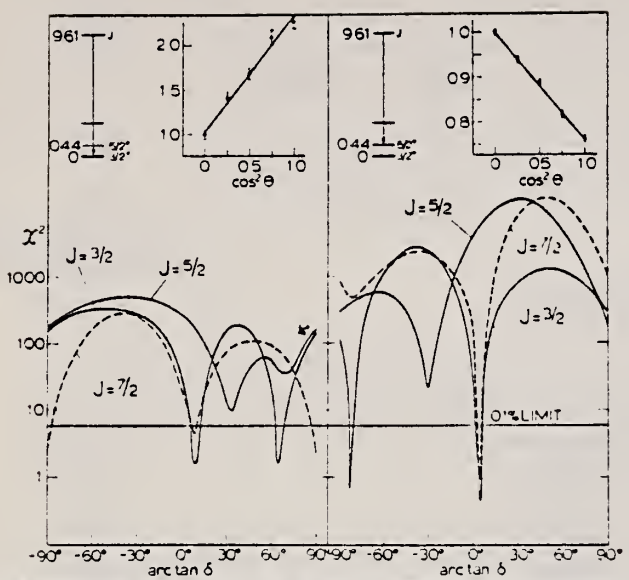

Fig. 4. Summary of results from the angular γ-distribution measurements of the 9.61 → 0 and 9.61 → 0.44 MeV transitions from the $E_p = 853$ keV resonance

REF.

Tatsuya Saito
Nippon Kagaku Zasshi 92, 164 (1971)

ELEM. SYM.	A	Z
Na	23	11

METHOD

REF. NO. 71 Sa 1 egf

REACTION	RESULT	EXCITATION ENERGY	SOURCE TYPE	SOURCE RANGE	DETECTOR TYPE	DETECTOR RANGE	ANGLE
G,N	ABY	12-68	C	10-68	ACT-I		4PI

Nippon Kagaku Zasshi, 92, 164~168(1971)

The Yields of Radioactivities Induced by (γ, n) Reactions with Bremsstrahlung up to 68 MeV

by Tatsuya SAITO

The (γ, n) yields of 12 target nuclides have been measured at 10, 13, 16, 30, 45 and 68 MeV bremsstrahlung by observing the induced activities.

The energy dependence of the yields has been investigated extensively in the same way as in the previous work at 20 MeV bremsstrahlung.

In the case of heavy nuclides, the yields rise greatly as a function of maximum bombarding energy up to 20 MeV, and rise gradually from 20 MeV up to 68 MeV. However, in the case of light nuclides, the yields rise greatly up to 30 MeV, because the neutron separation energies of light ones are larger than those of heavy ones, and the bremsstrahlung spectrum covers the giant resonance and so the yields rise gradually from 30 MeV up to 68 MeV.

The yields have approximately been estimated from the parameter of the giant resonance, that is the peak cross section and the half width, in order to compare with the experimental data. As a result, the experimental data of light nuclides and heavy ones are nearly in agreement with the estimated data of Nathans et al., Johns et al. and Montalbetti et al., but those of medium weight ones are relatively lower values.

Department of Chemistry, Faculty of Science, Tohoku University; Katahira-cho, Sendai-shi, Japan

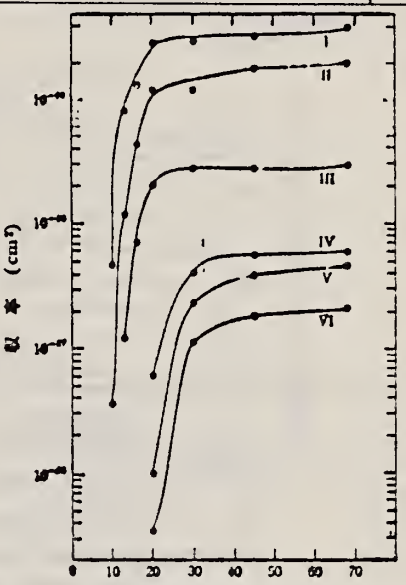

制動輻射最大エネルギー

I: $^{197}Au(\gamma, n)^{196}Au$, II: $^{127}I(\gamma, n)^{126}I$
III: $^{55}Mn(\gamma, n)^{54}Mn$, IV: $^{23}Na(\gamma, n)^{22}Na$
V: $^{16}O(\gamma, n)^{15}O$, VI: $^{12}C(\gamma, n)^{11}C$

図 3 (γ, n)反応の収率

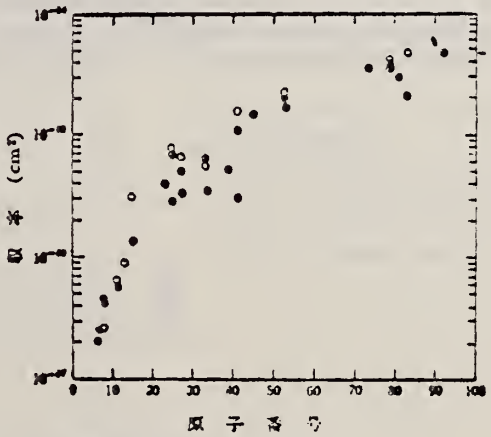

原子番号

●: 実験値, ⊕: Johns ら,
◑: Nathans ら, ○: Montalbetti ら

図 4 (γ, n)反応の収率の比較

REF. C. P. Swann
Nucl. Phys. A167, 201 (1971)

ELEM. SYM.	A	Z
Na	23	11

METHOD

REF. NO. 71 Sw 1 egf

REACTION	RESULT	EXCITATION ENERGY	SOURCE TYPE	SOURCE RANGE	DETECTOR TYPE	DETECTOR RANGE	ANGLE
G,G	LFT	7	D	7	SCD-D		DST

5 LEVELS

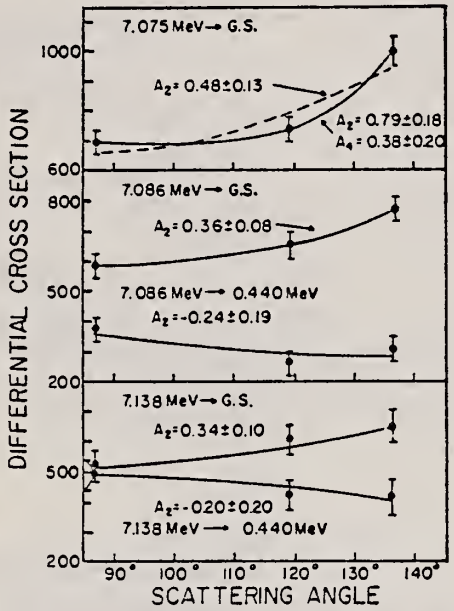

Fig. 3. Results of angular distribution measurements. The curves drawn were the least-square fits with the A_2 and/or A_4 coefficients given.

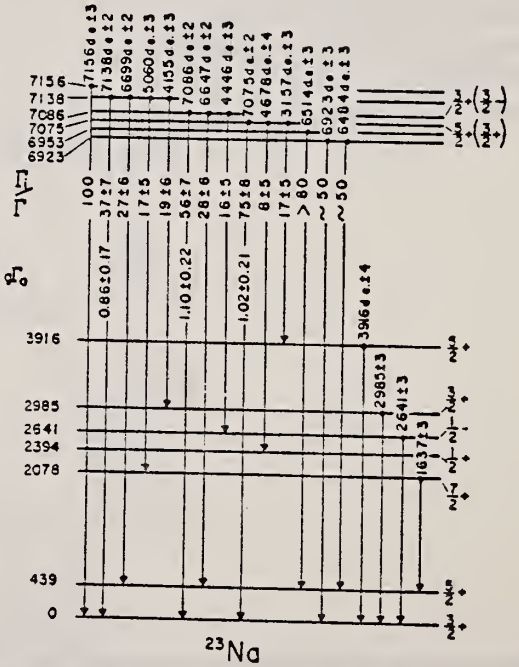

Fig. 2. Level scheme of observed γ-rays. The d.e. indicates that the double-escape peak was used in obtaining the energy. Given also are the branching ratios and some widths in eV for the ground state transitions. The spins and parities for the levels from 3.916 down were taken from Poletti *et al.* [7]) and Maier *et al.* [8]).

REF.

D.L. Friesel, T.J. Lewis, and W.C. Miller
Phys. Rev. C6, 846 (1972)

ELEM. SYM.	A	Z
Na	23	11

METHOD

REF. NO.	
72 Fr 4	hmg

REACTION	RESULT	EXCITATION ENERGY	SOURCE		DETECTOR		ANGLE
			TYPE	RANGE	TYPE	RANGE	
G,G	LFT	3-6	C	3-6	NAI-D		130

G-WIDTH, 5 LEVELS

Five levels in ^{23}Na were studied using nuclear resonance fluorescence. A previously reported level at 3.91 MeV was identified as a doublet with levels at 3914.0 ± 1.8 and 3916.3 ± 1.8 keV. Levels of 5375.8 ± 2.7, 5742.7 ± 2.9, and 5768.3 ± 2.9 keV have widths ($g\Gamma$) of $2.45^{+0.41}_{-0.41}$, $1.29^{+0.19}_{-0.09}$, and $0.62^{+0.05}_{-0.04}$ eV, respectively, as measured by self-absorption experiments. The γ-ray branching ratios for these levels were measured with a 40-cm^3 Ge(Li) spectrometer.

TABLE I. Experimental results.

Energy level (keV)	Transition (keV)	Branching ratio (present work)	Branching ratio (other work) [a]	Transmission $\Gamma=0$ [b]	Transmission experimental	Possible spin	$g\Gamma$ (meV)
3914.0 ± 1.8	3914		0.81	0.730	0.665 ± 0.058	$(\frac{5}{2}^+)$ [a]	28 ± 27
3916.3 ± 1.8	3916		0.81	0.730	0.622 ± 0.054	$(\frac{5}{2}^+)$ [a]	49 ± 27
5375.8 ± 2.7	5376	0.12 ± 0.08	0.14 ± 0.04	0.760	0.484 ± 0.029	$(\frac{5}{2}^+)$ [a]	2450^{+418}_{-418}
	4935	0.69 ± 0.15	0.63 ± 0.07				
	3297	0.19 ± 0.07	0.23 ± 0.05				
5742.7 ± 2.9	5743	0.71 ± 0.13	0.60 ± 0.10	0.766	0.298 ± 0.012	$(\frac{3}{2}^+, \frac{5}{2}^+)$ [a]	1400^{+120}_{-100}, 1290^{+109}_{-93}
	5302	0.29 ± 0.05	0.40 ± 0.10				
5768.3 ± 2.9	5768	0.73 ± 0.15		0.767	0.395 ± 0.029	$(\frac{5}{2}^+)$ [c]	800^{+122}_{-100}
	5327	0.27 ± 0.13					

[a] Branching ratios and spins reported by Poletti *et al.* (Refs. 1, 2, 8).
[b] Expected transmission if only electronic absorption were present (no resonant absorption).
[c] Spin of $\frac{5}{2}^+$ arbitrarily chosen to allow comparison with other widths.

[1] A.R. Poletti and D.F.H. Start, Phys. Rev. 147, 800 (1966).
[2] A.R. Poletti, J.A. Becker, and R.E. McDonald, Phys. Rev. C2, 964 (1970).
[8] A.R. Poletti et al., Phys. Rev. 184, 1130 (1969).

REF.

N. Shikazono and Y. Kawarasaki
Nucl. Phys. A188, 461 (1972)

ELEM.	S/M.	A	L
Na		23	11

METHOD

REF. NO. 72 Sh 2 egf

REACTION	RESULT	EXCITATION ENERGY	SOURCE		DETECTOR		ANGLE
			TYPE	RANGE	TYPE	RANGE	
G,G/	SPC	0-14	C	14	SCD-D		87

TABLE 2

Gamma-rays resulting from the photon bombardment of a NaOH target

E_γ (MeV)	Observed peak	Relative intensity	Transition
2.98	F	19 ±7	2.98 → 0
4.43	D, S, F	89 ±4	4.43 → 0
4.94	D, S, F	14.7±1.5,	5.38 → 0.44
5.30	D, S, F	7.7±1.6	5.74 → 0.44
5.33	D, S, F	6.3±1.6	5.77 → 0.44
5.74	D, S, F	27.3±1.2	5.74 → 0
5.77	D, S, F	15.1±1.2	5.77 → 0
6.30	(D)	3.4±0.8	8.37 → 2.07
6.64	(D)	3.4±1.0	7.09 → 0.44
6.70	D, (S)	2.8±0.9	7.14 → 0.44
6.74	D, S, (F)	8.6±0.9	6.74 → 0
7.07	D, (S), F	10.8±0.7	7.07 → 0
7.09	D, S, F	9.3±0.7	7.09 → 0
7.14	D, S, (F)	11.5±0.8	7.14 → 0
7.46	D, S, F	10.6±0.8	7.90 → 0.44
7.57	D, (S)	2.7±0.7	7.57 → 0
7.90	D, S, F	18.5±0.8	7.90 → 0
7.93	(D), (S)	7.3±0.7	8.37 → 0.44
8.37	D, S	12.0±0.7	8.37 → 0
8.65	D	6.5±0.6	8.65 → 0
8.67	D, S	12.7±0.6	8.67 → 0
9.15	D	7.5±0.6	9.15 → 0

(over)

TABLE 6

Excitation energies and ground state transition widths obtained from the $^{23}Na(\gamma,\gamma')^{23}Na$ reaction

Excitation energy (keV)		$J^\pi; T$	$\Gamma_{\gamma 0}/\Gamma_\gamma$ [a]	$(2J+1)\Gamma_{\gamma 0}$ (eV) [b]	
present work	previous work			present work	previous work
2979±6	2985± 6 [c]	$(\frac{3}{2}^+)$ [c]	0.51 [c]	0.20±0.08	0.28±0.04 [c]
4426±4	4431± 5 [c]	$\frac{1}{2}^+$ [d]	0.95 [c]	5.0 ±0.8	4.3±0.5 [c]
5376±4	5378± 5 [e]	$\frac{5}{2}^+$ [f]	0.13±0.01 [g]	1.6 ±0.3	
5744±4	5738± 8 [e]	$(\frac{3}{2}, \frac{5}{2})^+$ [h]	0.78±0.04	3.7 ±0.7	
5768±4	5762± 8 [e]		0.70±0.06	2.1 ±0.4	
6739±4	6731± 8 [e]	$(\frac{3}{2}, \frac{5}{2})^+$ [i]	1.0	1.5 ±0.3	
7074±5	7075± 2 [j]	$\frac{5}{2}^+$ [j]	1.0	3.0 ±0.5 [k]	4.1±0.8 [j]
7086±5	7086± 2 [j]	$\frac{3}{2}^+$ [j]	0.75±0.06 [l]	3.4 ±0.7 [k]	4.4±0.9 [j]
7137±5	7138± 2 [j]	$(\frac{3}{2}, \frac{5}{2}, \frac{7}{2})$ [j]	0.80±0.05	3.8 ±0.7 [k]	3.7±0.4 [c] 3.4±0.7 [j]
7572±6	7563± 7 [e]		1.0	0.7 ±0.2	
7896±5	7900±21 [m]	$\frac{5}{2}^+, T=\frac{3}{2}$ [m]	0.67±0.02 [l]	11 ±2	
8367±5	8357± 8 [e]	$(\frac{5}{2}, \frac{7}{2})$	0.53±0.03 [n]	12 ±2	
8652±6	8643± 7 [e]		1.0	3.1 ±0.6	
8669±5	8659±30 [d]	$\frac{1}{2}^+, T=\frac{3}{2}$ [d]	1.0	6.5 ±1.1	
9147±5			1.0	5.2 ±0.9 [o]	

[a]) The branchings are obtained from the relative intensities observed at the scattering angle of 87°. The effect of the angular distribution of the γ-rays is not taken into account.

[b]) The error for $(2J+1)\Gamma_{\gamma 0}$ only includes the statistical error. An estimate of the uncertainty associated with the shape of the incident bremsstrahlung is not included.

[c]) Ref. [8]).

[d]) Ref. [18]).

[e]) Ref. [19]).

[f]) Ref. [51]).

[g]) Ref. [52]).

[h]) Ref. [53]).

[i]) Ref. [8]). The energy of the state is given as 6727±20 keV in ref. [5]).

[j]) Ref. [20]).

[k]) This value is calculated by using the result of the angular distribution measurement given in ref. [20]).

[l]) This value is calculated on the assumption that the transitions to lower states are of pure dipole character.

[m]) Ref. [17]).

[n]) The 8.37 MeV state decays to three lower states. The branching to the 0.44 and 2.07 MeV states are 0.32±0.03 and 0.15±0.03, respectively.

[o]) The value given is not the $(2J+1)\Gamma_{\gamma 0}$ but the $(2J+1)\Gamma_{\gamma 0}\Gamma_\gamma/\Gamma$ value.

[8] P.M. Endt et al. Nucl. Phys. A105 (1967) 1.

[17] J.C. Hardy et al. Phys. Rev. 183 (1969) 854.

[18] J. Dubois, Nucl. Phys. A104 (1967) 657.

[19] H.J. Hay et al. Nucl. Phys. A98 (1967) 330.

[20] C.P. Swann, Nucl. Phys. A167 (1971) 201.

[51] E. Kramer et al. Nucl. Phys. A165 (1971) 353.

[52] M.F. da Silva et al. Nucl. Phys. A168 (1971) 663.

[53] A.R. Poletti et al. Phys. Rev. 184 (1969) 1130.

REF.

Z. B. du Toit, P. R. de Kock, J. H. Hough, and W. L. Mouton
Z. Physik 255, 97 (1972)

COMPOUND		
Na	23	11

METHOD

REF. NO.

72 To 3 egf

REACTION	RESULT	EXCITATION ENERGY	SOURCE		DETECTOR		ANGLE
			TYPE	RANGE	TYPE	RANGE	
G,MU-T	LFT	9	D	9	NAI-D		4PI

9.404, 9.700 MEV

Gamma rays of energy 9.404 and 9.700 MeV were obtained from the reaction $^{22}Ne(p, \gamma)^{23}Na$ at proton energies of 640 and 950 keV respectively and were resonantly absorbed in sodium metal. Isotopically separated ^{22}Ne targets on nickel backings were used. The following level widths for ^{23}Na were obtained:

The 9.404 MeV level:

$$\Gamma = 65 \pm 40 \text{ eV}$$
$$\Gamma_\gamma = 2.2 \pm 0.7 \text{ eV}.$$

The 9.700 MeV level:

$$\Gamma = 9.5^{+4.5}_{-1.0} \text{ eV}$$
$$\Gamma_\gamma = 5.6^{+1.2}_{-0.8} \text{ eV}.$$

The disagreement between the results for the 9.404 MeV level and the previously determined values can probably be ascribed to proton scattering in the window of the gas target used in the latter measurement.

REF.

M. Viitasalo, M. Piiparinen and A. Anttila
Z. Physik 250, 387 (1972)

ELEM.		
Na	23	11

METHOD

REF. NO. 72 Vi 1 egf

REACTION	RESULT	EXCITATION ENERGY	SOURCE		DETECTOR		ANGLE
			TYPE	RANGE	TYPE	RANGE	
P,G	NOX	9-10	D	0-1	SCD-D		DST

4 LEVELS, J-PI

Table 1. Experimental angular distribution coefficients

Resonance	Transition	a_2	a_4
E_p = 897 keV	$r \rightarrow$ 0	0.68 ± 0.08	0.12 ± 0.08
E_x = 9652 keV	$r \rightarrow$ 440	0.74 ± 0.06	0.06 ± 0.06
	$r \rightarrow$ 4775	−0.05 ± 0.05	−0.09 ± 0.07
	4775 → 440	0.18 ± 0.06	−0.17 ± 0.07
	4775 → 2076	0.33 ± 0.14	0.02 ± 0.13
E_p = 1006 keV	$r \rightarrow$ 0	0.22 ± 0.05	−0.10 ± 0.06
E_x = 9756 keV	$r \rightarrow$ 440	−0.22 ± 0.04	0.07 ± 0.05
	$r \rightarrow$ 2640	−0.44 ± 0.02	0.01 ± 0.03
	$r \rightarrow$ 3678	0.41 ± 0.04	−0.03 ± 0.04
	$r \rightarrow$ 3846	0.12 ± 0.05	0.03 ± 0.06
	3846 → 2076	−0.23 ± 0.04	0.02 ± 0.04
	3678 → 440	0.07 ± 0.03	−0.08 ± 0.03
	2640 → 0	0.00 ± 0.02	−0.03 ± 0.03
E_p = 1091 keV	$r \rightarrow$ 0	0.72 ± 0.04	0.00 ± 0.03
E_x = 9838 keV	$r \rightarrow$ 440	−0.16 ± 0.05	−0.09 ± 0.05
	$r \rightarrow$ 2391	−0.06 ± 0.05	−0.06 ± 0.06
	$r \rightarrow$ 3913	−0.06 ± 0.10	0.02 ± 0.11
	$r \rightarrow$ 4430	−0.14 ± 0.07	0.02 ± 0.08
	4430 → 0	0.01 ± 0.08	0.08 ± 0.09
	3913 → 0	−0.08 ± 0.06	0.03 ± 0.07
	2391 → 440	0.05 ± 0.06	−0.01 ± 0.07
	2391 → 0	0.05 ± 0.05	−0.03 ± 0.06
E_p = 1278 keV	$r \rightarrow$ 0	−0.64 ± 0.08	0.40 ± 0.10
E_x = 10016 keV	$r \rightarrow$ 440	0.22 ± 0.03	0.01 ± 0.03
	$r \rightarrow$ 2076	0.27 ± 0.04	−0.02 ± 0.04
	$r \rightarrow$ 2983	−0.43 ± 0.02	0.00 ± 0.02
	$r \rightarrow$ 3678	−0.40 ± 0.02	0.03 ± 0.03
	$r \rightarrow$ 3846	0.36 ± 0.07	0.01 ± 0.07
	$r \rightarrow$ 3913	0.51 ± 0.03	−0.03 ± 0.03
	$r \rightarrow$ 6617	0.25 ± 0.13	0.14 ± 0.15
	6617 → 440	−0.07 ± 0.06	−0.16 ± 0.07
	3913 → 0	−0.05 ± 0.02	0.01 ± 0.02
	3846 → 2076	−0.03 ± 0.06	−0.01 ± 0.07
	3678 → 440	−0.05 ± 0.02	0.03 ± 0.03
	3678 → 2640	−0.58 ± 0.03	−0.01 ± 0.04
	2983 → 0	0.44 ± 0.04	−0.04 ± 0.04
	2983 → 440	−0.19 ± 0.04	0.06 ± 0.04

$$W(\theta) = 1 + a_2 P_2 + a_4 P_4$$

(over)

Table 2. Multipole mixing ratios δ of the primary gamma-rays from the resonance levels measured in the present investigation

Resonance	Transition (E_x in keV)	$J_i \rightarrow J_f$	Mixing ratio δ
$E_p = 897$ keV	$r \rightarrow 0$	$5/2 \rightarrow 3/2$	0.63 ± 0.03
$E_x = 9652$ keV	$r \rightarrow 440$	$5/2 \rightarrow 5/2$	0.30 ± 0.04
	$r \rightarrow 4775$	$5/2 \rightarrow 7/2$	-0.07 ± 0.03
$E_p = 1006$ keV	$r \rightarrow 0$	$3/2 \rightarrow 3/2$	-0.11 ± 0.02
$E_x = 9756$ keV			7.0 ± 0.5
	$r \rightarrow 440$	$3/2 \rightarrow 5/2$	0.10 ± 0.01
			-9.0 ± 1.0
	$r \rightarrow 2640$	$3/2 \rightarrow 1/2$	0.04 ± 0.02
	$r \rightarrow 3678$	$3/2 \rightarrow 3/2$	0.01 ± 0.02
			3.9 ± 0.4
	$r \rightarrow 3846$	$3/2 \rightarrow 5/2$	-0.19 ± 0.04
		$3/2 \rightarrow 7/2$	0.03 ± 0.02
$E_p = 1091$ keV	$r \rightarrow 0$	$3/2 \rightarrow 3/2$	0.25 ± 0.02
$E_x = 9838$ keV			2.0 ± 0.1
	$r \rightarrow 440$	$3/2 \rightarrow 5/2$	0.04 ± 0.02
			-6.0 ± 0.5
	$r \rightarrow 2391$	$3/2 \rightarrow 1/2$	0.24 ± 0.06
			-3.2 ± 0.5
	$r \rightarrow 3913$	$3/2 \rightarrow 3/2$	-0.28 ± 0.03
			-18.0 ± 3.0
		$3/2 \rightarrow 5/2$	-0.03 ± 0.07
			-4.3 ± 0.7
	$r \rightarrow 4430$	$3/2 \rightarrow 1/2$	0.19 ± 0.03
			-3.2 ± 0.2
		$3/2 \rightarrow 3/2$	-0.38 ± 0.08
			-11.0 ± 1.0
$E_p = 1278$ keV	$r \rightarrow 0$	$5/2 \rightarrow 3/2$	-2.0 ± 0.2
$E_x = 10016$ keV	$r \rightarrow 440$	$5/2 \rightarrow 5/2$	-0.20 ± 0.02
	$r \rightarrow 2076$	$5/2 \rightarrow 7/2$	-0.30 ± 0.03
	$r \rightarrow 2983$	$5/2 \rightarrow 3/2$	-0.01 ± 0.01
	$r \rightarrow 3678$	$5/2 \rightarrow 3/2$	0.00 ± 0.01
	$r \rightarrow 3846$	$5/2 \rightarrow 5/2$	-0.06 ± 0.03
		$5/2 \rightarrow 7/2$	-0.50 ± 0.05
	$r \rightarrow 3913$	$5/2 \rightarrow 5/2$	0.05 ± 0.02
	$r \rightarrow 6617$	$5/2 \rightarrow 7/2$	-0.25 ± 0.05
			-3.0 ± 0.3

REF. E. Ventura
Phys. Rev. C7, 1900 (1973)

ELEM. SYM.	A	Z
Na	23	11

METHOD

REF. NO. 73 Ve 2 hmg

REACTION	RESULT	EXCITATION ENERGY	SOURCE		DETECTOR		ANGLE
			TYPE	RANGE	TYPE	RANGE	
P,G	ABX	14- 26	D	5- 18	NAI-D		90

G = G0 + G1
777

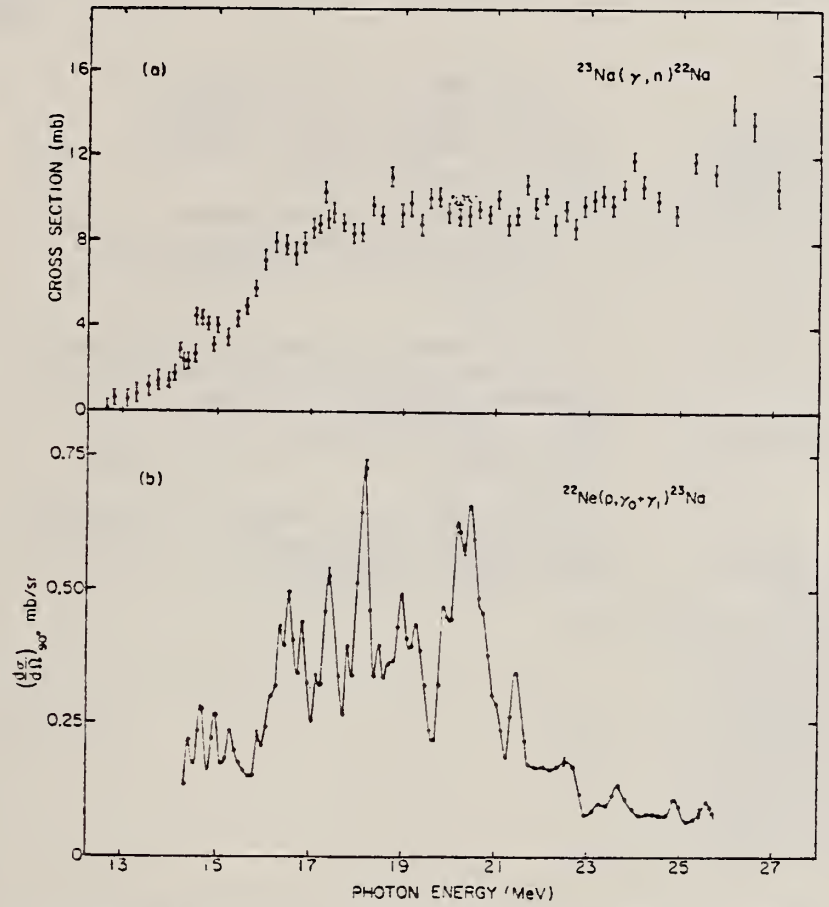

FIG. 2. (a) Photoneutron cross section for ^{23}Na as measured by Alvarez *et al.* (Ref. 8). (b) Differential cross section as a function of photon energy for $^{22}Ne(p,\gamma_0+\gamma_1)^{23}Na$ at $\theta_{lab}=90°$. The yield curve has been converted to a photodisintegration curve (in the conversion E_{γ_0} is used for the photon energy).

The differential cross section for the capture reaction $^{22}Ne(p,\gamma_0+\gamma_1)^{23}Na$ has been measured. Significant structure is observed in the giant-resonance region. Comparison with the reaction $^{23}Na(\gamma,n)^{22}Ne$ indicates a splitting of the dipole strength. Possible sources of this splitting are discussed.

REF.

V. DiNapoli and M.L. Terranova
J. Inorg. Nucl. Chem. 36, 3633 (1974)

Na	23	11

METHOD

REF. NO. 74 Di 7 egf

REACTION	RESULT	EXCITATION ENERGY	SOURCE TYPE	SOURCE RANGE	DETECTOR TYPE	DETECTOR RANGE	ANGLE
G,3P3N	ABY	THR* 1	C	300* 1	ACT-I		4PI

1=1 GEV

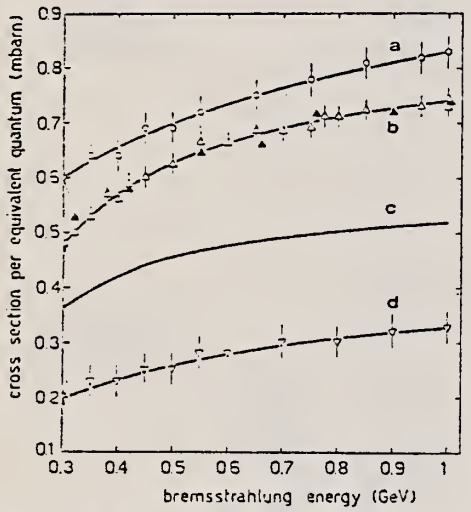

Fig. 1. Cross section per equivalent quantum σ_Q vs the bremsstrahlung maximum energy. Curve a is an eye-fit of the present work values (open circles) for the reaction $^{23}Na(\gamma, 2p\,3n)^{18}F$. Curve b is an eye-fit of the present work values (open triangles) and the values taken from Ref. [2] (filled triangles) for the reaction $^{27}Al(\gamma, 2p\,3n)^{22}Na$. Curve c is the best-fit of the present work values and values taken from Refs. [18, 20–22] for the reaction $^{12}C(\gamma, 2p\,3n)^{7}Be$; for the sake of simplicity, experimental points have not been reported. Curve d is an eye-fit of the present work values (reversed open triangles) for the reaction $^{16}O(\gamma, 2p\,3n)^{11}C$.

[2] V. di Napoli, A.M. Lacerenza, F. Salvetti, H.G. de Carvalho, and J.B. Martins, Nuovo Cimento Lettere 1, 835 (1971).

[18] V. di Napoli, D. Margadonna, F. Salvetti, H.G. de Carvalho, and J.B. Martins, Nucl.Inst.Meth. 93, 77 (1971).

[20] V. di Napoli, F. Dobici, O. Forina, F. Salvetti and H.G. de Carvalho, Lett. Nuovo Cimento 55B, 95 (1968).

[21] V. di Napoli, Nucl.Inst.Meth. 69, 155 (1969).

[22] V.I. Noga, Yu.N. Ranyuk, P.V. Sorokin, and V.A. Tkachenko, Ukr. J.Phys. 16, 1850 (1971) in Russian.

REF.

A. Veyssiere, H. Beil, R. Bergere, P. Carlos, A. Lepretre, and A. De Miniac
Nucl. Phys. A227, 513 (1974)

ELEM. SYM.	A	Z
Na	23	11

METHOD

REF. NO.	
74 Ve 1	egf

REACTION	RESULT	EXCITATION ENERGY	SOURCE		DETECTOR		ANGLE
			TYPE	RANGE	TYPE	RANGE	
* G,N	ABX	12- 30	D	12- 30	BF3-I		4PI
** G,2N	ABX	23- 30	D	23- 30	BF3-I		4PI

* 885+
** 884
883+

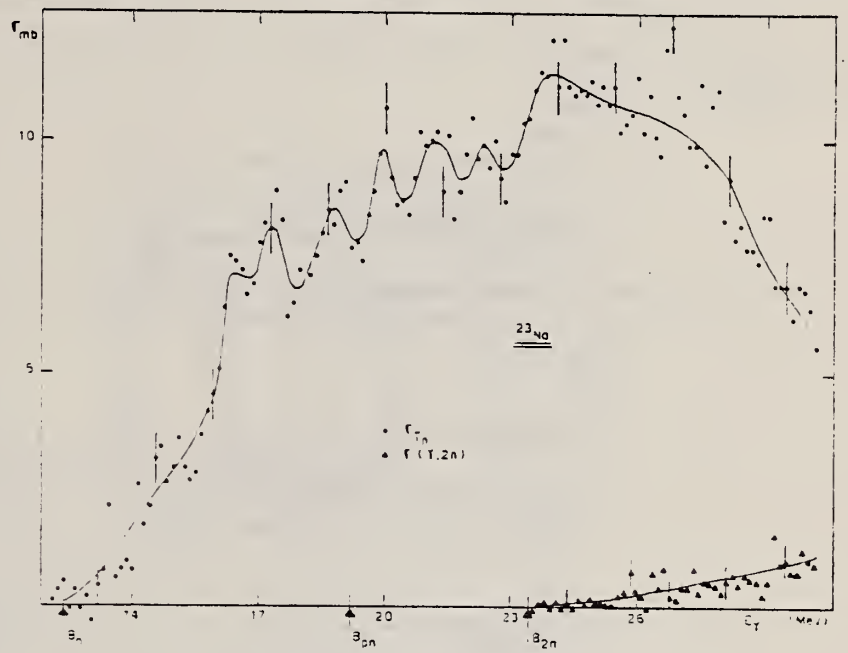

Fig. 5. Photoneutron cross sections $\sigma_{\gamma n}$ and $\sigma(\gamma, 2n)$ of ^{23}Na.

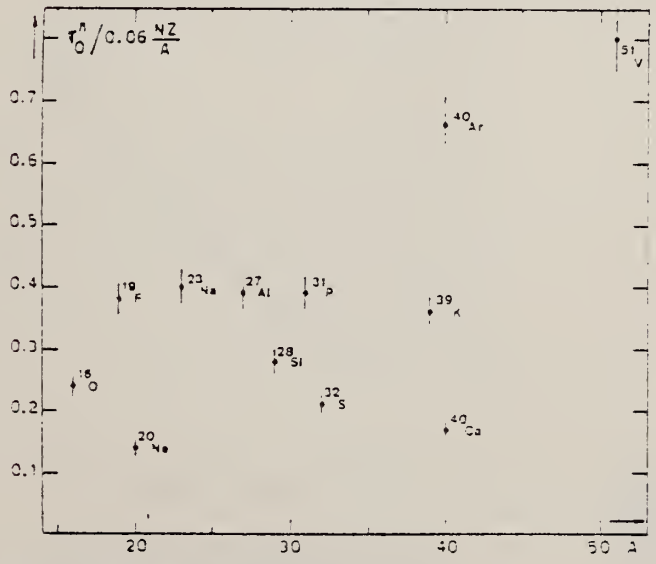

Fig. 22. Ratio of experimental integrated photoneutron cross section σ_0^n over the Thomas, Reiche and Kuhn sum rule [0.06 NZ/A]. Numerical values and upper integration limits E_M are taken from table 3. Also $\Delta\sigma_0^n = \pm 7\%$ for all nuclei.

(over)

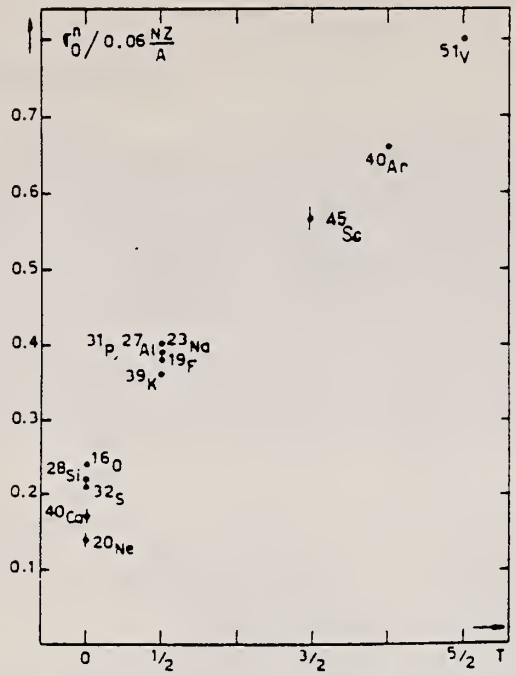

Fig. 24. The $[\sigma_0^n/(0.06\ NZ/A)]$ ratio as a function of isospin T. Possible overall errors of $\pm 7\%$ are to be applied to all nuclei shown.

TABLE 3

Experimental integrated photoneutron cross sections $\sigma_0^n = \int_0^{E_M} \sigma_{Tn}(E)dE$ compared with the classical sum rule $[0.06\ NZ/A]$ of Thomas, Reich and Kuhn

	$T=0$					$T=\frac{1}{2}$					$T=\frac{3}{2}$	$T=2$	$T=\frac{5}{2}$
Nucleus	^{16}O	^{20}Ne	^{28}Si	^{32}S	^{40}Ca	^{19}F	^{23}Na	^{27}Al	^{31}P	^{39}K	^{45}Sc	^{40}Ar	^{51}V
σ_0^n (MeV · mb)	58 ±4	42 ±3	94 ±7	98 ±7	100 ±7	108 ±7	137 ±9	158 ±10	182 ±12	210 ±14	383 ±25	393 ±28	602 ±42
$\sigma_0^n/(0.06NZ/A)$	0.24	0.14	0.22	0.21	0.17	0.38	0.40	0.39	0.39	0.36	0.57	0.66	0.8
E_{st} (MeV)	30	26.7	30	30	29.5	29	30	30	29	30	28.1	26.7	28

REF. V. di Napoli, G. Rosa, F. Salvetti, M. L. Terranova, H. G. de Carvalho, J. B. Martins, O. A. P. Tavares
J. Inorg. Nucl. Chem. 37, 1101 (75)

ELEM. SYM.	A	Z
Na	23	11

METHOD

REF. NO. 75 Di 4 egf

REACTION	RESULT	EXCITATION ENERGY	SOURCE		DETECTOR		ANGLE
			TYPE	RANGE	TYPE	RANGE	
G,F18	ABY	21-999	C	300-999	ACT-I		4PI
G,NA22	ABY	12-999	C	300-999	ACT-I		4PI

999 = 1 GEV

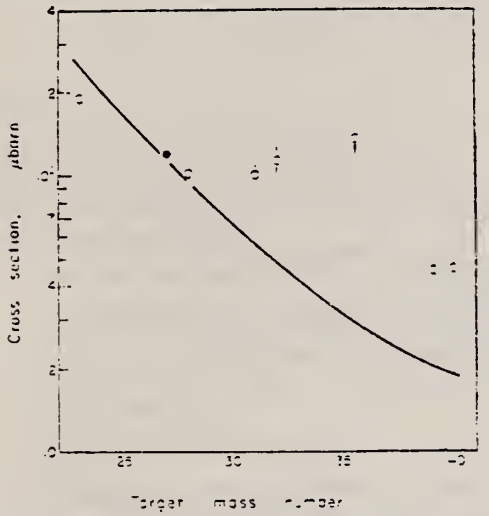

Fig. 2. Mean absolute cross section of ^{19}F photoproduction vs the target mass number. Open triangle: energy range 0·15–0·72 GeV, Ref. [18]. Filled circle: energy range 0·3–1 GeV, Ref. [3]. Open circles: present work. The curve has been calculated by means of Eqn (1).

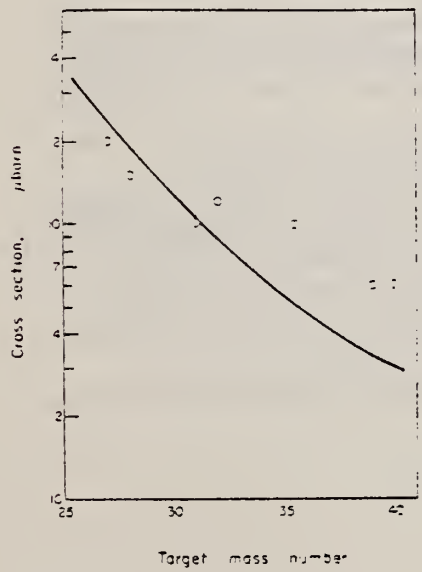

Fig. 3. Mean absolute cross section of ^{23}Na photoproduction vs the target mass number. The curve has been calculated by means of Eqn (1).

Table 2. Cross-section per equivalent quantum $\sigma_Q(\mu b)$ of photoproduction of ^{19}F

Target nucleus	Bremsstrahlung maximum energy E_0(GeV)				
	0·30	0·40	0·55	0·75	1·00
^{23}Na	590 ± 30	640 ± 30	720 ± 30	780 ± 30	830 ± 30
^{27}Al*	116 ± 7	172 ± 6	202 ± 6	245 ± 5	270 ± 5
^{28}Si	80 ± 10	110 ± 10	145 ± 10	170 ± 10	200 ± 10
^{31}P	60 ± 10	90 ± 10	130 ± 10	150 ± 10	180 ± 10
^{32}S	55 ± 10	90 ± 10	125 ± 10	160 ± 10	190 ± 10
^{35,37}Cl	185 ± 20	230 ± 20	270 ± 20	310 ± 20	350 ± 20
^{39}K	35 ± 5	50 ± 5	65 ± 5	75 ± 5	90 ± 5
^{40}Ca	5 ± 2	20 ± 3	35 ± 5	45 ± 5	60 ± 5

*The results for ^{27}Al have already been published (see[3]) and are reported for comparison.

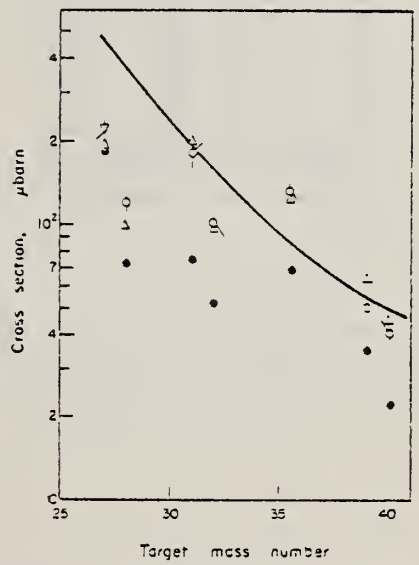

Fig. 4. Mean absolute cross section of ^{24}Na photoproduction vs the target mass number. Filled circles: energy range 0·1–1 GeV, Ref. [20]. Reversed open triangle: energy range 0·3–1 GeV, Ref. [8]. Open triangles: energy range 0·25–1 GeV, Ref. [19]. Open circles: present work. The curve has been calculated by means of Eqn (1).

(over)

Table 3. Cross-section per equivalent quantum $\sigma_Q(\mu b)$ of photoproduction of ^{22}Na

Target nucleus	Bremsstrahlung maximum energy E_0 (GeV)				
	0·30	0·40	0·55	0·75	1·00
^{27}Al	490 ± 20	560 ± 20	667 ± 20	690 ± 20	745 ± 20
^{28}Si	290 ± 20	330 ± 20	330 ± 20	430 ± 20	470 ± 20
^{31}P	230 ± 20	250 ± 20	290 ± 20	330 ± 20	350 ± 20
^{32}S	206 ± 10	240 ± 10	280 ± 10	320 ± 10	350 ± 10
$^{35,37}Cl$	230 ± 10	260 ± 10	290 ± 10	320 ± 10	350 ± 10
^{39}K	30 ± 3	50 ± 5	65 ± 5	80 ± 5	100 ± 5
^{40}Ca	5 ± 2	20 ± 3	45 ± 5	60 ± 5	60 ± 5

Table 4. Cross-section per equivalent quantum $\sigma_Q(\mu b)$ of photoproduction of ^{24}Na

Target nucleus	Bremsstrahlung maximum energy E_0 (GeV)				
	0·30	0·40	0·55	0·75	1·00
$^{27}Al^a$	370 ± 10	440 ± 10	500 ± 20	550 ± 20	660 ± 20
^{28}Si	100 ± 10	140 ± 10	160 ± 10	210 ± 10	240 ± 10
^{31}P	100 ± 20	160 ± 20	200 ± 20	270 ± 20	310 ± 20
^{32}S	120 ± 10	160 ± 10	150 ± 10	210 ± 10	240 ± 10
$^{35,37}Cl$	65 ± 10	100 ± 10	140 ± 10	190 ± 10	220 ± 10
^{39}K	20 ± 5	35 ± 5	55 ± 5	65 ± 5	80 ± 5
^{40}Ca	12 ± 3	25 ± 5	35 ± 5	50 ± 5	60 ± 5

[a]The results for ^{27}Al have already been published (see[3]) and are reported for comparison.

Table 5. Mean absolute cross-section $\bar{\sigma}_v(\mu b)$ in the energy range 0·3–1 GeV

Target nucleus	Produced radionuclide		
	^{18}F	^{22}Na	^{24}Na
^{23}Na	190 ± 30		
$^{27}Al^a$	120 ± 10	200 ± 20	220 ± 20
^{28}Si	100 ± 10	150 ± 20	120 ± 10
^{31}P	100 ± 10	100 ± 20	150 ± 20
^{32}S	110 ± 10	120 ± 10	100 ± 10
$^{35,37}Cl$	135 ± 20	100 ± 10	130 ± 10
^{39}K	45 ± 5	60 ± 5	50 ± 5
^{40}Ca	46 ± 5	60 ± 5	40 ± 5

[a]The results for the photoproduction of ^{18}F and ^{24}Na from ^{27}Al have already been published (Ref.[3] and [8], respectively).

2. V. di Napoli and M. L. Terranova, *J. inorg. nucl. Chem.* 36, 3633 (1974).
3. V. di Napoli, A. M. Lacerenza, F. Salvetti, S. M. Terenzi, H. G. de Carvalho and J. B. Martins, *J. inorg. nucl. Chem.* 35, 1419 (1973).
4. C. M. Lederer, J. M. Hollander and I. Perlman, *Table of Isotopes.* 6th Edn Wiley, New York (1967).
5. R. G. Korteling and A. A. Caretto, Jr., *J. inorg. nucl. Chem.* 29, 2863 (1967).
6. R. G. Korteling and A. A. Caretto, Jr., *Phys. Rev.* C1, 193 (1970).
7. R. G. Korteling and A. A. Caretto, Jr., *Phys. Rev.* C1, 1960 (1970).
8. V. di Napoli, A. M. Lacerenza, F. Salvetti, H. G. de Carvalho and J. B. Martins, *Lett. Nuovo Cimento* 1, 835 (1971).
9. I. Halpern, R. J. Debs, J. T. Eisinger, A. W. Fairhall and H. G. Richter, *Phys. Rev.* 97, 1327 (1955).
10. C. B. Fulmer, K. S. Toth, I. R. Williams, T. H. Handley, C. F. Dell, E. L. Callis, T. M. Jenkins and J. M. Wyckoff, *Phys. Rev.* C2, 1371 (1970).
11. G. J. Kumbartzki, U. Kim and C. K. Kwan, *Nucl Phys.* A160, 237 (1970).
12. G. J. Kumbartzki and U. Kim, *Nucl. Phys.* A176, 23 (1971).
13. K. Lindgren and G. G. Jonsson, *Nucl. Phys.* A197, 71 (1972).
14. C. E. Roos and V. Z. Peterson, *Phys. Rev.* 124, 1610 (1961).
15. T. A. Gabriel and R. G. Alsmiller, Jr., *Phys. Rev.* 182, 1035 (1969).
16. G. G. Jonsson and K. Lindgren, *Phys. Scr.* 7, 49 (1973).
17. G. Rudstam, *Z. Naturf.* 21a, 1027 (1966).
18. A. Masaike, *J. phys. Soc. Japan* 19, 427 (1964).
19. A. Jārund, B. Friberg and B. Forkman, Private communication to G. G. Jonsson and K. Lindgren, quoted in Ref.[16]; see also A. Jārund, B. Friberg and B. Forkman, University of Lund Report No. LUNP-7303, 1973 (unpublished).
20. V. I. Noga, Yu. N. Ranyuk and P. V. Sorokin, *Yad. Fiz.* 9, 1152 (1969) (transl.: *Sov. J. Nucl. Phys.* 9, 673 (1969)).
21. T. Methasiri and S. A. E. Johansson, *Nucl. Phys.* A167, 97 (1971).
22. J. R. Nix and E. Sassi, *Nucl. Phys.* 81, 61 (1966).
23. W. D. Myers and W. J. Swiatecki, *Nucl. Phys.* 81, 1 (1966).

REF. K. Masumoto, T. Kato, N. Suzuki
Nucl. Inst. Meth. 157, 567 (1978)

ELEM. SYM.	A	Z
Na	23	11

METHOD

REF. NO. 78 Ma 10 hg

REACTION	RESULT	EXCITATION ENERGY	SOURCE		DETECTOR		ANGLE
			TYPE	RANGE	TYPE	RANGE	
G,N	ABY	12-68	C	30-68	ACT-I		4PI

Analysis is made of reactions interfering with photon activation analysis procedures.

The activation yield curves have been presented for a number of photonuclear reactions in the energy range from 30 to 68 MeV, in order to evaluate quantitatively the interferences due to competing reactions in multielement photon activation analysis. The general features of the yields as functions of both target mass number and excitation energy were elucidated from the data obtained, discussion being given on the results in terms of the reaction mechanism.

Simultaneous neutron activation due to appreciable neutron production from the converter and surrounding materials has also been studied, and, finally, the magnitudes of interferences in real multielement analysis were given in the form of their energy dependences.

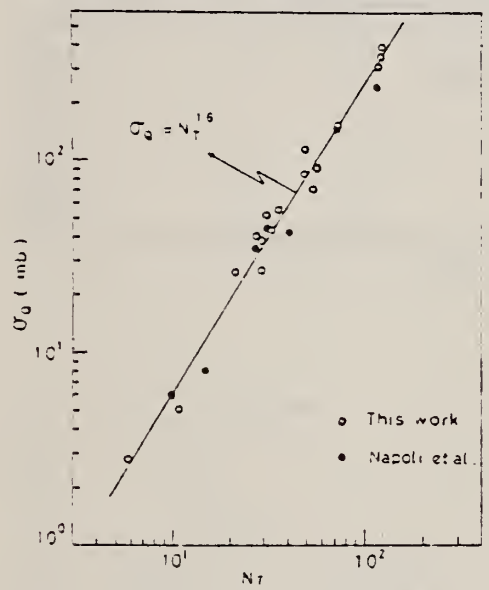

Fig. 2. Yield per equivalent quanta versus target neutron number.

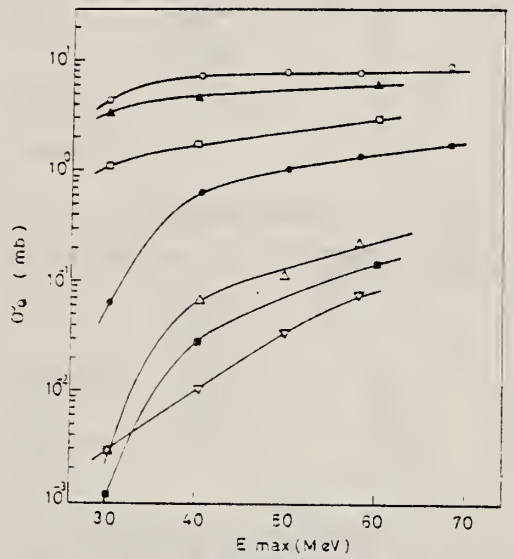

Fig. 3. Activation yield curves for the reactions on C, Na, Mg and Al.
□ $^{12}C(\gamma, n)^{11}C$, ■ $^{12}C(\gamma, xn)^{7}Be$, ▲ $^{23}Na(\gamma, n)^{22}Na$,
○ $^{25}Mg(\gamma, p)^{24}Na$, ● $^{24}Mg(\gamma, pn)^{22}Na$, △ $^{27}Al(\gamma, xn)^{22}Na$,
▽ $^{27}Al \rightarrow ^{24}Na$.

(over)

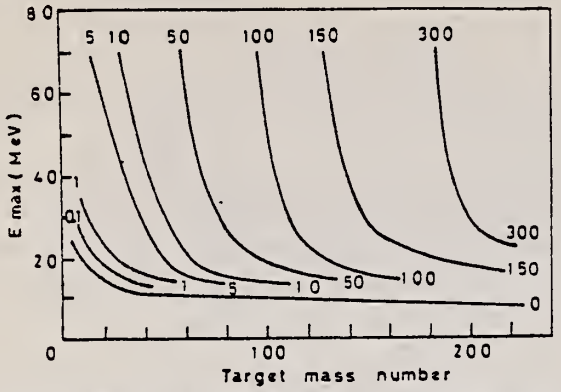

Fig. 9. Yields of the (γ, n) reactions as a function of bremsstrahlung maximum energy and target mass number. The numerical values in the figure are yields per equivalent quanta in mb.

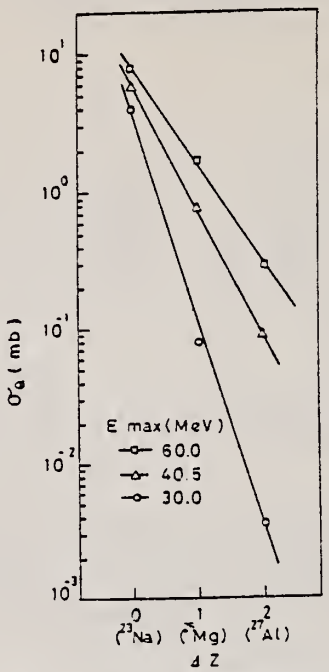

Fig. 12. The reaction yields leading to ^{22}Na as a function of difference in atomic number between target and product nuclides

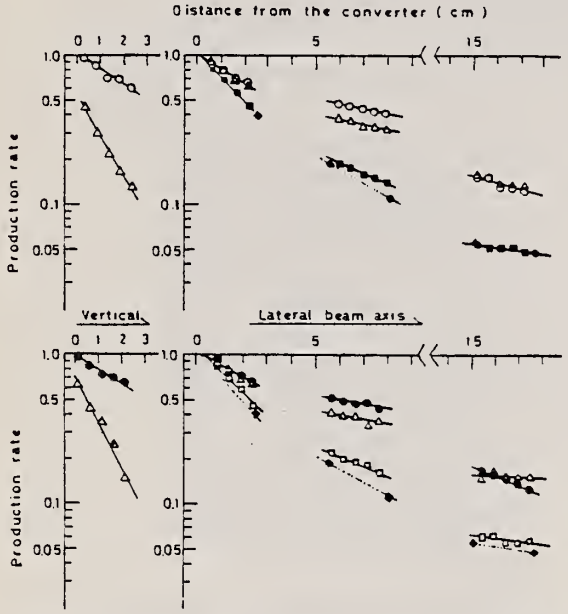

Fig. 13. Production rates of the neutron reactions and the photonuclear reactions as a function of distance from the converter in vertical and lateral directions.
○ ^{55}Mn(n, γ)^{56}Mn, ● ^{23}Na(n, γ)^{24}Na, △ ^{27}Al(n, x)^{24}Na,
■ ^{55}Mn(γ, n)^{54}Mn, □ ^{23}Na(γ, n)^{22}Na, ◆ ^{65}Cu(γ, n)^{64}Cu.

REF. B.S. Ishkhanov, V.I. Mokeev, Yu.A. Novikov, E.S. Omarov, I.M. Piskarev, A.M. Parlag, A.I. Gutii
Sov. J. Nucl. Phys. 32, 455 (1980)
Yad. Fiz. 32, 885 (1980)

ELEM. SYM.	A	Z
Na	23	11

METHOD

REF. NO. 80 Is 2 hg

REACTION	RESULT	EXCITATION ENERGY	SOURCE		DETECTOR		ANGLE
			TYPE	RANGE	TYPE	RANGE	
G,PG/	ABI	8-32	C	13-32	SCD-D		135
G,NG/	ABI	12-32	C	13-32	SCD-D		135

Energy spectra of photons from the reaction $^{23}Na(\gamma,X\gamma')$ have been measured. Integrated cross sections have been determined for population of the individual levels of the nuclei ^{22}Na and ^{22}Ne. The energy dependence of the cross section for excitation of the 1.27-MeV level of the ^{22}Ne nucleus in the $(\gamma,p\gamma')$ reaction is obtained. The results are compared with spectroscopic data existing in the literature.

(G,PG/) ABI FOR 5 LEVELS

(G,NG/) ABI FOR 3 LEVELS

PACS numbers: 25.20. + y, 27.30. + t

TABLE I. Levels populated in the reaction $^{23}Na(\gamma,X\gamma')$ at E_{max} = 32 MeV.

E_γ, MeV (Ref. 2)	Final nucleus	J^π, T [*]	Integrated cross section, MeV · mb (present work)	Spectroscopic factors C^2S	
				[*]	[*]
1.27±0.01	^{22}Ne	2+	15±4	1.2	
3.36±0.03		4+	5±2	0.41	
4.48		2+	≤2	0.15–0.3	
5.15		2−	≤20 *	1.7	
5.23; 5.36; 5.52; 5.64; 5.92			≤1	–	
1.95±0.02	^{22}Na	2+, 1	8±2		1.2
5.60±0.04		(1, 2)+	2±1		0.06
5.73±0.04		–	2±1		–

*Obtained on the assumption that the level width is 200 keV.

TABLE II. Values of errors in determination of the integrated cross section for population of levels

Photon energy, MeV	Error, MeV · mb
0.55	10
1.0	5
1.5	3
2–4	2
5–6	1

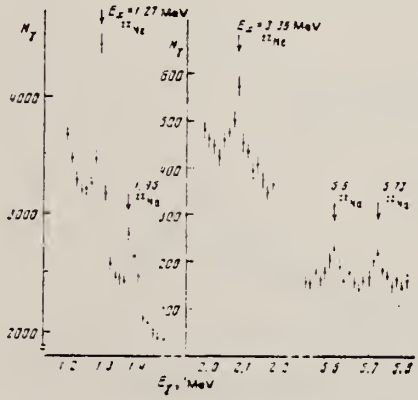

FIG. 1. Portions of the energy spectrum of γ rays from the reaction $^{23}Na(\gamma,X\gamma')$ for a bremsstrahlung maximum energy 32 MeV. The numbers by the arrows are values of E_γ.

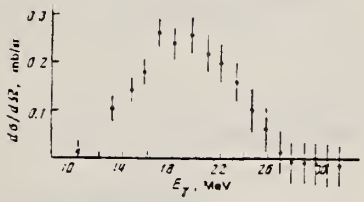

FIG. 2. Differential cross section for the reaction $^{23}Na(\gamma,p\gamma')$, leading to population of the 1.27-MeV level of the ^{22}Ne nucleus.

REF. M. Yagi, R. Amano
Int. J. Applied Radiat. Isotopes 31, 559 (1980)

ELEM. SYM.	A	Z
Na	23	11

METHOD

REF. NO. 80 Ya 2 hg

REACTION	RESULT	EXCITATION ENERGY	SOURCE		DETECTOR		ANGLE
			TYPE	RANGE	TYPE	RANGE	
G,F18	YLD	THR-60	C	30-60	ACT-I		4PI

The production rates of ^{18}F by the $^{20}Ne(\gamma, pn)^{18}F$ plus $^{20}Ne(\gamma, 2n)^{18}Ne \rightarrow {}^{18}F$, $^{23}Na(\gamma, \alpha n)^{18}F$, and $^{19}F(\gamma, n)^{18}F$ reactions were determined as a function of the maximum bremsstrahlung energies between 30 and 60 MeV. In addition, a simple and fast method to prepare anhydrous $H^{18}F$ was studied by using KHF_2 target.

TABLE I. Photonuclear reactions for ^{18}F production

Target nuclide (abundance, %)	Reaction type	Threshold energy (MeV)	Product nuclide
^{20}Ne (90.51)	$(\gamma, 2n)$	28.50	$^{18}Ne \rightarrow {}^{18}F$
^{21}Ne (0.27)	$(\gamma, 3n)$	35.27	$^{18}Ne \rightarrow {}^{18}F$
^{22}Ne (9.22)	$(\gamma, 4n)$	45.63	$^{18}Ne \rightarrow {}^{18}F$
^{20}Ne (90.51)	(γ, pn)	23.26	^{18}F
^{21}Ne (0.27)	$(\gamma, p2n)$	29.93	^{18}F
^{22}Ne (9.22)	$(\gamma, p3n)$	40.38	^{18}F
^{23}Na (100)	$(\gamma, \alpha n)$	20.89	^{18}F
^{19}F (100)	(γ, n)	10.43	^{18}F

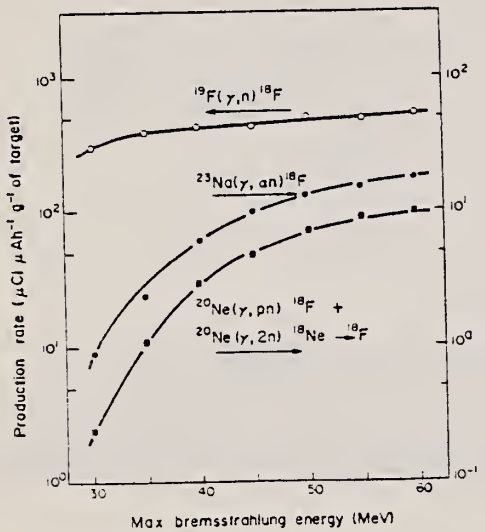

FIG. 1. Production rates of ^{18}F on Ne, Na and F targets as a function of the maximum bremsstrahlung energy.

REF. B.S. Ishkhanov, I.M. Kapitonov, V.I. Shvedunov, A.I. Gutii, A.M. Parlag
Sov. J. Nucl. Phys. 33, 303 (1981)
Yad. Fiz. 33, 581 (1981)

ELEM. SYM.	A	Z
Na	23	11

METHOD

REF. NO. 81 Is 3 hg

REACTION	RESULT	EXCITATION ENERGY	SOURCE		DETECTOR		ANGLE
			TYPE	RANGE	TYPE	RANGE	
G,P	ABX	8-30	C	16-30	TEL-D		90

Total $\sigma(\gamma,p)$ obtained by summing the various photoproton cross sections and multiplying by 4π.

$$\int_{Th}^{29.5} \sigma(\gamma,p)dE = 190 \pm 20 \text{ MEV}\cdot\text{mb}$$

The photoproton spectra from ^{23}Na have been measured in a bremsstrahlung beam. The bremsstrahlung maximum energy was varied over the range 16–30 MeV in 1-MeV steps. The photoproton spectra were analyzed to obtain cross sections for the reaction ^{23}Na$(\gamma,p)^{22}$Ne with formation of the final nucleus in various states. The experimental results are interpreted on the basis of spectroscopic information on the low-lying levels of ^{22}Ne obtained in the reaction ^{23}Na$(d,^3$He$)^{22}$Ne. An estimate is given of the contribution of $1p$–$1h$ configurations to formation of the proton channel of decay of the giant dipole resonance of ^{23}Na. The centers of gravity of the electric dipole transitions from various shells are determined.

PACS numbers: 25.20. + y, 27.30. + t, 23.20.Lv

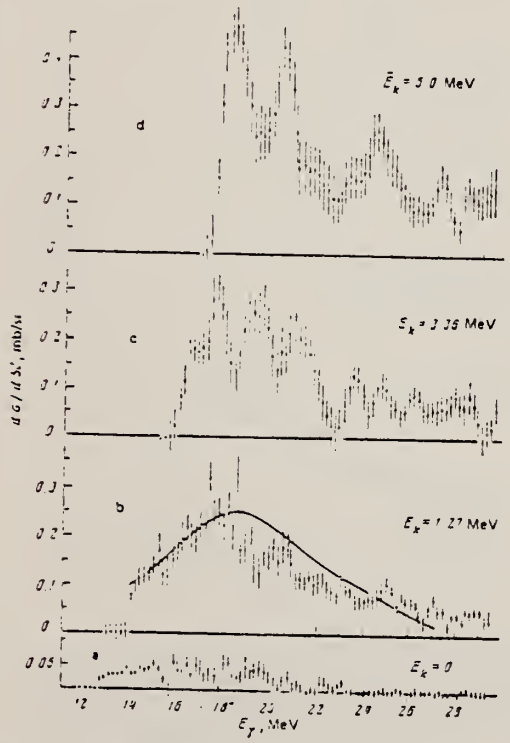

FIG. 4. Cross section for the reaction ^{23}Na$(\gamma,p)^{22}$Ne with formation of the final nucleus in the ground state (a), first excited state (b), second excited state (c), and also in the group of states at energy 5.0 MeV (d). The solid line in Fig. 4b shows the cross section obtained in Ref. 11.

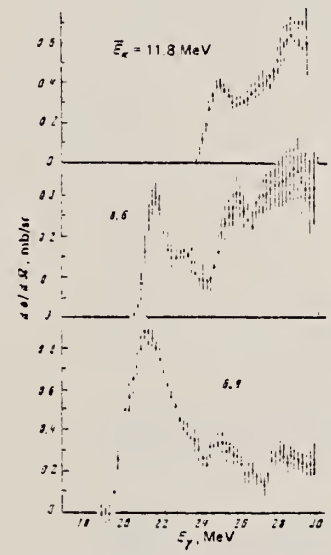

FIG. 5. Cross sections for the reaction ^{23}Na$(\gamma,p)^{22}$Ne with formation of the final nucleus in groups of states at energies 6.9, 8.9 and 11.8 MeV.

(OVER)

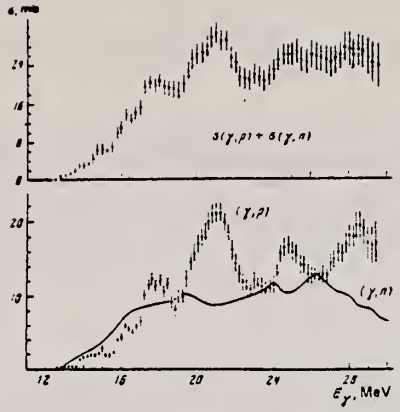

FIG. 6. Total cross section for the reaction $^{23}Na(\gamma,p)^{22}Ne$ (lower figure) and cross section for absorption of photons by ^{23}Na (upper figure) obtained by summation of the photoproton and photoneutron cross sections.[7,8] The latter is shown by the solid line in the lower figure.

REF. B.S. Ishkhanov, I.M. Kapitonov, V.I. Shvedunov, A.I. Gutiĭ, A.M. Parlag
Yad. Fiz. 33, 581 (1981)
Sov. J. Nucl. Phys. 33, 303 (1981)

ELEM. SYM.	A	Z
Na	23	11

METHOD

REF. NO. 81 Is 8 egf

REACTION	RESULT	EXCITATION ENERGY	SOURCE		DETECTOR		ANGLE
			TYPE	RANGE	TYPE	RANGE	
G,PØ	ABX	12-29	C	16-30	TEL-D		90
G,P1	ABX	14-29	C	16-30	TEL-D		90
G,P2	ABX	16-29	C	16-30	TEL-D		90
G,PN	ABX	19-29	C	16-30	TEL-D		90

The photoproton spectra from ^{23}Na have been measured in a bremsstrahlung beam. The bremsstrahlung maximum energy was varied over the range 16–30 MeV in 1-MeV steps. The photoproton spectra were analyzed to obtain cross sections for the reaction ^{23}Na$(\gamma, p)^{22}$Ne with formation of the final nucleus in various states. The experimental results are interpreted on the basis of spectroscopic information on the low-lying levels of ^{22}Ne obtained in the reaction ^{23}Na$(d, ^3$He$)^{22}$Ne. An estimate is given of the contribution of $1p$–$1h$ configurations to formation of the proton channel of decay of the giant dipole resonance of ^{23}Na. The centers of gravity of the electric dipole transitions from various shells are determined.

PACS numbers: 25.20. + y, 27.30. + t, 23.20.Lv

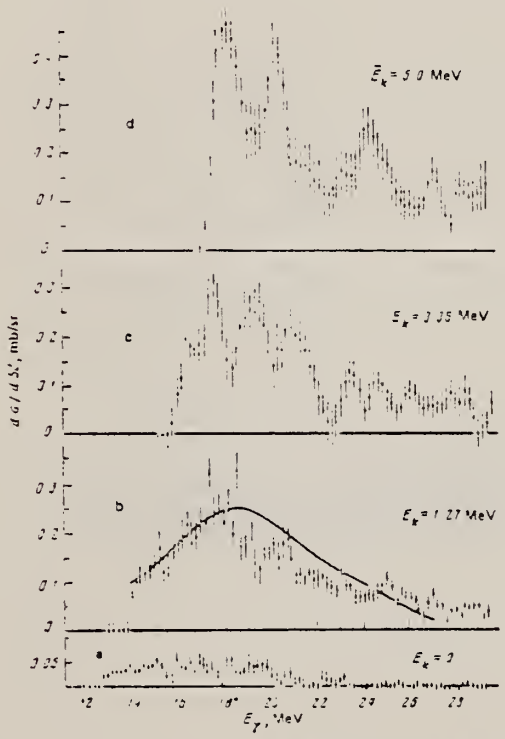

FIG. 4. Cross section for the reaction ^{23}Na$(\gamma, p)^{22}$Ne with formation of the final nucleus in the ground state (a), first excited state (b), second excited state (c), and also in the group of states at energy 5.0 MeV (d). The solid line in Fig. 4b shows the cross section obtained in Ref. 11.

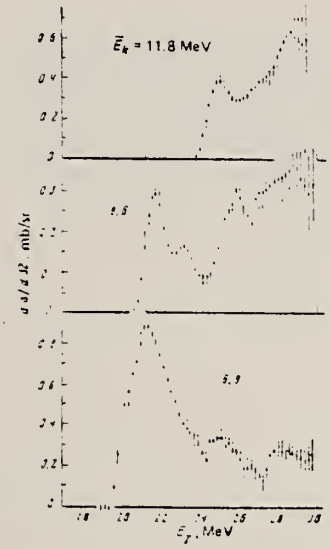

FIG. 5. Cross sections for the reaction ^{23}Na$(\gamma, p)^{22}$Ne with formation of the final nucleus in groups of states at energies 6.9, 8.9 and 11.8 MeV.

TABLE I. Energy resolution of partial cross sections and probability of formation of the ^{22}Ne nucleus in various states.

Number of partial cross section k	Energy ε_k of a final state of the ^{22}Ne nucleus or center of gravity $\bar{E}_k$ of the group of states, MeV		Energy resolution, MeV	Probability
	ε	$\bar{E}_k$		
1	0		0.4	0.02
2	1.27		0.3	0.12
3	3.36		1.0	0.11
4	4.46 5.14	5.0	1.2	0.15
5		6.9	1.5	0.27
6		8.9	1.5	0.17
7		11.8	2.0	0.16

(OVER)

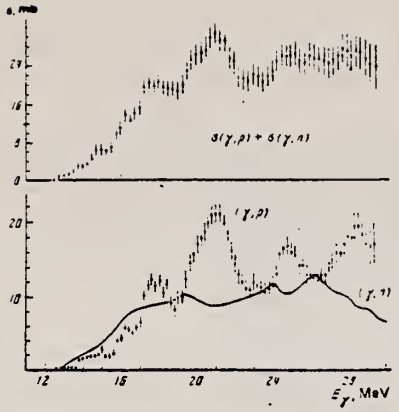

FIG. 6. Total cross section for the reaction $^{23}Na(\gamma,p)^{22}Ne$ (lower figure) and cross section for absorption of photons by ^{23}Na (upper figure) obtained by summation of the photoproton and photoneutron cross sections.[7,8] The latter is shown by the solid line in the lower figure.

REF. B.S. Ishkhanov, Yu.A. Novikov, E.S. Omarov, I.M. Piskarev, V.M. Sorvin, A.I. Gutii, A.M. Parlag
Yad. Fiz. 35, 3 (1982)
Sov. J. Nucl. Phys. 35, 1 (1982)

ELEM. SYM.	A	Z
Na	23	11

METHOD

REF. NO.: 82 Is 2 | egf

REACTION	RESULT	EXCITATION ENERGY	SOURCE TYPE	SOURCE RANGE	DETECTOR TYPE	DETECTOR RANGE	ANGLE
G,G	ABX	7-31	C	7-31	NAI-D		90

The cross section for elastic scattering of photons by the ^{23}Na nucleus has been measured in the energy ranges 7–14 and 16–31 MeV. At energies 16–31 MeV the cross sections for the nuclear Raman effect and for inelastic scattering of photons with population of the 2.08-MeV level are obtained. The results are discussed in the framework of the shell model. The contributions of various shell configurations to the formation of the giant resonance in ^{23}Na are evaluated.

PACS numbers: 25.20. + y, 27.30. + t

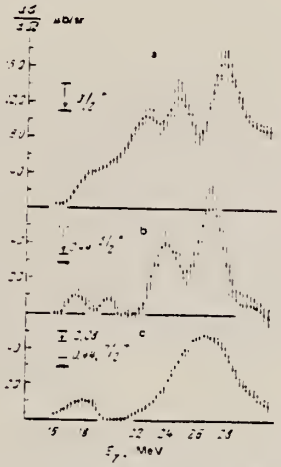

FIG. 2. Differential cross sections for photon-scattering channels in the region of the giant resonance: a—elastic scattering, b—nuclear Raman effect, c—inelastic scattering with excitation of the 2.08-MeV level.

TABLE II. Position of maxima in the cross sections for the various photon-scattering channels.

Elastic scattering, $J^\pi = 3/2^+$	NRE, 0.44 MeV, $J^\pi = 5/2^+$	Inelastic scattering with excitation of the 2.08-MeV level, $J^\pi = 7/2^-$	Elastic scattering, $J^\pi = 3/2^+$	NRE, 0.44 MeV, $J^\pi = 5/2^+$	Inelastic scattering with excitation of the 2.08-MeV level, $J^\pi = 7/2^-$
18.0±0.5	17.7±0.5	18.0±0.5	24.6±0.5	–	–
–	19.8±0.3	–	–	–	26.5±0.5
22.5±0.5	–	–	–	27.1±0.5	–
–	23.7±0.5	–	28.0±0.5	–	–

MAGNESIUM
Z=12

Because the metal is so reactive, man's first knowledge of magnesium came from its compounds. In 1618, Henry Wicker (or Wickes) noticed a small hole filled with water on the common at Epsom, Survey. Even though there was a draught, not one of his thirsty cattle would drink the water. The water, althougnt bitter, was found to be useful as an internal medicine and as a bath to heal external wounds. Within 30 years, Epsom became a famous spa and attracted visitors from all over the continent. The English botanist Nehemian Grew (1641-1712) in 1695 isolated the salts (magnesium sulphate) from this well and recognized it as a unique substance.

Mg

Sir Humphry Davy in 1808 produced a small amount of the metal by electrolyzing magnesium sulphate using metallic mercury as the cathode. This process yielded magnesium, not in a pure form, but as an amalgam. It was two years later in 1828 that the metal was first actually isolated. A. Bussy (1794-1882) obtained it by fusing magnesium chloride with metallic potassium. He called it magnium because as he said, the word magnesium is easily confused with manganese. Nevertheless, the word magnesium persisted.

Mg

REF.

D. Reagan
Phys. Rev. 100, 113-120 (1955)

ELEM. SYM.	A	Z
Mg		12

METHOD

Linac; counted delayed neutrons from N^{17}

REF. NO.	
55 Re 1	NVB

REACTION	RESULT	EXCITATION ENERGY	SOURCE		DETECTOR		ANGLE
			TYPE	RANGE	TYPE	RANGE	
G,N17	ABI	THR - 400	C	80-400	ACT-I		4PI

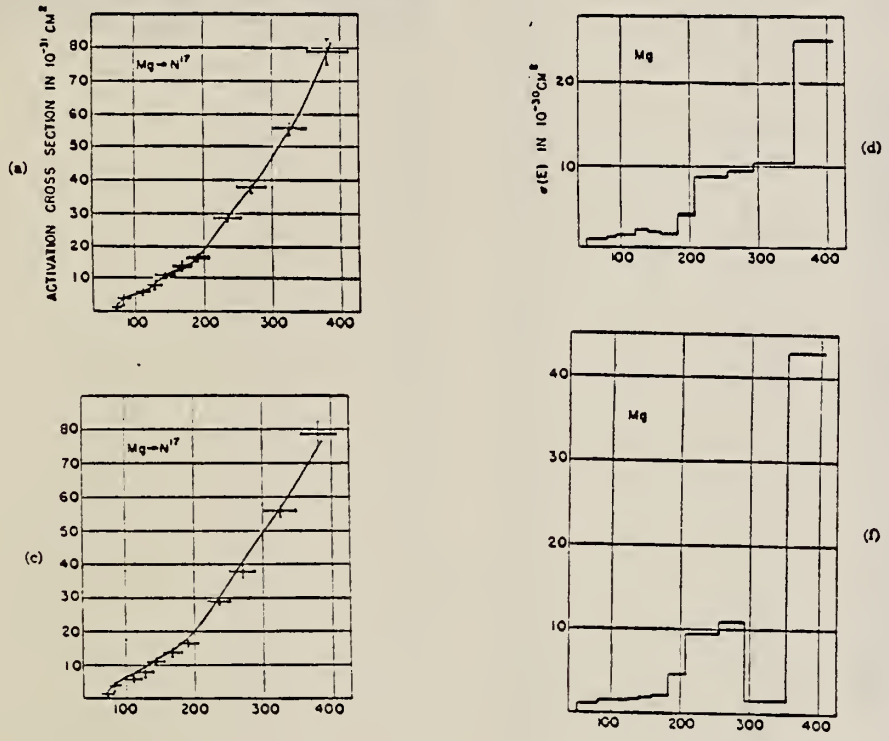

FIG. 5. Graphs a, b, and c show activation points for N^{17} yields in magnesium and aluminum. Graphs d, e, and f are the calculated photon cross sections, from which the solid lines in a, b, and c have been reconstructed. The third cross-section curve is actually the slightly modified result of an early aluminum run, and is included to illustrate the effects of moderate errors in data upon the photon cross section results.

Ref. E.G. Fuller, E. Hayward Phys. Rev. 101, 692 (1956)	Elem. Sym.	A	Z
	Mg		12
Method Betatron; photon scattering; NaI spectrometer	Ref. No.		
	56 Fu 1		EH

Reaction	E or ΔE	E_o	Γ	$\int \sigma dE$	Jπ	Notes
Mg (γ,γ)	Bremss. 4-40					Detector at 120°. Cross sections given here are 13% too high due to erroneous cos β factor in denominator of Eq. (5). [See footnote 8 in Phys. Rev. 106, 993 (1957)].

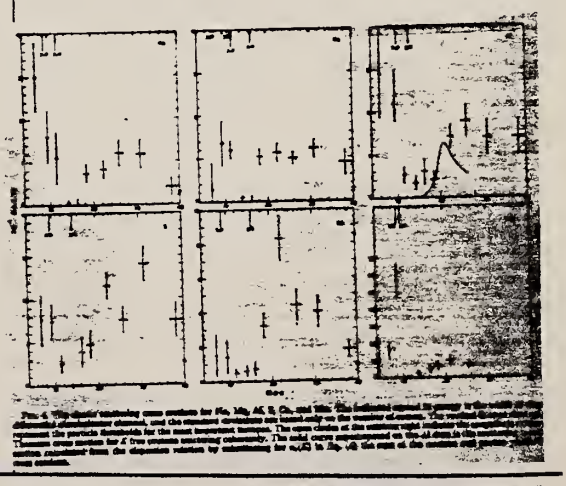

Ref. P.F. Yergin
Phys. Rev. 104, 1340 (1956)

Elem. Sym.	A	Z
Mg		12

Method Neutron detector; Bremsstrahlung.

Ref. No. 56 Ye 1 | EGF

Reaction	E or ΔE	E_o	Γ	$\int \sigma dE$	Jπ	Notes
(γ,xn)	7-23					$Mg^{24}(\gamma,n)_{th}$ = 16.57 MeV $Mg^{25}(\gamma,n)_{th}$ = 7.33 MeV $Mg^{26}(\gamma,n)_{th}$ = 11.12 MeV Figure 1: Yield of neutrons versus gamma-ray energy for natural magnesiu samples. Points shown with estimated error ellipses are for the present work. Crosses are from reference 2 [Katz et al, Canad. J. Phys. 32, 580 (1954)], scaled by a factor 0.74 to give agreement with the present work at 20 MeV. Triangles are the Mg^{25} yield data for reference 5 [Phys. Rev 98, 1296 (1954)], adjusted for the isotopic abundance of Mg^{25} in natural Mg. The (γ,n) thresholds for the 3 Mg isotopes are indicated along the abscissa. Over the energy range from threshold to about 16 MeV the yield values are plotted to a scale expanded 5 times over the scale given. Fro about 12.5 MeV to the upper energy limit of the data, the points are plotted to the scale shown. (The points from 12.5 to 16 MeV are plotte to both scales).

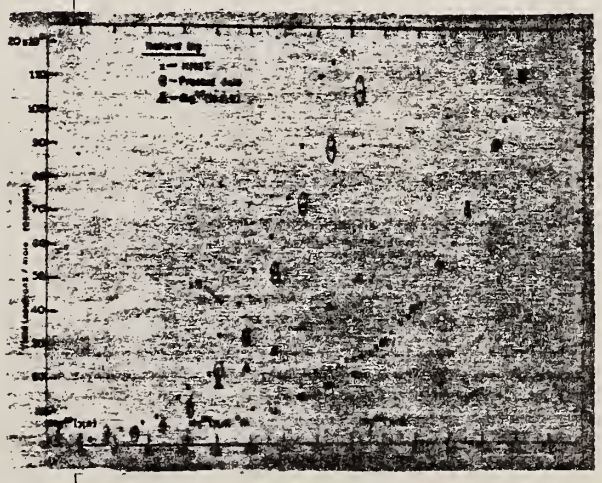

Ref. B.M. Spicer, F.R. Allum, J.E. Baglin, H.H. Thies
Australian J. Phys. 11, 273 (1958)

Elem. Sym.	A	Z
Mg		12

Method: 18 MeV electron synchrotron; BF_3 counters; 0.25 r Victoreen thimble ionization chamber; 8cm Lucite monitor.

Ref. No.: 58 Sp 2 EH

Reaction	E or ΔE	E_o	Γ	$\int \sigma dE$	Jπ	Notes
Mg (γ,n)	8-17	13.5				328 σ_{max} = 2.5 mb At E = 17 MeV, absolute yield of neutrons calculated to be 4×10^4 n $m^{-1} r^{-1}$.

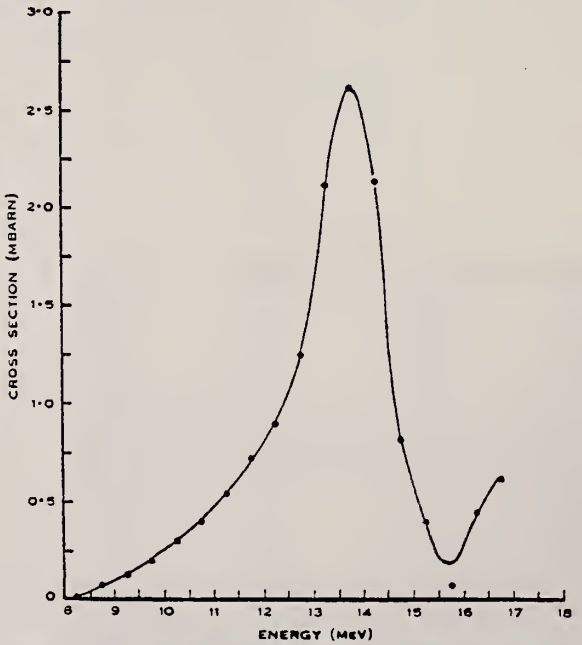

Fig. 2.—Cross section for photoneutron production from natural magnesium.

REF.

M. Langevin and A. Bussiere de Nercy
J. Phys. Radium 20, 831 (1959) (See 61 Bu 4)

ELEM. SYM.	A	Z
Mg		12

METHOD

REF. NO.	
59 La 1	EGF

REACTION	RESULT	EXCITATION ENERGY	SOURCE		DETECTOR		ANGLE
			TYPE	RANGE	TYPE	RANGE	
G,G	LFT	10	C	13	NAI-D	0 - 12	135
		(10.3±0.5)					

$\int \sigma_s dE = 2.24 \pm 0.44$ MeV-mb

$\Gamma_\gamma = 22 \pm 4$ eV

REF.

T.G. Walker, W.T. Morton
Proc. Phys. Soc. 75, 4 (1960)

ELEM. SYM.		
Mg		12

METHOD

Synchrotron; proton-neutron cross section; radioactivity

REF. NO.	
60 Wa 2	NVB

REACTION	RESULT	EXCITATION ENERGY	SOURCE		DETECTOR		ANGLE
			TYPE	RANGE	TYPE	RANGE	
G,2N3P	ABX	THR-240	C	240	ACT-I		4PI

$\sigma = (0.20 \pm 0.02)\ 10^{-27} cm^2$/equivalent quantum

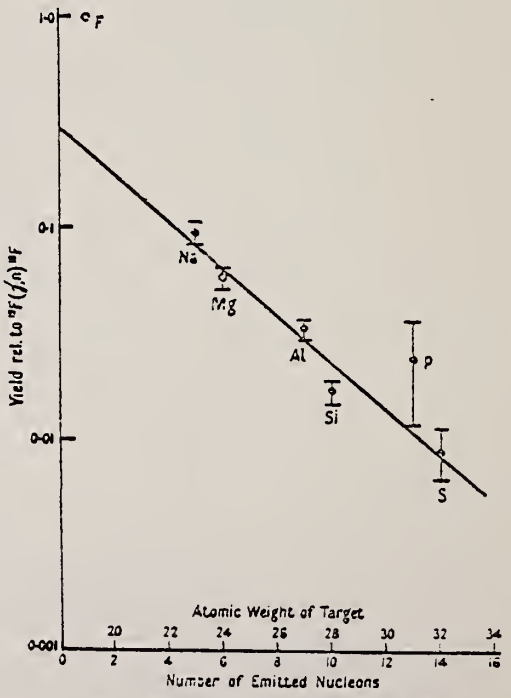

Yields relative to $^{19}F(\gamma, n)^{18}F$ at 240 Mev.

REF.

A. Bussiere de Nercy
Ann. Phys. (Paris) Third Series 6, 1379 (1961)

ELEM. SYM.	A	Z
Mg		12

METHOD

REF. NO.	
61 Bu 4	egf

REACTION	RESULT	EXCITATION ENERGY	SOURCE		DETECTOR		ANGLE
			TYPE	RANGE	TYPE	RANGE	
G,G	ABX	15-30	C	27,32	NAI-D		140

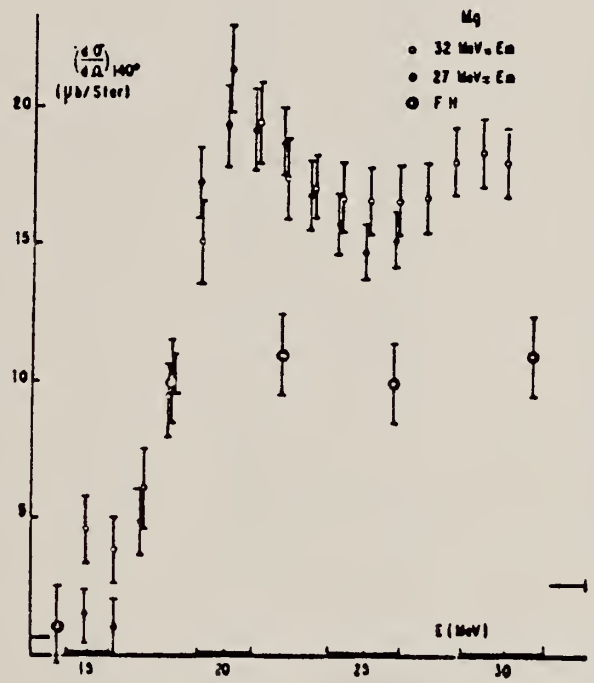

Fig 19. — Section efficace différentielle de diffusion (γ, γ) à 140° pour le magnésium.

Ref. M. Sugawara
J. Phys. Soc. Japan 16, 1857 (1961)

Elem. Sym.	A	Z
Mg		12

Method: 25 MeV betatron; photon scattering; NaI(Tℓ) spectrometer; ion chamber

Ref. No.: 61 Su 1 ,S — NVB

Reaction	E or ΔE	E_o	Γ	∫σdE	Jπ	Notes
Mg(γ,γ)	Bremss. 7-14	10.2	$3.8^{+1.2}_{-0.6}$ eV		1^+	
		9.3	0.9eV		1^+	Detector at 120°.

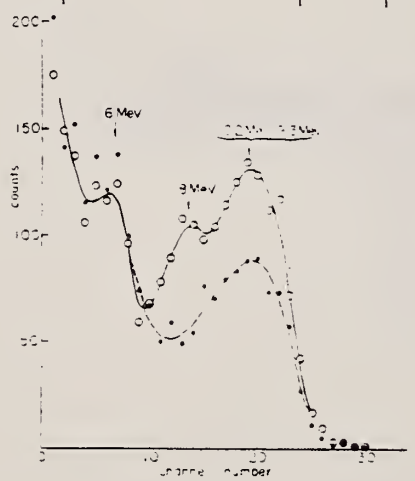

Fig. 3. The spectra of the scattered photons from the Mg scatterer. The solid line is the spectra measured without the Mg absorber and the broken line with the absorber. They are all normalized to the unit charge of the ionization chamber.

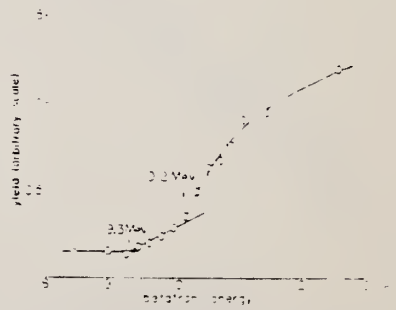

Fig. 4. The yield curve for Mg. The count at each bombarding energy of the incident bremsstrahlung was normalized to the unit charge from the monitor. The vertical lines show the statistical errors.

Ref. F.D. Seward
Phys. Rev. 125, 335 (1962)

Elem. Sym.	A	Z
Mg		12

Method: Linac; NaI; detector at 90°.

Ref. No.: 62 Se 1 | JHH

Reaction	E or ΔE	E_o	Γ	$\int \sigma dE$	Jπ	Notes
Mg (γ,γ)	Bremss; 16	10.6				Other, unresolved lines in region ~ 9.2 MeV indicated. Spectrum in contradiction with conclusion of Langevin and de Nercy [J. Phys. Rad. 20, 831 (1959)]; that peak results from two γ-rays: one to ground state; the other to first excited state.

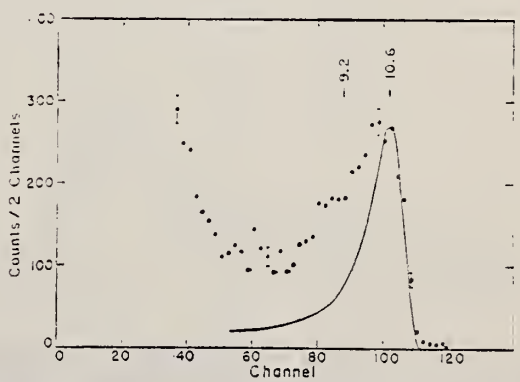

FIG. 7. Pulse-height spectrum for γ rays scattered from a Mg sample. Sample-out background has been subtracted. The solid line is a KS response function for a 10 6-Mev γ ray.

Ref. K. Shoda, K. Abe, T. Ishizuka, N. Kawamura, M. Kimura
J. Phys. Soc. Japan 17, 735 (1962)

Elem. Sym.	A	Z
Mg		12

Method: 25 MeV betatron; proton yield; scintillator; ion chamber.

Ref. No.: 62 Sh 11 NVB

Reaction	E or ΔE	E_o	Γ	$\int \sigma dE$	Jπ	Notes
Mg(γ,p) Thr-24	Bremss.	20	6 MeV	$\int_0^{23}$ = 0.070 MeV-b		σ_{max} = 16 mb. 6 Detectors at angles: 20° 55° 90° (2) 125° 160° Measured all protons above E_o = 1.5MeV

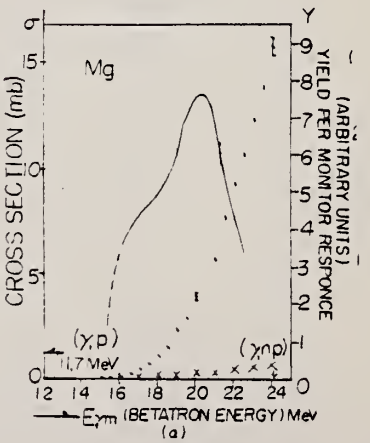

FORM NBS-418
(8-1-63)
USCOMM-DC 18556-P63

U.S. DEPARTMENT OF COMMERCE
NATIONAL BUREAU OF STANDARDS

Ref.		Elem. Sym.	A	Z
	S. Costa, F. Ferrero, S. Ferroni, B. Minetti, C. Molino E. Malvano Phys. Letters 6, 206 (1963)	Mg		12

Method	Ref. No.	
100 MeV Synchrotron; 4π neutron detector; calculated integrated cross sections - fitted with polynomial of degree n	63 Co 3	327

Reaction	E or ΔE	E_o	Γ	$\int \sigma dE$	$J\pi$	Notes
(γ, xn)						$\sigma_b = \frac{\sigma(E)_{dE}}{E}$ 327 gets $\langle \bar{v}_p \cdot \bar{v}_n - \bar{v}_n \cdot \bar{v}_n \rangle$ $= (R_n^2 - R_p^2 - \frac{3}{\pi^2} \frac{\Sigma\sigma}{\sigma^2} \sigma_b \frac{A-1}{A^2}) \times \frac{2}{A-2}$ See "Baron" for plots of this and σ dE/60 MZ/A.

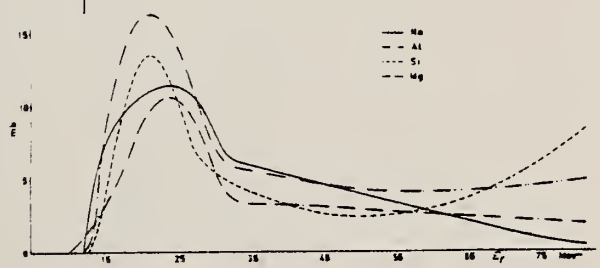

Figure 1: Photoneutron cross sections for several light elements versus γ-ray energy.

Ref. (a) M. Sugawara, S. Mori, A. Ono, A. Hotta, M. Kimura
J. Phys. Soc. Japan 18, 17 (1963)

Elem. Sym.	A	Z
Mg		12

Method: 25 MeV betatron; photon scattering; NaI spectrometer; NBS chamber

Ref. No.: 63 Su 1 (a) NVB

Reaction	E or ΔE	E_o	Γ	$\int \sigma dE$	Jπ	Notes
Mg(γ,γ)	Bremss. 4-14	10.2		$\int_4^{14}$ = 0.6 MeV-mb		Detector at 120° σ_{max} = 0.5 mb Corrects results of J. Phys. Soc. Japan 16, 1657 (1961)

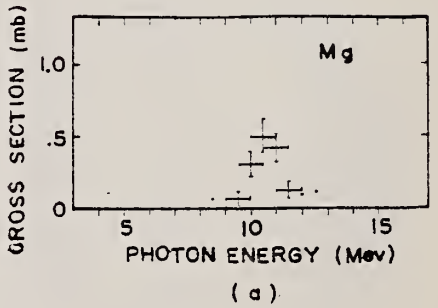

(a)

REF.

B. S. Dolbilkin, V. A. Zapevalov, V. I. Korin, L. E. Lazareva and F. A. Nikolaev
Proc. Paris Conference 1060 (1964)

ELEM. SYM.	A	Z
Mg		12

METHOD

Synchrotron

REF. NO.

64 Do 2 JDM

REACTION	RESULT	EXCITATION ENERGY	SOURCE		DETECTOR		ANGLE
			TYPE	RANGE	TYPE	RANGE	
MU-T	G,MU-T	12-30	C	250	MGP-D	12-30	4PI

$$\int_{12}^{30} \sigma dE = 332 \pm 40 \text{ MeV.mb}$$

$h\nu_{max.}$ (MeV)	13.9	17.0	18.9	20.3	23.1	24.8
$\sigma_{max.}$ (mb)	7	16	37	41	30	32
Half-width Γ (MeV)	~ 0.9	~ 0.7	~ 1.0	~ 1.0	~ 2.7	~ 0.9
$\int \sigma.d(h\nu)$ (MeV.mb)	14	20	55	64	95	53

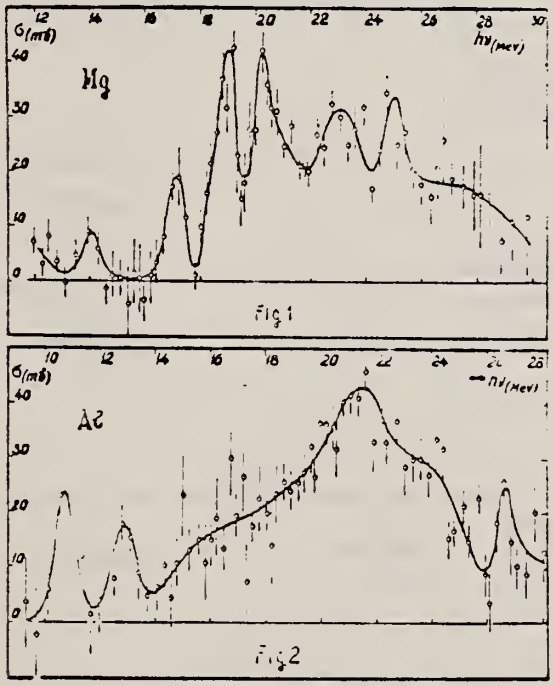

FIG. 1. — Nuclear γ-ray absorption cross-section of Mg(Mg[24] — 78.6, Mg[25] — 10.1, Mg[26] — 11.3 per cent).
The cross sections for Mg in the above figure have to be raised by 2.5 mb.
FIG. 2. — Nuclear γ-rays absorption cross-section of Al[27].

B. Forkman and W. Stiefler
Nucl. Phys. 56, 604-614 (1964)

ELEM.		
Mg		12

METHOD	REF. NO.	
Synchrotron Transmission Chamber	64 Fo 1	JOC

REACTION	RESULT	EXCITATION ENERGY	SOURCE		DETECTOR		ANGLE
			TYPE	RANGE	TYPE	RANGE	
G,P	SPC	THR - 40	C	20-40	EMU-D	1-18	DST

RLX

See following theory paper, Nucl. Phys. 56, 615-(1964)

TABLE 1

The α coefficient in the angular distribution $1+\alpha \sin^2\theta$ of the photoprotons from Mg^{24} at the different bremsstrahlung maximum energies

Proton energy (MeV)	E_{max} = 23 MeV	E_{max} = 26.5 MeV	E_{max} = 40 MeV
1.0—3.5	1.11±0.44	0.04±0.05	
3.5—5.7	0.18±0.16	−0.15±0.09	
5.7—7.3	−0.29±0.23	−0.26±0.14	
>7.3		−0.40±0.19	0.99±0.42

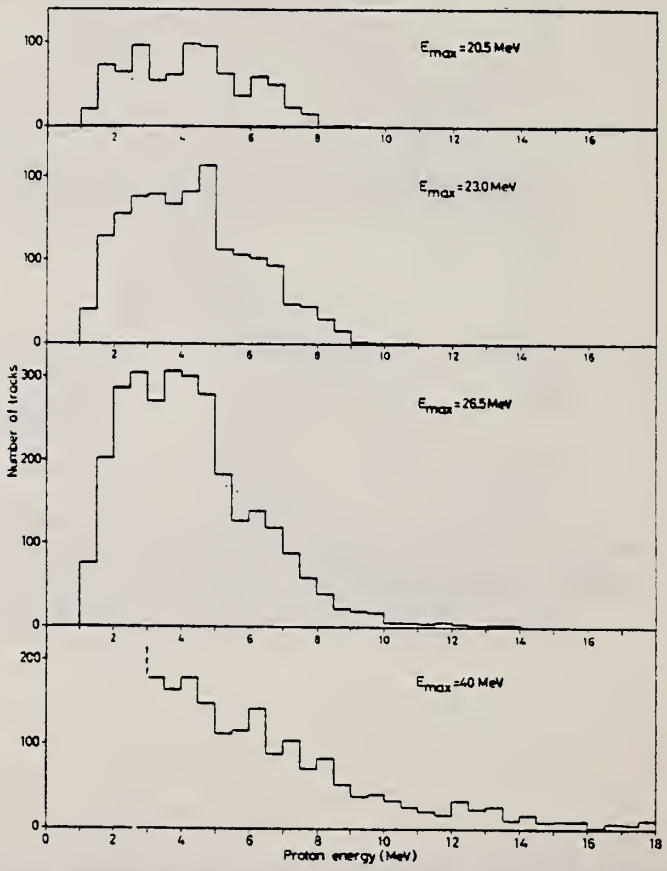

Fig. 2. Proton spectra for maximum bremsstrahlung energies of 20.5, 23, 26.5 and 40 MeV.

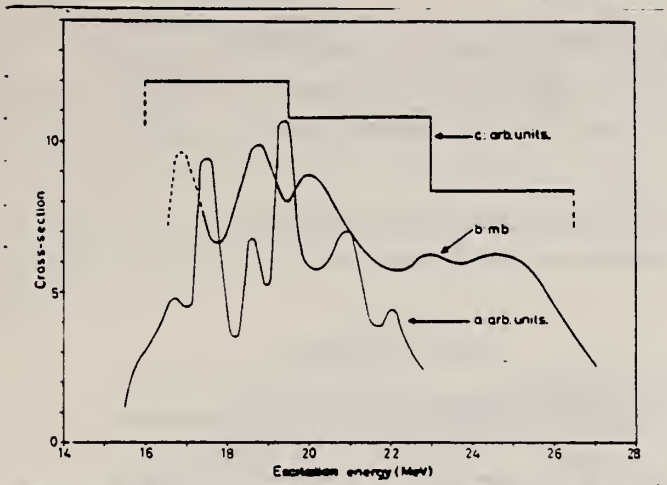

Fig. 4. Cross-section for photoprotons from magnesium. (a) The (γ, p_0) cross-section calculated from ref. [9]). (b) The (γ, p) cross-section calculated from the (γ, n) cross-section given ref. [9]) assuming ground-state transitions. (c) The relative (γ, p) cross-section from the present experiment.

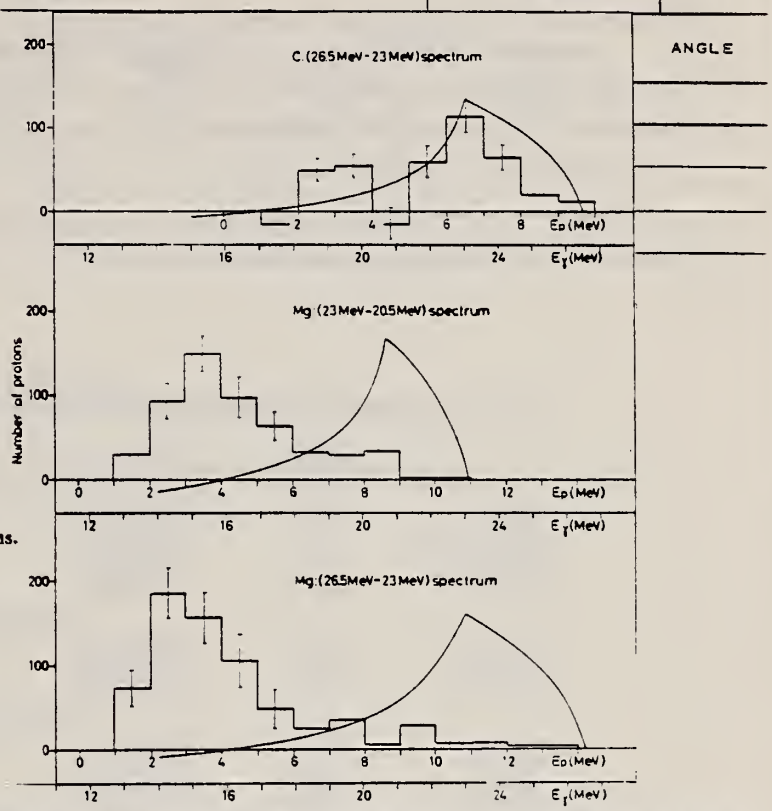

Fig. 6. Difference proton spectra between the 23 MeV and the 20.5 MeV exposures and the 26.5 MeV and the 23 MeV exposures for magnesium and carbon. The corresponding photon spectra are also given.

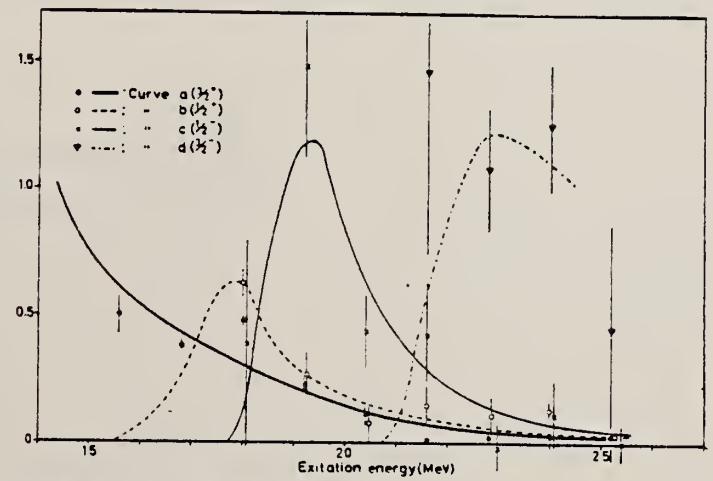

Fig. 7. Branching ratios to (a) the $\frac{5}{2}^+$ ground state [211 $\frac{5}{2}$], (b) the $\frac{1}{2}^+$ hole state [220 $\frac{1}{2}$] at 2.6 MeV, (c) the $\frac{1}{2}^-$ hole state [101 $\frac{1}{2}$] at 5 MeV, (d) the $\frac{1}{2}^-$ hole state [101 $\frac{1}{2}$] at 8 MeV in Na^{23} as a function of the excitation energy of Mg^{24}.

J. Goldemberg, W.C. Barber, F.H. Lewis, Jr., J.W. Walecka
Phys. Rev. 134, B1022 (1964)

ELEM. SYM.	A	
Mg		12

METHOD	REF. NO.	
Linac	64 Go 3	NVB

REACTION	RESULT	EXCITATION ENERGY	SOURCE		DETECTOR		ANGLE
			TYPE	RANGE	TYPE	RANGE	
E,E/	ABX	11	D	40-70	MAG-D		180

FMF

TABLE I. Data on $M1$ transitions.

	q MeV/c	Cross section[a]	Reference	$\lvert\langle J_f\rvert\lvert T_1^{\max}(q)\rvert\lvert J_i\rangle\rvert^2$ (10^{-3})	$(1/q^2)\lvert\langle J_f\rvert\lvert T_1^{\max}(q)\rvert\lvert J_i\rangle\rvert^2$ [10^{-6}(MeV/c)$^{-2}$]
		15.1-MeV level in C^{12}			
Photons	15.1	(2.05±0.27)	8	0.044	(0.19 ±0.025)
Electrons	68	(2.0 ±0.3)	this work	0.55	(0.12 ±0.018)
Electrons (160°)	68	(2.6 $\pm_{0.40}^{0.47}$)	5	0.69	(0.15 $\pm_{0.022}^{0.026}$)
Electrons	93	(2.0 ±0.3)	this work	0.87	(0.10 ±0.015)
Electrons	125	(1.5 ±0.25)	this work	1.10	(0.07 ±0.012)
		3.56-MeV level in Li^6			
Photons	3.56	(0.92$\pm_{0.18}^{0.20}$)	b	0.014	(1.10 $\pm_{0.18}^{0.24}$)
Electrons	76	(3.0 ±0.45)	this work	2.0	(0.38 ±0.057)
Electrons	106	(1.55±0.23)	this work	2.1	(0.19 ±0.028)
Electrons	136	(0.90±0.14)	this work	2.0	(0.11 ±0.017)
		11.6-MeV level in Si^{28}			
Photons	11.6	(9.8 ±2.6)	c	0.016	(1.2 ±0.32)
Electrons	71.5	(3.5 ±1.4)	d	0.92	(0.18 ±0.07)
Electrons	88.4	(3.0 ±0.75)	this work	1.2	(0.15 ±0.038)
Electrons	129.4	(1.8 ±0.45)	this work	1.5	(0.09 ±0.022)
		11-MeV level in Mg^{24}			
Photons	11	(13.1 ±3.8)	c	0.02	(1.7 ±0.50)
Electrons	83	(4.4 ±0.88)	6	1.5	(0.22 ±0.044)
Electrons	97	(3.5 ±0.70)	this work	1.6	(0.1 ±0.034)
Electrons	129	(1.8 ±0.36)	this work	1.3	(0.081±0.016)

[a] In units of 10^{-27} MeV-cm^2 for photons and 10^{-28} cm^2/sr for electrons.
[b] L. Cohen and R. A. Tobin, Nucl. Phys. 14, 243 (1960).
[c] A. B. de Nercy, Ann. Phys. (Paris) 6, 1379 (1961).
[d] R. D. Edge and G. A. Peterson, Phys. Rev. 128, 2750 (1962).

REF.

B. S. Ishkhanov, I. M. Kapitonov, V. G. Shevchenko and B. A. Yur'ev
Phys. Letters 9, 162 (1964)

ELEM. SYM.	A	Z
Mg		12

METHOD: Betatron

REF. NO.: 64 Is 1 JOC

REACTION	RESULT	EXCITATION ENERGY	SOURCE		DETECTOR		ANGLE
			TYPE	RANGE	TYPE	RANGE	
G,XP	ABX	THR - 32	C	15-32	SCI-D	0-3	4KN

336

Table 2
Measurements results

Element	Maximum cross section (b)	Peak position (MeV)	Peak half-width (MeV)	Integrated cross section $\int_0^{32} \sigma dE$ (MeV, b)
P	0.043	21	10	0.35 ± 0.06
S	0.050	21	9	0.37 ± 0.05
Mg	0.018 0.018	22.5 26.0	11	0.18 ± 0.04

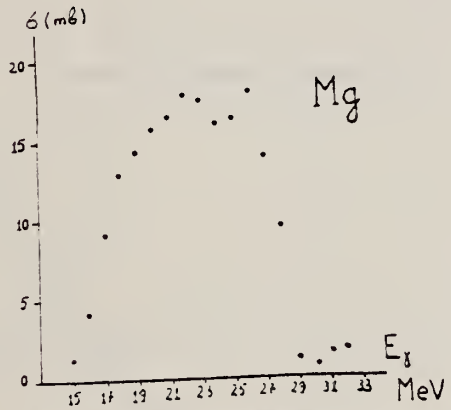

Fig. 2. The (γ,p) cross section for Mg.

B.S. Dolbilkin, V.I. Korin, L.E. Lazareva, F.A. Nikolaev and V.A. Zapevalov
Nuclear Phys. 72, 137 (1965)

ELEM. SYM.	A	Z
Mg		12

METHOD: Synchrotron

REF. NO.: 65 Do 2 | EGF

REACTION	RESULT	EXCITATION ENERGY	SOURCE TYPE	SOURCE RANGE	DETECTOR TYPE	DETECTOR RANGE	ANGLE
G,MU-T	ABX	11 - 30	C	260	MGP-D	10-30	

$$\int_{11}^{30} \sigma dE = 365^{+40}_{-20} \text{ MeV-mb}$$

$$\frac{\int E\sigma dE}{\int \sigma dE} = 21.6 \text{ MeV}$$

$\sigma_{-1} = 17.9$ mb

$\sigma_{-2} = 0.95$ mb/MeV

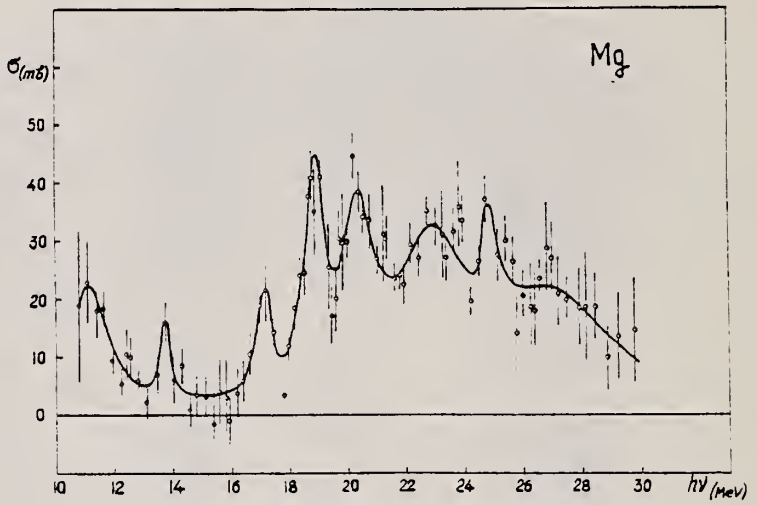

Fig. 2. The nuclear absorption cross section.

TABLE 1

Parameters of resonance peaks observed in the nuclear absorption cross section

$h\nu_{res}$ (MeV)	11.2	13.8	17.1	18.9	20.4	22.9	24.9	27.0
σ_{max} (mb)	21	13	20	37	29	26	20	19
Half-width Γ (MeV)	1.5	0.3	0.4	0.8	1.3	2.6	0.6	4.9
$\int \sigma(h\nu)\, d\,(h\nu)$ (MeV · mb)	48	7	14	44	57	106	18	146

REF.

G. Manuzio, G. Ricco and M. Sanzone
Il Nuovo Cimento 39, 1057 (1965)

ELEM. SYM.		
Mg		12

METHOD

REF. NO.	
65 Ma 4	JOC

REACTION	RESULT	EXCITATION ENERGY	SOURCE		DETECTOR		ANGLE
			TYPE	RANGE	TYPE	RANGE	
G,XP	SPC	THR - 31	C	31	SCD-D	3-14	

$Y(E_p > 3.5$ MeV) = 10^{-4} cm^2/mole MeV.

TABLE I. – *Energy levels in* ^{24}Mg.

(γ, n) (a)	(γ, n) (b)	Total absorption (c)	Total absorption (d)	Our experiment
—	—	—	—	16.3
17	17.5	17	17.5	17.8
—	18.8	18.9	19.2	18.9
19.5	—	—	—	—
—	20	20.3	20	20
21.5	—	—	—	—
23.5	23	23.1	—	—
25.5	25	25.8	—	—

(a) ref. (7)
(b) ref. (8)
(c) ref. (14)
(d) ref. (15)

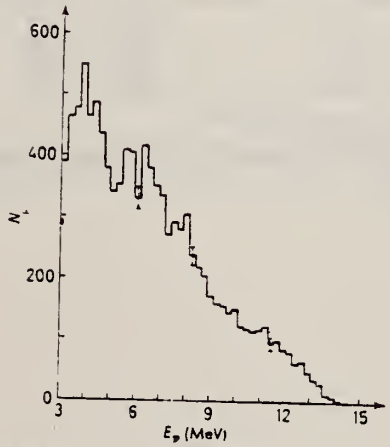

Fig. 2. – Photoproton spectrum from Mg.

REF.

K. Min, W. D. Whitehead
Phys. Rev. 137, B301-304 (1965)

ELEM. SYM.		
Mg		12

METHOD

Synchrotron; NBS chamber monitor

REF. NO.	
65 Mi 1	NVB

REACTION	RESULT	EXCITATION ENERGY	SOURCE		DETECTOR		ANGLE
			TYPE	RANGE	TYPE	RANGE	
G,XN	ABX	THR-30	C	THR-30	BF3-I		4PI

325

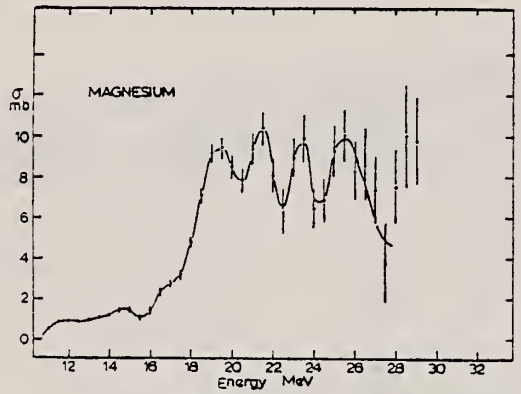

FIG. 3. Total photoneutron cross section of magnesium unfolded in 1-MeV intervals.

TABLE I. Isotopic abundance in the samples and threshold energies.

Isotope	Abundance (%)	(γ,n) (MeV)	(γ,pn) (MeV)	$(\gamma,2n)$ (MeV)
C^{12}	98.89	18.7	27.4	32.4
C^{13}	1.11	5.0	20.9	23.7
Mg^{24}	78.60	16.6	24.1	
Mg^{25}	10.11	7.3	19.0	23.9
Mg^{26}	11.29	11.1	23.2	18.4

TABLE III. Energy levels observed in magnesium (MeV).

Present work (γ,n)	Other experiments (γ,n)[a]	Other experiments Absorption[b]
17.0	17.5	17.0
19.5	18.8	19.0
21.5	20.0	20.0
23.5	23.0	23.0
25.5	25.0	25.0

$\int_{Th.}{}^{25}\sigma dE = 90.7$ MeV-mb

[a] Reference 9.
[b] Reference 23.

REF.

J.M. Wyckoff, B. Ziegler, H.W. Koch, and R. Uhlig
Phys. Rev. 137, B576-94 (1965)

ELEM. SYM.		
Mg		12

METHOD

Synchrotron; ion chamber monitor

REF. NO.	
65 Wy 1	NVB

REACTION	RESULT	EXCITATION ENERGY	SOURCE		DETECTOR		ANGLE
			TYPE	RANGE	TYPE	RANGE	
G,MU-T	ABX	10-70	C	90	SCI-D		4π

4π+

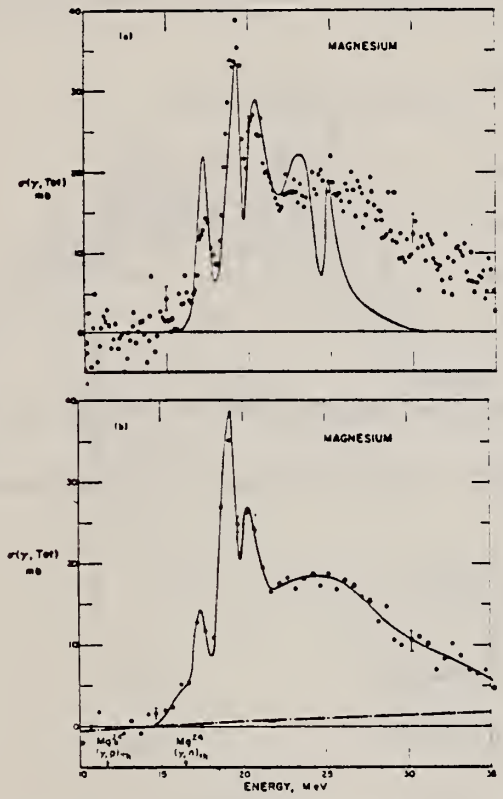

FIG. 13. Magnesium total photonuclear cross section. The solid line in (a) represents the Lebedev data moved up in energy by 375 keV.

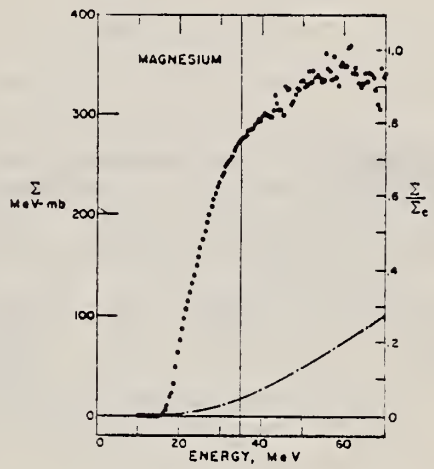

FIG. 14. Magnesium total photonuclear cross section integrated over energy. The dot-dashed line represents the corrected baseline resulting from the introduction of the calculated radiative corrections to the electronic cross sections.

REF. B. S. Dolbilkin, V. A. Zapevalov, V. I. Korin, L. E. Lazareva and F. A. Nikolaev
Izv. Akad. Nauk fiz. 30, 349 (1966)
Bull. Acad. Sci. USSR-Phys. 30, 354 (1966)

ELEM. SYM.	A	Z
Mg		12

METHOD

REF. NO.	
66 Do 2	EGF

REACTION	RESULT	EXCITATION ENERGY	SOURCE		DETECTOR		ANGLE
			TYPE	RANGE	TYPE	RANGE	
G-MU-T	ABX	8-30	C	260	MGP-D	6-30	4PI
							323

Resolution 120 keV 10 MeV
220 keV 20 MeV

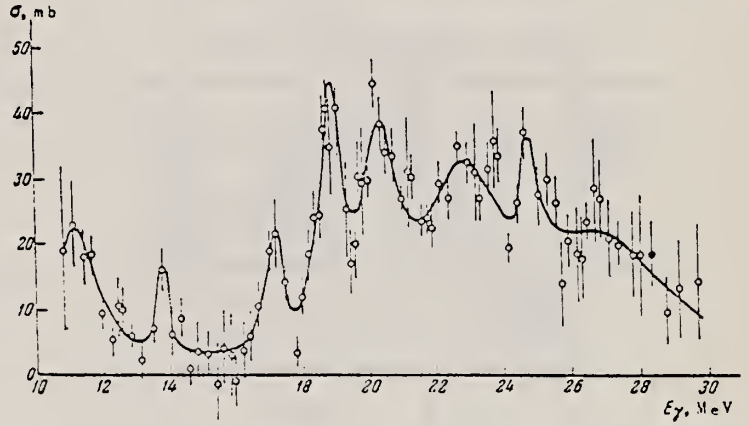

Fig.3. Nuclear absorption cross section of magnesium.

Table 2

Breit-Wigner resonance components of the Mg cross section (Fig.3)

E_{res}, MeV	σ_{max}, mb	Γ, MeV	$\int \sigma dE$, MeV·mb	E_{res}, MeV	σ_{max}, mb	Γ, MeV	$\int \sigma dE$, MeV·mb
11,2	21	1,5	48	20,4	29	1,3	57
13,8	13	0,3	7	22,9	26	2,6	106
17,1	20	0,4	14	24,9	20	0,6	18
18,9	37	0,8	44	27,0	19	4.9	15

REF.

F. W. K. Firk
Proc. Gatlinburg Conference 352 (1966)

ELEM. SYM.	A	Z
Mg		12

METHOD

REF. NO. 66 Fi 2 hmg

REACTION	RESULT	EXCITATION ENERGY	SOURCE		DETECTOR		ANGLE
			TYPE	RANGE	TYPE	RANGE	
G,XN	SPC	THR-65	C	65	TOF-D	5-40	90

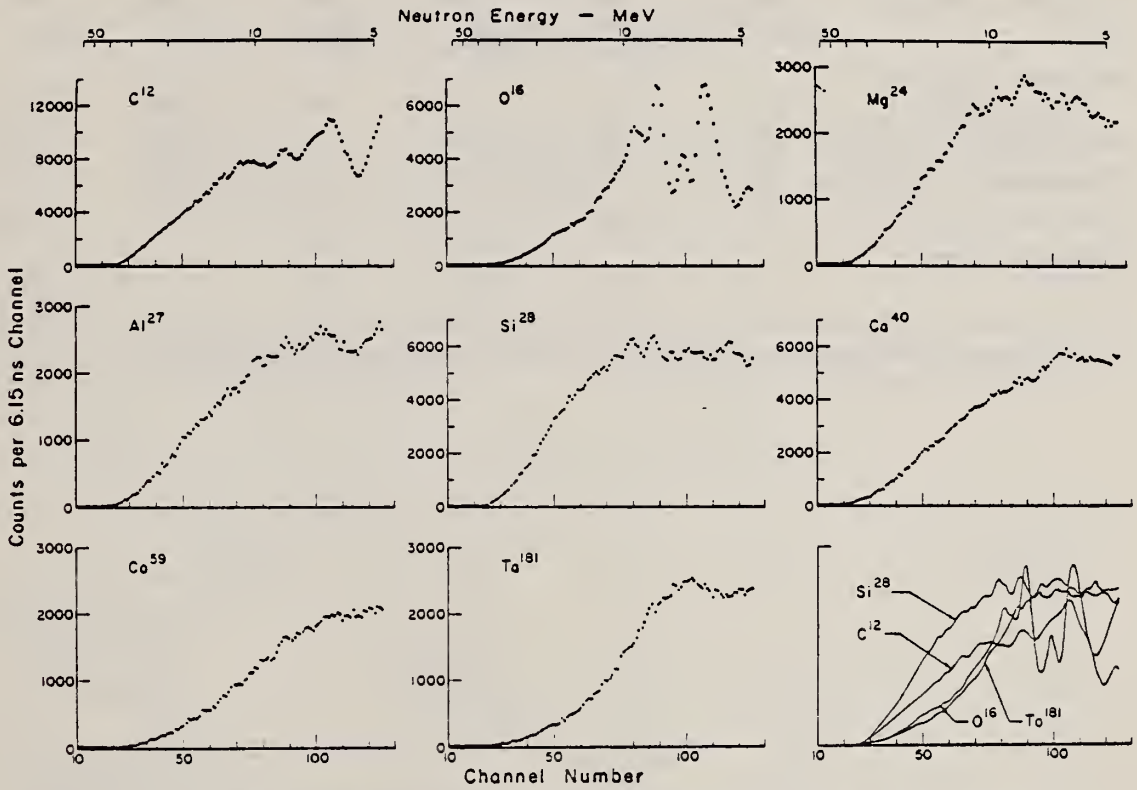

Fig. 1. Observed photoneutron time-of-flight spectra of C, O, Mg, Si, Ca, Co, V, and Ta.

REF.

H. Hoffmann, B. Prowe and H. Ullrich
Nuclear Phys. 85, 631 (1966)

ELEM. SYM.		
Mg		12

METHOD	REF. NO.	
Betatron	66 Ho 3	JDM

REACTION	RESULT	EXCITATION ENERGY	SOURCE		DETECTOR		ANGLE
			TYPE	RANGE	TYPE	RANGE	
G,A	SPC	THR-31	C	31	SCD-D	2-13	130

TABLE 1

Experimental data and results

Element	Mg	Al	S	Ni	Cu	Zn	Error (%)
target thickness (mg/cm²)	0.81	1.54	0.80	2.50	2.68	3.00	5 [a]
dose (r)	6190	25400	23200	3880	5840	4220	10
yield absolute (10^5/mole · r) for $E_m > 3.16$ MeV	0.61	0.93	1.46	1.65	0.92	2.42	11 [a]
yield relative to Ni	0.36	0.56	0.88	1	0.55	1.43	5 [a]
$Y_{\gamma,\alpha}/Y_{\gamma,tot}$(%)	9.6	11.4	12.4	7.0	3.2	[b]	
nuclear temp. θ (MeV)	1.43	1.48	1.46	1.04		0.91	10
level density parameter a (MeV^{-1})	5.1	4.8	4.9	8.6		10.8	10

[a] For S, the error of the target thickness has been 10 %, of the absolute yield 14 % and of the relative yield 10 %.
[b] For Zn $\sigma_{\gamma,tot}$ is not known.

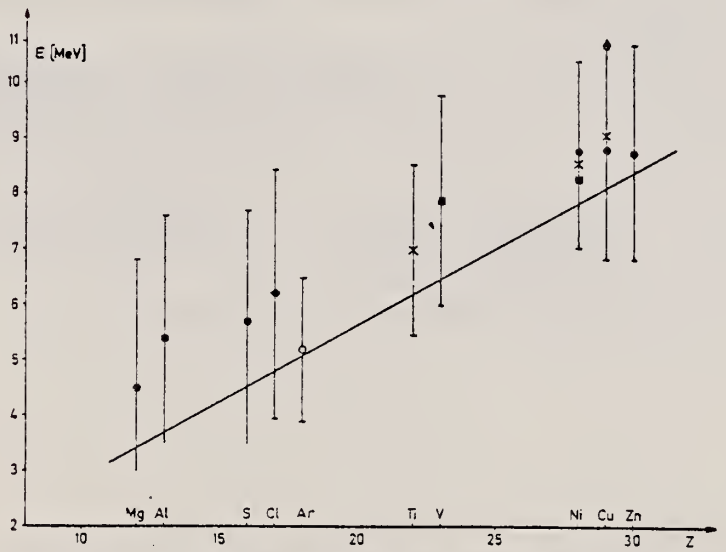

Fig. 4. Position of the peaks in different photoalpha spectra plotted against Z of the target nuclei. × : Scheer *et al*[10]), ■ : Kregar and Povh[9]). ▲ : Meneghetti and Vitale[5]), ◆ : Erdös *et al*[1]), ○ : Komar *et al*[7]), ● : this work. The signs show the position of the maximum, the bars give the widhs at half maximum. The curve shows the height of the Coulomb barrier.

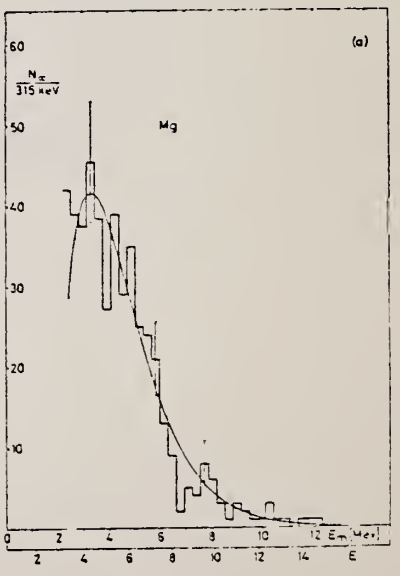

Fig. 3 (a)

REF.

J. M. Loiseaux, J. M. Maison, and M. Langevin
J. de Physique 28, 11 (1967)

ELEM. SYM.	A	Z
Mg		12

METHOD

REF. NO.	
67 Lo 1	JOC

REACTION	RESULT	EXCITATION ENERGY	SOURCE		DETECTOR		ANGLE
			TYPE	RANGE	TYPE	RANGE	
G,G/	ABX	16-32	C	34	NAI-D		DST

TABLEAU I

COEFFICIENT a DES DISTRIBUTIONS ANGULAIRES

$$W(\theta) = 1 - a\cos^2\theta$$

^{16}O.....	a(19-25 MeV) $= 1 \pm 0,1$		
^{23}Na.....	a(15-18 MeV) $= 0,1 \pm 0,1$	a(18,5-23 MeV) $= 0,4 \pm 0,15$	a(25-30 MeV) $= 0,85 \pm 0,2$
^{24}Mg	a(16,5-20 MeV) $= 0,3 \pm 0,1$	a(20-25 MeV) $= 0,5 \pm 0,1$	a(25,5-32 MeV) $= 0,5 \pm 0,1$
^{28}Si	a(15-17,5 MeV) $= 0,87 \pm 0,1$	a(18-23 MeV) $= 0,7 \pm 0,1$	a(25,5-32 MeV) $= 0,5 \pm 0,1$
^{39}K	a(14,5-18,5 MeV) $= 0,5 \pm 0,1$	a(19-24,5 MeV) $= 1 \pm 0,1$	a(25-32 MeV) $= 1 \pm 0,1$

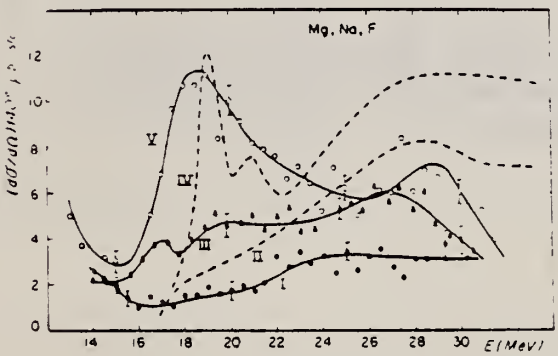

FIG. 6.

Sections efficaces différentielles de diffusion à 110° pour ^{19}F (I), ^{23}Na (III) et Mg (V).

Section efficace prévue par la relation de dispersion pour ^{23}Na (courbe II) et Mg (courbe IV).

G. A. Savitskii, N. G. Afanas'ev, I. S. Gul'karov, V. M. Khvastunov, A. A. Khomich, and N. G. Shevchenko
Yad. Fiz. 7, 1181 (1968)
Sov. J. Nucl. Phys. 7, 705 (1968)

ELEM. SYM.		
Mg		12

METHOD

REF. NO.	
68 Sa 1	HMG

REACTION	RESULT	EXCITATION ENERGY	SOURCE		DETECTOR		ANGLE
			TYPE	RANGE	TYPE	RANGE	
E,E/	FMF	1-8	D	100-260	MAG-D		

Observed inelastic scattering peaks at
1.4±.2, 4.1±.2, 6.0±.3, 6.9±.3, 7.6±.3 MeV.
Results compared with the prediction of the α-particle model.

3 PEAKS 1.4-6.0

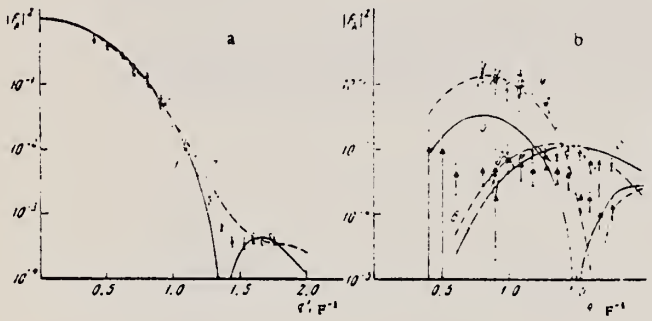

FIG. 1. Form factors for scattering of electrons by the nucleus Mg^{24}: a – elastic scattering form factor; b – form factors corresponding to excitation of the levels 1.37 MeV (2^+) – O; 6.0 MeV (4^+) – X; and doublet 4.1 MeV (2^+ and 4^+) – ▲; the curves are calculated according to the α-particle model.

REACTION	RESULT	EXCITATION ENERGY	SOURCE TYPE	SOURCE RANGE	DETECTOR TYPE	DETECTOR RANGE	ANGLE
E,E/	FMF	1-8	D	99-229	MAG-D	99-229	DST
		(1.4-7.6)					

B(EL) 1-8 MEV

Table 2

Squared form factor for inelastic scattering of electrons with excitation of levels in ^{24}Mg

Q = 1.37 MeV		(4.1±0.2) MeV		(6.0±0.2) MeV		(6.9±0.3) MeV		(7.6±0.3) MeV	
q, fermi^{-1}	F_λ^2, 10^{-4}	q, fermi^{-1}	F_λ^2, 10^{-4}	q, fermi^{-1}	F_λ^2, 10^{-4}	q, fermi^{-1}	F_λ^2, 10^{-4}	q, fermi^{-1}	F_λ^2, 10^{-4}
0,804	161±68	0,409	9,8±9,8	0,899	6,5±3,5	0,409	5,2±1,3	0,899	11,1±6,6
0,804	147±46	0,509	9,4±9,4	0,902	4,8±3,0	0,509	5,0±1,4	0,902	11,5±3,9
0,902	101±32	0,609	4,0±2,0	0,993	8,5±3,3	0,609	3,1±1,1	0,993	15,1±3,9
0,903	114±35	0,804	4,7±2,0	1,09	7,9±2,3	0,706	2,3±0,8	1,09	19,6±4,7
0,904	131±41	0,899	5,1±2,6	1,18	9,6±2,0	0,707	2,2±0,7	1,18	21±5
0,993	79,2±24,6	0,902	1,8±1,6	1,27	8,6±2,3	0,804	1,4±0,4	1,27	15,9±3,7
1,08	64,2±26,4	0,993	6,8±2,1	1,36	8,1±1,6			1,36	15,3±3,4
1,09	113±24	1,09	5,7±2,0	1,44	10,0±1,8			1,44	10,5±2,3
1,09	90,0±18,9	1,09	5,9±3,0	1,53	8,3±1,4			1,53	12,1±2,7
1,09	137±28	1,18	4,6±1,9	1,60	6,3±1,3			1,60	7,8±2,0
1,18	60,6±12,7	1,27	7,7±2,7	1,67	6,3±1,5			1,67	6,4±1,7
1,27	52,2±11,0	1,36	4,5±1,6	1,76	6,1±1,4			1,76	4,8±1,4
1,28	50,4±13,1	1,44	3,8±1,4						
1,36	37,2±5,7	1,53	1,8±0,6						
1,44	19,9±4,2	1,60	1,7±0,6						
1,53	9,92±1,65	1,67	0,95±0,33						
1,60	5,31±1,52	1,76	1,20±0,43						
1,67	2,40±0,52								

Table 5

Characteristics of some electron-excited transitions in ^{24}Mg

Method	Parameters and method of determination	6,0±0,2 MeV, λ = 4	6,9±0,3 MeV, λ = 1	7,6±0,3 MeV, λ = 3
1	β_λ, 10^{-2}	25,8±5,4	2,25±0,33	16,7±4,8
	$B(E\lambda, I_i \to I_f)$, e^2 fermi$^{2\lambda}$	(4,1±0,9)·10^4	2,8±0,4	(2,4±0,7)·10^3
	G	15,0±3,2	1,7±0,3	10,3±3,0
2	A_λ, fermi$^{\lambda-2}$	0,61±0,04	1,41±0,07	0,84±0,04
	B_λ, fermi^2	0,38±0,05	1,00±0,14	0,32±0,04
	$B(E\lambda, I_i \to I_f)$, e^2fermi$^{2\lambda}$	(6,6±0,7)·10^4	1,20±0,12	(1,55±0,12)·10^3
	G	24,6±2,6	0,73±0,08	6,6±0,6
	R_{trans}, fermi	4,76±0,12	4,05±0,17	4,18±0,08

[over]

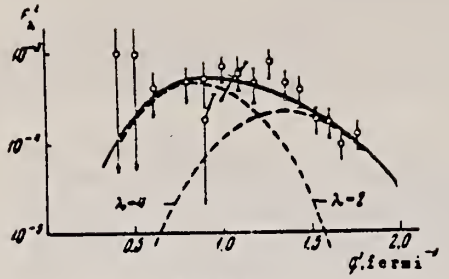

Fig.4

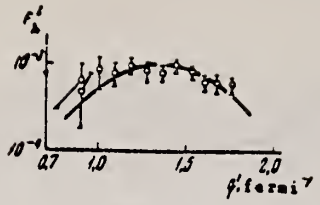

Fig.5

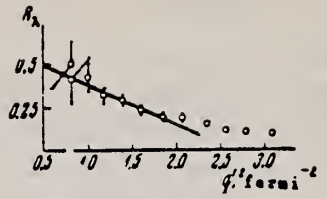

Fig.6

Fig.4. Squared form factor for excitation of ^{24}Mg levels at 4.12 and 4.23 MeV, as a function of q'. Solid curves - calculated by method 1 for a $\lambda = 1$ plus $\lambda = 4$ multipole mixture and fitted to the experimental points ($\beta_2 = 0.0112$ and $\beta_4 = 0.0566$). Dashed curves - contributions of the individual multipoles.

Fig.5. The same as Fig.4, but for the 6.0 MeV level. ($\lambda = 4$, $\beta_4 = 0.258$).

Fig.6. R_λ (Ref. 8) as a function of q'^2 for the 6.0 MeV level in ^{24}Mg. The straight line is described by the equation $R_\lambda = A_\lambda \cdot (1 - B_\lambda\ q'^2)$ with $\lambda = 4$, $A_\lambda = 0.61$, and $B_\lambda = 0.38$ fermi^2.

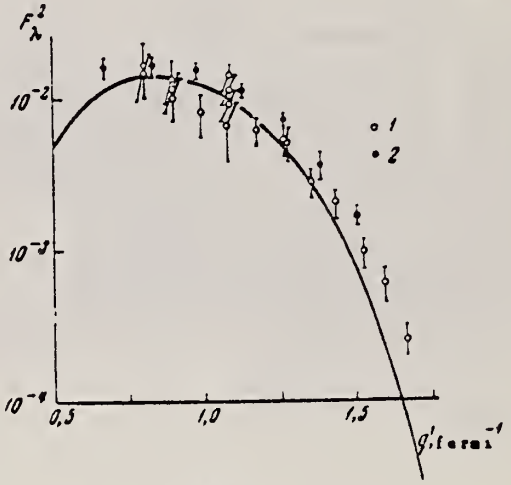

Fig.3

Fig.3. Squared form factor for inelastic scattering of electrons by ^{24}Mg with excitation of the 1.37 MeV level, as a function of q': 1 - our data; 2 - Helm's data[4]. The curve is a least-squares fit to our experimental points, calculated by method 1 ($\lambda = 2$, $\beta_2 = 0.35$).

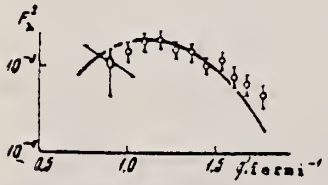

Fig.7. The same as Fig.4 but for the 7.6 MeV level ($\lambda = 3$, $\beta_3 = 0.167$).

REF. S.C. Fultz, R.A. Alvarez, B.L. Berman, M.A. Kelly, D.R. Lasher, T.W. Phillips, J. McElhinney
Phys. Rev. C4, 149 (1971)

ELEM. SYM.	A	Z
Mg		12

METHOD

REF. NO.	
71 Fu 2	hmg

REACTION	RESULT	EXCITATION ENERGY	SOURCE		DETECTOR		ANGLE
			TYPE	RANGE	TYPE	RANGE	
G,XN	ABX	THR-29	D	10-29	BF3-I		4PI

14 LEVEL FIT 342

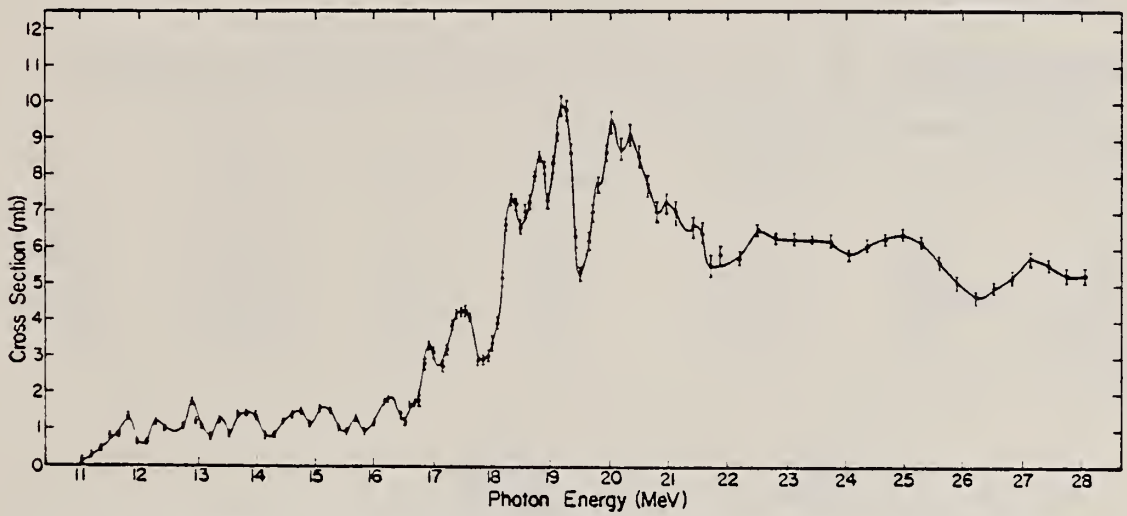

FIG. 8. Natural magnesium total cross section $\sigma((\gamma,n)+(\gamma,pn)+(\gamma,2n))$ showing detailed structure. The solid line is merely to guide the eye through the data points.

TABLE II. Integrated cross sections of magnesium isotopes.

Isotope	$\int_{E_{thr}}^{28}\sigma(\gamma,n_{tot})dE$ (MeV mb)	$\int_{E_{thr}}^{28}\sigma(\gamma,2n)dE$ (MeV mb)
^{24}Mg	50	...
^{26}Mg	226	68
Natural magnesium	76	...

REF.

Tatsuya Saito
Bull. Chem. Soc. Japan 44, 1800 (1971)

ELEM. S / M.		
Mg		12

METHOD

REF. NO.	
71 Sa 2	egf

REACTION	RESULT	EXCITATION ENERGY	SOURCE		DETECTOR		ANGLE
			TYPE	RANGE	TYPE	RANGE	
G,P	ABX	THR-250	C	20-250	ACT-I		4PI

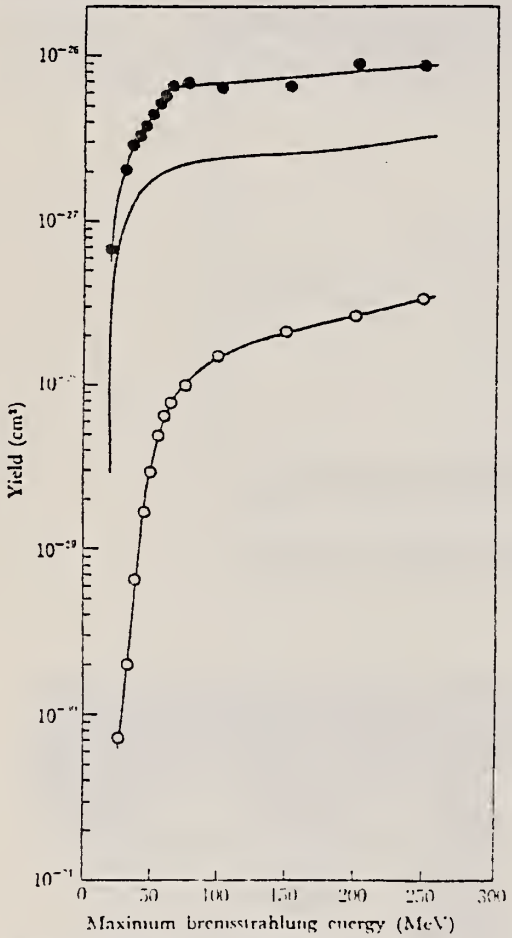

Fig. 3. The yield curves for the reactions $^{25}Mg(\gamma,p)^{24}Na$, $^{27}Al \rightarrow ^{24}Na$, and $^{12}C(\gamma,n)^{11}C$ as a monitor.
●: $^{25}Mg(\gamma,p)^{24}Na$, ○: $^{27}Al \rightarrow ^{24}Na$, ——: $^{12}C(\gamma,n)^{11}C$

REF. Z. Berant, R. Moreh and S. Kahane
Phys. Lett. 69B, 281 (1977)

ELEM SYM.	A	Z
Mg		12

METHOD

REF. NO. 77 Be 3 egf

REACTION	RESULT	EXCITATION ENERGY	SOURCE		DETECTOR		ANGLE
			TYPE	RANGE	TYPE	RANGE	
G,G	ABX	5 - 8	D	5-8	SCD-D		140

5.5-7.2 MeV

Table 1
Differential cross sections (μb/sr) for elastic scattering from C and Mg targets at an angle of 140°. The theoretical values include the combined effect of NT, NR and D scattering; The R contribution was ignored. The values for pure NT scattering are also given.

E	C(Z = 6)			Mg(Z = 12)		
(keV)	Experiment	Theory	Thomson	Experiment	Theory	Thomson
5516	0.17 ± 0.04	0.16	0.17	0.64 ± 0.15	0.61	0.67
5752	0.20 ± 0.06	0.15	0.17	0.66 ± 0.15	0.61	0.67
6465	0.17 ± 0.04	0.15	0.17	0.64 ± 0.15	0.59	0.67
6517	0.16 ± 0.04	0.15	0.17	0.63 ± 0.15	0.59	0.67
6874	0.18 ± 0.04	0.15	0.17	0.59 ± 0.15	0.58	0.67
7163	0.16 ± 0.04	0.14	0.17	0.50 ± 0.15	0.57	0.67

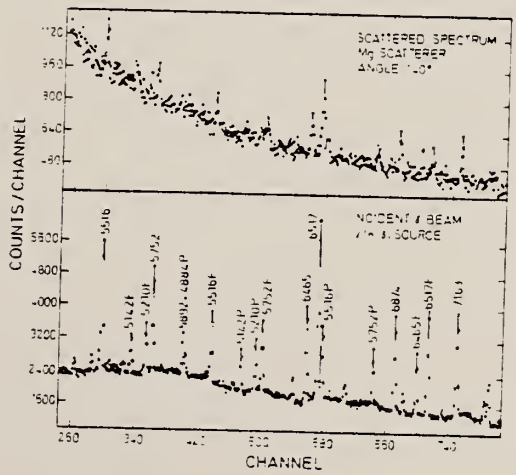

Fig. 1. High-energy part of the elastic scattering spectrum from a Mg target at 140° as measured by a 40 cm³ Ge(Li) detector, and of the incident V(n, γ) spectrum. Lines indicated by P and F denote photopeaks and first-escape peaks. Other lines denote double-escape peaks.

MG
A=24

MG
A=24

Ref. R. Nathans, P.F. Yergin
Phys. Rev. 98, 1296 (1955)

Elem. Sym.	A	Z
Mg	24	12

Method BF_3 counters; 24 MeV Bremms. betatron.

Ref. No. 55 Na 1 EGF

Reaction	E or ΔE	E_o	Γ	$\int \sigma dE$	Jπ	Notes
(γ,xn)	9.3 - 24	19.5	7-8	0.055 MeV-mb		E_{th} = 16.6 MeV; σ_{max} = 8.4 mb. No corrections. [NOTE: Figure 1 - "KBM" - Katz, Baker, Montalbetti, Can. J. Phys. 31, 250 (1953).]

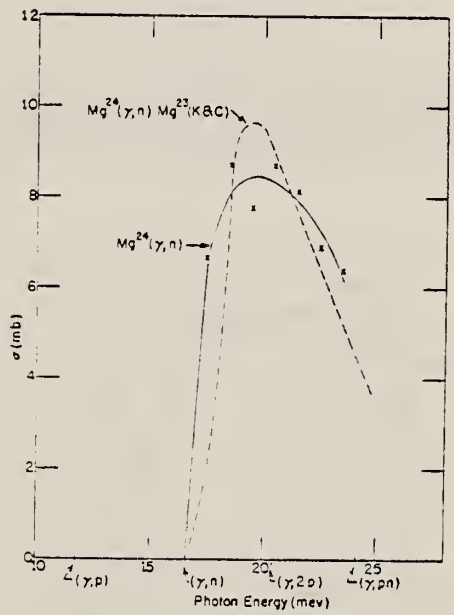

FIG. 1. (γ,n) cross section for Mg^{24}. The ordinate scale is in millibarns (10^{-27} cm^2). The locations of the thresholds for various reactions are indicated by arrows. The crosses are the points calculated from the yield data. The solid curve is drawn to fit the points. The dashed curve represents results previously reported by others for $Mg^{24}(\gamma,n)Mg^{23}$ by the residual activity method (see reference 8).

[8] Katz, Baker, and Montalbetti, Can. J. Phys. 31, 250 (1953).

R. H. Helm
Phys. Rev. 104, 1466 (1956)

ELEM. SYM.	A	Z
Mg	24	12

METHOD

REF. NO. 56 He 3 hmg

REACTION	RESULT	EXCITATION ENERGY	SOURCE		DETECTOR		ANGLE
			TYPE	RANGE	TYPE	RANGE	
E,E/	FMF	1-7	D	187	MAG-D		DST

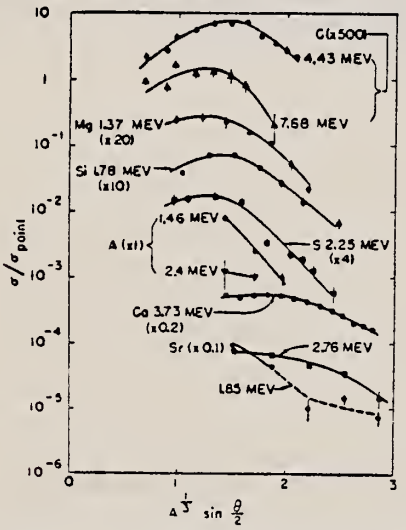

FIG. 3. Inelastic angular distributions (observed cross section divided by Feshbach point-charge cross sections). The results of Hahn *et al.* (reference 8) for Ca and of Fregeau and Hofstadter (reference 11) are included for comparison.

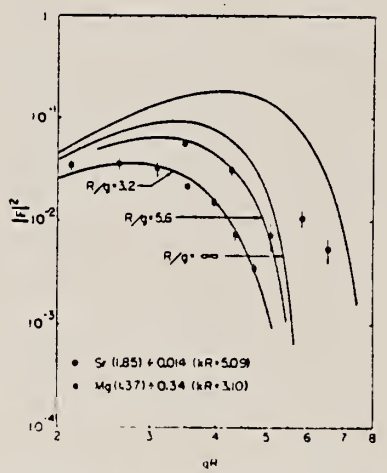

FIG. 6. Comparison of typical experimental and calculated squared inelastic form factors. Both the Sr (1.85 Mev) and Mg (1.37 Mev) are known to be 2+ levels. The calculated curves are for a "smeared δ-function" transition charge density (see Sec. V) with values of R/q taken from the elastic results. The abscissae for the experimental data are scaled by values of R taken from the elastic results [Table III (a)]. Shown for comparison (upper curve) is a squared form factor calculated from a quadrupole transition charge density whose radial dependence is constant for $r<R$, zero for $r>R$. This would give a poorer fit to the data than the δ-function distribution, indicating that the quadrupole vibrational mode is approximated better by a transverse wave in an incompressible nuclear fluid than by some sort of a compressional body wave.

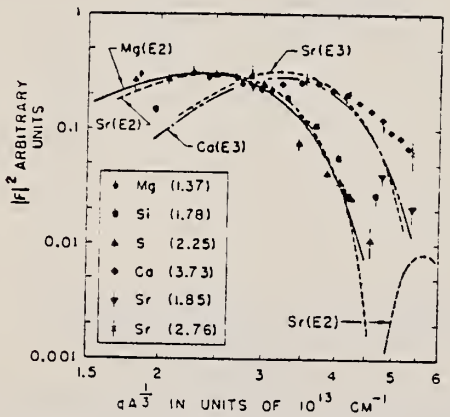

FIG. 7. Inelastic "universal curves." A composite plot of inelastic data from Mg, Si, S, Ca, and Sr against $qA^{\frac{1}{3}}$. The various form factors are arbitrarily normalized to minimize the spread of points. The point from sulfur and the point from silicon which seem to deviate from the "universal curve" are assumed to contain undetected experimental errors. The curves labeled Mg($E2$), Sr($E2$), Ca($E3$), and Sr($E3$) are calculated for electric-quadrupole and-octupole transitions using the "smeared δ-function" transition charge densities of Sec. V, and are arbitrarily normalized.

N. A. Burgov and Yu. V. Terekhov
J. Nucl. Energy II, 1958, Vol. 7, pp. 247 to 254.
Pergamon Press Ltd., London

Mg	24	12

METHOD

REF. NO. 58 Bu 1 | EGF

REACTION	RESULT	EXCITATION ENERGY	SOURCE		DETECTOR		ANGLE
			TYPE	RANGE	TYPE	RANGE	
G,G	LFT	1	D	1	SCI-D	1	4PI
		1.38 MeV					

$\Gamma \geq 3.2 \times 10^{-4}$ eV.

Lifetime by Doppler recoil method. Used recoil from 2.76 MeV γ.

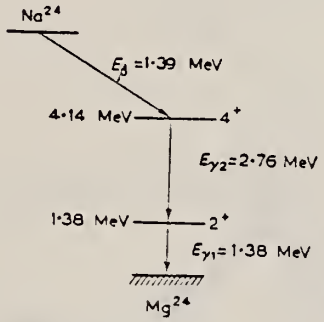

FIG. 1.—The decay scheme of ^{24}Na.

A. Bussière de Nercy
Compt. Rend. 250, 1252 (1960)

(See 61 Bu 4)

Mg	24	12

METHOD

REF. NO. 60 Bu 2 | EGF

REACTION	RESULT	EXCITATION ENERGY	SOURCE		DETECTOR		ANGLE
			TYPE	RANGE	TYPE	RANGE	
G,G	LFT	10.5	C		NAI-D		DST

x = scattering target thickness
y = absorber thickness

Peak absorption cross section 7 ± 2 barns.

Ground state radiation width 180 ± 50 eV.

Total width 1.7 ± 0.4 keV.

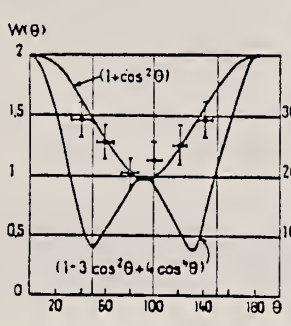

Fig. 1.

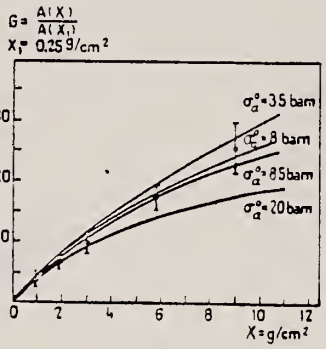

Fig. 2.

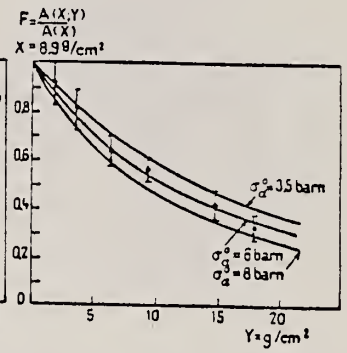

Fig. 3.

A. Bussiere de Nercy and M. Langevin
J. Phys. Radium 21, 293 (1960) (See 61 Bu 4)

Mg	24	12

METHOD

REF. NO. 60 Bu 3 | EGF

REACTION	RESULT	EXCITATION ENERGY	SOURCE		DETECTOR		ANGLE
			TYPE	RANGE	TYPE	RANGE	
G,G	LFT	10	C	23	NAI-D		DST

Includes inelastic to 1st excited state.

$\int \sigma dE = 1.98 \pm 0.4$ MeV-mb

$\Gamma_\gamma = 110 \pm 30$ eV

$\Gamma = 1 \pm .3$ keV

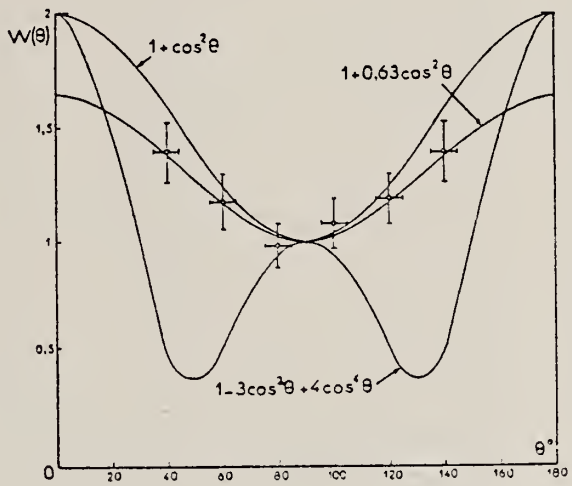

Fig. 1.

Ref. J.D. King, W.J. McDonald
Nuclear Phys. 19, 94 (1960)

Elem. Sym.	A	Z
Mg	24	12

Method 25 MeV betatron; activation; 2 NaI in coinc. to count annihilation radiation of β^+ from Mg^{23}.

Ref. No. 60 Ki 1 | JHH

Reaction	E or ΔE	E_o	Γ	$\int \sigma dE$	$J\pi$	Notes 3.9
(γ,n)	Bremss. 16.6-25	17.2±0.2 19.2±0.2				σ(γ,n) (19.2 MeV) = 6.7 mb Lower σ(γ,n) value [9.8 mb, Katz and Cameron, Phys. Rev. 84, 1115 (1951); 8.4 mb, Nathens and Yergin, Phys. Rev. 98, 1296 (1955) - our reference (55 Na 1)] attributed to use of Leiss and Penfold data analysis instead of photon difference method.

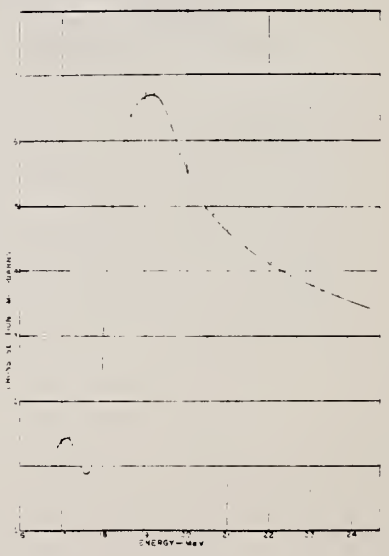

Fig. 5 Cross section for $Mg^{24}(\gamma,n)Mg^{23}$

Ref. F.R. Metzger, C.P. Swann, V.K. Rasmussen
Nuclear Phys. 16, 568 (1960)

Elem. Sym.	A	Z
Mg	24	12

Method: Protons from Bartol-ONR generator; (p,p'γ), etc. reactions for γ source; ring scatterer; NaI.

Ref. No.: 60 Me 1 JHH

Reaction	E or ΔE	E_o	Γ	$\int \sigma dE$	Jπ	Notes
(γ,γ)	1.37		$4.2 \pm 1.5 \times 10^{-4}$ ev		2^+	Assumed $f(\theta) = 1.25 - 3.75 \cos^2\theta + 5 \cos^4\theta$, corresponding to 0—2—0 spin sequence.

Ref. R.A. Tobin
Phys. Rev. 120, 175 (1960)

Elem. Sym.	A	Z
Mg	24	12

Method: Betatron; Mg absorber and scatterer; NaI

Ref. No.: 60 To 1 | JHH

Reaction	E or ΔE	E_o	Γ	$\int \sigma dE$	Jπ	Notes
$Mg^{24}(\gamma,\gamma)$	Bremss. 13.1		$4.80^{+1.56}_{-1.43}$ eV		1	E_{th} = 10.15±0.06 MeV Detector at 118°.

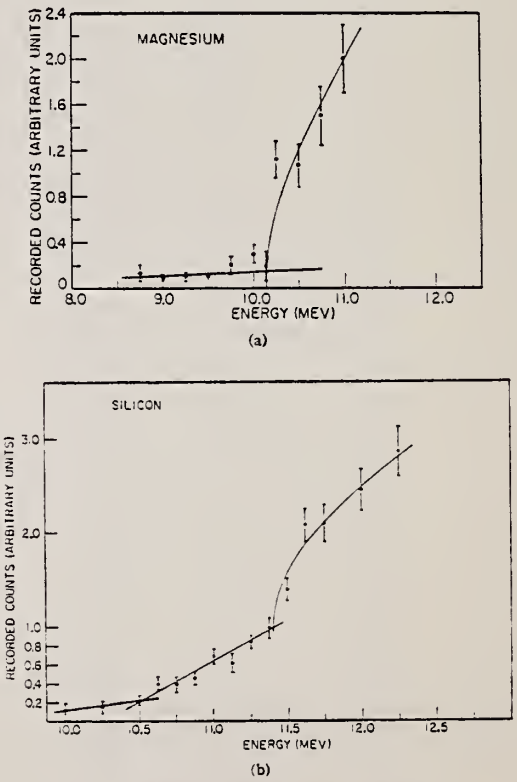

FIG. 4. Thresholds for the levels in Mg and Si.

Ref. H.E. Gove, A.E. Litherland, R. Batchelor
Nuclear Phys. 26, 480 (1961)

Elem. Sym.	A	Z
Mg	24	12

Method: Tandem accelerator; NaI

Ref. No.: 61 Go 1 EH

Reaction	E or ΔE	E_o	Γ	∫σdE	Jπ	Notes
$Na^{23}(p,\gamma)$	2.6-11.4	17.4	Γ_p=4.9MeV			E_{p_o} = ~ 6 MeV
		20.6	=4.9MeV			E_{p_o} ~ 9 MeV

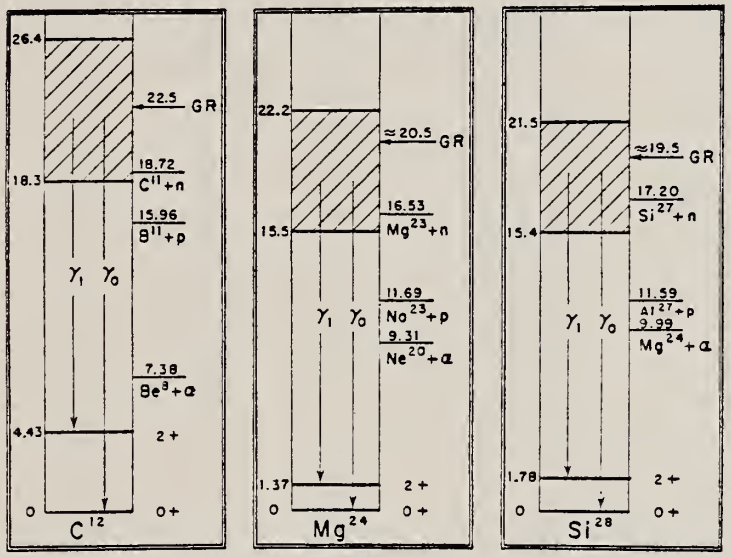

Fig. 1. Partial energy level diagrams for C^{12}, Mg^{24} and Na^{23} showing the region of excitation energy covered (shaded). the positions of the first excited states and the energies at which each nucleus becomes unstable against neutron, proton and alpha particle emission. The approximate position of the peak of the giant resonance (GR) is also indicated.

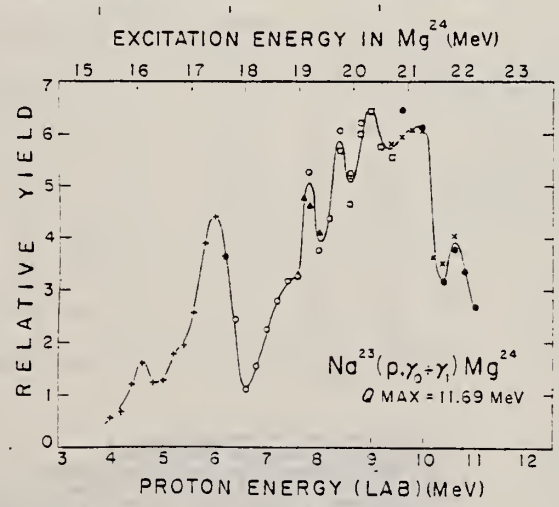

Fig. 19. The combined yield of gamma rays leading to the ground and first excited state of Mg^{24} resulting from proton capture in Na^{23} and measured at 90° to the incident beam. The different symbols on the yield curve represent separate runs. The abscissa is marked both in terms of the incident laboratory proton energy and in excitation energy in the compound nucleus Mg^{24}.

Ref. E.C. Booth, K.A. Wright
Nuclear Phys. 35, 472 (1962)

Elem. Sym.	A	Z
Mg	24	12

Method 4 MeV electron Van de Graaff; bremss.; nuclear resonance scattering, ring scatterer; NaI

Ref. No. 62 Bo 6 JHH

Reaction	E or ΔE	E_o	Γ	$\int \sigma dE$	Jπ	Notes
$Mg^{24}(\gamma,\gamma)$	Bremss. 0 - 4					

TABLE 2
Comparison of mean lifetime measurements

Nucleus	Energy	%	Spins	g	Γ_0/Γ	$W(\theta)$	τ × 10¹⁴ sec		
							This work	Other	
Li^6	3.56	7	$1^+ - 0$	$\frac{1}{2}$	(1)	1	0.012	0.0072 $^{+0.0015}_{-0.0013}$	[10]
								0.0105 ±0.001	[12]
B^{11}	2.14	81	$\frac{1}{2}^- - (\frac{1}{2})$	$\frac{1}{2}$	1	1	0.53	0.47 ±0.06	[14]
Al^{27}	2.21	100	$\frac{1}{2}^+ - \frac{1}{2}^-$	$\frac{1}{2}$	(1)	1	3.2	2.7 ±0.3	[15]
Al^{27}	1.01	100	$\frac{1}{2}^+ - \frac{1}{2}^+$	$\frac{1}{2}$	0.98	1	320	170 ±50	[15]
Si^{28}	1.78	92	$0^+ - 2^+$	5	1	0.63	88	73 ±22	[16]
S^{32}	2.24	95	$0^+ - 2^-$	5	1	0.63	26	≈16	[16]
Mg^{24}	1.37	78.6	$0^+ - 2^-$	5	1	0.63	220	155 ±40	[15]
Mg^{25}	1.61	25	$\frac{1}{2}^+ - \frac{1}{2}^-$	$\frac{1}{2}$	(1)	1	3.6	2.5 $^{+0.6}_{-0.4}$	[17]
Cu^{63}	0.963	69	$\frac{3}{2} - \frac{1}{2}$	$\frac{1}{2}$	1	0.92	230	72 ±18	[18]
								90 ±15	[18]
Cu^{63}	0.67	69	$\frac{1}{2} - \frac{1}{2}$	$\frac{1}{2}$	1	1	100	31 ±3	[18]

The factor g equals $(2I+1)(2I_0+1)^{-1}$.

10) R. C. Heim, Phys. Rev. 140 (1965) 1466
11) S. Vegors, L. Marsden and R. Heath, IDO-16870
12) Leslie Cohen and Ralph Tobias, Nuclear Physics 14 (1959) 542
13) W. C. Barber, F. Berthold, G. Friesia and F. E. Guddam, Phys. Rev. 120 (1960) 2128
14) F. R. Metzger, C. P. Swann and V. K. Rasmussen, Phys. Rev. 110 (1958) 906
15) F. R. Metzger, C. P. Swann and V. K. Rasmussen, Nuclear Physics 16 (1960) 568
16) S. Ofer and A. Schwarzschild, Phys. Rev. Lett. 3 (1959) 384
17) V. K. Rasmussen, F. R. Metzger and C. P. Swann, Phys. Rev. 123 (1961) 1386
18) J. B. Cummings, A. Schwarzschild, A. W. Sunyar and N. T. Porile, Phys. Rev. 120 (1960) 2123
19) T. Rothen, F. R. Metzger and C. P. Swann, Nuclear Physics 22 (1961) 505

Ref., P.W.M. Glaudemans, P.M. Endt
Nuclear Phys. 30, 30 (1962)

Elem. Sym.	A	Z
Mg	24	12

Method: Cockroft-Walton generator; NaI

Ref. No.: 62·Gl 1

Reaction	E or ΔE	E_o	Γ	$\int \sigma dE$	Jπ	Notes
(p,γ)	300-750 kev	12.18				E_{p_o} = 511 kev. 6% of decays are by this ground state transition. E_{p_o} resonances also at 308, 591, 676, 738 and 743 kev, but γ_o transitions ≤ 2.9%. Detector at 55°.

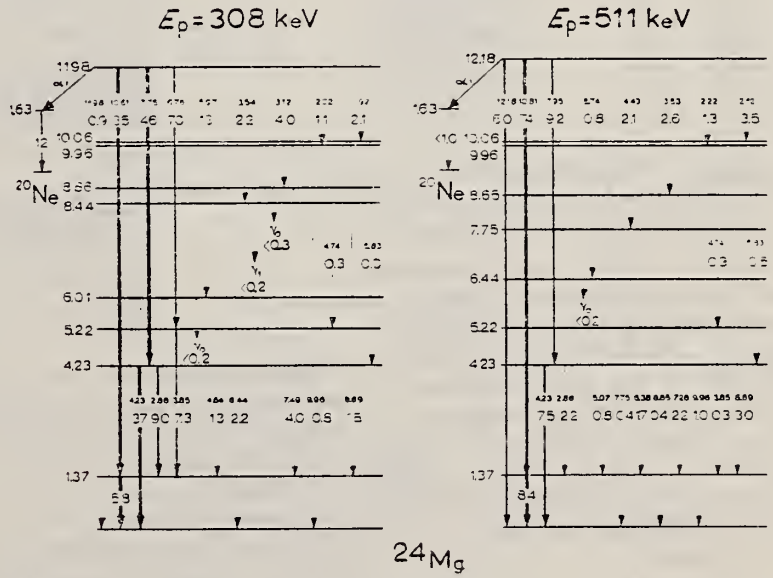

Fig. 4. Decay schemes of the ^{23}Na(p, γ)^{24}Mg resonances at E_p = 308 and 511 keV.

Ref. F.W. Prosser, Jr., W.P. Unruh, B.H. Wildenthal, R.W. Krone
Phys. Rev. 125, 594 (1962)

Elem. Sym.	A	Z
Mg	24	12

Method
[proton source not given]; NaI

Ref. No. 62 Pr 1 JHH

Reaction	E or ΔE	E_o
$Na^{23}(p,\gamma)$	0.58-1.42	12.532
		12.809
		12.819
		12.958

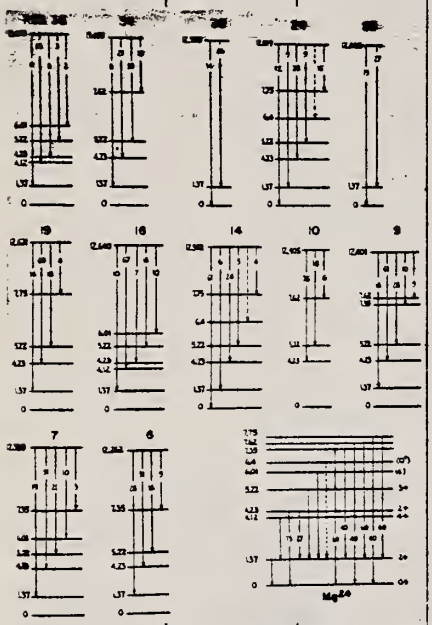

Fig. 1: Relative intensities and proposed cascades for 12 resonances in the reaction $Na^{23}(p,\gamma)Mg^{24}$. The numbering of the resonances is that proposed in ref. 6 [Prosser et al, Phys. Rev. 104, 369 (1956)]; the corresponding proton bombarding energies are listed in Table 1. The dashed lines represent transitions the existence of which are uncertain at that resonance.

TABLE I. Relative intensities of the γ rays observed at the resonances in the $Na^{23}(p,\gamma)Mg^{24}$ reaction. The relative intensities, with their standard errors, are given parenthetically following the energies of the γ rays and are in arbitrary units based on 100 for the strongest high-energy γ ray in the spectrum. The energies of the γ rays whose presence in the spectra are less certain or which were not fitted into a decay scheme are shown in italics.

Resonance	Proton energy (kev)	Excitation energy (Mev)	γ-ray energy (Mev) and relative intensity
6	594	12.262	10.89 (56±5); 8.03 (100±5); 7.04 (32±5); 6.05 (9±2); 4.90 (8±2); 4.23 (80±4); 3.85 (46±4); 2.86 (31±6); 1.37 (144±20)
7	675	12.338	10.97 (30±4); *8.30* (4±2); 8.10 (100±8); 7.35 (13±5); 7.11 (41±7); 6.32 (11±4); 5.98 (15±4); 4.98 (19±4); 4.64 (6±3); 4.23 (76±4); 3.85 (40±4); 2.86 (30±4); 1.37 (120±4)
9	740	12.401	11.03 (42±5); *9.2* (20±6); *8.8* (13±4); 8.17 (100±5); 7.62 (13±6); 7.35 (27±8); 7.18 (64±8); 6.30 (10±4); 5.98 (13±5); 5.05 (23±4); 4.78 (13±4); 4.23 (84±6); 3.85 (48±6); 2.86 (38±6); 1.37 (120±15)
10	744	12.405	8.18 (100±5); 7.18 (24±4); 6.29 (7±3); 4.75 (8±3); 4.23 (78±5); 3.85 (22±4); 2.86 (27±5); 1.37 (49±7)
14	877	12.532	12.53 (100±3); 11.16 (11±2); 9.3 (2±1); 8.30 (39±2); 7.72 (5±2); 7.31 (8±4); 6.30 (5±3); 6.00 (4±2); 5.00 (4±2); 4.80 (7±3); 4.23 (31±4); 3.85 (11±3); 2.86 (9±3); 1.37 (44±8)
16	989	12.640	11.27 (13±3); *9.4* (5±2); 8.52 (100±4); 7.45 (7±2); 6.60 (13±2); 4.62 (12±2); 4.23 (8±2); 3.85 (10±2); 2.75 (84±4); 1.37 (110±10)
19	1022	12.671	11.30 (24±3); 8.44 (100±4); 7.45 (30±4); 6.35 (6±2); 4.94 (14±3); 4.23 (85±5); 3.85 (29±4); 2.86 (25±3); 1.37 (94±10)
23	1166	12.809	12.81 (100±10); 11.44 (37±7)
24	1176	12.819	12.82 (100±10); 11.44 (21±4); 9.4 (12±4); 8.58 (66±5); 7.75 (13±6); 7.60 (13±6); 6.40 (37±7); 5.05 (38±7); 4.23 (70±20); 3.85 (12±5); 2.86 (25±8); 1.37 (94±15)
30	1321	12.958	12.96 (16±3); 11.59 (100±4); 1.37 (93±5)
34	1398	13.033	11.66 (14±2); 8.80 (55±4); 7.81 (100±8); 7.6 (6±3); 6.27 (11±3); 5.40 (19±4); 4.23 (42±5); 3.86 (99±8); 2.86 (27±5); 1.37 (160±16)
35	1419	13.053	11.68 (7±2); *10.1* (4±2); 8.93 (100±3); 4.60 (2±1); 4.23 (4±1); 3.85 (3±1); 2.75 (100±3); 1.37 (112±5)

[a] This resonance has been assigned energies from 869 keV to 877 keV in various studies. Using a thin target deliberately contaminated with F^{19}, we find that the resonance is 1.4±0.4 k above the strong resonance in $F^{19}(p,\alpha\gamma)O^{16}$ reaction.

Notes

14 Identification numbers assigned
23 to γ transitions to ground
24 state in Mg^{24}.
30

Data for these and other transitions are in Table II.

Detector at 55°.

TABLE II. Absolute yields of the reaction $Na^{23}(p,\gamma)Mg^{24}$. The thick target yields are those for an evaporated target of Na_2SO_4. The assumptions used in the calculation of $(2J+1)\Gamma_\gamma$ are discussed in the text.

Resonance	Thick-target yield (γ's/proton×10^{11})	ωγ (ev)	$(2J+1)\Gamma_\gamma$ (ev)
6	5.4	0.21	1.9
7	16.6	0.70	5.6
9	3.7	0.16	1.3
10	4.6	0.20	1.6
14	12.1	0.58	5.1
16	5.9	0.29	2.4
19	45.2	2.3	20
23	5.3	0.28	4.4[a]
24	28.4	1.5	17
30	146	7.9	63
34	34.7	1.9	22
35	92.5	5.1	81[a]

[a] Γ_p assumed to be 0.5Γ.

Ref.	Elem. Sym.	A	Z
W.C.Barber, J.Goldemberg, G.A.Peterson, Y.Torizuka Nuclear Phys. 41, 461 (1963); erratum to be published (as of 9/5/63)	Mg	24	12

Method	Ref. No.	
Linac (Stanford Mark II) - counter telescope	63Bal	BG

Reaction	E or ΔE	E_o	Γ	$\int \sigma dE$	Jπ	Notes
			eV			
(e,e')	41.5					Inelastic electron scattering cross section at 180°(cm^2/sr x10^{-32})
		11.0	21.0	1.76		4.4±20%
		~14	15.8	0.83		1.5±30%
						The rad. widths correspond to transitions from the 0^+ state to 1^+ excited states.
						*Mg has 3 isotopes. Most abundant $_{12}Mg^{24}$(78.8%). Observed structure attributed to this isotope.

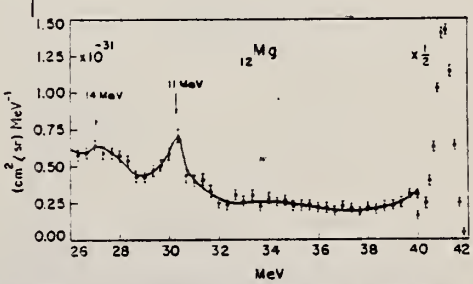

Fig. 12. Spectrum of 41.5 MeV electrons scattered from a magnesium target at 180°.

Ref. H.E. Gove
Nuclear Phys. 49, 279 (1963)

Elem. Sym.	A	Z
Mg	24	12

Method: Tandem accelerator; γ-ray yield, spectra; NaI

Ref. No.: 63 Go 3 JHH

Reaction	E or ΔE	E_o	Γ	$\int \sigma dE$	Jπ	Notes 942
$Na^{23}(p,\gamma)$	3.8-11.6	~ 15-23				Detector at 90°.

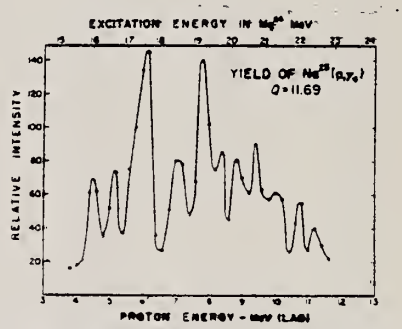

Fig. 2. The yield of gamma rays leading to the ground state of Mg^{24} from the reaction $Na^{23}(p,\gamma_0)Mg^{24}$ as a function of incident proton energy. Q = 11.69.

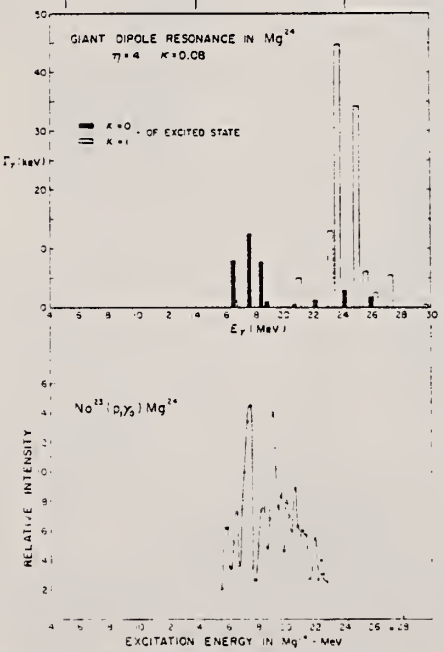

Fig. 5. A comparison between the experimental results for the $Na^{23}(p,\gamma_0)Mg^{24}$ reaction yield (lower half) and the predictions of Nilsson, Sawicki and Glendenning (upper half), where the Ferrell-Visscher exchange mixture correlations are included. See ref. [10].

10) S. G. Nilsson, J. Sawicki and N. K. Glendenning, Nuclear Physics 33 (1962) 239

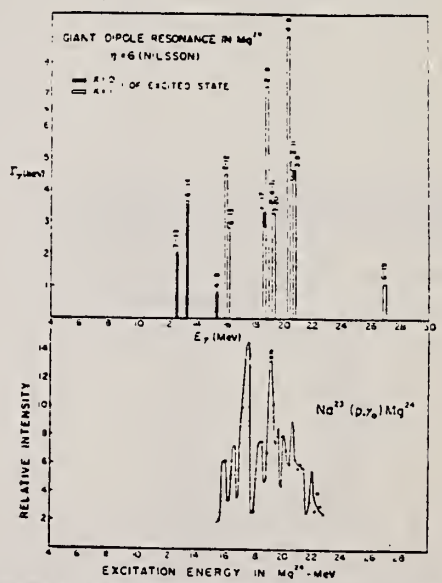

Fig. 4. A comparison between the experimental results for the $Na^{23}(p,\gamma_0)Mg^{24}$ reaction yield (lower half) and the predictions of the Nilsson model (upper half). Note 1. Orbit 7, 8 and 6 are "valence" orbits, 2 orbits 2, 3, 8 and 4 are "core" orbits, 3. 4 MeV pairing energy has been added to the Nilsson scale.

Ref. N.K. Sherman
Phys. Letters 4, 138 (1963)

Elem. Sym.	A	Z
Mg	24	12

Method emulsions

Ref. No. 63 Sh 3 JHH

Reaction	E or ΔE	E_o	Γ	$\int \sigma dE$	Jπ	Notes
$Mg^{24}(\gamma, C^{12*})$	Bremss. 70					Of 15 6-α events, at least two are consistent with $Mg^{24}(\gamma, C^{12*})C^{12*}$.

Ref. N. Yamamuro

J. Phys. Soc. Japan 18, 11 (1963)

Elem. Sym.	A	Z
Mg	24	12

Method
synchrotron; foils; emulsions

Ref. No. 63Ya1

BG

Reaction	E or ΔE	E_o	Γ	$\int \sigma dE$	Jπ	Notes
(γ,p)	bremss.: E_{pmax}= 21.5			(4.1×10^5 protons/ mole/roentgen; see Table I)		Energy distributions of p's (Figs. 1, 2, 4) Angular distributions fitted to $a + b\sin^2\theta$ (Table III, Fig. 3)

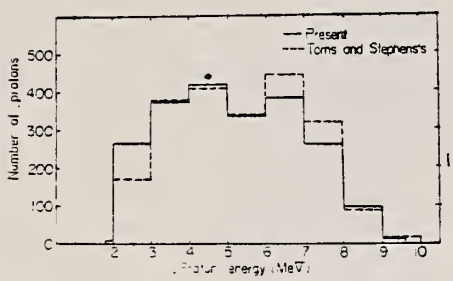

Fig. 1. Energy spectrum of photoprotons from Mg. (I) The solid line shows present and the dotted line is Toms and Stephens' result.

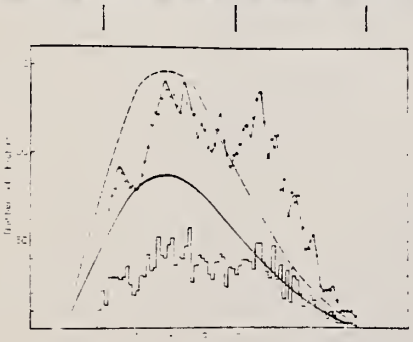

Fig. 2. Energy spectrum of photoprotons from Mg. (I) Histogram is shown as width of 100 KeV and solid line through black circles shows the smoothed spectrum averaged over the energy resolution of detection. The calculated distribution of the evaporative process is shown by the dotted curve and that multiplied by 0.6 is shown by the solid curve.

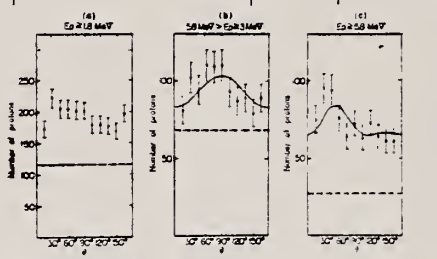

Fig. 3. Angular distributions of emitted protons from Mg.
a) all protons of energies above 1.4 MeV. b) protons of energy region from 3 to 5.8 MeV.
c) protons of energy region above 5.8 MeV.

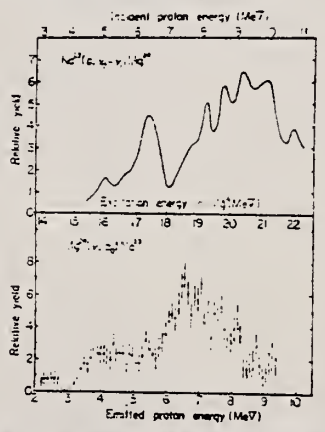

Fig. 4. The relative yield of $Mg^{24}(\gamma, p_0)$. Vertical lines represent the statistical error. The yield of $Na^{23}(p, \gamma_0+\gamma_1)$ is taken from Gove et al.'s result, which is measured at 90° to the incident beam.

Table I. Photoproton yield from magnesium.

Element	Yield (protons/mole/ roentgen)	Bremsstrahlung peak energy (Mev)	Ref.
Mg	7×10^5	23.5	8)
Mg	4.1×10^5	21.5	present
Mg	1.86×10^5	22.5	6)
Mg^{24}	1.74×10^5	24	6)

Table II. Abundance ratios and thresholds for (γ, p) reaction of the isotopes of magnesium.

	Abundance (%)	Threshold (MeV)
Mg^{24}	78.8	11.7
Mg^{25}	10.1	12.1
Mg^{26}	11.1	14.3

Table III. The ratios of unisotropic part to isotropic part in the angular distribution of protons. b/a is the ratio for all process and b/a' for direct process.

Proton energy (Mev)	b/a	b/a'
$5.8 > E_p \geq 3$	0.24 ± 0.04	1.33
$E_p \geq 5.8$	0.09 ± 0.02	0.15

REF. E. C. Booth, B. Chasan and K. A. Wright
Nucl. Phys. 57, 403-420 (1964)

ELEM. SYM.	A	Z
Mg	24	12

METHOD

REF. NO. 64 Bo 1 NVB

REACTION	RESULT	EXCITATION ENERGY	SOURCE		DETECTOR		ANGLE
			TYPE	RANGE	TYPE	RANGE	
G,G	LFT	1-3	C	1 - 3	NAI-D		100

ABI

TABLE 1
Cases of observed resonance fluorescence

Nucleus multipol.	State (MeV)	Spin	Γ_0/Γ	$T(g w \Gamma_0^2/\Gamma^2)^{-1}$ (sec).	Mean lifetime T BCW (sec)	Mean lifetime T other (sec)	Ref.	Γ_0/Γ_W BCW
Mg^{24}	0.00	0^+						
E2	1.37	2^+	1	$4.1\pm1.3\times10^{-13}$	$13\pm4\times10^{-13}$	$16^{+8}_{-4}\times10^{-13}$	10)	50
Mg^{24}	0.00	0^+						
E2[a])	1.83	2^+	1	$12\pm5\times10^{-14}$	$37\pm15\times10^{-14}$	$70\pm30\times10^{-14}$	11)	22

REF.

F. W. K. Firk and E. M. Bowey
Proc. Paris Conference 1013 (1964)

ELEM. SYM.	A	Z
Mg	24	12

METHOD

Linac

REF. NO.	
64 Fi 2	JDM

REACTION	RESULT	EXCITATION ENERGY	SOURCE		DETECTOR		ANGLE
			TYPE	RANGE	TYPE	RANGE	
G,N	RLY	18-26	C	27-32	TØF-D	1-9	

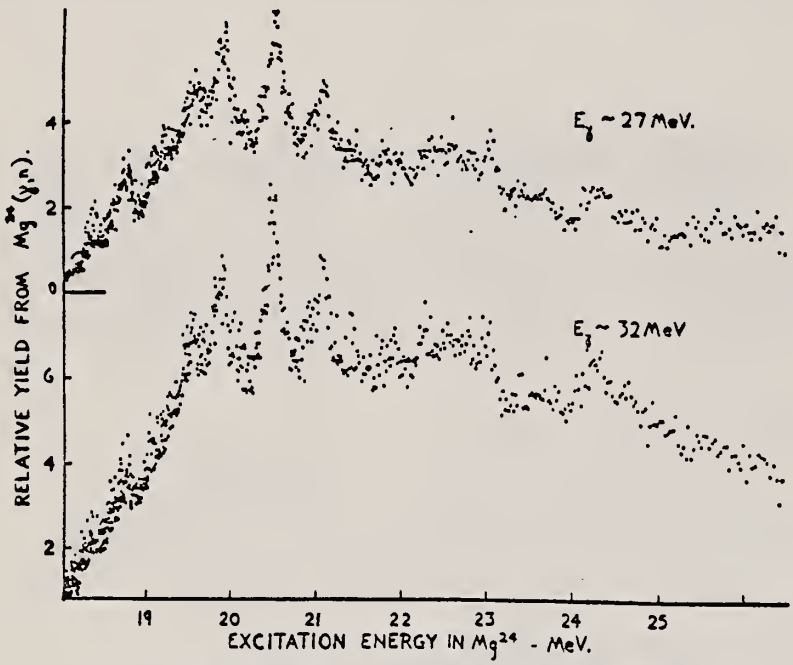

FIG. 1. — The observed relative yield of neutrons from Mg (γ, n) for bremsstrahlung energies of 27 and 32 MeV (assuming ground state transitions).

REF.

N. K. Sherman
Proc. Paris Conference 1051 (1964)

ELEM.	A	Z
Mg	24	12

METHOD

100 MeV Linac; $^{24}Mg(\gamma, ^{12}B)^{12}N$

REF. NO. 64 Sh 6 JDM

REACTION	RESULT	EXCITATION ENERGY	SOURCE		DETECTOR		ANGLE
			TYPE	RANGE	TYPE	RANGE	
G,F	ABY	THR-100	C	100	ACT-I		4PI

Y > 50 MeV-μb

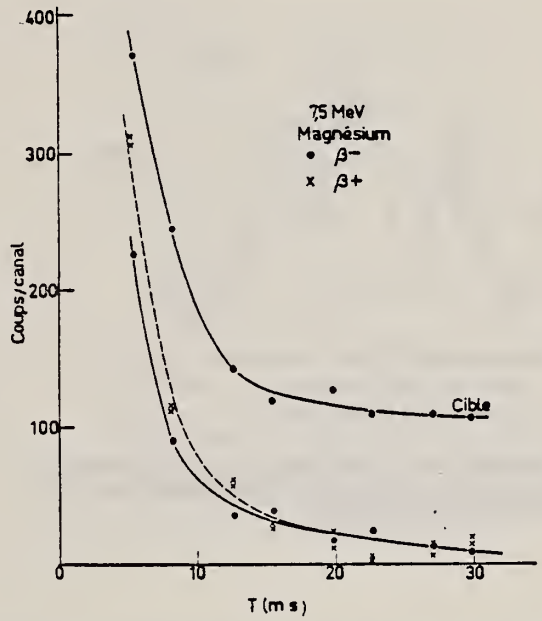

Fig. 1. — Comptages observés pendant des intervalles de 7 ms centrés à des temps T suivant l'impulsion de synchronisation de l'accélérateur.

REF. H. Artus, P. Brix, H. G. Clerc, F. Eigenbrod, A. Goldmann, F. Gudden, E. Spamer, P. Strehl, M. Stroetzel, O. Titze, and K. J. Wetzel
Proc. Gatlinburg Conference, 314 (1966)

ELEM. SYM.	A	Z
Mg	24	12

METHOD

REF. NO. 66 Ar 2 hmg

REACTION	RESULT	EXCITATION ENERGY	SOURCE		DETECTOR		ANGLE
			TYPE	RANGE	TYPE	RANGE	
E,E/	LFT	9-22	D	52	MAG-D		141

945

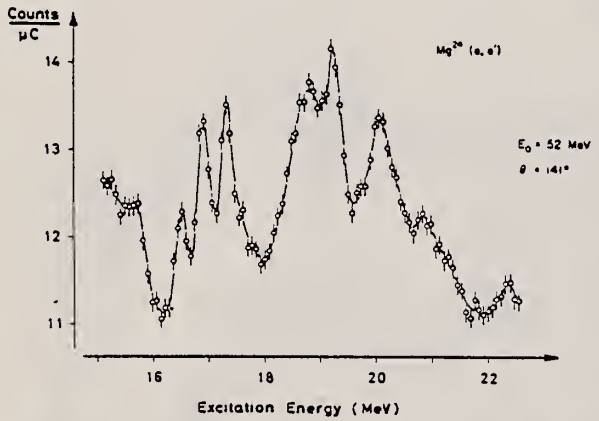

Fig. 1. Electron scattering from an isotopically enriched ^{24}Mg target in the giant resonance region. Note the suppressed zero of the ordinate scale. The elastic peak has 9.10^3 units of the ordinate scale.

TABLE 1

Summary of Experimental Results[a]

Nuclide	E_x (MeV)	Type	Γ_γ^0(eV)	Γ_γ^0/Γ_w	R_{tr} (F)
^{6}Li	2.18	E2	(3.9 ± 0.5) × 10^{-4}	14.4	3.77 ± 0.48
	3.56	M1	8.9 ± 0.4	9.4	2.96 ± 0.11
^{7}Li	11.28 ± 0.05	(M1) or	(1.3 ± 0.4)/g[b]	0.043/g	—
		(M2)	(0.026 ± 0.008)/g	2.6/g	—
^{9}Be	15.97 ± 0.03	M1	(3.7 ± 0.8)/g	0.043/g	—
^{11}B	4.46	E2 and	0.0173 ± 0.0021	8.2	3.44 ± 0.50
		M1	0.64 ± 0.08	0.34	2.60 ± 0.35
	5.04	M1	1.84 ± 0.14	0.69	2.60 ± 0.11
^{12}C	4.43	E2	0.0122 ± 0.0008	5.30	3.14 ± 0.30
^{16}O	6.92	E2	0.100 ± 0.015	3.28	3.82 ± 0.46
	11.52	E2	0.52 ± 0.13	1.31	—
^{24}Mg	9.85 ± 0.04	M1	7.95 ± 1.2	0.38	3.50 ± 0.49
	9.97 ± 0.03				
	10.35 ± 0.03	E2	0.24 ± 0.05	0.58	5.05 ± 0.50
	10.70 ± 0.03	M1	22.2 ± 2.4	0.86	3.60 ± 0.36
	10.93 ± 0.04	E2	0.26 ± 0.11	0.50	—
^{28}Si	4.97 ± 0.02	C0	(2.0 ± 0.5) × 10^{-5}[c]	—	6.90 ± 1.20
^{40}Ca	6.89 ± 0.05	E2	0.29 ± 0.04	2.85	4.60 ± 0.50

[a] The Born approximation has been used except for ^{16}O and ^{40}Ca.
[b] $g = (2I_f + 1)/(2I_i + 1)$.
[c] $\Gamma_e^{\pm}$ equivalent to ME = (8.87 ± 1.00) F^2.

REF. B. S. Ishkhanov, I. M. Kapitonov, V. G. Shevchenko and B. A. Yur'ev
Izv. Akad. Nauk Fiz. 30, 378 (1966)
Bull. Acad. Sci. USSR-Phys. 30, 383 (1966)

ELEM. SYM.	A	Z
Mg	24	12

METHOD

REF. NO. 66 Is 1 EGF

REACTION	RESULT	EXCITATION ENERGY	SOURCE		DETECTOR		ANGLE
			TYPE	RANGE	TYPE	RANGE	
G,P	ABX	THR-34	C	15-30	EMU-D	2-14	DST

771

Fig.1. Energy distribution of photoprotons from magnesium irradiated with $E_{\gamma max}$ = 23 MeV bremsstrahlung.

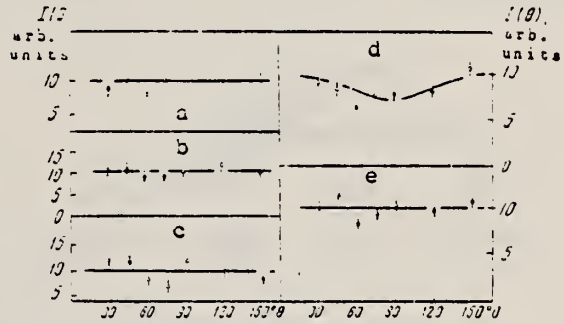

Fig.3. Angular distributions of photoprotons from magnesium irradiated with $E_{\gamma max}$ = 23 MeV bremsstrahlung. The different curves are for photoprotons with energies in the following ranges (in MeV): a) 3.8-4.5, b) 4.6-5.5, c) 5.6-6.6, d) $\geqslant$ 6.7, e) $\geqslant$ 1.9.

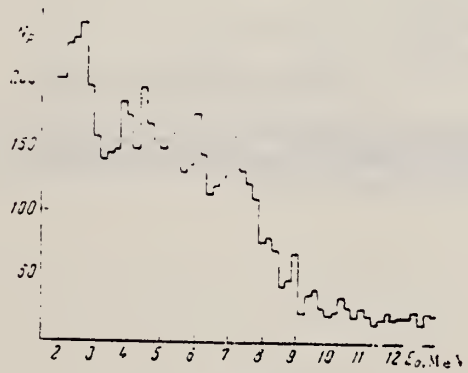

Fig.2. Energy distribution of photoprotons from magnesium irradiated with $E_{\gamma max}$ = 34 MeV bremsstrahlung.

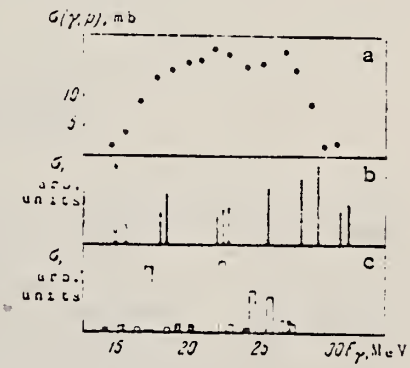

Fig.4. Photoproton production cross sections of magnesium: a - the present measurements; b - calculated cross sections of Ref. 3; c - calculated cross sections of Ref. 2.

REF.

J. Miller, C. Schuhl, G. Tamas, C. Tzara
J. de Physique 27, 8 (1966)

ELEM. SYM.	A	Z
Mg	24	12

METHOD

REF. NO.: 66 Mi 2 egf

REACTION	RESULT	EXCITATION ENERGY	SOURCE		DETECTOR		ANGLE
			TYPE	RANGE	TYPE	RANGE	
G,N	ABX	16-27	D	16-27	BF3-I		4PI

324

TABLEAU V

σ_{int} à 26 MeV en MeV.mb

	^{16}O	^{40}Ca	^{12}C	Mg
γ, n	$41{,}5 \pm 4$	73 ± 7	$29{,}4 \pm 3$	58 ± 6

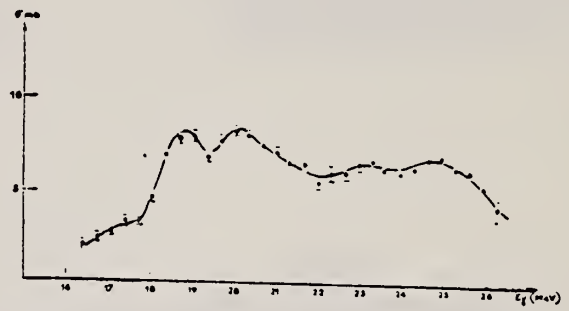

FIG. 4. — $\sigma(\gamma, n)$ dans ^{24}Mg. Points expérimentaux de mai 1963. La courbe tient compte de la largeur finie de la raie de photons (400 keV).

REF. O. Titze and E. Spamer
Z. Naturforschg. 21a, 1504 (1966)

ELEM. SYM.	A	Z
Mg	24	12

METHOD

REF. NO. 66 Ti 1 egf

REACTION	RESULT	EXCITATION ENERGY	SOURCE TYPE	SOURCE RANGE	DETECTOR TYPE	DETECTOR RANGE	ANGLE
E,E/	LFT	7-15	D	51	MAG-D	36-51	DST

Angular distribution measured for q = 0.48, 0.41, 0.32 fm^{-1}.

DST CONST Q

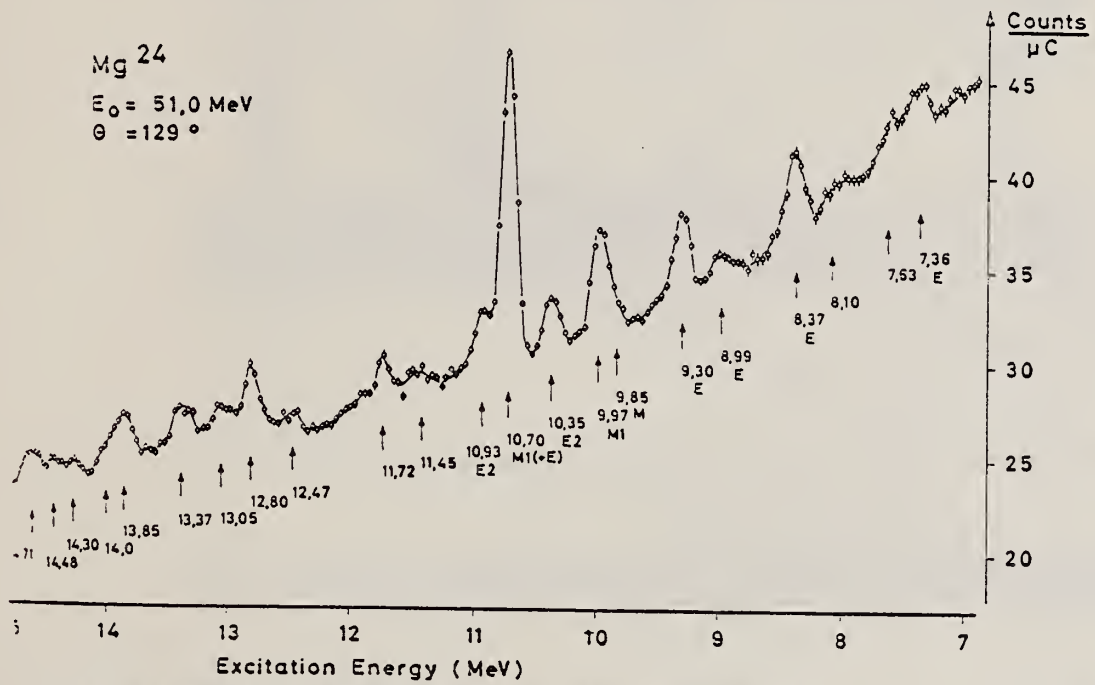

Fig. 1. Spectrum of inelastically scattered electrons from ^{24}Mg. The effective target thickness was 50 mg/cm². The arrows indicate the measured excitation energies in MeV. The type of transition [electric (E) or magnetic (M)] is labeled. Note the suppressed zero of the ordinate scale. The elastic peak has a height of 2.4×10^4 units of the ordinate scale.

E_x (MeV)		Γ_γ^0 (eV)	Γ_γ^0/Γ_W	R_{tr} (fm)
9.85 ± 0.04 9.97 ± 0.03	M1	7.95 ± 1.2	0.38	3.50 ± 0.49
10.35 ± 0.03	E2	0.24 ± 0.05	0.58	5.05 ± 0.50
10.70 ± 0.03	M1	22.2 ± 2.4	0.86	3.60 ± 0.36
10.93 ± 0.04	E2	0.26 ± 0.11 *	0.50	—

* Calculated with R_{tr} from 10.35 MeV transition.

Table 1. Results for ^{24}Mg. The first two columns give excitation energies and multipolarities as determined from this work. Column 3 to 5 show the ground state radiation widths Γ_γ^0, the transition strengths in Weisskopf units Γ_W and the transiton radii R_{tr}. The Bohr approximation has been used.

[over]

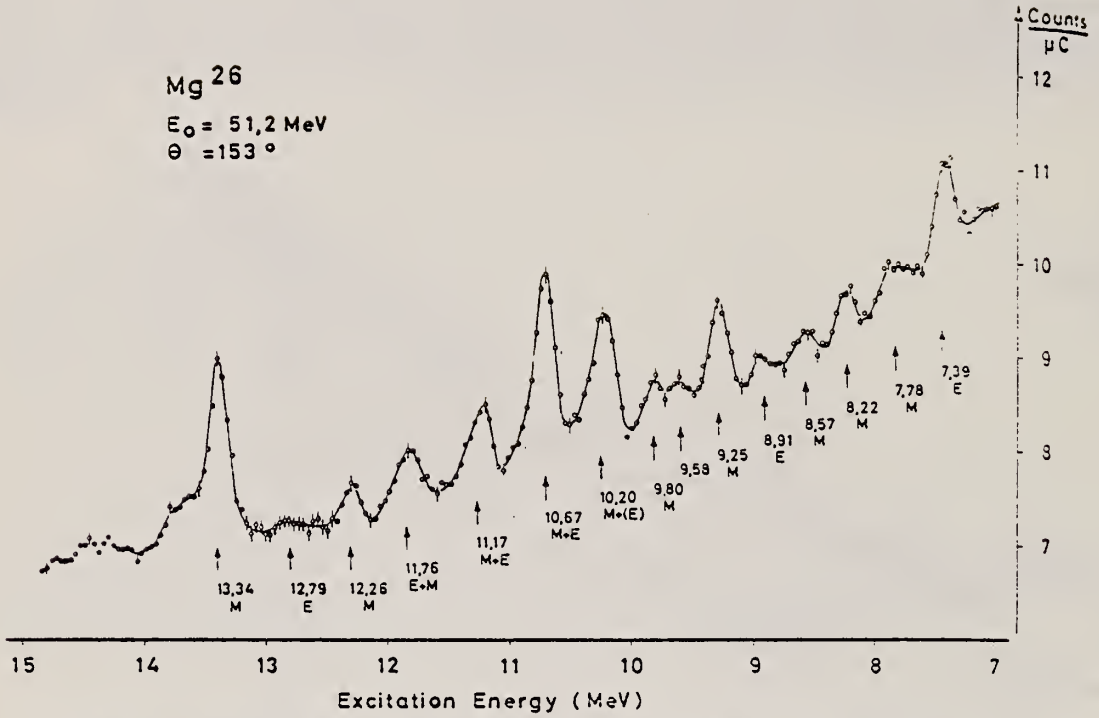

Fig. 2. Spectrum of inelastically scattered electrons from ^{26}Mg. The effective target thickness was 170 mg/cm^2. The arrows indicate the measured excitation energies in MeV. The type of transition [electric (E) or magnetic (M)] is labeled. Note the suppressed zero of the ordinate scale. The elastic peak has a height of 2.5×10^3 units of the ordinate scale.

REF. H. W. Kuehne, P. Axel, and D. C. Sutton
Phys. Rev. 163, 1278 (1967)

ELEM. SYM.	A	Z
Mg	24	12

METHOD

REF. NO. 67 Ku 2 HMG

REACTION	RESULT	EXCITATION ENERGY	SOURCE		DETECTOR		ANGLE
			TYPE	RANGE	TYPE	RANGE	
G,G	LFT	9-11	D	9-11	NAI-D	9-11	135

Photons, defined in energy to about 1% with the aid of a bremsstrahlung monochromator, were scattered by isolated energy levels in C, Mg, and Si. Parameters for the six observed levels are:

Isotope	Energy (MeV)	Γ_0^2/Γ (eV)	Γ_0/Γ	$B(M1)/(e\hbar/2M_pc)^2$
C^{13}	15.11	36	1	0.93
Mg^{24}	10.66±0.02	14	0.8	1.21
Si^{28}	11.42±0.02	23	1	1.33
Si^{28}	12.33±0.03			
Mg^{24}	9.92±0.03	3.0	0.5	0.49
Mg^{26}	10.07±0.05	4.2		≥0.36

The 15.11-MeV level in C^{13}, the 9.92- and 10.66-MeV levels in Mg^{24}, and the 11.42-MeV level in Si^{28} are $T=1$, $T_z=0$ analogs of low-lying 1+ states in the neighboring odd-odd nuclei. These levels exhaust most of the magnetic dipole transition strength of the respective nuclei, and therefore give information about the expectation value of l·s in the ground state.

REF. J. R. Leslie and I. G. Main
Nuovo Cimento 50B, 389 (1967)

ELEM. SYM.	A	Z
Mg	24	12

METHOD

REF. NO.	
67 Le 1	egf

REACTION	RESULT	EXCITATION ENERGY	SOURCE		DETECTOR		ANGLE
			TYPE	RANGE	TYPE	RANGE	
P,G	ABX	16-25	D	5-14	MGP-D	8-25	90

943

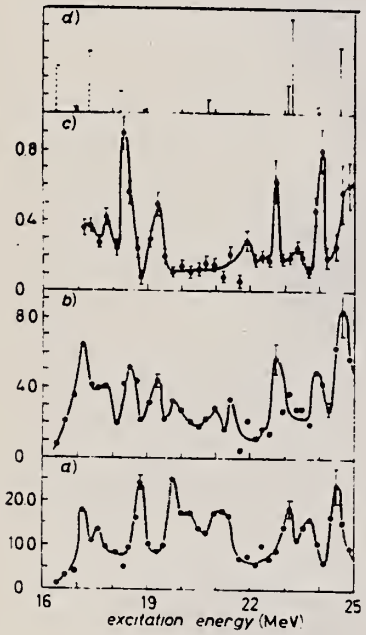

Fig. 2. - *a*) The 90° yield for the reaction $^{23}Na(p, \gamma_1)^{24}Mg$ as a function of excitation energy in ^{24}Mg. The ordinate unit is μb/sr. *b*) As *a*) for the reaction $^{23}Na(p, \gamma_0)$. *c*) The ratio of these two yields. *d*) The results of one of the calculations by NILSSON *et al.*(7), using a Ferrell-Visscher interaction and considering ground-state correlations. —— $K = 1$, — — — $K = 0$.

REF. O. Titze, E. Spamer and A. Goldmann
Phys. Letters 24B, 169 (1967)

ELEM. SYM.	A	Z
Mg	24	12

METHOD

REF. NO. 67 T1 1 EGF

REACTION	RESULT	EXCITATION ENERGY	SOURCE		DETECTOR		ANGLE
			TYPE	RANGE	TYPE	RANGE	
E,E/	SPC	15-26	D	45-54	MAG-D		DST

944

Spectrometer resolution 145-180 keV.

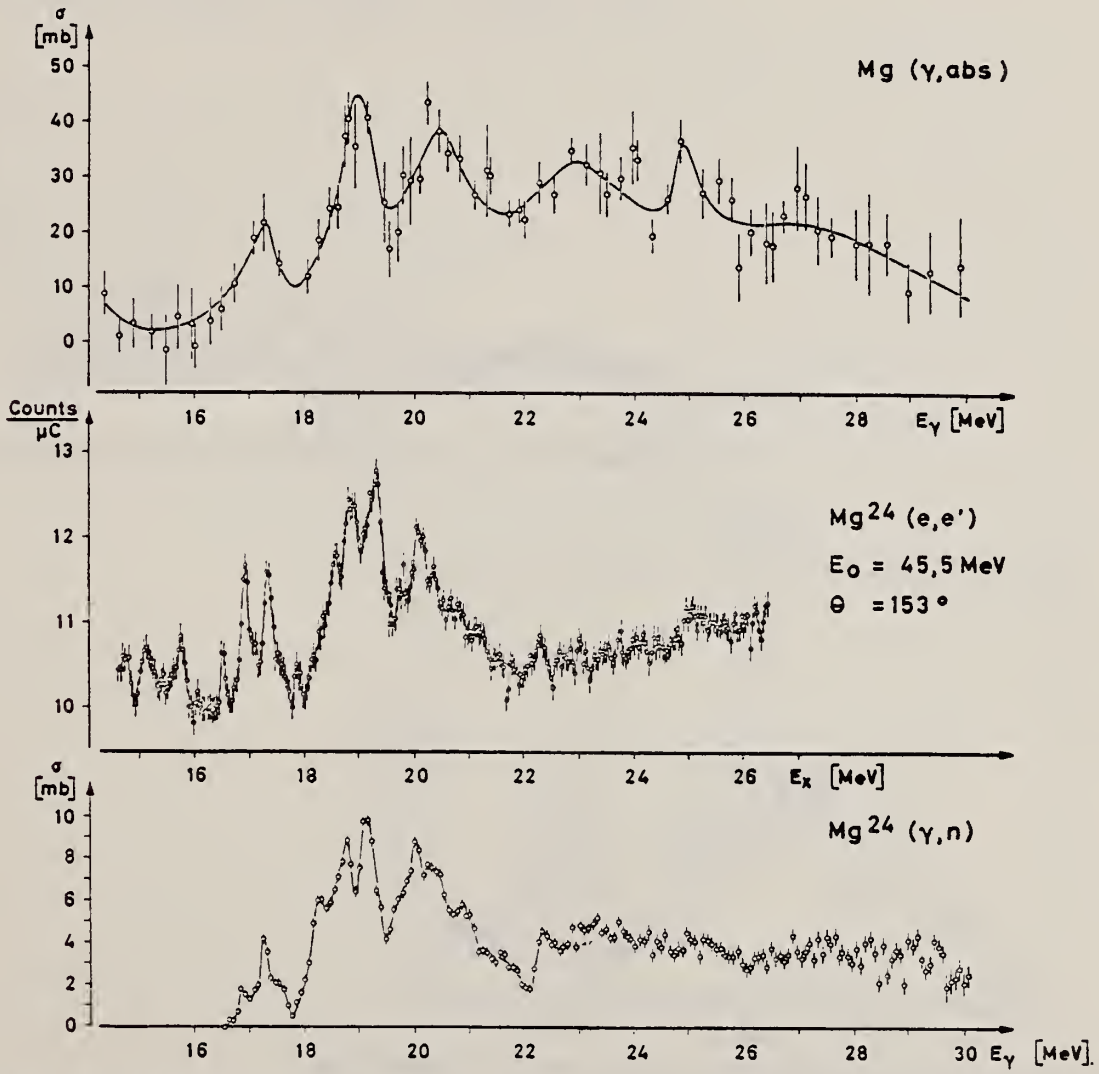

Fig.1. Giant resonance of ^{24}Mg. The upper part gives the photonuclear cross section for natural magnesium [2], the lower the photoneutron cross section of ^{24}Mg [3]. The center shows a spectrum of inelastically scattered electrons. Note the suppressed zero of the ordinate scale. The effective target thickness was 86 mg/cm^2. The height of the elastic peak is 8×10^3 units of the ordinate scale. E_x, E_γ are excitation energy and photon energy, respectiveiy.

REF. R. C. Bearse, L. Meyer-Schutzmeister and R. E. Segel
Nucl. Phys. A116, 682 (1968)

ELEM. SYM.	A	Z
Mg	24	12

METHOD

REF. NO.

 68 Be 3 egf

REACTION	RESULT	EXCITATION ENERGY	SOURCE		DETECTOR		ANGLE
			TYPE	RANGE	TYPE	RANGE	
P,G	ABX	16-24	D	4-13	NAI-D	16-24	DST

798+

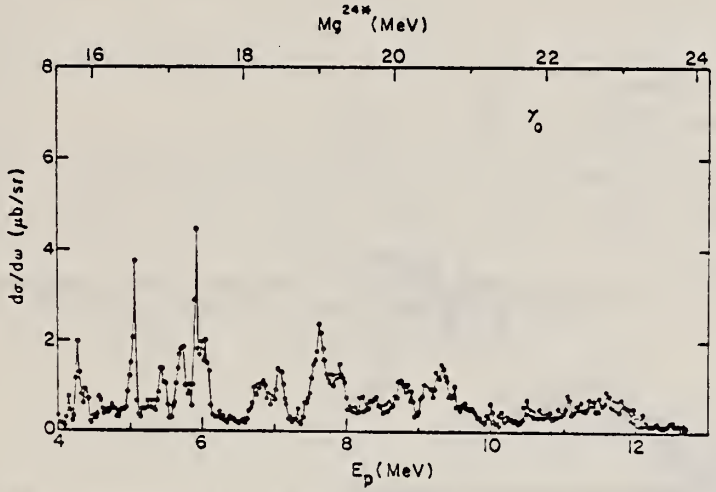

Fig. 2. Yield curve at 90° of the ground-state gamma ray from the $^{23}Na(p,\gamma)$ reaction.

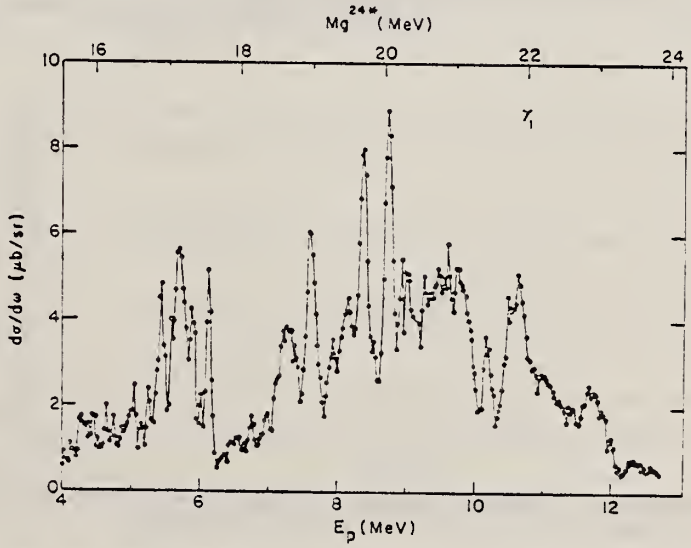

Fig. 3. Yield curve at 90° of the gamma ray to the 1.37 MeV first excited state in ^{24}Mg from the ^{23}Na (p,γ) reaction.

[over]

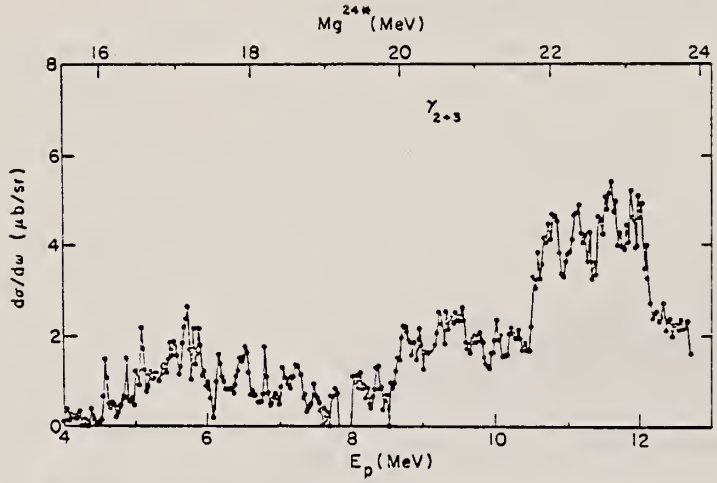

Fig. 4. Yield curve at 90° of the (unresolved) gamma rays feeding the doublet at 4.12 and 4.23 MeV in ^{24}Mg from the ^{23}Na(p,γ) reaction.

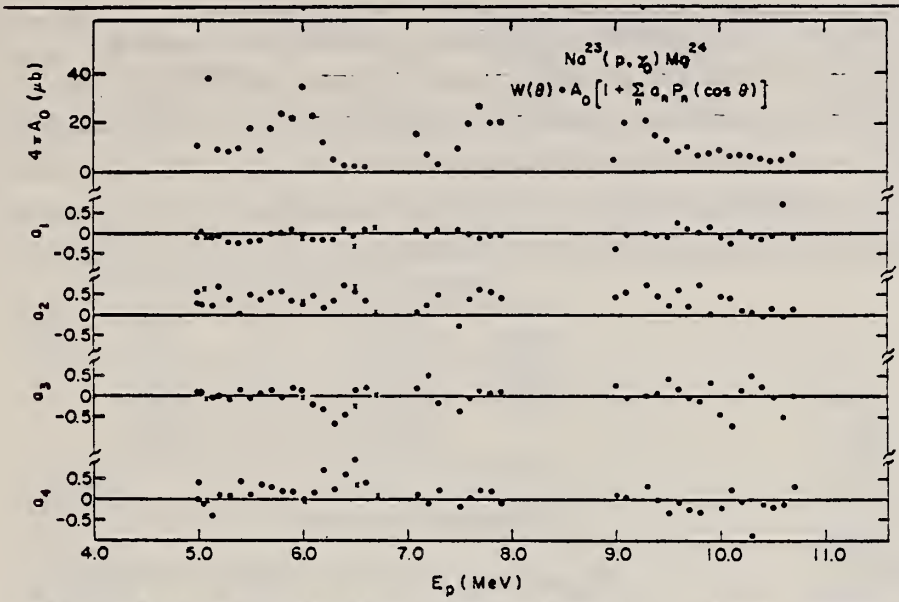

Fig. 10. Coefficients obtained in fitting series of Legendre polynomials to the angular distributions for $^{23}Na(p,\gamma_0)^{24}Mg$. The data were taken with 100 keV resolution.

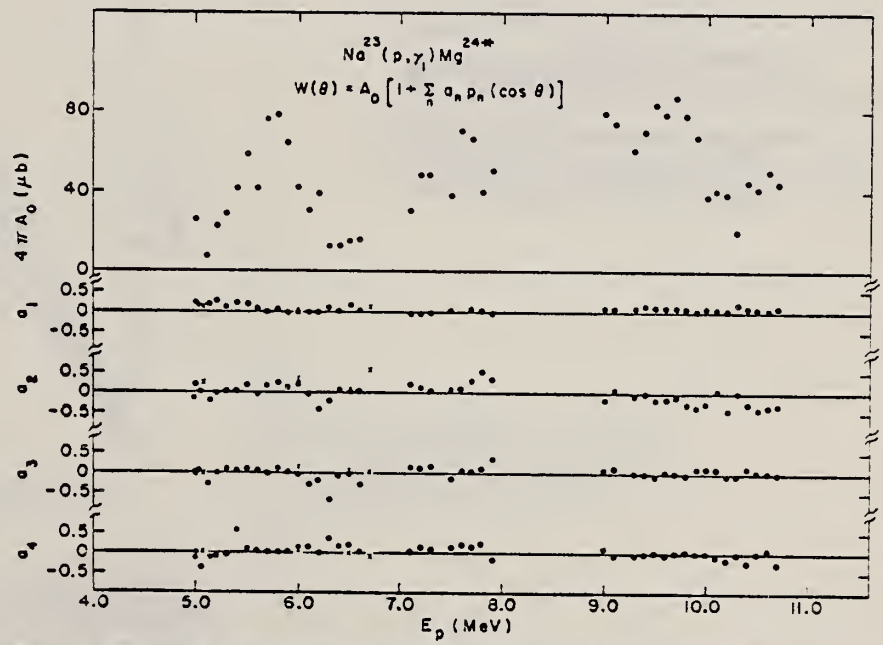

Fig. 11. Coefficients obtained in fitting series of Legendre polynomials to the angular distributions for $^{23}Na(p,\gamma_1)^{24*}Mg$. The data were taken with 100 keV resolution.

REF. B. C. Cook, D. W. Anderson, T. J. Englert
Phys. Letters 26B, 341 (1968)

ELEM. SYM.	A	Z
Mg	24	12

METHOD

REF. NO.	
68 Co 1	HMG

REACTION	RESULT	EXCITATION ENERGY	SOURCE		DETECTOR		ANGLE
			TYPE	RANGE	TYPE	RANGE	
G,N	RLX	THR- 65	C	13-65	ACT-I		4PI

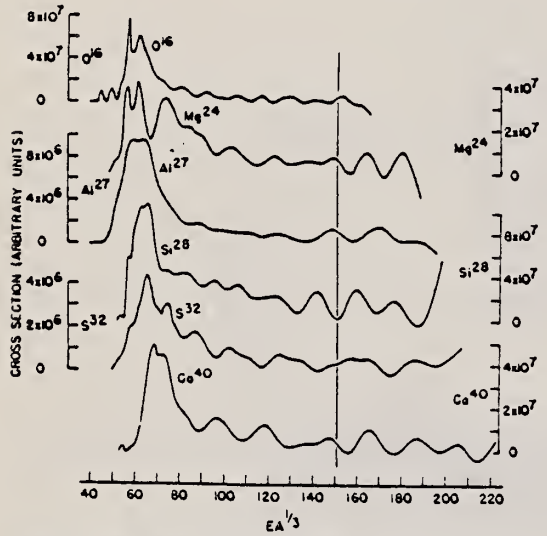

Fig. 1. Cross section for elements in the s-d shell as a function of $EA^{1/3}$. The vertical line is only an aid to the eye. Universal curves expected for the hydrodynamical model are not evident.

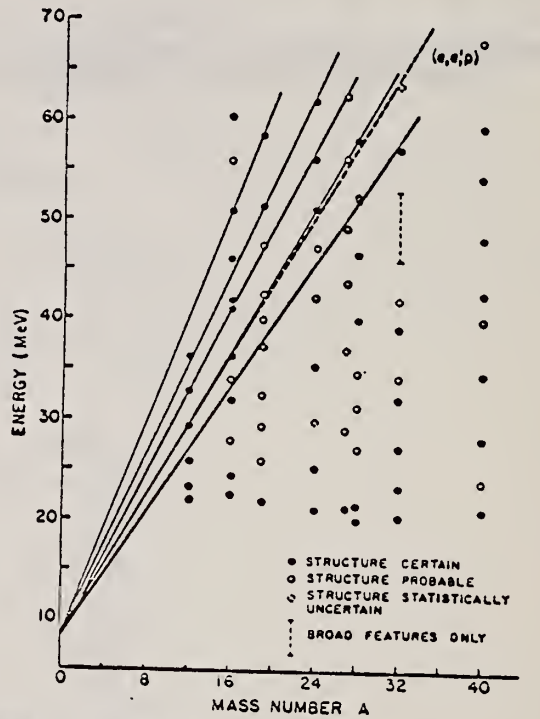

Fig. 2. A dependence of structure. A qualitative estimate for the statistical validity for structure is also indicated. The solid straight lines have the form mA + + 8 MeV while the dashed line represents the position of the 1s level as determined from (e,e'p) experiments.

REF. L. W. Fagg, W. L. Bendel, R. A. Tobin and H. F. Kaiser
Phys. Rev. 171, 1250 (1968)

ELEM. SYM.	A	Z
Mg	24	12

METHOD

FOR REANALYSIS OF THIS DATA SEE: 70 Fa 1

REF. NO. 68 Fa 1 egf

REACTION	RESULT	EXCITATION ENERGY	SOURCE		DETECTOR		ANGLE
			TYPE	RANGE	TYPE	RANGE	
E,E/	LFT	7-28	D	39,56	MAG-D	28-56	180

DETAILS 9.9; 10.7

TABLE I. Values of transition widths and radii.

Transition parameter	Energy (MeV)	Present work	Titze and Spamer[a]	Kuehne *et al.*[b]
Γ(eV)	9.94±0.03	11.9±2.7	7.95±1.2	5.6±3.0[c]
	10.70±0.03	18.9±3.7	22.2 ±2.4	17.0±4.0
R(F)	9.94±0.03	3.5±0.2	3.50±0.49	
	10.70±0.03	3.0±0.2	3.60±0.36	

[a] Reference 6.
[b] Reference 5.
[c] Error not given by authors; it is estimated here from information given in Ref. 5.

[5] H. W. Kuehne, P. Axel, and D. C. Sutton, Phys. Rev. 163, 1278 (1967).
[6] O. Titze and E. Spamer, Z. Naturforsch. 21a, 1504 (1966).
[7] M. Rosen, R. Raphael, and H. Überall, Phys. Rev. 163, 927 (1967).

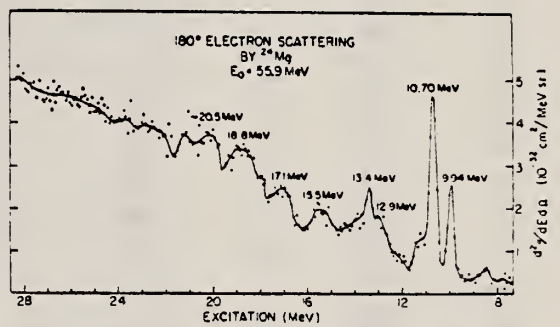

FIG. 1. Differential cross section for 180° electron scattering from ^{24}Mg at E_0 = 55.9 MeV covering the excitation energy range from about 7 to 28 MeV.

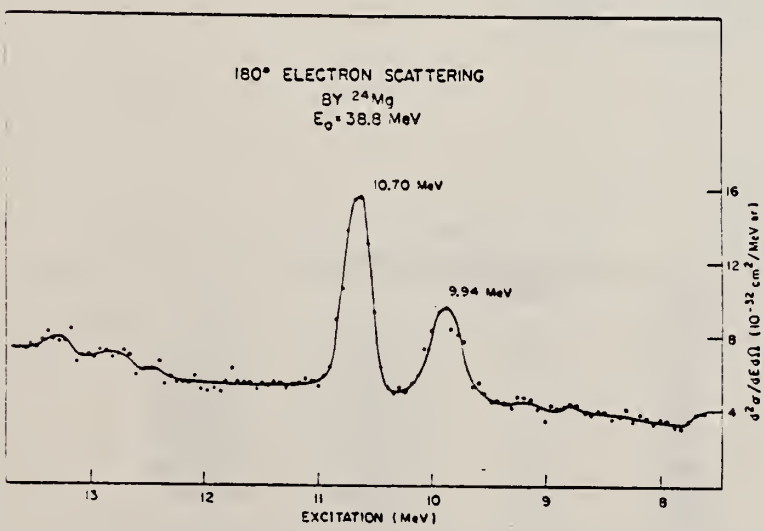

FIG. 2. Differential cross section for 180° electron scattering from ^{24}Mg at E_0 = 38.8 MeV covering the excitation energy range from 8 to 14 MeV.

REF.
G. J. Highland and T. T. Thwaites
Nucl. Phys. A109, 163 (1968)

ELEM. SYM.	A	Z
Mg	24	12

METHOD

REF. NO. 68 Hi 1 EGF

REACTION	RESULT	EXCITATION ENERGY	SOURCE		DETECTOR		ANGLE
			TYPE	RANGE	TYPE	RANGE	
A,G	RLX	11-14	D	3-6	NAI-D	7-16	DST

J-PI, G-WIDTH

TABLE 1

Resonances in $^{20}Ne(\alpha,\gamma)^{24}Mg$ reaction

E_α (MeV)	E_x (MeV) [a]	J^π	γ_0	γ_1	$\gamma_2+\gamma_3$	$(2J+1)\Gamma_\alpha\Gamma_\gamma/\Gamma$ (eV)
3.056	11.863	1^-	1	0.7		2.4 [c]
3.187	11.972	2^+	0.3	1		0.7 [c]
3.245	12.020		<0.3	1		2.0
3.289	12.057		<0.05	<0.2	1	≦33 [d]
3.422	12.168	$(2^+, 4^+)$	<0.3	1	0.9	5.8
3.715	12.412		<0.2	<0.2	1(γ_3)	20
3.792	12.476	2^+	0.4	1		2.3
3.836	12.513	$(2^+, 4^+)$	<0.3	1	0.3	7.3
3.920	12.583	2^+	1	0.1	0.1	0.9
3.997	12.647		<0.03	<0.2	1	12
4.109	12.740	2^+	0.7	1	0.2	0.7
4.193	12.810	2^+	1	0.4		1.8
4.483	13.052		<0.04	<0.1	1	25
4.528	13.089	2^+	1	0.07	0.7	2.0
4.913	13.410	$(1^-, 2^+)$	0.09	1		2.9
(4.944) [b]	(13.436)					
5.653	14.026	1^-	0.6	1		12
5.720	14.082		<0.07	<0.3	1(γ_2)	9.8
5.743 [b]	14.101					
5.796	14.146		<0.07	<0.2	1(γ_2)	12
6.017	14.330	$2^+, 3^-, 4^+$	<0.07	0.36	1(γ_2)	10
all ±5 keV						all ±50 %

[a]) Calculated using $Q = 9.317$ MeV, ref. [22]).
[b]) Energy uncertainty ±10 keV.
[c]) Ref. [14]).
[d]) See subsect. 3.3.

TABLE 2

Angular distribution coefficients

E_x (MeV)	Transition	A_2	A_4
3.245	γ_1	+0.07±0.10	+0.03±0.13
3.422	γ_1	+0.47±0.14	−0.30±0.18
3.715	γ_3	+0.47±0.04	−0.04±0.06
3.836	γ_1	+0.49±0.04	−0.42±0.06
3.920	γ_0	+0.42±0.30	−2.05±0.43
4.109	γ_1	+0.56±0.22	−0.42±0.28
4.913	γ_1	+0.31±0.13	−0.11±0.17
5.653	γ_0	−0.99±0.13	
5.720	γ_2	+0.38±0.09	−0.17±0.11

REF. Y. Oka, T. Kato and A. Yamadera
Bull. Chem. Soc. Japan 41, 1606 (1968)

ELEM. SYM.	A	Z
Mg	24	12

METHOD

REF. NO. 68 Ok 2 egf

REACTION	RESULT	EXCITATION ENERGY	SOURCE		DETECTOR		ANGLE
			TYPE	RANGE	TYPE	RANGE	
G,N	ABY	THR-20	C	20	ACT-I		4PI

ISOMERIC YIELD

TABLE 1. THE PARTICULARS OF THE (γ,n) REACTION PRODUCTS AND THE DATA OBTAINED WITH 20 MeV BREMSSTRAHLUNG

Nuclide		Half-life of product (sec)	Gamma-ray determined			Limit of detection (μg)	Yield ($mol^{-1} \cdot R^{-1}$)
Parent (Natural abundance, %)	Residual		Energy (MeV)	Branching ratio (%)	Photopeak activity (cpm/mg)[a]		
$^{24}Mg(78.60)$	^{23}Mg	9.9	0.511	200	2.04×10^{6}	0.49	8.1×10^{4}
$^{76}Ge(7.67)$	^{75m}Ge	48	0.139	100	6.37×10^{5}	1.6	1.1×10^{4}
$^{78}Se(23.52)$	^{77m}Se	17	0.162	100	1.82×10^{6}	0.55	1.2×10^{4}
$^{92}Mo(15.86)$	^{91m}Mo	65	0.650	57	2.22×10^{5}	4.5	2.7×10^{4}
$^{140}Ce(88.48)$	^{139m}Ce	58	0.745	100	1.06×10^{6}	0.95	1.3×10^{4}
$^{142}Nd(27.13)$	^{141m}Nd	64	0.760	100	3.19×10^{5}	3.1	1.4×10^{4}
$^{159}Tb(100)$	^{158m}Tb	11	0.111	100	2.56×10^{5}	3.8	2.2×10^{4}

a) The value corrected at the end of one-minute irradiation with the dose rate of 10^{7} R/min; Counting geometry is 20% with a 3"dia.×3"NaI(Tl) detector.

REF. D. W. Anderson, B. C. Cook and T. J. Englert
Nucl. Phys. A127, 474 (1969)

ELEM. SYM.	A	Z
Mg	24	12

METHOD

REF. NO. 69 An 2 egf

REACTION	RESULT	EXCITATION ENERGY	SOURCE TYPE	SOURCE RANGE	DETECTOR TYPE	DETECTOR RANGE	ANGLE
G,XN	ABX	THR-65	C	16-64	ACT-I		4PI
							321

MEAS TOT ACT

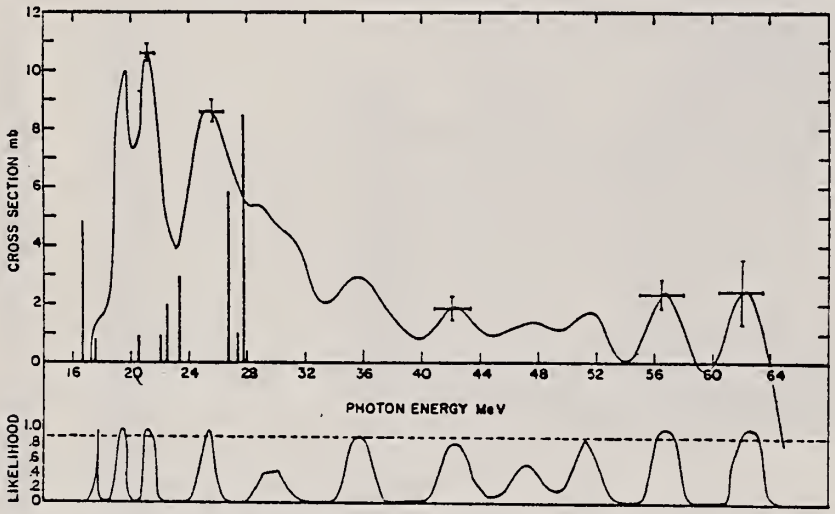

Fig. 2. The least structure cross-section solution for $\sigma_n + 0.6\,\sigma_{2n}$. The coefficient for σ_{2n} results because the experimental timing cycle used was less efficient for accumulating yield data for $^{23}Mg(\tau_{\frac{1}{2}} = 3.9$ sec) than for $^{23}Mg(\tau_{\frac{1}{2}} = 11.2$ sec). A likelihood estimate for the statistical significance of peaks is also shown. Peaks with likelihood of 0.9 are considered significant. The vertical lines represent Γ_γ of the strongest transitions of a calculation by Bassichis and Scheck [23]).

[23] W.H.Bassichis and F.Scheck, Phys.Lett.19 (1965)509.

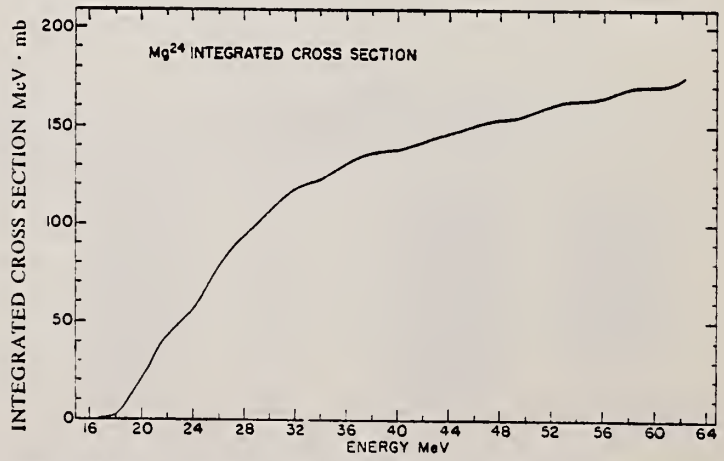

Fig. 3. The integrated cross section $\Sigma(E) = \int_0^E (\sigma_n + 0.6\,\sigma_{2n})dE$ shown as a function of energy.

REF. Otto Titze
Z. Physik 220, 66 (1969)

ELEM. SYM.	A	Z
Mg	24	12

METHOD

REF. NO. 69 Ti 1 egf

REACTION	RESULT	EXCITATION ENERGY	SOURCE		DETECTOR		ANGLE
			TYPE	RANGE	TYPE	RANGE	
E,E/	FMF	1-12	D	37-51	MAG-D	26-51	DST

TABULAR DATA

Tabelle 2. *Zusammenstellung der Ergebnisse. Spalten 1—6 zeigen die Ergebnisse dieser Arbeit, Spalten 7—9 enthalten Vergleichswerte anderer Autoren. Hier sind die Werte E_x, I^π Ref.[1] entnommen (ME: Matrixelement für E0, BA: ausgewertet in Bornscher Näherung aus σ', $G = \Gamma_\gamma^0/\Gamma_\omega$)*

E_x [MeV]	I^π	$B(\lambda, 0)$ [fm$^{2\lambda}$]	Γ_γ^0 [eV]	R_{tr} [fm]	G	Vergleichswerte		
						E_x	I^π	G
1,366 (10)	2^+	455 (12)	3,49 (36) 10^{-4}	4,37 (35)	21,7 (25)	1,36857 (4)	2^+	viele, Mittelwert 25,9 ± 2,5 nach [33]
4,228 (10)	2^+	24,1 (20)	5,26 (92) 10^{-3}	4,12 (66)	1,15 (20)	4,233 (7)	2^+	> 14,7[35], 1,10 (20)[33], 2,29 (46)[7], (1,66)[41]
6,436 (15)	$0^+(2^+)$	6,23 (62) ME	—	5,66 (85)	—	6,436 (16)	0^+	
7,355 (20)	2^+	8,01 (79)	2,78 (58) 10^{-2}	4,60 (75)	0,38 (8)	7,349 (8)	2^+	1,30 (17)[5], 3,9[6], 0,73[41]
7,600 (21)	3^-	1,60 (31) 10^3 BA	1,26 (43) 10^{-4}	5,2 (12)	6,5 (22)	7,620 (10)	3^- [2]	4,96[5], 2,34[4]
8,375 (18)	3^-	2,60 (22) 10^3 BA	4,04 (67) 10^{-4}	4,12 (76)	10,5 (17)	8,357 (10)	(3^-)[4]	2,60[5], 1,33[6], 2,9[4], 4,17[41]
8,995 (21)	2^+	3,57 (38)	3,39 (78) 10^{-2}	4,22 (84)	0,17 (4)	9,004 (12)	2^+ [2]	
9,304 (19)	$2^+(0^+)$	11,22 (91)	0,126 (23)	4,34 (64)	0,534 (97)	9,282 (12)		
9,846 (20)	1^+	3,14 (27) 10^{-3}	1,05 (26)	3,30 (60)	0,052 (13)	9,826 (12)		
9,972 (17)	1^+	1,300 (44) 10^{-2}	4,50 (73)	3,05 (44)	0,216 (35)	9,984 (16)	(1^+)	0,269 (48)[14], 0,9[8], 0,57 (13)[15]
10,363 (19)	$2^+(0^+)$	7,56 (61)	0,146 (31)	4,31 (86)	0,360 (76)	10,353 (20)		
10,716 (18)	(0^+)	3,79 (65) ME	—	(5,66)	—	10,683 (5)	0^+ [3]	
	1^+	3,71 (16)	15,9 (24)	3,22 (47)	0,616 (93)	10,737 (9)	(1^+)	3,8 $\left(\begin{smallmatrix}+12\\-6\end{smallmatrix}\right)^8$, 4,8 $\left(\begin{smallmatrix}+16\\-14\end{smallmatrix}\right)^9$, 5,3 (17)[10], 0,90 (18)[11], 0,66 (10)[14], 0,73 (14)[15]
10,939 (20)	2^+	7,28 (10)	0,184 (58)	4,7 (10)	0,34 (11)	10,924 (5)	2^+ [3]	> 0,37[3]
11,474 (30)	(2^+)	5,33 (38)	0,177 (44)	(4,30)	0,26 (7)	11,459 (5)	2^+ [3]	> 0,13[3]
						11,460 (5)	0^+	

[over]

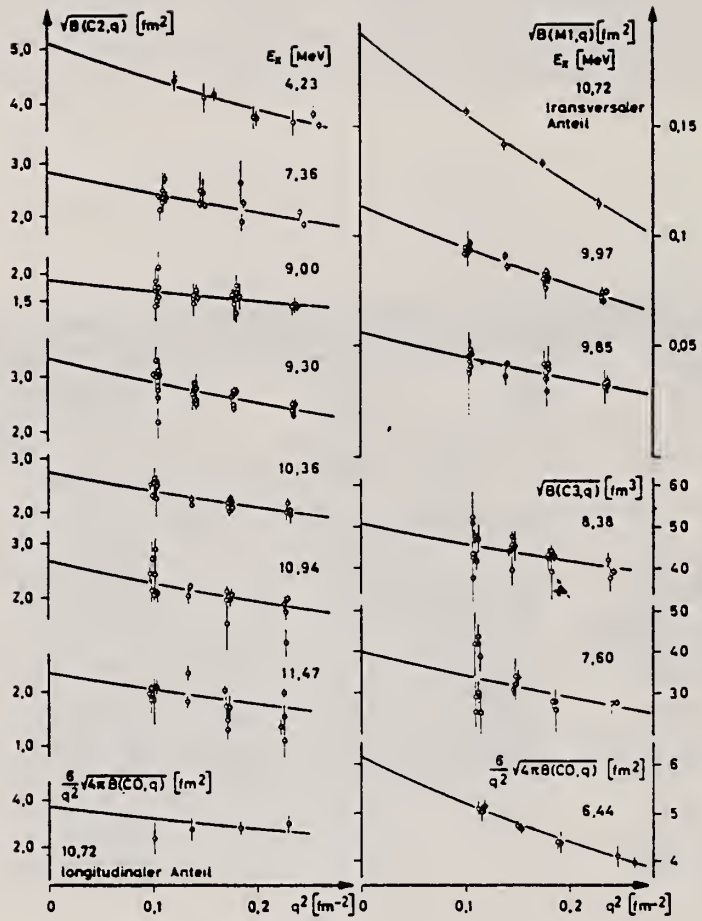

Fig. 2. Zusammenstellung der aus den korrigierten Wirkungsquerschnitten berechneten $B(X\lambda, q)$ Werte als Funktion von q^2. Für C 3-Übergänge sind die unkorrigierten Werte angegeben, berechnet aus σ' (s. Gl. (14))

REF. L. W. Fagg, W. L. Bendel, S. K. Numrich and B. T. Chertok
Phys. Rev. C1, 1137 (1970)

ELEM. SYM.	A	Z
Mg	24	12

METHOD

REF. NO. 70 Fa 1 hmg

REACTION	RESULT	EXCITATION ENERGY	SOURCE		DETECTOR		ANGLE
			TYPE	RANGE	TYPE	RANGE	
E,E/	LFT	9-14	D	39,56	MAG-D		180

No new data-analysis of data found in 68 Fa 1. REANALYSIS OF 68FA1

The data of an earlier paper presenting the results of 180° electron scattering from ^{24}Mg have been re-examined using more refined data-treatment techniques. Present results favor an assignment of 2^- for $T=1$ states at 12.91 and 13.37 MeV with estimates for radiation widths Γ_0 of 0.11 and 0.13 eV, respectively. Revised transition widths for the 1^+, $T=1$ states at 9.94 and 10.70 MeV are found to be 7.6 and 17.6 eV, respectively, in better agreement with results of other workers.

TABLE I. Values of differential cross sections, spin and parity, transition radii, and radiation widths for energy levels excited in ^{24}Mg. Transition radii and radiation widths have been corrected to the distorted-wave theory.

Level energy (MeV)	$(d\sigma/d\Omega)_{56}$ (10^{-34} cm^2/sr)	$(d\sigma/d\Omega)_{30}$ (10^{-34} cm^2/sr)	J^π	R_M (fm)	Γ_0 (eV)
9.94±0.03	104±5	202±15	1^+	$2.94_{-0.30}^{+0.18}$	$7.6_{-1.6}^{+1.6}$
10.70±0.03	194±7	372±21	1^+	$2.94_{-0.15}^{+0.13}$	$17.6_{-3.5}^{+3.5}$
12.91±0.06	76±18	58±33	(2^-)	$3.9_{-0.5}^{+1.6}$	$0.11_{-0.03}^{+0.14}$
13.37±0.05	95±18	63±38	(2^-)	$3.5_{-0.5}^{+1.5}$	$0.13_{-0.03}^{+0.15}$

REF. A. Goldmann
Z. Physik 234, 144 (1970)

ELEM. SYM.	A	Z
Mg	24	12

METHOD

REF. NO. 70 Go 3 egf

REACTION	RESULT	EXCITATION ENERGY	SOURCE		DETECTOR		ANGLE
			TYPE	RANGE	TYPE	RANGE	
E,E/	ABX	15-26	D	45-55	MAG-D		DST

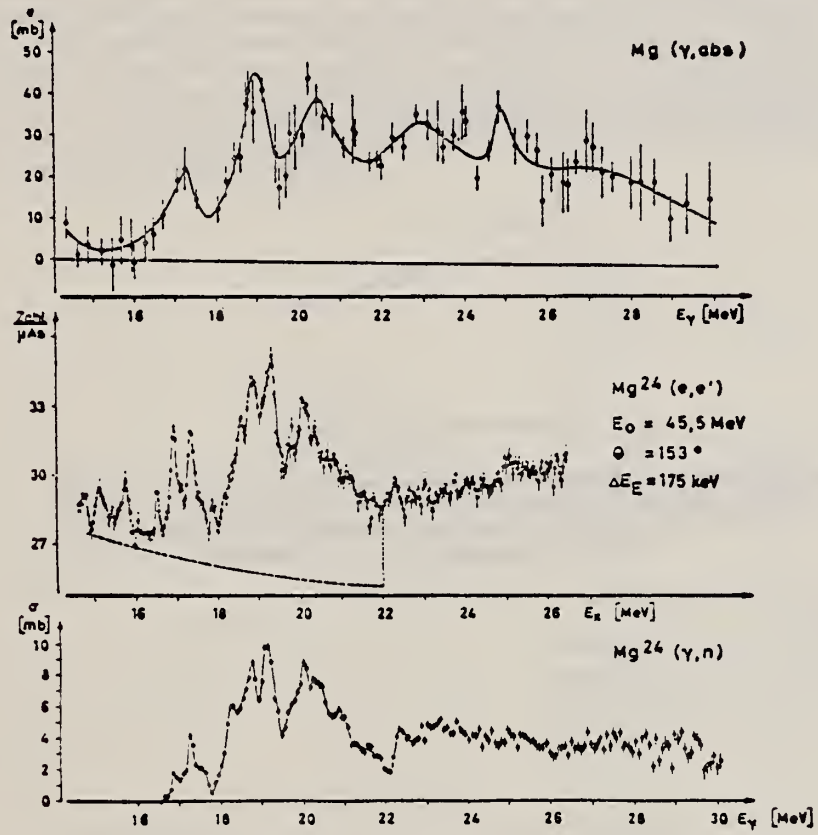

Fig. 1. Riesenresonanz von ^{24}Mg. Oben: Absorptionswirkungsquerschnitt nach Dolbolkin et al.[3], unten: $\sigma(\gamma, n)$ nach Fultz et al.[29]. Mitte: Spektrum unelastisch gestreuter Elektronen. Der Strahlenschwanz wurde *nicht* subtrahiert, der Nullpunkt stark unterdrückt. E_x und E_γ sind Anregungs- bzw. Photonenenergien. Der zur Flächenbestimmung angenommene Untergrund und die Integrationsgrenzen sind gestrichelt eingezeichnet. Die Fläche der elastischen Linie ist $A_E = 5{,}0 \cdot 10^3$ MeV/μAs

[over]

Tabelle 2. *Ergebnisse an ^{24}Mg. Bei allen Werten ist $A_E = 5{,}0 \cdot 10^3$ MeV/μAs. Die Flächen A_f wurden von 16,0 bis 22,0 MeV integriert. Bei der Auswertung wurden die im Text erwähnten Strahlungskorrekturen[22,23] nur an der elastischen Fläche angebracht ($K_f = 1{,}0$ in Gl. (2)). Die getrennte Auswertung der Bereiche von $E_x = 16{,}0$ bis 18,0 MeV und von $E_x = 18{,}0$ bis 22,0 MeV liefert mit den obigen Daten konsistente Ergebnisse*

E_0 [MeV]	Θ [Grad]	q^2 [fm^{-2}][a]	$A_f \left[\frac{\text{MeV}}{\mu\text{As}}\right]$	G [10^{-6}][b]	$B(C1, q)$ [fm^2]
54,5	129	0,17	24,5	4,53	1,01
50,4	153	0,16	48,0	2,45	0,95
15,3	153	0,12	26,5	2,41	1,05

[a] bei $E_x = 19{,}7$ MeV. [b] $G = (d\sigma/d\Omega)_f (k_i^2/V_T)$.

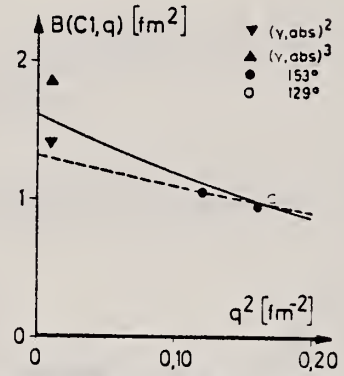

Fig. 2. Reduzierte Matrixelemente für den Bereich von 16,0 bis 22,0 MeV in ^{24}Mg. Die Photonenwerte (▲ entspricht 145 MeV mb, ▼ entspricht 110 MeV mb) wurden aus[3,2] berechnet. Die Kurven zeigen die Extrapolation zum Photonenpunkt für $R_{tr} = 1{,}3\ R_m$ (ausgezogen) bzw. $R_{tr} = R_m$ (gestrichelt)

REF. V.M. Khvastunov, N.G. Afanas'ev, V.D. Afanas'ev, E.V. Bondarenko, I.S. Gul'karov, G.A. Savitskii, and N.G. Shevchenko
Yad. Fiz. 12, 9 (1970)
Sov. J. Nucl. Phys. 12, 5 (1971)

ELEM. SYM.	A	Z
Mg	24	12

METHOD

REF. NO. 70 Kh 1 hmg

REACTION	RESULT	EXCITATION ENERGY	SOURCE		DETECTOR		ANGLE
			TYPE	RANGE	TYPE	RANGE	
E,E/	FMF	1	D	225	MAG-D		DST
		(1.37)					

1 = 1.37

Elastic and inelastic scattering of 225-MeV electrons by the isotopes Mg^{24} and Mg^{26} have been measured. Analysis of the data was carried out in the Born approximation. From analysis of the elastic scattering for a uniform-Gaussian charge-distribution model it is found that addition of two neutrons to the Mg^{24} nucleus leads to an increase in the parameter R by 0.03 ± 0.02 F and a decrease in g by 0.07 ± 0.04 F, which corresponds to a decrease in the mean-square radius of the Mg^{26} nucleus by (1.6 ± 1.3)% in comparison with Mg^{24}. Analysis of the inelastic scattering with excitation of the first 2^+ level shows that the internal quadrupole moments of the nuclei Mg^{24} and Mg^{26} are identical within experimental error.

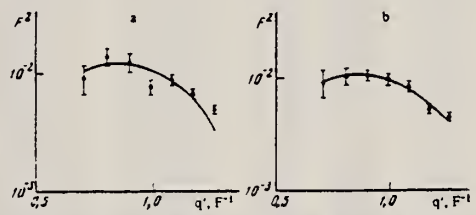

FIG. 3. Form factors for inelastic scattering with excitation of the first 2^+ levels, 1.37 MeV in Mg^{24} (a) and 1.81 MeV in Mg^{26} (b). The solid lines are theoretical curves calculated with Eq. (3).

Characteristics of the first 2^+ levels of the nuclei Mg^{24} and Mg^{26}

Nucleus	Level energy, MeV	$\beta_2(0^+, 2^+)$	$B(E2\uparrow)$, e^2F^4	τ, 10^{-13} sec	G	Q_0, F^2
Mg^{24}	1.37	0.31 ±0.02	412 ±43	20.5±2.1	20.1 ±2.1	64 ±4
Mg^{26}	1.81	0.25 ±0.01	349 ±30	6.04±0.52	15.2 ±1.3	59 ±3

REF. P. Strehl
Z. Physik 234, 416 (1970)

ELEM. SYM.	A	Z
Mg	24	12

METHOD

REF. NO. 70 St 2 egf

REACTION	RESULT	EXCITATION ENERGY	SOURCE TYPE	SOURCE RANGE	DETECTOR TYPE	DETECTOR RANGE	ANGLE
E,E/	ABX	6	D	31-59	MAG-D		DST
		(6.44)					

6 = 6.44 0+

Tabelle 3. *Experimentelle Parameter und Meßwerte. E_0, Θ Primärenergie, Streuwinkel im Laborsystem. q unelastischer Impulsübertrag. σ/σ_E gemessenes Verhältnis von unelastischem zu elastischem differentiellen Wirkungsquerschnitt; in Klammer ist der statistische Fehler in % angegeben. $d\sigma/d\Omega$ inelastischer differentieller Wirkungsquerschnitt; wegen der Fehlerangaben vgl. Text. Die Meßwerte für Si und S sind als Ergebnisse für ^{nat}Si und ^{nat}S aufzufassen (vgl. Text)*

	E_0 (MeV)	Θ (°)	q^2 (fm^{-2})	σ/σ_E (10^{-4})	$d\sigma/d\Omega$ (10^{-33} cm^2/ster.)
^{12}C 7,65 MeV	59,58	117,04	0,231	14,90 (0,6)	24,69 ±1,60
	56,94	129,02	0,231	13,79 (1,0)	13,68 ±0,96
	54,12	141,11	0,229	14,98 (0,7)	8,15 ±0,55
	52,75	153,15	0,231	15,24 (1,0)	6,62 ±0,47
	51,90	165,05	0,231	15,78 (1,8)	1,16 ±0,09
	51,18	104,98	0,145	5,80 (0,7)	28,80 ±1,69
	47,90	117,04	0,145	5,51 (0,7)	17,19 ±1,01
	45,48	129,02	0,145	5,97 (1,2)	11,14 ±0,71
	43,57	141,11	0,143	5,95 (1,1)	6,09 ±0,38
	42,54	153,15	0,145	5,82 (1,4)	2,67 ±0,18
	37,51	104,98	0,074	1,41 (1,4)	15,38 ±1,07
	35,08	117,04	0,073	1,33 (1,6)	9,14 ±0,57
	33,39	129,02	0,073	1,44 (1,7)	5,89 ±0,37
	32,04	141,11	0,073	1,39 (2,0)	3,11 ±0,21
	31,36	153,15	0,073	1,39 (3,2)	1,39 ±0,11
^{24}Mg 6,44 MeV	59,01	116,94	0,232	5,53 (2,2)	28,28 ±2,24
	55,81	129,03	0,231	5,41 (1,5)	16,65 ±1,20
	53,64	140,95	0,231	5,65 (1,6)	9,51 ±0,70
	52,14	153,00	0,231	5,17 (2,1)	3,95 ±0,32
	[illegible]	104,96	0,074	0,59 (2,6)	25,08 ±1,78
	[illegible]	116,94	0,074	0,56 (3,2)	15,09 ±1,16
	[illegible]	129,03	0,074	0,58 (2,8)	9,37 ±0,68
	31,72	140,95	0,074	0,58 (3,1)	5,10 ±0,39
	30,86	153,00	0,074	0,68 (5,5)	2,69 ±0,27
Si 4,98 MeV	58,38	116,94	0,232	5,61 (1,9)	38,70 ±2,68
	55,12	129,03	0,231	5,27 (0,9)	21,98 ±1,34
	52,87	141,11	0,231	5,58 (1,3)	12,72 ±0,81
	51,28	153,00	0,230	5,69 (1,9)	6,00 ±0,42
	49,93	104,96	0,145	2,05 (1,6)	49,60 ±3,13
	49,97	104,96	0,146	2,10 (1,4)	50,68 ±3,09
	46,77	116,94	0,146	2,23 (2,2)	33,90 ±2,31
	44,28	129,03	0,146	2,14 (2,0)	19,48 ±1,29
	42,44	141,11	0,146	2,20 (1,7)	10,98 ±0,70
	41,23	153,00	0,145	2,45 (2,1)	5,64 ±0,38
	41,37	153,00	0,146	2,48 (2,5)	5,67 ±0,40
	36,28	104,96	0,074	0,53 (4,5)	32,51 ±2,90
	36,26	104,96	0,074	0,56 (4,0)	34,35 ±2,89
	33,98	116,94	0,074	0,55 (4,3)	21,28 ±1,83
	32,17	129,03	0,074	0,52 (4,0)	11,98 ±1,00
	30,87	141,11	0,073	0,59 (5,3)	7,54 ±0,73
	29,96	153,00	0,073	0,66 (5,7)	3,89 ±0,39
	30,09	153,00	0,074	0,60 (5,0)	3,52 ±0,33
Si 6,69 MeV	58,38	116,94	0,225	0,48 (25)	3,30 ±1,00
S 3,78 MeV	59,19	104,96	0,210	0,32 (37)	5,17 ±3,36
	58,80	104,96	0,209	0,27 (45)	4,40 ±3,30
^{40}Ca 3,35 MeV	53,98	140,95	0,250	0,92 (9)	3,03 ±1,21

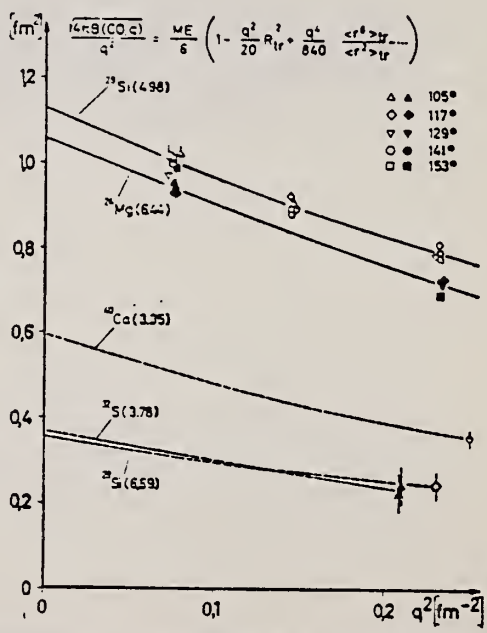

Fig. 3. Meßergebnisse für Monopolübergänge in ^{24}Mg(6,44 MeV), ^{28}Si(4,98 und 6,69 MeV), ^{32}S(3,78 MeV) und ^{40}Ca(3,35 MeV) als Funktion von q^2. Die eingetragenen Meßpunkte und die zugehörigen Kurven gelten für eine Auswertung mit f_c, x_1 und x_2 nach Modell I. Für ^{28}Si(4,98) sind nur die aus σ/σ_E und D_{exp}^{BA} berechneten longitudinalen Anteile aufgetragen (vgl. 5.1), wobei die Meßpunkte bei gleicher Impulsübertragung und gleichem Streuwinkel (vgl. Tabelle 3) zusammengefaßt wurden. Die gestrichelten Kurven zeigen die Extrapolation nach $q=0$ mit vorgegebenem Übergangsradius

REF. D. V. Webb, E. G. Muirhead and B. M. Spicer
Nucl. Phys. A159, 81 (1970)

ELEM. SYM.	A	Z
Mg	24	12

METHOD

REF. NO.: 70 We 1 egf

REACTION	RESULT	EXCITATION ENERGY	SOURCE		DETECTOR		ANGLE
			TYPE	RANGE	TYPE	RANGE	
G,N	ABX	17-32	C	17-32	ACT-I		4PI

322+

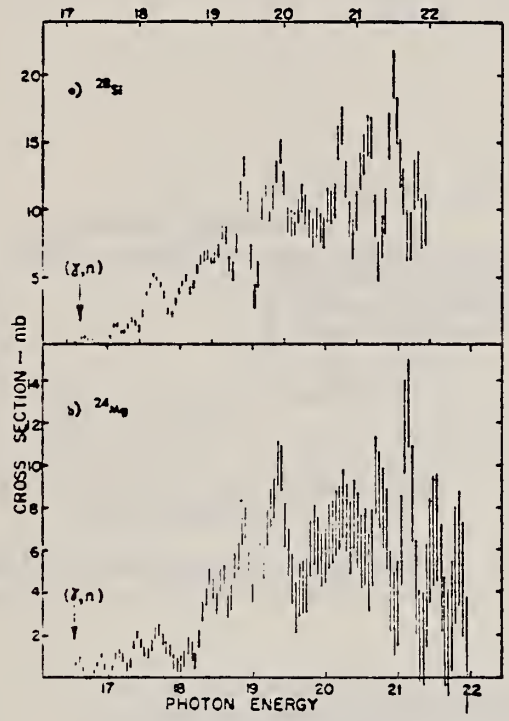

Fig. 2. Analysis of the Δ_i = 50 keV data to 22 MeV in Δ_o = 100 keV bins for the photoneutron cross sections of (a) silicon and (b) magnesium.

TABLE 3
Integrated cross sections for magnesium

Source	$\int_0^{24\,\mathrm{MeV}} \sigma dE$ (MeV · mb)	$\int_0^{31\,\mathrm{MeV}} \sigma dE$ (MeV · mb)
this experiment	35±4	72±7 (62.8±6 to 29 MeV)
Fultz *et al.* [24])	33.7	66.8 (to 29 MeV)
Anderson *et al.* [27])	52	115
Miller *et al.* [25])	45±7	
Min and Whitehead [26])	60	

[24])S.C. Fultz, J.T. Caldwell, B.L. Berman, R.R. Harvey and M. Kelly, Bull.Am.Phys.Soc. 14 (1969) 103.
[25])J. Miller, C. Schul, G. Tamas and C. Tzara, J.de Phys.27 (1966)8.
[26])K. Min and W.D. Whitehead, Phys. Rev. 137B (1965)301.
[27])D.W. Anderson, B.C. Cook and T.J. Englert, Nucl. Phys. A127 (1969) 474.

[over]

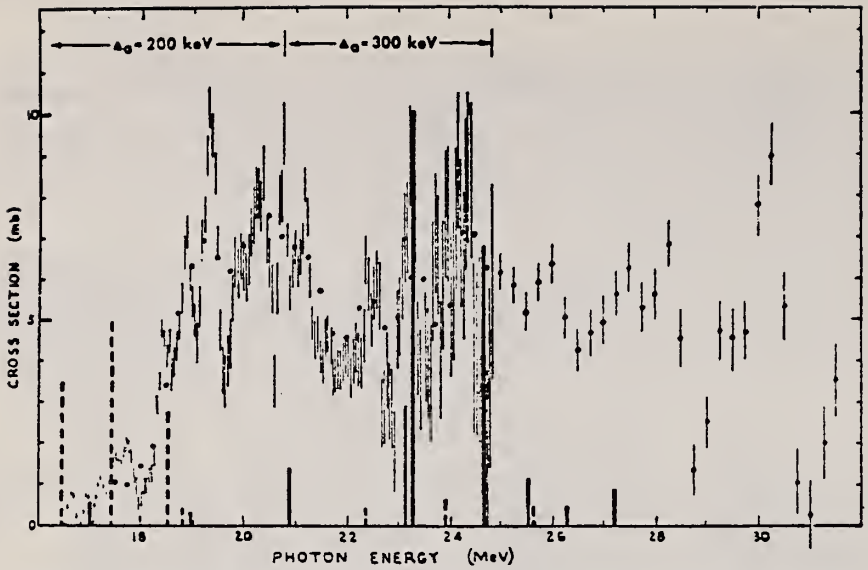

Fig. 5. The photoneutron cross section for natural magnesium. The full circles indicate the coarse resolution measurement ($\Delta_c = 250$ keV, $\Delta_s = 500$ keV). The higher resolution measurement ($\Delta_c = 50$ keV, $\Delta_s = 200$ keV) is presented by the error bars up to 25 MeV. The predictions of Nilsson *et al.* [9]) are shown by the heavy dashed ($K = 0$) and continuous ($K = 1$) bars.

[9])S.G. Nilsson, J. Sawicki and N.K. Glendenning, Nucl. Phys.33 (1962)239.

REF. R. J. Baglan, C. D. Bowman and B. L. Berman
Phys. Rev. C3, 672 (1971)

ELEM. SYM.	A	Z
Mg	24	12

METHOD

REF. NO. 71 Ba 2 hmg

REACTION	RESULT	EXCITATION ENERGY	SOURCE TYPE	SOURCE RANGE	DETECTOR TYPE	DETECTOR RANGE	ANGLE
G,N	ABX	16 - 20	C	17,20	TOF-D		135
		(16.6 - 19.5)					

941

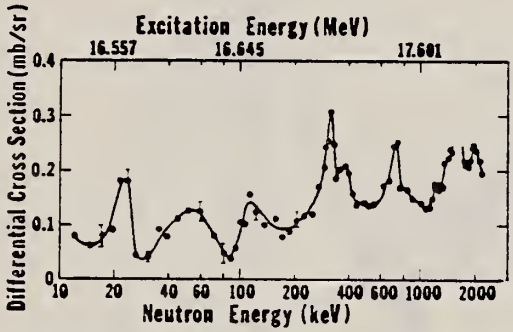

FIG. 15. The 135° differential threshold photoneutron cross section for ^{24}Mg (see caption to Fig. 4).

FIG. 4. The 135° differential threshold photoneutron cross section for ^{207}Pb at low energies versus the energy of the emitted neutron (lower scale) and the excitation energy (upper scale). The arrows indicate peaks which decay to excited states of the residual nucleus (ES), or peaks owing to contaminating isotopes in the photoneutron sample. The inset shows the ^{207}Pb(γ, n) cross section averaged with a square 40-keV wide smoothing function.

Also see:
R. J. Baglan et al.
Phys. Rev. C3, 2475
(1971)

[over]

TABLE VII. Resonance parameters for ^{24,25,26}Mg, ^{19}F, and ^{31}P. For all resonances, the area under the peak in the 135° differential cross section is multiplied by 4π to yield approximate values for $g_\gamma\Gamma_{\gamma 0}\Gamma_n/\Gamma \simeq g_\gamma\Gamma_{\gamma 0}$. For those resonances where J^π is known, the differential area is multiplied by the appropriate factor F from Table I to obtain $\Gamma_{\gamma 0}$. E_L is the laboratory neutron energy for the (γ,n) reaction and E_n is the corresponding laboratory neutron energy for a neutron-induced reaction. Column 5 labels the peak as a ground-state (GS) or excited-state (ES) transition as determined in this work alone.

Nucleus	E_L (keV)	E_{ex} (MeV)	$g_\gamma\Gamma_{\gamma 0}\Gamma_n/\Gamma$ (eV)	GS or ES	J^π	$\Gamma_{\gamma 0}$ (eV)	E_n (keV) (This work)
^{24}Mg	22	16.559	0.61		(1^-)	0.40	28
	55	16.596	2.4	GS	(1^-)	1.6	66
	110	16.656	4.0	GS	(1^-)	2.7	128
	312	16.871	10.7		(1^-)	7.1 [a]	354
	382	16.95					432
	717	17.30	19.5		(1^-)	13.0 [a]	804
	1210	17.83					1348
	1620	18.26					1799
	1955	18.61					2168
							46.8
^{25}Mg	41.1	7.374	0.09	GS			
	45.1	8.746	0.31	ES			
	74.9	7.410	0.36	GS	$\frac{3}{2}^-$ [b]	1.1	84.1 [b]
	208	8.920	0.29	ES			
	236	7.580	0.09	GS			261
	404	7.756	0.03				445
	439	7.793	0.05		$\frac{5}{2}^+$ [c]		484
	472	7.828	0.06				520
	515	7.873	0.46	GS	$\frac{3}{2}^+$ [c]		567
	601	7.964	0.18				661
	781	8.152	1.51	GS			857
	912	8.292	0.72				1003
	1236	9.999	2.4 [c]	ES	$\frac{3}{2}^+$ or $\frac{5}{2}^+$ [c]		
	1707	9.12					1869
	1764	9.18					1931
^{26}Mg	54.3	11.155	2.6	GS	$1^-(1^+,2^+)$	1.75	62.3
	63.2	11.164	0.05			0.034	72.2
	181	11.289	1.0	GS	$1^-(1^+,2^+)$	0.68	202
	222	11.333	1.9	GS	$1^-(1^+,2^+)$	1.3	248
	391	11.511	5.1	GS	$1^-(1^+,2^+)$	3.5	433
	621	11.753	32.5	GS	$1^-(1^+,2^+)$	22.2	684
	738		15.0 [d]	ES		5.1	
	1122	12.279	14.7	GS	$1^-(1^+,2^+)$	10.0	1232
^{19}F	100	10.542	1.8	GS			118
^{31}P	109	12.429	0.86				121
	280	12.609	0.60				307
	398	12.732	0.59				434
	678	13.026	0.90				737
	939	13.297	4.4				1018

[a] These values for $\Gamma_{\gamma 0}$, when increased by approximately a factor of 2 in order to include the relatively high cross sections in the valleys, agree very well with corresponding values from Ref. 8 (see Ref. 4).

[b] This resonance was seen at E_n = 83 and 84 keV in Refs. 24 and 25, respectively.

[c] Analogs of states in ^{25}Na (see text). The value for $g_\gamma\Gamma_{\gamma 0}\Gamma_n/\Gamma$ given in Ref. 26 was not corrected with the multiplicative factor in Table II.

[d] Assuming a first-excited-state transition.

[4] R.L. Van Hemert, C.D. Bowman, R.J. Baglan, and B.L. Berman (to be published); R.L. Van Hemert, University of California Lawrence Radiation Laboratory Report No. UCRL-50442, 1968 (unpublished).

[8] S.C. Fultz, M.A. Kelly, J.T. Caldwell, R.R. Harvey, and B.L. Berman, Bull. Am. Phys. Soc. 14, 103 (1969), and private communication.

[24] H.W. Newson, R.C. Block, P.F. Nichols, A. Taylor, A.K. Furr, and E. Merzbacher, Ann. Phys. (N.Y.) 8, 211 (1959).

[25] D.J. Hughes and R.B. Schwartz, Neutron Cross Sections (U.S. Government Printing Office, Washington, D.C., 1966), 2nd ed., 2nd Suppl., Vol. IIc.

REF. S.C. Fultz, R.A. Alvarez, B.L. Berman, M.A. Kelly, D.R. Lasher, T.W. Phillips, J. McElhinney
Phys. Rev. C4, 149 (1971)

ELEM. SYM.	A	Z
Mg	24	12

METHOD

REF. NO. 71 Fu 2 hmg

REACTION	RESULT	EXCITATION ENERGY	SOURCE TYPE	SOURCE RANGE	DETECTOR TYPE	DETECTOR RANGE	ANGLE
G,N	ABX	16-29	D	16-30	BF3-I		4PI
							343

14 LEVEL FIT

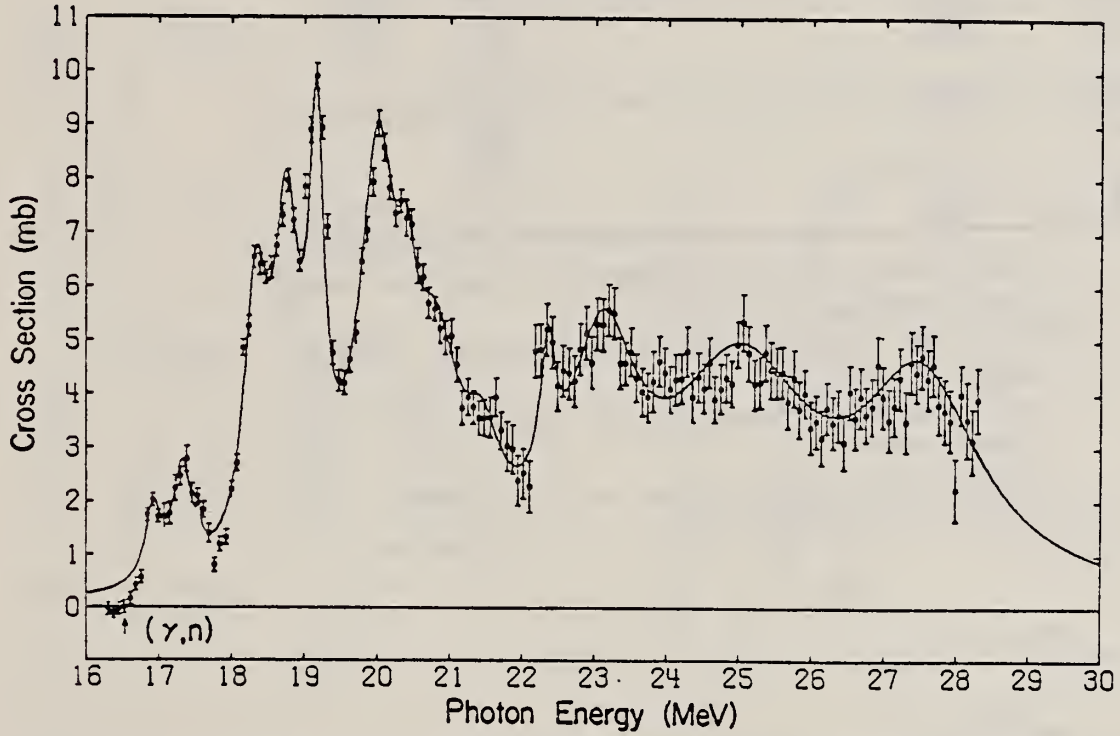

FIG. 3. ^{24}Mg total cross section $\sigma(\gamma,n)+(\gamma,p n))$ fitted with a calculated cross-section curve. The solid line is the sum of the 14 Lorentz lines whose parameters were adjusted to fit the data.

TABLE II. Integrated cross sections of magnesium isotopes.

Isotope	$\int_{E_{thr}}^{28} \sigma(\gamma, n_{tot})dE$ (MeV mb)	$\int_{E_{thr}}^{28} \sigma(\gamma, 2n)dE$ (MeV mb)
^{24}Mg	50	...
^{26}Mg	226	68
Natural magnesium	76	...

[over]

TABLE III. Analytical and experimental resonance energies for ^{24}Mg (MeV).

Resonance number	Analytical energy	Experimental energies: Present data (γ, n_{tot})	Livermore (Ref. 15) (γ, n_0)	Yale (Ref. 14) (γ, n_0)	Darmstadt (Ref. 12) (e, e')	Argonne (Ref. 2) (γ, p_0)
1	16.92	16.90	16.871		16.90	16.9
			16.95		17.08	17.2
2	17.32	17.30	17.30		17.33	17.35
3	17.55	17.65	17.83	17.83	17.60	17.5
				17.95	17.90	
				18.15	18.21	
4	18.33	18.30	18.26	18.36	18.50	18.25
5	18.75	18.82	18.61	18.58	18.85	18.5
6	19.16	19.17		19.21	19.23	19.0
				19.48		19.3
7	20.00	20.05		19.95	20.10	20.1
8	20.40	20.36			20.35	20.4
9	20.80	20.90			20.77	20.7
					21.16	
10	21.45	21.45			21.50	
11	22.35	22.35			22.28	
12	23.10	23.10			23.02	
					23.42	
13	25.00	25.00			25.05	
14	27.50	27.50				

[2] R.C. Bearse, L. Meyer-Schutzmeister, and R.E. Segel, Nucl. Phys. A116, 682 (1968).

[12] O. Titze, E. Spamer, and A. Goldman, Phys. Letters 24B, 169 (1967).

[14] C.-P. Wu, Ph.D. Thesis, Yale University, 1968 (unpublished).

[15] R. J. Baglan, C. D. Bowman, and B. L. Berman, Phys. Rev. C3, 672 (1971).

Y. Horikawa, Y. Torizuka, A. Nakada, S. Mitsunobu, Y. Kojima, and M. Kimura
Phys. Letters 36B, 9 (1971)

Mg	24	12

METHOD

REF. NO. 71 Ho 1 | egf

REACTION	RESULT	EXCITATION ENERGY	SOURCE		DETECTOR		ANGLE
			TYPE	RANGE	TYPE	RANGE	
E,E/	FMF	1,4	D	183,250	MAG-D		DST

1.37, 4.12 MEV

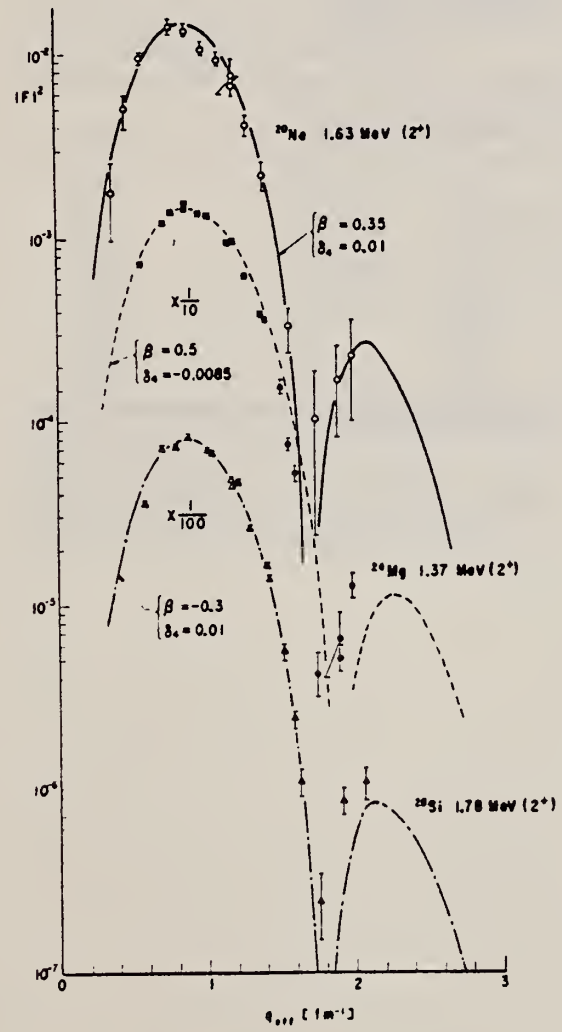

Fig.1. The experimental form factors for the 2$^+$ members of the ground-state rotational bands in ^{20}Ne, ^{24}Mg and ^{28}Si are shown as a function of the q_{eff} [3].

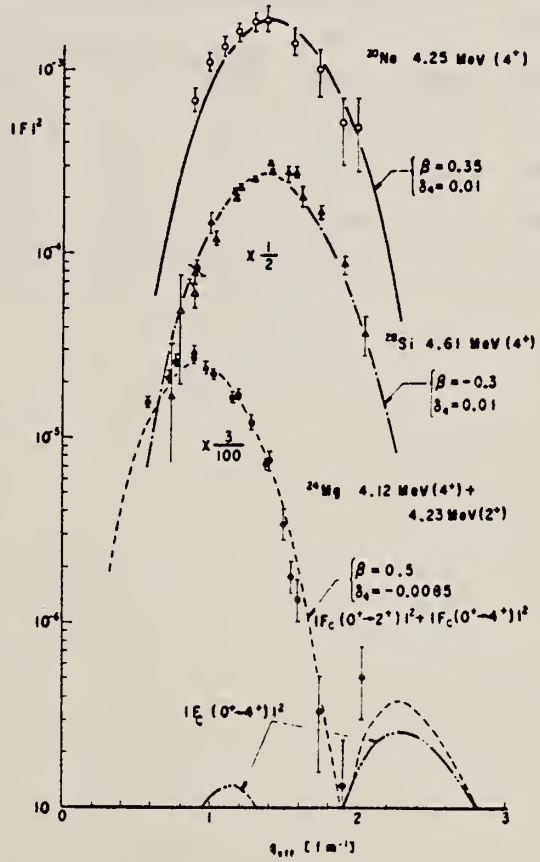

Fig.2. The same as for fig. 1 except for the 4$^+$ members. The unresolved data of the 4.12 MeV (4$^+$) and 4.23 MeV(2$^+_2$) states is presented in the case of ^{24}Mg.

(over)

(2) R. de Swiniarski, D. Glashausser, D. L. Hendrie, J. Sherman, A. D. Bacher, and E. A. McClatchie, Phys. Rev. Letters 23 (1964) 317.
(3) D. G. Ravenhall, quoted in: R. Hofstater, Rev. Mod. Phys. 28 (1956) 214.
(5) H. Rebel, G. W. Schweimer, J. Specht, G. Schatz, R. Lohken, D. Habs, G. Hanser and H. Klewe-Nebenius, Phys. Rev. Letters 26 (1971) 1190.

Table 1
The values obtained from the Nilsson orbits which provide the best fit form factors. The signs of the moments were determined by the characteristic of the orbits. The β_2 and β_4 values of the present study are compared with those of the (p, p') [2] and (α, α') [5] reactions.

	$\langle r^2 \rangle^{1/2}$ (fm)	$\langle r^4 \rangle^{1/4}$ (fm)	Q_o (efm^2)	H_o (efm^4)	β_2 present (e, e')	β_2 (p, p')	β_2 (α, α')	β_4 present (e, e')	β_4 (p, p')	β_4 (α, α')
^{20}Ne	2.91	3.14	+58 ±3	+249 ±27	+0.40	+0.47	+0.35 ±0.01	+0.19	+0.28 ±0.05	+0.11 ±0.01
^{24}Mg	3.03	3.24	+69 ±3	+ 48 ±16	+0.45	+0.47		-0.06	-0.05 ±0.08	
^{28}Si	3.14	3.35	-64 ±3	+205 ±33	-0.39	-0.37	-0.32 ±0.01	+0.10	+0.25 ±0.08	+0.08 ±0.01

REF.

E. J. Moniz, I. Sick, R. R. Whitney, J. R. Ficenec, R. G. Kephart and W. P. Trower
Phys. Rev. Letters 26, 445 (1971)

ELEM. SYM.	A	Z
Mg	24	12

METHOD

REF. NO.: 71 Mo 3 | hmg

REACTION	RESULT	EXCITATION ENERGY	SOURCE		DETECTOR		ANGLE
			TYPE	RANGE	TYPE	RANGE	
E,E/	ABX	0-240	D	500	MAG-D		60

Table I. Nuclear Fermi momentum k_F and average nucleon interaction energy $\bar{\epsilon}$ determined by least-squares fit of theory to quasielastic peak.

Nucleus	k_F (MeV/c)[a]	$\bar{\epsilon}$ (MeV)[b]
$_3Li^6$	169	17
$_6C^{12}$	221	25
$_{12}Mg^{24}$	235	32
$_{20}Ca^{40}$	251	28
$_{28}Ni^{58.7}$	260	36
$_{39}Y^{89}$	254	39
$_{50}Sn^{118.7}$	260	42
$_{73}Ta^{181}$	265	42
$_{82}Pb^{208}$	265	44

[a]The fitting uncertainty in these numbers is approximately ±5 MeV/c.

[b]The fitting uncertainty in these numbers is approximately ±3 MeV. Simple estimates for $\bar{\epsilon}$ give numbers in reasonable agreement with those in the table.

REF. C. P. Swann
Phys. Rev. C4, 1489 (1971)

ELEM. SYM.	A	Z
Mg	24	12

METHOD

REF. NO. 71 Sw 2 hmg

REACTION	RESULT	EXCITATION ENERGY	SOURCE		DETECTOR		ANGLE
			TYPE	RANGE	TYPE	RANGE	
G,G	LFT	1	D	1	SCD-D		127
		(1.368)		(1.468)			

1.368 MEV 2+ STATE

A mean life of 1.92 ± 0.15 psec has been obtained for the 1.368-MeV 2^+ state of ^{24}Mg by comparing the resonant scattering of γ rays through the ^{24}Mg level and through the 1.333-MeV 2^+ state of ^{60}Ni, the lifetime of which is known accurately. This value is in good agreement with recent Coulomb-excitation results but differs markedly from a recent resonance-fluorescence self-absorption result.

TABLE I. Mean lifetime of the 1.368-MeV level of ^{24}Mg.

Method	τ (psec)	Reference
Resonance-fluorescence scattering	1.92 ± 0.15	Present
Resonance-fluorescence scattering	1.95 ± 0.26	3
Resonance-fluorescence scattering	1.11 ± 0.13	2
Inelastic electron scattering	1.9 ± 0.2	5
Coulomb excitation	2.00 ± 0.10	1
Coulomb excitation	2.04 ± 0.14	4

REF.

B.S. Ishkhanov, I.M. Kapitonov, E.V. Lazutin, I.M. Piskarev, and V.G. Shevchenko
Nucl. Phys. A186, 438 (1972)

ELEM. SYM.	A	Z
Mg	24	12

METHOD

REF. NO. 72 Is 1 egf

REACTION	RESULT	EXCITATION ENERGY	SOURCE		DETECTOR		ANGLE
			TYPE	RANGE	TYPE	RANGE	
G,XN	ABX	16-30	C	16-30	BF3-I		4PI

548

TABLE 2

The maxima of the fine structure of the giant resonance in ^{24}Mg and the corresponding resonances of intermediate structure

Ref. [16])	Ref. [12])	Ref. [10])	Present work	Resonances of intermediate structure (MeV)
16.52		16.6		
16.90	16.92	17.0	16.85 ± 0.08	
(17.08)				
17.33	17.32	17.2	17.40 ± 0.08	17
(17.60)	(17.55)	17.6		
17.90		17.8		
(18.21)				
18.50	18.33	18.5	18.30 ± 0.09	
18.85	18.75	18.9	18.85 ± 0.09	19
19.23	19.16	19.3	19.30 ± 0.10	
19.74				
20.10	20.00	20.3	20.20 ± 0.10	
20.35	20.40			
(20.77)	(20.80)	20.7		20–21
(21.16)		21.2		
(21.50)	21.45		21.45 ± 0.13	
22.28	22.35	22.5	22.50 ± 0.15	
(23.02)	23.10	23.2	23.35 ± 0.15	23
(23.42)				
(24.06)		24.1		
25.05	25.00	(25.8)	24.6 ± 0.2	25
			26.3 ± 0.2	

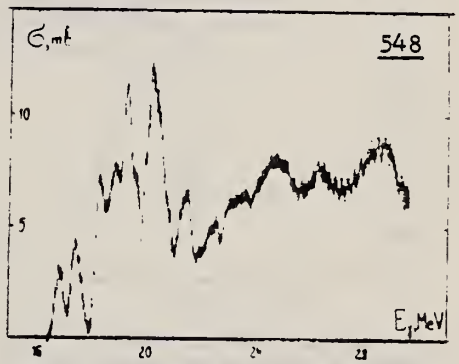

Fig. 1. Cross section for ^{24}Mg(γ, n)+(γ, np).

[10] D.V. Webb et al., Nucl. Phys. A159 (1970) 81

[12] S.C. Fultz et al., Phys. Rev. C4 (1971) 149

[16] O. Titze et al., Phys. Lett. 24B (1967) 169

REF.

A. Nakada & Y. Torizuka
J. Phys. Soc. Japan 32, 1 (1972)

ELEM. SYM.		
Mg	24	12

METHOD

REF. NO. 72 Na 1 egf

REACTION	RESULT	EXCITATION ENERGY	SOURCE TYPE	SOURCE RANGE	DETECTOR TYPE	DETECTOR RANGE	ANGLE
E,E/	LFT	1-6	D	183-250	MAG-D		DST

1.37,4.23,6.00 MEV

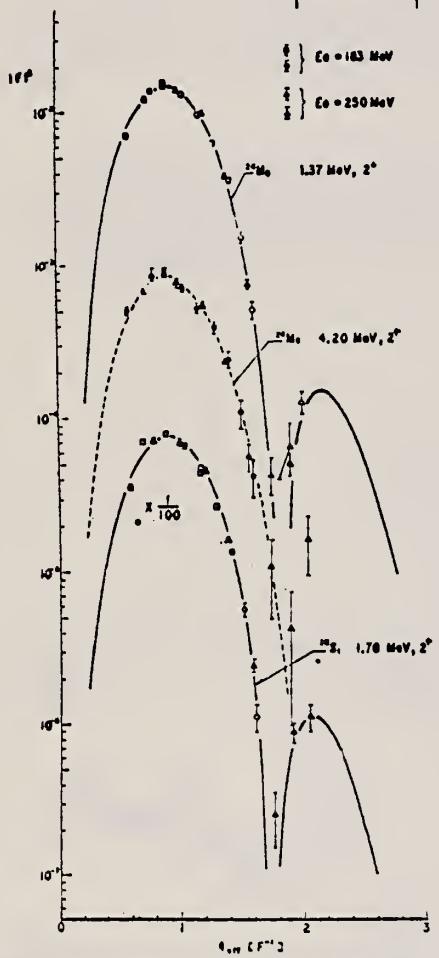

Fig. 5. The inelastic form factors for the 1.37-(2+), 4.20-MeV (2+) states in ^{24}Mg and for the 1.78-MeV (2+) in ^{28}Si are shown as a function of q_{eff}. The curves are the best fit form factors calculated with the Born approximation.

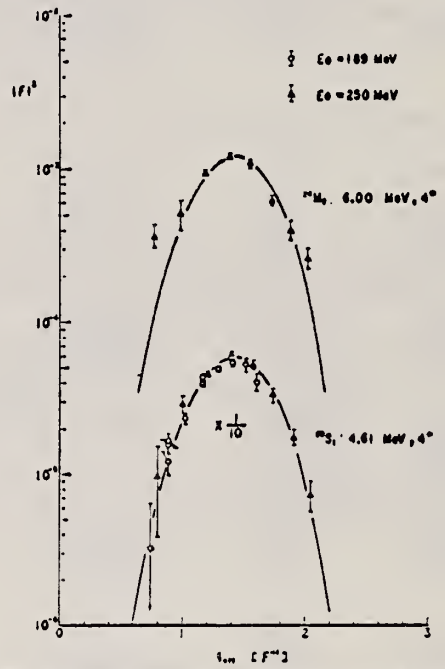

Fig. 7. The inelastic form factors for the 6.00-MeV(4+) state in ^{24}Mg and 4.61-MeV(4+) state in ^{28}Si.

Table II. The $B(EL)$ values extracted from the experimental form factors.

			Born approx.		DWBA	
Nucleus	E_x (MeV)	J^π	$B(EL)$ (W.U.)	$B(EL)$ (e^2F^{2L})	$B(EL)$ (W.U.)	$B(EL)$ (e^2F^{2L})
^{24}Mg	1.37	2+	18.1±1.7	(3.27±0.35)×10^3	21.7±2.2	(4.46±0.45)×10^3
	4.23	2+	1.11±0.18	(2.28±0.37)×10		
	6.00	4+	10.6	2.87×10^4		
^{28}Si	1.78	2+	11.1±1.5	(2.80±0.38)×10^3	13.7±1.3	(3.46±0.33)×10^3
	4.61	4+	4.35±0.49	(1.78×0.20)×10^4		
	6.88	3−	8.99±0.71	(2.93±0.23)×10^3		
	9.70	3−	1.88±0.30	(6.13±0.98)×10^3		

REF. A.H. Chung, W.T. Diamond, A.E. Litherland, H.L. Pai, and J. Goldemberg
Phys. Lett. 53B, 244 (1974)

ELEM. SYM.	A	Z
Mg	24	12

METHOD

REF. NO. 74 Ch 9 egf

REACTION	RESULT	EXCITATION ENERGY	SOURCE		DETECTOR		ANGLE
			TYPE	RANGE	TYPE	RANGE	
E,C12	NOX	24- 29	D	25- 29	TRK-I		DST

$$\int_{24}^{29} \sigma dE \geq 3.0 \pm 0.6 \ \mu b\text{-MeV}$$

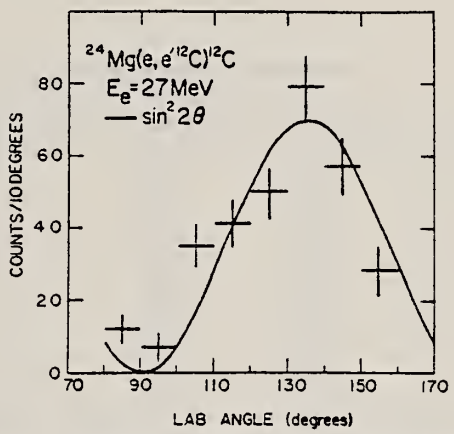

Fig. 1. The angular distribution of ground-state carbon nuclei from the electron induced fission of ^{24}Mg at E_e = 27 MeV is shown together with the function sin$^2 2\theta$.

The electron induced fission of ^{24}Mg leading to the ground states of two carbon nuclei has been studied using 25 to 45 MeV electrons. The observed sin$^2 2\theta$ angular distribution of the carbon nuclei indicates the dominance of E2 virtual photon absorption. The yield of ground state carbon nuclei is observed to decrease with increasing excitation energy in ^{24}Mg above 24 MeV.

REF. A. Johnston and T.E. Drake
J.Phys.A: Math., Nucl.Gen. 7, 898 (1974)

EL EM. SYM.	A	Z
Mg	24	12

METHOD

REF. NO. 74 Jo 4 egf

REACTION	RESULT	EXCITATION ENERGY	SOURCE TYPE	SOURCE RANGE	DETECTOR TYPE	DETECTOR RANGE	ANGLE
E,E/	LFT	1- 14	D	64-116	MAG-D		DST

19 STATES

$F^2(q)$, $F_T^2(q)$ plots given.

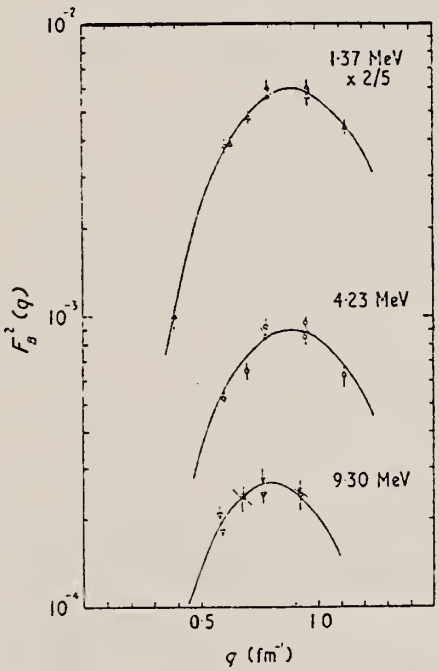

Figure 5. $F_h^2(q)$ for the 2⁻ states at 1·37 MeV, 4·23 MeV and 9·30 MeV.

Table 1. Kinematics of the experimental runs.

Run Number	Energy (MeV)	Angle (deg)	q_{EL} (fm^{-1})
1	91·50	120·0	0·80
2	81·66	154·0	0·80
3	110·82	120·0	0·97
4	99·21	153·0	0·97
5	64·94	154·0	0·64
6	70·92	120·0	0·62
7	73·81	153·0	0·72
8	110·07	80·0	0·72
9	115·67	153·0	1·14
10	72·6	65·0	0·40

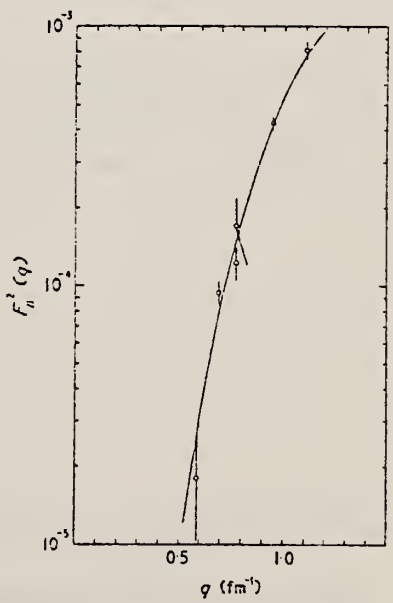

Figure 6. $F_h^2(q)$ for the 4⁺ state at 6·00 MeV.

(over)

Table 5. Results for the states with $E_x < 11$ MeV.

		Tassie model				Helm model		
E_x (MeV)	J^π	c(fm)	t(fm)	$B(XL\uparrow)e^2\,\mathrm{fm}^{2L}$	R_{tr}(fm)	R(fm)	$B(XL\uparrow)e^2\,\mathrm{fm}^{2L}$	R_{tr}(fm)
1·37	2^+	2·88	2·06	420 ± 25	$4{\cdot}11 \pm 0{\cdot}08$	3·03	411 ± 23	$4{\cdot}03 \pm 0{\cdot}07$
4·23	2^+	2·91	2·08	$26{\cdot}3 \pm 6{\cdot}0$	$4{\cdot}14 \pm 0{\cdot}30$	3·10	$25{\cdot}5 \pm 4{\cdot}0$	$4{\cdot}09 \pm 0{\cdot}20$
6·00	4^+	2·48	1·93	$(4{\cdot}2 \pm 1{\cdot}0) \times 10^4$	$4{\cdot}90 \pm 0{\cdot}70$	3·0	$(3{\cdot}6 \pm 1{\cdot}0) \times 10^4$	$4{\cdot}50 \pm 0{\cdot}50$
6·43	0^+					5·14	$6{\cdot}7 \pm 0{\cdot}4$(ME)	$6{\cdot}05 \pm 0{\cdot}20$
7·59	3^-	2·68	2·08	$(1{\cdot}36 \pm 0{\cdot}22) \times 10^3$	$4{\cdot}57 \pm 0{\cdot}40$	3·17	$(1{\cdot}30 \pm 0{\cdot}16) \times 10^3$	$4{\cdot}39 \pm 0{\cdot}22$
8·37	3^-	2·61	2·09	$(2{\cdot}0 \pm 0{\cdot}2) \times 10^3$	$4{\cdot}55 \pm 0{\cdot}38$	3·03	$(1{\cdot}80 \pm 0{\cdot}20) \times 10^3$	$4{\cdot}28 \pm 0{\cdot}22$
9·30	2^+	3·18	2·36	$12{\cdot}0 \pm 2{\cdot}0$	$4{\cdot}62 \pm 0{\cdot}30$	3·56	$11{\cdot}3 \pm 1{\cdot}5$	$4{\cdot}45 \pm 0{\cdot}19$
9·97	1^+	2·45	2·90	$(1{\cdot}38 \pm 0{\cdot}20) \times 10^{-2}$	$2{\cdot}83 \pm 0{\cdot}30$		$(1{\cdot}34 \pm 0{\cdot}15) \times 10^{-2}$	$2{\cdot}70 \pm 0{\cdot}20$
10·35	4^+					3·0	$(1{\cdot}2 \pm 0{\cdot}4) \times 10^4$	4·5
10·70	1^+	2·64	2·90	$(3{\cdot}11 \pm 0{\cdot}40) \times 10^{-2}$	$2{\cdot}91 \pm 0{\cdot}40$		$(3{\cdot}15 \pm 0{\cdot}30) \times 10^{-2}$	$2{\cdot}74 \pm 0{\cdot}30$

Table 6. Results for the states with $E_x > 11$ MeV.

		Helm model			
E_x (MeV)	J^π	R(fm)	γ^0	$B(XL\uparrow)e^2\mathrm{fm}^{2L}$	R_{tr}(fm)
11·1	3^-	3·03†	2·0	$6{\cdot}2 \times 10^2$	4·3
11·38	2^+	3·10†	$0{\cdot}4 \pm 0{\cdot}2$	$2{\cdot}5 \pm 0{\cdot}7$	4·1
11·86	$(1^-, 3^-)$	3·03†	—	$2{\cdot}6 \times 10^{-6}$(E1) $(3{\cdot}4 \pm 0{\cdot}5) \times 10^2$(E3)	4·3
11·99	3^-	3·03†	$1{\cdot}0 \pm 0{\cdot}2$	$(1{\cdot}4 \pm 0{\cdot}2) \times 10^2$	4·3
12·39	3^-	3·03†	—	$(2{\cdot}0 \pm 0{\cdot}2) \times 10^2$	4·3
12·52	2^+	3·10†	$0{\cdot}63 \pm 0{\cdot}05$	$2{\cdot}2 \pm 0{\cdot}4$	4·1
12·7‡	2^-	$0{\cdot}42 \pm 0{\cdot}08$	$1{\cdot}6 \pm 0{\cdot}3$	$0{\cdot}26 \pm 0{\cdot}10$	$2{\cdot}5 \pm 1{\cdot}0$
12·99	2^+	3·10†	$0{\cdot}85 \pm 0{\cdot}05$	$3{\cdot}7 \pm 0{\cdot}6$	4·1
13·37‡	2^-	$0{\cdot}63 \pm 0{\cdot}11$	$2{\cdot}2 \pm 0{\cdot}4$	$0{\cdot}58 \pm 0{\cdot}20$	$2{\cdot}5 \pm 1{\cdot}0$

† Parameter fixed at value obtained for a lower energy transition of the same multipolarity.
‡ γ^- and γ^+ are given under R and γ^0 respectively.

REF.

G. C. Li, M. R. Yearian, and I. Sick
Phys. Rev. C9, 1861 (1974)

ELEM. SYM.	A	Z
Mg	24	12

METHOD

REF. NO.: 74 Li 2 hmg

REACTION	RESULT	EXCITATION ENERGY	SOURCE TYPE	SOURCE RANGE	DETECTOR TYPE	DETECTOR RANGE	ANGLE
E,E/	FMF	1- 6	C	250,500	MAG-D		DST

Detailed elastic scattering data tables for ^{24}Mg, ^{27}Al, ^{28}Si, and ^{32}S.

4 LEVELS 1.37 to 6.00

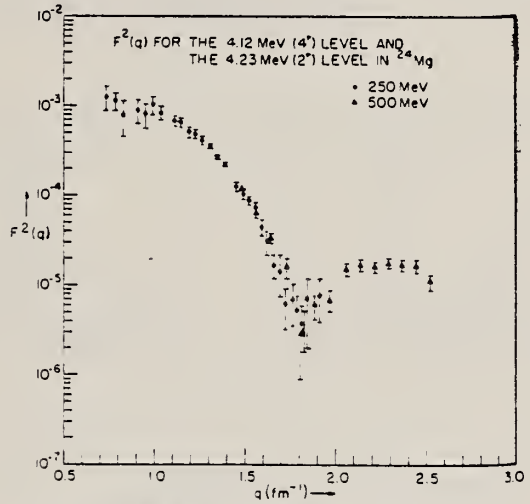

FIG. 10. Experimental form factor of the 4.12-MeV (4⁺) and the 4.23-MeV (2⁺) levels in ^{24}Mg.

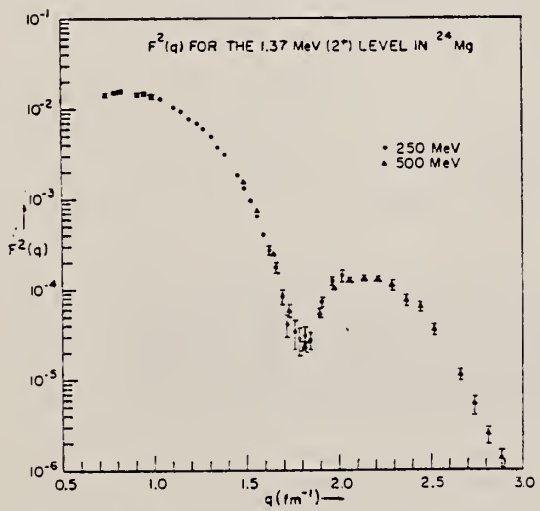

FIG. 9. Experimental form factor of the 1.37-MeV (2⁺) level in ^{24}Mg.

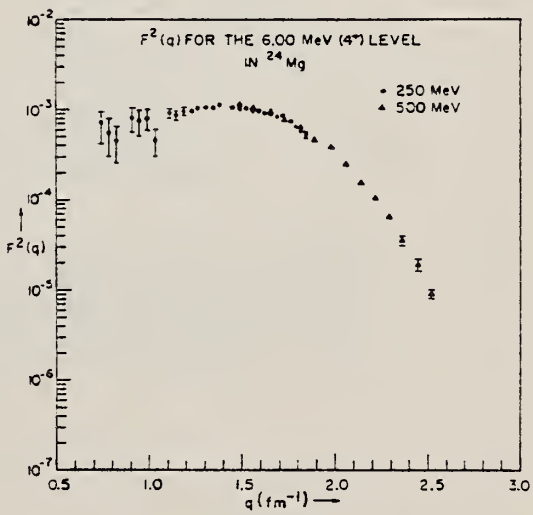

FIG. 11. Experimental form factor of the 6.00-MeV (4⁺) level in ^{24}Mg.

REF. R.R. Whitney, I. Sick, J.R. Ficenec, R.D. Kephart, and W.P. Trower
Phys. Rev. C9, 2230 (1974)

ELEM. SYM.	A	Z
Mg	24	12

METHOD

REF. NO. 74 Wh 3 hmg

REACTION	RESULT	EXCITATION ENERGY	SOURCE		DETECTOR		ANGLE
			TYPE	RANGE	TYPE	RANGE	
E,E/	ABX	0-300	D	500	MAG-D		60

See further analysis of this data in reference 79Zil

QUASIELASTIC SCAT

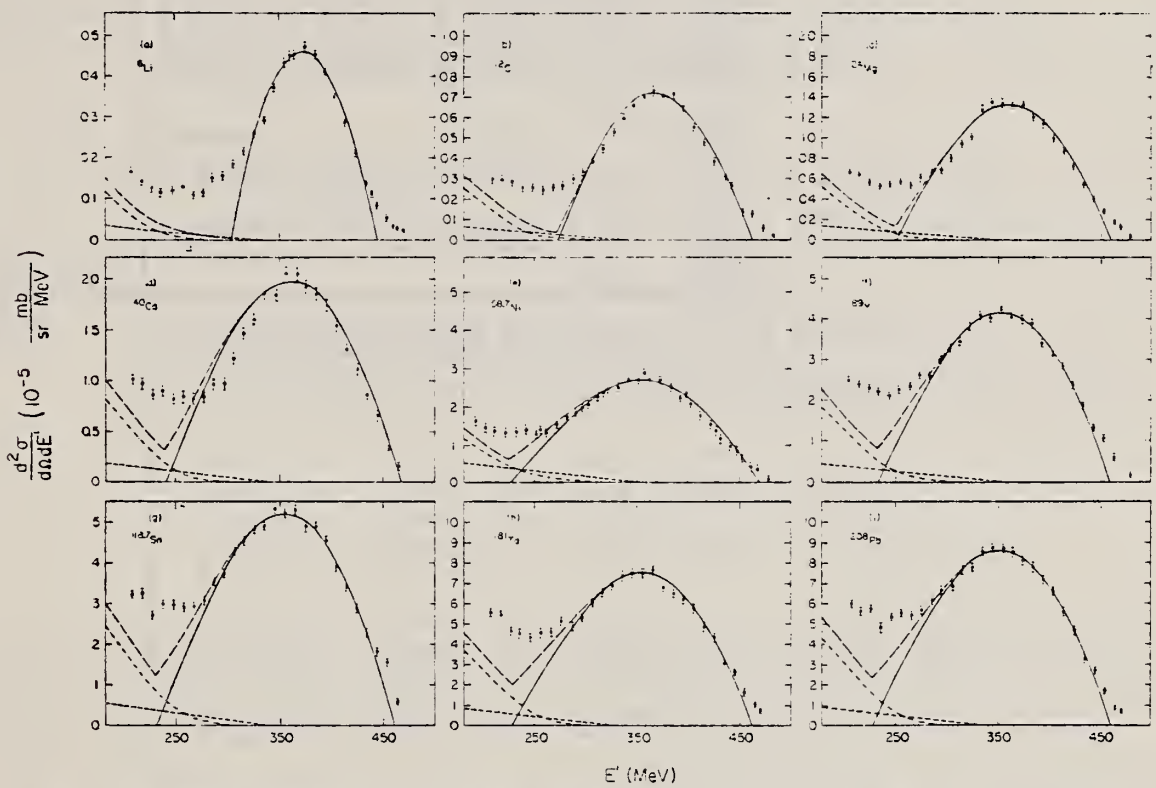

FIG. 1. The measured quasielastic peaks; the errors on the data points do not include an over-all 3% normalization uncertainty. The solid curve is a fit by the Fermi-gas model which yielded k_F (in MeV/c) and $\bar{\epsilon}$ (in MeV) as follows: (a) ^{6}Li (169, 17); (b) ^{12}C (221, 25); (c) ^{24}Mg (235, 32); (d) ^{40}Ca (249, 33); (e) $^{58.7}$Ni (260, 36); (f) ^{89}Y (254, 39); (g) $^{118.7}$Sm (260, 42); (h) ^{181}Ta (265, 42); (i) ^{208}Pb (265, 44). The fitting uncertainty in k_F is ±5 MeV/c and in $\bar{\epsilon}$ it is ±3 MeV. The small-amplitude dashed curve is the s-wave π-production contribution, the dot-dashed curve is the isobar excitation, and the large-amplitude dashed curve is the total result.

(over)

TABLE I. Proton-normalized and radiative-corrected cross sections $d^2\sigma/d\Omega dE' = (N \pm \Delta N) \times 10^{-n}$ in mb/sr MeV, for $E = 500$ MeV and $\theta = 60°$.

E'	^{6}Li			^{12}C			^{27}Al$_{fg}$			^{40}Ca			$^{58.7}$Ni			^{89}Y			$^{118.7}$Sn			$^{180.95}$Ta			^{208}Pb		
(MeV)	N	ΔN	n	N	ΔN	n	N	ΔN	n	N	ΔN	n	N	ΔN	n	N	ΔN	n	N	ΔN	n	N	ΔN	n	N	ΔN	n
480.0	···			1.79	0.19	7	3.83	0.42	7	···			1.22	0.17	6	1.71	0.19	6	···			···			···		
474.0	···			1.02	0.13	7	···			···			···			···			···			···			···		
470.0	1.72	0.18	7	5.75	0.52	7	1.55	0.15	6	···			3.90	0.29	6	5.85	0.41	6	···			7.09	0.67	6	7.00	0.68	6
464.0	2.49	0.29	7	1.39	0.11	6	1.91	0.17	6	2.72	0.15	6	4.48	0.33	6	5.68	0.37	6	8.32	0.71	6	1.16	0.08	5	9.82	0.79	6
460.0	2.96	0.30	7	1.20	0.09	6	2.58	0.19	6	···			···			···			···			1.54	0.10	5	1.81	0.10	5
454.1	5.02	0.17	7	9.21	0.71	7	2.96	0.20	6	1.20	0.17	6	7.00	0.41	6	1.07	0.05	5	1.85	0.09	5	1.70	0.11	5	2.31	0.11	5
450.0	···			···			···			···			8.92	0.17	6	1.03	0.05	5	1.83	0.09	5	···			···		
444.3	8.68	0.58	7	1.26	0.07	6	4.11	0.25	6	6.67	0.27	6	1.02	0.05	5	1.33	0.05	5	···			2.77	0.14	5	2.74	0.12	5
440.0	1.11	0.06	6	2.59	0.13	6	5.23	0.26	6	···			···			···			···			3.43	0.16	5	3.24	0.13	5
434.2	1.32	0.06	6	2.99	0.14	6	5.50	0.26	6	8.74	0.35	6	1.19	0.05	5	1.90	0.07	5	2.27	0.09	5	3.14	0.15	5	3.34	0.14	5
430.0	···			···			···			···			1.40	0.07	5	2.11	0.08	5	2.77	0.11	5	···			···		
424.3	2.12	0.08	6	3.75	0.15	6	7.31	0.29	6	1.12	0.04	5	1.54	0.08	5	2.31	0.09	5	2.88	0.12	5	4.43	0.18	5	4.74	0.19	5
414.4	2.88	0.12	6	4.75	0.19	6	8.78	0.35	6	1.32	0.05	5	1.78	0.10	5	2.88	0.11	5	3.40	0.14	5	4.98	0.20	5	5.64	0.23	5
404.5	3.51	0.11	6	5.46	0.22	6	1.02	0.04	5	1.56	0.06	5	2.09	0.08	5	3.09	0.12	5	3.90	0.16	5	5.89	0.24	5	6.57	0.26	5
400.0	···			6.25	0.25	6	1.09	0.04	5	···			2.35	0.09	5	3.34	0.13	5	4.29	0.17	5	6.56	0.27	5	7.00	0.28	5
394.7	4.16	0.17	6	6.32	0.26	6	1.15	0.05	5	1.75	0.07	5	2.22	0.09	5	3.41	0.14	5	4.56	0.18	5	6.29	0.25	5	7.25	0.29	5
385.7	4.55	0.18	6	7.09	0.28	6	1.21	0.05	5	1.86	0.07	5	2.51	0.10	5	3.91	0.16	5	4.88	0.19	5	6.36	0.26	5	7.88	0.32	5
374.9	4.76	0.19	6	6.97	0.28	6	1.33	0.05	5	1.94	0.08	5	2.72	0.11	5	4.02	0.16	5	4.88	0.19	5	6.87	0.28	5	8.19	0.33	5
365.0	4.56	0.18	6	7.28	0.29	6	1.32	0.05	5	2.08	0.08	5	2.69	0.10	5	4.04	0.16	5	5.34	0.21	5	7.77	0.31	5	8.61	0.34	5
360.0	4.50	0.18	6	6.61	0.28	6	1.32	0.05	5	···			2.88	0.11	5	4.11	0.16	5	5.69	0.23	5	7.92	0.33	5	8.42	0.34	5
355.2	4.35	0.17	6	6.97	0.28	6	1.36	0.05	5	2.08	0.08	5	2.69	0.11	5	4.23	0.17	5	5.22	0.21	5	7.51	0.30	5	···		
345.3	3.68	0.15	6	6.54	0.26	6	1.35	0.05	5	1.85	0.07	5	2.72	0.11	5	4.02	0.16	5	5.37	0.21	5	7.59	0.30	5	8.83	0.35	5
335.4	2.90	0.12	6	5.91	0.24	6	1.29	0.05	5	1.87	0.08	5	2.48	0.10	5	4.08	0.16	5	4.92	0.19	5	7.44	0.29	5	8.68	0.35	5
325.5	2.59	0.10	6	5.23	0.21	6	1.05	0.04	5	1.61	0.07	5	2.48	0.11	5	3.78	0.15	5	4.83	0.19	5	6.93	0.28	5	7.81	0.31	5
320.0	···			···			···			···			2.35	0.09	5	3.34	0.14	5	4.53	0.18	5	···			···		
315.7	2.16	0.10	6	4.43	0.18	6	9.41	0.38	6	1.47	0.06	5	2.26	0.09	5	3.43	0.14	5	4.34	0.17	5	6.61	0.26	5	7.76	0.31	5
305.8	1.84	0.09	6	3.79	0.15	6	8.61	0.32	6	1.23	0.05	5	2.03	0.08	5	3.27	0.13	5	4.32	0.17	5	6.11	0.24	5	6.92	0.28	5
300.0	···			···			···			···			1.97	0.08	5	3.11	0.12	5	4.03	0.16	5	···			···		
295.9	1.55	0.09	6	3.38	0.14	6	6.77	0.29	6	9.97	0.40	6	1.80	0.07	5	3.02	0.12	5	3.74	0.15	5	5.38	0.22	5	6.73	0.27	5
285.9	1.50	0.09	6	2.96	0.14	6	6.64	0.31	6	9.73	0.39	6	1.72	0.07	5	2.60	0.13	5	3.55	0.15	5	4.92	0.23	5	6.30	0.29	5
276.2	1.14	0.08	6	2.64	0.13	6	6.03	0.32	6	8.35	0.41	6	1.50	0.07	5	2.64	0.13	5	3.10	0.15	5	5.22	0.24	5	5.73	0.30	5
266.3	1.08	0.08	6	2.61	0.14	6	5.32	0.33	6	8.57	0.43	6	1.31	0.08	5	2.37	0.14	5	2.72	0.16	5	4.62	0.26	5	5.51	0.31	5
260.0	···			···			···			···			1.39	0.08	5	1.95	0.13	5	2.94	0.18	5	···			···		
256.4	1.28	0.09	6	2.43	0.15	6	5.71	0.35	6	8.33	0.45	6	1.27	0.08	5	2.27	0.14	5	2.87	0.18	5	4.57	0.28	5	5.63	0.33	5
246.6	1.20	0.09	6	2.55	0.16	6	5.47	0.36	6	8.55	0.48	6	1.39	0.09	5	2.14	0.14	5	2.95	0.19	5	4.33	0.28	5	5.40	0.35	5
236.7	1.15	0.10	6	2.54	0.16	6	5.18	0.38	6	8.71	0.51	6	1.31	0.09	5	2.24	0.15	5	3.02	0.20	5	4.35	0.30	5	4.90	0.34	5
226.8	1.27	0.11	6	2.88	0.19	6	5.62	0.42	6	8.72	0.51	6	1.29	0.10	5	2.29	0.16	5	2.73	0.20	5	4.57	0.30	5	5.88	0.37	5
216.9	1.43	0.14	6	2.91	0.21	6	6.35	0.49	6	9.81	0.56	6	1.34	0.10	5	2.38	0.17	5	3.26	0.22	5	5.42	0.36	5	5.76	0.38	5
207.0	1.66	0.16	6	2.91	0.21	6	6.59	0.52	6	1.02	0.06	5	1.13	0.11	5	2.51	0.18	5	3.24	0.22	5	5.58	0.37	5	6.11	0.40	5
197.2	1.78	0.17	6	3.42	0.24	6	7.01	0.59	6	···			1.59	0.12	5	2.77	0.20	5	3.43	0.24	5	5.67	0.38	5	5.99	0.41	5

REF. U. E. P. Berg, K. Wienhard, H. Wolf
Phys. Rev. C11, 1851 (1975)

ELEM. SYM.	A	Z
Mg	24	12

METHOD

REF. NO.: 75 Be 1 hmg

REACTION	RESULT	EXCITATION ENERGY	SOURCE TYPE	SOURCE RANGE	DETECTOR TYPE	DETECTOR RANGE	ANGLE
G,G	LFT	9- 11	C	29	SCD-D		125
		(9.83-10.73)		(28.7)			

9.827,9.965,10.731 LEVELS

TABLE II. Integrated scattering cross sections I_s and derived γ-decay widths.

Transition (Energy in MeV)	Titze [a] Γ_γ^0 (eV)	Fagg [b] Γ_γ^0 (eV)	This work Γ_γ^0 (eV)	This work Γ_γ^1 (eV)	This work I_s (MeV mb)
10.71 — g.s.	15.9 ± 2.4	$17.6^{+3.5}_{-3.0}$	$17.8^{+8.9}_{-5.6}$		$1.45^{+0.64}_{-0.44}$
10.71 — 1.38				$4.2^{+1.8}_{-1.6}$	$0.33^{+0.17}_{-0.12}$
9.97 — g.s.	4.50 ± 0.73		$6.2^{+2.7}_{-2.2}$		$0.48^{+0.23}_{-0.16}$
9.97 — 1.38		$\Sigma = 7.6^{+1.5}_{-1.4}$		$2.8^{+1.2}_{-1.0}$	$0.22^{+0.11}_{-0.08}$
9.83 — g.s.	1.05 ± 0.26		$1.7^{+1.0}_{-0.7}$		$0.16^{+0.08}_{-0.06}$
9.83 — 1.38				$0.5^{+0.5}_{-0.4}$ [c]	$0.045^{+0.043}_{-0.036}$

[a] Reference 2.
[b] Reference 3.

[2] O. Titze, Z. Phys. 220, 66 (1969).
[3] L.W. Fagg et al., Phys. Rev. C1, 1137 (1970).

REF. E. Kuhlmann, E. Ventura, J. R. Calarco, D. G. Mavis, S. S. Hanna
Phys. Rev. C11, 1525 (1975)

ELEM. SYM.	A	Z
Mg	24	12

METHOD

REF. NO. 75 Ku 4 hmg

REACTION	RESULT	EXCITATION ENERGY	SOURCE TYPE	SOURCE RANGE	DETECTOR TYPE	DETECTOR RANGE	ANGLE
A,G	ABX	11- 26	D	3- 20	NAI-D		DST

SEE ANALYSIS 79KU5

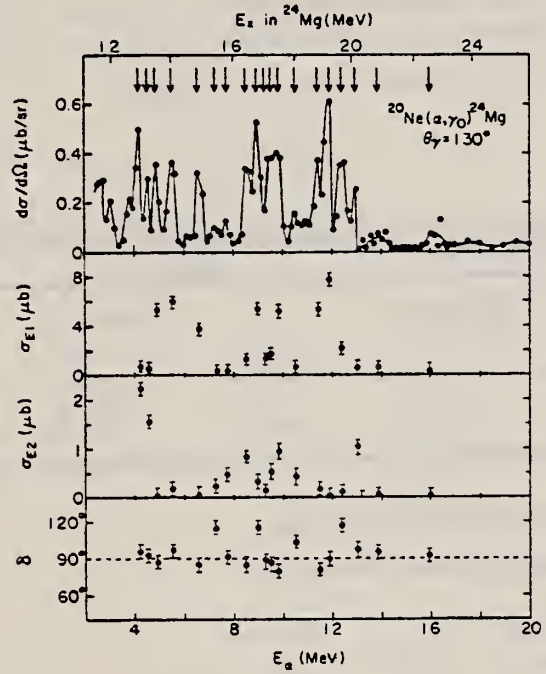

FIG. 2. Top: excitation function at $\theta = 130°$ for the reaction ^{20}Ne$(\alpha, \gamma_0)^{24}$Mg. The arrows indicate energies at which angular distributions were studied. Middle: the extracted $E1$ and $E2$ total cross sections for the (α, γ_0) reaction. Bottom: the $E2$ phase δ, relative to the $E1$ phase, which is arbitrarily set to zero.

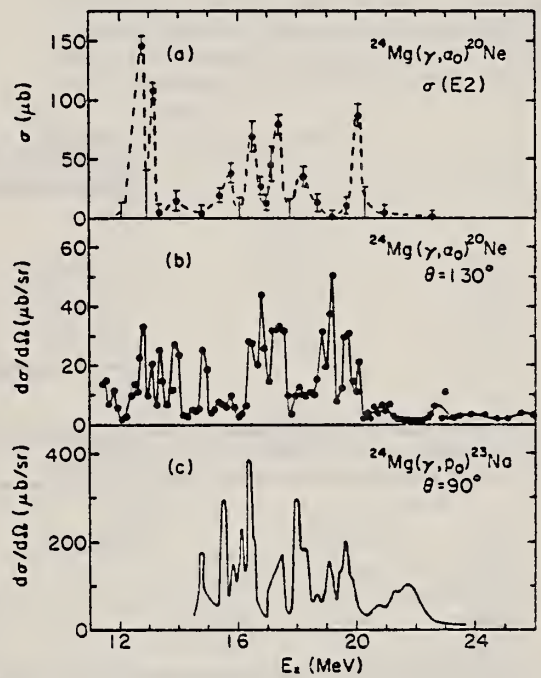

FIG. 4. (a) the extracted total $E2$ cross section converted by detailed balance to that for the reaction ^{24}Mg$(\gamma, \alpha_0)^{20}$Ne. (b) the 130° excitation function $(E1 + E2)$ for ^{24}Mg$(\gamma, \alpha_0)^{20}$Ne. (c) the excitation function at $\theta = 90°$ for ^{24}Mg$(\gamma, p_0)^{23}$Na obtained by detailed balance from ^{23}Na$(p, \gamma_0)^{24}$Mg (Ref. 14).

(over)

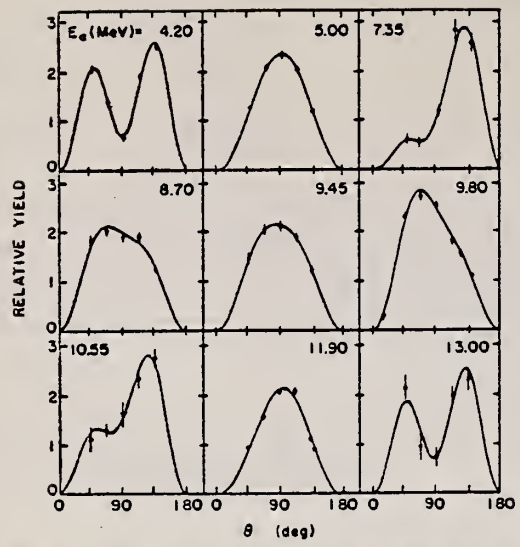

FIG. 3. Typical angular distributions for the reaction ^{20}Ne(α, γ_0)^{24}Mg. Note the almost pure $E1$ character of the distributions at E_α = 5.00 and 11.90 MeV in marked contrast to the predominantly $E2$ character at 4.20 and 13.00 MeV. The solid lines are fits in terms of Eq. (3).

TABLE I. The averaged absolute cross sections $\bar{\sigma}(\alpha,\gamma_0)$ and $\bar{\sigma}(\alpha,\gamma_1)$ for the reactions ^{20}Ne(α,γ)^{24}Mg and ^{22}Ne(α,γ)^{26}Mg.

	^{20}Ne(α,γ)^{24}Mg		^{22}Ne(α,γ)^{26}Mg	
ΔE_x (MeV)	$\bar{\sigma}(\alpha,\gamma_0)$ [a] (μb)	$\bar{\sigma}(\alpha,\gamma_1)$ [b] (μb)	$\bar{\sigma}(\alpha,\gamma_0)$ [a] (μb)	$\bar{\sigma}(\alpha,\gamma_1)$ [b] (μb)
11.4–14.4	3.2	3.9	...	...
14.4–17.8	3.1	4.8	9.2	8.6
17.8–20.2	3.6	9.6	3.0	4.5
20.2–23.8	0.6	1.8	0.9	2.8
23.8–26.0	0.4	0.6	...	...

[a] Angular distribution assumed to be of the form $W(\theta) = \sin^2\theta$.
[b] Angular distribution assumed to be isotropic.

TABLE II. Summary of $E2$ strengths in ^{24,26}Mg(γ, α_0) (see text) given in percent of the $E2$ sum rule [Eq. (5)].

Nucleus	ΔE (MeV)	$\int\sigma(E2)/E^2dE$ (%)	ΔE (MeV)	$\int\sigma_{tot}^{CN}(E2)/E^2dE$ (%)
^{24}Mg	12.0–22.5	11.8 ± 1.0	0–22.5	120 ± 30
^{26}Mg	15.0–21.4	6.0 ± 2.0	0–21.4	290 ± 80

TABLE III. A comparison of the integrated $E1$ strengths found in various reactions in the GDR's of ^{24}Mg and ^{26}Mg. The strengths are given in percent of the $E1$ sum rule [Eq. (4)].

	(γ, α)		(γ, p_0) [a]		(γ, n) [b]		(e, e') [c]	
Nucleus	ΔE (MeV)	$\int\sigma(E1)dE$ (%)	ΔE (MeV)	$\int\sigma(E1)dE$ (%)	ΔE (MeV)	$\int\sigma(E1)dE$ (%)	ΔE (MeV)	$\int\sigma(E1)dE$ (%)
^{24}Mg	14.6–20.6	0.33	15.5–23.0	3.3	16.5–28.0	14.0	16.0–22.0	30.0
^{26}Mg	14.8–21.0	0.70	...	...	11.0–28.0	58.0	14.5–28.0	48.0

[a] Reference 14.
[b] Reference 15.
[c] References 19 and 27.

14 R.C. Bearse et al., Nucl. Phys. A116, 682 (1968).

15 S.C. Fultz et al., Phys. Rev. C4, 149 (1971).

19 O. Titze et al., Phys. Lett. 24B, 169 (1967); A. Goldmann, Z. Phys. 234, 144 (1970).

27 O. Titze et al., Phys. Lett. 31B, 565 (1970).

REF. K. Bangert, U.E.P. Berg, G. Junghans, R. Stock, K. Wienhard
H. Wolf
Nucl. Phys. A261, 149 (1976)

EL EM. SYM.	A	Z
Mg	24	12

METHOD

REF. NO. 76 Ba 2 egf

REACTION	RESULT	EXCITATION ENERGY	SOURCE		DETECTOR		ANGLE
			TYPE	RANGE	TYPE	RANGE	
G,P	SPC	13- 30	C	18- 30	TEL-D		90
G,PG	ABY	12- 30	C	18- 30	SCD-D		125
G,NG	ABY	17- 30	C	18- 30	SCD-D		125
G,A	ABX	18- 22	C	30	TEL-D		90

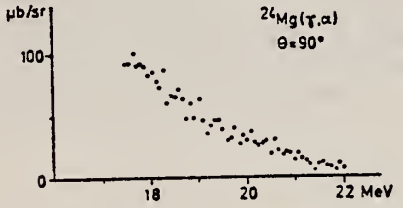

Fig. 2. The $^{24}Mg(\gamma, \alpha)$ differential cross section obtained from the 30.0 MeV α-particle spectrum.

TABLE 1
Structures in the $^{24}Mg(\gamma, p)$ spectra [a])

Run (MeV)	18	19.5	21	23	30
Peaks at	2.63	2.76	2.82		2.8
(MeV)	3.00	2.92	3.03	2.92	3.02
	3.83		3.78	3.88	3.96
	4.26	4.18	4.07	4.10	4.20
		4.63	4.65	4.75	4.73
	4.80				
		5.06	5.11	5.13	
	5.35		5.43		
	5.55	5.58	5.66		
	5.76			5.8	5.73
					5.96
		6.32	6.26	6.43	6.42
			6.84	6.86	6.80
				7.06	7.03
				7.70	7.66
				7.98	7.95
				8.4	8.4
				8.7	8.6
				8.9	8.9
				10.4	10.6
					10.9
					12.5

[a]) Peak energies are corrected for energy loss in the target and for recoil energy, assuming direct (γ, p) reactions.

(over)

TABLE 2

Results of the $^{24}Mg(\gamma, x\gamma')$ experiment, giving the "bremsstrahlung-weighted" integrated cross sections in MeV · mb for the population of excited residual nuclear states

	Bremsstrahlung endpoint energy (MeV)				
	18.0	19.5	21.0	23.0	30.5
(a) ^{23}Na states					
g.s. $\frac{3}{2}^+$ [a])	0.67	1.02	1.52	2.07	2.59
440 keV, $\frac{5}{2}^+$	?	?	?	?	?
2076 keV, $\frac{7}{2}^+$	<1.25	<2.24	<2.74	<5.49	<8.90
2391 keV, $\frac{1}{2}^+$	0.99	2.73	4.68	7.45	10.56
2640 keV, $\frac{1}{2}^-$	0.80	1.41	2.27	4.52	8.02
2704 keV, $\frac{3}{2}^+$				<1.25	<2.80
2982 keV, $\frac{3}{2}^+$		0.85	1.77	3.13	5.73
3678 keV, $\frac{3}{2}^-$		0.65	1.34	2.72	4.44
3848 keV, $\frac{5}{2}^-$				0.82	2.03
3915 keV, $\frac{5}{2}^+$		0.57	0.94	2.27	6.27
4432 keV, $\frac{1}{2}^+$		0.94	1.78	3.22	6.53
5380 keV, $(\frac{3}{2}, \frac{5}{2})^+$			0.7	1.31	1.89
5967 keV, $(\frac{1}{2}, \frac{3}{2})^-$		0.3	0.51	1.81	<3.5
(b) ^{23}Mg states					
g.s. $\frac{3}{2}^+$	?	?	?	?	?
451 keV, $\frac{5}{2}^+$	?	?	?	?	?
2051 keV, $\frac{7}{2}^+$					0.85
2359 keV, $\frac{1}{2}^+$				1.46	2.13
2715 keV, $\frac{5}{2}^+$				<1.18	<1.79
2771 keV, $\frac{1}{2}^-$				0.93	3.05
4356 keV, $\frac{1}{2}^+$				0.3	0.55
(c) ^{22}Ne states					
1275 keV, 2^+					1.17
(d) ^{20}Ne states					
1634 keV, 2^+	<1.25	<2.24	<2.74	<5.49	<8.9
Sum of observed (γ, p) excited states cross sections	1.79	7.18	13.99	28.50	51.77
Sum of observed (γ, n) excited states cross sections				3.87	8.37
Total (γ, n) yield [b])	0.57	3.16	6.91	11.97	21.41
Total photoabsorption yield [c])	7.46	16.23	32.42	52.62	104.55

The bremsstrahlung spectra are normalized at 10.71 MeV.

[a]) Calculated from the data of ref. [14]).

[b]) Calculated from the data of ref. [2]).

[c]) Calculated from the data of ref. [22]).

[2] S.C. Fultz et al., Phys. Rev. C4, 149 (1971); R.A. Alvarez et al., Phys. Rev. C4, 1673 (1971).

[14] R.C. Bearse et al., Nucl. Phys. A116, 682 (1968).

[22] B.S. Dolbilkin et al., Bull. Acad. Sci. USSR 30, 354 (1966.

REF. H. Zarek, B. O. Pich, T. E. Drake, D. J. Rowe, W. Bertozzi, C. Creswell, A. Hirsch, M. V. Hynes, S. Kowalski, B. Norum, F. N. Rad, C. P. Sargent, C. F. Williamson and R. A. Lindgren
Phys. Rev. Lett. 38, 750 (1977)

ELEM. SYM.	A	Z
Mg	24	12

METHOD

REF. NO. 77 Za 2 hmg

REACTION	RESULT	EXCITATION ENERGY	SOURCE		DETECTOR		ANGLE
			TYPE	RANGE	TYPE	RANGE	
E,E/	FMF	15	D	108-260	MAG-D		DST

15.045 MeV

The unique high-resolution and high-energy features of the electron-scattering facility at the MIT–Bates Accelerator were used to locate a dominant narrow resonance at 15.045 ± 0.035 MeV in ^{24}Mg. A spin-parity assignment of 6^- and an isospin $T = 1$ assignment were made. The $M6$ form factor was measured and compared to the prediction of a theoretical calculation which uses the open-shell random-phase approximation on a shell-model ground state for ^{24}Mg.

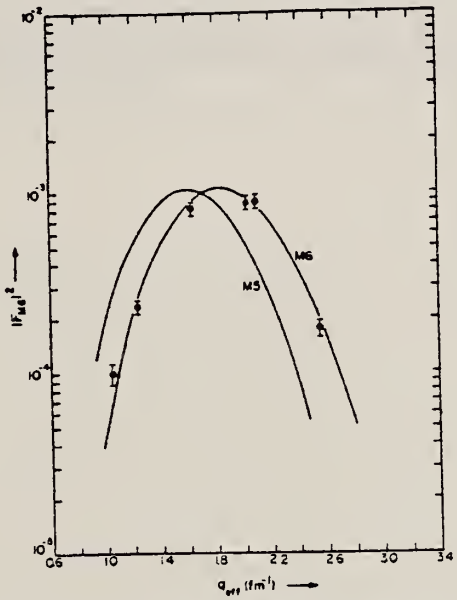

FIG. 3. The form factor $|F_{M6}(q)|^2$ for the 6^-, $T=1$ resonance at 15.045± 0.035 MeV in ^{24}Mg. The open-shell random-phase approximation calculation for $M6$ is shown as a solid line. An $M5$ curve (see text) is added for comparison purposes.

REF. L.K. Fifield, M.J. Hurst, T.J.M. Symons, F. Watt, C.H. Zimmerman, and K.W. Allen
Nuclear Physics A309, 77 (1978)

ELEM. SYM.	A	Z
Mg	24	12

METHOD

REF. NO. 78 Fi 6 hg

REACTION	RESULT	EXCITATION ENERGY	SOURCE		DETECTOR		ANGLE
			TYPE	RANGE	TYPE	RANGE	
A,G	LFT	12-15	C	3-6	SCD-D		DST
		(12.00-14.15)		(3.05-5.8)			

8 LEVELS STUDIED

Abstract: The $^{20}Ne(\alpha, \gamma)^{24}Mg$ reaction has been used to measure radiative decay rates for known high spin levels at 12.86(6^+), 13.44(6^-) and 14.15(8^-) MeV in ^{24}Mg, and for previously unidentified levels at 12.00, 13.04 and 14.08 MeV. Gamma-ray angular distributions indicate that the 12.00 and 14.08 MeV levels are probably 6^+ levels, while the 13.04 MeV level is the lowest 0^+ $T = 1$ state. A new level at 11.005 MeV, populated in the radiative decay of the 14.08 MeV level, is most likely the lowest 5^+ $T = 1$ state in ^{24}Mg. Alpha-particle widths have also been measured for several of these levels and for the known 6^+ level at 13.85 MeV using the $^{20}Ne(\alpha, \alpha'\gamma)^{20}Ne$ reaction and previously determined branching ratios. The results for both radiative and particle decay widths are compared with recent shell-model calculations performed within a full $(sd)^8$ basis.

E NUCLEAR REACTIONS $^{20}Ne(\alpha, \gamma)$, $^{20}Ne(\alpha, \alpha'\gamma)$, $E = 3.0$–6.0 MeV; measured $\sigma(E_\alpha, E_\gamma, \theta_\gamma)$. ^{24}Mg deduced levels, J, π, T, γ-ray branching ratios, radiative widths, α-particle widths. Windowless gas target.

TABLE 4

Alpha particle widths of 6^+ and 8^+ levels in ^{24}Mg

Level	E_x (MeV)	$\omega\gamma_a$ [a] (eV)	Γ_{a_0}/Γ [b]	Ground-state transitions			Transitions to 1.63 MeV state		
				Γ_{a_0} (eV)	$\vartheta^2_{a_0}$ [c]	A^2_{NL} [d]	Γ_{a_1} (eV)	$\vartheta^2_{a_1}$ [c]	A^2_{NL} [d]
6_3	12.00	[e]		> 0.022	> 7.6×10^{-3}	5.1×10^{-3}			
6_4	12.86	2.4 ± 0.3	0.35 ± 0.04	0.33 ± 0.04	$(4.0\pm0.5)\times10^{-3}$	8.6×10^{-3}	0.54 ± 0.08	0.10 ± 0.02	3.5×10^{-4}
6_5	13.44	15 ± 5	0.23 ± 0.03	1.6 ± 0.6	$(3.5\pm1.3)\times10^{-3}$	3.5×10^{-3}	4.9 ± 1.7	0.03 ± 0.01	2.5×10^{-3}
6_6	13.85	40 ± 10	0.03 ± 0.01	3.0 ± 1.3	$(2.6\pm1.1)\times10^{-3}$	2.2×10^{-2}	100 ± 40	0.13 ± 0.05	1.1×10^{-4}
6_7	14.08	1160 ± 165	> 0.7 [f]	250 < Γ_{a_0} < 1000	0.13 < $\vartheta^2_{a_0}$ < 0.51	[g]	105 ± 25 [h]	0.06 ± 0.014	[g]
8_1	11.86			< 1.2×10^{-4} [i]	< 3.4×10^{-2}	2.7×10^{-3}			
8_2	13.21			< 2.2×10^{-3} [i]	< 1.6×10^{-3}	2.8×10^{-3}			
8_3	14.15		0.22 ± 0.04	0.075 ± 0.016 [j]	$(3.7\pm0.8)\times10^{-3}$	8.0×10^{-3}	0.18 ± 0.05 [j]	$(6.9\pm1.9)\times10^{-3}$	2.5×10^{-2}

[a]) $\omega\gamma_a = (2J+1)\Gamma_{a_0}\Gamma_{a_1}/\Gamma$.
[b]) Derived from the present work and from α-particle branching ratios in ref. [9]). Errors were estimated from data in ref. [9]).
[c]) $\vartheta^2_a = \Gamma_a/(2\hbar^2 P_L/\mu R^2)$, where μ is the reduced mass of the ^{20}Ne + α system, $R = r_0(20^{1/3}+4^{1/3})$ fm, $P_L(kR)$ is the penetrability factor for relative orbital angular momentum L and wave number k.
[d]) Ref. [11]).
[e]) The 12.00 MeV level was not observed as a ^{20}Ne(α, α′)^{20}Ne* resonance.
[f]) See text.
[g]) Calculations are not available for this level.
[h]) Using $\Gamma_{a_0}/\Gamma = 0.85\pm0.15$.
[i]) Ref. [9]).
[j]) Derived from known α-particle and γ-ray branching ratios [9]) using our measured value of Γ_γ.

Alpha-particle widths. Alpha-particle widths of 6^+ and 8^+ levels in ^{24}Mg are summarised in table 4. With the exception of the 11.86 and 13.21 MeV 8^+ levels, all the values are from the present work using branching ratios from ref. [9]) where appropriate. The spectroscopic factors, ϑ^2_a, were derived from the measured widths using a radius parameter r_0 of 1.2 fm; increasing r_0 to 1.4 fm decreases ϑ^2_a by a factor between 4 and 10 depending on the transition. Theoretical calculations by Kelvin *et al.* [11]), using wave functions generated with the CWC interaction, are tabulated in the final column. The quantity A^2_{NL} is as defined by Ichimura *et al.* [22]), and when calculated with harmonic oscillator wave functions should be approximately equal to ϑ^2_a. The N and L are the oscillator quantum numbers for the c.m. of the α-particle, where $2N+L = 8$ if the same oscillator length parameters are used for the internal structure of the α-particle and for the sd shell wave functions. In deriving $\vartheta^2_{a_0}$ for the 14.08 MeV level, we have assumed a conservative upper limit of 30 % on an α-particle branch to the 1.63 MeV level in ^{20}Ne, and have used $\Gamma_{a_0}/\Gamma = 0.85\pm0.15$ in deriving $\vartheta^2_{a_1}$.

Ref. 9 -- L.K. Fifield, R.W. Zurmühle and D.P. Balamuth, Phys. Rev. C8, (1973) 2217
Ref. 11 - D. Kelvin, A. Watt and R.R. Whitehead, to be published
Ref. 22 - M. Ichimura, A. Arima, E.C. Halbert and T. Terasawa, Nucl. Phys. A204, (1973) 225

REF. K. Masumoto, T. Kato, N. Suzuki
Nucl. Inst. Meth. 157, 567 (1978)

ELEM. SYM.	A	Z
Mg	24	12

METHOD

REF. NO. 78 Ma 10 hg

REACTION	RESULT	EXCITATION ENERGY	SOURCE		DETECTOR		ANGLE
			TYPE	RANGE	TYPE	RANGE	
G,PN	ABY	26-68	C	30-68	ACT-I		4PI

Analysis is made of reactions interfering with photon activation analysis procedures.

The activation yield curves have been presented for a number of photonuclear reactions in the energy range from 30 to 68 MeV, in order to evaluate quantitatively the interferences due to competing reactions in multielement photon activation analysis. The general features of the yields as functions of both target mass number and excitation energy were elucidated from the data obtained, discussion being given on the results in terms of the reaction mechanism.

Simultaneous neutron activation due to appreciable neutron production from the converter and surrounding materials has also been studied, and, finally, the magnitudes of interferences in real multielement analysis were given in the form of their energy dependences.

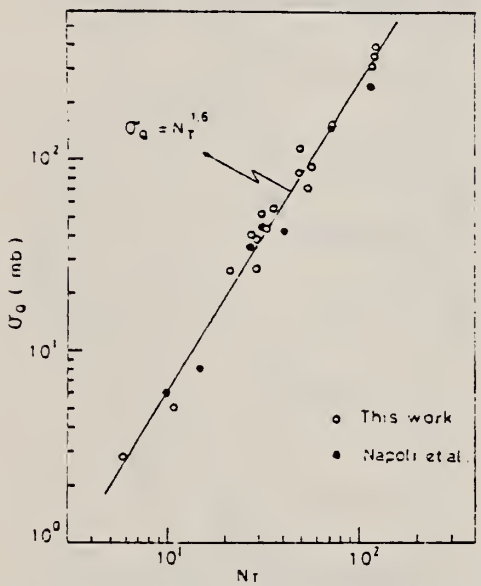

Fig. 2. Yield per equivalent quanta versus target neutron number.

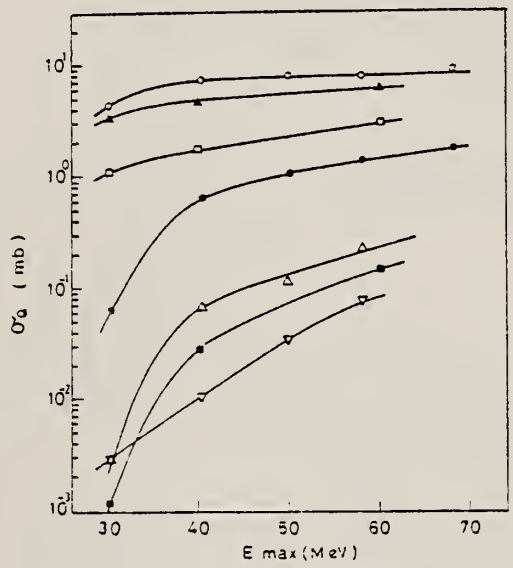

Fig. 3. Activation yield curves for the reactions on C, Na, Mg and Al.
□ $^{12}C(\gamma, n)^{11}C$, ■ $^{12}C(\gamma, xn)^{7}Be$, ▲ $^{23}Na(\gamma, n)^{22}Na$,
○ $^{25}Mg(\gamma, p)^{24}Na$, ● $^{24}Mg(\gamma, pn)^{23}Na$, △ $^{27}Al(\gamma, xn)^{22}Na$,
▽ $^{27}Al - ^{24}Na$.

(over)

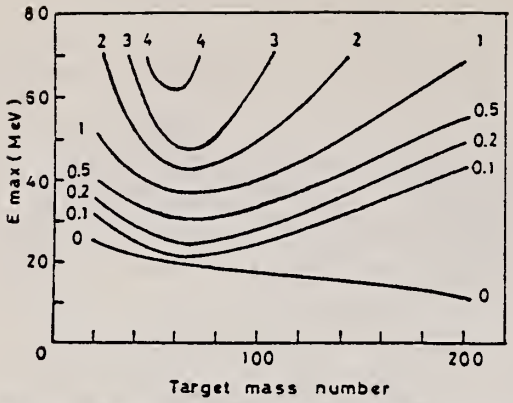

Fig. 11. Yields of the (γ, pn) reactions as a function of bremsstrahlung maximum energy and target mass number. The numerical values in the figure are yields per equivalent quanta in mb.

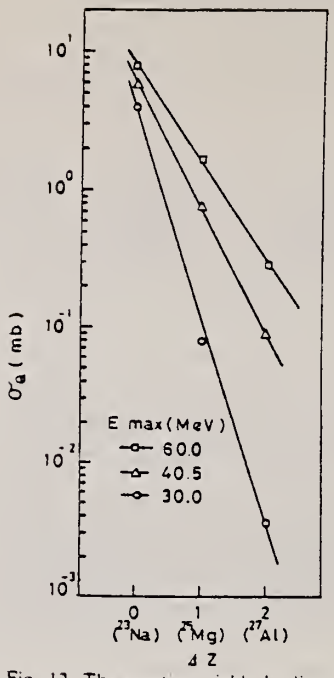

Fig. 12. The reaction yields leading to ^{22}Na as a function of difference in atomic number between target and product nuclides.

REF. A.M. Sandorfi and A.M. Nathan
Phys. Rev. Lett. 40, 1252 (1978)

ELEM. SYM.	A	Z
Mg	24	12

METHOD

REF. NO. 78 Sa 3 rs

REACTION	RESULT	EXCITATION ENERGY	SOURCE TYPE	SOURCE RANGE	DETECTOR TYPE	DETECTOR RANGE	ANGLE
C12,G	ABX	18- 28	D	4- 14	NAI-D		45°

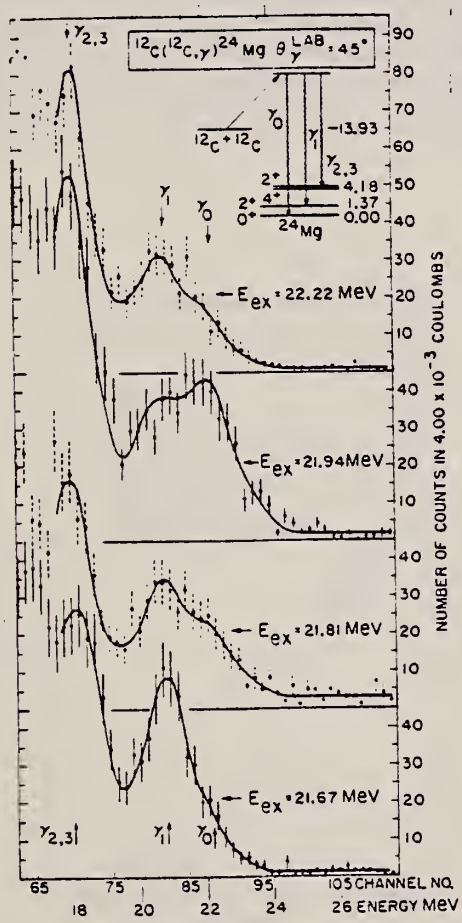

FIG. 1. The high-energy portion of the γ-ray spectra, taken at incident beam energies of 15.70, 15.98, 16.25, and 16.80 MeV with a 230-keV- (c.m.) thick target, are shown here. The spectra are labeled with the Doppler-shift-corrected excitation energies at the middle of the target and have been shifted linearly in channel number to compensate for the differences in energy. As displayed, all share a common energy scale with the data at 21.81 MeV excitation. The position of the centroids of γ_0, γ_1, and $\gamma_{2,3}$ are indicated. The variations of the Doppler shifts and of the peak widths are negligible for these spectra. The intensities of the high-energy γ-ray lines may thus be compared directly. The solid curves are three-peak fits to the data points (see text).

The yield curves of high-energy capture γ rays from $^{12}C(^{12}C,\gamma_0)$ and $^{12}C(^{12}C,\gamma_1)$ were measured at θ_{lab} = 45° from $E_{c.m.}$ = 5.0 to 11.0 MeV. A $J^\pi = 2^+$ resonance, with a width (full width at half-maximum) of 261± 74 keV and a peak cross section at 45° of 44.3± 4.5 nb/sr, was observed in $^{12}C(^{12}C,\gamma_0)$ at (21.98± 0.03) MeV excitation in ^{24}Mg. Several other resonant features were also observed in the γ-ray yields.

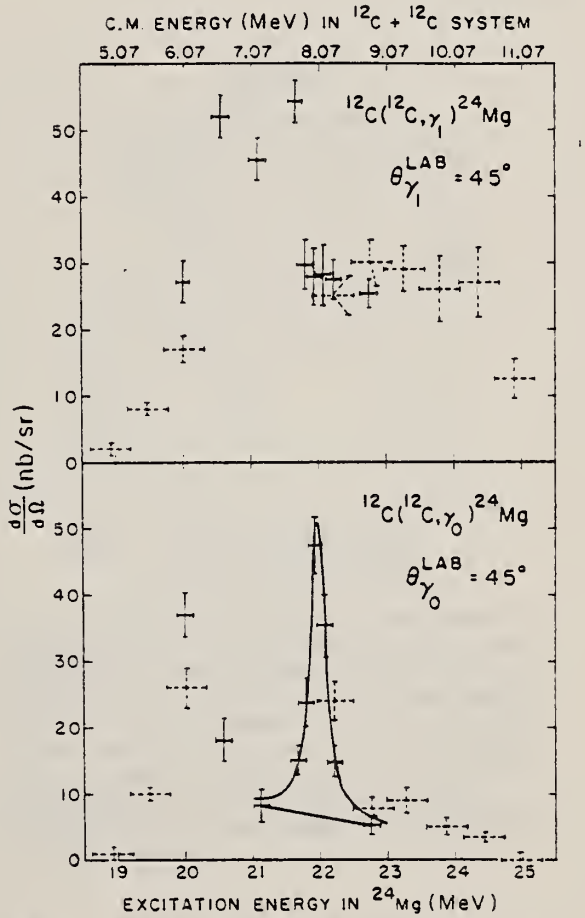

FIG. 2. The solid points on the excitation functions shown here were taken with a 74-μg/cm² ^{12}C(99.9%) target. The dashed data points were collected with a 280-μg/cm² natural carbon foil. The horizontal bars indicate the target thickness. The solid curve is a fit to the data assuming a single Breit-Wigner resonance (see text).

REF. A.M. Sandorfi, L.R. Kilius, H.W. Lee, and A.E. Litherland
Phys. Rev. Lett. 40, 1248 (1978)

ELEM. SYM.	A	Z
Mg	24	12

METHOD

REF. NO. 78 Sa 4 rs

REACTION	RESULT	EXCITATION ENERGY	SOURCE TYPE	SOURCE RANGE	DETECTOR TYPE	DETECTOR RANGE	ANGLE
E,F	ABX	20- 28	D	21- 32	TRK-D		DST

We report the electron-induced fission of ^{24}Mg into two ground-state ^{12}C nuclei following monopole excitation at energies between 20 and 22 MeV. The observed cross section exhausts at least (8±2)% of the linear energy-weighted monopole sum rule $S(E0)$ and may form a part of the giant monopole resonance. In addition, we have observed a peak in the $\theta_{^{12}C} = 45°$ excitation function between 22.0 and 23.5 MeV with a width (full width at half-maximum) < 1 MeV and a ^{12}C angular distribution, $\sin^2(2\theta_{c.m.})$, indicating $J^\pi = 2^+$.

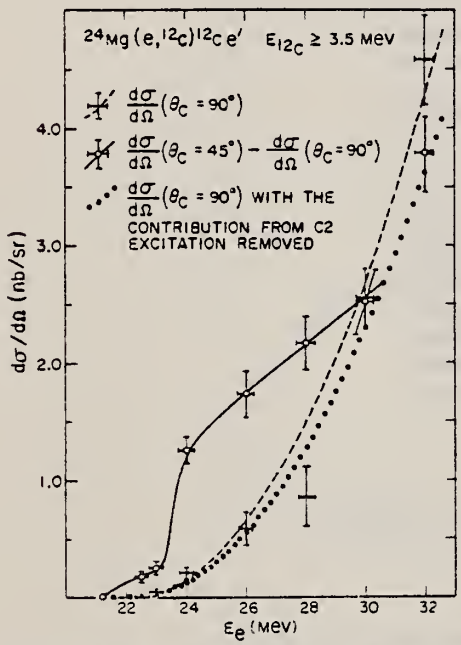

FIG. 1. Differential electrofission cross sections are shown here. The solid curve follows a form calculated assuming E2 excitation [Ref. 6, Eq. (14)]. The dashed and dotted curves are fits to the data assuming the quadratic energy dependence characteristic of "Coulomb" excitation (see text).

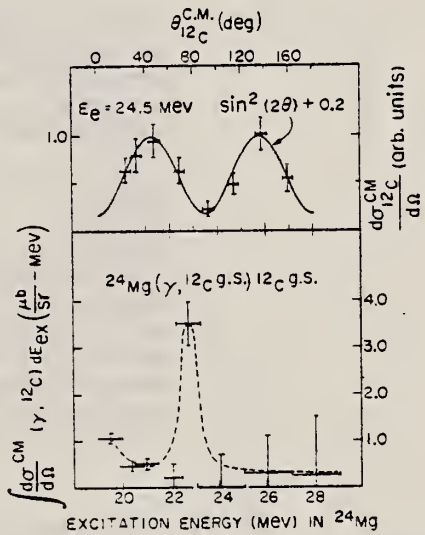

FIG. 2. The equivalent photofission cross section (bottom) was deduced from the data points on the solid curve of Fig. 1. The points shown here result from integrals over the regions of excitation energy denoted by the horizontal bars. Below 21 MeV, the cross sections are uncertain within a factor of 2, in addition to the errors shown (see text). The dashed curve is merely a guide to the eye. The ^{12}C angular distribution (top) indicates a $J^\pi = 2^-$ assignment to the peak centered at 22.7 MeV (bottom).

[6]G. Bishop, in "Nuclear Structure and Electromagnetic Interactions, Scottish Universities Summer School, Edinburgh, Scotland, 1964," edited by N. MacDonald (Oliver and Boyd, Edinburgh, Scotland, 1964).

over

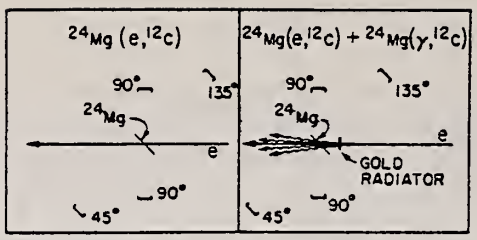

FIG. 3. The inability to excite 0^+ states with real photons was utilized, in the experiment shown here schematically, to verify the association of the 90° yield of Fig. 1 with monopole excitation (see text and Table I).

TABLE I. ^{12}C production cross sections (nb/sr) with and without a photon converter. This data has not been corrected for $^{16}O(e/\gamma, ^{12}C)$ (10% of the yield at this electron energy). $E_{^{12}C} \geq 3.5$ MeV.

$\theta(^{12}C)$	45°	90°	135° [a]
Radiator out	2.0 ± 0.2	0.6 ± 0.1	0.4 ± 0.1
Radiator in	4.1 ± 0.3	0.8 ± 0.1	1.1 ± 0.2

[a]The 135° and 45° data differ because they are presented for a fixed detector development time (see Ref. 2). This results in an angle-dependent detector efficiency due to the varying kinematic shifts between laboratory and center-of-mass frames. This dependence was removed from the angular distribution measurements of Fig. 2 (see text).

[2]R. Fleischer, P. Price and R. Walker, "Nuclear Tracks in Solids (Univ. of California Press, Berkeley, 1975), pp. 136-137.

REF. H. Zarek, S. Yen, B.O. Pich, T.E. Drake, C.F. Williamson, S. Kowalski, C.P. Sargent, W. Chung, B.H. Wildenthal, M. Harvey and H.C. Lee
Phys. Lett. 80B, 26 (1978)

ELEM. SYM.	A	Z
Mg	24	12

METHOD

REF. NO. 78 Za 2 rs

REACTION	RESULT	EXCITATION ENERGY	SOURCE TYPE	SOURCE RANGE	DETECTOR TYPE	DETECTOR RANGE	ANGLE
E,E/	FMF	4	D	1* 2	MAG-D		DST

.8*2.2 FM-1,SEE 81ZA1

The high-resolution electron scattering facility at the MIT-Bates accelerator was used to resolve the 4_1^+ 4.12 MeV and 2_2^+ 4.24 MeV levels in ^{24}Mg. The respective E2 and E4 Coulomb form factors were measured and compared to form factors calculated theoretically; the 4_1^+ form factor exhibits a momentum-transfer dependence which strongly suggests that K is a good quantum number in ^{24}Mg.

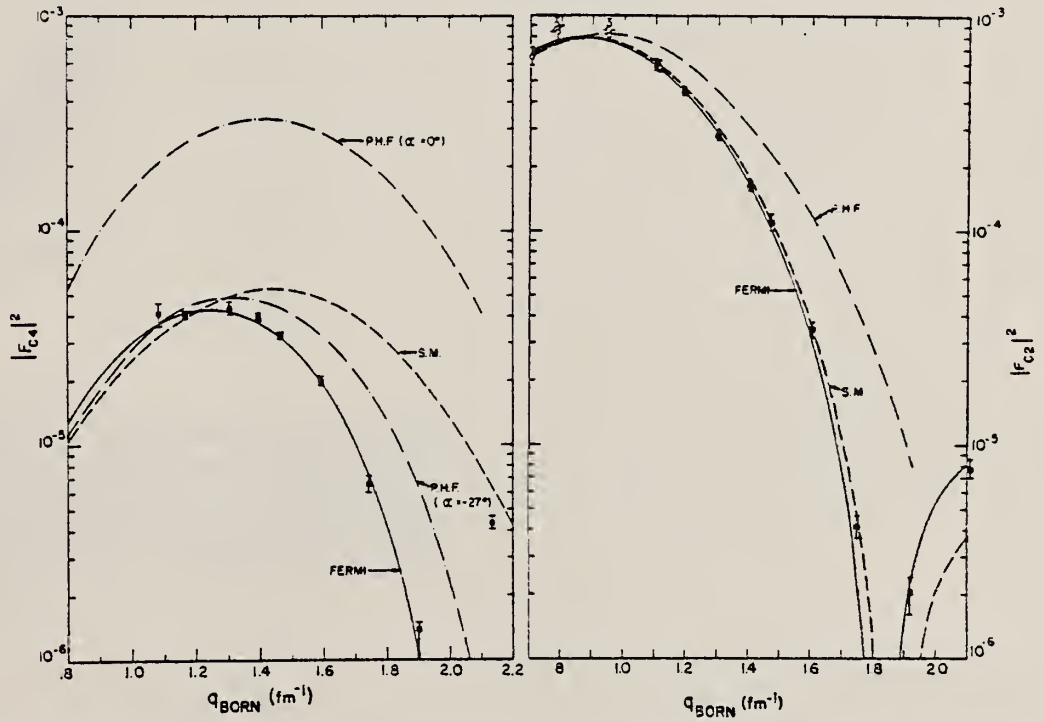

Fig. 2. The form factor for the 4_1^+ 4.12 MeV level of ^{24}Mg is on the left, and for the 2_2^+ 4.24 MeV level on the right. The Fermi-density form factors are shown as a solid line, shell-model form factors as a dashed line and the PHF form factors as a dash–dot line.

over

Table 1
Parameters for Fermi transition charge densities to the 2^+ and 4^+ $K = 0$ and 2 states in ^{24}Mg.

J^π	c(fm)	t(fm)	$B(E\lambda\uparrow)$
2_1^+	2.77	2.35	$453 \pm 35\ e^2\text{fm}^4$
2_2^+	2.77	2.35	$27.4 \pm 3.0\ e^2\text{fm}^4$
4_1^+	3.625	1.85	$(2.0 \pm 0.3) \times 10^3\ e^2\text{fm}^8$
4_2^+	2.725	1.91	$(4.3 \pm 0.6) \times 10^4\ e^2\text{fm}^8$

REF. K. Sh. Egiyan
Yad. Fiz. 30, 890 (1979)
Sov. J. Nucl. Phys. 30, 461 (1979)

ELEM. SYM.	A	Z
Mg	24	12

METHOD

REF. NO. 79 Eg 3 hg

REACTION	RESULT	EXCITATION ENERGY	SOURCE		DETECTOR		ANGLE
			TYPE	RANGE	TYPE	RANGE	
G,XP	RLY	12-250	C	130,250	MAG-D		DST

Experimental data are presented on the inclusive photoproduction of protons in the nuclei ^{12}C, ^{24}Mg, ^{63}Cu, ^{118}Sn, and ^{208}Pb irradiated by bremsstrahlung with maximum energies 0.13 and 0.25 GeV. The regions of angles 30–90° and of photoproton momenta 0.24–0.48 GeV/c were studied.

PACS numbers: 25.20. + y

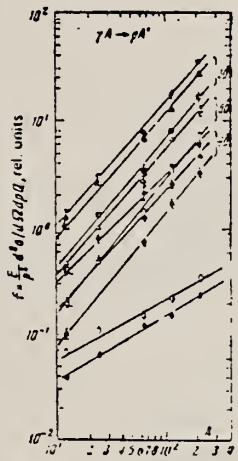

FIG. 5. A-dependence of the photoproton yield in reactions (2) and (3). Experimental points for $E_{\gamma\,max} = 0.25$ GeV: circles—$p_p = 0.29$ GeV/c; triangles—$p_p = 0.34$ GeV/c, squares—$p_p = 0.40$ GeV/c; half-open symbols—for $\vartheta_p = 30°$, open symbols—$\vartheta_p = 60°$, solid symbols—$\vartheta_p = 90°$, for $E_{\gamma\,max} = 0.13$ GeV: ◇—$p_p = 0.29$ GeV/c, $\vartheta_p = 30°$; ♦—$p_p = 0.34$ GeV/c, $\vartheta_p = 30°$. The lines have been drawn through the experimental points by the method of least squares.

REF. V.V. Varlamov, B.S. Ishkhanov, I.M. Kapitonov, Yu.I. Prokopchuk, V.I. Shvedunov
Yad. Fiz. 30, 1185 (1979)
Sov. J. Nucl. Phys. 30, 617 (1979)

ELEM. SYM.	A	Z
Mg	24	12

METHOD

REF. NO. 79 Va 3 egf

REACTION	RESULT	EXCITATION ENERGY	SOURCE		DETECTOR		ANGLE
			TYPE	RANGE	TYPE	RANGE	
G,P	ABX	11-30	C	17-30	SCD-D		90

Photoproton spectra from ^{24}Mg have been measured in a bremsstrahlung beam. The end-point energy was varied over the range 17–30 MeV with a 1-MeV step. From the photoproton spectra we calculated the distributions of the fraction of transitions to various states of the ^{23}Na final nucleus and determined the partial cross sections corresponding to these transitions. The giant resonance of ^{24}Mg is broken down into components associated with electric dipole transitions from the $1d$–$2s$ outer shell and the $1p$ inner shell. An estimate is given of the contribution of $1p$–$1h$ configurations. The results are compared with theory.

PACS numbers: 25.20. + y

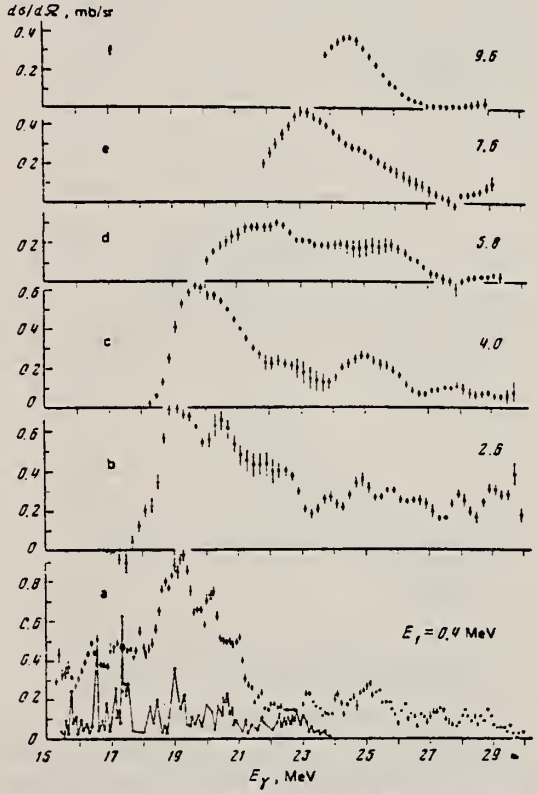

FIG. 3. Partial cross sections for the reaction ^{24}Mg$(\gamma,p)^{23}$Na with formation of the final nucleus in groups of states with centers of gravity at 0.4, 2.6, 4.0, and 5.8, 7.6, and 9.6 MeV. In the lower figure we have also shown the cross section for the (γ,p_0) reaction from Ref. 11.

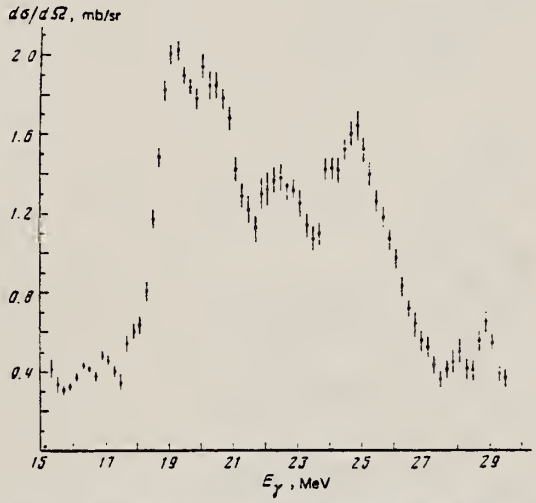

FIG. 4. Sum of the partial cross sections for the reaction ^{24}Mg$(\gamma,p)^{23}$Na.

TABLE III. The main characteristics of electric dipole transitions which form the giant resonance of ^{24}Mg.

Transitions from $1d$-$2s$ shell			Transitions from $1p$ shell			Difference of centers of gravity of transitions from different shell, MeV	Location of strongest transitions, MeV	Contribution of $1p$-$1h$ configurations, %	Reference
Center of gravity, MeV	Energy spread, MeV	Fraction in integrated cross section	Center of gravity, MeV	Energy spread, MeV	Fraction in integrated cross section				
17.3	5.0	0.47	27.0	4.8	0.53	9.7	25–28	100	[2]
18.5	6.4	0.24	25.4	7.2	0.76	6.9	26–27	100	[3]
22.1	5.8	0.57	21.4	6.3	0.43	−0.7	23–25	100	[4]
21.6	6.8	0.65	23.6	5.1	0.35	2.0	19–21	75	Present work

(over)

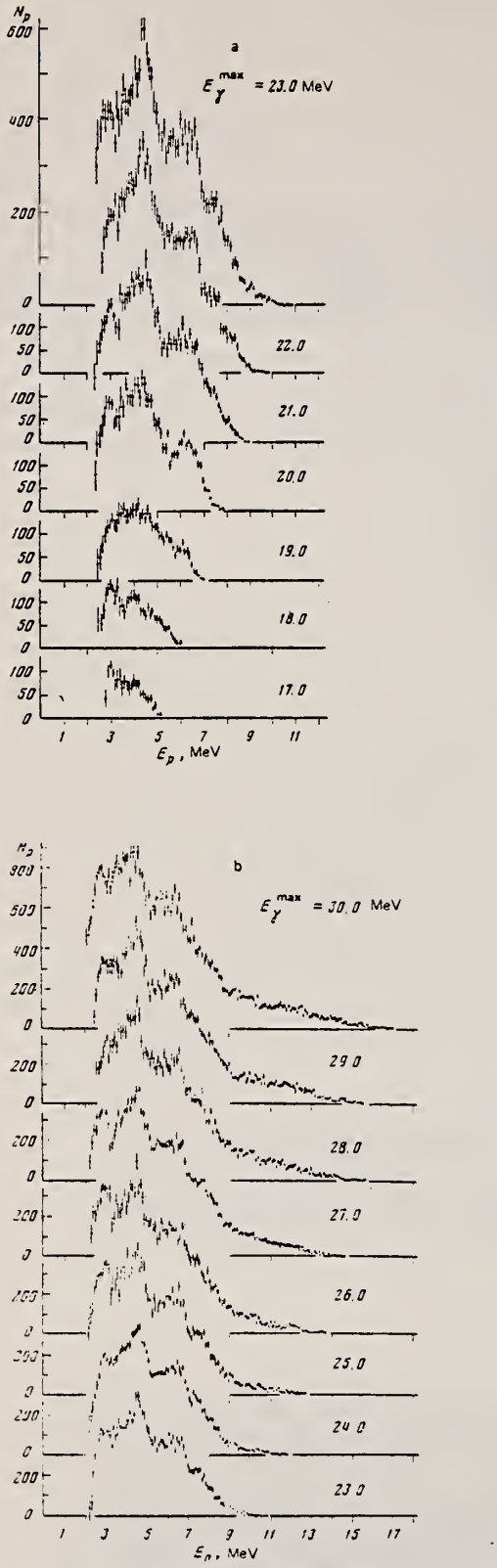

FIG. 1. Photoproton spectra for $E_\gamma^{max} = 17-23$ MeV (a) and $E_\gamma^{max} = 23-30$ MeV (b).

REF. A.M. Sandorfi, J.R. Calarco, R.E. Rand, H.A. Schwettman
Phys. Rev. Lett. 45, 1615 (1980)

ELEM. SYM.	A	Z
Mg	24	12

METHOD

REF. NO.	
80 Sa 4	hg

REACTION	RESULT	EXCITATION ENERGY	SOURCE		DETECTOR		ANGLE
			TYPE	RANGE	TYPE	RANGE	
E,F	ABX	13-29	D	26-40	TEL-D		90

FISS PROD COINC

Coincidence measurements of electrodisintegration products have been used to simultaneously study the $^{12}C + ^{12}C$, $^{16}O + ^{8}Be$, and $^{20}Ne + \alpha$ decay channels of ^{24}Mg. Asymmetric fission into $^{16}O + ^{8}Be$, is concentrated between 18 and 28 MeV in ^{24}Mg and exhibits resonances with cross sections ten times those of symmetric fission. There is little correlation among resonances in the three decay channels. The fission yields are not consistent with statistical decays from giant resonances, and suggest highly clustered states in ^{24}Mg.

PACS numbers: 24.30.-v, 24.75.+i, 25.85.Ge

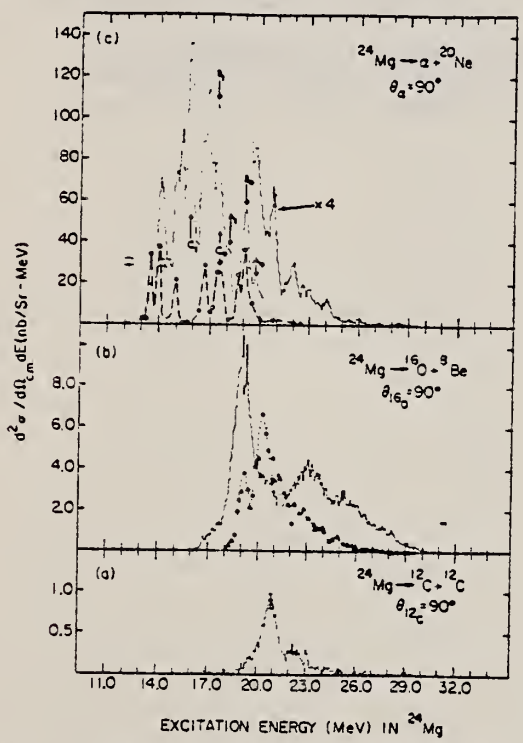

FIG. 3. The 90° cross sections (in nanobarn/steradian per megaelectronvolt excitation) for $^{24}Mg(e,f_1f_3)e'$ are histogrammed here for the main decay channels of Fig. 1. A vertical bar on each spectrum at E_{ex} = 20.8 MeV indicates the level of statistical uncertainty. The α_0 yield predicted by the data of Ref. 9 is shown as open circles in (c). Peaks that could result from decays to $^{20}Ne^{2+}$(1.63 MeV) are labeled with a subscript 1. (The energy scale is appropriate to α_0 decays.) The triangle points in (b) are the predictions of a H-F calculation for the decay of the GDR.

(over)

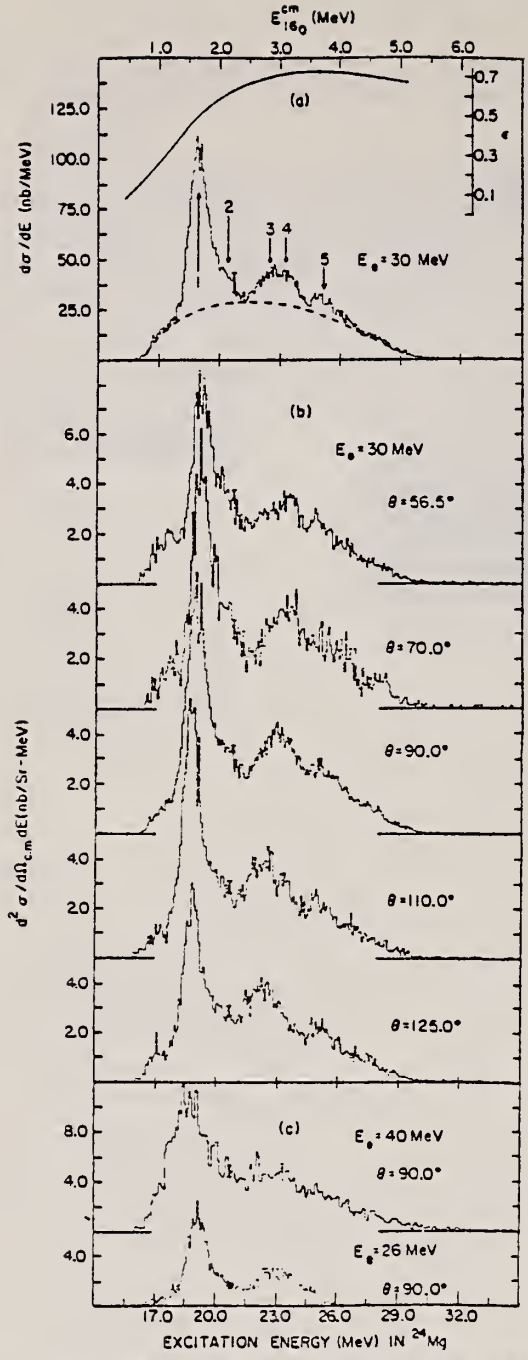

FIG. 2. Cross sections (in nanobarn/steradian per megaelectronvolt of excitation) for ^{24}Mg$(e, ^{16}$O ^{8}Be$)e'$ are shown in (b) and (c). The angle-integrated spectrum, is shown in (a). The detection efficiency follows the solid curve in (a) with its scale on the right. A vertical bar on each spectrum at E_{ex} = 20.8 MeV indicates the level of statistical uncertainty.

REF.

Y. Cauchois, H. Ben Abdelaziz, R. Khérouf, C. Schloesing-Möller
J. Phys. G7, 1539 (1981)

ELEM. SYM.	A	Z
Mg	24	12

METHOD

REF. NO.	
81 Ca 2	hg

REACTION	RESULT	EXCITATION ENERGY	SOURCE		DETECTOR		ANGLE
			TYPE	RANGE	TYPE	RANGE	
G,G	LFT	1	C	0 - 2	SCD-D		
		(1.368)					

Abstract. Lifetimes of 49 excited states below 1.65 MeV have been measured in ^{24}Mg, ^{27}Al, ^{48}Ti, ^{58}Ni, ^{59}Co, ^{61,62}Ni, ^{63,65}Cu, ^{64,66,68}Zn, ^{75}As, ^{103}Rh, ^{113,115}In, ^{116,118,120}Sn and ^{121,123}Sb by means of nuclear resonance fluorescence experiments. The levels are excited by bremsstrahlung x-ray photons. The self-absorption technique applied to suitable cases provides nuclear absorption cross sections, widths and lifetimes from which the x-ray spectral distributions are also obtained. Scattering experiments are performed for all other cases in order to obtain widths and lifetimes from these x-ray photon curves. The Compton effect in the sample is taken into account. Self-absorption provides $g\Gamma_0$ from which Γ is deduced using adopted J^π and Γ_0/Γ values; scattering provides $u = g(\Gamma_0^2/\Gamma)W(\theta)$ from which Γ is also deduced with J, Γ_0/Γ and mixing ratios taken from the literature. Thanks to simultaneous determination of the x-ray spectra all the lifetimes as given by our programs with their statistical errors form an unusually coherent set of values.

1.358 MeV

NUCLEAR REACTIONS (γ, γ'), bremsstrahlung excitation: natural isotopes; ^{24}Mg, ^{27}Al, ^{48}Ti, ^{58}Ni, ^{59}Co, ^{61,62}Ni, ^{63,65}Cu, ^{64,66,68}Zn, ^{75}As, ^{103}Rh, ^{113,115}In, ^{116,118,120}Sn and ^{121,123}Sb; $E \simeq 0.5$–1.65 MeV; measured $g\Gamma_0$ or $g(\Gamma_0^2/\Gamma)W(\theta)$; deduced $T_{1/2}$.

(OVER)

Tableau 3. Résultats des mesures des niveaux étudiés par diffusion.

Table 3. Results obtained using the diffusion method.

Isotope	Energie (keV)	J^π	J_0^π	Γ_0/Γ	δ	$u=g(\Gamma_0^2/\Gamma)W(\theta)$ (meV)	τ (ps) ce travail	$\tau_{réf}$ (ps)	Références†
^{24}Mg	1368,59(4)	2^+	0^+	1	E2	1,08(13)	1,76(21)	1,98(4)	Endt et van der Leun (1978)
^{27}Al	1014,45(3)	$\frac{1}{2}^+$	$\frac{1}{2}^+$	0,971	+0,351(12)	0,186(13)	2,20(16)	2,12(8)	Endt et van der Leun (1978)
^{48}Ti	983,512(3)	2^+	0^+	1	E2	0,282(23)	6,74(55)	6,1(13)	Been (1978)
^{58}Ni	1454,45(15)	2^+	0^+	1	E2	2,11(26)	0,90(11)	0,92(3)	Kocher et Auble (1976)
^{59}Co	1099,224(25)	$\frac{1}{2}^-$	$\frac{7}{2}^-$	1	(E2)	0,069(8)	4,79(55)	3,17(58)	Kim (1976)
^{59}Co	1458,8(3)	$\frac{5}{2}^-$	$\frac{7}{2}^-$	0,91	(E2)	0,68(8)	1,17(14)	1,52(16)	Kim (1976)
^{59}Co	1480,9(3)	$\frac{5}{2}^-$	$\frac{7}{2}^-$	0,8	$<0.35^a$	1,23(15)	0,254(31)	0,31(3)	Kim (1976)
^{61}Ni	1185,7(6)	$\frac{3}{2}^-$	$\frac{3}{2}^-$	0,77(8)[i]	$\lvert 0,14\rvert$	1,88(49)	0,21(5)	0,16(3)	Andreev *et al* (1974)
^{62}Ni	1172,91(9)	2^+	0^+	1	E2	0,88(17)	2,15(42)	2,09(3)	Halbert (1979a)
^{63}Cu	1327,00(7)	$\frac{7}{2}^-$	$\frac{3}{2}^-$	0,84	(E2)	1,04(14)	0,84(11)	0,88(4)	Auble (1979b)
^{63}Cu	1412,05(4)	$\frac{5}{2}^-$	$\frac{3}{2}^-$	0,72	$+0.61\{^{+29}_{-28}\}$	0,260(38)	1,90(28)	1,61(3)	Auble (1979b)
^{64}Zn	991,54(7)	2^+	0^+	1	E2	0,640(54)	2,97(25)	2,60(13)	Halbert (1979b)
^{63}Cu	1481,83(5)	$\frac{7}{2}^-$	$\frac{3}{2}^-$	0,85	(E2)	1,13(19)	0,79(13)	0,49(5)	Auble (1975a)
^{64}Zn	1039,37(6)	2^+	0^+	1	E2	0,70(6)	2,71(23)	2,25(15)	Auble (1975b)
^{68}Zn	1077,38(5)	2^+	0^+	1	E2	0,70(6)	2,71(23)	2,34(23)	Lewis (1975)
^{75}As	572,5(10)	$\frac{5}{2}^-$	$\frac{3}{2}^-$	1[d]	0,39[b]	0,236(26)	4,14(46)	3,5(9)	Horen et Lewis (1975)
^{75}As	823,0(10)	$\frac{7}{2}^-$	$\frac{3}{2}^-$	0,86[d]	(E2)	0,214(22)	4,27(43)	3,5(3)	Robinson *et al* (1967)
^{75}As	865,5(10)	$\frac{5}{2}^+$	$\frac{3}{2}^-$	0,83[d]	—[c]	0,78(6)	0,863(68)	0,60(12)	Celliers *et al* (1977)
^{75}As	1076,0(10)	$\frac{7}{2}^-$	$\frac{3}{2}^-$	0,94[d]	0,38[d]	1,97(13)	0,287(19)	0,32(7)	Celliers *et al* (1977)
^{75}As	1128,5(10)	$\frac{5}{2}^+$	$\frac{3}{2}^-$	1	E1[d]	0,224(24)	1,47(16)	—	
^{75}As	1349,0(10)	$\frac{7}{2}^-$	$\frac{3}{2}^-$	0,67[d]	0,20[d]	1,61(29)	0,180(32)	0,12(3)	Wilson (1970)
^{75}As	1370,0(10)	$\frac{9}{2}^-$	$\frac{3}{2}^-$	0,47[d]	0,47[d]	0,64(13)	0,218(44)	—	
^{103}Rh	803,1(2)	$\frac{7}{2}^+$	$\frac{1}{2}^-$	0,70	M1	1,85(16)	0,174(15)	—	Harmatz (1979)
^{103}Rh	1277,0(2)	$\frac{7}{2}^+$	$\frac{1}{2}^-$	0,75	$-0.62(30)^c$	0,81(9)	0,87(10)	1,3(9)	Harmatz (1979)
^{113}In	1177(1)	$\frac{11}{2}^+$	$\frac{9}{2}^+$	1	+0,5(2)	9,1(8)	0,086(8)	0,10(6)	Tuttle *et al* (1976)
^{113}In	1510(1)	$\frac{7}{2}^+$	$\frac{9}{2}^+$	0,935	$-0.5\{^{+1.0}_{-2.0}\}$	6,4(9)	0,071(10)	$0.11\{^{+.43}_{-.25}\}$	Tuttle *et al* (1976)
^{115}In	1077,7(10)	$\frac{7}{2}^+$	$\frac{9}{2}^+$	0,81[f]	(E2)	0,159(24)	1,61(24)	1,23(7)	Tuttle *et al* (1976)
^{115}In	1290,59(3)	$\frac{11}{2}^+$	$\frac{9}{2}^+$	0,98[f]	(E2)	1,31(11)	0,66(6)	0,55(4)	Tuttle *et al* (1976)
^{115}In	1448,78(3)	$\frac{7}{2}^+$	$\frac{9}{2}^+$	0,86	-8^f	0,90(11)	0,50(6)	0,52(20)	Tuttle *et al* (1976)
^{115}In	1486,1(1)	$\frac{5}{2}^+$	$\frac{9}{2}^+$	0,787	-0.8^f	0,63(9)	0,63(9)	0,4(3)	Tuttle *et al* (1976)
^{115}In	1497,2(4)	$(\frac{5}{2}^+)$	$\frac{9}{2}^+$	<1	(E2)	1,33(16)	$<0.30(4)$	—	
^{115}In	1607,8(15)	$(\frac{5}{2}^+)$	$\frac{9}{2}^+$	$\leqslant 1$	(E2)	1,54(24)	$\leqslant 0.26(4)$	—	
^{116}Sn	1293,54(2)	2^+	0^+	1	E2	3,58(37)	0,53(6)	0,522(14)	Carlson *et al* (1975)
^{118}Sn	1229,64(4)	2^+	0^+	1	E2	2,75(28)	0,69(7)	0,67(2)	Carlson *et al* (1976)
^{120}Sn	1171,6(2)	2^+	0^+	1	E2	1,83(16)	1,04(9)	0,91(2)	Kocher (1976)
^{121}Sb	1023,5(10)	$\frac{7}{2}^+$	$\frac{5}{2}^+$	1	$\lvert 0.57\rvert^g$	3,69(34)	0,228(21)	0,20(7)[h]	Tamura *et al* (1979)
^{121}Sb	1105,5(10)	$\frac{5}{2}^+$	$\frac{5}{2}^+$	0,4	—	0,47(4)	0,42(4)	—	
^{121}Sb	1142,5(10)	$\frac{9}{2}^+$	$\frac{5}{2}^+$	0,6	(E2)	0,85(8)	0,449(40)	0,41(8)[h]	Booth *et al* (1973)
^{121}Sb	1384,0(10)	$\frac{7}{2}^+$	$\frac{5}{2}^+$	1	$\lvert 0.45\rvert^g$	4,7(5)	0,092(10)	0,088(14)[h]	Booth *et al* (1973)
^{123}Sb	1029,5(10)	$\frac{9}{2}^+$	$\frac{7}{2}^+$	1	$\lvert 0.57\rvert^g$	2,96(27)	0,272(25)	0,26(4)[h]	Booth *et al* (1973)
^{123}Sb	1086,5(10)	$\frac{7}{2}^+$	$\frac{7}{2}^+$	1	$\lvert\delta\rvert > 1.26^g$	1,06(9)	0,67(6)	0,72(15)[h]	Booth *et al* (1973)

† References pour les colonnes 3, 4, 5, 6 et 9 de chaque ligne, sauf indication appelée au bas de ce tableau. Pour les autres données se reporter au texte.

Remarque. Pour calculer δ^2 quand nous ne disposons que de $B(E2)$, pour un mélange (E2) + (M1), nous déduisons $g\Gamma_0(E2) \propto B(E2)E_\gamma^5$; en admettant $W(\theta)=1$ et connaissant Γ_0/Γ, notre détermination de u donne une première approximation de $g\Gamma_0$ d'où une valeur de $\delta^2=(g\Gamma_0(E2))/(g\Gamma_0-g\Gamma_0(E2))$ qui permet d'améliorer $W(\theta)$ et $g\Gamma_0$ de proche en proche.

[a] Swann (1971); [b] Robinson *et al* (1967); [c] $W(\theta)=0.99$ calculé d'après la formule de Celliers *et al* (1977); [d] Abbondanno *et al* (1978); [e] Sayer *et al* (1972); [f] Tuttle *et al* (1976); [g] d'après $B(E2)$ de Barnes *et al* (1966); [h] calculé d'après Booth *et al* (1973); [i] Williams *et al* (1975); [j] Dietrich *et al* (1970).

REF. K. Itoh, S. Ohsawa, Y. Torizuka, T. Saito, T. Terasawa
Phys. Rev. C23, 945 (1981)

EL EM. SYM.	A	Z
Mg	24	12

METHOD

REF. NO. 81 It 1 hg

REACTION	RESULT	EXCITATION ENERGY	SOURCE TYPE	SOURCE RANGE	DETECTOR TYPE	DETECTOR RANGE	ANGLE
E,E/	ABX	9-34	D	102-200	MAG-D		DST

Highly excited multipole resonances of ^{24}Mg between 9 and 34 MeV excitation energy have been investigated by inelastic electron scattering for incident energies in the 102 and 200 MeV range. Prominent giant dipole resonances were observed at 18.9 and 20 MeV excitation energy, with a shape which is very similar to the shape of the photoneutron cross section. Over twenty-five quadrupole and twenty octupole resonances were identified and separated by means of the multipole expansion method. The giant dipole strength exhausts (85^{+9}_{-17})% of the isovector dipole energy-weighted sum rule. The quadrupole and the octupole strength exhaust (117 ± 23)% and (115 ± 23)% of the corresponding isoscalar energy-weighted sum rule, respectively. Evidence for the excitation of higher multipole states such as hexadecapole transitions was also found in the excitation energy region studied.

[NUCLEAR REACTIONS ^{24}Mg(e,e'), E = 102, 125, 150, 200 MeV, q = 0.37–1.3 fm^{-1}, measured $\sigma(E',\theta)$ up to 34 MeV in excitation energy; deduced dipole, quadrupole, and octupole strengths in giant resonance region. Enriched targets.]

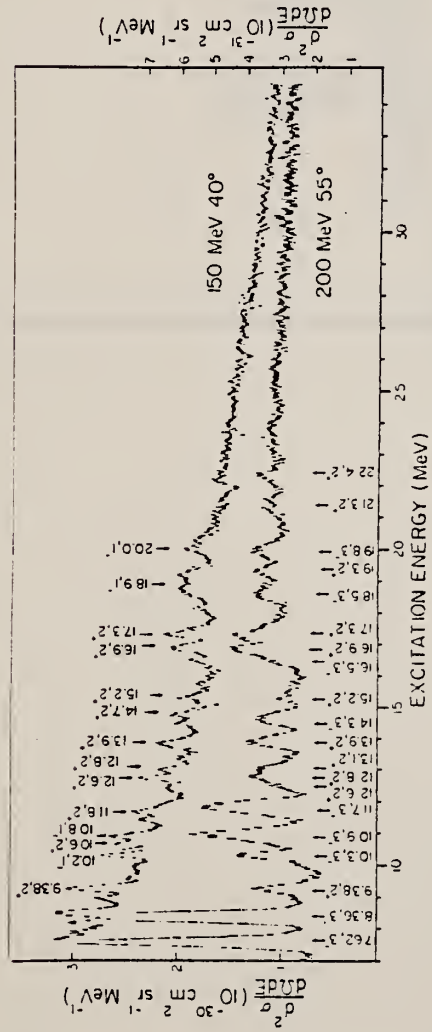

FIG. 1. Typical scattered electron spectra from ^{24}Mg obtained at 150 and 200 MeV incident electron energy and scattering angles of 40° and 55°, respectively. The right-hand scale is for the 200 MeV spectrum, and the left-hand scale for the 150 MeV spectrum.

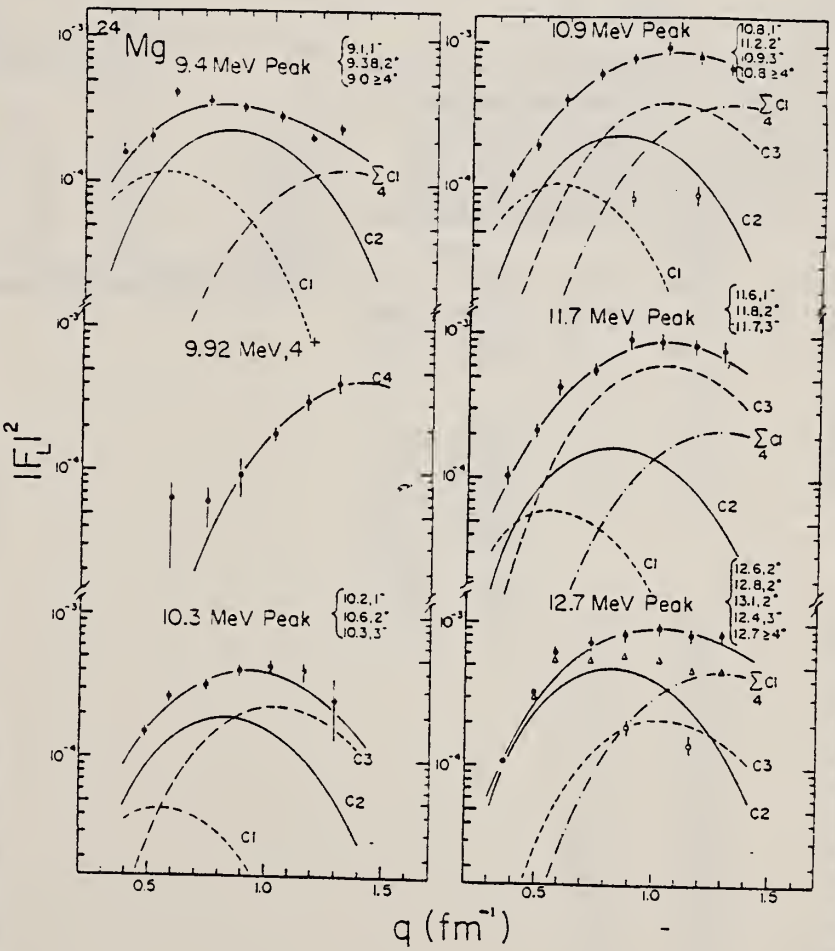

FIG. 9. Longitudinal form factors as decomposed according to the multipole expansion. Open circles indicate the contributions of the transverse excitations. The triangles are the form factors obtained by subtracting the phenomenological shape for the underlying continuum, as described in the text.

(OVER)

TABLE I. Reduced transition probabilities $B(C1,\uparrow)$ and percentage of the isovector energy-weighted sum rule S_1. The errors are +10%, −20%. The (γ,n) data were taken from Ref. 14.

	Present		(γ,n)	
E_x (MeV)	$B(C1,\uparrow)$ (e^2fm^2)	S_1 (%)	E_x (MeV)	S_1 (%)
9.1	0.11	1.1		
10.2	0.039	0.44		
10.8	0.10	1.2		
11.6	0.054	0.71		
13.7	0.043	0.67		
14.4	0.077	1.2		
15.0	0.026	0.45		
16.7	0.22	4.2	16.9	0.16
17.1	0.12	2.3	17.3	0.29
			17.6	0.015
			18.3	0.84
18.9(17.7–19.5)	0.75	15.9	18.8	1.1
			19.2	0.79
20.0(19.5–20.3)	0.33	7.5	20.1	2.0
			20.4	0.29
20.3–21.4	0.28	6.5	20.9	1.2
21.4–25.0	0.77	20.0	21.5	0.41
			22.4	0.27
			23.1	2.0
25.0–28.0	0.39	10.5	25.0	4.2
			27.5	3.2
			16.5–28.0	16.7
28.0–31.0	0.22	6.5		
31.0–34.0	0.16	5.8		
9.0–34.0	3.69	84.9		

TABLE II. $B(C2,\uparrow)$ and percentage of the isoscalar quadrupole EWSR S_2. The errors are ±10% up to 15.7 MeV, ±20% above 16 MeV in excitation energy. $B(C2,\uparrow)$ for the two lowest states were taken from the (e,e') work of Ref. 22. The α-particle scattering data were taken from Ref. 7. S_2 for the α-capture reaction were calculated by Bertrand *et al.* (Ref. 7) using the data of Ref. 3. The previous (e,e') data were taken from Ref. 12.

	Present		(α,α')		(α,γ_0)		(e,e')	
E_x (MeV)	$B(C2,\uparrow)$ (e^2fm^4)	S_2 (%)	E_x (MeV)	S_2 (%)	E_x (MeV)	S_2 (%)	E_x (MeV)	S_2 (%)
1.37	446	13.3					1.37	12.4
4.23	22.8	2.1					4.23	2.4
7.34	0.9	0.2						
9.38	9.4	1.9					9.30	2.4
10.6	7.6	1.7						
11.2	9.7	2.4					11.38	0.6
11.8	6.8	1.8						
12.6							12.52	0.6
12.8	20.0	5.6	12.8	3.5	12.8	4.0	12.99	0.6
13.1			13.1	3.6	13.1	2.8		
13.9	11.3	3.4	13.9	3.0	13.9	0.4		
14.7	10.7	3.4	14.5	3.3				
			14.9	2.5				
15.2	11.0	3.7			15.8	0.6		
15.7								
			16.6	2.3	16.5	1.1		
16.9	7.5	2.7	17.0	5.3				
17.3	19.0	7.1	17.4	8.4	17.4	1.2		
			17.8	3.1				
			18.2	2.5	18.2	0.5		
19.3	6.3	2.6	18.8	4.8				
			19.1	2.0				
			19.6	5.2				
20.1	10.0	4.3	20.0	2.3	20.0	1.0		
			20.4	6.8				
20.8	2.1	0.9	21.1	(2.7)				
21.3	7.8	3.6	21.4	(2.8)				
22.4	8.4	4.1	21.7	5.4				
22.7–25.0	20.6	10.1	24.0	7.9				
25.0–28.0	29.4	17.0						
28.0–31.0	28.5	18.3						
31.0–34.0	10.0	7.0						
0–34.0	705	117						

TABLE III. $B(C3,\uparrow)$ and percentage of the isoscalar octupole EWSR S_3. The errors are ±10% up to 16.5 MeV, ±25% above 17 MeV. $B(C3)$ for the lowest two states were taken from previous (e,e') work of Ref. 12. The result of the (p,p') was taken from Ref. 9.

	Present		(p,p')	
E_x (MeV)	$B(C3,\uparrow)$ 10^3 e^2fm^6	S_3 (%)	E_x (MeV)	S_3 (%)
7.62	1.33	5.3	7.616	4.99
8.36	1.90	8.2	8.356	4.26
9.1	0.04	0.2		
10.3	0.26	1.4		
10.9	0.47	2.7	11.157	1.24
			11.318	0.31
11.7	0.71	4.3	12.016	0.58
12.4	0.24	1.5	12.261	0.39
			12.663	0.39
			12.850	0.30
				0.77
			13.344	0.33
			13.440	0.60
13.7	0.21	1.5		
14.3	0.31	2.3		
16.5	0.78	6.6		
17.1	0.18	1.6		
17.9	0.18	1.7		
18.5	0.36	3.5		
19.1	0.13	1.3		
19.8	0.34	3.5		
20.7	0.12	1.3		
21.1	0.23	2.5		
21.6	0.20	2.2		
22.0	0.42	4.8		
22.8	0.18	2.1		
23.4	0.41	4.9		
23.9–25.0	0.26	3.3		
25.0–28.0	1.04	9.3		
28.0–31.0	0.92	14.1		
31.0–34.0	1.51	25.5		
0–34.0	12.7	115		

REF. H. Zarek, S. Yen, B.O. Pich, T.E. Drake, C.F. Williamson, S. Kowalski, C.P. Sargent, W. Chung, B.H. Wildenthal, M. Harvey, H.C. Lee
Phys. Lett. 104B , 499 (1981)

ELEM. SYM.	A	Z
Mg	24	12

METHOD

REF. NO. 81 Za 1 egf

REACTION	RESULT	EXCITATION ENERGY	SOURCE		DETECTOR		ANGLE
			TYPE	RANGE	TYPE	RANGE	
E,E/	FMF	4	D	1*2	MAG-D		DST

ERRATA FOR 78ZA2

ERRATA

H. Zarek et al., Electroexcitation and the determination of the K-band structure in ^{24}Mg, Phys. Lett. 80B (1978) 26.

On page 27 in table 1, $B(E4\uparrow)$ to the 4_1^+ state is $(3.8 \pm 0.3) \times 10^3\ e^2\text{fm}^8$ and *not* $(2.0 \pm 0.3) \times 10^3\ e^2\text{fm}^8$.

* * *

Mg
A=25

Mg
A=25

Ref. R. Nathans, P.F. Yergin
Phys. Rev. 98, 1296 (1955)

Elem. Sym.	A	Z
Mg	25	12

Method BF_3 counters; 24 MeV Bremss Betatron.

Ref. No. 55 Na 1 EGF

Reaction	E or ΔE	E_o	Γ	$\int \sigma dE$	Jπ	Notes 320
(γ,xn)	9.3-24	20.3	5	0.096 MeV-mb		E_{th} = 7.3 MeV; σ_{max} = 16.5 mb. No corrections. [NOTE: Figure 2: Ref 8: Katz, Baker, Montalbetti, Can. J. Phys. 31, 250 (1953). Ref 5: Katz, Haslam, Goldemberg, Taylor, Can. J. Phys. 32, 580 (1954). Ref 9: Katz and Cameron, Phys. Rev. 84, 1115 (1951). Ref 10: Toms, Stephens, Phys. Rev. 82, 709 (1951).]

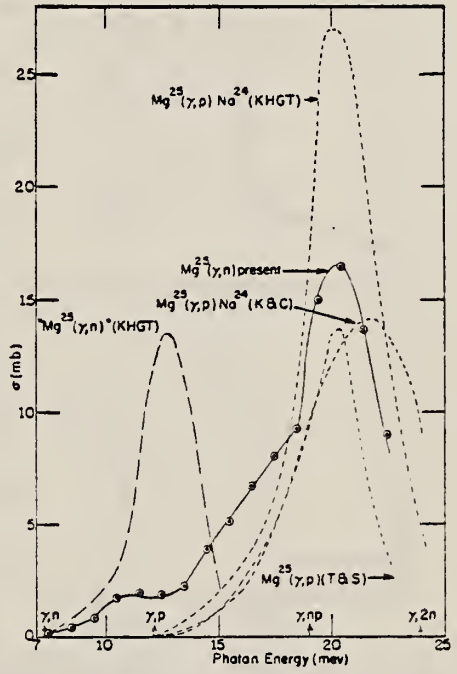

FIG. 2. (γ,n) cross section for Mg^{25}. The ordinate scale is in millibarns (10^{-27} cm^2). The locations of the thresholds for various reactions are indicated by arrows. The circles are the points calculated from the yield data. The solid curve is drawn to fit the points. The three dotted curves are the previously reported $Mg^{25}(\gamma,p)Na^{24}$ cross sections (see references 5, 9, and 10). The dashed curve is the estimate of the $Mg^{25}(\gamma,n)$ cross section made previously by subtracting the $Mg^{24}(\gamma,n)$ of reference 8 from the measured cross section for natural Mg (see reference 5).

FORM NBS-418
(8-1-63)
USCOMM-DC 18556-P63

U.S. DEPARTMENT OF COMMERCE
NATIONAL BUREAU OF STANDARDS

Ref. F.R. Metzger, C.P. Swann, V. K. Rasmussen
Nuclear Phys. 16, 568 (1960)

Elem. Sym.	A	Z
Mg	25	12

Method
Protons from Bartol-ONR generator; $(p,p'\gamma)$, etc. reactions for γ source; ring scatterer; NaI.

Ref. No. 60 Me 1 JHH

Reaction	E or ΔE	E_o	Γ	$\int \sigma dE$	$J\pi$	Notes
(γ,γ)	1.61		$3.0 \pm 1.5 \times 10^{-2}$ ev		$3/2^+$	

Ref. V.K. Rasmussen, F.R. Metzger, C.P. Swan
Phys. Rev. 123, 1386 (1961)

Elem. Sym.	A	Z
Mg	25	12

Method Van de Graaff; 1.61 MeV γ source by $Mg^{25}(p,p'\gamma)$ with 4.0 MeV protons; ring scatterer; NaI.

Ref. No. 61 Ra 1 JHH

Reaction	E or ΔE	E_o	Γ	$\int \sigma dE$	$J\pi$	Notes
(γ,γ)	1.61	1.61			(7/2+)	Assuming level to be 7/2+, mean life is $(2.5^{+0.6}_{-0.4}) \times 10^{-14}$ sec. Angular distribution fitted to $1+(0.42\pm0.03)P_2 \cos\theta + (0.03\pm0.003)P_4 \cos\theta$ but P_4 term probably about zero.

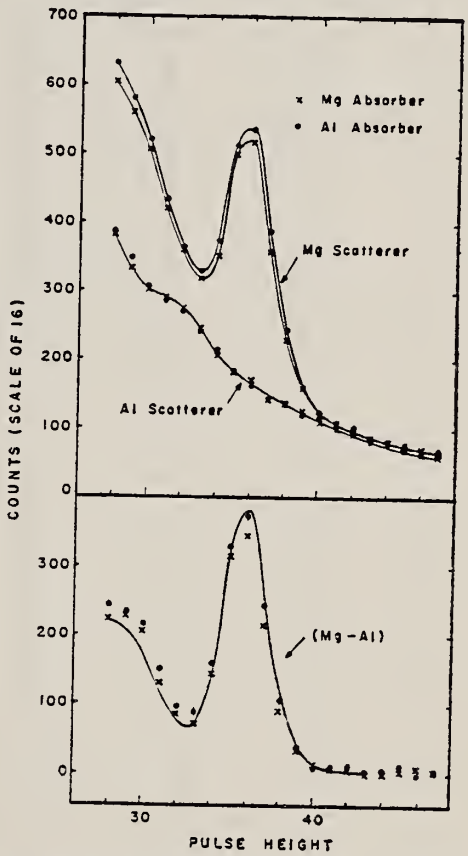

FIG. 3. Resonant scattering of the 1.61-Mev γ ray from Mg^{25}. The upper curves give the original data for the scatterer-absorber combinations noted. Statistical errors can be estimated from the left-hand scale which gives the total number of counts for each point. Magnesium scatterer-aluminum scatterer differences are shown in the lower plot, where the solid curve drawn is the shape found for an isolated 1.61-Mev γ ray from a radioactive source and is normalized to the aluminum absorber data. The sum of the counts for pulse heights 34 to 37 was taken to represent the resonance effect.

Ref. E.C. Booth, K.A. Wright
Nuclear Phys. 35, 472 (1962)

Elem. Sym.	A	Z
Mg	25	12

Method 4 MeV electron Van de Graaff; bremss.; nuclear resonance scattering, ring scatterer; NaI

Ref. No. 62 Bo-6 JHH

Reaction	E or ΔE	E_0	Γ	$\int \sigma dE$	Jπ	Notes
$Mg^{25}(\gamma,\gamma)$	Bremss. 0 - 4					

TABLE 2
Comparison of mean lifetime measurements

Nucleus	Energy	%	Spins	g	Γ_0/Γ	$W'(\theta)$	$\tau \times 10^{14}$ sec This work	Other	
Li^6	3.56	7	$1^+ - 0$	½	(1)	1	0.012	$0.0072^{+0.0015}_{-0.0013}$	[9]
								0.0105 ± 0.001	[10]
B^{11}	2.14	81	$\frac{1}{2}^- - (\frac{1}{2})$	½	1	1	0.53	0.47 ± 0.06	[10]
Al^{27}	2.21	100	$\frac{1}{2}^+ - \frac{1}{2}^-$	½	(1)	1	3.2	2.7 ± 0.3	[10]
Al^{27}	1.01	100	$\frac{1}{2}^+ - \frac{1}{2}^+$	½	0.98	1	320	170 ± 50	[11]
Si^{28}	1.78	92	$0^+ - 2^-$	5	1	0.63	88	73 ± 22	[10]
S^{32}	2.24	96	$0^+ - 2^-$	5	1	0.63	28	≈16	[10]
Mg^{24}	1.37	78.6	$0^+ - 2^-$	5	1	0.63	220	155 ± 40	[10]
Mg^{25}	1.61	25	$\frac{1}{2}^+ - \frac{3}{2}^-$	½	(1)	1	3.6	2.5 ± 0.6 -0.4	[17]
Cu^{63}	0.963	69	$\frac{3}{2} - \frac{1}{2}$	½	1	0.92	230	72 ± 18	[18]
								90 ± 15	[19]
Cu^{65}	0.67	69	$\frac{3}{2} - \frac{1}{2}$	½	1	1	100	31 ± 3	[18]

The factor g equals $(2I+1)(2M_0+1)^{-1}$.

10) R. C. Hoisn, Phys. Rev. 140 (1966) 1466
11) S. Vegors, L. Marsden and R. Heath, IDO-16870
12) Leslie Cohen and Ralph Tobias, Nuclear Physics 16 (1960) 342
13) W. C. Barber, F. Berthold, G. Frieks and F. E. Gudden, Phys. Rev. 120 (1960) 2128
14) F. R. Metzger, C. P. Swann and V. K. Rasmussen, Phys. Rev. 110 (1958) 906
15) F. R. Metzger, C. P. Swann and V. K. Rasmussen, Nuclear Physics 16 (1960) 568
16) S. Ofer and A. Schwarzschild, Phys. Rev. Lett. 3 (1959) 384
17) V. K. Rasmussen, F. R. Metzger and C. P. Swann, Phys. Rev. 123 (1961) 1386
18) J. B. Cummings, A. Schwarzschild, A. W. Sunyar and N. T. Porile, Phys. Rev. 120 (1960) 2128
19) T. Rothen, F. R. Metzger and C. P. Swann, Nuclear Physics 22 (1961) 505

REF. E.C. Booth, B. Chasan and K.A. Wright
Nucl. Phys. 57, 403-420 (1964)

ELEM. SYM.	A	Z
Mg	25	12

METHOD
Van de Graaff; resonance fluorescence

REF. NO.: 64 Bo 1 NVB

REACTION	RESULT	EXCITATION ENERGY	SOURCE		DETECTOR		ANGLE
			TYPE	RANGE	TYPE	RANGE	
G,G	LFT	1-3	C	1 - 3	NAI-D		100
		(0.5 - 3.0)		(0.5 - 3.0)			

ABI

TABLE I
Cases of observed resonance fluorescence

Nucleus multipol.	State (MeV)	Spin	Γ_0/Γ	$T(g w \Gamma_0^2/\Gamma^2)^{-1}$ (sec).	Mean lifetime T BCW (sec)	Mean lifetime T other (sec)	Ref.	Γ_0/Γ_W BCW
Mg^{25}	0.00	$\frac{5}{2}^+$						
M1	1.61	$\frac{7}{2}^-$	1	$21 \pm 5 \times 10^{-15}$	$28 \pm 7 \times 10^{-15}$	$25^{+6}_{-4} \times 10^{-15}$	11)	0.085

REF.

I. Bergqvist, J. A. Biggerstaff, J. H. Gibbons, W. M. Good
Phys. Rev. 158, 1049 (1967)

ELEM. SYM.	A	Z
Mg	25	12

METHOD

REF. NO.: 67 Be 7 egf

REACTION	RESULT	EXCITATION ENERGY	SOURCE		DETECTOR		ANGLE
			TYPE	RANGE	TYPE	RANGE	
N,G	LFT	7	D	1	NAI-D	0-7	90

SOURCE 84 KEV

TABLE IV. Gamma rays from $^{24}Mg(n,\gamma)^{25}Mg$; $E_n = 84$ keV, $J^\pi = \frac{1}{2}^-$.

E_γ (MeV)	I_γ (per 100 captures)	Assignment	$J_i^\pi \rightarrow J_f^\pi$	Γ_{γ_i} (meV)	$1000\|M\|^2$
7.41	18±1	$C \rightarrow 0$	$\frac{1}{2}^- \rightarrow \frac{1}{2}^+$	630	2.7
6.83	67±2	$C \rightarrow 0.58$	$\frac{1}{2}^- \rightarrow \frac{1}{2}^+$	2350	13.
5.45	2.5±1.0	$C \rightarrow 1.96$	$\frac{1}{2}^- \rightarrow \frac{1}{2}^+$	85	0.9
4.84	12.5±1.5	$C \rightarrow 2.57$	$\frac{1}{2}^- \rightarrow \frac{1}{2}^+$	440	6.7
(3.9)*	(1.4)				
(3.25)	(1.2)				
(2.8)	(2)				
(2.5)	(2.4)				
1.98	11.1±0.9	$2.57 \rightarrow 0.58$ $1.96 \rightarrow 0$	$\frac{1}{2}^+ \rightarrow \frac{1}{2}^+$ $\frac{1}{2}^+ \rightarrow \frac{1}{2}^-$		
1.58	3.3±0.4	$2.57 \rightarrow 0.98$ $(1.61 \rightarrow 0)$	$\frac{1}{2}^+ \rightarrow \frac{1}{2}^+$ $((\frac{1}{2}^+) \rightarrow \frac{1}{2}^+)$		
1.38	2.4±0.4	$1.96 \rightarrow 0.58$	$\frac{1}{2}^+ \rightarrow \frac{1}{2}^+$		
0.98	5.7±0.8	$1.96 \rightarrow 0.98$ $0.98 \rightarrow 0$	$\frac{1}{2}^+ \rightarrow \frac{1}{2}^+$ $\frac{1}{2}^+ \rightarrow \frac{1}{2}^+$		

* Parentheses imply marginal credibility.

REF. Y. Oka, T. Kato, K. Nomura, T. Saito, Hui-Tuh Tsai
Bull. Chem. Soc. Japan 41, 380 (1968)

ELEM. SYM.	A	Z
Mg	25	12

METHOD

REF. NO. 68 Ok 3 egf

REACTION	RESULT	EXCITATION ENERGY	SOURCE TYPE	SOURCE RANGE	DETECTOR TYPE	DETECTOR RANGE	ANGLE
G,P	ABY	THR-20	C	20	ACT-I		4PI

TABLE 1. SUMMARY OF DATA ON (γ, p) REACTIONS WITH 20 MeV BREMSSTRAHLUNG

Nuclide: Parent (Natural abundance, %)	Nuclide: Residual (Half-life)	S_p (MeV)	Observed γ-ray: Energy (MeV)	Branching ratio (%)	Type of multipole transition	Yield determined: μCi/mg[a]	Yield/mol·R
^{25}Mg (10.11)	^{24}Na (15 hr)	12.06	1.37	100	$E2$	1.48×10^{-1}	1.7×10^{5}
^{29}Si (4.71)	^{28}Al (2.27 min)	12.33	1.78	100	$E2$	1.91	2.8×10^{5}
^{30}Si (3.12)	^{29}Al (6.56 min)	13.59	1.28	93.8	$E2+M1$	6.51×10^{-1}	1.5×10^{5}
^{44}Ca (2.06)	^{43}K (22.4 hr)	12.17	0.374	85	$E2+M1$	7.86×10^{-2}	1.3×10^{5}
^{47}Ti (7.32)	^{46}Sc (84.1 d)	10.47	0.887	100	$E2$	7.11×10^{-4}	3.1×10^{5}
^{48}Ti (73.99)	^{47}Sc (3.4 d)	11.44	0.160	100	$E2+M1$	6.83×10^{-2}	1.2×10^{5}
^{49}Ti (5.46)	^{48}Sc (1.8 d)	11.35	1.31	100	$E2$	4.40×10^{-3}	5.8×10^{4}
^{52}Cr (9.55)	^{52}V (3.8 min)	11.15	1.43	100	$E2$	5.01×10^{-1}	6.6×10^{4}
^{57}Fe (2.17)	^{56}Mn (2.58 hr)	10.57	1.81	23.5	$E2+M1$	8.10×10^{-2}	2.1×10^{5}
^{74}Ge (36.74)	^{73}Ga (4.8 hr)	10.92	0.295	97	$(E2)$	3.70×10^{-1}	1.3×10^{5}
^{77}Se (7.58)	^{76}As (26.5 hr)	9.61	0.559	41	$E2$	1.48×10^{-2}	1.3×10^{5}
^{87}Sr (7.02)	^{86}Rb (19 d)	9.41	1.08	9	$E2$	5.15×10^{-4}	9.9×10^{4}
^{113}Cd (12.26)	^{112}Ag (3.2 hr)	9.74	1.39	35	$E2$	1.91×10^{-2}	2.1×10^{4}
^{117}Sn (7.57)	^{116m}In (54 min)	9.58	1.27	84	$E2$	9.80×10^{-3}	6.9×10^{3}
^{137}Ba (11.32)	^{136}Cs (13 d)	8.67	0.830	100	$E2$	1.68×10^{-4}	2.2×10^{4}
^{199}Hg (16.84)	^{198}Au (2.7 d)	7.27	0.412	100	$E2$	8.43×10^{-4}	2.2×10^{4}

a) The value corrected at the end of 1 hr irradiation (9.4×10^{6} R/min).

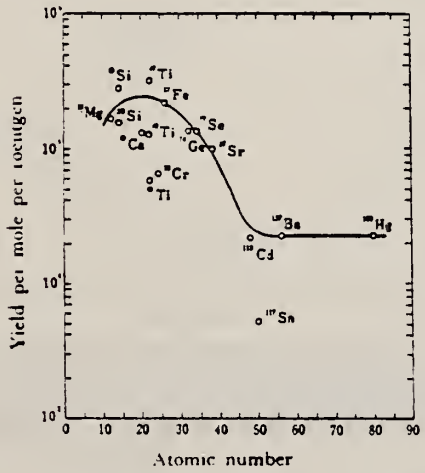

Fig. 2. The yield curve for the (γ, p) reaction with 20 MeV bremsstrahlung.

L. W. Fagg, W. L. Bendel, E. C. Jones, Jr., H. F. Kaiser, and T. F. Godlove
Phys. Rev. 187, 1384 (1969)

Mg	25	12

METHOD

REF. NO. 69 Fa 2 | hmg

REACTION	RESULT	EXCITATION ENERGY	SOURCE TYPE	SOURCE RANGE	DETECTOR TYPE	DETECTOR RANGE	ANGLE
E,E/	ABX	0-27	D	39,56	MAG-D	30-56	180
				(38.9,55.9)			
							203 +

J-PI, B(ML)

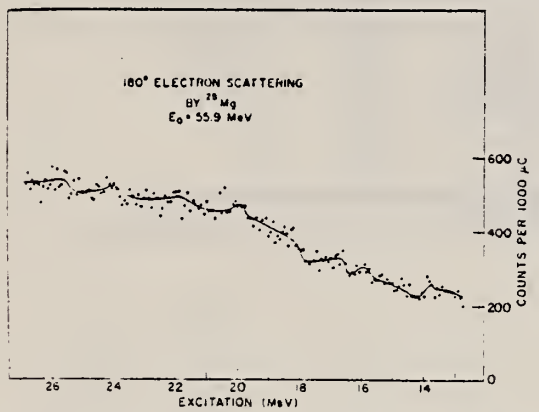

FIG. 1. Spectrum obtained from 180° electron scattering by ^{25}Mg with $E_0 = 55.9$ MeV, covering the excitation energy range 12–27 MeV.

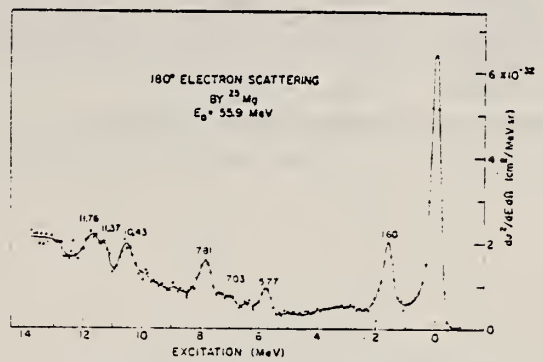

FIG. 2. Differential cross section for 180° electron scattering from ^{25}Mg with $E_0 = 55.9$ MeV, covering the excitation energy range 0–12 MeV.

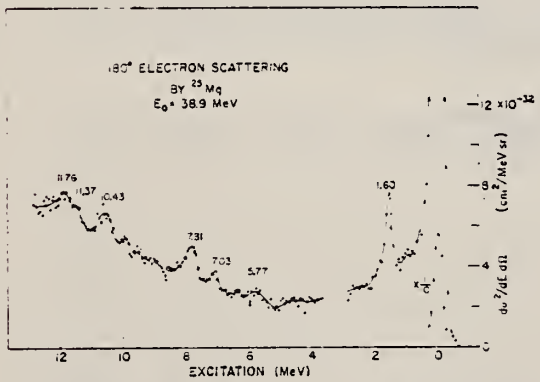

FIG. 3. Differential cross section for 180° electron scattering from ^{25}Mg with $E_0 = 38.9$ MeV, covering the excitation energy range 0–12 MeV. The gap in the spectrum arises from the fact that a preliminary survey, as well as the 56-MeV data, showed no structure of interest in this region; thus presentable data were not accumulated here.

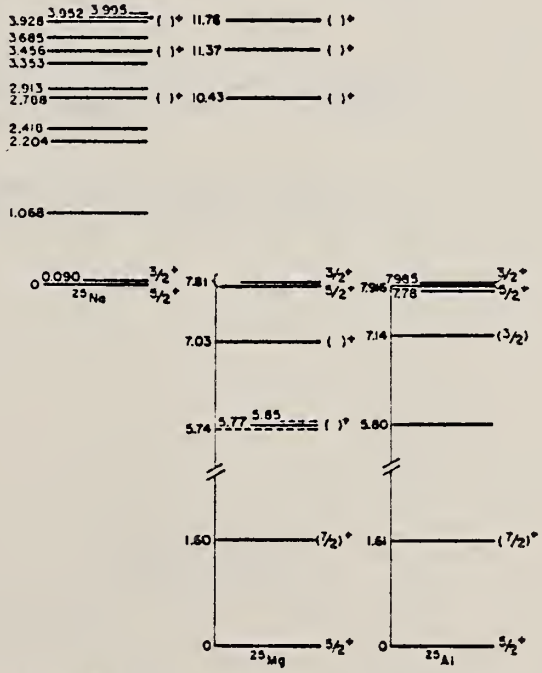

FIG. 4. Energy-level diagram adjusted for the Coulomb displacement showing ^{25}Na, ^{25}Mg, and ^{25}Al analog states. In the ^{25}Mg scheme only states excited and analyzed in this work are shown with solid lines. Some corresponding ^{25}Al states are shown. Energy values given in the ^{25}Na and ^{25}Al level schemes are those quoted from Ref. 18 except for the 7.916- and 7.985-MeV levels quoted from Ref. 5.

[5] G.C. Morrison, D.H. Youngblood, R.C. Bearse, R.E. Segel, Phys.Rev. 174, 1366('68).
[18] P.M. Endt, C. Van der Leun, Nucl. Phys. A105, 1 (1967).

[over]

TABLE I. Values of differential cross section, isospin, spin and parity, spin projection on the nuclear axis, transition radius, and radiation width for energy levels excited in ^{25}Mg.

Level energy (MeV)	$(d\sigma/d\Omega)_{56}$ (10^{-34} cm^2/sr)	$(d\sigma/d\Omega)_{28}$ (10^{-34} cm^2/sr)	T	J^π	K^π	Plane-wave Born approximation R_M (fm)	Plane-wave Born approximation $\frac{2J+1}{2J_0+1}\Gamma_0$ (eV)	DWBA corrections R_M (fm)	DWBA corrections $\frac{2J+1}{2J_0+1}\Gamma_0$ (eV)
1.60±0.02	91±7	158±15	$\frac{1}{2}$	$\frac{3}{2}^+$	$\frac{3}{2}^+$	2.7	0.078	$2.4_{-0.4}^{+0.2}$	$0.055_{-0.012}^{+0.014}$
5.77±0.04	27±3	38±8	$\frac{1}{2}$	$(\frac{3}{2}^+)$	$(\frac{3}{2}^+)$	2.4	0.83	$2.0_{-1.5}^{+0.6}$	$0.61_{-0.22}^{+0.28}$
7.03±0.05	13±4	42±8	$\frac{1}{2}$	$(\frac{3}{2}^+)$	$(\frac{3}{2}^+)$	3.8	2.9	3.7±0.5	$2.2_{-0.8}^{+1.0}$
7.81±0.03	59±4	100±10	$\frac{1}{2}$	$\frac{3}{2}^+$, $\frac{5}{2}^+$	$\frac{3}{2}^+$	2.9	6.5	$2.6_{-0.4}^{+0.2}$	$4.7_{-1.0}^{+1.2}$
10.43±0.05	39±6	104±15	$(\frac{3}{2})$	( )[a]	( )[a]	3.7	22	3.5±0.3	17±5
11.37±0.07	34±8	68±15	$(\frac{3}{2})$	( )[a]	( )[a]	3.3	16	$3.0_{-0.8}^{+0.6}$	12_{-6}^{+6}
11.76±0.06	41±8	87±16	$(\frac{3}{2})$	( )[a]	( )[a]	3.4	24	$3.2_{-0.6}^{+0.4}$	18_{-6}^{+7}

[a] $\frac{3}{2}^-$, $\frac{5}{2}^+$, or $\frac{7}{2}^+$.

REF. B. L. Berman, R. J. Baglan, and C. D. Bowman
Phys. Rev. Letters 24, 319 (1970)

ELEM. SYM.	A	Z
Mg	25	12

METHOD

REF. NO. 70 Be 5 hmg

REACTION	RESULT	EXCITATION ENERGY	SOURCE		DETECTOR		ANGLE
			TYPE	RANGE	TYPE	RANGE	
G,N	ABX	7-10	C	11	TOF-D		135
							9474

The photoneutron cross section for Mg^{25} has been measured from 30 to 2000 keV above threshold. The locations of the isobaric analogs of the ground and first excited states of Na^{25} have been assigned and lower limits for their neutron-decay widths have been determined.

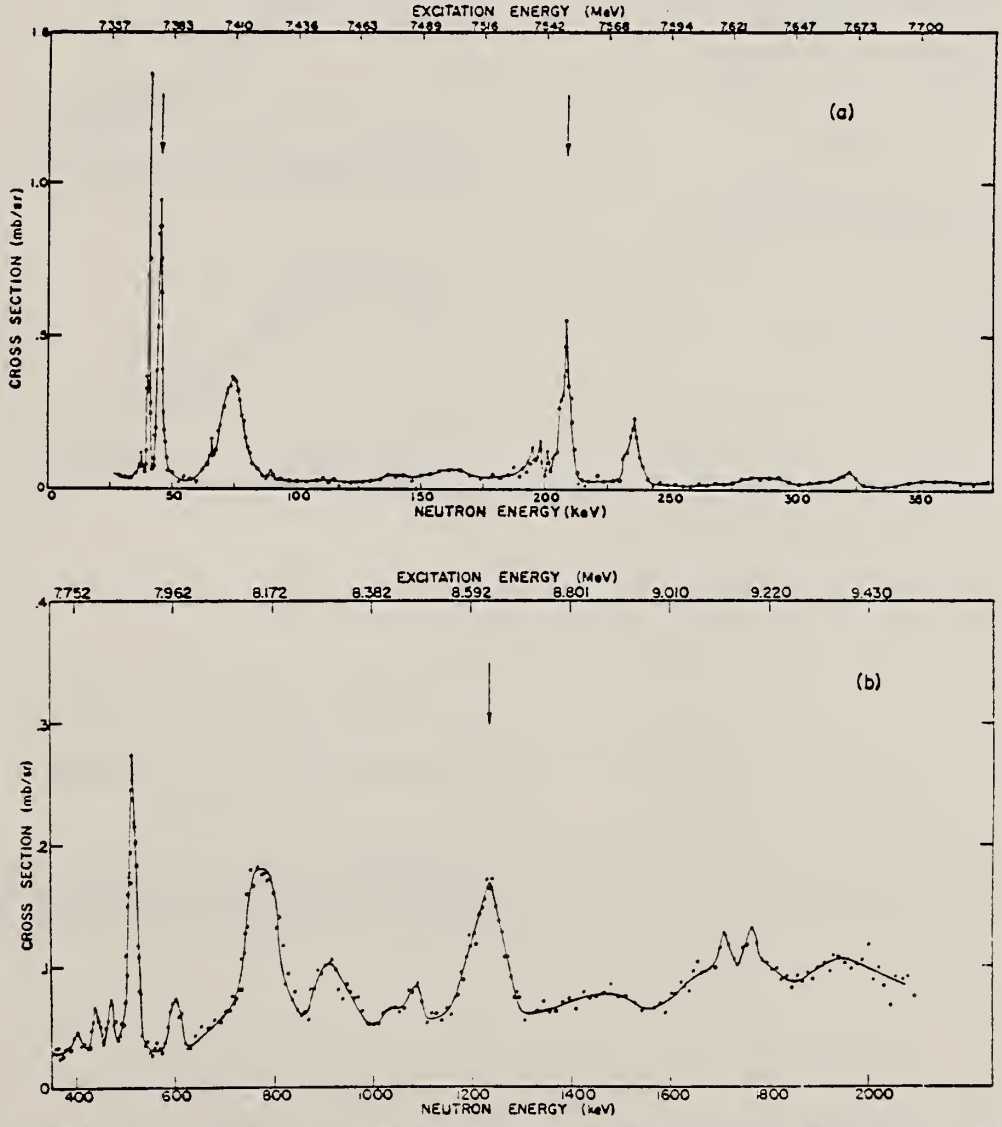

FIG. 1. Differential photoneutron cross section for Mg^{25} at 135° as a function of laboratory neutron energy (lower scale) and of excitation energy (upper scale). The arrows refer to peaks resulting from transitions to the first excited state of Mg^{24}. (a) Low-energy cross section; (b) high-energy cross section.

REF.

R. A. Alvarez, B. L. Berman, D. R. Lasher, T. W. Phillips, and S. C. Fultz
Phys. Rev. C4, 1673 (1971)

ELEM. SYM.	A	Z
Mg	25	12

METHOD

REF. NO.	
71 A1 1	hmg

REACTION	RESULT	EXCITATION ENERGY	SOURCE		DETECTOR		ANGLE
			TYPE	RANGE	TYPE	RANGE	
G,N 352	ABX	7-29	D	7-29	BF3-I		4PI *
G,2N 353†	ABX	23-29	D	23-29	BF3-I		4PI

* INCLUDES G,NP 352+

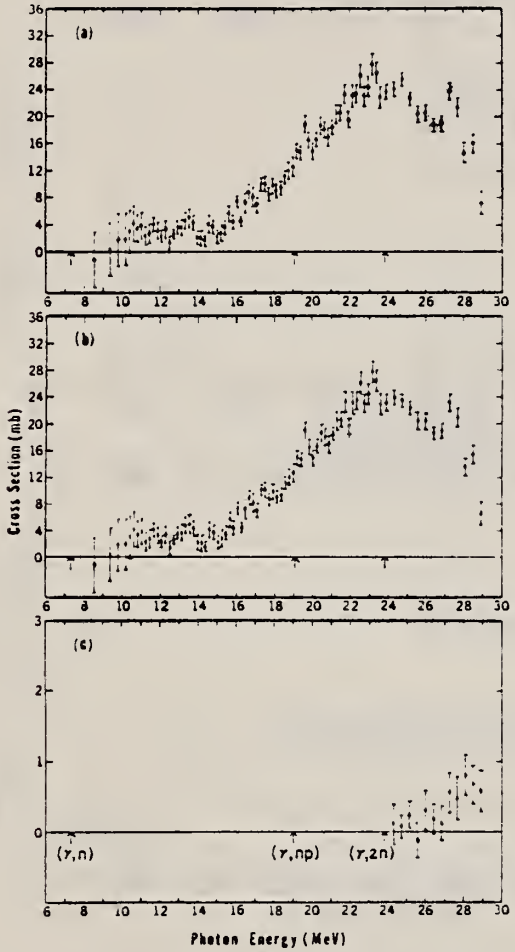

FIG. 3. Cross sections for ^{25}Mg. (a) Total photoneutron cross section, $\sigma[(\gamma,n)+(\gamma,np)+(\gamma,2n)]$. (b) Single-photoneutron cross section, $\sigma[(\gamma,n)+(\gamma,np)]$. (c) Double-photoneutron cross section, $\sigma(\gamma,2n)$.

TABLE II. Integrated total photoneutron cross sections and their moments.

Nucleus	$E_{\gamma max}$ (MeV)	σ_{int} [a] (MeV mb)	σ_{-1} [b] (mb)	σ_{-2} [b] (mb MeV^{-1})
^{23}Na	27	119	5.74	0.288
^{25}Mg	29	249	11.7	0.584

[a] $\sigma_{int} \equiv \int_{E_{thr}}^{E_{\gamma max}} \sigma_{tot} dE$.

[b] $\sigma_{-n} \equiv \int_{E_{thr}}^{E_{\gamma max}} \sigma_{tot} E^{-n} dE$.

(over)

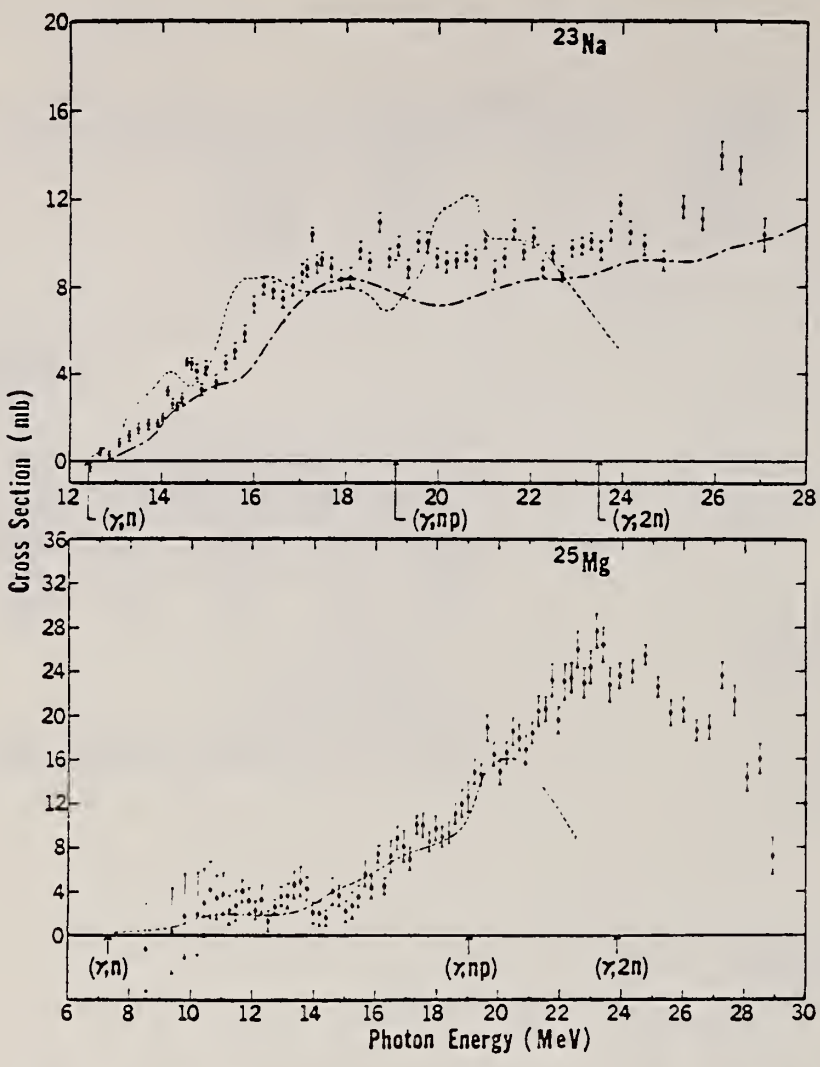

FIG. 4. Comparison of the present total photoneutron cross sections with previous measurements. The dashed curves indicate the results of Sato (Ref. 11) for ^{23}Na and of Nathans and Yergin (Ref. 13) for ^{25}Mg; the dash-dot curve represents the ^{23}Na data of Fielder, Bolen, and Whitehead (Ref. 12).

REF. R. J. Baglan, C. D. Bowman and B. L. Berman
Phys. Rev. C3, 672 (1971)

ELEM. SYM.	A	Z
Mg	25	12

METHOD

REF. NO. 71 Ba 2 hmg

REACTION	RESULT	EXCITATION ENERGY	SOURCE		DETECTOR		ANGLE
			TYPE	RANGE	TYPE	RANGE	
G,N	ABX	7 - 11	C	8,11	TOF-D		135
		(7.3-11.0)					

205

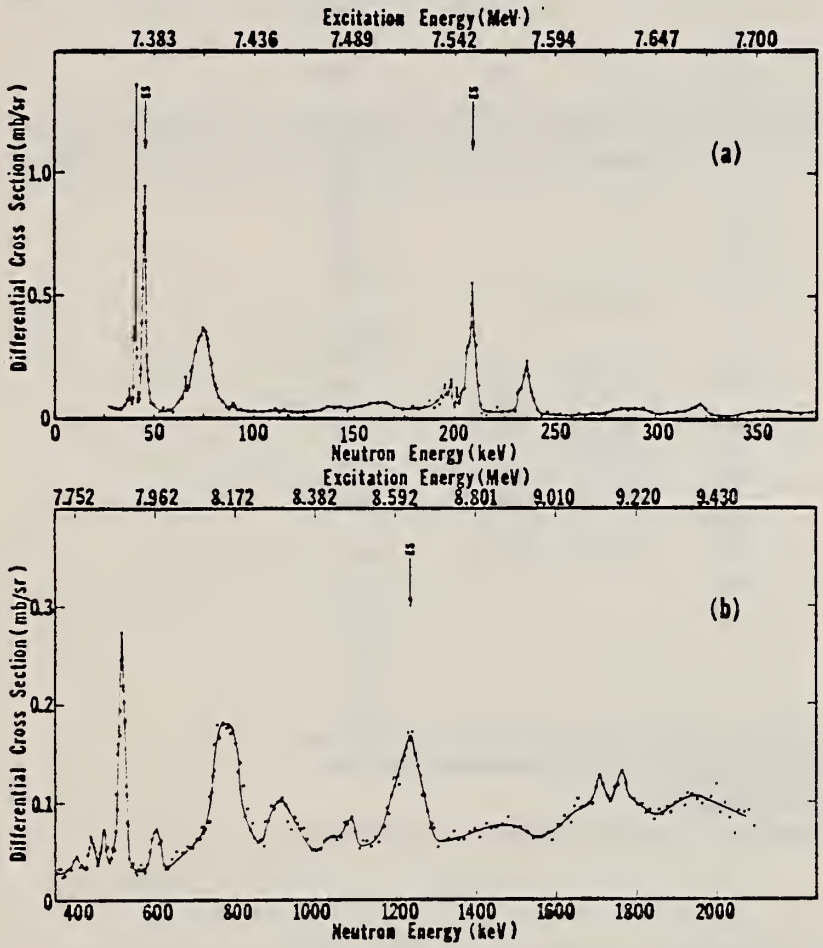

FIG. 16. The 135° differential threshold photoneutron cross section for ^{25}Mg (see caption to Fig. 4).

FIG. 4. The 135° differential threshold photoneutron cross section for ^{207}Pb at low energies versus the energy of the emitted neutron (lower scale) and the excitation energy (upper scale). The arrows indicate peaks which decay to excited states of the residual nucleus (ES), or peaks owing to contaminating isotopes in the photoneutron sample. The inset shows the ^{207}Pb(γ, n) cross section averaged with a square 40-keV wide smoothing function.

Also see:
R. J. Baglan et al.
Phys. Rev. C3, 2475 (1971)

[over]

TABLE VII. Resonance parameters for ^{24,25,26}Mg, ^{19}F, and ^{31}P. For all resonances, the area under the peak in the 135° differential cross section is multiplied by 4π to yield approximate values for $g_\gamma\Gamma_{\gamma 0}\Gamma_n/\Gamma \simeq g_\gamma\Gamma_{\gamma 0}$. For those resonances where J^π is known, the differential area is multiplied by the appropriate factor F from Table I to obtain $\Gamma_{\gamma 0}$. E_L is the laboratory neutron energy for the (γ,n) reaction and E_n is the corresponding laboratory neutron energy for a neutron-induced reaction. Column 5 labels the peak as a ground-state (GS) or excited-state (ES) transition as determined in this work alone.

Nucleus	E_L (keV)	E_{ex} (MeV)	$g_\gamma\Gamma_{\gamma 0}\Gamma_n/\Gamma$ (eV)	GS or ES	J^π	$\Gamma_{\gamma 0}$ (eV)	E_n (keV) (This work)
^{24}Mg	22	16.559	0.61		(1^-)	0.40	28
	55	16.596	2.4	GS	(1^-)	1.6	66
	110	16.656	4.0	GS	(1^-)	2.7	128
	312	16.871	10.7		(1^-)	7.1[a]	354
	382	16.95					432
	717	17.30	19.5		(1^-)	13.0[a]	804
	1210	17.83					1348
	1620	18.26					1799
	1955	18.61					2168
^{25}Mg	41.1	7.374	0.09	GS			46.8
	45.1	8.746	0.31	ES			
	74.9	7.410	0.36	GS	$\frac{3}{2}^-$[b]	1.1	84.1[b]
	208	8.920	0.29	ES			
	236	7.580	0.09	GS			261
	404	7.756	0.03				445
	439	7.793	0.05		$\frac{5}{2}^+$[c]		484
	472	7.828	0.06				520
	515	7.873	0.46	GS	$\frac{3}{2}^+$[c]		567
	601	7.964	0.18				661
	781	8.152	1.51	GS			857
	912	8.292	0.72				1003
	1236	9.999	2.4[c]	ES	$\frac{3}{2}^+$ or $\frac{5}{2}^+$[c]		
	1707	9.12					1869
	1764	9.18					1931
^{26}Mg	54.3	11.155	2.6	GS	$1^-(1^+,2^+)$	1.75	62.3
	63.2	11.164	0.05			0.034	72.2
	181	11.289	1.0	GS	$1^-(1^+,2^+)$	0.68	202
	222	11.333	1.9	GS	$1^-(1^+,2^+)$	1.3	248
	391	11.511	5.1	GS	$1^-(1^+,2^+)$	3.5	433
	621	11.753	32.5	GS	$1^-(1^+,2^+)$	22.2	684
	738		15.0[d]	ES		5.1	
	1122	12.279	14.7	GS	$1^-(1^+,2^+)$	10.0	1232
^{19}F	100	10.542	1.8	GS			118
^{31}P	109	12.429	0.86				121
	280	12.609	0.60				307
	398	12.732	0.59				434
	678	13.026	0.90				737
	939	13.297	4.4				1018

[a]These values for $\Gamma_{\gamma 0}$, when increased by approximately a factor of 2 in order to include the relatively high cross sections in the valleys, agree very well with corresponding values from Ref. 8 (see Ref. 4).

[b]This resonance was seen at E_n = 83 and 84 keV in Refs. 24 and 25, respectively.

[c]Analogs of states in ^{25}Na (see text). The value for $g_\gamma\Gamma_{\gamma 0}\Gamma_n/\Gamma$ given in Ref. 26 was not corrected with the multiplicative factor in Table II.

[d]Assuming a first-excited-state transition.

[4]R.L. Van Hemert, C.D. Bowman, R.J. Baglan, and B.L. Berman (to be published); R.L. Van Hemert, University of California Lawrence Radiation Laboratory Report No. UCRL-50442, 1968 (unpublished).

[8]S.C. Fultz, M.A. Kelly, J.T. Caldwell, R.R. Harvey, and B.L. Berman, Bull. Am. Phys. Soc. 14, 103 (1969), and private communication.

[24]H.W. Newson, R.C. Block, P.F. Nichols, A. Taylor, A.K. Furr, and E. Merzbacher, Ann. Phys. (N.Y.) 8, 211 (1959).

[25]D.J. Hughes and R.B. Schwartz, Neutron Cross Sections (U.S. Government Printing Office, Washington, D.C., 1966), 2nd ed., 2nd Suppl., Vol. IIc.

REF.

B. L. Berman and T. W. Phillips
Phys. Rev. C6, 2295 (1972)

ELEM. SYM.	A	Z
Mg	25	12

METHOD

REF. NO.	
72 Be 9	hmg

REACTION	RESULT	EXCITATION ENERGY	SOURCE		DETECTOR		ANGLE
			TYPE	RANGE	TYPE	RANGE	
G,N	NOX	7	C	UKN	TOF-D		90
		(7.864)					

Repeat of previous experiment.

SEE 70BE5

The location in ^{25}Mg of the isobaric analog of the first excited state of ^{25}Na has been measured to be 7864.5±1.2 keV. Combining this result with other data yields a value for the coefficient of the cubic term in the isobaric-multiplet mass equation of −0.2±4 keV.

REF.

E. W. Lees, C. S. Curran, S. W. Brain, W. A. Gillespie, A. Johnston, R. P. Singhal
J. Phys. G1, L13 (1975)

ELEM. SYM.	A	Z
Mg	25	12

METHOD

REF. NO.	
75 Le 3	egf

REACTION	RESULT	EXCITATION ENERGY	SOURCE		DETECTOR		ANGLE
			TYPE	RANGE	TYPE	RANGE	
E,E/	LFT	0- 4	D	62-119	MAG-D		DST

1.611,3.405 MEV

Abstract. The members of the ground state band of ^{25}Mg have been studied in the momentum transfer range 0·2 to 1·15 fm^{-1}. The reduced transition probabilities and transition radii were measured for the 1·612 MeV and 3·405 MeV levels. The transition probabilities are shown to be considerably more precise than existing measurements and are compared with various theoretical predictions. The hexadecupole strength to the $\frac{11}{2}^+$ levels is also discussed.

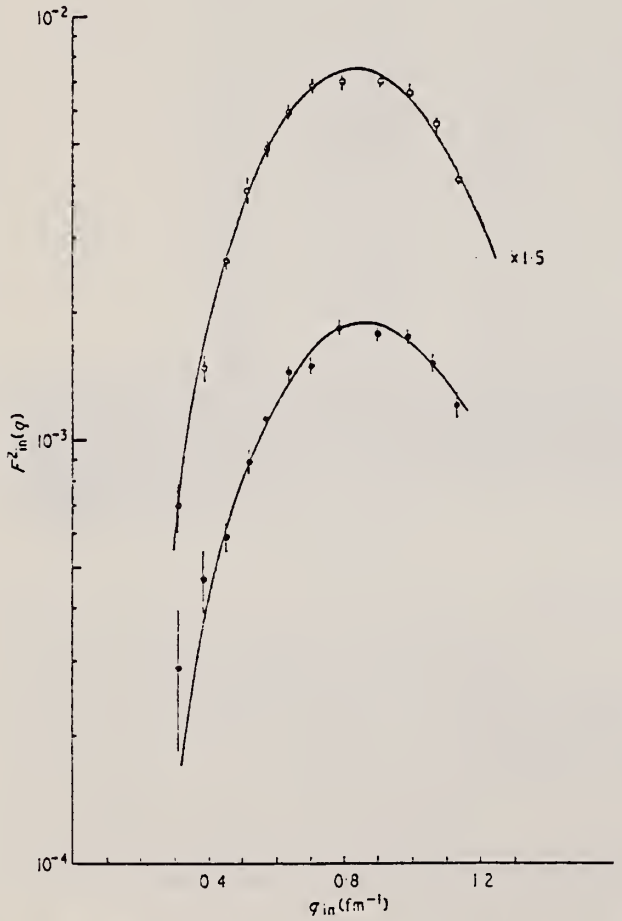

Figure 1. Inelastic form factors for the $\frac{7}{2}^+$ level in ^{25}Mg at 1·612 MeV (○) and for the $\frac{9}{2}^+$ level at 3·405 MeV (●). The full curves are the corresponding best-fit DWBA Coulomb form factors for an $L = 2$ transition. The upper curve is multiplied by a scale factor of 1·5. See text for further details.

Table 1. Best fit DWBA parameters.

E_x (MeV)	c_{tr} (fm)	t_{tr} (fm)	R_{tr}† (fm)	B(E2,↑)‡ (e^2 fm^4)	χ^2 pdf§
1·611±0·004	2·85±0·20	2·21±0·23	4·25±0·11	158±7	1·0
3·405±0·007	2·48±0·43	2·42±0·32	4·28±0·18	57±4	0·7

† R_{tr} is the transition radius.
‡ B(E2,↑) is the E2 reduced transition probability from the ground state.
§ χ^2 pdf is χ^2 per degree of freedom.

Table 2. Comparison of B(E2,↑) deduced from lifetime measurements and present results. See text for references to individual measurements.

E_x (MeV)	J^π	Lifetime (fs)	Mixing ratio	Ground state branching ratio	B(E2,↑) (e^2 fm^4)	B(E2,↑)c, e′ (e^2 fm^4)
1·612	$\frac{7}{2}^+$	20·6±2·6[a]	0·20±0·02	100%	187±43	158±7
		24·5±3·3[b]	0·20±0·02	100%	157±37	158±7
3·405	$\frac{9}{2}^+$	10±5	0	18±1%	54±27	57±4

[a] Includes the measurement by Fagg *et al* (1969).
[b] Excludes the measurement by Fagg *et al* (1969).

Phys. Rev. 187, 1384 (69)

REF.	ELEM. SYM.	A	Z
K. Bangert, U.E.P. Berg, G. Junghans, R. Stock, K. Wienhard, H. Wolf Nucl. Phys. A261, 149 (1976)	Mg	25	12

METHOD	REF. NO.
	76 Ba 2 egf

REACTION	RESULT	EXCITATION ENERGY	SOURCE		DETECTOR		ANGLE
			TYPE	RANGE	TYPE	RANGE	
G,P	ABX	14- 18	C	19- 29	TEL-D		90
G,A	ABX	18- 24	C	29	TEL-D		90
G,D	ABX	19- 24	C	29	TEL-D		90
G,PG	ABY	13- 29	C	19- 29	SCD-D		90
G,NG	ABY	8- 29	C	19- 29	SCD-D		90

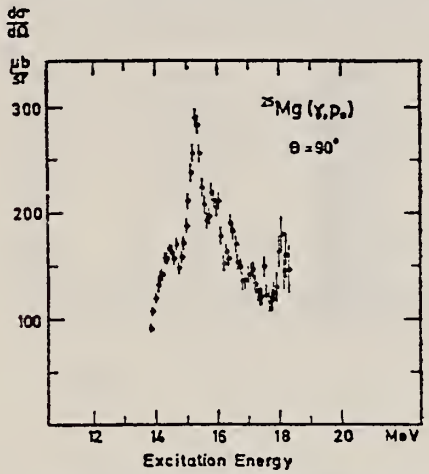

Fig. 6. The 90° ^{25}Mg(γ, p_0) differential cross section as derived from the 18.5 MeV proton spectrum, assuming ground-state transitions.

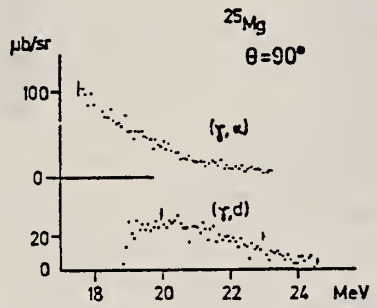

Fig. 7. The 90° ^{25}Mg(γ, d) and ^{25}Mg(γ, α) differential cross sections derived from the 28.7 MeV particle spectra.

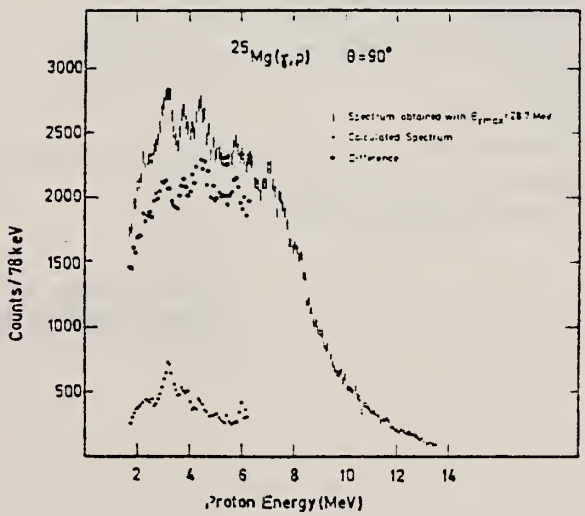

Fig. 8. A comparison between the 28.7 MeV ^{25}Mg photoproton spectrum and a "(γ, p_0)" spectrum derived from the ^{25}Mg(γ, p_0) differential cross section of fig. 6.

(over)

TABLE 4

Results of the $^{25}Mg(\gamma, x\gamma')$ experiment, giving the "bremsstrahlung-weighted" integrated cross sections in MeV · mb for the population of excited residual nuclear states

	Bremsstrahlung endpoint energy (MeV)		
	18.5	21.0	28.7
(a) ^{24}Na states			
g.s. 4^+			
472 keV, 1^+	?	?	?
563 keV, 2^+	?	?	?
1341 keV, ?+1347 keV, 1^+		0.89	6.09
1345 keV, 3		0.52	2.20
1511 keV, $(3, 5)^+$		0.33	2.21
1885 keV, $(2, 3)^+$		0.41	3.72
2513 keV, (1–3)		0.15	1.25
2561 keV, $(1–4)^+$		0.49	3.67
2909 keV, 3^+		0.23	1.15
(b) ^{24}Mg states			
g.s. 0^+	13.04 [a])	24.9 [a])	?
1369 keV, 2^+	4.30	4.76	12.84
4123 keV, 4^+	1.32	2.12	5.18
4239 keV, 2^+	1.04	1.34	3.64
5236 keV, 3^+	0.82	0.93	2.65
6010 keV, 4^+	0.55	0.58	1.56
7616 keV, 3^-	0.18	0.42	1.63
8436 keV, 4^+	0.29	1.03	2.94
9515 keV, 4^+ $T = 1$		0.78	2.84
9827 keV, 1^+ $T = ?$		0.29	1.28
9967 keV, 1^+ $T = 1$		0.55	1.05
10059 keV, $(1, 2)^+$ $T = 1$		0.32	1.38
10822 keV, ?			1.42
(c) ^{23}Na states			
404 keV, $\frac{5}{2}^+$	?	?	?
2076 keV, $\frac{7}{2}^+$			3.11
(d) ^{21}Ne states			
350 keV, $\frac{5}{2}^+$	?	?	?
1746 keV, $\frac{7}{2}^+$			<1.32
Sum of observed (γ, p) excited states cross sections		3.07	20.29
Sum of observed (γ, n) excited states cross sections	8.5	13.12	38.42
Proton yield		12.15	77.10
$(\gamma, n)+(\gamma, np)$ yield [a])	21.54	38.02	106.11

Bremsstrahlung spectra are normalized at 11.44 MeV.
[a]) Calculated from the data of ref. [2]).

[2] S.C. Fultz et al., Phys. Rev. C4, 149 (1971);
R.A. Alvarez et al., Phys. Rev. C4, 1673 (1971).

REF. E. W. Lees, C. S. Curran, T. E. Drake, W. A. Gillespie, A. Johnston, and R. P. Singhal
J. Phys. (London) G2, 341 (1976)

ELEM. SYM.	A	Z
Mg	25	12

METHOD

REF. NO. 76 Le 3 egf

REACTION	RESULT	EXCITATION ENERGY	SOURCE TYPE	SOURCE RANGE	DETECTOR TYPE	DETECTOR RANGE	ANGLE
E,E/	FMF	1- 4	D	62-119	MAG_D		DST

7 LEVELS,.98-4.1 MEV

Table 3. Results for the DWBA analysis of the present data using an $L = 2$ transition within the framework of the Tassie model. The accepted values have been used for the excitation energies, spins and parities of the states.

E_x (MeV)	J^π	c_{tr} (fm)	t_{tr} (fm)	R_{tr} (fm)	$B(E2,\uparrow)$ (e^2 fm^4)
0·975	$\frac{1}{2}^+$	2·85†	2·21†	4·25†	2·3 ± 0·6
1·612	$\frac{7}{2}^+$	2·85 ± 0·20	2·21 ± 0·23	4·25 ± 0·11	156 ± 7
1·965	$\frac{5}{2}^+$	2·85†	2·21†	4·25†	3·0 ± 0·5
2·563	$\frac{1}{2}^-$	2·45	2·21†	4·01	4·3 ± 0·8
2·801	$\frac{3}{2}^+$	2·45†	2·21†	4·01†	5·2 ± 0·4
3·405	$\frac{9}{2}^+$	2·48 ± 0·43	2·42 ± 0·32	4·28 ± 0·18	57 ± 4
4·059	$\frac{9}{2}^+$	2·66	2·21†	4·13	9·6 ± 1·0

† Denotes that the radial parameter for this level was fixed.

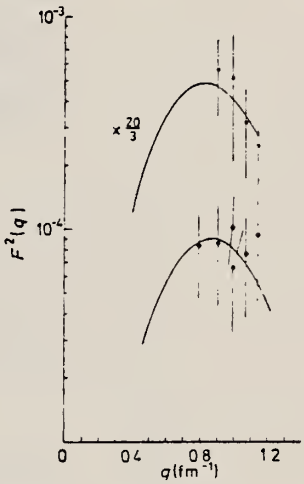

Figure 3. Inelastic form factors for the transitions in ^{25}Mg to the levels at 0·975 MeV (○) and 1·965 MeV (●). The full curves are the corresponding best-fit $L = 2$ Coulomb form factors calculated in DWBA. The upper curve and data are multiplied by a scale factor of $\frac{20}{3}$.

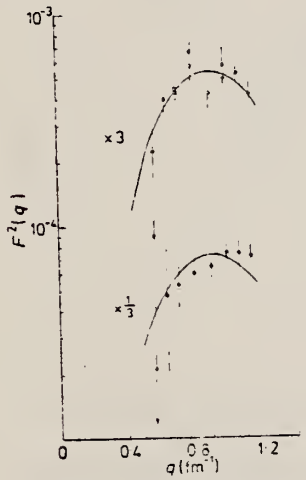

Figure 4. Inelastic form factors for the transitions in ^{25}Mg to the levels at 2·564 MeV (○) and 2·801 MeV (●). The full curves are the corresponding best-fit $L = 2$ Coulomb form factors calculated in DWBA. The upper curve and data are multiplied by a scale factor of 3 and the lower ones by $\frac{1}{3}$.

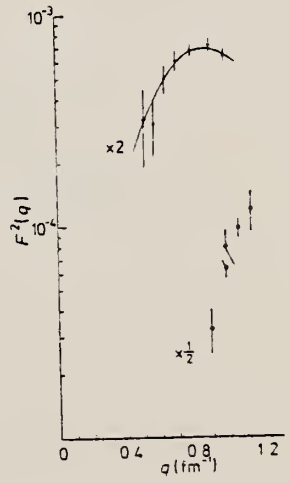

Figure 5. Inelastic form factors for the transitions in ^{25}Mg to the levels at 4·056 MeV (○) and 5·252 MeV (●). The full curve is the corresponding best-fit $L = 2$ Coulomb form factor calculated in DWBA. The upper curve and data are multiplied by a scale factor of 2 and the lower data by $\frac{1}{2}$.

REF. K. Masumoto, T. Kato, N. Suzuki
Nucl. Inst. Meth. 157, 567 (1978)

ELEM. SYM.	A	Z
Mg	25	12

METHOD

REF. NO. 78 Ma 10 hg

REACTION	RESULT	EXCITATION ENERGY	SOURCE		DETECTOR		ANGLE
			TYPE	RANGE	TYPE	RANGE	
G,P	ABY	12-68	C	30-68	ACT		4PI

Analysis is made of reactions interfering with photon activation analysis procedures.

The activation yield curves have been presented for a number of photonuclear reactions in the energy range from 30 to 68 MeV, in order to evaluate quantitatively the interferences due to competing reactions in multielement photon activation analysis. The general features of the yields as functions of both target mass number and excitation energy were elucidated from the data obtained, discussion being given on the results in terms of the reaction mechanism.

Simultaneous neutron activation due to appreciable neutron production from the converter and surrounding materials has also been studied, and, finally, the magnitudes of interferences in real multielement analysis were given in the form of their energy dependences.

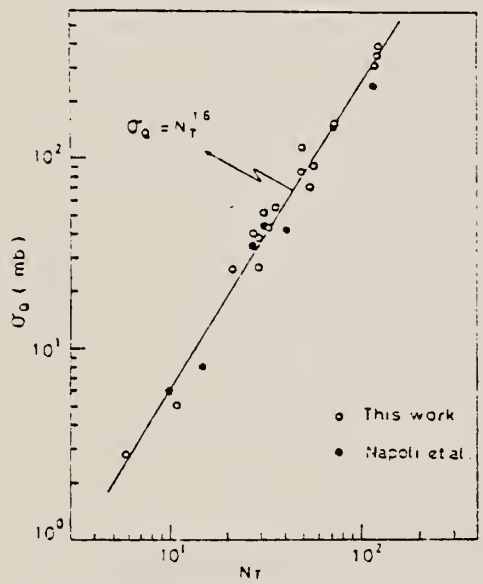

Fig. 2. Yield per equivalent quanta versus target neutron number.

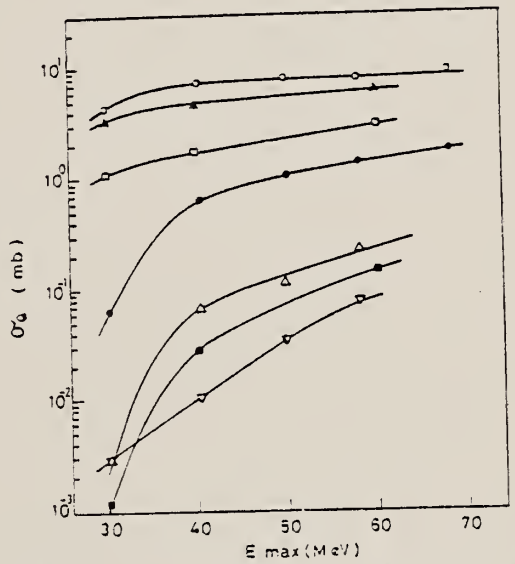

Fig. 3. Activation yield curves for the reactions on C, Na, Mg and Al.
□ $^{12}C(\gamma, n)^{11}C$, ■ $^{12}C(\gamma, \pi n)^{7}Be$, ▲ $^{23}Na(\gamma, n)^{22}Na$,
○ $^{25}Mg(\gamma, p)^{24}Na$, ● $^{24}Mg(\gamma, pn)^{23}Na$, △ $^{27}Al(\gamma, \pi n)^{22}Na$,
▽ $^{27}Al - ^{24}Na$.

(over)

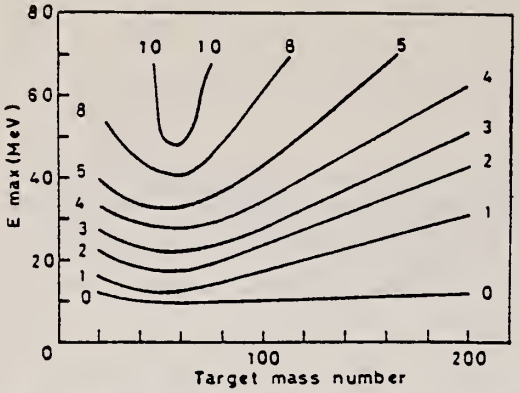

Fig. 10. Yields of the (γ, p) reactions as a function of bremsstrahlung maximum energy and target mass number. The numerical values in the figure are yields per equivalent quanta in mb.

MG
A=26

MG
A=26

Ref. V.K. Rasmussen, F.R. Metzger, C.P. Swan
Phys. Rev. 123, 1386 (1961)

Elem. Sym.	A	Z
Mg	26	12

Method
Van de Graaff; 1.83 MeV γ source by $Mg^{26}(p,p'\gamma)$ with 4.4 MeV protons; ring scatterer; NaI.

Ref. No. 61 Ra 1 JHH

Reaction	E or ΔE	E_o	Γ	$\int \sigma dE$	$J\pi$	Notes
(γ,γ)	1.83	1.83				Mean life = $(7\pm3) \times 10^{-13}$ sec.

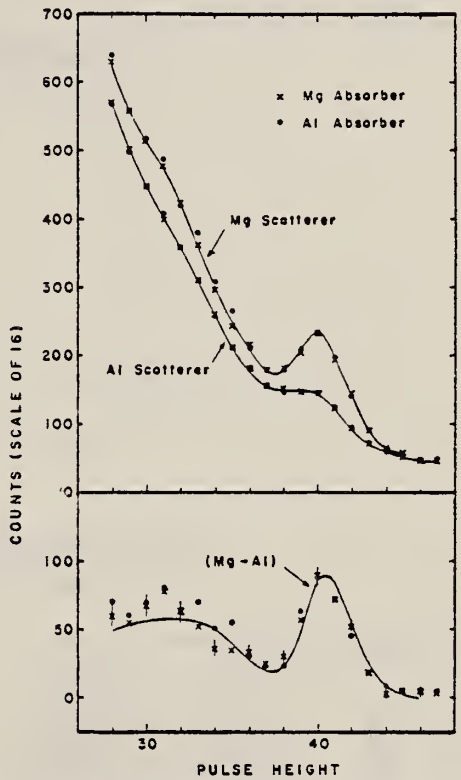

FIG. 6. Resonant scattering of the 1.83-Mev γ ray from Mg^{26}. The upper curves give the original data for the scatterer-absorber combinations noted. Statistical errors can be estimated from the left-hand scale which gives the total number of counts for each point. Mg scatterer–Al scatterer differences are shown in the lower plots, where the solid curve is that obtained when the counter is exposed to direct radiation from the target. The sum of counts for pulse heights 39 to 42 was taken to represent the resonance effect.

REF. E. C. Booth, B. Chasan and K. A. Wright
Nucl. Phys. 57, 403-420 (1964)

ELEM. SYM.	A	Z
Mg	26	12

METHOD
Van de Graaff; resonance fluorescence

REF. NO. 64 Bo 1 NVB

REACTION	RESULT	EXCITATION ENERGY	SOURCE TYPE	SOURCE RANGE	DETECTOR TYPE	DETECTOR RANGE	ANGLE
G,G	LFT	1-3	C	1 - 3	NAI-D		100
		(0.5 - 3.0)		(0.5 - 3.0)			

ABI

TABLE I
Cases of observed resonance fluorescence

Nucleus multipol.	State (MeV)	Spin	Γ_0/Γ	$T(g w \Gamma_0^2/\Gamma^2)^{-1}$ (sec).	Mean lifetime T BCW (sec)	Mean lifetime T other (sec)	Ref.	Γ_0/Γ_W BCW
Mg^{26}	0.00	0^+						
E2	1.83	2^+	1	$12 \pm 5 \times 10^{-14}$	$37 \pm 15 \times 10^{-14}$	$70 \pm 30 \times 10^{-14}$	11)	22

REF. O. Titze and E. Spamer
Z. Naturforschg. 21a, 1504 (1966)

ELEM. SYM.	A	Z
Mg	26	12

METHOD

REF. NO. 66 Ti 1 egf

REACTION	RESULT	EXCITATION ENERGY	SOURCE		DETECTOR		ANGLE
			TYPE	RANGE	TYPE	RANGE	
E,E/	LFT	7-15	D	51	MAG-D	36-51	DST

Angular distribution measured for q = 0.48, 0.41, 0.32 fm^{-1}.

DST CONST O

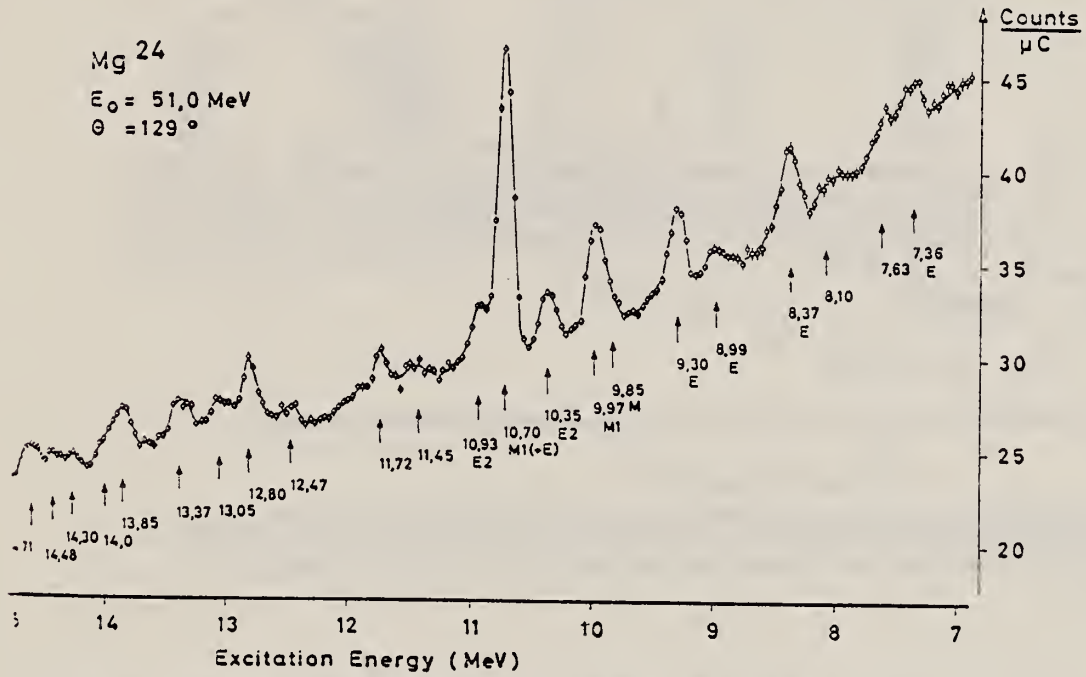

Fig. 1. Spectrum of inelastically scattered electrons from ^{24}Mg. The effective target thickness was 50 mg/cm². The arrows indicate the measured excitation energies in MeV. The type of transition [electric (E) or magnetic (M)] is labeled. Note the suppressed zero of the ordinate scale. The elastic peak has a height of 2.4×10^4 units of the ordinate scale.

E_x (MeV)		$\Gamma_\gamma{}^0$ (eV)	$\Gamma_\gamma{}^0/\Gamma_W$	R_{tr} (fm)
9.85 ± 0.04 9.97 ± 0.03	M1	7.95 ± 1.2	0.38	3.50 ± 0.49
10.35 ± 0.03	E2	0.24 ± 0.05	0.58	5.05 ± 0.50
10.70 ± 0.03	M1	22.2 ± 2.4	0.86	3.60 ± 0.36
10.93 ± 0.04	E2	0.26 ± 0.11 *	0.50	—

* Calculated with R_{tr} from 10.35 MeV transition.

Table 1. Results for ^{24}Mg. The first two columns give excitation energies and multipolarities as determined from this work. Column 3 to 5 show the ground state radiation widths $\Gamma_\gamma{}^0$, the transition strengths in Weisskopf units Γ_W and the transiton radii R_{tr}. The Bohr approximation has been used.

over

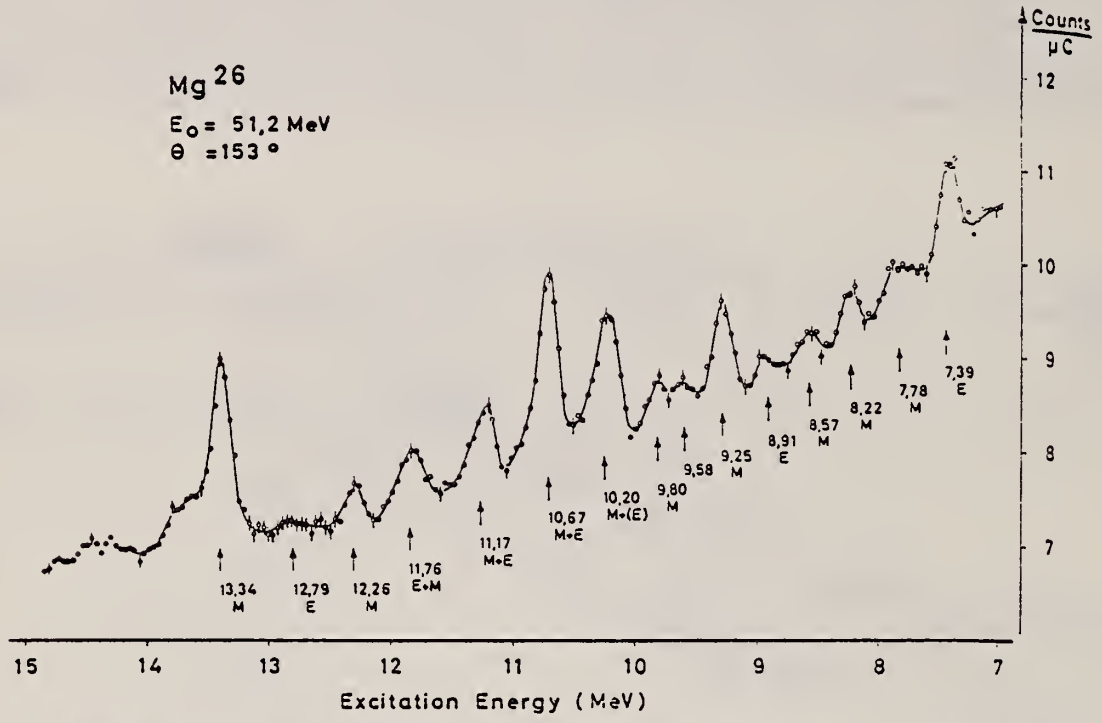

Fig. 2. Spectrum of inelastically scattered electrons from ^{26}Mg. The effective target thickness was 170 mg/cm^2. The arrows indicate the measured excitation energies in MeV. The type of transition [electric (E) or magnetic (M)] is labeled. Note the suppressed zero of the ordinate scale. The elastic peak has a height of 2.5×10^3 units of the ordinate scale.

REF.

H. W. Kuehne, P. Axel, and D. C. Sutton
Phys. Rev. 163, 1278 (1967)

ELEM. SYM.	A	Z
Mg	26	12

METHOD

REF. NO.	
67 Ku 2	HMG

REACTION	RESULT	EXCITATION ENERGY	SOURCE		DETECTOR		ANGLE
			TYPE	RANGE	TYPE	RANGE	
G,G	LFT	10	D	10	NAI-D	10	135

Photons, defined in energy to about 1% with the aid of a bremsstrahlung monochromator, were scattered by isolated energy levels in C, Mg, and Si. Parameters for the six observed levels are:

Isotope	Energy (MeV)	Γ_0^2/Γ (eV)	Γ_0/Γ	$B(M1)/(e\hbar/2M_pc)^2$
C^{13}	15.11	36	1	0.93
Mg^{24}	10.66±0.02	14	0.8	1.21
Si^{28}	11.42±0.02	23	1	1.33
Si^{28}	12.33±0.03			
Mg^{24}	9.92±0.03	3.0	0.5	0.49
Mg^{26}	10.07±0.05	4.2		≥0.36

The 15.11-MeV level in C^{13}, the 9.92- and 10.66-MeV levels in Mg^{24}, and the 11.42-MeV level in Si^{28} are $T=1$, $T_z=0$ analogs of low-lying 1+ states in the neighboring odd-odd nuclei. These levels exhaust most of of the magnetic dipole transition strength of the respective nuclei, and therefore give information about the expectation value of l·s in the ground state.

REF. W. L. Bendel, L. W. Fagg, R. A. Tobin, H. F. Kaiser
Phys. Rev. 173, 1103 (1968)

ELEM. SYM.	A	Z
Mg	26	12

METHOD

REF. NO. 68 Be 2 HMG

REACTION	RESULT	EXCITATION ENERGY	SOURCE		DETECTOR		ANGLE
			TYPE	RANGE	TYPE	RANGE	
E,E/	ABX	8-14	D	39,56	MAG-D		180

TABLE I. Levels at 8 to 14 MeV in ^{26}Mg found in electron scattering. The differential cross sections are in units of 10^{-34} cm^2 per sr.

Energy (MeV)	$(d\sigma/d\Omega)_{56\ MeV}$	$(d\sigma/d\Omega)_{39\ MeV}$	Parameters as $M1$ transitions R (fm)	Γ_0 (eV)	Energy and type, Titze and Spamer[a]
8.52±0.05	81±22	159±57	$3.2_{-1.4}^{+0.6}$	$0.5_{-0.2}^{+0.4}$	8.22 M 8.57 M
9.24±0.03	268±26	695±63	$3.62_{-0.19}^{+0.17}$	$3.3_{-0.7}^{+0.9}$	8.91 E
9.67±0.05	246±26	409±69	$2.90_{-0.54}^{+0.36}$	$1.7_{-0.6}^{+0.8}$	9.25 M
10.18±0.03	447±30	968±77	$3.40_{-0.19}^{+0.16}$	$5.7_{-1.2}^{+1.3}$	9.58, 9.80 M
10.63±0.03	593±42	1332±77	3.47 ± 0.14	$9.1_{-1.7}^{+2.0}$	10.20 $M+(E)$
11.20±0.05	274±26	525±68	$3.23_{-0.33}^{+0.26}$	$3.9_{-1.1}^{+1.3}$	10.67 $M+E$
11.67, 11.82					11.17 $M+E$
12.31	62±26	<97	<3.8	<1.2	11.76 $E+M$ 12.26 M
13.33±0.03	689±35	1174±90	$3.10_{-0.21}^{+0.17}$	$14.5_{-3.0}^{+3.3}$	12.79 E
13.66±0.06	110±31	180±76	$3.0_{-3.0}^{+0.8}$	$2.3_{-1.5}^{+2.4}$	13.34 M

[a] See Ref. 10.

[10] O. Titze and E. Spamer, Z. Naturforsch. 21a, 1504 (1966).

B. L. Berman, R. L. Van Hemert, C. D. Bowman
Phys. Rev. Letters 23, 386 (1969)

Mg	26	12

METHOD

REF. NO. 69 Be 3 egf

REACTION	RESULT	EXCITATION ENERGY	SOURCE		DETECTOR		ANGLE
			TYPE	RANGE	TYPE	RANGE	
G,N	ABX	11-13	C	13	TOF-D	0	135
							949

0= 10 to 1200 KEV

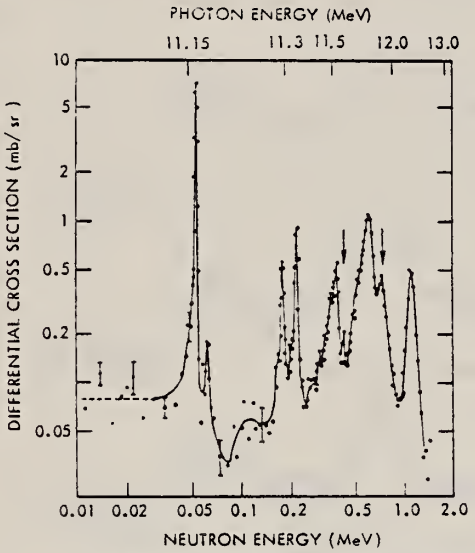

FIG. 1. Threshold photoneutron cross section for Mg^{26} at 135° as a function both of photon energy and of laboratory neutron energy. The solid line drawn through the data points is to guide the eye. The arrows indicate excited-state transitions. The electron beam energy was 13.3 MeV.

REF. A. Goldmann
Z. Physik 234, 144 (1970)

ELEM. SYM.	A	Z
Mg	26	12

METHOD

REF. NO.	
70 Go 3	egf

REACTION	RESULT	EXCITATION ENERGY	SOURCE		DETECTOR		ANGLE
			TYPE	RANGE	TYPE	RANGE	
E,E/	ABX	15-26	D	45-55	MAG-D		DST

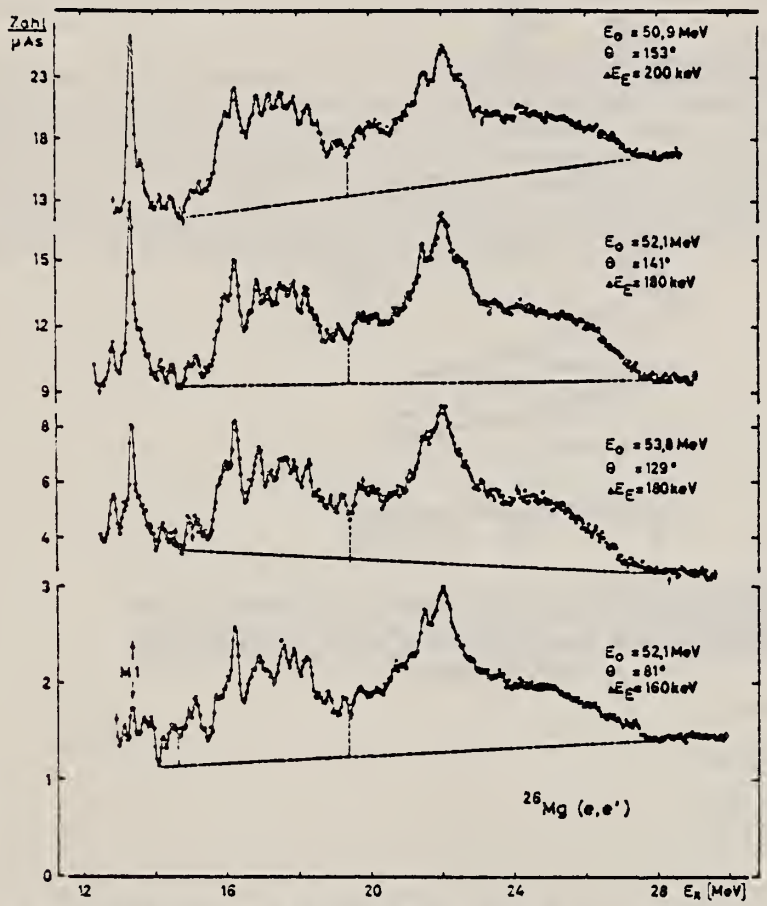

Fig. 3. Riesenresonanz von ^{26}Mg. Die von den Meßspektren bereits subtrahierten Anteile sind in Tabelle I zusammengestellt. Die gestrichelten Linien geben den zur Auswertung angenommenen Untergrund und die Integrationsgrenzen an. Alle Spektren sind auf gleiche elastische Fläche $A_E = 5{,}0 \cdot 10^3$ MeV/μAs normiert

[over]

Tabelle 3. *Ergebnisse an ^{26}Mg. Bei allen Werten ist $A_E = 5{,}0 \cdot 10^3$ MeV/μAs. Die Flächen A_I wurden jeweils in den Bereichen 14,5 bis 19,5 MeV („$E_x = 17$ MeV") und 19,5 bis 28,0 MeV („$E_x = 22$ MeV") integriert. Bezüglich der Strahlungskorrekturen siehe Unterschrift zu Tabelle 2*

E_0 [MeV]	Θ [Grad]	E_x [MeV]	q^2 [fm^{-2}]	A_I [MeV/μAs]	G [10^{-6}]*	$B(C1, q)$ [fm^2]
50,9	153	17	0,180	28,3	1,31	0,72
		22	0,155	45,8	2,51	1,05
52,1	141	17	0,180	13,9	1,38	0,54
		22	0,155	27,9	3,22	1,07
53,8	129	17	0,180	11,3	1,94	0,54
		22	0,155	18,2	3,63	0,91
52,1	81	17	0,087	3,2	3,55	0,65
		22	0,080	5,5	7,31	1,30

* $G = (d\sigma/d\Omega)_t (k_i^2/V_T)$.

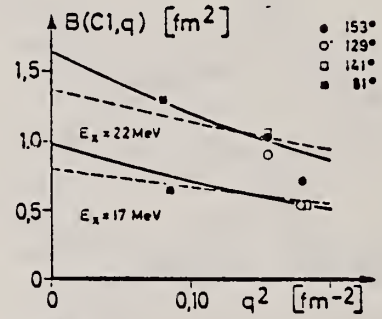

Fig 5

Fig. 4. Reduzierte Matrixelemente für ^{26}Mg, integriert in den Bereichen 14,5 bis 19,5 MeV („$E_x = 17$ MeV") und 19,5 bis 28,0 MeV („$E_x = 22$ MeV"). Die Kurven zeigen die Extrapolation zum Photonenpunkt für $R_{tr} = 1{,}3\ R_m$ (ausgezogen) bzw. $R_{tr} = R_m$ (gestrichelt)

REF. V.M. Khvastunov, N.G. Afanas'ev, V.D. Afanas'ev, E.V. Bondarenko, I.S. Gul'karov, G.A. Savitskii, and N.G. Shevchenko
Yad. Fiz. 12, 9 (1970)
Sov. J. Nucl. Phys. 12, 5 (1971)

ELEM. SYM.	A	Z
Mg	26	12

METHOD

REF. NO. 70 Kh 1 hmg

REACTION	RESULT	EXCITATION ENERGY	SOURCE		DETECTOR		ANGLE
			TYPE	RANGE	TYPE	RANGE	
E,E/	FMF	1	D	225	MAG-D		DST
		(1.81)					

1 = 1.81

Elastic and inelastic scattering of 225-MeV electrons by the isotopes Mg^{24} and Mg^{26} have been measured. Analysis of the data was carried out in the Born approximation. From analysis of the elastic scattering for a uniform-Gaussian charge-distribution model it is found that addition of two neutrons to the Mg^{24} nucleus leads to an increase in the parameter R by 0.03 ± 0.02 F and a decrease in g by 0.07 ± 0.04 F, which corresponds to a decrease in the mean-square radius of the Mg^{26} nucleus by (1.6 ± 1.3)% in comparison with Mg^{24}. Analysis of the inelastic scattering with excitation of the first 2⁺ level shows that the internal quadrupole moments of the nuclei Mg^{24} and Mg^{26} are identical within experimental error.

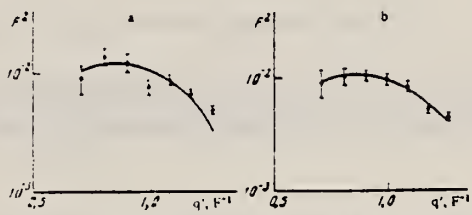

FIG. 3. Form factors for inelastic scattering with excitation of the first 2⁺ levels, 1.37 MeV in Mg^{24} (a) and 1.81 MeV in Mg^{26} (b). The solid lines are theoretical curves calculated with Eq. (3).

Characteristics of the first 2⁺ levels of the nuclei Mg^{24} and Mg^{26}

Nucleus	Level energy, MeV	$\beta_2(0^+, 2^+)$	$B(E2\uparrow)$, e^2F^4	τ, 10^{-13} sec	G	Q_0, F^2
Mg^{24}	1.37	0.31 ±0.02	412 ±43	20.5 ±2.1	20.1 ±2.1	64 ±4
Mg^{26}	1.81	0.25 ±0.01	349 ±30	6.04 ±0.52	15.2 ±1.3	59 ±3

REF. O. Titze, A. Goldmann, and E. Spamer
Phys. Letters 31B, 565 (1970)

ELEM. SYM.	A	Z
Mg	26	12

METHOD

REF. NO. 70 Ti 1 egf

REACTION	RESULT	EXCITATION ENERGY	SOURCE		DETECTOR		ANGLE
			TYPE	RANGE	TYPE	RANGE	
E,E/	SPC	12-28	D	50-54	MAG-D		DST
							953

CONST Q = .41 FM-1

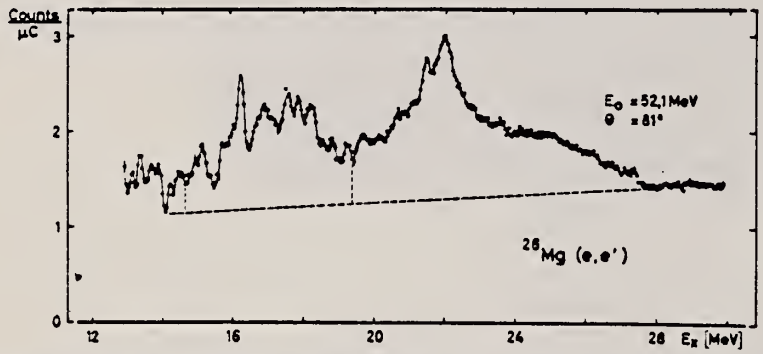

Fig. 1. Spectrum of electrons scattered inelastically from ^{26}Mg at primary energy 52.1 MeV and scattering angle 81°, after subtraction of the calculated [6] elastic radiation tail; E_x = excitation energy. The energy resolution at E_x = 20 MeV is about 130 keV. The dashed lines indicate the background subtraction and the separation of the two "bumps".

REF. C. P. Wu, F. W. K. Firk, and B. L. Berman
Phys. Letters 32B, 675 (1970)

ELEM. SYM.	A	Z
Mg	26	12

METHOD

REF. NO.	
70 Wu 2	egf

REACTION	RESULT	EXCITATION ENERGY	SOURCE		DETECTOR		ANGLE
			TYPE	RANGE	TYPE	RANGE	
G,XN	SPC	11-23	C	19,23	TOF-D		XX

Data taken but not given at $E_{\gamma max}$ = 21.4 and 27.5 MeV.

XX = NOT GIVEN

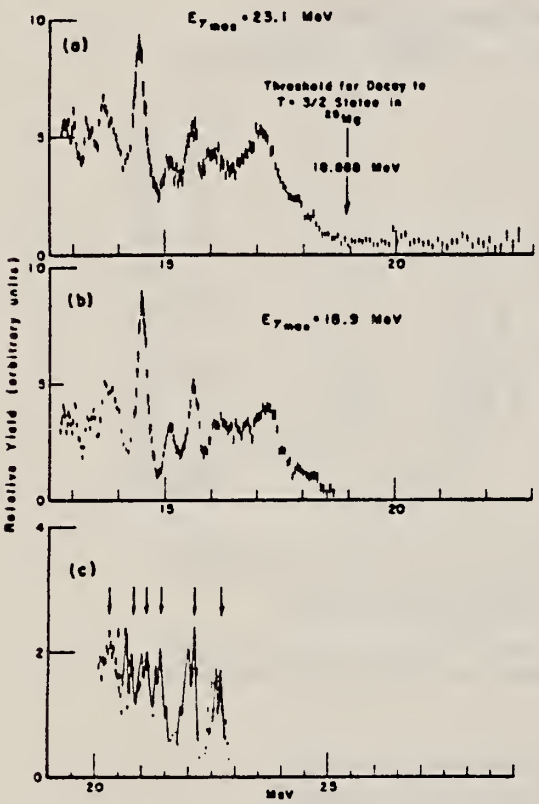

Fig. 2. a) The observed energy spectrum of photoneutrons from the reaction ^{26}Mg (γ, n) ^{25}Mg for a bremsstrahlung end-point energy $E_{\gamma max}$ = 23.1 MeV. The energy scale assumes groundstate transitions. b) The observed energy spectrum of photoneutrons from the reaction ^{26}Mg (γ, n) ^{25}Mg with $E_{\gamma max}$ = 18.9 MeV. The energy scale assumes ground-state transitions. c) The difference spectrum obtained from the two spectra with $E_{\gamma max}$ = 23.1 and 18.9 MeV. The energy scale assumes transitions to the first $T = \frac{1}{2}$ state in ^{25}Mg at an energy of 7.7926 MeV (in ^{25}Mg). Note the appearance of doublets for the strong transitions: these are attributed to transitions to the 7.7926 and 7.8729 MeV states in ^{25}Mg. The arrows point to the states seen in the work of ref. [1] and [5].

REF. R. J. Baglan, C. D. Bowman and B. L. Berman
Phys. Rev. C3, 672 (1971)

ELEM. SYM.	A	Z
Mg	26	12

METHOD

REF. NO. 71 Ba 2 hmg

REACTION	RESULT	EXCITATION ENERGY	SOURCE TYPE	SOURCE RANGE	DETECTOR TYPE	DETECTOR RANGE	ANGLE
G,N	ABX	11-14	C	11,14	TOF-D		DST
		(11.1-13.3)					

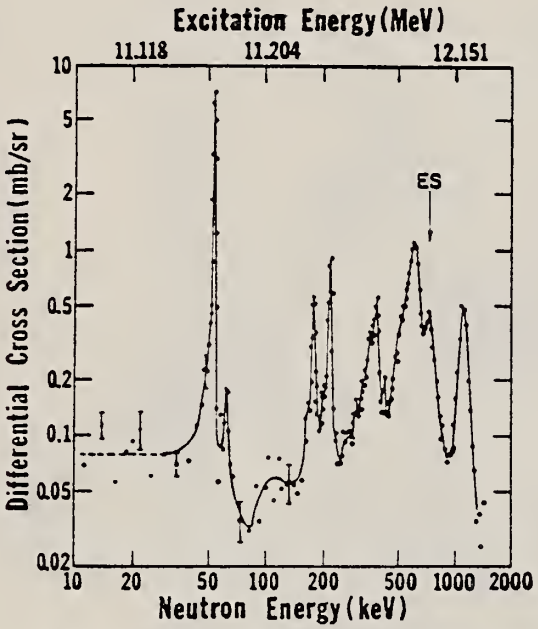

FIG. 17. The 135° differential threshold photoneutron cross section for ^{26}Mg (see caption to Fig. 4).

FIG. 4. The 135° differential threshold photoneutron cross section for ^{207}Pb at low energies versus the energy of the emitted neutron (lower scale) and the excitation energy (upper scale). The arrows indicate peaks which decay to excited states of the residual nucleus (ES), or peaks owing to contaminating isotopes in the photoneutron sample. The inset shows the ^{207}Pb(γ, n) cross section averaged with a square 40-keV wide smoothing function.

Also see:
R. J. Baglan et al.
Phys. Rev. C3, 2475
(1971)

[over]

TABLE VII. **Resonance parameters for ^{24,25,26}Mg, ^{19}F, and ^{31}P. For all resonances, the area under the peak in the** 135° differential cross section is multiplied by 4π to yield approximate values for $g_\gamma\Gamma_{\gamma 0}\Gamma_n/\Gamma \simeq g_\gamma\Gamma_{\gamma 0}$. For those resonances where J^π is known, the differential area is multiplied by the appropriate factor F from Table I to obtain $\Gamma_{\gamma 0}$. E_L is the laboratory neutron energy for the (γ,n) reaction and E_n is the corresponding laboratory neutron energy for a neutron-induced reaction. Column 5 labels the peak as a ground-state (GS) or excited-state (ES) transition as determined in this work alone.

Nucleus	E_L (keV)	E_{ex} (MeV)	$g_\gamma\Gamma_{\gamma 0}\Gamma_n/\Gamma$ (eV)	GS or ES	J^π	$\Gamma_{\gamma 0}$ (eV)	E_n (keV) (This work)
^{24}Mg	22	16.559	0.61		(1^-)	0.40	28
	55	16.596	2.4	GS	(1^-)	1.6	66
	110	16.656	4.0	GS	(1^-)	2.7	128
	312	16.871	10.7		(1^-)	7.1 [a]	354
	382	16.95					432
	717	17.30	19.5		(1^-)	13.0 [a]	804
	1210	17.83					1348
	1620	18.26					1799
	1955	18.61					2168
^{25}Mg	41.1	7.374	0.09	GS			46.8
	45.1	8.746	0.31	ES			
	74.9	7.410	0.36	GS	$\frac{3}{2}^-$ [b]	1.1	84.1 [b]
	208	8.920	0.29	ES			
	236	7.580	0.09	GS			261
	404	7.756	0.03				445
	439	7.793	0.05		$\frac{3}{2}^+$ [c]		484
	472	7.828	0.06				520
	515	7.873	0.46	GS	$\frac{3}{2}^+$ [c]		567
	601	7.964	0.18				661
	781	8.152	1.51	GS			857
	912	8.292	0.72				1003
	1236	9.999	2.4 [c]	ES	$\frac{3}{2}^+$ or $\frac{5}{2}^+$ [c]		
	1707	9.12					1869
	1764	9.18					1931
^{26}Mg	54.3	11.155	2.6	GS	$1^-(1^+,2^-)$	1.75	62.3
	63.2	11.164	0.05			0.034	72.2
	181	11.289	1.0	GS	$1^-(1^+,2^+)$	0.68	202
	222	11.333	1.9	GS	$1^-(1^+,2^+)$	1.3	248
	391	11.511	5.1	GS	$1^-(1^+,2^+)$	3.5	433
	621	11.753	32.5	GS	$1^-(1^+,2^-)$	22.2	684
	738		15.0 [d]	ES		5.1	
	1122	12.279	14.7	GS	$1^-(1^+,2^+)$	10.0	1232
^{19}F	100	10.542	1.8	GS			118
^{31}P	109	12.429	0.36				121
	280	12.609	0.60				307
	398	12.732	0.59				434
	678	13.026	0.90				737
	939	13.297	4.4				1013

[a] These values for $\Gamma_{\gamma 0}$, when increased by approximately a factor of 2 in order to include the relatively high cross sections in the valleys, agree very well with corresponding values from Ref. 8 (see Ref. 4).

[b] This resonance was seen at E_n = 83 and 84 keV in Refs. 24 and 25, respectively.

[c] Analogs of states in ^{25}Na (see text). The value for $g_\gamma\Gamma_{\gamma 0}\Gamma_n/\Gamma$ given in Ref. 26 was not corrected with the multiplicative factor in Table II.

[d] Assuming a first-excited-state transition.

[4] R.L. Van Hemert, C.D. Bowman, R.J. Baglan, and B.L. Berman (to be published); R.L. Van Hemert, University of California Lawrence Radiation Laboratory Report No. UCRL-50442, 1968 (unpublished).

[8] S.C. Fultz, M.A. Kelly, J.T. Caldwell, R.R. Harvey, and B.L. Berman, Bull. Am. Phys. Soc. 14, 103 (1969), and private communication.

[24] H.W. Newson, R.C. Block, P.F. Nichols, A. Taylor, A.K. Furr, and E. Merzbacher, Ann. Phys. (N.Y.) 8, 211 (1959).

[25] D.J. Hughes and R.B. Schwartz, Neutron Cross Sections (U.S. Government Printing Office, Washington, D.C., 1966), 2nd ed., 2nd Suppl., Vol. IIc.

REF. S.C. Fultz, R.A. Alvarez, B.L. Berman, M.A. Kelly, D.R. Lasher, T.W. Phillips, J. McElhinney
Phys. Rev. C4, 149 (1971)

ELEM. SYM.	A	Z
Mg	26	12

METHOD

REF. NO.	
71 Fu 2	hmg

REACTION	RESULT	EXCITATION ENERGY	SOURCE		DETECTOR		ANGLE
			TYPE	RANGE	TYPE	RANGE	
G,N 344+	ABX	10-29	D	10-29	BF3-I		4PI
G,2N 345	ABX	18-29	D	18-29	BF3-I		4PI

32 LEVEL FIT
344+

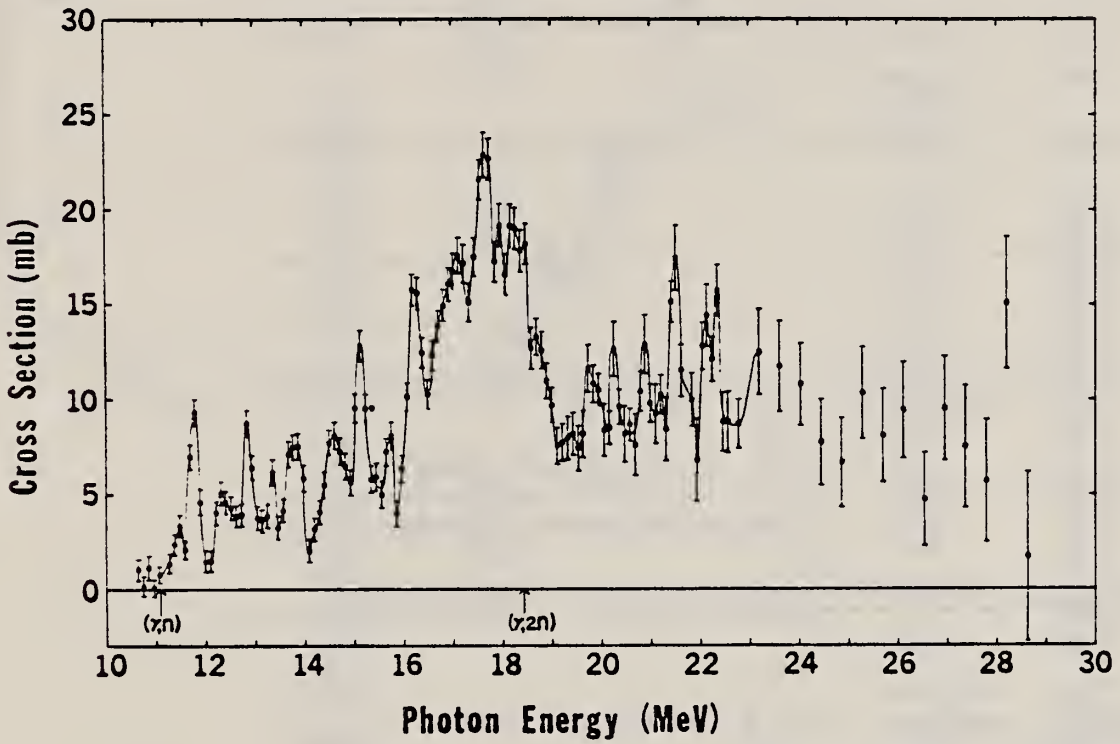

FIG. 4. Single-photoneutron cross section $\sigma(\gamma,n)+(\gamma,pn))$ for ^{26}Mg.

TABLE II. Integrated cross sections of magnesium isotopes.

Isotope	$\int_{E_{thr}}^{28}\sigma(\gamma,n_{tot})dE$ (MeV mb)	$\int_{E_{thr}}^{28}\sigma(\gamma,2n)dE$ (MeV mb)
^{24}Mg	30	...
^{26}Mg	226	68
Natural magnesium	76	...

[over]

TABLE V. Analytical and experimental resonance energies for ^{26}Mg (MeV).

Resonance number	Analytical energy	Experimental energies: Present data (γ, n_{tot})	Present data ($\gamma, 2n$)	Livermore (Ref. 15) (γ, n_0)	Yale (Ref. 17) (γ, n_0)	Darmstadt (Ref. 13) (e, e')
1	11.17	11.15		11.155		
				11.164		
				11.289		
				11.333		
2	11.46	11.47		11.511		
3	11.75	11.75		11.753		
4	12.35	12.30		12.279		
5	12.80	12.80			12.81	
					12.90	
					13.04	13.12
6	13.30	13.35			13.33	13.35
					13.44	
7	13.75	13.75			13.67	13.70
		13.83				13.89
						14.22
8	14.60	14.60			14.49	14.50
						14.91
9	15.15	15.15			15.10	15.12
10	15.70	15.70			15.59	15.73
11	16.25	16.20				16.25
12	16.70	16.70				16.90
13	17.05	17.15				17.16
14	17.65	17.65				17.52
15	17.95	17.95				17.83
16	18.20	18.20				18.19
17	18.45	18.45				18.51
18	18.75	18.75	18.80			18.79
19	19.30	19.30	19.32			19.21
20	19.75	19.75	19.63			19.66
21	20.25	20.25	20.05		20.37	20.12
22	20.82	20.87	20.68		20.77	20.59
23	21.20	21.30	21.30		21.16	21.09
24	21.50	21.50			21.37	21.42
25	21.85		21.93			21.93
26	22.15	22.15			22.13	
27	22.30		22.25			22.74
28	23.50	23.00				23.15
			24.9			23.60
29	25.35	25.25				
30	26.10					
31	27.00	27.00				27.32
32	28.20	28.20				

[13] O. Titze, A. Goldmann, and E. Spamer, Phys. Letters 31B, 565 (1970).

[15] R. J. Baglan, C.D. Bowman, and B.L. Berman, Phys. Rev. C3, 672 (1971).

[17] C.-P. Wu, F.W.K. Firk, and B.L. Berman, Phys. Letters 32B, 675 (1970).

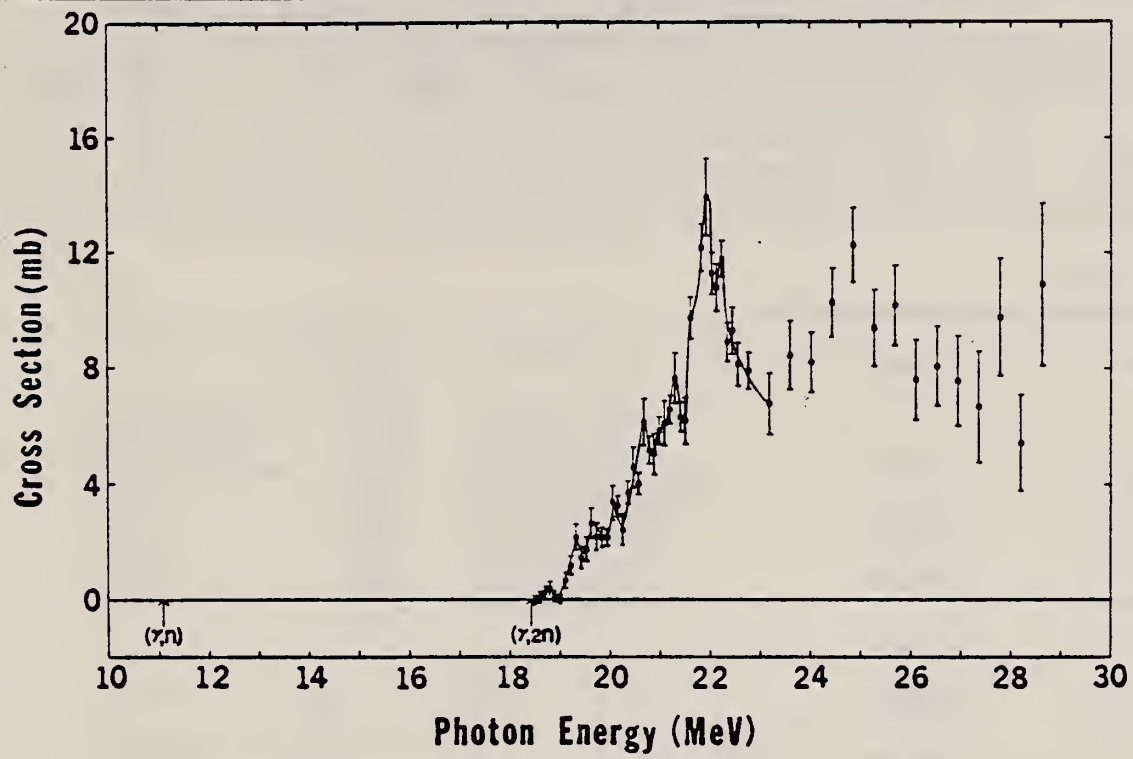

FIG. 5. Double-photoneutron cross section $\sigma(\gamma, 2n)$ for ^{26}Mg.

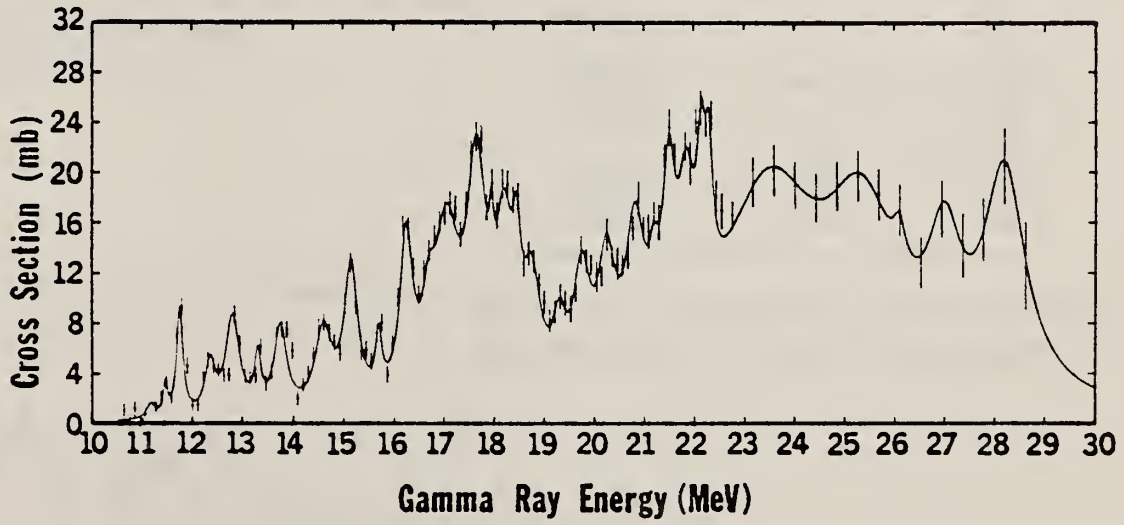

FIG. 7. Total photoneutron cross section $\sigma(\gamma,n)+(\gamma,pn)+(\gamma,2n))$ for ^{26}Mg. The solid line is the sum of 32 Lorentz lines with parameters listed in Table VI.

REF.

B. S. Ishkhanov, I.M. Kapitonov, E. V. Lazutin, I. M. Piskarev, and V. G. Shevchenko
Nucl. Phys. A186, 438 (1972)

ELEM. SYM.	A	Z
Mg	26	12

METHOD

REF. NO. 72 Is 1 egf

REACTION	RESULT	EXCITATION ENERGY	SOURCE		DETECTOR		ANGLE
			TYPE	RANGE	TYPE	RANGE	
G,XN	ABX	11-30	C	11-30	BF3-I		4PI

549

TABLE 3

The position of the structural features (MeV) of the giant resonance for ^{26}Mg

Ref. [17])	Ref. [12])	The present work
	11.11	
	11.53	11.40 ± 0.05
	11.84	
	12.37	12.35 ± 0.05
13.1	13.00	13.15 ± 0.05
13.3	13.45	
13.7		13.60 ± 0.05
13.9	13.84	
14.2		
14.5	14.67	14.45 ± 0.06
14.9		
15.1	15.31	15.25 ± 0.07
15.8		15.85 ± 0.07
16.2	16.33	
16.9		16.80 ± 0.08
17.6		17.50 ± 0.08
17.9	17.80	
18.2		
18.8		18.75 ± 0.10
19.2		
19.6		19.40 ± 0.10
20.1	20.20	20.10 ± 0.10
20.7		20.85 ± 0.12
21.1		
21.4		
22.0	22.0	22.25 ± 0.15
23.6	23.6	
24.5	24.8	24.5 ± 0.2

[12] S. C. Fultz et al., Phys. Rev. C4 (1971) 149
[17] O. Titze et al., Phys. Lett. 31B (1970) 565

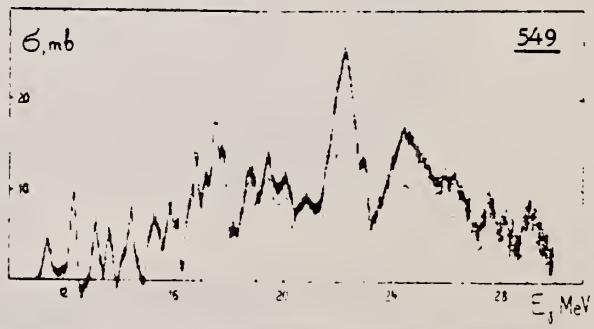

Fig. 2. Cross section for ^{26}Mg(γ, xn). The dashed line shows the expected behaviour of the (γ, n)+(γ, 2n)+(γ, np) reaction cross section above the (γ, 2n) reaction threshold.

REF.

E.W. Lees, A. Johnston, S.W. Brain, C.S. Curran, W.A. Gillespie, and R.P. Singhal
J. Phys.A: Math., Nucl.Gen., 6, L116 (1973)

C.CM. SYM.		
Mg	26	12

METHOD

REF. NO.	
73 Le 6	egf

REACTION	RESULT	EXCITATION ENERGY	SOURCE		DETECTOR		ANGLE
			TYPE	RANGE	TYPE	RANGE	
E,E/	LFT	2	D	0.4*1.2	MAG-D		UKN

2=1.809MeV,*=FM-1

Table 1.

(*a*) Method	B(E2, ↑) (e^2 fm^4)	Reference
Resonance fluorescence	305 ± 131	Rasmussen *et al* (1961)
Coulomb excitation	370 ± 96	Andreev *et al* (1961)
Resonance fluorescence†	570 ± 231	Booth *et al* (1964)
DSA (α, α′γ)	370^{+37}_{-34}	Robinson and Bent (1968)
DSA (p,p′γ)	397 ± 75	Hausser *et al* (1968)
DSA (p,p′γ)	703^{+234}_{-141}	de Kock *et al* (1970)
Recoil distance	305 ± 131	McDonald *et al* (1971)
DSA (α,pγ)	346 ± 57‡	Durell *et al* (1972)
(e,e′)	299 ± 29§	Present work

(*b*) Method	Q_0 (fm^2)	B(E2, ↑) (e^2 fm^4)	Reference
(α,α′) 104 MeV	(−)44 ± 3	193 ± 26	Rebel *et al* (1972)
Reorientation	+ 56 ± 14	311 ± 156	Schwalm et al (1972)
	(+42 ± 14)	(175 ± 117)	

† A natural magnesium target used in this experiment.
‡ ±25% additional uncertainty in slowing down theory.
§ Corrected for model dependence (see text).

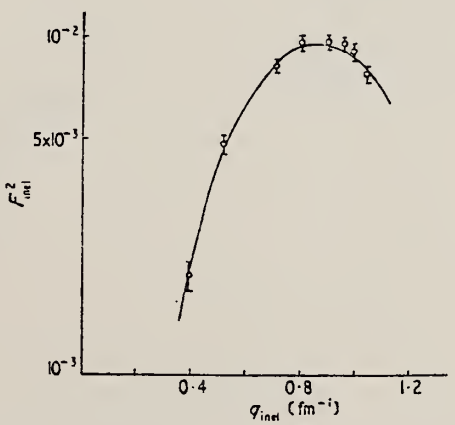

Figure 1. Inelastic form factor for the 1·809 MeV, 2⁺ level in ^{26}Mg. The full curve is the best-fit DWBA form factor.

REF.

V.V. Varlamov, B.S. Ishkhanov, I.M. Kapitonov, Zh.L. Kocharova, I.M. Piskarev, and O.P. Shevchenko
ZhETF Pis. Red. 18, 170 (1973)
JETP Letters 18, 99 (1974)

Mg	26	12

METHOD

REF. NO.	
73 Va 7	hmg

REACTION	RESULT	EXCITATION ENERGY	SOURCE		DETECTOR		ANGLE
			TYPE	RANGE	TYPE	RANGE	
G,P	SPC	14- 30	C	32	SCD-D		UKN

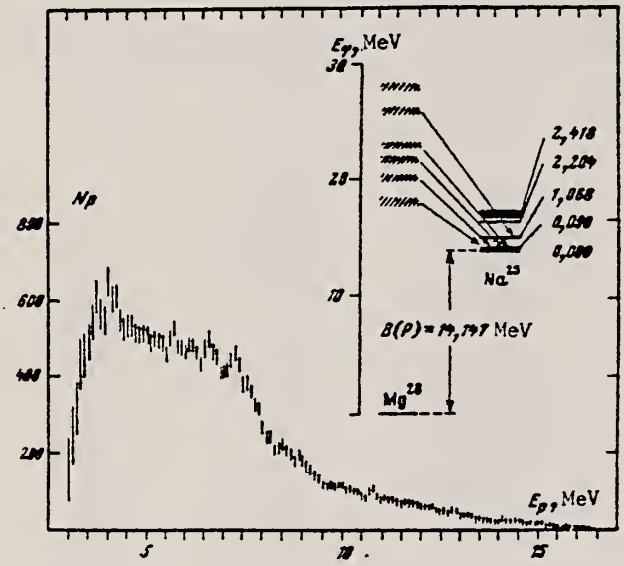

REF.

D.W. Anderson, R.F. Petry, and H.J. Fischbeck
Phys. Rev. C9, 1919 (1974)

Mg	26	12

METHOD

REF. NO. 74 An 1 hmg

REACTION	RESULT	EXCITATION ENERGY	SOURCE		DETECTOR		ANGLE
			TYPE	RANGE	TYPE	RANGE	
G,P	ABX	15-60	C	15- 60	ACT-I		4PI

950

The cross section for the reaction $^{26}Mg(\gamma,p)^{25}Na$ has been measured from 15 to 60 MeV using bremsstrahlung activation methods to obtain the yield curve. The peak cross section of 15.7 mb occurs at 22.6 MeV. Prominent secondary maxima occur at 29.6, 49.0, and 57.9 MeV. The cross section integrated to 28 MeV is 80 ± 9 MeV mb. The cross section integrated to 60 MeV is 161 ± 18 MeV mb. A discussion of our results and comparison with photoneutron data for ^{26}Mg from other sources is given.

[NUCLEAR REACTIONS $^{26}Mg(\gamma,p)$, E=15–60 MeV; measured bremsstrahlung yield; deduced $\sigma(E)$.]

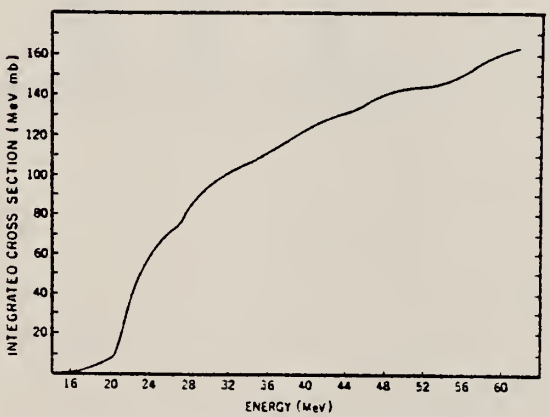

FIG. 5. The integrated cross section for the $^{26}Mg(\gamma,p)^{25}Na$ reaction is displayed as a function of energy.

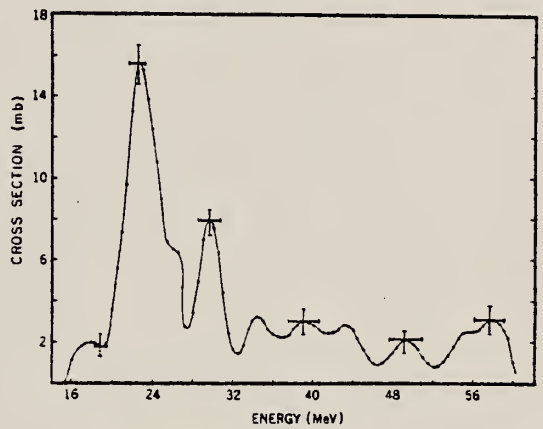

FIG. 3. The cross section for the $^{26}Mg(\gamma,p)^{25}Na$ reaction is shown.

REF. E.W. Lees, A. Johnston, S.W. Brain, C.S. Curran, W.A. Gillespie and R.P. Singhal
J.Phys.:Math.Nucl. Gen. 7, 936 (1974)

ELEM. SYM.	A	Z
Mg	26	12

METHOD

REF. NO. 74 Le 4 egf

REACTION	RESULT	EXCITATION ENERGY	SOURCE TYPE	SOURCE RANGE	DETECTOR TYPE	DETECTOR RANGE	ANGLE
E,E/	LFT	1- 11	D	56-111	MAG-D		DST

$F^2(q)$ plots given

26 LEVELS

Table 2. Electron energies and angles employed in the present experiment.

Run	E_i (MeV)	θ (deg)	q_{EL} (fm^{-1})
1	95·74	120	0·84
2	110·71	120	0·97
3	82·75	120	0·73
4	85·09	90	0·61
5	110·45	140	1·05
6	56·89	120	0·50
7	91·28	120	0·80
8	84·16	140	0·80
9	81·36	153	0·80

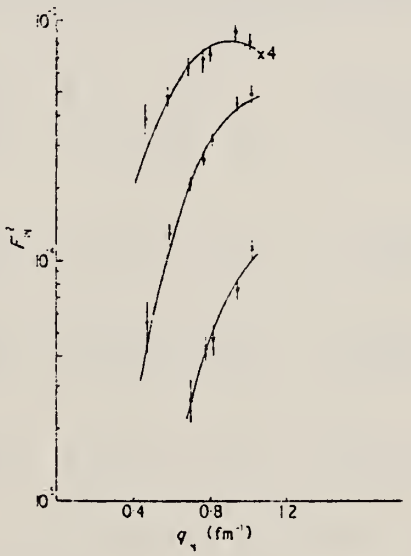

Figure 7. Inelastic form factors for the 2^+ level at 8·892 MeV (○), the 3^- level at 6·876 MeV (●) and the 4^+ level at 5·720 MeV (×). The full curves are the corresponding best-fit DWBA form factors.

(over)

Table 7. Results for the analysis of the present data using the Tassie model and the generalized Helm model

		Tassie model				Generalized Helm model				
E_x (MeV)	J^π	c_{tr} (fm)	t_{tr} (fm)	R_{tr} (fm)	$B(iL,\uparrow)$† (e^2 fm^{2L})	β	γ^0	R (fm)	R_{tr} (fm)	$B(iL,\uparrow)$† (e^2 fm^{2L})
1·809	2^+	2·76	2·16	4·13 ± 0·12	275 ± 20	1·937		2·90 ± 0·09	4·04 ± 0·06	266 ± 16
2·945	2^+	1·92	2·61	4·27	7·4	0·346		2·71 ± 0·34	3·90 ± 0·23	6·5 ± 1·4
3·579	0^+					$4·46 \times 10^{-2}$		5·18 ± 0·35	6·17 ± 0·30	17·9 ± 3·9§
4·337	2^+	2·47	2·26	4·08	2·7	0·212		2·75 ± 0·56	3·93 ± 0·39	2·6 ± 1·0
4·875	4^+	1·83	2·31‡	5·59	$3·4 \times 10^4$	1·11		3·47 ± 0·60	4·94 ± 0·42	$(2·6 \pm 0·7) \times 10^4$
4·979	0^+					$3·31 \times 10^{-2}$		5·32 ± 0·31	6·29 ± 0·27	11·1 ± 1·3§
5·294	2^+	1·82	2·20	3·68	3·6	0·404	$0·156^{+0·130}_{0·136}$	2·13 ± 0·38	3·52 ± 0·23	3·3 ± 0·6
5·449	4^+	2·75‡	2·39‡	5·94‡	$4·6 \times 10^3$	0·248		3·91‡	5·26‡	$3·4 \times 10^3$
5·720	4^+	2·75	2·39	5·94	$1·7 \times 10^4$	0·480		3·91 ± 0·66	5·26 ± 0·49	$(1·3 \pm 0·5) \times 10^4$
6·216	0^+					$2·14 \times 10^{-2}$		5·25‡	6·23‡	$4·4^{+3·1}_{-1·3}$§
6·876	3^-	2·27	2·47	5·07	750	0·677		3·34 ± 0·33	4·62 ± 0·24	638 ± 101
7·082	2^+					0·240	$0·177^{+0·143}_{0·177}$	2·79 ± 0·30	3·96 ± 0·21	3·5 ± 0·6
7·364	2^+					0·704	0·409 ± 0·081	2·12 ± 0·15	3·52 ± 0·09	10·0 ± 0·6
7·691	3^-	2·27‡	2·47‡	5·07‡	531	0·577		$3·32^{+0·69}_{-1·00}$	$4·60^{+0·50}_{-0·72}$	446 ± 223
7·830	3^-					0·813	0·617 ± 0·200	3·06 ± 0·23	4·42 ± 0·16	546 ± 59
8·181	3^-	3·06	2·31‡	5·11	1050	0·643		3·63 ± 0·26	4·83 ± 0·20	947 ± 154
8·526	2^+					0·195	0·508 ± 0·068	2·13‡	‖	$0·78^{+0·33}_{-0·30}$
8·892	2^+	1·86	2·63	4·27	5·4	0·293		2·74 ± 0·35	3·93 ± 0·24	4·8 ± 1·0
9·287	2^+	2·45	2·31‡	4·13	1·6	0·159		2·79 ± 0·63	3·96 ± 0·44	1·5 ± 0·5
9·860	2^+					$9·82 \times 10^{-2}$	0·293 ± 0·135	3·40 ± 1·59	‖	$1·3^{+1·4}_{-0·9}$
10·199	1^+	3·85	2·40	3·29	$1·14 \times 10^{-2}$	0·619 ± 0·168¶	0·623 ± 0·198¶		3·32 ± 0·20	$(1·3 \pm 0·9) \times 10^{-2}$
10·330	3^-					0·350	$0·264^{+0·315}_{-0·264}$	3·53 ± 0·88	4·76 ± 0·65	238 ± 115
10·491	2^+					0·304	0·258 ± 0·120	$1·98^{+0·92}_{-1·40}$	$3·44^{+0·32}_{-0·79}$	1·4 ± 0·6
10·65	1^+	3·85‡	2·40‡	3·29‡	$1·3 \times 10^{-2}$	0·632¶	0·669¶		3·34	$1·5 \times 10^{-2}$
10·680	4^+	2·75‡	2·39‡	5·94‡	$9·7 \times 10^3$	0·368		3·91‡	$5·26^{+0·82}_{-2·72}$	$(7·4^{+3·7}_{-6·7}) \times 10^3$
10·838	2^+	2·38	2·31‡	4·09	4·5	0·278		2·72 ± 0·62	3·91 ± 0·42	4·3 ± 1·2
10·990	2^+	2·13	2·31‡	3·97	3·7	0·295		2·51 ± 0·50	3·76 ± 0·33	3·4 ± 0·8

† $B(iL,\uparrow)$ (I = E or M) is the ground state reduced transition probability for excitation to the level of spin L.
‡ Denotes that the radius parameter for this level was fixed.
§ The value of the square of the matrix element is quoted for this level in e^2 fm^4.
‖ R_{tr} not evaluated since this level has a strong transverse component.
¶ Values for γ^+ and γ^- for magnetic states are given under the columns β and γ^0 respectively.

REF.

V.V. Varlamov, B.S. Ishkhanov, I.M. Kapitonov, I.M. Piskarev, V.G. Shevchenko, and O.P. Shevchenko
Nucl. Phys. A222, 548 (1974)

ELEM. SYM.	A	Z
Mg	26	12

METHOD

REF. NO.: 74 Va 2 egf

REACTION	RESULT	EXCITATION ENERGY	SOURCE		DETECTOR		ANGLE
			TYPE	RANGE	TYPE	RANGE	
G,XP	ABX	15- 29	C	8- 29	ION-I		4PI

951

$$\int_{15}^{29} \sigma_{xp} = 140 \pm 20 \text{ MeV-mb}$$

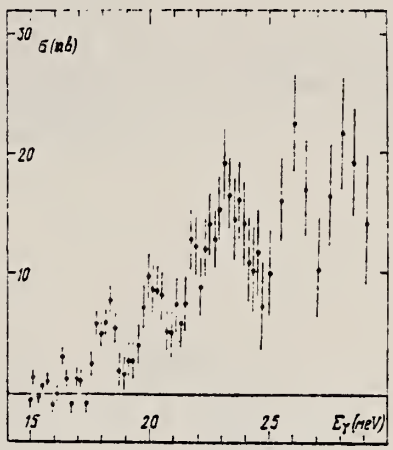

Fig. 2. The $^{26}Mg(\gamma, xp)$ reaction effective cross section.

REF. H. Wolf, R. Stock, U.E.P. Berg, and K. Wienhard
Nucl. Phys. A234, 365 (1974)

EL EM. SYM.	A	Z
Mg	26	12

METHOD

REF. NO. 74 Wo 5 egf

REACTION	RESULT	EXCITATION ENERGY	SOURCE		DETECTOR		ANGLE
			TYPE	RANGE	TYPE	RANGE	
G,P	ABY	16- 23	C	24, 31	TEL-D		DST
G,A	ABY	16- 23	C	24, 31	SCD-D		90

Assumes all ground-state transitions to obtain a cross section. The total ground-state cross sections used to obtain the integrals given in Table 2 were obtained by assuming that the angular distribution measured for presumed ground-state protons produced by 22.1 MeV photons held for all photon energies below 23 MeV.

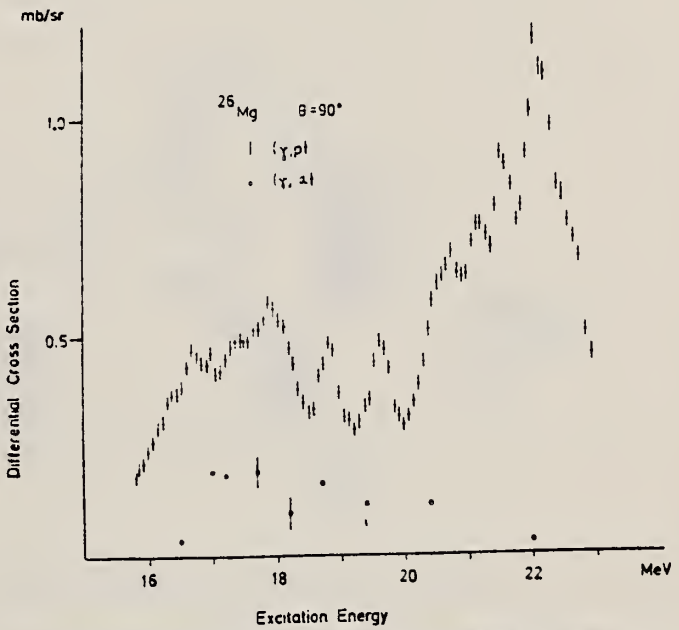

Fig. 2. The 90° ^{26}Mg(γ, p) and ^{26}Mg(γ, α) differential cross sections.

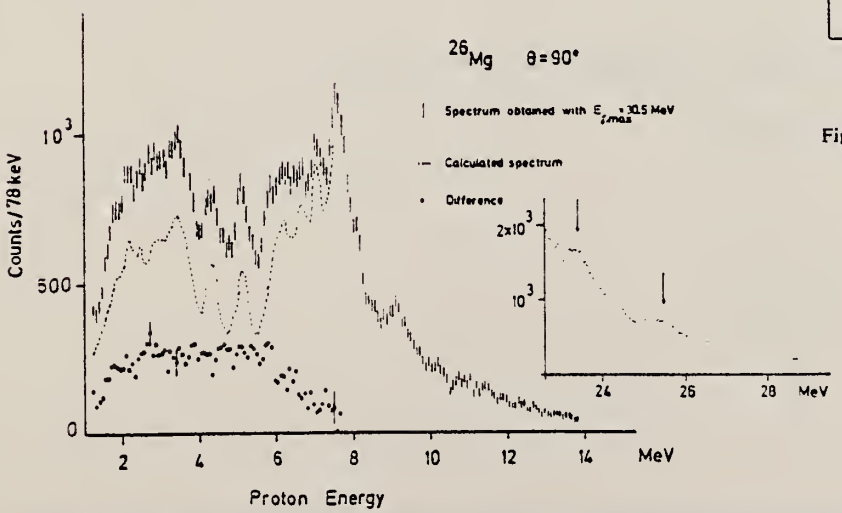

Fig. 3. The ^{26}Mg(γ, p) proton spectrum obtained at 30.5 MeV bremsstrahlung endpoint energy, showing a large excess of low-energy protons.

(over)

TABLE 2

Integrated and "bremsstrahlung-weighted" integrated proton and neutron cross sections

Excitation energy region of integration (MeV)	$\int \sigma(E)dE$ (MeV · mb)			$\int (\sigma(E)/E)dE$ (mb)		
	(γ, p)	(γ, n_{tot})	$(\gamma, p)+(\gamma, n_{tot})$	(γ, p)	(γ, n_{tot})	$(\gamma, p)+(\gamma, n_{tot})$
16.0–18.5	9.4	41.67	51.1	0.56	2.4	2.96
16.0–20.0	14.3	59.16	73.44	0.81	3.31	4.12
16.0–23.0	32.8	112.4	142.5	1.66	5.86	7.52

REF. H. Wolf, U. Berg, and K. Wienhard
Phys. Lett. 50B, 244 (1974)

ELEM. SYM.	A	Z
Mg	26	12

METHOD

REF. NO. 74 Wo 7 egf

REACTION	RESULT	EXCITATION ENERGY	SOURCE		DETECTOR		ANGLE
			TYPE	RANGE	TYPE	RANGE	
G,NG	ABI	19- 23	C	30	SCD-D		90

The population of $T = 3/2$ states in ^{25}Mg from the giant dipole resonance in ^{26}Mg was observed by the ^{26}Mg $(\gamma, n\gamma')$ reaction. The previously reported result, that neutron decay between 18.9 MeV and 23.0 MeV proceeds mainly to these states, could not be confirmed. Therefore the isospin splitting of the giant resonance of ^{26}Mg remains questionable.

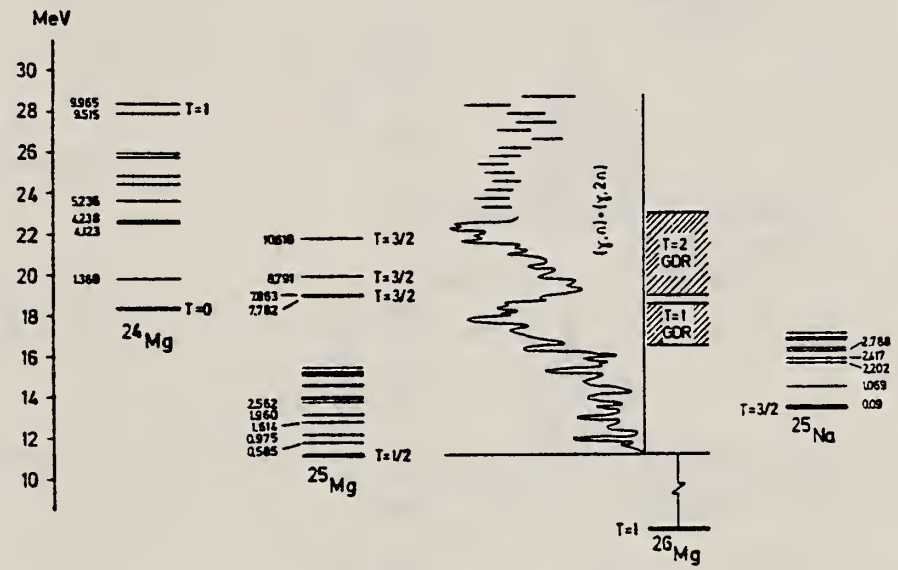

Fig. 1. Energy levels of residual nuclei from the ^{26}Mg $(\gamma, x\gamma')$ reaction. The $(\gamma, n) + (\gamma, 2n)$ curve and data points are from ref. [5].

[5] S.C. Fultz et al., Phys. Rev. C4 (1971) 149.

REF. E. Kuhlmann, E. Ventura, J. R. Calarco, D. G. Mavis, S. S. Hanna
Phys. Rev. C11, 1525 (1975)

ELEM. SYM.	A	Z
Mg	26	12

METHOD

REF. NO. 75 Ku 4 hmg

REACTION	RESULT	EXCITATION ENERGY	SOURCE TYPE	SOURCE RANGE	DETECTOR TYPE	DETECTOR RANGE	ANGLE
A,G	ABX	14- 24	D	5- 16	NAI-D		DST

SEE ANALYSIS 79KU5

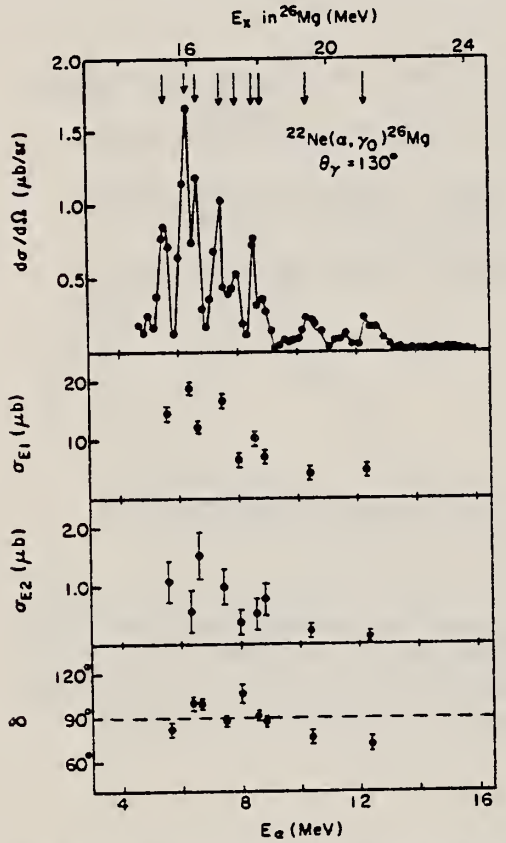

FIG. 6. Top: excitation function for the reaction ^{22}Ne(α, γ$_0$) at θ = 130°. Middle: the extracted $E1$ and $E2$ total cross sections for the (α, γ$_0$) reaction. Bottom: the $E2$ phase relative to the $E1$ phase.

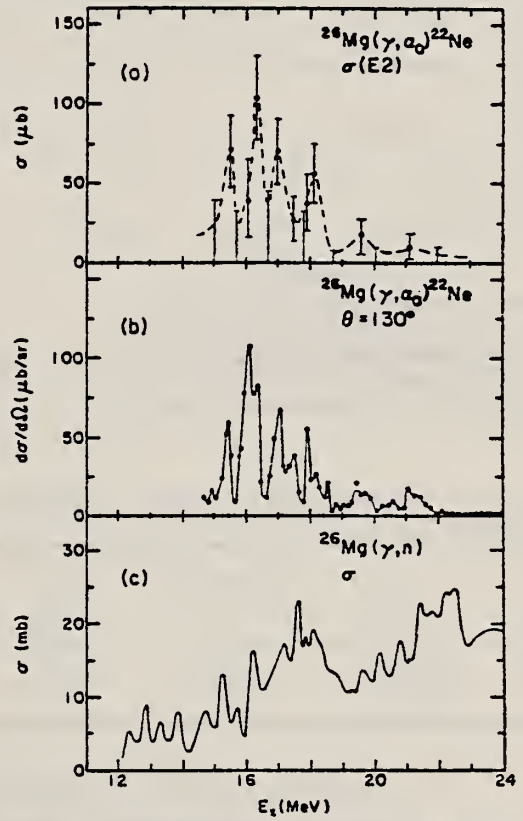

FIG. 7. (a) the extracted $E2$ cross section converted by detailed balance to the total $E2$ cross section for the reaction ^{26}Mg(γ, α$_0$)^{22}Ne. (b) the excitation function ($E1 + E2$) at θ = 130° for the reaction ^{26}Mg(γ, α$_0$)^{22}Ne. (c) the cross section for ^{26}Mg(γ, n) obtained with monoenergetic photons (Ref. 15).

(over)

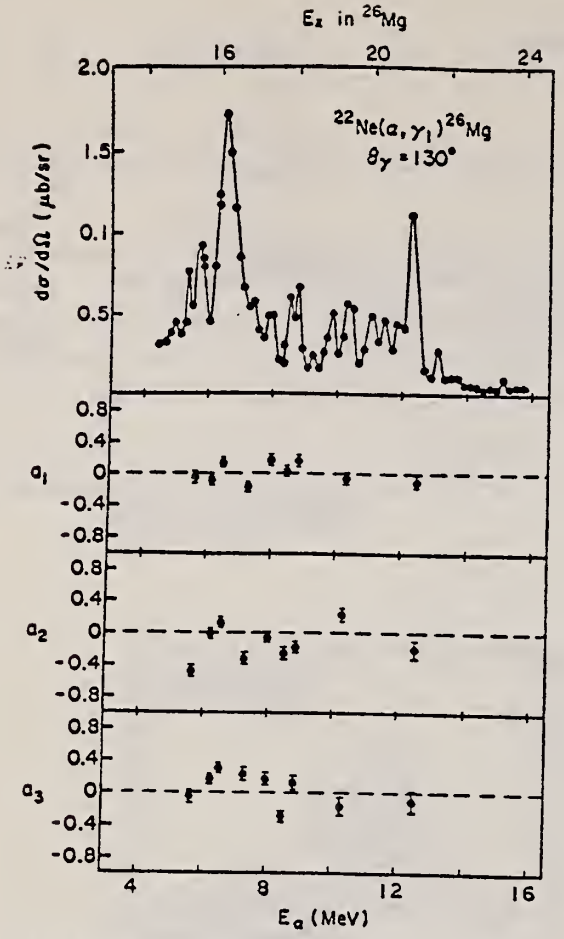

FIG. 8. The excitation function at $\theta = 130°$ and the coefficients a_1, a_2, and a_3 from a Legendre polynomial fit to the angular distributions for the reaction ^{22}Ne$(\alpha, \gamma_1)^{26}$Mg* (1.81 MeV). In this case the a_2 fluctuates about a value of −0.12 in contrast to the behavior for ^{20}Ne(α, γ_1).

TABLE I. The averaged absolute cross sections $\bar{\sigma}(\alpha, \gamma_0)$ and $\bar{\sigma}(\alpha, \gamma_1)$ for the reactions ^{20}Ne$(\alpha, \gamma)^{24}$Mg and ^{22}Ne$(\alpha, \gamma)^{26}$Mg.

	^{20}Ne$(\alpha, \gamma)^{24}$Mg		^{22}Ne$(\alpha, \gamma)^{26}$Mg	
ΔE_x (MeV)	$\bar{\sigma}(\alpha, \gamma_0)$ [a] (μb)	$\bar{\sigma}(\alpha, \gamma_1)$ [b] (μb)	$\bar{\sigma}(\alpha, \gamma_0)$ [a] (μb)	$\bar{\sigma}(\alpha, \gamma_1)$ [b] (μb)
11.4–14.4	3.2	3.9	...	...
14.4–17.8	3.1	4.8	9.2	8.6
17.8–20.2	3.6	9.6	3.0	4.5
20.2–23.8	0.6	1.8	0.9	2.8
23.8–26.0	0.4	0.6	...	...

[a] Angular distribution assumed to be of the form $W(\theta) = \sin^2\theta$.
[b] Angular distribution assumed to be isotropic.

14 R.C. Bearse et al., Nucl. Phys. A116, 682 (1968).
15 S.C. Fultz et al., Phys. Rev. C4, 149 (1971).
19 O. Titze et al., Phys. Lett. 24B, 169 (1967); A. Goldmann, Z. Phys. 234, 144 (1970).
27 O. Titze et al., Phys. Lett. 31B, 565 (1970).

TABLE II. Summary of $E2$ strengths in ^{24,26}Mg(γ, α_0) (see text) given in percent of the $E2$ sum rule [Eq. (5)].

Nucleus	ΔE (MeV)	$\int \sigma(E2)/E^2 dE$ (%)	ΔE (MeV)	$\int \sigma^{CN}_{tot}(E2)/E^2 dE$ (%)
^{24}Mg	12.0–22.5	11.8 ± 1.0	0–22.5	120 ± 30
^{26}Mg	15.0–21.4	6.0 ± 2.0	0–21.4	290 ± 80

TABLE III. A comparison of the integrated $E1$ strengths found in various reactions in the GDR's of ^{24}Mg and ^{26}Mg. The strengths are given in percent of the $E1$ sum rule [Eq. (4)].

	(γ, α)		(γ, p_0) [a]		(γ, n) [b]		(e, e') [c]	
Nucleus	ΔE (MeV)	$\int \sigma(E1)dE$ (%)	ΔE (MeV)	$\int \sigma(E1)dE$ (%)	ΔE (MeV)	$\int \sigma(E1)dE$ (%)	ΔE (MeV)	$\int \sigma(E1)dE$ (%)
^{24}Mg	14.6–20.6	0.33	15.5–23.0	3.3	16.5–28.0	14.0	16.0–22.0	30.0
^{26}Mg	14.8–21.0	0.70	...	...	11.0–28.0	58.0	14.5–28.0	48.0

[a] Reference 14.
[b] Reference 15.
[c] References 19 and 27.

REF.

V.V. Varlamov, F.A. Zhivopistsev, B.S. Ishkhanov, A.V. Lukashev
Izv. Akad. Nauk SSSR. Ser. Fiz. 39, 131 (1975)
Bull. Acad. Sci. USSR Phys. Ser. 39, 113 (1975)

ELEM. SYM.	A	Z
Mg	26	12

METHOD

REF. NO.: 75 Va 3 hmg

REACTION	RESULT	EXCITATION ENERGY	SOURCE		DETECTOR		ANGLE
			TYPE	RANGE	TYPE	RANGE	
G,P	SPC	17- 32	C	32	SCD-D		UKN

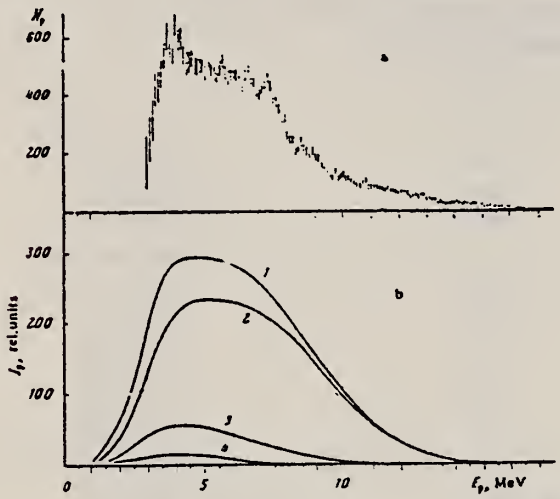

Fig. 1. Comparison of the results of the calculation with experimental data: a) experimental photoproton spectrum; b) calculated spectra of the protons escaping at various stages of the process involving linkages with more complex states: 1) (2p-2h) + (3p-3h) + (4p-4h); 2) (2p-2h); 3) (3p-3h); 4) (4p-4h).

REF.		ELEM. SYM.	A	Z
	V.V. Varlamov, B.S. Ishkhanov, I.M. Kapitonov, Zh.L. Kocharova, V.I. Shvedunov, and O.P. Shevchenko Izv. Akad. Nauk SSSR, Ser. Fiz. 39, 1744 (1975) Bull. Acad. Sci. USSR Phys. Ser. 39, 150 (1975)	Mg	26	12
METHOD		REF. NO.		
		75 Va 4		hmg

REACTION	RESULT	EXCITATION ENERGY	SOURCE		DETECTOR		ANGLE
			TYPE	RANGE	TYPE	RANGE	
G,P	SPC	14- 32	C	19- 32	SCD-I		90

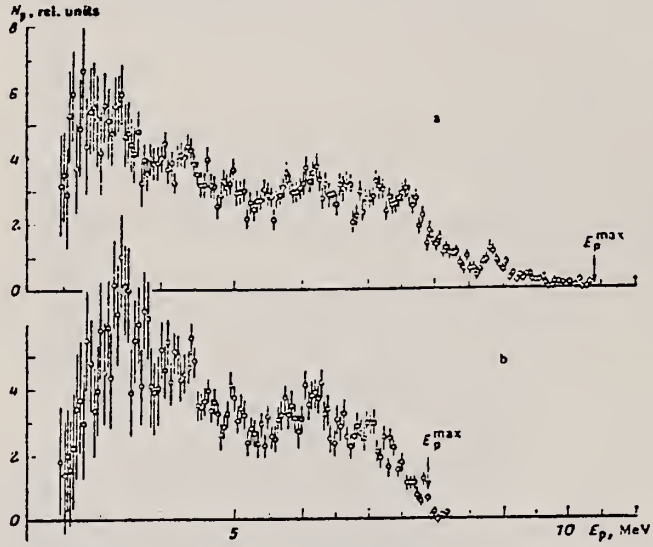

Fig. 1. Spectra of photoprotons from ^{26}Mg obtained for two values of E_γ^{max}: 24.5 MeV (a) and 22.0 MeV (b).

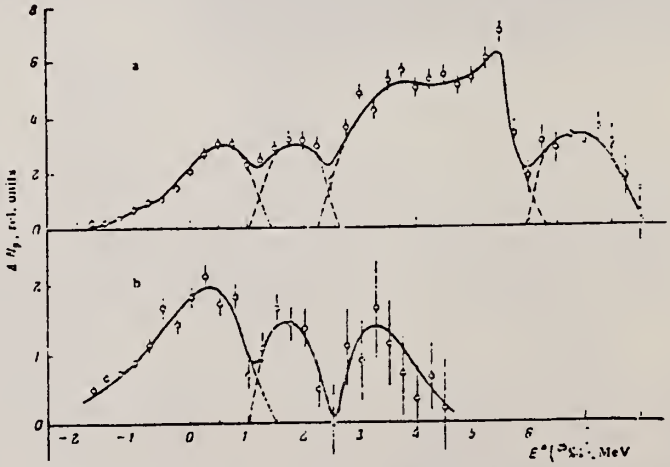

Fig. 2. Resultant distribution of $\Delta N_p(E_{f.n.}^*)$ obtained for different excitation-energy bands of ^{26}Mg: a) 22.0-27.0 MeV; b) 19.5-22.0 MeV.

REF. K. Bangert, U.E.P. Berg, G. Junghans, R. Stock, K. Wienhard, H. Wolf
Nucl. Phys. A261, 149 (1976)

ELEM. SYM.	A	Z
Mg	26	12

METHOD

REF. NO. 76 Ba 2 egf

REACTION	RESULT	EXCITATION ENERGY	SOURCE		DETECTOR		ANGLE
			TYPE	RANGE	TYPE	RANGE	
G,PG	ABY	15- 30	C	24, 30	SCD-D		90
G,NG	ABY	12- 30	C	24, 30	SCD-D		90

TABLE 5

Results of the ^{26}Mg(γ, $x\gamma'$) experiment, giving "bremsstrahlung-weighted" integrated cross sections in MeV · mb for the population of excited residual nuclear states

	Bremsstrahlung endpoint energy (MeV	
	23.5	30.0
(a) ^{25}Na states		
g.s. $\frac{5}{2}^+$	10.10 [a])	?
90 keV, $(\frac{1}{2}, \frac{3}{2})^+$		
1069 keV, $\frac{1}{2}^+$	<1.9	<2.7
2914 keV, $(\frac{1}{2}, \frac{3}{2})^+$	0.8	1.0
(b) ^{25}Mg states		
g.s. $\frac{5}{2}^+$	35.93 [b])	?
585 keV, $\frac{1}{2}^+$	<3.6	<3.5
974 keV, $\frac{3}{2}^+$	4.0	3.2 (?)
1611 keV, $\frac{7}{2}^+$	1.9	2.7
1965 keV, $\frac{3}{2}^+$	1.1	2.1
2564 keV, $\frac{1}{2}^+$	3.2	4.1
2801 keV, $\frac{3}{2}^+$	2.0	2.8
3901 keV, $(\frac{3}{2}, \frac{5}{2})^+$	0.8	1.8
4354 keV, $\frac{1}{2}^+$	1.7	1.63 (?)
4715 keV, ?	1.2	1.08 (?)
7784 keV, $(\frac{3}{2}, \frac{5}{2})^+$ $T = \frac{1}{2}$	2.57	3.1
7864 keV, $(\frac{3}{2}, \frac{5}{2})^+$ $T = \frac{1}{2}$	0.3	0.35
(c) ^{24}Mg states		
1369 keV, 2^+	0.8	2.6
(d) ^{22}Ne states		
1275 keV, 2^+	1.6	2.03
Sum of observed (γ, p) excited state cross section	2.7	3.7
Sum of observed (γ, n) excited state cross section	22.37	26.35
Proton yield [a])	12.8	
(γ, n)+(γ, np) yield [b])	58.31	80.2
(γ, 2n) yield [b])	7.2	25.22

Bremsstrahlung spectra normalized at 10.6 MeV.
[a]) Calculated from the data of ref. [4]).
[b]) Calculated from the data of ref. [2]).

[2] S.C. Fultz et al., Phys. Rev. C4, 149 (1971); R.A. Alvarez et al., Phys. Rev. C4, 1673 (1971).

[4] H. Wolf et al., Nucl. Phys. A234, 365 (1974).

REF. K. Wienhard, K. Bangert, U.E.P. Berg, G. Junghans, R. Stock and H. Wolf
Nucl. Phys. A280, 109 (1977)

ELEM. SYM.	A	Z
Mg	26	12

METHOD

REF. NO.: 77 Wi 1 egf

REACTION	RESULT	EXCITATION ENERGY	SOURCE		DETECTOR		ANGLE
			TYPE	RANGE	TYPE	RANGE	
G,P	ABX	16-24	C	24	TEL-D		DST
				(23.5)			

Assumes all ground state transitions

TABLE 1
Integrated and "bremsstrahlung-weighted" integrated proton cross sections

Excitation energy region of integration (MeV)	$\int\sigma(\gamma, p)dE$ (MeV · mb)	$\int(\sigma(\gamma, p)/E)dE$ (mb)
16.0—18.5	14.8	0.88
16.0—20.0	22.1	1.26
16.0—23.0	52.0	2.64

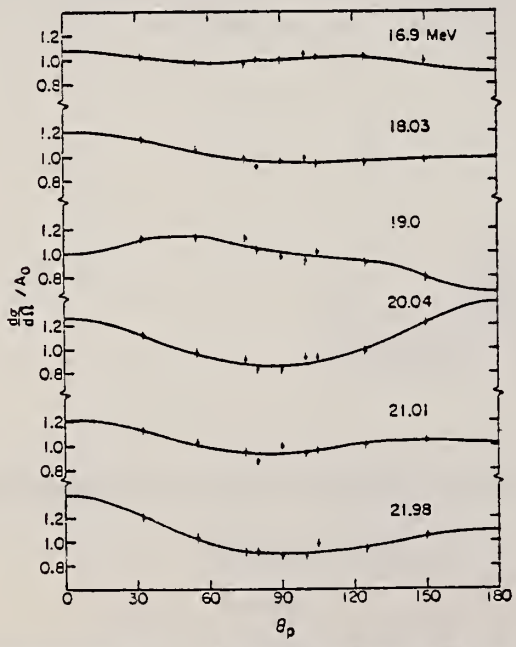

Fig. 1. Some angular distributions of the $^{26}Mg(\gamma, p)$ reaction. The solid lines through the data points are Legendre polynomial fits as discussed in the text. The error bars represent statistical uncertainties only.

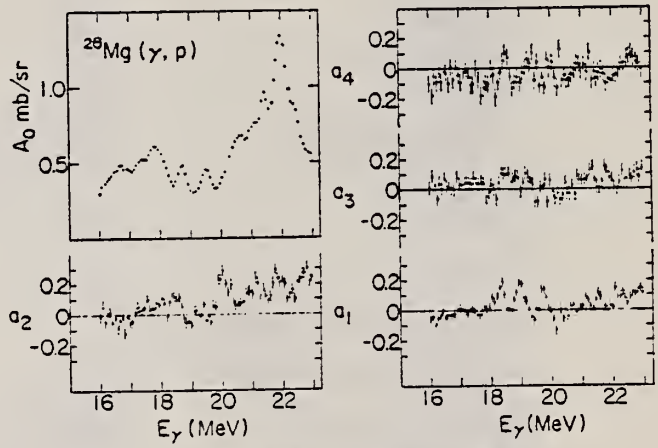

Fig. 2. Angular distribution coefficients.

REF. B.S. Ishkhanov, I.M. Kapitonov, V.N. Orlin, I.M. Piskarev, V.I. Shvedunov, V.V. Varlamov
Nucl. Phys. A313, 317 (1979)

ELEM. SYM.	A	Z
Mg	26	12

METHOD

REF. NO. 79 Is 2 hg

REACTION	RESULT	EXCITATION ENERGY	SOURCE		DETECTOR		ANGLE
			TYPE	RANGE	TYPE	RANGE	
G,PJ	ABX	14-27	C	19-27	MAG-D		UKN

J=0+1,3,6

Abstract: The energy spectra of photoprotons from ^{26}Mg have been measured with bremsstrahlung at five values of the end-point energy E^{max}, namely, at 19.5, 20.5, 22.0, 24.5 and 27.0 MeV. Using the difference spectra technique, we have determined the main decay channels of the states of the giant dipole resonance (GDR) of ^{26}Mg. The photoproton spectra have been used to obtain the cross sections for the formation of the final nucleus of the ^{26}Mg(γ,p)^{25}Na reaction in its various states. The magnitude of the configurational splitting of the GDR of ^{26}Mg has been estimated. Relevant data from other studies have been utilized to calculate the isospin components of the GDR of ^{26}Mg within the framework of a combined model for the decay of the giant resonance, with isospin taken into account. A new isospin interpretation of the cross sections for the photoproton and photoneutron reactions on the ^{26}Mg nucleus is proposed.

E NUCLEAR REACTION ^{26}Mg(γ, p), E = 19.5, 20.5, 22.0, 24.5, 27.0 MeV; measured photoproton energy spectra; deduced σ for different final states. Configurational and isospin splitting of GDR discussed. Enriched target.

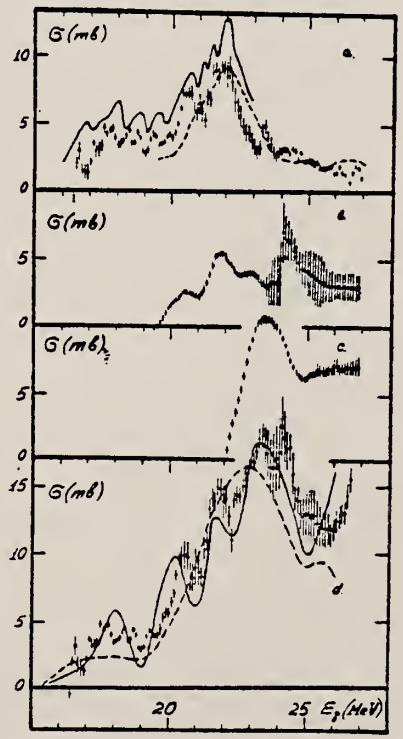

Fig. 4. Results of the calculation of the partial cross sections for the photoproton reaction on ^{26}Mg. (a) The cross section σ_{γ,p_0+p_1}; solid curve: data of ref. [8]), dotted curve: data of ref. [9]). (b) The cross section $\sigma_{\gamma,p_{2+3}}$. (c) The cross sections $\sigma_{\gamma,p_{4-6}}$. (d) The sum of the cross sections $\sigma_{\gamma,p_0+p_1}+\sigma_{\gamma,p_{2+3}}+\sigma_{\gamma,p_{4-6}}$; solid curve: data of ref. [4]); dotted curve: data of ref. [5]).

TABLE 1
Integrated cross sections for the partial photoproton reactions on ^{26}Mg

Reaction	ΔE (MeV)	Integrated cross sections (MeV · mb)		
		$\int_{E_{th}}^{20.9}\sigma dE$	$\int_{E_{th}}^{24.7}\sigma dE$	$\int_{E_{th}}^{27.0}\sigma dE$
(γ, p_0+p_1)	0.3	19.8±1.2	37.9±2.4	41.2± 2.6
(γ, p_{2+3})	0.8	2.9±0.2	18.1±1.6	26.8± 3.1
(γ, p_{4-6})	1.0		15.9±1.2	39.2± 1.4
(γ, p)		20.9±3.0	66.3±9.5	101.3±14.4

(over)

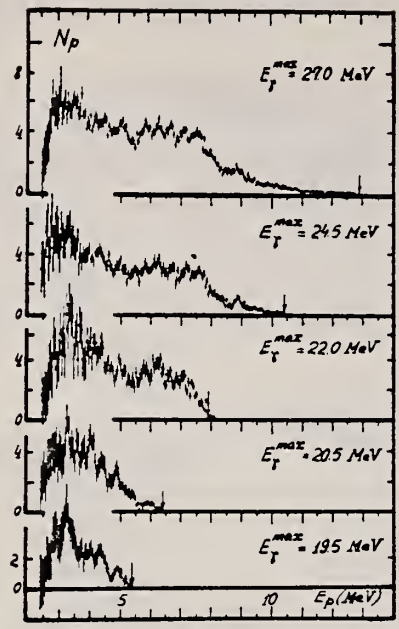

Fig. 1. Spectra of photoprotons (arb. units) from ^{26}Mg obtained for the various endpoint energies of the bremsstrahlung γ-radiation E_γ^{max}.

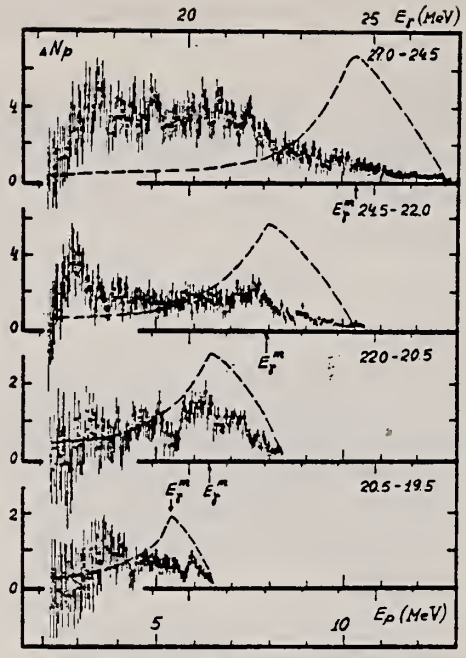

Fig. 2. Difference photoproton spectra (arb. units). The dotted curves indicate the difference photon spectra (E_γ^m is the energy at the maxima).

DEFINITIONS OF ABBREVIATIONS AND SYMBOLS

Note: In this list definitions are given for various photoneutron reactions in which the following symbols are used: N, NL, nN, SN and XN. Corresponding definitions apply for reactions involving other nuclear particles where the symbols N (neutron) is replaced by, e.g. P, D, T, HE, A etc. Where unknown reactions result in the production of a specific radionuclide, the chemical symbol and mass number is listed as the reaction product, e.g. a G,NA22 reaction in ^{59}Co.

A	alpha particle
ANAL	analysis
ABI	absolute integrated cross-section data
ABX	absolute cross-section data
ABY	absolute yield data. Often means cross-section per equivalent quantum is listed.
ACT	measurement of induced radioactivity of the target
ASM	asymmetric, asymmetry
AVG	average
BBL	bubble chamber
BEL B(EL)	reduced electric radiative transition probability
BF3	BF_3 neutron counter with moderator e.g., Halpern detector, long counter
BML	reduced magnetic radiative transition probability, B(ML)
BREAKS	levels located by "breaks" in the yield curve
BRKUP	breakup
BRMS	bremsstrahlung
BTW	between
C	continuous. Used to describe a photon source or a detector response function. Contrast with D = discrete.
CCH	cloud chamber
CF	compared with
CHRGD	charged
CMPT	Compton
COIN COINC	coincidence, coincide
COH	coherent
CK	Cerenkov
D	deuteron or discrete. When discrete, it is used to describe a photon source or a detector response function. Contrast with C = continuous.
DLTE	energy loss
DLTQ	momentum transfer
DST	distribution
DT BAL	detailed balance
E	electron
E/	inelastically scattered electron
E+	positron
EDST	energy distribution or spectrum
E/N	used only to indicate a coincidence experiment as in (E,E/N).

	N stands for any outgoing particle measured in coincidence with an inelastically scattered electron. Distinguish from eg., (E,N) which is used to represent an electron induced reaction when only the outgoing particle N is detected.
EMU	emulsions (photographic plates)
EXCIT	excited
F	fission
FMF	form factor
FM-1	inverse femtometers
FRAG	fragment
G	photon
G/	inelastically scattered photon
G-WIDTH	gamma-ray transition width
HAD	hadrons, hadron production
HE He3	^{3}He particle
INT	interaction, integral, intensity
INC	includes
ION	ionization chamber
ISOB	isobaric
ISM	isomer
J	multiplicity of particle defined by following symbol e.g. (G,PJN) with remark J = 2,3,5,7
JPI J-PI	spin and parity of a nuclear state
K	second multiplicity index, e.g. (G,JPKN) with both J & K positive integers greater than 1
KE	kinetic energy
L	may be an integer or zero that always follows a reaction product symbol. This is used to indicate transitions to specific states in the residual nuclide. When the letter is used as in (G,NL) the cross section given is that for the sum of transitions to two or more specific final states.
LFT	excited state lifetime
LIM	limit
LV,LVS	level, levels
LQD	liquid
MAG	magnetic spectrometer
MEAS	measurement(s)
MGC	magnetic Compton spectrometer
MGP	magnetic pair spectrometer
MOD	moderated neutron detector <u>not</u> employing a BF_3 counter, e.g. rhodium foil, Szilard-Chalmers reaction, ^{3}He, ^{6}Li reactions, GD loaded liquid scintillator, etc.
MSP	mass spectrometer
MULT	multiple, multipole, multiplicity
MU-T	used only in combination with G to indicate a total photon absorption cross section measurement, i.e. (G,MU-T)
N	neutron (see also XN and SN). The notation (G,N) is used to indicate a reaction in which only a single neutron is emitted, i.e. the reaction that can, in many cases, be measured by observing the radioactive decay of the residual nuclide.

nN	where n is any integer. (G,nN) indicates the sum over all reaction cross sections in which n neutrons are emitted.
NAI	NaI(Tl) spectrometer
NEUT	neutron(s)
NOX	no cross-section data
P	proton (see also XP)
PART	particle(s)
PHOT	photon(s)
PI	pion, usually written as PI+, PI-, PIO to indicate charge
POL	polarized or polarization
Q-SQUAR	momentum transfer squared (q^2)
RCL	recoil
REL	relative
RLI	relative integrated cross-section data
RLX	relative cross-section data
RSP	reaction spectrometer
RLY	relative yield data
SCTD	scattered
SCD	semiconductor (solid state) detector
SCI	scintillator detector other than NaI, e.g., CsI, KI, organic (liquid or solid), stilbene, He
SEP	separation
SEP ISOTP	separated isotope used
SIG	SIGMA (cross section)
SN	sum of neutron producing reactions, $\sigma(\gamma,SN)=\sigma(\gamma,N) + \sigma(\gamma,NP) + \sigma(\gamma,2N) + \sigma(\gamma,3N)$ + etc.
SPC	photon or particle energy spectrum
SPK	spark chamber
SPL	spallation
STAT	statistical
SYM	symetric, symmetry
T	triton
TEL	counter telescope
THR	threshold for reaction or threshold detector, e.g., $^{29}Si(n,p)^{29}Al$.
TOF	time-of-flight detector
TRK	tracks of particles or fragments observed in solid materials (glass, mylar, etc.)
TRNS	transition
UKN UNK	unknown
VIB	vibrational
VIR PHOT	virtual photon(s)
XN	all neutrons, total neutron yield, $\sigma(\gamma,XN) = \sigma(\gamma,N) + 2\sigma(\gamma,2N) + 3\sigma(\gamma,3N) + \sigma(\gamma,NP)$ + etc.
XP	all protons, total proton yield $\sigma(\gamma,XP) = \sigma(\gamma,P) + \sigma(\gamma,NP) + 2\sigma(\gamma,2P)$ + etc.
XX XXX	reaction products defined in REMARKS
YLD	yield

4PI	a 4π geometry was used or a method like radioactivity or a total absorption measurement		products was determined. The polarized particle is indicated in REMARKS.
999	energy defined in REMARKS	* or @	symbols used to indicate that the units associated with the numerals on one or both sides of the symbol in a specific column are not MeV. The units are defined in REMARKS.
$	indicates the measurement involved beams or targets that were either polarized or aligned, or that the polarization of the reaction		

NBS-114A (REV. 2-8C)

U.S. DEPT. OF COMM. BIBLIOGRAPHIC DATA SHEET (See instructions)	1. PUBLICATION OR REPORT NO.	2. Performing Organ. Report No.	3. Publication Date

4. TITLE AND SUBTITLE

Photonuclear Data-Abstract Sheets
1955-1982

5. AUTHOR(S)

E.G. Fuller and Henry Gerstenberg

6. PERFORMING ORGANIZATION (If joint or other than NBS, see instructions)

NATIONAL BUREAU OF STANDARDS
DEPARTMENT OF COMMERCE
WASHINGTON, D.C. 20234

7. Contract/Grant No.

8. Type of Report & Period Covered

9. SPONSORING ORGANIZATION NAME AND COMPLETE ADDRESS (Street, City, State, ZIP)

10. SUPPLEMENTARY NOTES

☐ Document describes a computer program; SF-185, FIPS Software Summary, is attached.

11. ABSTRACT (A 200-word or less factual summary of most significant information. If document includes a significant bibliography or literature survey, mention it here)

These abstract sheets cover most classes of experimental photonuclear data leading to information of the electromagnetic matrix element between the ground and excited states of a given nucleus. This fifteen volume work contains nearly 7200 abstract sheets and covers 89 chemical elements from hydrogen through americium. It represents a twenty-seven year history of the study of electromagnetic interactions. The sheets are ordered by target element, target isotope, and by an assigned bibliographic reference code. Information is given on the type of measurement, excitation energies studied, source type and energies, detector type, and angular ranges covered in the measurement. For a given reference, the relevant figures and tables are mounted on a separate sheet for each nuclide studied.

12. KEY WORDS (Six to twelve entries; alphabetical order; capitalize only proper names; and separate key words by semicolons)

data-abstract sheets, elements, experimental, isotopes, nuclear physics, photonuclear reactions

13. AVAILABILITY

☐ Unlimited

☒ For Official Distribution. Do Not Release to NTIS

☐ Order From Superintendent of Documents, U.S. Government Printing Office, Washington, D.C. 20402.

☐ Order From National Technical Information Service (NTIS), Springfield, VA. 22161

14. NO. OF PRINTED PAGES

15. Price

USCOMM-DC 6043-P80